HYDROLOGICAL MODELING TO STUDY THE INTERACTIONS OF LAND USE−CLIMATE−HYDROLOGY FOR SUSTAINABLE RIVER BASIN MANAGEMENT

Ph.D. THESIS

by

PALMATE SANTOSH SUBHASH

DEPARTMENT OF WATER RESOURCES DEVELOPMENT & MANAGEMENT
INDIAN INSTITUTE OF TECHNOLOGY ROORKEE
ROORKEE - 247 667 (INDIA)
DECEMBER, 2018

HYDROLOGICAL MODELING TO STUDY THE INTERACTIONS OF LAND USE−CLIMATE−HYDROLOGY FOR SUSTAINABLE RIVER BASIN MANAGEMENT

A THESIS

Submitted in partial fulfilment of the requirements for the award of the degree

of

DOCTOR OF PHILOSOPHY

in

WATER RESOURCES DEVELOPMENT AND MANAGEMENT

by

PALMATE SANTOSH SUBHASH

DEPARTMENT OF WATER RESOURCES DEVELOPMENT & MANAGEMENT
INDIAN INSTITUTE OF TECHNOLOGY ROORKEE
ROORKEE - 247 667 (INDIA)
DECEMBER, 2018

INDIAN INSTITUTE OF TECHNOLOGY ROORKEE
ROORKEE

CANDIDATE'S DECLARATION

I hereby certify that the work which is being presented in the thesis entitled **"HYDROLOGICAL MODELING TO STUDY THE INTERACTIONS OF LAND USE−CLIMATE−HYDROLOGY FOR SUSTAINABLE RIVER BASIN MANAGEMENT"** in partial fulfilment of the requirement for the award of the Degree of Doctor of Philosophy and submitted in the Department of Water Resources Development and Management of the Indian Institute of Technology Roorkee, Roorkee is an authentic record of my own work carried out during a period from July, 2013 to December, 2018 under the supervision of Dr. Ashish Pandey, Associate Professor, Department of Water Resources Development and Management, Indian Institute of Technology Roorkee, Roorkee.

The matter presented in this thesis has not been submitted by me for the award of any other degree of this or any other Institute.

(PALMATE SANTOSH SUBHASH)

This is to certify that the above statement made by the candidate is correct to the best of my knowledge.

(Ashish Pandey)
Supervisor

The Ph.D Viva-Voce Examination of Mr. Palmate Santosh Subhash, Research Scholar, has been held on.....

Chairman, SRC **Signature of External Examiner**

This is to certify that student has made all the corrections in the thesis.

Signature of Supervisor **Head of the Department**

Date: …….

ABSTRACT

Sustainable natural resources management at local and regional scale is a prime concern for growth, development, conservation, and protection of the environment, and prosperity of the nation. To mitigate the present and future anthropogenic activities and climatic change, field-based investigations of land and water resources are time-consuming and challenging to manage and sustain the agriculture food production in developing countries like India. Indian River basins are one of the most influencing natural systems owing to land dynamics and the uncertain climatic events, such as cloud bursting and heavy rainfall occurred in Uttarakhand during the year 2013, then in Chennai (2015), and the recently in Kerala (2018). The present study has been focused to model the complex hydrological process of the Betwa River basin, part of the lower Yamuna River basin located in central India, for sustainable management of land and water resources considering future climate change and land use change. In this context, hydrological modelling can be considered as a valuable technique for the simulation of basin-wide various hydrologic components i.e. stream flow (FLOW), sediment yield (SYLD), evapotranspiration (ET) and water yield (WYLD) etc.

In this study, various satellite imageries have been utilized to prepare the historical land use/land cover (LU/LC) maps for the years 1972, 1976, 1991, 2001, 2007, 2010 and 2013 using a maximum likelihood supervised classification method. Further, an integrated Cellular Automata-Markov Chain (CA-MC) model based on Geographical Information System (GIS)-based Multi-Criteria Evaluation (MCE) and the Multi-Objective Land Allocation (MOLA) methods has been employed to predict the future LU/LC maps for the years 2020, 2040, 2060, 2080 and 2100. Future problems such as food security and surface water resources availability are successfully discovered through CA-MC model.

To study the relationships between land cover dynamics and hydro-climatic variables, the MODIS NDVI (MOD13Q1) and land cover (MCD12Q1) time-series datasets have been used for correlation analysis, and then Multiple Linear Regression (MLR) models were prepared at monthly, seasonal and annual time-scale over the period of 2001-2013. The Savitzky-Golay filtering method was employed to de-noise and smoothing of the NDVI time-series data using TIMESAT software. The land greening and land degradation under dry spell, wet spell and combined dry and wet spells were analyzed employing a conceptual framework, representing four concepts of climatic greening, climatic degradation, non-climatic greening and non-climatic degradation etc. The developed conceptual framework approach can be applied effectively in other river basins having different land cover and hydro-climatic conditions.

Further, hydrological modelling considering numerous medium to large sized water storages (7 reservoirs and 2 weirs) located on main channel as well as tributary channel of the Betwa river has been carried out using the Soil and Water Assessment Tool (SWAT). With the required spatial, storage and outflow information, these water storages were successfully implemented and managed for reliable hydrological simulation using the SWAT model. Monthly calibration, validation, sensitivity and uncertainty analyses have been carried out using the SWAT-Calibration and Uncertainty Programs (CUP) Sequential Uncertainty Fitting version-2 (SUFI-2) algorithm for the years 2003-2013. The observed and simulated hydrographs for both the streamflow and sediment indicates a good performance of the SWAT model. The model

performance was high for the Garrauli gauging site without any upstream water storage structure, as compared to the gauging sites with upstream water storage structures. This analysis shows that better information of the water storage structures promises a significantly improved hydrological simulation using the SWAT model.

The India Meteorological Department (IMD) data benchmarked in calibrated and validated SWAT model was replaced by the downscaled and bias-corrected (quantile mapping method) Global Climate Model (GCM) data of the Max-Planck-Institute-Earth System Model-Medium Resolution (MPI-ESM-MR) model. In this study, the MPI-ESM-MR model data of RCP 8.5, a worst-case climate scenario, has been considered for hydrologic simulation at the severe climate condition in future. Land use data of the years 2013 and 2040, and the GCM-derived climate variables were categorized into five periods i.e. baseline 1986 (1986-2005), horizon 2020 (2020-2039), horizon 2040 (2040-2059), horizon 2060 (2060-2079), and horizon 2080 (2080-2099) and used to assess the land use and climate change impact on hydrological simulation of streamflow (FLOW), sediment yield (SYLD), Evapotranspiration (ET) and water yield (WYLD). It was found that climate change impact is dominant over the impact of land use change in future. Further, a conceptual framework has been developed to assess the individual as well as combined impacts of land use and climate change. The proposed conceptual framework can be used effectively for watershed analysis with given limitations.

Furthermore, based on the future simulations, critical sub-watersheds of the study area were identified and then prioritized for effective implementation of Best Management Practices (BMPs). In this study, the over-land as well as in-stream BMPs has been implemented to reduce the streamflow and sediment yield in future. Four over-land BMPs namely tillage management, contour farming, residue management and strip cropping for agriculture land, and five in-stream BMPs namely grassed waterways, streambank stabilization, grade stabilization structures, porous gully plugs and recharge structures for main and tributary river channels have been considered in this study. Sensitivity and uncertainty analysis of BMPs parameters were also carried out for an effective management and implementation of BMPs in the river basin. The effectiveness of BMPs implementation was estimated by percent reduction and sensitivity index of the model parameters. It was found that strip cropping is the most effective agriculture land operation which reduces streamflow in the range of 11.07% to 13.97% and sediment yield in the range of 21.04% to 37.28% for soil and water conservation of the river basin in future. Furthermore, the in-stream BMPs namely grassed waterways and streambank stabilization can be an effective intervention for sediment yield reduction (about 20% to 60%), and grade stabilization structures for streamflow reduction (about 6% to 10%) within the main river channel.

Overall, this study provides connectivity of land use change, climate change, and hydrological modelling for the research communities focusing sustainable river basin management, and may also provide valuable guidelines to the users interested in water resources development, planning and management in agriculture dominant large river basin.

ACKNOWLEDGEMENT

I wish to express my deep sense of gratitude to my supervisor Dr. Ashish Pandey, Associate Professor, Department of Water Resources Development and Management (WRD&M), Indian Institute of Technology (IIT) Roorkee, for his invaluable guidance, thought provoking discussions and untiring efforts throughout the course of this work. His timely help, encouragement, constructive criticism, and painstaking efforts made it possible to present the work carried out by me in the form of this thesis.

I am thankful to Prof. Ajit Kumar Chaturvedi, Director, IIT Roorkee; Prof. S. K. Mishra, Head, Department of WRD&M; Prof. Deepak Khare, Chairman, DRC, SRC & Internal Member (SRC); Dr. Sumit Sen, Department of Hydrology & External Member (SRC) for providing constructive suggestions and boosting moral during the study period. I thankfully acknowledge the moral and technical support received from my friends. I am thankful to my volleyball team players and coach for their faithful support to my extra-curricular activities during Ph.D. study.

It will be unjust on my part to bind in words the spirits of unparalleled sacrifices made by my parents, my father Late Shri Palmate Subhash Shivdas, and my mother Smt. Palmate Suman S., and my brothers, sisters, uncles and aunties for their blessings. The moral support of my grand-parents, my grandfather Shri Palmate Shivdas Paran, and my grandmother Smt. Palmate Kisabai S., always encouraged me to pursue the higher studies. I also feel obliged to my family members who have always supported me spiritually throughout the study and my life in general.

I sincerely acknowledge the Ministry of Human Resource Development (MHRD), Government of India (GoI) to provide financial support in the form of scholarship during the study period in IIT Roorkee. I would like to acknowledge the support under the 'World Bank Robert S. McNamara (RSM) Fellowship Programme-2017' to take research guidance of Prof. Dr. Nicola Fohrer in the Department of Hydrology and Water Resources Management, Institute for Natural Resource Conservation, Kiel University, Germany. Also, I am thankful to Dr. Paul D. Wagner for providing constructive suggestions and technical support during RSMFP-2017. Furthermore, the scholarship provided by 'University of Bergen, Norway' to attend 'Bergen Summer Research School-2016' on 'Water, Climate and Society: Modeling the complexities of water, climate and society'; the partial fellowship provided by the 'University Network for Climate and Ecosystems Change Adaptation Research (UN-CECAR), United Nations University (UNU)' to attend the training course on 'Climate Change Adaptation Approaches and Applications (CCDAA)-2015', the Early Career Scientist's Travel Support provided to present my Ph.D. Research work in the 'European Geosciences Union (EGU) General Assembly 2017', and the travel support provided by ITS (DST), GoI to present my research work in the 'EGU-2019' conference at Vienna, Austria is greatly acknowledged.

Further, my humble thanks are due to all those who in any manner, directly or indirectly, put a helping hand in every bit of completion of this research work.

(Palmate Santosh Subhash)

TABLE OF CONTENT

LIST OF FIGURES

LIST OF TABLES

LIST OF ABBREVIATIONS & SYMBOLS

Abbreviation/ Symbol		Description
%	:	Percentage
°C	:	Degree Celsius
95PPU	:	95 Percentile Prediction Uncertainty
ADJ_PKR	:	Peak rate adjustment factor for sediment routing in the sub-watershed (tributary channels
AI	:	Aridity Index
ALPHA_BF	:	Baseflow alpha factor
A_o	:	Overall accuracy
A_p	:	Producer's accuracy
ARS	:	Agricultural Research Service
A_u	:	User's accuracy
BMP	:	Best Management Practice
BRB	:	Betwa River Basin
BSV	:	Barren or sparsely vegetated
CA-MC	:	Cellular Automata - Markov Chain
CH_COV1	:	Channel erodibility factor
CH_COV2	:	Channel cover factor
CH_EROD	:	Channel erodibility factor
CH_ERODMO	:	Jan. channel erodability factor
CH_K1	:	Changing hydraulic conductivity
CH_N1	:	Manning's roughness coefficient 'n' of tributary main channel
CH_N2	:	Manning's roughness coefficient 'n' of main channel
CH_S2	:	Slope of the main channel segment
CL	:	Crop Land
CN2	:	Curve Number for moisture condition II
CN2	:	Initial SCS runoff curve number for moisture condition II
CSL	:	Closed Shrub Land
CWC	:	Central Water Commission
DBF	:	Deciduous Broadleaf Forest
DEM	:	Digital Elevation Model
DEPTIL	:	Depth of Tillage
DNF	:	Deciduous Needleleaf Forest
EBF	:	Evergreen Broadleaf Forest
EFFMIX	:	Tillage mixing efficiency
ENF	:	Evergreen Needleleaf Forest
EOS	:	Earth Observing System
ESCO	:	Soil evaporation compensation factor

ET	:	Evapotranspiration
ETM+	:	Enhanced Thematic Mapper Plus
FLOW	:	Streamflow
FSI	:	Forest Survey of India
g/l	:	Gram per liter
GCM	:	Global Circulation Model
GDRAIN	:	Drain tile lag time
GDS	:	Gauge Discharge Sediment
GIS	:	Geographical Information System
GL	:	Grass Land
GloVis	:	Global Visualization viewer
GPS	:	Global Positioning System
GW_DELAY	:	Groundwater delay time
GWQMN	:	Threshold depth of water in the shallow aquifer required for return flow to occur
ha	:	Hectare
HO	:	Hydrologic Observatory
hr	:	Hour
HRU	:	Hydrological Response Unit
IDW	:	Inverse Distance Weighted
IFLOD1R	:	Beginning month of non-flood season
IFLOD2R	:	Ending month of non-flood season
IMD	:	India Meteorological Department
IRS	:	Indian Remote Sensing
K_c	:	Kappa coefficient
KIA	:	Kappa Index of Agreement
km	:	Kilometer
km^2	:	Square Kilometer
LAI	:	Leaf Area Index
LAT_SED	:	Sediment concentration in lateral flow and groundwater flow
LISS	:	Linear Imaging and Self Scanning
LP DAAC	:	Land Processes Distributed Active Archive Center
LU/LC	:	Land Use/Land Cover
m	:	Meter
m.s.l.	:	Mean sea level
m^2	:	Square meter
m^3/s	:	Cubic meter per second
MCE	:	Multi-Criteria Evaluation
MCM	:	Million Cubic Meters
MLR	:	Multiple Linear Regression

mm	:	Millimeters
mm/day	:	Millimeter per day
MODIS	:	MODerate resolution Imaging Spectro-radiometer
MOLA	:	Multi-Objective Land Allocation
MP	:	Madhya Pradesh
MPI-ESM-MR	:	Max Planck Institute-Earth System Model-Medium Resolution
MRT	:	MODIS Reprojection Tool
MSS	:	Multi-Spectral Scanner
MUSLE	:	Modified Universal Soil Loss Equation
MXF	:	Mixed Forest
NBSS&LUP	:	National Bureau of Soil Survey and Land Use Planning
NCCS	:	NASA Center for Climate Simulation
NDTARGR	:	Number of days required to achieve a target storage from the current reservoir storage
NDVI	:	Normalized Difference Vegetation Index
NDWI	:	Normalized Difference Water Index
NEX-GDDP	:	NASA Earth Exchange Global Daily Downscaled Projections
NRCS	:	National Resource Conservation Services
NRSC	:	National Remote Sensing Centre
NSE	:	Nash-Sutcliffe Efficiency
NV	:	Natural Vegetation
NWDA	:	National Water Development Agency
OAT	:	One-At-a-Time sensitivity analysis
OLI	:	Operational Land Imager
OSL	:	Open Shrublands
OV_N	:	Manning's roughness coefficient for overland flow
P	:	Precipitation
PBIAS	:	Percent Bias
PET	:	Potential Evapotranspiration
PRF	:	Peak rate adjustment factor for sediment routing in the main channel
PWL	:	Permanent Wetlands
Q	:	Discharge
QA	:	Quality Assessment
r	:	Coefficient of correlation
R^2	:	Coefficient of Determination
RCHRG_DP	:	Deep aquifer percolation fraction
RCM	:	Regional Climate Model
RCP	:	Representative Concentration Pathway
RES_NSED	:	Equilibrium sediment concentration in the reservoir

RES_RR	:	Average daily principle spillway release rate
RES_SED	:	Initial sediment concentration in the reservoir
RES_STLR_CO	:	Reservoir sediment settling coefficient
R_H	:	Relative Humidity
RMSE	:	Root Mean Square Error
RMSE	:	Root Mean Square Error
RSR	:	RMSE-Observations Standard Deviation Ratio
S&I	:	Snow and Ice
SCS	:	Soil Conservation Services
SD	:	Standard eviation
SI	:	Sensitivity Index
SOL_AWC	:	Available water capacity of the soil layer
SPEXP	:	xponent parameter for calculating sediment re-entrained in channel sediment routing
SRTM	:	Shuttle Radar Topography Mission
STARG	:	Monthly target reservoir storage
STDEV	:	Standard Deviation
SUFI-2	:	Sequential Uncertainty Fitting version 2
SURLAG	:	Surface runoff lag coefficient
SV	:	Savannas
SW	:	Sub-Watershed
SWAT	:	Soil and Water Assessment Tool
SWAT-CUP	:	SWAT- Calibration and Uncertainty Programs
SYLD	:	Sediment yield
$t\ ha^{-1}\ yr^{-1}$	:	Tonnes per hectare per year
TAM	:	Transition Area Matrix
Tdiff	:	Difference of Maximum and Minimum Temperature
TM	:	Thematic Mapper
Tmax	:	Maximum Temperature
Tmin	:	Minimum Temperature
TPM	:	Transition Probability Matrix
TSM	:	Transition Suitability Map
U&B	:	Urban and builtup
UP	:	Uttar Pradesh
USDA	:	United States Department of Agriculture
USGS	:	United States Geological Survey
USLE	:	Universal Soil Loss Equation
USLE_C	:	Minimum value of USLE C factor
USLE_K	:	USLE equation soil erodibility
USLE_P	:	USLE equation support practice factor

UTM	:	Universal Transverse Mercator
WGS	:	World Geodetic System
WRIS	:	Water Resources Information System
WSV	:	Woody Savannas
WTR	:	Water
WYLD	:	Water yield
YBO	:	Yamuna Basin Organization
β	:	Beta coefficient

CHAPTER 1
INTRODUCTION

1.1 GENERAL BACKGROUND OF THE STUDY

Sustainable management of land and water resources in a river basin is vital for growth and development of the rural livelihood, conservation and protection of the environment, and prosperity of the Nation. Efficient management of natural resources in a large river basin is difficult and time-consuming (Griffin, 1999; Muro and Jeffrey, 2008); instead the GIS-based hydrological modelling can provide a framework to simulate the complex hydrological process and evaluate the management practices for decision and policy making (Abu-Zreig et al., 2004; Newham et al., 2004; Oxley et al., 2004; Pandey et al., 2007; Christianson et al., 2008; Jackson et al., 2008; Pandey et al., 2009 & 2011; Sardar et al., 2012; Kumar et al., 2014). Precise simulation of hydrological components, such as streamflow and sediment, addresses the issues/problems in environmental management and socio-economic development. The progressively developed hydrological models, and the advanced freely-available global datasets such as digital elevation models (DEM), remote sensing imagery data, and spatial data of land use and soil, have been employed in the published literature (Tripathi et al., 2003, 2004 & 2005; Karydas et al., 2014; Prabhanjan et al., 2014; Kumari et al., 2016; Golmohammadi et al., 2017b).

Hydrological models vary from a simple empirical equation to complex physically distributed models based on spatial and temporal scales, in-build process, and algorithm used (Borah and Bera, 2003; Naik et al., 2009; Ale et al., 2012; Devia et al., 2015). In this perspective, selection of an appropriate hydrological model is difficult and challenging for the potential users to simulate the complex hydrological process and resolve the land and water resources management problems. The vulnerability of extreme hydrological changes has already been exposed showing the pronounced impact on human life and natural system. The changes in availability of water resources are expected to be among the most significant consequences of climatic change (Kingston and Taylor, 2010; Cibin et al., 2017). Consequently, the spatial and temporal hydrological changes can significantly alter the ongoing management and development in agriculture, industry, and urban sectors (Frederick et al., 1997; Matsuno et al., 2007; Hutchinson et al., 2011; Matsuno et al., 2013; Stang et al., 2016; Her et al., 2017; Mauget et al., 2017; McDonough et al., 2017). Thus, awareness of the environmental change due to anthropogenic activities has been presently accelerating, and could also be continued in future for sustainable planning, management and development of a watershed.

From last few decades, changes in land use and climate have been gradually studied world-wide as they are expected to alter the hydrological cycle of a watershed, i.e. especially vulnerable to the available land and water resources (Vörösmarty, 2000; Bekker and Matsuno, 2001; Mishra et al., 2007b; Gitau et al., 2010; Mango et al., 2011; Craine et al., 2012; Golmohammadi et al., 2013; Singh et al., 2014; Bhave et al., 2016; Dey and Mishra, 2017; Sinha and Eldho, 2018). Land use changes are attributed to the spatiotemporal changes in dominant area of the watershed such as agriculture, forest, settlement, and barren land (Fohrer et al., 2001; Weber et al. 2001; Chiang et al., 2010; Palmate et al., 2017). Climate change is attributed to long-term changes in the meteorological variables such as precipitation and temperature (Chien et al., 2013; Reddy et al., 2016). Effect of precipitation changes on hydrological response has been studied independently, as well as in combination with temperature change by Shen et al. (2009). In reality, both the precipitation and temperature variables are likely to vary spatially and temporally, and may have pronounced impact on components of the hydrological cycle.

The scientific/research community has realized that the hydrological response of a watershed/catchment/river basin to the changes in land use and climate are more complex than it was originally believed. Hydrological response depends on the physical characteristics, climatic conditions, and sources of runoff of the river basin (Fontaine et al., 2001; Golmohammadi et al., 2017a; Park et al., 2017; Zhang et al., 2018). It is widely acknowledged that an empirical equation between hydrological response and changes in land use and climate derived by spatiotemporal analysis can be used as an alternative or complement to the physical hydrological modelling (Wagener, 2007; Bulygina et al., 2012). In some regions, the hydrological response has been affected by rapid land use changes, and the sources of hydrological alterations that may complicate the spatial generalization (Chiew et al., 2009; Peel and Blöschl, 2011). Furthermore, climate change forms interactive system by linking a human action, viz. settlement and industrialization inducing the land use change, which in turn renders the complex hydrological process (Schulze, 2000). These changes have significant impact on hydrological components such as frequency and distribution pattern of precipitation, surface-runoff, groundwater, sediment, evapotranspiration, soil moisture etc., and thus, affect the available land and water resources. Therefore, the study on hydrological response of a river basin under the consideration of changes in land use and climate is pre-requisite for sustainable planning and management in present and future years.

Physically based hydrological modelling has always been the primary choice of the researchers while dealing with complex hydrological process and the simulation problems. In general, GIS

provides a framework to different hydrologic models globally developed for environmental application and evolution (Chowdary et al., 2009 & 2013). Thus, the GIS-based hydrologic models are being used to assess the effect of land use and climate changes for a watershed. Hydrological models are broadly classified into several categories, i.e. empirical (*black-box / metric*) model, conceptual (*grey-box / parametric*) model, and physically based distributed (*white-box / mechanistic*) model. Empirical models, such as ANN (*Artificial neural network*) and unit hydrograph, can only relate the input to output through some transform function, but not explicitly consider the governing physically based hydrological processes involved (Gupta et al., 1980; Jakeman et al., 1990; Minns and Hall, 1996; Dawson and Wilby, 2001). Conceptual models, such as SWM (*Stanford Watershed Model IV*) and HBV (*Hydrologiska Byrans Vattenavdelning Model*), represent the effective measurement of an entire catchment, without attempting to characterize the spatial variability (Bergström and Forsman, 1973; Harlin, 1991; Crawford and Linsley, 1996; Kumar and Warsi, 1998). Lumped models, such as MIKE 11, are defective to represent the spatial variability of hydrologic processes and catchment parameters (Refsgaard, 1987; Moore et al., 1991). The physically based distributed models, such as SHE (*Systeme Hydrologique European*)/MIKESHE and SWAT (*Soil and Water Assessment Tool*), are those which are able to explicitly represent spatial variability of the important land surface characteristics such as topographic elevation, land slope, aspect ratio, vegetation cover, soil type, as well as the climatic parameters including precipitation, and temperature (Refsgaard et la., 1992; Havnø et al., 1995; Refsgaard, 1995; Arnold et al., 2012b). Nowadays, the SWAT model is being widely acknowledged and used to simulate the quantity and quality of water-flow and sediment, and to evaluate the land management practices for a watershed (Arnold and Fohrer, 2005; Moriasi et al., 2013; Daggupati et al., 2015; Chen et al., 2017; Mishra et al., 2007a). Therefore, in this study the SWAT model has been used to simulate the complex hydrological process for sustainable management of an Indian River basin.

1.2 NEED OF HYDROLOGICAL MODELLING STUDY IN INDIAN RIVER BASINS

The vulnerability of land use and climate change in Indian subcontinent is vital to study their impacts on hydrology, natural resources, agricultural productivity, and the economy of India. Due to the poor capacity to cope up with and adapt changes, these impacts in the developing countries like India are going to be most severe again (Kulkarni and Karyakarte, 2014). Among major rivers of the Indian subcontinent, the Ganga, Brahmaputra and Indus Rivers, originates from the Himalayas, and substantially contribute the flow from snow and glaciers, are expected to be more vulnerable due to the anthropogenic activities and the land use and climatic changes

(Tiwari et al., 2000; Bookhagen and Burbank, 2010; Immerzeel et al., 2010; Nepal and Shrestha, 2015). For in these river basins, little emphasis has been given on the study of possible future impacts of land use and climate changes employing hydrological modelling approach (Miller et al., 2012; Nepal and Shrestha, 2015). Mehrotra and Mehrotra (1995) studied the impact of climate change on hydrology of the Indian River basin, considering substantial changes in precipitation at spatial and temporal scales. The frequency of heavy precipitation events showed increasing trends over the central part of India (Goswami et al., 2006). Thus, it is necessary to study the possible changes in available land and water resources employing hydrological modelling approach.

1.3 MOTIVATION AND STATEMENT OF THE PROBLEMS

In the present study, an attempt has been made to investigate the impacts of land use and climate changes on hydrology of the Betwa River basin located in central India which is a part of the Yamuna River, a tributary of Ganga River system. The Betwa River basin has dominant agriculture land which plays important role in rural livelihood. Forest is thick in hillier South-East region and covers about one-fourth area of the total basin. Betwa basin falls under semi-arid to dry sub-humid climate region of the India. The air of the Betwa basin is being mostly dry with exception of south-west monsoon season. It has generally mild winter and hot summer climate. Increase in winter temperature may adversely affect the growth of Rabi crops (wheat and mustard) in the Betwa basin (Suryavanshi et al., 2014). Thus, it is essential to study the impacts of land use and climate changes for present and future years employing hydrological modelling approach for the Betwa basin. This study can be helpful for the sustainable land and water resources management and development of the Betwa River basin.

The Betwa basin is classified as an agricultural river basin in the central part of India. The runoff/streamflow and sediment in the Betwa basin is strongly influenced by changes in land use and climate. Hydrological modelling of a river basin can render better land and water resources in agriculture and river channels for sustainable management of available resources. Besides, the application of feasible management practices can protect the degradation of the critical areas due to flooding situation and unconventional field treatments. Intensive use of unconventional agricultural practices is one of the main reasons for increasing land and water resources problems in the Betwa river basin. The excessive change in vegetation cover may cause looseness in the soil which may further washed off by surface runoff. In addition, improper management of dominant agriculture area and river channel network can negatively affect surface water flow and sediment in the Betwa River basin.

1.4 OBJECTIVES OF THE STUDY

Keeping the aforementioned, the present study has been planned with the following specific objectives:

1. To study the spatiotemporal land use/land cover (LU/LC) changes of the Betwa River basin and its modelling for future analysis.
2. To study the relationship between hydro-climatic variables and land cover dynamics under dry and wet spells over Betwa Basin.
3. Hydrological modelling of water storages in the Betwa River basin using Soil and Water Assessment Tool (SWAT).
4. Development and application of a conceptual framework to study the individual as well as combined impact of land use and climate change on hydrology of the Betwa River basin.
5. Evaluation of the over-land and in-stream best management practices (BMPs) for sustainable development of the Betwa River basin.

1.5 ORGANIZATION OF THESIS

The thesis has been organized in nine chapters as follows:

Chapter 1: This chapter briefly describes the general background of the study and the present state-of-the-art knowledge of land use change, climate change, and hydrological modelling. Furthermore, the motivation of study, need of hydrological modelling study in the Betwa River basin, and specific research objectives are provided.

Chapter 2: This chapter deals with the literature reviews on land use change, climate change, their impact on river basin hydrology, use of hydrological models, and the BMP application for sustainable management. Critics in the literature review have been also included in this chapter.

Chapter 3: This chapter includes details of the study area characteristics, acquisition of hydro-meteorological data, remote sensing data, generation of thematic maps, ground truth verification, field visits, present land management practices, and water resources in the Betwa River basin.

Chapter 4: This chapter deals with the spatiotemporal land use/land cover (LU/LC) analysis for historical and future years. An integrated Cellular Automata and Markov Chain (CA-MC) model has been used for future LU/LC prediction. Furthermore, the LU/LC change analysis has been carried out for two inter-state regions, i.e. Madhya Pradesh (MP) and Uttar Pradesh (UP), covered within the Betwa basin.

Chapter 5: This chapter deals with the relationship analysis between hydro-climatic variables and land cover dynamics at monthly, seasonal and annual time-scale. The time-series MODIS data of NDVI and land cover has been employed to study climatic greening, non-climatic greening, climatic degradation and non-climatic degradation employing a conceptual framework, and spatial change analysis.

Chapter 6: This chapter emphasizes description of the SWAT model, input and output files, model set-up and run, water storages (7 reservoirs and 2 weirs) management, sensitivity and uncertainty analysis, model calibration and validation, model evaluation for the simulation of streamflow and sediment at four gauging sites, i.e. Basoda, Garrauli, Mohana, and Shahijina, of the Betwa river basin.

Chapter 7: This chapter deals with the comprehensive analysis of individual land use change impact, individual climate change impact, and combined land use and climate change impact on streamflow, sediment yield, evapotranspiration and water yield in future. Further, the conceptual framework has been developed and employed for individual as well as combined impact assessment.

Chapter 8: This chapter deals with the identification and prioritization of critical areas based on future hydrological simulation, implementation of over-land as well as in-stream BMPs, sensitivity and uncertainty analysis of BMP parameters in SWAT, and percent reduction in streamflow and sediment yield. Based on pre-BMP and post-BMP simulations, the optimal BMP has been recommended for sustainable management of agriculture land and river channel.

Chapter 9: This chapter discusses the summary and conclusions of the study. The major research contributions and future research scope has been also discussed at the end of this chapter.

Furthermore, few appendices which includes (A) field visit photographs, (B) LU/LC modelling statistical (confusion matrix) tables, (C) relationship equations, (D) hydrological response unit (HRU) distribution table of the SWAT model, and (E) the sub-watershed wise model simulation tables under land use and climate change, have been provided for more detailed information of the analyses carried out in the present research study.

CHAPTER 2
LITERATURE REVIEW

This chapter encompasses review of the relevant literatures on hydrological modelling and land use change modelling, and their application studies. Further, the application of SWAT model in land use change and climate change impact assessment, critical area identification and prioritization, best management practices application and evaluation has been also discussed. The last section deals with the sustainable river basin management and development employing hydrological modelling approach, and the critiques in literature review.

2.1 NECESSITY AND CONSTRAINTS OF MODELLING APPROACH

Limited field measurements create difficulty to understand the hydrological processes of a watershed/river basin. Long term remote sensing datasets of land use/land cover (LU/LC) and climate are required as inputs to the Geographical Information System (GIS) for investigation of spatiotemporal changes. GIS-based models use the field measurements of soil, topography and management practices to build and study the complex hydrological process. It is very important to ensure the accuracy of such remotely sensed data products and field measurements for feasible application and simulation using the modelling approach. Numerous models are progressively developed to account such difficulties in modelling approach (Singh, 1996, 2002). It includes the land use change models, the climate change models, the conceptual models, and the hydrological models etc. These models vary with their input data requirement, in-build process algorithm, spatiotemporal accountability, practical application, types of output, capability and complexity of the model simulation (Pandey et al., 2016b). To ensures the validity and applicability of a model in the same/other study area having similar environmental conditions, these models can be calibrated and validated using the field measurements/data (Govers, 2011). Thus, selection of a model should include minimum data inputs, ability to account the changes in land use, climate and management practices, model reliability, acceptability, and robustness in nature.

Progressive development in the remote sensing and GIS promises the potential applicability of hydrological modelling approach employing various datasets including land use, climate, soil, slope, and management practices at spatiotemporal scales. Remotely sensed satellite data is used for land use classification and their change detection. GIS facilitate an environment for data collection, analysis, mapping, and scaling. The Digital Elevation Model (DEM) data is used to extract topographic variables such as slope, aspect, stream-network, and basin geometry.

2.2 LAND USE/LAND COVER (LU/LC) CHANGE MODELLING

The LU/LC plays an important role in global environmental changes. It is most important linkage between socio-economic processes associated with land development, agricultural activities, natural resource management strategies, and the ways that these changes affect the structure and function of ecosystems (Roy and Tomar, 2001). In the mid 1930's, the LU/LC mapping began using the available aerial Gemini and Apollo space photographs and the photo-interpretation techniques, and continued to use until early 1970's (MacPhail and Campbell, 1970). Operational use of space-borne multispectral data began only after the launch of the Earth Resources Technology Satellite (ERTS-I), later renamed as Landsat-1, in July-1972. The Landsat Multispectral Scanner (MSS) imagery provides synoptic view of a fairly large area at regular intervals which was exploited for LU/LC change mapping and monitoring by the United States Geological Survey (USGS) (Anderson, 1971).

Various change detection techniques have been developed and utilized, i.e. (i) based on spectral classification of input data (*categorical method*), post-classification comparison (Mas, 1999) and direct two-date classification (Yeh and Li, 1997), and (ii) based on radiometric change between acquisition dates, including (a) image algebra method, such as band differencing (Weismiller et al., 1977), rationing (Howarth and Wickware, 1981) and vegetation indices (Nelson, 1983), (b) regression analysis (Singh, 1986), (c) principal component analysis (Byrne et al., 1980; Gong, 1993), and (d) change-vector analysis (CVA; Malila, 1980). In addition, hybrid approaches involving a mixture of categorical and radiometric change information have also been proposed and evaluated (Colwell and Weber, 1981). Future, LU/LC prediction is also required to emulate the implications of human activity for sustainability of natural system (Turner II et al., 1995). Several LU/LC models are available to reflect the current and future trends that can serve as the benchmarks against process-oriented models. These models involve historical pattern of LU/LC change, and then extending these patterns for future prediction. Best LU/LC prediction model represents: (a) amount of future LU/LC changes, (b) location of changes, and (c) spatial pattern of changes. Although some existing models address the first two of these conditions (Veldkamp and Fresco, 1996**a**; Landis and Zhang, 1998), there are few models which are specifically aimed to reproduce the spatial patterns of LU/LC changes. Mainly, there are two types of LU/LC prediction models i.e. regression type models and spatial transition-based models (Theobald and Hobbs, 1998).

Agarwal et al. (2002) reported 19 LU/LC change models for spatial, temporal and human decision-making characteristics for reviewing and comparing LU/LC models (Table 2.1a). Furthermore, recently developed LU/LC models are summarized in Table 2.1b.

Table 2.1a: Land use change models

Sr. No.	Model Name	Author(s) [Year]
1.	GEM (General Ecosystem Model)	Fitz et al. (1996)
2.	PLM (Patuxent Landscape Model)	Voinov et al. (1999)
3.	CLUE model (Conversion of Land Use and its Effects)	Veldkamp and Fresco (1996**a**)
4.	CLUE-CR (Conversion of Land Use and its Effects – Costa Rica)	Veldkamp and Fresco (1996**b**)
5.	Area base model	Hardie and Parks (1997)
6.	Univariate spatial models	Mertens and Lambin (1997)
7.	Econometric (multinomial logit) model	Chomitz and Gray (1996)
8.	Spatial dynamic model	Gilruth et al. (1995)
9.	Spatial Markov model	Roy et al. (2001)
10.	CUF (California Urban Futures)	Landis (1994); Landis and Zhang (1998)
11.	LUCAS (Land Use Change Analysis System)	Berry et al. (1996)
12.	Simple log weights	Wear et al. (1998)
13.	Logit model	Wear et al. (1996)
14.	Dynamic model	Swallow et al. (1997)
15.	NELUP (Natural Environment Research Council (NERC)– Economic and Social Research Council (ESRC): NERC/ESRC Land Use Programme (NELUP))	O'Callaghan (1995)
16.	NELUP - Extension	Oglethorpe (1995); O'Callaghan (1995)
17.	FASOM (Forest and Agriculture Sector Optimization Model)	Adams et al. (1996)
18.	CURBA (California Urban and Biodiversity Analysis Model)	Landis et al. (1998)
19.	CA (Cellular Automata) model	Clarke et al. (1997); Kirtland et al. (2000)

Table 2.1b: Recently developed land use change models

Sr. No.	Model Name	Author(s) [Year]
1.	GEOMOD & GEOMOD 2	Pontius et al. (2001)
2.	LTM (Land Transformation Model)	Pijanowski et al. (2002)
3.	SELUTH (Slope, Land use, Exclusion, Urban extent, Transportation, Hill shade)	Clarke et al. (1997)
4.	Environment Explorer	de Nijs et al. (2004)

5.	CLUE-S (2005)	Verburg and Veldkamp (2004)
6.	Land Use Scanner	Koomen et al. (2005)
7.	SAMBA	Castella et al. (2005a)
8.	Land Change Modeler – for Ecological Sustainability	Clark Labs (2006)
9.	Earth Trends Modeler	Clark Labs (2007)
10.	MABEL (Multi Agent-Based Economic Landscape) Model	Konstantinos et al. (2008)

2.3 HYDROLOGICAL MODELLING

Hydrological models are diverse in data handling and computational requirements. Several watershed models have drawbacks due to the requirement of large datasets, lack of user-friendliness, conditions of their applicability and improper measure of reliability. Spatial scale play important role in the selection of the models, and to study the complex processes of river basin. Based on the degree to which spatial parameters affect the modelling process, the watershed models are categorized as lumped, semi-distributed and distributed model.

1. In lumped models, spatial variability of processes, input data, watershed characteristics, and boundary conditions are not taken into account.
2. However, the distributed models accounts the spatial variability of processes and outputs (Zhang et al., 1996).
3. The semi-distributed models lies in between lumped and distributed models by dividing river basin into sub-watersheds and reasonably homogeneous regions employing hydrological response units (HRUs) or quasi-statistical approach, or combination of both (Schumann, 1993).

Furthermore, the temporal scale of model is also important due to variation in hydrological processes at different time periods. Based on the temporal scale, the models are categorized as event based (single or multi-event), or continuous. Both the spatial and temporal scales are important in the modelling approach, thus, the models are classified as field-scale or watershed-scale models (Singh, 1989).

1. Generally, the field-scale models have spatially uniform rainfall, single land use, homogeneous slope and soil, and single management practice.
2. On other hand, the watershed-scale models are reasonably advanced, and they can have non-uniform rainfall distribution, different land use, slope, soil and management practices.

Further, based on the area of the watershed, the models are again re-classified into small- (<100 km^2), medium- (100-1000 km^2), and large- (>1000 km^2) watershed scale models. The small area scale studies focus on on-site impacts, whereas larger area scale studies focus on off-site impacts of surface flow.

Hydrological models are mainly grouped into three categories i.e. empirical, conceptual, and physical based (Singh, 1995; Singh and Woolhiser, 2002; Singh and Frevert, 2006).

1. Empirical models require less data, as compared to the conceptual and physically-based models, and capable of working with coarser and limited measurements/data (Wheater et al., 1993; Jakeman et al., 1999). Further, empirical models can be reclassified as stochastic, deterministic or mixed type models (Singh, 1988). These models ignore the heterogeneity of watershed characteristics, and involve the unrealistic assumptions for physical process of watershed (Wheater et al., 1993).
2. Conceptual models represent the watershed as a series of internal storages with the parameters having limited physical interpretability. It includes only general description of watershed processes, but not the specific details of process interactions and detailed watershed information. Thus, conceptual model plays an intermediate role between empirical and physically based models (Beck, 1987).
3. Physical models include fundamental physical equations accounting hydrology of a watershed. These models represent the water flow by the conservation of mass and momentum equations and the sediment by the conservation of mass equation (Kandel et al., 2004). In physical models, the inputs data of land use, soil, climate, topography, geology, vegetation, and river flow characteristics uses to represent and simulate the complex hydrological processes. Limitation of such models is that such models require more number of input datasets and parameters for hydrological simulation (Jetten et al., 2003). Generally, use of more number of data/parameters provides better simulation results, but not always in case models with limited number of parameters (Perrin et al., 2001). Some most popular physically-based hydrological models are listed in Table 2.2.

Table 2.2: List of physically-based hydrological model (Pandey et al., 2016b)

Sr. No.	Model Name	Author(s) [Year]	Remarks
1.	ACTMO (Agricultural Chemical Transport Model)	Frere et al. (1975)	Lumped, event based, farm scale model
2.	AGNPS (Agricultural Non-point Source model)	Young et al. (1989)	Distributed, event based, watershed scale model
3.	AnnAGNPS (Annualized Agricultural Non-point Source model)	Bingner et al. (2011)	Continuous simulation, watershed scale model
4.	ANSWERS (Areal Nonpoint Source Watershed Environment Response Simulation)	Beasley et al. (1980)	Distributed, deterministic, event based, watershed scale simulation model
5.	ANSWERS-continuous (Areal Nonpoint Source Watershed Environment Response Simulation-Continuous)	Bouraoui and Dillaha (1996)	Continuous, process-oriented, distributed, simulation model
6.	APEX (Agricultural Policy/Environmental eXtender) [EPIC model extension]	Williams and Izaurralde (2006)	Continuous simulation, farm scale or small watershed model
7.	CASC2D (CASCade of planes in 2-Dimensions)	Julien and Saghafian (1991)	Unsteady, distributed, event based Hortonian simulation model
8.	CREAMS (Chemicals, Runoff and Erosion from Agricultural Management Systems)	Knisel (1980)	Lumped, process-oriented, field-scale model
9.	DWSM (Dynamic Watershed Simulation Model)	Borah et al. (1999)	Process-oriented, single storm event based, distributed simulation model
10.	EPIC (Erosion Productivity Impact Calculator)	William et al. (1984)	Process-oriented, lumped, field scale continuous simulation model
11.	EROSION-2D/3D	Schmidt (1991)	Single storm event based, simulation model
12.	EUROSEM (European Soil Erosion Model)	Morgan et al. (1993)	Process-oriented, single event, dynamic distributed model
13.	GLEAMS (Groundwater Loading Effects of Agricultural Management Systems)	Leonard et al. (1987), Knisel et al. (1993)	Lumped, process-oriented, event based, Field-scale model
14.	GSSHA (Gridded Surface Subsurface hydrologic Analysis)	Downer and Ogden (2004)	Process-oriented, distributed simulation model
15.	GUEST (Griffith University Erosion System	Misra and Rose (1996)	Process-oriented, steady state, event based, soil erosion model

	Template)		
16.	HYPE (Hydrological Predictions for the environment)	Lindstrom et al. (2010)	Process-oriented, semi-distributed, continuous simulation model
17.	IDEAL (Integrated Design and Evaluation of loading Models)	Barfield et al. (2006b)	Process-oriented, simulation model
18	IQQM (Integrated Water quality and quantity model)	Simons et al. (1996)	Event based, watershed scale model.
19.	KINEROS (KINematic runoff and EROSion model)	Woolhiser et al. (1990)	Process-oriented, single storm event based, distributed simulation model
20.	LASCAM (Large Scale Catchment Model)	Viney and Sivapalan (1999)	Distributed, continuous model
21.	MEDALUS (Mediterranean Desertification and Land Use research programme Model)	Kirkby et al. (1993); Kirkby (1998)	Process-oriented, event based, hillslope field-scale model
22.	MEFIDIS (Modelo de ErosaoFIsico e DIStribuido)	Nunes et al. (2005)	Deterministic, spatially distributed, time dynamic model
23.	MIKE 11	MIKE (1995)	Watershed scale, dynamic computer model
24.	MULTSED (MULTiple watershed storm water and SEDiment runoff Simulation model)	Melching and Wenzel (1985)	Distributed, deterministic, single event based simulation model
25.	OPUS	Smith (1992)	Continuous field-scale, simulation model
26.	PALMS (Precision Agricultural Landscape Modeling System)	Bonilla et al. (2008)	Process-oriented, event based, distributed, landscape model
27.	PERFECT (Productivity, Erosion and Runoff, Functions to Evaluate Conservation Techniques)	Littleboy et al. (1992)	Mix of empirical, conceptual and physics based field scale model
28.	PESERA (Pan-European Soil Erosion Risk Assessment)	Kirkby et al. (2004)	Process-oriented, spatially distributed, single storm event based model
29.	PRMS (Precipitation Runoff Modelling System)	Leavesley et al. (1983)	Modular design, single storm event based, distributed simulation model
30.	RHEM (Rangeland Hydrology and Erosion Model)	Nearing et al. (2011)	Process-oriented, event based, rangeland management model
31.	RillGrow	Favis-Mortlock (1996)	Distributed, process-oriented, single event based, hillslope rill erosion model
32.	RUNOFF	Borah (1989)	Event based, distributed, deterministic model

33.	SEDIMOT (Sedimentology by Distributed Modelling Technique-Version III)	Barfield et al. (2006a)	Single event based, field scale model
34.	SHE/SHESED (SystemeHydrologiqueEuropian/ SystemeHydrologiqueEuropian Sediment)	Abbott et al. (1986a, b)	Distributed, continuous basinscale, simulation model
35.	SHETRAN (SystemeHydrologiqueEuropian-TRANsport)	Ewen et al. (2000)	Spatially-distributed, basin-scale, simulation model
36.	SMODERP (Simulation Model of OverlanD Flow and ERosion Process)	Holy et al. (1988)	Single storm event based, simulation model
37.	SPUR (Simulating Production and Utilization of Rangeland)	Carlson et al. (1995); Teague and Foy (2002)	Lumped, continuous, field scale, rangeland simulation model
38	SWAT (Soil and Water Assessment Tool)	Arnold et al. (1998)	Semi-distributed, physically-based, continuous simulation model
39.	SWIM (Soil and Water Integrated Model)	Krysanova et al. (1998)	Spatially distributed watershed model
40.	SWM [Stanford Watershed Model/ Hydrological Simulation Program-Fortran (HSPF)]	Bicknell et al. (1993)	Process-oriented, lumped parameter, continuous simulation model
41.	SWRRB (Simulator for Water Resources in Rural Basins)	Williams et al. (1985)	Semi-distributed, process-oriented simulation model
42.	TOPMODEL (TOPography based hydrological MODEL)	Beven and Kirkby (1979)	Distributed, continuous hydrologic, watershed scale simulation model
43.	TOPOG	Vertessy et al.(1990)	Deterministic, distributed, event based catchment model
44.	WEPP (Water Erosion Prediction Project)	Laflen et al. (1991)	Process-oriented, distributed, continuous simulation model
45.	WESP (Watershed erosion simulation program)	Lopes (1987)	Distributed, event based, nonlinear, numerical model

2.4 DESCRIPTION OF THE SWAT MODEL

Physically-based models have mathematical expressions for individual hydrological process. Practically, none physical model is fully physically-based because it includes many assumptions and considerations of empirical/conceptual approaches. But, physically based models can help to study complex hydrological processes in a short time and with limited investments. Mainly physically-based models provide accurate representation of different land use, erosion processes, and complex conditions under varying soil properties (Lane et al., 2001). Among different physically-based models given in Table 2.2, the SWAT model is a

physically-based, continuous-time, long-term, distributed river basin or watershed scale hydrologic model (Arnold et al., 1998; Arnold and Fohrer, 2005) developed by USDA's Agricultural Research Service (ARS) to predict the impact of land management practices on water, sediment and contaminant in complex and large river basin with varying land use, soil and management practices over long periods of time.

The SWAT model, developed in the early 1990s, is an outgrowth of the SWRRB model. It has features of CREAMS, GLEAMS and EPIC models that contributed initial development. It has undergone continued review and expansion of capabilities. The most significant improvements of the SWAT model are as follows:

- **SWAT94.2**: In this version multiple hydrologic response units (HRUs) were incorporated.
- **SWAT96.2**: In this version, auto-fertilization and auto-irrigation were added as management options. Further, canopy storage of water and, a CO_2 component was also added to crop growth model for climatic change studies. Penman-Monteith potential evapotranspiration equation was also added. Lateral flow of water in the soil based on kinematic storages model was incorporated. In-stream nutrient water quality equations from QUAL2E and in-stream pesticide routing were included in the model.
- **SWAT98.1**: In this version, snow melt routines and in-stream water quality module was improved. Nutrient cycling routines were expanded. Grazing, manure applications, and tile flow drainage were added as management options. Also, the model was modified for use in Southern Hemisphere.
- **SWAT99.2**: In this version, nutrient cycling routines and rice/wetland routines were improved. Reservoir/pond/wetland nutrient removal by settling, bank storage of water in reach and routing of metals through reach were added in the model. All year references in model were changed from last 2 digits of year to 4-digit year. Urban build up/wash off equations from SWMM were added along with regression equations from USGS.
- **SWAT2000**: In this version, bacteria transport routines and Green & Ampt infiltration were added. The weather generator was improved by allowing to be read or generated the daily solar radiation, relative humidity, and wind speed. Also, allowed the potential ET values for watershed to be read in or calculated. All potential ET methods were reviewed. Elevation band processes were improved. Simulation of unlimited number of reservoirs was enabled. Muskingum routing method was added. Also, the dormancy calculations for proper simulation in tropical areas were modified.
- **SWAT2005**: In this version, the bacteria transport routines were improved. Weather forecast scenarios and sub-daily precipitation generator were added. The retention

parameter was used in the daily CN calculation, which may be a function of soil water content or plant evapotranspiration.

- **SWAT2009**: In this version, vegetative filter strip model was updated. Wet and dry deposition of nitrate and ammonium was improved. Also, modelling of on-site wastewater systems was added.
- **SWAT2012**: In this version, the CROP table to include several new crops in the SWAT2012 database was updated. The writing of atmo.atm file was modified to only write the file if an average annual value option is chosen. Also, an option to provide own atmo.atm monthly values by choosing an IATMO value of "1" was added. The same deposition values specified in the .BSN file were written as one line for every sub-watershed. The DEM, land use, and soils raster datasets were allowed to read from a file geo-database. The header line in the .RES files was modified to be compatible with SWAT-CUP. The handling of split sub-landuses during HRU delineation has been modified for the case exempt land uses are specified (if a parent land use is specified as being "exempt" from the land use threshold, then all sub-land uses will also be exempt). New parameters in the HRU table and .hru files were added to the interface. New parameters in the BSN table and .bsn file were added to the interface. And, the SWAT executable was updated to version 627.

In addition to the changes listed above, interfaces for the model have been developed in Windows (Visual Basic), GRASS, and ArcView. The SWAT model has also undergone extensive validation.

The SWAT-CUP (SWAT-Calibration and Uncertainty Programs) a decision-making framework was developed for calibration of the SWAT model which also enables sensitivity and uncertainty analysis (Abbaspour, 2007; Arnold et al., 2012b). For evaluation of the SWAT model simulation, different statistical tools, guidelines and recommendations have been provided by Moriasi et al. (2007). Abbaspour et al. (2015) modelled the hydrology of entire European continent with SWAT and improved SWAT-CUP to include parallel processing and visualization. Fu et al. (2014) revised and tested the SWAT model to generate SWAT-CS a version representing hydrological processes dominating forested Canadian Shield catchments. A version SWAT-G was also developed for application to low mountain range catchments of Germany (Eckhardt and Arnold, 2001; Eckhardt et al., 2002). In order to identify potential model application problems SWAT-Check was developed to make modelling applications more reliable and user friendly (White et al., 2014). Although, storm event based high and peak flows are not well simulated by the SWAT model, which needs improvement.

Global applications of SWAT model over the past 20 years have revealed limitations, and identified model development needs. Water resources modelling using the SWAT code have undergone numerous additions and modifications of the model components which made the code increasingly difficult to manage and maintain, resulting in SWAT+, a completely revised version of the model (Arnold et al., 2018). Keeping the basic processing algorithms same, the code (object based) and the input files (rational based) are considerably modified in terms of its structure and organization (Bieger et al., 2017). This is expected to facilitate model maintenance, future code modifications, and foster collaboration with other researchers to integrate new science into SWAT modules. The SWAT+ provides a more flexible spatial representation of interactions and processes within a watershed.

2.5 APPLICATION OF THE SWAT MODEL

With the enhanced features and in-build several hydrological processes, the SWAT has been widely employed for different applications such as calibration, sensitivity, and/or uncertainty analysis (Arnold et al., 2012b; Abbaspour et al., 2015), land use change impact assessment (Dixon and Earls, 2012), climate change impact assessment (Raneesh and Thampi Santosh, 2011; Records et al., 2014), non-point source pollutant cycling/loss and transport study (Niraula et al., 2012; Moriasi et al., 2013; Malagó et al., 2017), BMP evaluation (Pandey et al., 2009a; Betrie et al., 2011; Lampurlanés et al., 2016), snowmelt and/or glacier melt processes (Stehr et al., 2009; Rahman et al., 2013; Omani et al., 2017), hydropower projects (Piman et al., 2012; Pandey et al., 2015), groundwater and/or soil water impacts (Mishra et al., 2007; Sultan et al., 2011; Sun et al., 2016), plant parameters or crop growth/yield (Barron et al., 2010; Iizumi et al., 2013; Sinnathamby et al., 2017), evapotranspiration assessment (Immerzeel and Droogers, 2008; Licciardello et al., 2011; Aouissi et al., 2016) etc.

Bingner (1996) simulated runoff of the Goodwin Creek watershed in Northern Mississippi using the SWAT model. Results revealed that SWAT can simulate the relative trends of runoff on a daily and annual basis from multiple sub-watersheds. Analysis showed that SWAT model has capability to adequately simulate the effects on runoff from the temporal and spatial variability of watershed characteristics.

Van Liew and Garbrecht (2003) applied the SWAT model to predict streamflow under varying climatic conditions for three nested sub-watersheds in the Little Washita River Experimental Watershed in South-Western Oklahoma. Results showed that the model can adequately simulate runoff for dry, average, and wet climatic conditions at a sub-watershed level, following calibration for relatively wet years in two sub-watersheds.

Tripathi et al. (2004) performed the SWAT-based hydrological modelling for runoff and sediment yield estimation of a small agricultural watershed in Eastern India using generated precipitation. Results showed that the model can satisfactorily employ the generated monthly average rainfall values to simulate the monthly surface runoff and sediment yield close to the observed data. This study was found suitable to develop a multi-year management plans for the critical soil erosion prone areas of a watershed.

Schuol et al. (2008) employed the SWAT model to quantify freshwater availability of 4 million km^2 area covering 18 countries in West Africa. This study demonstrated that modelling uncertainties were generally within reasonable ranges, but in sub-watersheds containing features such as dams and wetlands or sub-watersheds with inadequate climate or land use information, the modelling uncertainties became higher.

Vazquez-Amabile and Engel (2008) applied the SWAT model to generate long time-series data to forecast short-term monthly groundwater depth and streamflow. The SWAT with the fitted time-series model performed good for groundwater depth simulation and forecasting. However, time-series fitted to the SWAT model data and the historical data resulted similar performance, but monthly streamflow forecast was poor.

Dhar and Mazumdar (2009) evaluated the projected parameters for agricultural activities using the SWAT model over the Kangsabati river watershed of West Bengal, India. Parameters such as ET, transmission losses, potential ET and lateral flow to reach were evaluated for the years 2041-2050 in order to render a picture for sustainable management and development of the river basin and its inhabitants.

Golmohammadi et al. (2017) employed the SWATDRAIN model to evaluate the impacts of tile drainage on alterations in discharge, sediment and water balance components of an agricultural watershed of Ontario, Canada. The results showed that discharge was not significantly affected by tile drainage, while removing the tile drain resulted in 55% increase in sediment load, and 37.1% increase in surface runoff from the watershed.

Application of the SWAT model in different hydrological applications is presented in Table 2.3.

Table 2.3: Application of the SWAT model in different hydrological studies

Researcher(s) and Year	Study Region(s)	Area (ha) approx.	Broad Application Category	Major Findings/Remarks
Chu and Shirmohammadi (2004)	Maryland	340	Surface and sub-surface flow prediction	The study revealed that SWAT underestimated total stream flow and sub-surface flow, especially during wet periods. During wet season, considerable groundwater contribution from outside the watershed was reported. Even after adjustments to measured data, SWAT model was found unable to simulate the extremely wet hydrologic conditions.
Mendas et al. (2008)	Macta watershed, NW region of Algeria	1423500	Water balance	The study showed that SWAT reproduces the parameters of streamflow, climate and water balance. A good correlation was observed between observed and simulated variables for the adopted model. Simulation results may help in decision-making and water resources management at watershed scale.
Rostamian et al. (2008)	Beheshtaba d and Vanak watersheds, Iran	386000 and 319800	Runoff and sediment simulation	The study indicates accounting of uncertainties and a fair model performance; P factor (0.31-0.86 and 0.71-0.80); D factor (0.3-1.1 and 0.771.16) for Beheshtabad and Vanak watersheds, respectively.
Schmalz et al. (2008)	Mesoscale lowland river basins	5000 to 51700	Water balance	Some groundwater parameters were found to be highly sensitive and they turned out to be the most influential factors for improving simulated water discharge. The dominating hydrological processes were found to be mainly controlled by groundwater dynamics and storage, drainage, wetlands and ponds.
Ficklin et al. (2009)	San Joaquin watershed, California	1498300	Variations of atmospheric CO_2, Temp and Rainfall	The study revealed that rainfall, temperature and atmospheric CO_2 change have major influence on ET, water yield, streamflow and irrigation water use. Finally, the selected watershed was found more sensitive to potential future climate change.

Pisinaras et al. (2010)	Kosynthos River watershed, NE Greece	44000	Hydrological and water quality modelling	A good correlation was observed between observed and simulated data for the adopted model. The study suggested that the SWAT model can be used effectively in testing management scenarios in Mediterranean watersheds, if properly validated.
Wang et al. (2010)	Cowhouse Creek watershed, Texas	117845	land use–soil interactive effects on water and sediment yields	Annual sediment and water yield increase in all soils with conversion of range brush to range grass. For the removal of range brush on a soil that is adjacent to the stream channels, the increase in water yield was found larger.
Oeurng et al. (2011)	Save catchment, South-west France	111000	Hydrologic & pollutant simulation	An empirical correlation was developed between annual water yield, annual sediment and organic carbon yield. The value of annual soil loss was found to vary spatially from 0.1 to 6 t ha^{-1} according to the agricultural practices and slope at the catchment scale. Critical source areas of erosion were also identified using the model.
Garg et al. (2012)	Upper Bhima river basin, southern India	4606600	Crop water productivity assessment	Different cropping patterns scenarios were tested with the goal of increasing economic water productivity values in the Ujjani Irrigation Scheme. The study suggested that maximization of the area by provision of supplemental irrigation to rain-fed areas as well as better on-farm water management practices can provide opportunities for improving water productivity.
Himanshu et al. (2017**c**)	Ken River basin, India	2867200	Runoff, sediment and water balance simulation	Satisfactory model performance for both runoff and sediment yield. The water balance study of the basin showed that evapotranspiration is more predominant accounting for about 44.6% of the average annual precipitation falling over the area. The average annual sediment yield of the basin was found to be 15.41 t/ha/year.
Suryavanshi et al. (2017)	Betwa River basin, India	4350000	Runoff and water balance simulation	Satisfactory model performance was observed for both runoff and seasonal water balance simulation. The seasonal water balance study of the basin showed that about 90% of annual rainfall and 97% of annual runoff occurred in the monsoon season.

2.5.1 Assessment of land use change impact using SWAT

Ghaffari et al. (2010) investigated the hydrological effects of land use changes over 1967, 1994 and 2007 in Zanjanrood basin, Iran using the SWAT model. In this study, the SWAT model was applied to simulate the main components of the hydrological cycle. Results revealed that hydrological response to the overgrazing and replacement of the rangelands with rain-fed agriculture and bare ground is nonlinear and exhibits a threshold effect.

Cai et al. (2012) assessed the impacts of land-use change on sediment yield of Upper Huaihe River basin, China. Results revealed that under the same condition of terrain slope and soil texture, the sensitivity of rainfall–sediment yield relationship to rainfall and the advantage for sediment yield descended by paddy field, woodland and farmland. The outcome of the research can provide references for river health protection, and soil and water conservation.

Du et al. (2013) quantified the hydrological processes in a rapid urbanization region of the Qinhuai River basin using SWAT model. They used regression equations to develop parameterization strategy with SWAT parameters as dependent variables and catchment impermeable area as independent variable. They concluded that, this modeling approach could provide an essential reference for the study of assessing the impact of LU/LC changes on hydrology in other regions.

Zhang et al. (2014) investigated an effect of land use change on sediment yield in Lixici watershed, China. The rate of soil erosion was found to be most severe in areas with slopes >25°. Use of grassland or forestland has been recommended rather than farmland in the areas with slopes >25°. This study revealed that SWAT model is suitable for developing sustainable soil conservation actions to reduce soil erosion.

Wei et al. (2016) analyzed the effects of four different land use scenarios changes on runoff of the Qiaoyu River Basin, China employing the SWAT model. Land use scenario-1 had the greatest impact on the annual runoff and the runoff reduction, while scenario 3 was the worst. At sub-watershed level, the water yield has greater impact of scenario-1 and scenario-2 in the upper and middle part of the basin. Scenario-3 and scenario-4 have a greater impact on the water yield in the middle and lower part of the basin. Thus, land use change has significant control on the downstream water yield. The effect of four land use scenarios was found to be in the order of Scenario1 > Scenario 2 > Scenario 4 > Scenario 3.

Kundu et al. (2017b) assessed the impact of land use change on the water balance of the past, present and future years in the part of Narmada River basin, India using the SWAT model.

Result showed that a water yield increases by 6.98% in past and 17.5% in future, while actual ET decreases by 3.37% in past and 8.40% in future due to impacts of land use change.

Napoli et al. (2017) quantified hydrological responses of land use and climate in a rural hilly basin, Italy using the SWAT model. Results showed that under a given same climatic conditions, the land use change affects both peak and total runoff. SWAT model can effectively simulate the basin response to climate and land use changes.

Setyorini et al. (2017) assessed the impact of LU/LC change and climate variability on hydrological processes in Upper Brantas River basin, Indonesia using SWAT model. Result showed that deforestation and expansion of agricultural area can lead to increase in annual surface runoff, evapotranspiration, streamflow, and the decrease in groundwater and lateral flow. Surface runoff is the more sensitive to LU/LC changes than other hydrological components.

Sun et al. (2017) evaluated hydrological relationships with the land use change in the Lake Dongting watershed, China using SWAT model. The evaluation of hydrological components in response to changing land use scenarios indicates that the water yield, as well as the distribution of runoff components associated with surface runoff, interflow, and groundwater flow, exhibit considerable changes under varying land use patterns. Results revealed that, in the forest-prone scenario, both water yield and surface runoff decreased simultaneously.

Table 2.4: Application of the SWAT model for land use change impact assessment

Researcher(s) and Year	**Study Region(s)**	**Area (ha) approx.**	**Broad Application Category**	**Major Findings/Remarks**
Chen et al. (2017)	Double Mountain Fork Brazos watershed, USA	600000	Impact of land use change on hydrology and water quality	Integrated APEX-SWAT model to evaluate an average annual surface runoff from the baseline cotton areas decreased significantly by 88%, and percolation increased by 28%. Due to perennial grass, the Nitrate-Nitrogen (NO3-N) and Organic-N loads in surface runoff and NO3-N leaching to groundwater reduced significantly by 86%, 98%, and 100%, respectively.
Boongaling et al. (2018)	Calumpang watershed, Philippines	35400	Impact of land use change on hydrological processes	Investigated solid connection between land use change and hydrological processes. Surface runoff increases by 5% and sediment yield (by 6%), and the base-flow reduces by −11% due to land use change.
da Silva et al.	Lower-Middle São Francisco	11045	Hydrological response to land	Surface runoff and sediment yield increases under the scenario of

(2018)	River sub-basin (LMSFR), Brazil		use changes	devastation (scenario III) of land use. Sustainable land use practices such as pasture land is replaced by natural vegetation should be applied in the study area.
Gashaw et al. (2018)	Andassa watershed, Ethiopia	58760	Land use/land cover change impacts on hydrology	Changes in cultivated land, forest, shrub-land, grassland and built-up area contributed changes in annual and wet season flow, dry season flow, and to the different water balance components
Guzha et al. (2018)	Catchments from East Africa	500 to 3100000	Impacts of land use/land cover change on surface runoff and low flows	Examined the effects of wood cover misfortune on hydrological transitions, particularly release and surface overflow. Deforestation results in increased surface runoff, mean annual, and peak river discharges.
Molina-Navarro et al. (2018)	Odense Fjord catchment, Denmark	106100	Effects of agriculture scenarios and climate change on hydrology	Changes in land use alone affected total catchment runoff in small extent. Combined land use and climate change showed impact on the river discharge (and its individual flow components), and the loads of organic nutrients and inorganic-P. The discharge variations mainly being influenced by the climate impacts.
Prasanchum and Kangrang (2018)	Upper Lampao Reservoir, Thailand	328200	Land use and climate change impact on reservoir operation	Average of the annual future inflows decreased under land use expansion of rubber trees area, evergreen forest and pasture, and the A2 and B2 climate scenarios of PRECIS model.
Zhang et al. (2018b)	Upper Heihe river basin in North-West China	1000000	Separating land use and climate change impacts on hydrology	Land use change slightly affected the water yield and ET at the same magnitude, while the climate change substantially affects at different magnitudes. This study revealed that influence of baseline period choices on the partitioning of hydrological impacts vary significantly between different hydrological models.

2.5.2 Assessment of climate change impact using SWAT

Gosain et al. (2006) simulated the impacts of climate change scenarios (A2 and B2) on the streamflow of twelve major river basins of India using SWAT model. Results showed that surface runoff was generally decreased, and the severity of both floods and droughts has been increased in response to the climate change.

Abbaspour et al. (2009) studied an impact of future climate change on the Iranian water resources using the hydrological model SWAT. Effect of future climate on precipitation, blue

water, green water, and yield of wheat crop across the country were analyzed. Results showed increase in the crop yield is small but statistically insignificant in winter wheat. The irrigated wheat production in the southern and eastern regions of Iran has significant negative impact of climate change as groundwater recharge decreases in future.

Carvalho-Santos et al. (2010) studied the construction of a new reservoir (two-reservoir system) of Alto Sabor watershed, Portugal by considering future climate projections. The SWAT model simulation resulted that the volume of water stored in the reservoirs will decrease, especially during spring and summer. In future, the reliability of existing water supply from two reservoirs will decrease under scenario RCP 8.5 during the years 2041–2060.

Lakshmanan et al. (2011) assessed the impacts of climate change on hydrology and rice yield in Bhavani basin of India. The SWAT model was applied as a decision support tool under a changing climate scenario to frame the adaptation strategies, such as fertilizer management and change in cultivation method.

Zhang et al. (2012a) investigated the impact of climate change and human activates on the runoff of the Huifa River Basin, Northeast China using the SWAT model. Results revealed that both climate change and human activities are responsible for the decrease in runoff. Climate change could result in decrease or increase of runoff depending on the changes in precipitation, temperature, radiation variation etc. Further, the human activities such as regulation and storage of the water projects also contributed significant decrease in the runoff during wet years.

Golmohammadi et al. (2013) used SWAT-DRAIN model to evaluate climate change impact on hydrology of Canagagigue watershed, located in Canada. The climate scenario under consideration in this study (2016-2044) was based on projections from SDSM downscaling based on historical weather data. With downscaling of the regional model results for the specified watershed, the future weather scenarios were the input for calibrated and validated hydrologic model, SWAT-DRAIN, for stream flow.

Zabaleta et al. (2014) assessed an impact of climate change on runoff and sediment yield of the Aixola watershed, Spain. The SWAT model performance was found to be satisfactory but underestimated the runoff and sediment yield when used CGCM2 and ECHAM4 climate models. Analysis under different climate model combinations suggested that runoff and sediments would decrease by 0.13 to 0.45 $m^3 s^{-1}$ and 0.11 to 0.43 tonne, respectively every year from 2011 to 2100.

Xu and Luo (2015) evaluated the spatiotemporal heterogeneity of climate change impacts on hydrological processes, mainly river discharge, for River Huangfuchuan in semi-arid regions of Northern China and River Xiangxi in humid Southern China. In this study, uncertainty in projected discharge for three time periods (2020s, 2050s and 2080s) was assessed using seven equally weighted GCMs (global climate models) for the SRES (special reports on emissions scenarios) A1B scenario.

Table 2.5: Application of the SWAT model for climate change impact assessment

Researcher(s) and Year	**Study Region(s)**	**Area (ha) approx.**	**Broad Application Category**	**Major Findings/Remarks**
Cibin et al. (2017)	Two agricultural dominant (Wildcat Creek and St. Joseph) watersheds of Indiana, USA	204500 and 280000	Climate and land use change impact on ecosystems services	Quantified ecosystem services of bio-energy based on land use and potential climatic changes. Results revealed that the impacts of land use change on ecosystem services are expected to be greater than the climate change and variability impacts. Climate change had more impact on food and fuel provisioning compared to other ecosystem services.
Duan et al. (2017)	Upper Ishikari River basin, Japan	345000	Future climate change impact on streamflow	Annual mean streamflow may increase in the future periods except the 2090s under the A2a scenario. Largest increase about 7.56% is possibly observed in the 2030s for A2a scenario. Uncertainties within the GCM, the downscaling method, and the hydrological model were probably enlarged because only one single GCM (HaDCM3) used.
Golmohammadi et al. (2017)	Canagagigue Creek watershed of Ontario, Canada	14300	Current and future climate impact on model simulation	The annual flow is expected to decrease due to increased temperature in the future, which will lead to a decrease in the sediment loads in the river.
Hammouri et al. (2017)	Yarmouk River basin in Jordan	679000	Impacts of climate change on water resources	Climate change impact was assessed on surface flow using three GCM models (CSIROMK3, ECHAM5OM and HADGEM1) as climatic input data in the SWAT. An average drop in future flow rates could be about 22% which would increase the stress on the already highly stressed water resources in Jordan.

Islam et al. (2017)	Brahmaputra River basin	53000000	Climate change impact on glacier melt	The pre-monsoon flow exhibits an increase at the end of the century, and results revealed major uncertainty of the changes in future flow during March, April, and May. The uncertainty probability in pre-monsoon flow will be more dominant than the uncertainty probability of in monsoon flow.
Ponce et al. (2017)	Vergara river basin, Chile	426000	Impacts of climate change on water resources	Assessed the distributional climate change impact on considering the geographical location of each farmer's community and the spatial allocation of water resources. Results revealed that rain-fed agriculture produces facing largest burden of climate change and the substantial land allocation activities.
Thai et al. (2017)	Upper Cau River basin, Thailand	283500	Impacts of climate change on erosion and water flow	Presented inflow variation in flood and dry season in future periods. Climate trends are leading to severe conditions for runoff generation as well as erosion status due to increase in evaporation and rainfall during the period of 2020-2099.
Wu et al. (2017)	Yanhe River basin, China	748500	Hydrological response to climate change and human activities	Quantified dominant role of climate change on the total runoff decrease accounted by 46-68%. And, 39-54% decrease was attributed to the human activities. The study revealed that climate change impact assessment obtained by hydrological modelling was substantially different from those obtained by empirical statistics.
Čerkasova et al. (2018)	Neris River basin, Europe	1090888	Impact of climate change on trans-boundary hydrology and water quality	Demonstrated the model performance with enhanced HRU definition to assess the trans-boundary hydrology and water quality. This study assessed the possible future nutrient loads that could be transported from Belarus to Lithuania under two climate change scenarios (RCP 4.5 and 8.5).

Leta et al. (2018)	Kalihi and Nuuanu watersheds, Oahu, Hawaii	51300	Impact of Climate Change on Daily Streamflow and Its Extreme Values	The extreme peak flows are expected to increase by 22% especially under the RCP 8.5 scenario, however, a consistent decrease in extreme low flows by 60%. The extreme values are more sensitive to rainfall change in comparison to temperature and solar radiation changes. Amplified climate change impacts by the end of this century and may cause earlier occurrence of hydrological droughts suggesting implementation of mitigation measures to climate change.

2.5.3 Identification of critical area and prioritization of watershed

In order to reduce the losses from the critical areas of the watersheds, effective watershed management practices are being implemented and evaluated employing the SWAT model. Critical areas have high rate of soil erosion and nutrient losses with the exceeded runoff/streamflow affecting natural resources of a watershed. It is required to know a priority order of critical areas to implement the targeted management practices.

Tripathi et al. (2003) identified and prioritized the critical sub-watersheds of Nagwan watershed of Jharkhand, India on the basis of average annual sediment yield and nutrient losses. The SWAT model was used to obtain sediment and nutrient loads to develop an effective management plan at sub-watershed level.

Behera and Panda (2006) identified critical sub-watersheds of the Kapgari watershed, India on the basis of sediment yield and nutrient load and then prioritized according the critical losses. Further, the SWAT model was used for development of best management practices in the critical areas of Kapgari watershed.

Agrawal et al. (2009) used the SWAT model for identification and prioritization of critical sub-watersheds of a small watershed. The critical sub-watersheds were identified and prioritized on the basis of annual average sediment yield and nutrient losses.

Besalatpour et al. (2012) employed the SWAT model to identify and prioritize the critical sub-basins in a highly mountainous Bazoft watershed of Iran, using imprecise and uncertain data. Critical areas were assigned to develop management plans to control erosion from critical areas.

Giri et al. (2012) prioritized three types of critical areas (high, medium, and low) on the basis of different factors such as pollutant concentration, load and yield. In this study, the SWAT model performance was evaluated using different targeting methods for identification of priority areas. Then, ten BMPs were implemented and evaluated using SWAT model.

Rocha et al. (2012) identified critical areas of runoff, sediment and nutrient losses, and then implemented the conservation practices for reducing these losses using the SWAT model in the São Bartolomeu stream watershed, Brazil. Results showed that an increase in water infiltration can reduces the average annual runoff, annual sediment yield, total nitrogen and total phosphorus.

Sardar et al. (2012) identified critical soil erosion areas of the Barakar Basin, India using the SWAT model for adaptation of the suitable soil conservation measures, and improvement in reservoir life. The study revealed that the SWAT model can be effectively used to identify critical sub-watersheds and to develop watershed management plans to control soil erosion by reducing the reservoir sedimentation rate.

Niraula et al. (2013) identified critical non-point source pollution areas using SWAT simulation, and generalized watershed loading function (GWLF) in the Saugahatchee Creek watershed of east central Alabama. This study revealed that use of different models will affect the identification of critical source areas of a watershed.

Previous studies carried out by the various researchers on the critical area identification and prioritization for watershed management are presented in Table 2.6.

Table 2.6: Identification and prioritization of critical areas for watershed management

Researcher(s) and Year	**Study Region(s)**	**Area (ha)**	**Major Findings/Remarks**
Jain and Goel (2002)	Ukai reservoir, Tapi river, Gujarat, India	6222500	Investigated vulnerability of watersheds to erosion for planning and management of soil conservation measures. A priority rating of the watersheds was recommended for soil conservation planning based on an integrated index.
Pandey et al. (2007)	Karso watershed, Jharkhand, India	2793	Average annual sediment yield on grid basis was carried out using USLE, GIS and remote sensing. Watershed was divided into 200×200 grid cells, and average annual sediment yields were estimated for each grid cell of the watershed to identify the critical erosion prone areas of watershed for prioritization purpose.
Dabral et al. (2008)	Dikrong river basin, Arunachal Pradesh, India	155600	Soil erosion assessment was carried out using USLE method. USLE parameters for soil erosion assessment were generated using GIS and remote sensing techniques.

Chen et al. (2011**b**)	Xiangxi watershed, China	309900	Identified critical soil erosion prone areas for land use prioritization and soil conservation. The watershed was distributed to critical and sub-critical areas, and erosion hazard maps were generated.
Pandey et al. (2011)	Karso watershed, Jharkhand, India	2793	GIS and remote sensing along with other datasets (existing maps and field observation data) were used for identification of suitable sites for soil and water conservation structures. They suggested construction of check dams across 2nd and 3rd order streams, and conversion of waste-land into crop-land for soil conservation measures.
Da Silva et al. (2012)	Tapacura´ catchment, Brazil	47000	Identification and prioritization of the critical sub-watersheds were carried out on the basis of average annual soil loss employing USLE. A total of 14 sub-watersheds were delineated, and erosion hazard maps were generated.
Chowdary et al. (2013)	Mayurakshi watershed Jharkhand, India	186000	Prioritization of micro-watersheds was carried out using AHP based SYI model (AHP-SYI) within GIS environment. The information of sediment delivery ratio, potential erosion index (PEI) and indicative of transport capacity were used by this method.
Malekian et al. (2016)	Shemshak watershed, Tehran	8177	Integrated Shannon's Entropy and VIKOR techniques were applied for prioritization of flood risk areas. The proposed methodology included two different types of sensitivity analysis for investigating the impacts of criteria weights modifications on the final ranking.
Rahmati et al. (2016)	Gorganrood river basin, Iran	1188815	Assessed the accuracy of GIS-based AHP method for watershed prioritization to locate the critical areas of flood hazard. The results of this study provide guidelines for planners and managers to determine priority of sub-watersheds based on both anthropogenic and natural components.
Sabbaghian et al. (2016)	Honeyoey Creek-Pine Creek watershed, USA	106131	MCDA was applied for selection of the best agricultural scenario for effective watershed management. The proposed methodology was successfully employed to evaluate various BMP scenarios, and to determine the best solution for both the stakeholders and the overall stream health.

2.5.4 Best Management Practices (BMP) using SWAT

The Best Management Practices (BMPs) have gained focus of concern with the enhanced awareness of soil and water conservation, and natural drainage system protection and restoration. BMP can be evaluated for identified and prioritized critical areas, and recommended for conservation and protection treatments (Srinivasan et al., 1998). The SWAT model is used to analyze future BMP scenarios for critical sub-watersheds of the study area (Daggupati et al., 2015). BMP interventions may be structural and non-structural without affecting available natural resources in a watershed. The watershed management implies the

wise use of soil and water resources within the study area which enables sustainable production, and minimizes floods, sediment yields and nutrient loads.

Pandey et al. (2005) employed the SWAT model for the prioritization of sub-watersheds and development of management scenarios in the Banikdih agricultural watershed in Jharkhand, India. Implementation of zero tillage and conservation tillage treatments effectively reduced the sediment yield by 11% and 5%, respectively, as compared to the conventional tillage. Rice crop cannot be replaced by other crops in order to minimize the sediment and nutrient losses.

Arabi et al. (2006) evaluated different BMPs using the SWAT model to examine their effectiveness at field and watershed scales in Maumee River Basin, Indiana. Sediment and nutrient outputs at pre- and post-BMP conditions were compared for effectiveness measurement at various watershed subdivision levels. This study concluded that subdivision of watershed helps in modelling, and to represent the influence of BMP effectiveness in watershed.

Zhang and Zhang (2011) evaluated effectiveness of agricultural BMPs including vegetated ditches, sediment ponds, buffer strips and their combinations in Orestimba Creek watershed to reduce organophosphate pesticides in surface runoff and sediment load. The study revealed that the SWAT hydrologic model is capable of predicting BMP effectiveness at the watershed scale.

Bossa et al. (2012) evaluated the impacts of crop patterns and management scenarios on nitrogen and phosphorous loads to groundwater and surface water using the SWAT model in the Donga-Pont river catchment, West Africa. Results revealed that management practices such as fertilizer inputs are main principal factors controlling on nitrogen and phosphorous loads dynamic.

Lam et al. (2011) assessed the long-term impact of agricultural BMPs on sediment and nutrient loads in the North German lowland catchment using the SWAT model. Results revealed that BMPs would reduce fairly the average annual loads of nitrate and total nitrogen. However, implementation of the BMPs does not have significant impact on reduction in the average annual loads of sediment and total phosphorus.

Maharjan et al. (2013) predicted the runoff flow from agricultural watershed using SWAT model. They used Green-Ampt infiltration method to carried out sub-daily simulation, and proven to be efficient for runoff estimation at field sized watershed with higher accuracies, that could be efficiently used to develop site specific Best Management Practices (BMPs) considering rainfall intensity, rather than simply using daily rainfall data.

Woznicki and Nejadhashemi (2014) quantified the level of uncertainty in performance of seven agricultural BMPs due to climate change in reducing sediment, total nitrogen and total phosphorus loads. The SWAT model was coupled with mid-21st century climate data to develop climate change scenarios for the Tuttle Creek Lake Watershed of Kansas and Nebraska. Results demonstrated that uncertainty in BMP performance was amplified in the extreme climate scenario.

Udias et al. (2016) employed a multi-objective, spatially explicit analysis tool, the R-SWAT-DM framework, to investigate an efficient, spatially-targeted solution of nitrate abatement in the Upper Danube Basin. Result of optimal spatial conservation strategies indicated that it could be possible to reduce Nitrate loads by more than 50%, while providing a higher income.

Christopher et al. (2017) evaluated an effectiveness of the two-stage ditch in improving water quality in the River Raisin watershed using SWAT model. Nutrient reduction efficiency for the two-stage ditch was found well as compared to the other conservation practices; both in terms of percent load reduction and cost.

Noor et al. (2017) evaluated the cost-effectiveness of different BMP scenarios on sediment yield simulation using the SWAT model. Analysis was carried out using different watershed management scenarios developed with non-dominated Sorting Genetic Algorithm. The study recommended implementation of optimal type of land uses and locations of BMPs in the watershed.

Seo et al. (2017) applied Low Impact Development (LID) practices using SWAT model. Results of the study demonstrated a decrease in surface runoff and pollutant loadings for all land uses.

Other literatures studies on application of the SWAT model for BMP implementation and evaluation are presented in Table 2.7.

Table 2.7: Application of the SWAT model for BMP evaluation

Researcher(s) and Year	Region(s)	Area (ha)	Management Practices Used	Results/Remarks/ Conclusion
Tripathi et al. (2005)	Nagwan watershed, India	9023	Tillage treatments, fertilizer treatments and crops treatments	The field cultivator was recommended to replace conventional tillage treatment. Rice crop cannot be replaced by other crops in order to minimize the sediment and nutrient losses
Behera and Panda (2006)	Kapgari watershed, India	973	Tillage treatments, fertilizer treatments and crops treatments	Conservation tillage was found to be more effective than the existing conventional tillage in controlling sediment yield and nutrient losses. Rice crop cannot be replaced by other crops in order to minimize the sediment and nutrient losses
Bracmort et al. (2006)	Black Creek watershed, USA	5000	Grassed waterways, parallel terrace, field border, and grade stabilization structure.	Evaluated the impacts of structural BMPs on long-term water quality using SWAT model. The current condition of the BMPs was determined using field evaluation results obtained from a previously developed BMP condition evaluation tool.
Arabi et al. (2008)	Smith Fry watershed, USA	730	Agricultural conservation practices and the river channel protection practices.	Identified hydrologic and water quality processes that are affected by practice implementation, parameter selection, parameter sensitivity, function of conservation practices, and reasonableness of the SWAT.
Ullrich and Volk (2009)	Parthe watershed, Saxony, Germany	31500	Management practices, crops treatments and varying operation dates	Model was found very sensitive to applied crop rotations and in some cases even to small variations of management practices. Soil cover over time and duration of vegetation period followed by soil cover characteristics of applied crops were found most sensitive.
Lee et al. (2010)	Gyeongancheon watershed, South Korea	25540	Vegetation filter strip, riparian buffer system, USLE P factor, and the fertilizing control amount for crops	Sediment reduced by 30% with the installation of a 60 m buffer zone. The best nutrients removal efficiency results were found in the land use change from a bare field to grassland.

Tuppad et al. (2010)	Bosque River Watershed, Texas, USA	428200	Porous gully plugs, recharge structures, conservation tillage, terrace, contour farming, and filter strip.	Several BMPs were proposed to simulate and assess their long-term impacts on sediment and nutrient loads at different spatial levels for pollution reduction and watershed protection using the hydrological SWAT model.
Phomcha et al. (2012)	Lam Sonthi River Watershed, Thailand	35700	Different combinations of reforestation, mulching, strip cropping	Sediment yields reduction under the combination of reforestation and mulching was found to be most effective. The study indicates that the SWAT model is capable of predicting monthly stream flow and sediment load.
Rocha et al. (2015)	Vouga catchment, Portugal	368500	N-application methods (single, split and slowrelease)	Results revealed that NO_3 exportation rates and crop yields decrease with reductions in N-application rates. Lower Single N-fertilizer application lead to higher NO_3 exportation rates and lower crop yields as compared to split and slow-release.
Lemann et al. (2016)	Gerda catchment, Upper Blue Nile basin, Ethiopia	4818	Terracing	It was found that discharge did not change significantly with implementation of soil and water conservation measures; however sediment yield was reduced substantially. The sediment yield from the study area was reduced to 17 t/ha from 37 t/ha after implementation of soil and water conservation measures.
Maharjan et al. (2016)	Haean catchment, South Korea	6270	Split fertilizer application (SF), winter cover crop cultivation (CC)	Cultivation of cover crops showed significant reductions of sediment and nitrate load while crop yields increased. Although split fertilizer application resulted in reduction of nitrate pollution while sediment and crop yield were found unchanged relative to the baseline scenario.
Strehmel et al. (2016)	Xiangxi catchment, China	310500	Changes in fertilizer amounts and the conditions of bench terraces	They found that reduction of fertilizer amounts did not reduced the phosphorus loads considerably without hindering crop productivity. The soil erosion and phosphorus releases from agricultural areas affected by the condition of terraces in the catchment.

Her et al. (2017)	St. Joseph River watershed, USA	280900	Conservation cover, conservation crop rotation, no-till, mulch till, cover crops, filter strips, nutrient management, water and sediment control basin, split nitrogen application	Conservation practices were found effective in reduction of sediment and total phosphorous load. Effectiveness of conservation practices for sediment and total phosphorous was found strongly correlated to the field slopes; however, load reductions were not associated with other features of fields such as curve number, saturated hydraulic conductivity, and soil erodibility.
Jang et al. (2017)	Haean catchment, South Korea	6270	Vegetation filter strip installation, fertilizer control, and rice straw mulching	Evaluated reduction of non-point source (NPS) pollution discharges applying BMPs of rice straw mulching (RSM), fertilizer control (FC) and vegetation filter strip installation (VFS), employing the SWAT model. The BMP using VFS demonstrated the best performance to reduce the sediment from highland crop areas.
Kalcic et al. (2018)	Upper Mississippi River Basin, USA	49200000	Agricultural ditches and wetlands for improving water quality	Developed the model to evaluate combinations of practices from the farm scale to the watershed scale. The study revealed characteristics, benefits, and drawbacks of agricultural ditches and wetlands, as well as strategies for applying agricultural best management practices (BMPs)
Mtibaa et al. (2018)	Joumine watershed, Northern Tunisia	41800	Contour ridges in critical source areas (CSAs) for reduction of soil erosion	Determined the most cost effective management scenario for controlling sediment yield. Results revealed that Contour ridges were the most effective individual BMP in terms of sediment yield reduction (reduced by 61.84% with a benefit/cost ratio).

2.6 CRITIQUES ON LITERATURE REVIEW

The relevant literature review reveals importance of hydrological modelling for sustainable management of a river basin considering changes in the land use and climate. Most of the hydrological models were originally developed and tested using the local data and field measurements, mainly in developed countries. However, before application these hydrological models need to be tested and employed in the developing countries like India, where the topography, soil, rainfall pattern and cultivation practices are prevalent and entirely different from those in other parts of the world. In India, the present inter-state disputes are raising land and water resources problems, and may be more in future years. The LU/LC patterns rapidly changes historically, due to human activities and climatic variability/changes, and have significant impact on the hydrological processes of a river basin. The above shortcomings can be overcome by using hydrological modelling approach, as it is crucial to quantify their applicability and feasibility in Indian River basins, where ongoing land use and climatic changes have pronounced impacts.

Literature perceives an importance of application of remote sensing data products and GIS techniques for river basin management. It is mostly devoted to monitor and predict the site specific LU/LC changes using satellite data and land use change models. The present study is the first of its kind for application of an integrated Cellular Automata−Markov Chain (CA−MC) model for prediction of the future LU/LC dynamics in an Indian River basin. The CA-MC model has been evaluated widely for land use change studies. However, no such study has been reported in literature for inter-state river basin in which future LU/LC changes are studied. Furthermore, the relationship between changes in LU/LC and hydro-climatic variables needs to be studied for their spatial and temporal interactions historically. Thus, the study on response of hydro-climatic changes to the land degradation and land greening/browning is essential for sustainable land resource management.

Literature reveals that each hydrological model has its own performance capabilities, and its application depends upon the study objectives and accuracy desired (Pandey et al., 2016b). Physically based hydrological modelling has always been the primary choice of the researchers while dealing with complex problems of streamflow and sediment, and their sustainable management. In India, human activity, such as dam/barrage construction, disturbs the virgin (or naturalized) flow of a river which is essential for agriculture and urban sectors. Hence, such influence is imperative in hydrological modelling study to incorporate the flow regulation and water utilization from small-sized ponds to large-sized reservoirs of a river basin. To test the suitability of hydrological (SWAT) model in a river basin under Indian conditions,

management of various water storages (like reservoirs or weirs), sensitivity/uncertainty analysis of various model parameters and field measurement/data is crucial before its useful implementation. Furthermore, the literature manifested that both the land use and climate have pronounced impacts on hydrology of a river basin. Very limited studies are carried out in which individual and combined impacts of land use and climate changes are explored. Therefore, new approach/method/framework needs to be developed to separate such impacts on river basin hydrology. Also, it is essential to assess these possible impacts on future river basin hydrology to deal with the sustainable management issues.

Although, the SWAT model has been successfully tested in various countries and proved its applicability on global scale; no such study has been reported in literature which focuses identification of critical soil erosion prone areas for prioritization and evaluation of BMPs to restrain sediment yield of the Betwa River basin. Further, no such study has been reported in literature in which SWAT model has been employed to evaluate both the over-land as well as in-stream BMPs for an Indian River basin. Therefore, this study will provide valuable guidelines not only to implement water storage structure information in hydrological model SWAT, but also to develop soil and water conservation practices in agriculture field, and to restore and protect the river channels for its sustainable river basin management. The present study will bridge the gap between the hydrologic prediction community and the remote sensing and GIS technologies development community, and the users interested in land and water resources planning, management and development. The review of literature presented in this chapter have facilitated comprehensive insights on the prime research issues of LU/LC, climate and hydrology interactions for investigation in this study.

CHAPTER 3
STUDY AREA AND DATA DESCRIPTION

This chapter encompasses description of the study area and data acquisitions of different hydro-meteorological variables used in this study. Further, generation of the various thematic maps (i.e. elevation map, slope map, soil map etc.), remote sensing datasets (i.e. Landsat, IRS, MODIS etc.) and the GCM (MPI-ESM-MR) data used in the study has been also discussed briefly. The details of the water resources/storages structures available in the study area also included in this chapter.

3.1 THE STUDY AREA

Betwa River basin is the study area selected in the present research work. Details of location, climate, major crops and the existing practices in the study area are discussed as follows:

3.1.1 Location of the Betwa basin

Betwa River is tributary of the Yamuna River (which is mainly a tributary of Ganga River) located in the Central India. It flows from South-Western to North-Eastern direction. The total length of the river, from its origin to its confluence with the Yamuna River, is 590 km, out of which 232 km lies in Madhya Pradesh (MP) and the rest 358 km in Uttar Pradesh (UP). It is an interstate river between MP and UP. It originates from the Barkhera in Raisen district of MP and then joins with the Yamuna River near Hamirpur in UP. Before the confluence with the Yamuna, the Betwa River is joined by a number of tributaries and sub-tributaries.

The Betwa River basin extends from 77º 05' 38" E to 80º 13' 48" E longitude and 22º 51' 51" N to 26º 3' 5" N latitude, and in the geo-graphical context of MP (68.90%) and UP States (31.10%) covering large geo-graphical area approximately 43900 km^2 as shown in Figures 3.1a and 3.1b. The elevation of the Betwa basin varies from 61 m to 715 m above mean sea level (m.s.l.). It has undulating topography with the land slope varying from 0 to 67%. The study area is dominated by black cotton soil, and bounded by Southern Vindhyan plateau and Northern alluvial plains. Betwa basin has flat wheat-growing agriculture to steep forest hilly area with varying vegetation and topography in complex pattern. Forest is dense in South-East, apart from the clay plains. Also, some Northern part of the Betwa basin covers partially distributed degraded or open forest area.

3.1.2 Climate of the Betwa Basin

The climate of Betwa basin is semi-humid to dry sub-humid (Suryavanshi et al., 2014). The climate of the Betwa basin is moderate, mostly dry except during the southwest monsoons. The

average annual rainfall of the study area varies from 700 to 1,200 mm with an average annual rainfall of 1,138 mm. The daily mean temperature ranges from a minimum of 8.1°C to a maximum of 42.3°C. The daily mean relative humidity varies from a minimum of 18 % (April and May) to a maximum of 90 % (August). The average annual evaporation losses are about 1,830 mm, and the average annual runoff is about 13,430 million cubic meters (MCM), out of which nearly 80 % occurs in monsoon season (Chaube 1988).

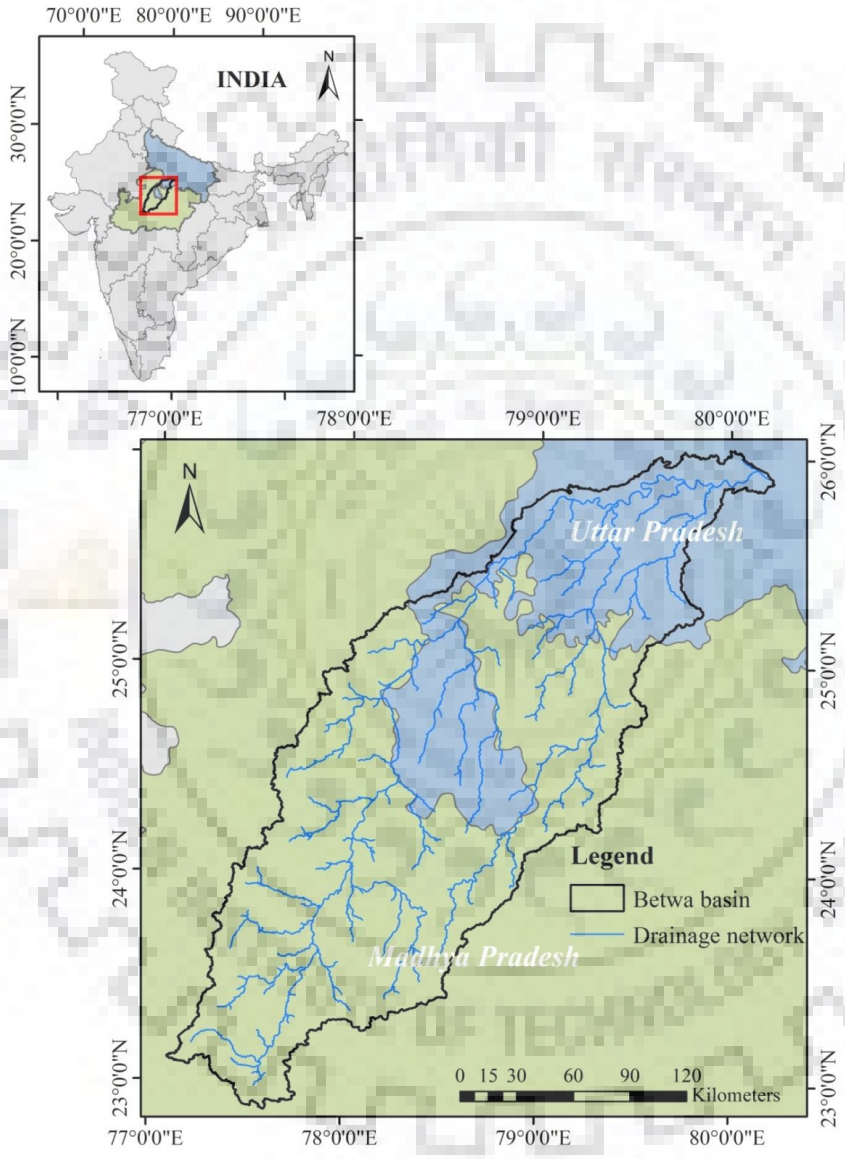

Figure 3.1a: Location map of the study area (Betwa river basin)

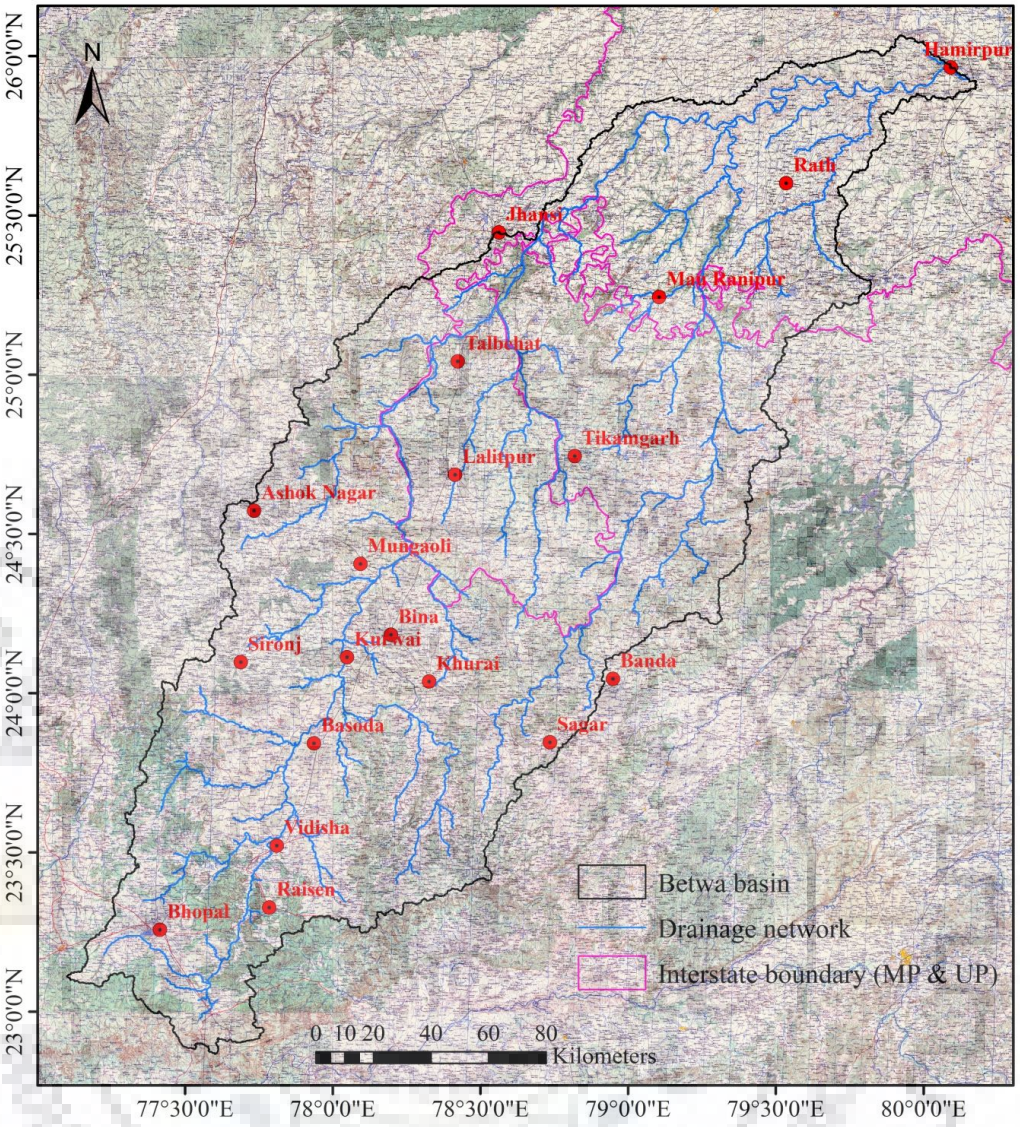

Figure 3.1b: Toposheet of the study area (Betwa river basin)

To understand the rainfall distribution pattern, spatial change analysis has been carried out for rainfall, minimum and maximum temperature (Figure 3.2). Also, the information of seasonal variation in these variables has been presented in Figure 3.3. It shows that most of the rainfall (about 87-93%) occurs during rainy (monsoon) season and mainly contribute to the total annual rainfall of the Betwa basin. Both minimum and maximum temperature has large variation in pre-monsoon, as compared to other seasons. Average maximum temperature decreases seasonally from pre-monsoon to winter. Average minimum temperature also decreases in the similar way, except in the monsoon season where it is higher than other seasonal mean values.

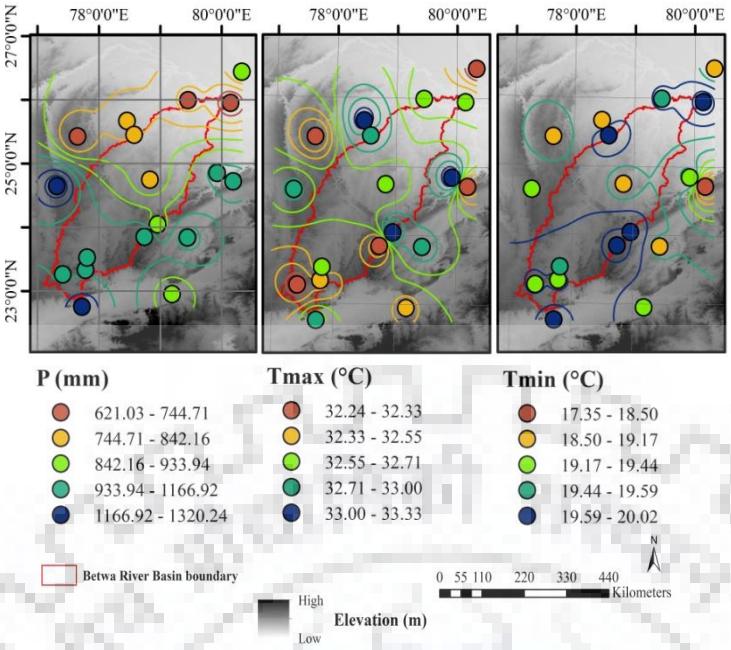

Figure 3.2: Spatial distribution of rainfall, maximum temperature, and minimum temperature over the Betwa River basin

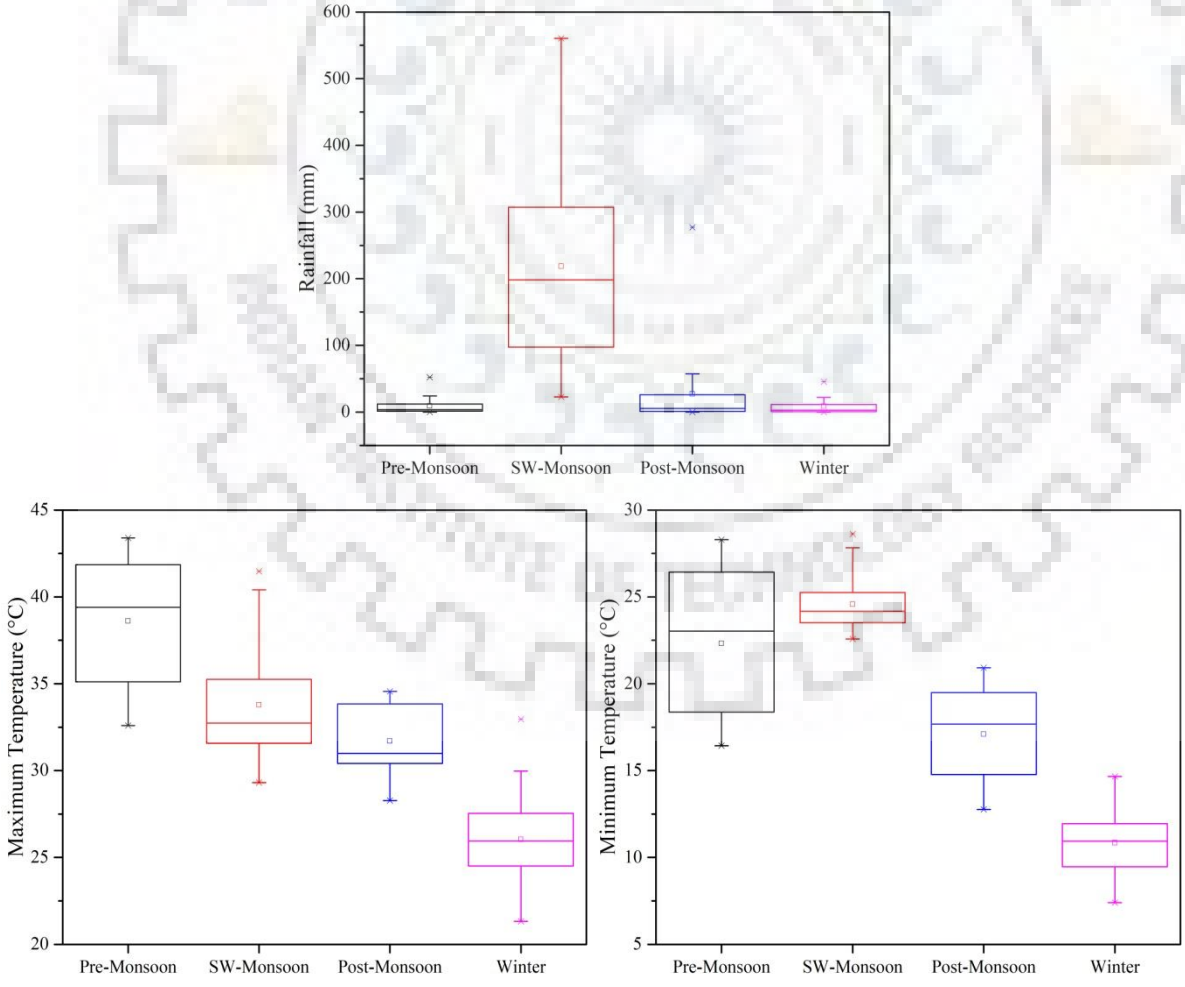

Figure 3.3: Seasonal variation of rainfall, maximum temperature and minimum temperature in the Betwa River basin

3.1.3 Major crops grown in Betwa basin

The major crops grown in the Betwa basin are cereals, pulses, oil seed, food grain vegetables and fodder. It includes cultivation of paddy, jowar, maize, groundnut, soyabean, tur (red gram), urad (black gram) and moong (green gram) as Kharif crops, and the wheat, gram, peas, lentil as Rabi crops. The agriculture informatics Division of National Informatics Centre, Ministry of Communication & Information Technology, Government of India (http://dacnet.nic.in, presently http://www.nic.in/) has suggested wheat, paddy, maize and sorghum as the most suitable crop rotation in this region.

3.2 DATA ACQUISITION

Followings are the details of several types of datasets, such as meteorological, hydrological, DEM, soil, remote sensing, and GCM, which have been used for the hydrological modelling.

3.2.1 Meteorological data

Daily observed data of precipitation (P), minimum and maximum temperature (Tmin and Tmax) and relative humidity (R_H) were obtained from the India Meteorological Department (IMD) Pune for the period of January-2001 to December-2013. The Betwa basin area has 18 gauging stations located in and near the basin area (Figure 3.4). Prior to the analysis, meteorological data was firstly checked, and then few missing data were filled by employing Inverse Distance Weighted (IDW) interpolation method (Spadavecchia & Williams, 2009; Di Piazza et al., 2011; Wagner et al., 2012).

3.2.2 Hydrological data

Further, daily discharge (Q) and sediment data of the Betwa basin gauges, i.e. Basoda, Garrauli, Mohana and Shahijina gauging station was procured from the Yamuna Basin Organization (YBO), Central Water Commission (CWC), New Delhi. However, sediment data was available only for Garrauli and Shahijina stations only. The location of CWC gauges is presented in Figure 3.4.

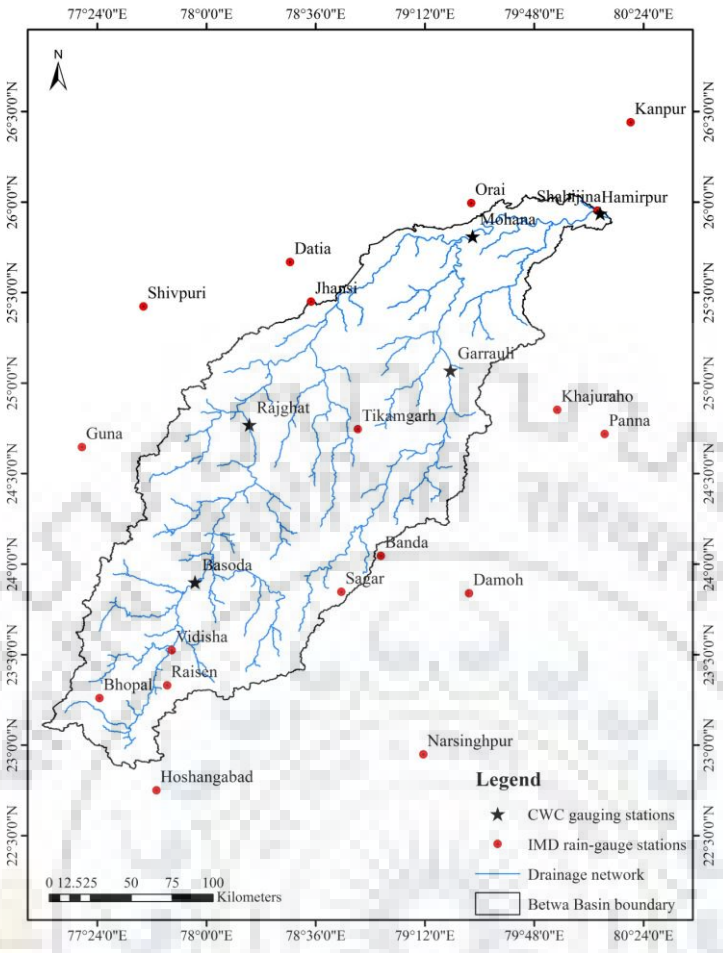

Figure 3.4: Gauging stations of IMD and CWC in the Betwa basin

3.2.3 DEM data

An immensely upgraded and freely available Shuttle Radar Topography Mission (SRTM) data of 30 m spatial resolution were processed for generation of the DEM, and then utilized for delineation of the study area. This SRTM data (Figure 3.5a) was downloaded from the Earth Explorer user interface available on public domain (https://earthexplorer.usgs.gov/) of the United States Geological Survey (USGS). The study area was delineated by using spatial analyst tools of the ArcGIS 10.2.2 version software package. Then, the basin boundary was used to extract and analyze MODIS land cover data of the study area. Furthermore, the DEM data was used to prepare and study the land slope variations (Figure 3.5b). This data was also used as an input to the SWAT model.

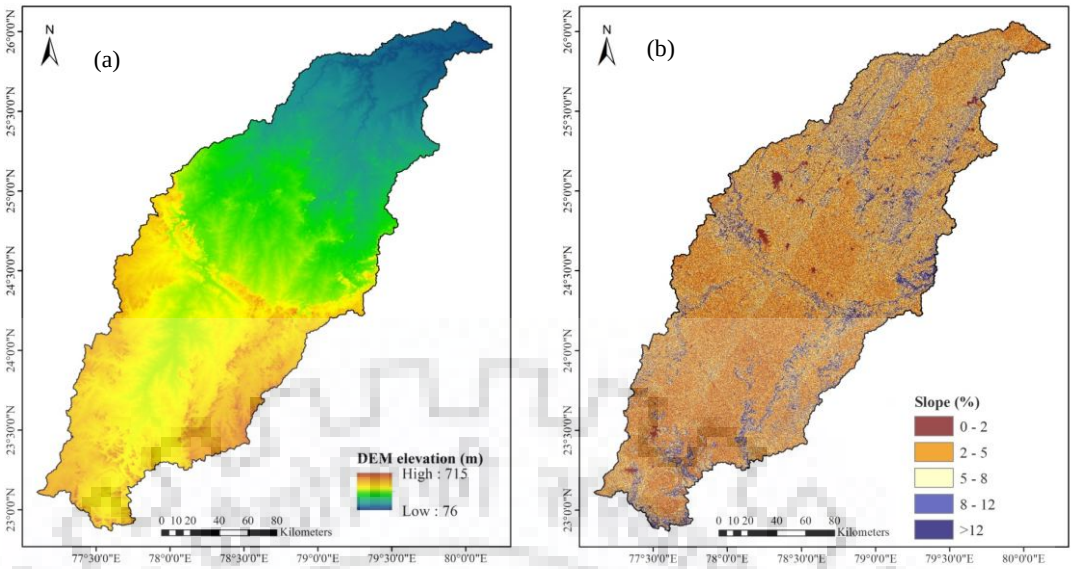

Figure 3.5: (a) DEM elevation (m), and (b) slope (%) map of the study area

Table 3.1: Detailed information of satellite imagery data

Year	Data type	Path - Row	Date of imagery	Spatial resolution (m)	Data source
1972	Landsat-1 Multispectral Scanner (MSS)	155 - 42, 43, 44	30-Nov-1972	60 m	USGS GloVis website (http://glovis.usgs.gov/)
		156 - 42, 43, 44	01-Dec-1972		
1976	Landsat-2 MSS	155 - 42, 43, 44	13-Oct-1976	60 m	
		156 - 42, 43, 44	01-Nov-1976		
1991	Landsat-5 Thematic Mapper (TM)	144 - 42, 43, 44	13-Dec-1991	30 m	
		145 – 42, 43	03-Feb-1991		
		145 - 44	19-Feb-1991		
2001	Landsat-7 Enhanced Thematic Mapper Plus (ETM+)	144 - 42, 43	27-Sep-2001	30 m	
		144 - 44	29-Oct-2001		
		145 - 42, 43, 44	21-Nov-2001		
2007	Indian Remote-sensing Satellite (IRS-P6) Linear Imaging and Self Scanning (LISS) III	97 - 54, 55, 56	27-Nov-2007	23.5 m	NRSC Hyderabad
		98 - 53, 54, 55, 56	08-Nov-2007		
		99 - 53, 54, 55, 56	13-Nov-2007		
		100 - 53	18-Nov-2007		
2010	Landsat-5 TM	144 - 42, 43, 44	15-Nov-2010	30 m	USGS GloVis website (http://glovis.usgs.gov/)
		145 - 42, 43, 44	21-Oct-2010		
2013	Landsat-8 Operational Land Imager (OLI)	144 - 42, 43, 44	22-Oct-2013	30 m	
		145 - 42, 43, 44	29-Oct-2013		

3.2.4 Remote sensing data

3.2.4.1 Satellite imagery data

In this study, historical LU/LC change analysis has been carried out using spatiotemporal satellite imagery data of the post-monsoon season (Table 3.1). These imageries were obtained from the United States Geological Survey (USGS) Global Visualization Viewer (GloVis) website (http://glovis.usgs.gov/) for the years 1972, 1976, 1991, 2001, 2010, and 2013. In addition, the IRS-P6 imagery of LISS-III sensor was procured from National Remote Sensing Centre (NRSC) Hyderabad for the year 2007. The problem of different spatial resolution has been removed by scaling IRS-P6 (LISS-II) imagery data from high (23.5 m) to coarse (30 m) resolution. Then, these scaled images were utilized for LU/LC change analysis to avoid errors while predicting consistent LU/LC maps.

3.2.4.2 MODIS datasets

In this study, remotely sensed time-series MODIS NDVI data sets of (collection 5) Terra (MOD13Q1) and MODIS Land Cover Type (MCD12Q1) products have been used to assess the relationship with hydro-climatic variables. The MOD13Q1 Terra NDVI data is available from February-2000 to present on 16-days temporal resolution and 250 m spatial resolution. In this study, NDVI data sets were retrieved for the period of January 2001 to December, 2013. The MCD12Q1 land cover data products are available on annual scale and at a spatial resolution of 500 m. These data sets were retrieved from the online Reverb tool (http://reverb.echo.nasa.gov/reverb/, presently https://search.earthdata.nasa.gov/search) of the NASA's Earth Observing System (EOS) Clearing House (ECHO), courtesy of the NASA EOSDIS Land Processes Distributed Active Archive Center (LP DAAC). The present study area is covered within one MODIS tile (number h25v06).

This study uses the MODIS C5 datasets, which has improved quality and accuracy, for land monitoring studies. The accuracy of the MODIS land cover data (MCD12Q1) product is significant about 74.8% globally, with a 95% confidence interval of 72.3 to 77.4%. The validation and accuracies of MCD12Q1 data is already examined by the developers (Friedl et al., 2010; Sulla-Menashe et al., 2011). Further, the MODIS data product has been extensively used for spatiotemporal land cover analysis in last decade (Zeng et al., 2010; Broxton et al., 2014; Liang et al., 2015; Pandey & Palmate, 2018). Information regarding the data accuracy is available on the website (https://landval.gsfc.nasa.gov/ProductStatus.php?ProductID=MOD12). Also, the accuracy of MOD13Q1 data is available on the NASA website (https://landval.gsfc.nasa.gov/ProductStatus.php?ProductID=MOD13).

3.2.5 CMIP5 GCM data

In this study, climate scenarios used are obtained from the NASA Earth Exchange Global Daily Downscaled Projections (NEX-GDDP) dataset, prepared by the Climate Analytics Group and NASA Ames Research Center using the NASA Earth Exchange, and distributed by the NASA Center for Climate Simulation (NCCS). In this study, the Max-Planck-Institute-Earth System Model-Medium Resolution (MPI-ESM-MR) model has been employed. From the recent literature, the MPI-ESM-MR model the best performing Coupled Model Intercomparison Project Phase 5 (CMIP5) GCM data was selected for the present study based on the model performance and climate change impacts study over Indian regions (Sharmila et al., 2015; Guo et al., 2016; Roxy et la., 2016; Das et al., 2018). Therefore, the CMIP5 datasets of the MPI-ESM-MR model has been used in this study. Future daily precipitation, minimum temperature and maximum temperature data of the MPI-ESM-MR model was obtained from the Centre for Climate Change Research, Indian Institute of Tropical Meteorology, Pune (http://cccr.tropmet.res.in/).

The MPI-ESM-MR dataset at 0.25°×0.25° spatial resolution was used to prepare climate change data for simulation of the SWAT model. In this study, RCP 8.5 scenario has been used for future hydrological modelling, because it is considered as the worst-case scenario and represents the most severe conditions, i.e. this scenario would be the upper limit for potential climate change impacts and responses. Firstly, future data was extracted for each station, and then bias-corrected by quantile mapping method (Thrasher et al., 2012). Based on empirical relationships between observed and simulated discharge and sediment datasets, the downscaled and bias-corrected MPI-ESM-MR dataset were further divided into five different time-periods. One historical period was used as baseline 1986 (1986-2005), and four future periods, i.e. horizon 2020 (2020-2039), horizon 2040 (2040-2059), horizon 2060 (2060-2079) and horizon 2080 (2080-2099) were used for future climate change impact studies.

3.2.6 Soil data

The Betwa basin area is dominated by black cotton soil, and bounded by southern Vindhyan plateau and Northern alluvial plains. The Betwa basin falls under the Vindhyan sandstone, Deccan traps and Bundelkhand granite. Soils survey of the region has been carried out by the National Bureau of Soil Survey and Land Use Planning (NBSS&LUP), Nagpur. Based on the NBSS&LUP data, soils of the basin are classified as clay, silty clay, clay loam and sandy loam.

Table 3.2: Physical and chemical properties of the soils in Betwa basin

Soil properties		Depth (mm)	MBD (Mg/m^3)	OCC (%)	Clay (%)	Silt (%)	Sand (%)	SHC (mm/hr)	USLE K factor	HYDGRP
Clay	Layer 1	140	1.32	0.7	52.1	32.3	15.6	11.45	0.2	D
	Layer 2	280	1.43	0.6	55.3	27.3	17	11.45	0.17	
	Layer 3	280	1.48	0.5	64.2	27.1	8.7	11.45	0.12	
	Layer 4	600	1.53	0.2	65.1	19.8	15.1	5.6	0.12	
Clay Loam	Layer 1	60	1.47	1.65	34.2	38.1	22.7	29.5	0.28	C / D
	Layer 2	80	1.71	1.56	37.1	22.4	40.5	29.5	0.26	
Sandy Loam	Layer 1	100	1.7	1.42	14.2	22.3	63.5	10.4	0.55	A / C
	Layer 2	120	1.7	1.36	35.7	20.7	43.6	10.4	0.3	
Silty Clay	Layer 1	110	1.35	0.48	46.4	43.2	10.4	12.1	0.25	B / D
	Layer 2	290	1.43	0.36	48.6	44.8	6.66	12.1	0.24	
	Layer 3	300	1.53	0.3	49.8	45.8	4.2	12.1	0.23	
	Layer 4	350	1.57	0.24	48.3	44.3	7.4	4.3	0.24	
	Layer 5	300	1.58	0.24	43.1	50.2	6.7	4.3	0.29	
	Layer 6	350	1.58	0.21	38.5	48.1	13.4	4.3	0.34	

Note: MBD = Moist Bulk Density, OCC = Organic Carbon Content, SHC = Soil Hydraulic Conductivity, HYDGRP = Soil Hydrologic Group

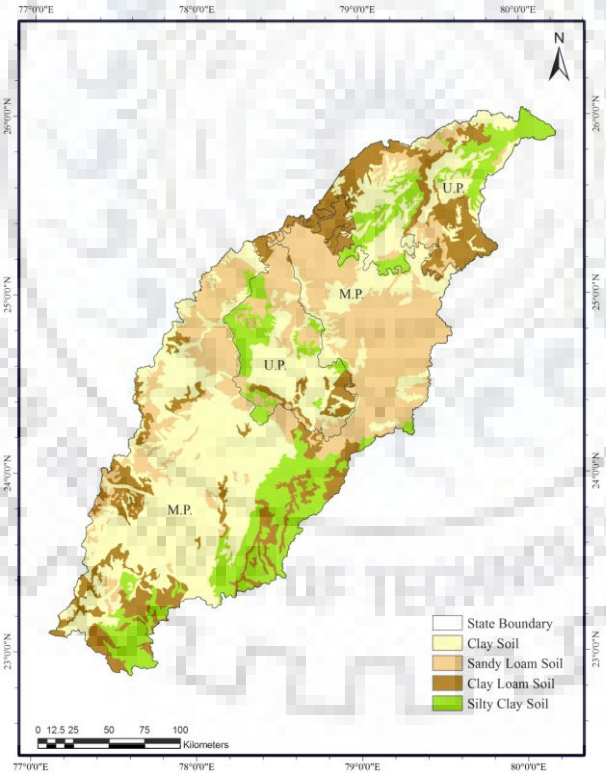

Figure 3.6: Soil map of the Betwa basin

Soil data in the form of maps (Madhya Pradesh: 9 sheets and Uttar Pradesh: 6 sheets), soil series booklet and bulletin format were procured from the National Bureau of Soil Survey & Land Use Planning (NBSS&LUP) Nagpur. These soil maps were scanned first and then geometrically rectified to generate thematic layer for the Betwa River basin (Figure 3.6). Based on the NBSS&LUP data, soils of the basin are classified as clay (40.89 %), Silty Clay (15.89

%), Clay Loam (16.25 %) and Sandy loam (26.97 %) with an area of 17782.8 km^2, 6912.15 km^2, 7068.75 km^2, 11727.6 km^2 respectively (Figure 3.6). The physical and chemical properties of the soils are taken from Soils of MP (NBSS, 1996) and are presented in Table 3.2. Also, the soil hydrologic groups used for runoff calculations are provided in Table 3.2.

3.2.7 Ground truth verification and field visits

In this study, several field visits were carried out to collect the ground truth points for accuracy assessment of LU/LC maps, and to collect the existing practices used in the agriculture area of the Betwa basin. Accuracy assessment of the LU/LC map is essential to understand the accurate and valid results of the classified imagery, without which the LU/LC map is a simply an untested hypothesis. In this study, ground truth verification of the LU/LC maps was carried out using Global Positioning System (GPS). These field visits were performed during August-2013, May-2014, November-2014 and November-2016 (Figure 3.7). The locations of the study area visited and their photos are given in Annexure-A.

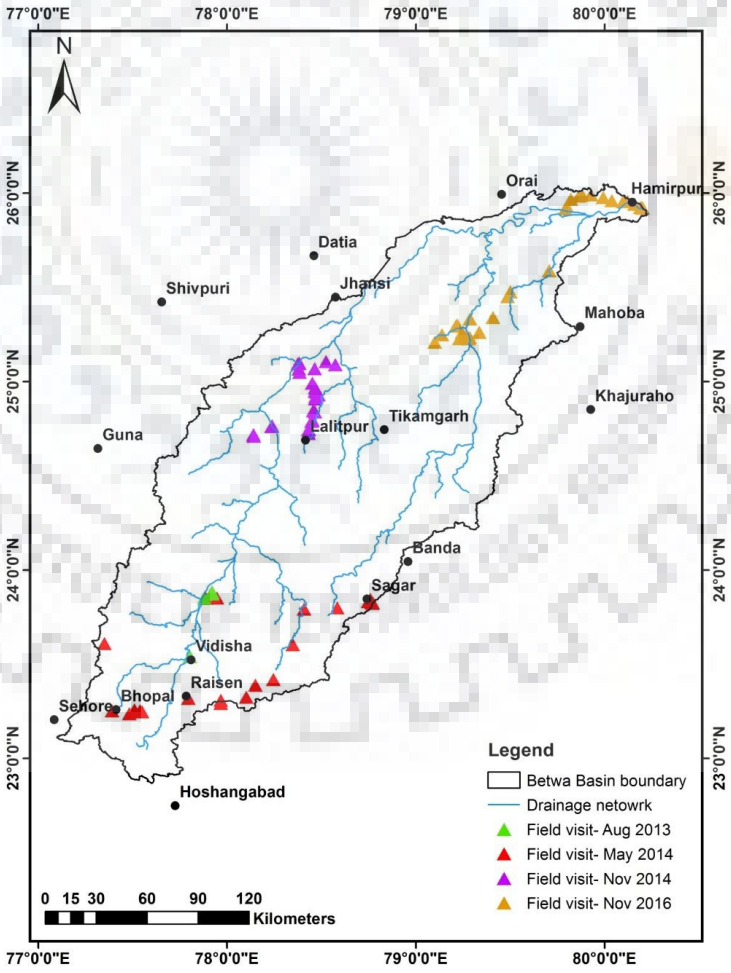

Figure 3.7: GPS locations during ground truth verification

3.2.8 Details of present operations/practices in Betwa basin

During field visits, the detail of operations in the agriculture area including ploughing, planting, irrigation, manure and fertilizer application, inter-culture operations, and harvesting were obtained and collected for hydrological modelling (Table 3.3).

Table 3.3: Schedule of field operations for the major crops in the Betwa basin

Sr. No.	Particulars	Crops							
		Wheat		Rice		Maize		Sorghum	
A	**Crop field management**								
1	1st ploughing	1st week of Oct.		25 April-15 may		Up to 15 may		Up to 15 may	
2	2nd ploughing (Cultivator twice)	15 Oct		After 1 week of 1st Ploughing		After 1 week of 1st Ploughing		After 1 week of 1st Ploughing	
3	First Planking (Cloud Breaking)	Just after 2nd Ploughing		Just after 2nd Ploughing		Just after 2nd Ploughing		Just after 2nd Ploughing	
4	3rd ploughing (Cultivator twice in cross direction)	At sowing Time		Two days before planting		At sowing Time		At sowing Time	
5	Final Planking	After sowing		At the time of planting		After sowing		After sowing	
6	Puddling*			1st week of July					
7	Sowing Time	First fortnight of November		Nursery 15-25 June		Kharif-15 June-15 July		First fortnight of July	
8	Transplanting			1st week of July					
B	**Irrigation**	**DAS**	**Qty.**	**DAP**	**Qty.**	**DAS**	**Qty.**	**DAS**	**Qty.**
1	1st irrigation	21	5 cm	Each 15 days interval as per need and rainfall distribution	2	30	5	30	5
2	2nd irrigation	45-50	5 cm		5	50-55	5	50	5
3	3rd irrigation	65-70	5 cm		5	70	5		
4	4th irrigation	85-90	5 cm		5				
5	5th irrigation	105-120	5 cm		5				
6	6th irrigation	130	3 cm		5				
C	**Manures and Fertilizer application**								
1	FYM/Compost (At the time of 2nd Ploughing)	10-15 ton		10-15 ton		10-15 ton		10-15 ton	
2	Basal dressing N:P:K (at the time of sowing)	60:60:40		60:60:40		Hybrid-60:60:40 Composite-40:30:20		60:50:40	
3	1st top dressing (After 1st Irrigation)	30 kg N		30 kg N		Hybrid-30 kg N Composite- 20 kg N (30-35 DAS)		30 kg N	
4	2nd top dressing	30 kg N		30 kg N		Hybrid-30 kg N Composite- 20 kg N (65 DAS)		30 kg N	
5	Others	5 kg Zn		25 kg Zn		20-25 kg Zn (30-35 DAS)		---	
D	**Intercultural Operations**								
1	1st weeding	25 DAS		25-30 DAS		30 DAS		30 DAS	
2	2nd weeding	40-45 DAS		45-50 DAS		40-45 DAS			
E	**Harvesting**	110-140 DAS		110-130 DAS		80-110 DAS		90-120 DAS	

*All the information given here on hectare (10000M^2) basis; *Only in Rice, ** Only in Maize*
DAS- Days after sowing, DAP- Days after planting

3.3 WATER RESOURCES OF THE BETWA BASIN

3.3.1 Rivers

The Betwa River basin joins a number of tributaries and sub-tributaries, among them the most important rivers are Bina, Jamini, Dhasan, and Birma on the right bank, and Kaliasote, Halali, Bah, Sagar, Narain, and Kaithan on the left Bank of the Betwa river. The rivers in the Bundelkhand swell up with floods during rainy season, and dry up in the summers. Even in the Betwa River basin which is the mightiest river of the region, discharge remains only a few cusecs during the summer months. Therefore, if the water is not stored during the monsoon months, water shortage conditions are created during the remaining time of the year. Even drinking water becomes scarcely available. Due to this, about 600 small tanks were constructed in this area during the time of Chandelas (9^{th} century CE to 13^{th} Century CE). Some of these tanks are still useful.

3.3.2 Reservoirs and weirs

Parichha dam was originally constructed in 1881 for 48.14 MCM and Betwa canal opened for irrigation in the year 1886. The storage fell short of the demand and, therefore, 6 ft high shutters were provided on the spillway weir in the year 1898 to increase its capacity to 68.64 MCM which was further increased. The supplies did not prove sufficient for the demand, and were augmented by another dam on Betwa River at Dhukwan in 1909. Originally the storage capacity of Dhukwan dam was 68.93 MCM after installation of 8 ft high shutters on the crest. The present storage capacities of the Parichha and Dhukwan, dams are 78.75 MCM and 64.67 MCM, respectively. In order to supplement Dhukwan reservoir, the Matatila dam (a major project in UP) was constructed in 1958.

In the present condition the role of Parricha weir and Dhukwan dam is more or less limited to diversion only whereas Rajghat and Matatila dam in the basin acts as major storage reservoirs for irrigation, power production, municipal and industrial water supply and to feed water through water through Dhukwan and Parricha weir for irrigation releases.

In addition, nine minor to major water storage structures are also available in the study area, i.e. lakes, ponds, reservoirs, weirs etc. (Figure 3.8). These structures have direct impact on hydrology of the Betwa basin, thus considered in the study. In the SWAT model, the required informations of these water storages were obtained from India-WRIS (Water Resources Information System) website (http://india-wris.nrsc.gov.in/) for precise hydrological simulation.

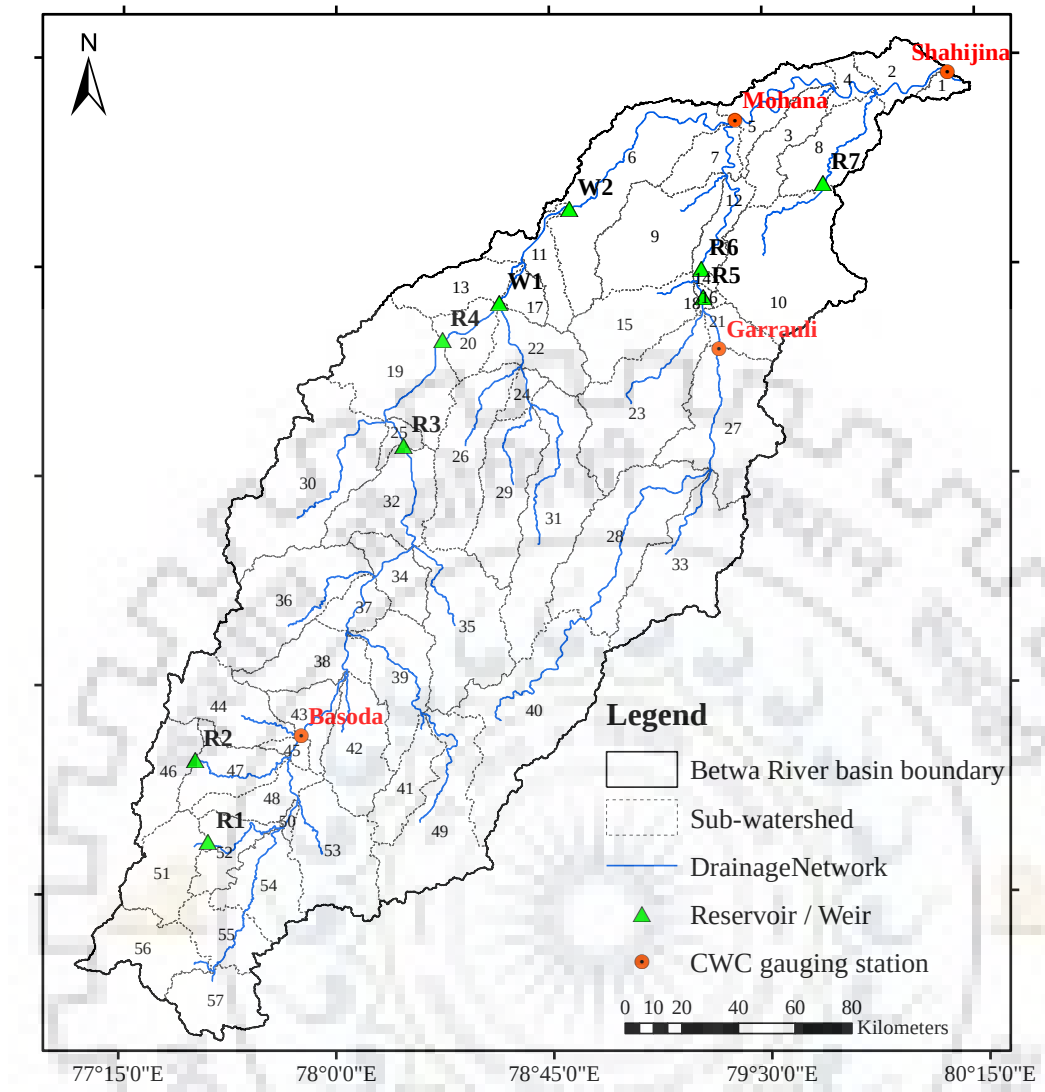

- R1: Samrat Ashok Sagar (Halali) dam
- R2: Bah dam
- R3: Rajghat (Rani Lakshmi Bai Sagar) dam
- R4: Matatila dam
- R5: Devri dam
- R6: Lahchura dam
- R7: Maudaha (Swami Brahmanand) dam
- W1: Dhukwan weir
- W2: Paricha weir

Figure 3.8: Water storage structures and CWC gauges in the Betwa river basin

CHAPTER 4

SPATIOTEMPORAL LAND USE/LAND COVER CHANGES AND ITS MODELLING FOR FUTURE ANALYSIS

In this chapter, spatiotemporal land use/land cover (LU/LC) change analysis has been carried out to address changes in land resources of the Betwa river basin, central India using various satellite data sets. The Supervised classification method has been used to prepare the LU/LC maps for historical years 1972, 1976, 1991, 2001, 2007, 2010 and 2013. Further, an integrated Cellular Automata (CA) - Markov Chain (MC) model has been employed to simulate the future LU/LC maps of the years 2020, 2040, 2060, 2080 and 2100. The integrated CA-MC modelling approach can interactively predict the future LU/LC maps, and provide solutions to the current land resources problems.

4.1 BACKGROUND OF THE STUDY

The trans-boundary river basins have major disputes of natural resources management (Wolf and Hamner, 2000; Dhliwayo, 2002) due to political and legislations issues (Kindt, 1986; Dedina, 1995; Singh and Gosain, 2004) that can potentially affects agrarian livelihood (Wolmer, 2003; Makalle et al., 2008). The Indian territory constitutes of major and medium trans-boundary rivers, and therefore adaptive land management strategies and environmental cooperation between countries/states are necessary for conservation of natural resources (Agrawal, 2000). Nowadays, changes in the land resources have been investigated using advanced remote sensing and GIS techniques. The land use/land cover (LU/LC) change analysis has been extensively carried out to understand spatiotemporal land dynamics for the studies on climate, ecology and food security (Vitousek, 1994; Fuchs et al., 2015). This information reveals ongoing process of deforestation (Geoghegan et al., 2001), biodiversity (Falcucci et al., 2007) and urbanization (Dewan and Yamaguchi, 2009). Also, LU/LC change has significant impact on hydrologic response (Shaw et al., 2014), stream-flow (Zheng et al., 2012), water quality (Goldshleger et al., 2014; Wang et al., 2014) and snow cover (Szczypta et al., 2015). It can significantly affect hydrology of the trans-boundary river basin (Mati et al., 2008). Therefore, spatiotemporal LU/LC maps are vital to monitor LU/LC changes (Herold et al., 2008), addresses climate change mitigation and adaptation (Turner and Annamalai, 2012), ecosystem evaluation (Nelson et al., 2009) and natural resources management (Tallis and Polasky, 2009; Bagan & Yamagata, 2012).

Previous research studies have used different datasets (historic maps and remotely sensed data) to carry out LU/LC change analysis for the local or regional studies (Čarni et al., 1998; Bičík et

al., 2001; Petit and Lambin, 2002; Kuemmerle et al., 2006). These datasets are pre-requisite to prioritize and evaluate spatially explicit future LU/LC (Torrens, 2006). Nowadays, advanced geo-spatial data sets have been extensively used for monitoring important LU/LC features to explore human-environment interaction (Hoalst-Pullen and Patterson, 2010). Moreover, several advanced geospatial and statistical LU/LC models such as Markov Chain (MC) (Kamusoko et al., 2009), Cellular Automata (CA) (Han et al., 2009; Mitsova et al., 2011), logistic regression model (Hu and Lo, 2007) and machine learning algorithms (Huang et al., 2010) are currently being used to understand and, to predict possible LU/LC pattern (Costanza and Ruth, 1998). Kamusoko et al. (2009) predicted future LU/LC for Zimbabwe, and reported increase in barren land area as potential threat to rural sustainability up to 2030. Guan et al. (2011) studied decrease in agriculture and forest area with increase in settlement area for the period of 2015 to 2042 in Saga, Japan. He et al. (2013) assessed impact of farmland preservation policies on urban sprawl and food security in China. They concluded that urban land could increase in the future, and have susceptible impact on future land resources. Moreover, future LU/LC maps were predicted by Paegelow and Olmedo (2005) for the Garrotxes (France) and Alta Alpujarra Granadina (Spain). Huang et al. (2012) studied LU/LC transition intensity effect on the regional economic and ecological health in Southeast China. Thus, it is observed that LU/LC modelling can significantly use to find out land resources problems.

Many researchers suggested that integration of two or more models will be useful to improve reliability of LU/LC prediction (Myint and Wang, 2006; Qiu and Chen, 2008; Kamusoko et al., 2009; Liu et al., 2010; Mondal and Southworth, 2010; Guan et al., 2011; Sang e al., 2011; Arsanjani et al., 2011). This approach has been employed effectively for LU/LC simulation using an integrated Cellular Automata (CA)-Markov Chain (MC) model (Myint and Wang, 2006; Kamusoko et al., 2009; Mondal and Southworth, 2010). The CA-MC model has been widely used for spatial analysis, due to remote sensing and GIS ability to efficiently use temporal datasets in the model (Kamusoko et al., 2009). It has a more significant effect on the transition maps, which determine the quantity and location of the LU/LC changes. This model integrates Markovian transition probabilities and CA spatial filter which facilitate to significantly simulate future LU/LC maps based on historical LU/LC changes (Kamusoko et al., 2009). It addresses improved CA-MC model functions i.e. MC model reveals transition rules of CA model for future simulation (Liu et al., 2008). Hence, CA-MC modelling is a robust approach in which, MC computes transition matrices based on amount of temporal changes among different LU/LC classes (López et al., 2001), and CA controls spatial change pattern through local-raster based contiguity filter or transitional maps (Clarke et al., 1994; Li

and Yeh, 2004) to predict future LU/LC at discrete time steps (Guan et al., 2011). Thus, CA-MC model employed in the present study has capability to simulate future LU/LC pattern.

In this study, historical and future LU/LC change analysis has been carried out for a trans-boundary/interstate river basin i.e. Betwa River Basin (BRB) of Central India. The study area has agriculture and water resources management problems due to disputes in the two territories of Madhya Pradesh and Uttar Pradesh States. Therefore, this chapter has been planned with the specific objective of spatiotemporal analysis of historical LU/LC dynamics, and use of integrated CA-MC model for future simulation to identify possible land resources problems in the Betwa River Basin. This study also emphasized the need of understanding changes in agriculture area corresponds to water resources availability in Central India.

4.2 MATERIALS AND METHODS

4.2.1 Study area and data acquisition

The detailed description of the study area and the satellite data pertaining to this study are briefly given in Chapter-3. The detailed methodology flowchart adopted in the present study is provided in Figure 4.1.

4.2.2 Historical LU/LC classification

The supervised classification algorithm is usually appropriate when relatively few classes are to be identified, or when training sites have been selected. It is the most common and easy image classification method, compared to other methods, uses spectral signatures in the training site. Therefore, in this study supervised classification method has been employed to prepare the LU/LC maps of the study area. Processing of satellite imagery data and their interpretation were carried out using ERDAS Imagine-2014 and ArcGIS 10.2.2 version software packages, respectively. The BRB area was classified into six LU/LC classes, i.e. dense forest, degraded/open forest, agriculture area, barren land, waterbody and settlement. The dense and degraded forest types were classified based on their canopy density. According to Forest Survey of India (FSI), land with canopy density more than 40% and less than 40% are termed as dense forest and degraded/open forest respectively. Difference in spectral resolution of forest canopy facilitated to distinguish these classes in the present study. Furthermore, agriculture class has been classified including both cultivated and non-cultivated crop land area.

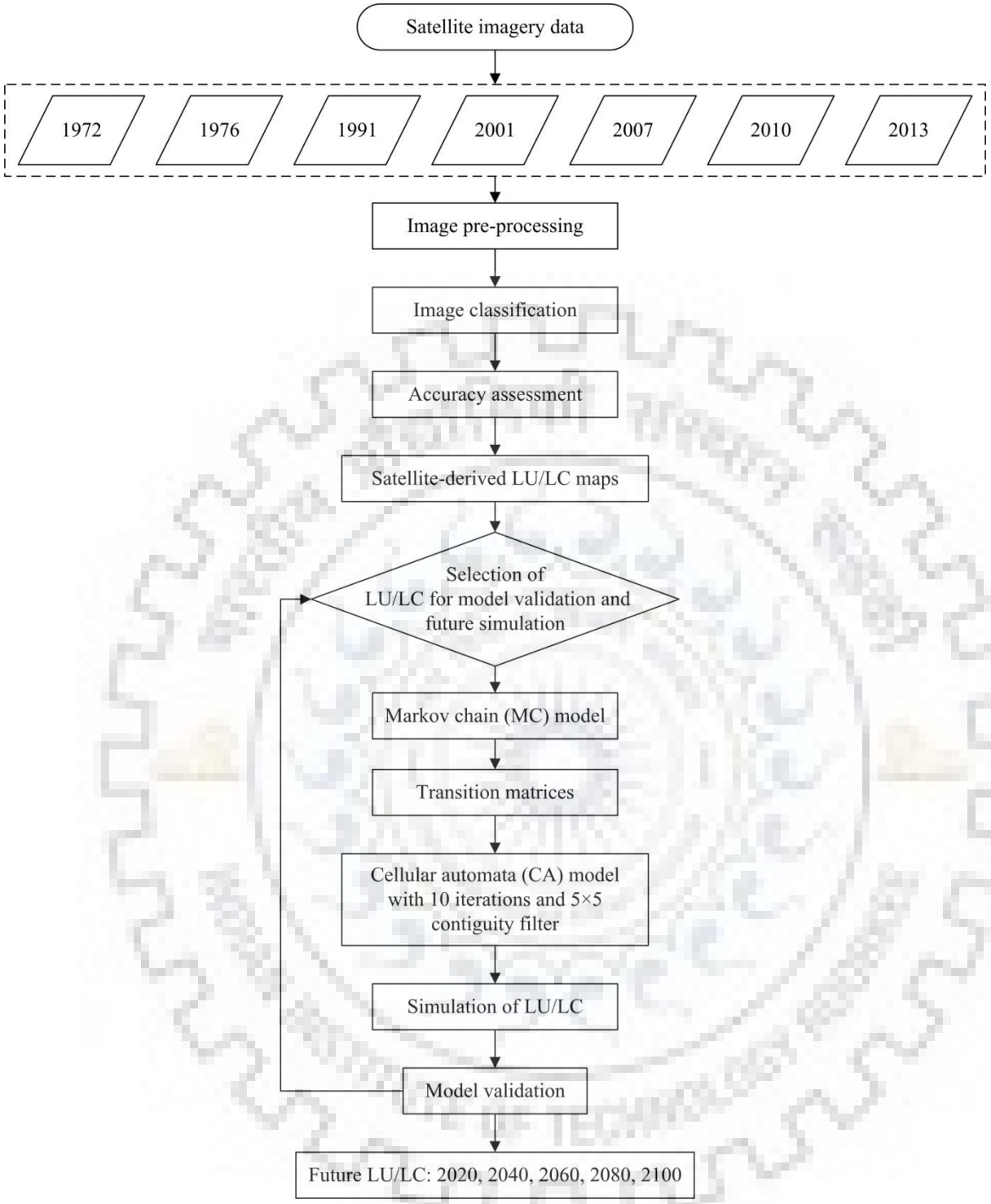

Figure 4.1: Flowchart of methodology used in the present study

For accuracy assessment, five hundred random points were generated across each LU/LC map. These points were then cross-checked with the reference data. In this study, Google Earth integrated in ERDAS Imagine software package has been used as reference data for accuracy assessment. In addition to this, ground truth verification was carried out through field visit of the study area using Global Positioning System (GPS) during August 2-3, 2013. These GPS points were also utilized for classification accuracy assessment. In this analysis, matching

points in both satellite-derived LU/LC map and reference map were denoted by the same class number; otherwise it was replaced with corrected class number. Then, accuracy assessment statistics were generated from the population error matrix of these maps. Table 4.1 shows the population error matrix which can be prepared when all the classes available on satellite-derived LU/LC map and reference image are same. The error matrix represents map accuracy, and allows to calculate specific accuracy measures such as user's accuracy (A_u), producer's accuracy (A_p), overall accuracy (A_o) and Kappa coefficient (K_c) as follows:

Table 4.1: Population error matrix with p_{ij} representing the proportion of area in the mapped land cover category i and the reference land cover category j

Classification	**Reference**				
	Class 1	**Class 2**	**...**	**Class *m***	**Row proportion**
Class 1	p_{11}	p_{12}	...	p_{1m}	p_{1+}
Class 2	p_{21}	p_{22}	...	p_{2m}	p_{2+}
.	.	.	...	.	.
.	.	.	...	.	.
.	.	.	...	.	.
Class *m*	p_{m1}	p_{m2}	...	p_{mm}	p_{m+}
Column proportion	p_{+1}	p_{+2}	...	p_{+m}	

User's accuracy: $A_u = p_{ii} / p_{i+}$ …(4.1)

Producer's accuracy: $A_p = p_{ii} / p_{+i}$ …(4.2)

Overall accuracy: $A_o = \frac{\sum_{i=1}^{m} p_{ii}}{n} \times 100$ …(4.3)

Kappa coefficient: $K_c = \frac{n\sum_{i=1}^{m} p_{ii} - \sum_{i=1}^{m} p_{i+} \times p_{+i}}{n^2 - \sum_{i=1}^{m} p_{i+} \times p_{+i}}$ …(4.4)

where, 1) p_{ii} is the LU/LC area proportion of classified class and reference class; 2) $p_{i+} = p_{+i} = \sum_{j=1}^{m} p_{ii}$ is the LU/LC area proportion of classified classes and true reference classes.

In this study, overall classification accuracy varies from 77% to 87% and, Kappa coefficient varies from 0.709 to 0.836 as shown in Table 4.2. The accuracy assessment results were affirmed the use of satellite-derived LU/LC maps for future analysis. Due to multi-spatial

resolution, small difference in the total area may cause an error and uncertainty in CA-MC model simulation. Therefore, datasets of the years 2001, 2007 and 2010 were brought into the same spatial resolution, i.e. 30 m, for future analysis.

Table 4.2: Accuracy assessment results of historical land use/land cover classification

LU/LC class	Accuracy type	Classification Accuracy Assessment (%)						
		1972	1976	1991	2001	2007	2010	2013
Dense forest	Producers Accuracy	94.44	88.24	92.31	93.33	93.33	100.00	93.75
	Users Accuracy	85.00	75.00	60.00	70.00	70.00	90.00	75.00
Degraded forest	Producers Accuracy	73.91	88.89	71.43	83.33	83.33	77.27	77.27
	Users Accuracy	85.00	80.00	75.00	75.00	75.00	85.00	85.00
Agriculture area	Producers Accuracy	78.79	71.79	68.42	65.79	79.41	81.82	80.65
	Users Accuracy	86.67	93.33	86.67	83.33	90.00	90.00	83.33
Barren land	Producers Accuracy	100.00	88.89	63.64	66.67	53.85	77.78	58.33
	Users Accuracy	80.00	80.00	70.00	80.00	70.00	70.00	70.00
Waterbody	Producers Accuracy	100.00	100.00	100.00	100.00	100.00	100.00	100.00
	Users Accuracy	100.00	100.00	90.00	90.00	100.00	100.00	90.00
Settlement	Producers Accuracy	100.00	100.00	100.00	90.00	90.00	100.00	100.00
	Users Accuracy	80.00	70.00	80.00	70.00	90.00	80.00	90.00
Overall Classification Accuracy (%)		86.00	84.00	77.00	78.00	82.00	87.00	82.00
Kappa coefficient		0.824	0.797	0.709	0.723	0.775	0.836	0.775

4.2.3 Future prediction using integrated CA-MC model

This study employed an integrated CA-MC model that uses satellite-derived LU/LC maps to predict spatial distribution of future LU/LC pattern. The CA-MC model is inbuilt module of the IDRISI Selva, a raster-based spatial analysis software package, developed by Clark Labs at Clark University. The methodology flowchart is presented in Figure 4.1.

For the future analysis, satellite-derived LU/LC maps of the years 2001, 2007 and 2010 were used to generate transition area matrix (TAM) and transition probability matrix (TPM), and then multi-criteria evaluation (MCE) procedure was followed to generate transition suitability maps (TSM) using MC model (Appendix-A). The TAM and TSM change dynamics were recalled and processed in the CA-MC model with 10 CA iterations and standard 5×5 contiguity filter. Iterations establishes the time steps in which, each LU/LC classes becomes host category and all other classes act as claimant classes to compete for future class using the multi-objective land allocation (MOLA) method. Finally, MOLA outputs were overlaid to produce future LU/LC map. In this study, future LU/LC maps were predicted for the years 2020, 2040,

2060, 2080 and 2100 employing integrated CA-MC model. Future LU/LC maps were simulated up to year 2100 for understanding possible trend of LU/LC dynamics. Due to uncertainty in LU/LC modelling, it is impossible to use these maps in policy planning. However, this can be used as an input data in hydrological modelling studies, or/and it could be an early-warning information for land planners, managers and developers.

The CA-MC model was validated twice for the years 2010 using input LU/LC data of the years 2001 and 2007, and for the year 2013 using input LU/LC data of the years 2007 and 2010 to provide confidence in future LU/LC modelling. The VALIDATE module of IDRISI Selva has been used to assess the level of agreement between simulated map and reference map (Mitsova et al., 2011). Furthermore, it is important to carry out visual inspection of the LU/LC to understand spatial pattern in the predicted maps. In visual inspection, satellite-derived and simulated LU/LC maps were compared graphically in clustered columns. The similar relative comparison method was also employed by the previous researchers for model validation (e.g. Kamusoko et al., 2009; Guan et al., 2011).

4.3 RESULTS

The results obtained from the spatiotemporal analysis of historical LU/LC pattern and future LU/LC prediction employing an integrated CA-MC model are presented in this section. Due to interstate river basin, results of LU/LC change analysis have been also discriminated for the Madhya Pradesh and Uttar Pradesh states.

4.3.1 Historical LU/LC change analysis

Area statistics of different LU/LC classes for the years 1972, 1976, 1991, 2001, 2007, 2010 and 2013 are presented in Tables 4.3a&b. In the study area, dense forest area has declined from 23.39% to 14.31% during the years 1972 to 2013 respectively, and resulted 9.08% decrease in the last four decades. However, the area under degraded forest has increased from 8.54% to 13.37%. Moreover, agriculture area has increased from 63.75% to 67.91%, barren land has decreased from 2.98% to 1.27%, waterbody surface area has increased from 1.22% to 2.84% and settlement area has increased from 0.12% to 0.31%. It is observed that dominant vegetation area, agriculture land, and waterbody were significantly changed during historical time-periods (Table 4.3b). These results of historical LU/LC analysis have been illustrated in the Figures 4.2 and 4.3.

Table 4.3a: Area (%) under historical land use/land cover classification

LU/LC class	Area (%) under land use/land cover classification						
	1972	1976	1991	2001	2007	2010	2013
Dense forest	23.39	21.16	18.02	14.84	11.97	12.91	14.31
Degraded/Open forest	8.54	9.68	9.15	12.65	14.46	13.91	13.37
Agriculture area	63.75	65.22	69.26	69.20	66.16	67.33	67.91
Barren land	2.98	2.42	2.55	1.31	5.96	4.45	1.27
Waterbody	1.22	1.40	0.84	1.78	1.17	1.11	2.84
Settlement	0.12	0.13	0.19	0.22	0.28	0.30	0.31
Total area (%)	100.00	100.00	100.00	100.00	100.00	100.00	100.00

Table 4.3: Percent change between historical time-periods

LU/LC class	Change (%) under land use/land cover classification					
	1972-1976	1976-1991	1991-2001	2001-2007	20072010	2010-2013
Dense forest	-2.23	-3.14	-3.18	-2.87	0.94	1.40
Degraded/Open forest	1.14	-0.53	3.50	1.81	-0.55	-0.54
Agriculture area	1.47	4.04	-0.06	-3.04	1.17	0.58
Barren land	-0.56	0.13	-1.24	4.65	-1.51	-3.18
Waterbody	0.18	-0.56	0.94	-0.61	-0.06	1.73
Settlement	0.01	0.06	0.03	0.06	0.02	0.01

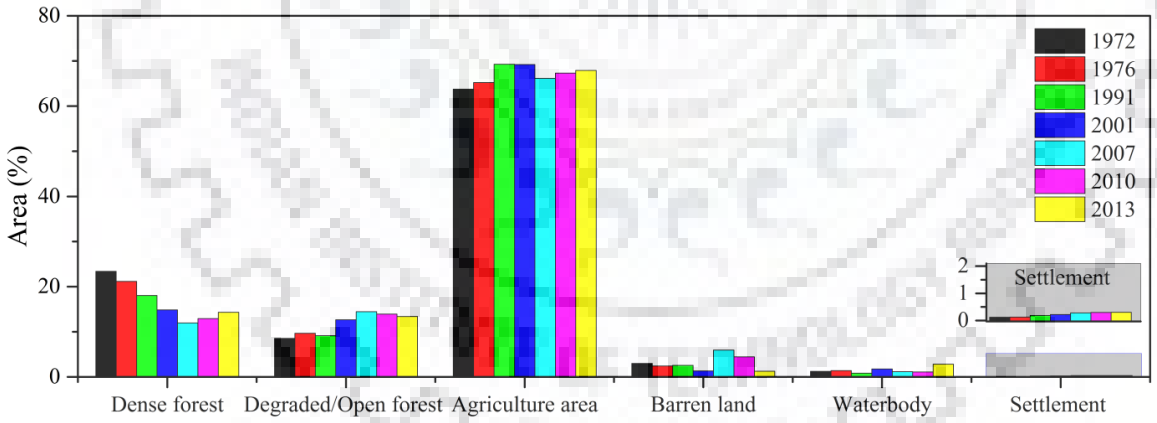

Figure 4.2: Graphical representation of historical land use/land cover

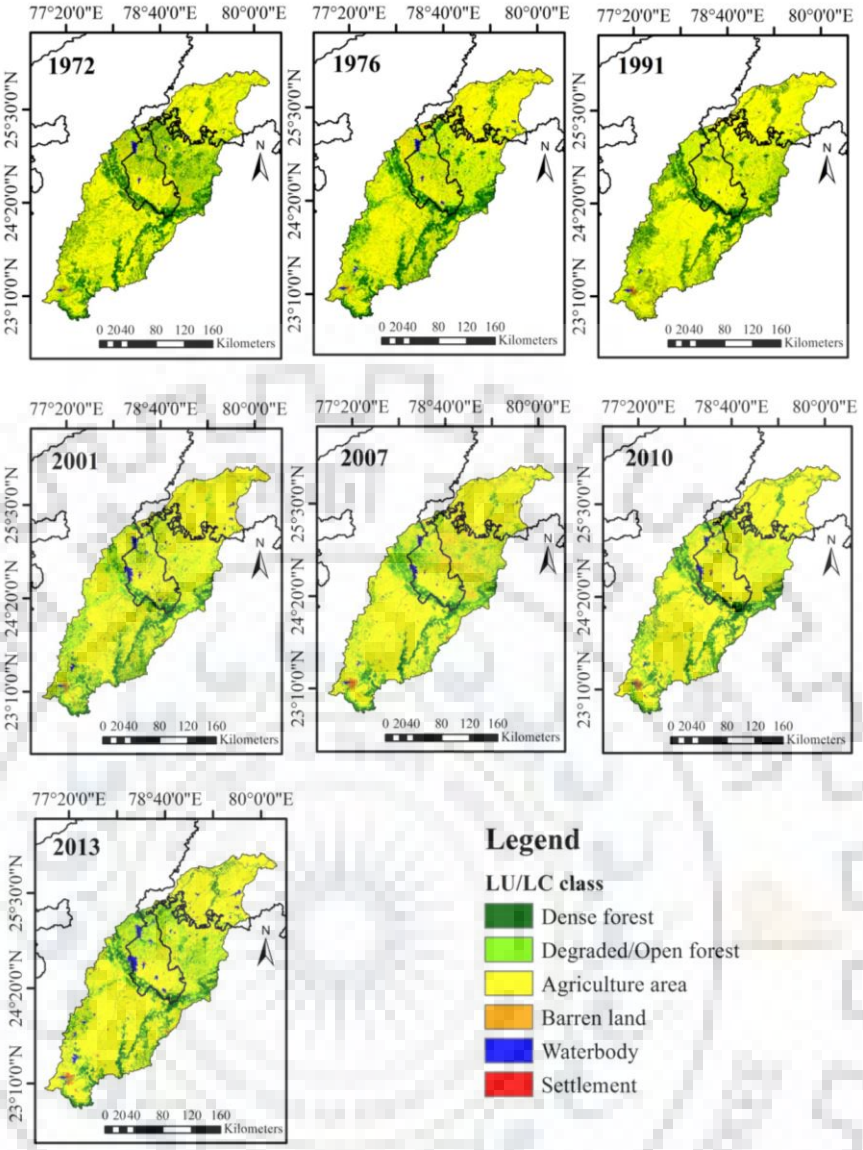

Figure 4.3: Satellite-derived LU/LC maps for the historical years 1972, 1976, 1991, 2001, 2007, 2010 and 2013

Furthermore, results of historical LU/LC change analysis have been discriminated into two geographical areas as shown in Figures 4.3 and 4.4. For Madhya Pradesh, decrease in dense forest and barren land by 7.67 % and 1.17 %, respectively have been found during 1972 to 2013. However, degraded forest, agriculture, waterbody and settlement were increased by 4.1%, 3.37 %, 0.85% and 0.16% respectively. Similarly, decrease in dense forest (1.41%) and barren land (0.54%), and increase in degraded forest (0.73%), agriculture area (0.43%), waterbody (0.77%) and settlement (0.03%) were also occurred in the Uttar Pradesh covered within the BRB area (Figure 4.4).

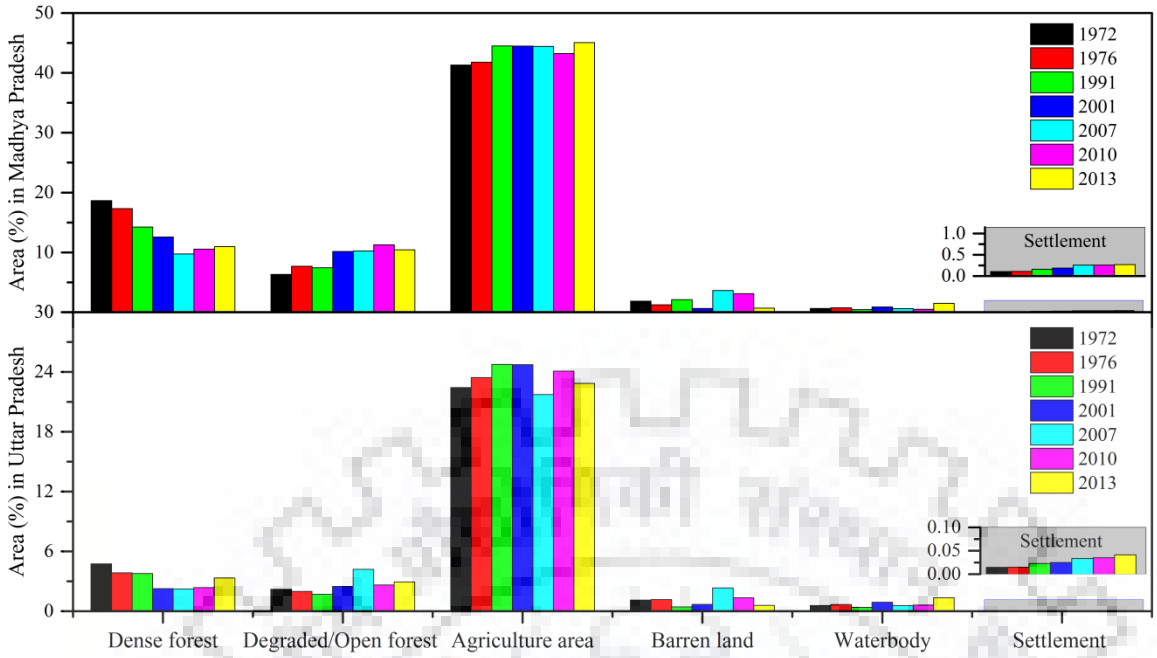

Figure 4.4: Area (%) wise distribution of historical LU/LC in Madhya Pradesh and Uttar Pradesh

From the year 2007, increase in the agriculture area by 0.62% and 1.13% was observed for Madhya Pradesh and Uttar Pradesh, respectively (Figure 4.4). Also, waterbody area was increased by 0.90% and 0.77% for the both trans-boundary States during 2007 to 2013 (Figure 4.4). Enhanced surface waterbody availability from 2007 has ensued to increase total agriculture area by 1.75% in the BRB.

4.3.2 Future LU/LC modelling

In this study, integrated CA-MC model and satellite-derived LU/LC maps have been employed to predict spatial distribution of future LU/LC for the BRB. On the basis of recent changes, the model can create simulations; therefore recent LU/LC maps of the years 2001, 2007, 2010 and 2013 are used for model validation and future prediction.

4.3.2.1 Validation of CA-MC model

In this analysis, simulated LU/LC maps have been compared with the satellite-derived maps which are attributed as reference map representing actual ground condition of the study area. The automated map comparison method was utilized to estimate the Kappa Index of Agreement (KIA) in terms of some unbiased summary statistics such as Kno values 0.850 and 0.867, Klocation values 0.788 and 0.812, KlocationStrata values 0.788 and 0.812 and Kstandard values 0.768 and 0.793 for the simulation years 2010 and 2013, respectively. The validation analysis reveals satisfactory Kappa indices, and verified CA-MC model simulation process which can be executed for future periods (Landis and Koch, 1977).

Moreover, as suggested (Kamusoko et al., 2009; Guan et al., 2011), area under simulated and satellite-derived LU/LC were compared by visual inspection analysis prior to check the model simulation results (Table 4.4). This method is simple and easy to interpret the comparison of LU/LC classes. Figure 4.5 depicts that the degraded forest, agriculture, waterbody and settlement in the simulated LU/LC map are comparatively similar to the corresponding classes in the satellite-derived LU/LC maps for the years 2010, while the dense forest and barren land classes are simulated poorly. However, Figure 4.5 shows that dense forest, degraded forest, agriculture area and settlement classes in the simulated LU/LC map are relatively close to corresponding classes in satellite-derived LU/LC map, while the waterbody and barren land classes are poorly simulated for the year 2013. This analysis also shows strong agreement between simulated and satellite-derived maps. Thus, CA-MC model has been found suitable for future prediction of satellite-derived LU/LC map of the BRB.

Table 4.4: Area (%) under satellite-derived and simulated LU/LC for 2010 and 2013

LU/LC class	2010		2013	
	Satellite-derived	Simulated	Satellite-derived	Simulated
Dense forest	12.91	11.27	14.31	13.28
Degraded/open forest	13.91	14.52	13.37	13.66
Agriculture area	67.33	65.58	67.91	67.53
Barren land	4.45	7.40	1.27	4.24
Waterbody	1.11	0.96	2.84	1.03
Settlement	0.30	0.26	0.31	0.25
Total area (%)	100.00	100.00	100.00	100.00

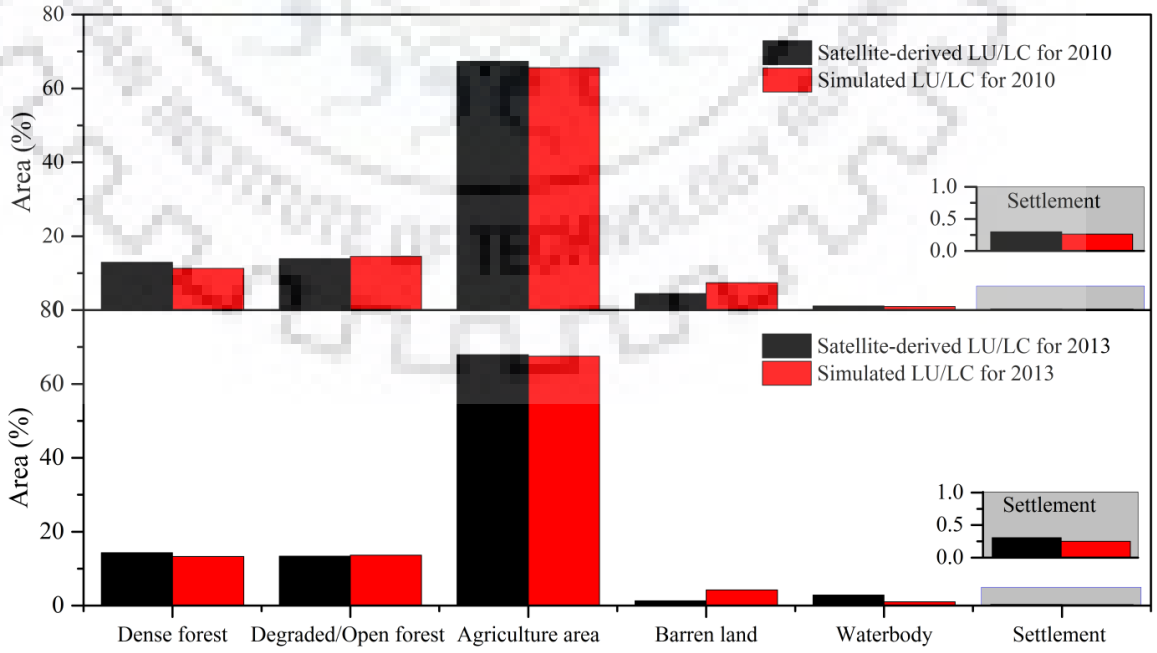

Figure 4.5: Comparison of satellite-derived and simulated LU/LC for the years 2010 and 2013

4.3.2.2 Future LU/LC prediction

After successful validation, the CA-MC model was further employed to simulate future LU/LC pattern. In this study, satellite-derived LU/LC maps of last decade (2001 and 2010) were used to simulate the LU/LC for the years 2020, 2040, 2060, 2080 and 2100. Tables 4.5a&b show percent area and changes of future LU/LC classes for the years 2020 to 2100. It shows that future agriculture and waterbody would have significant changes, compared to other LU/LC classes (Table 4.5b) Future analysis shows that, increase in the area of degraded forest from 14.82% to 18.82%, barren land from 5.80% to 10.03% and settlement from 0.36% to 0.64% could takes place in the BRB. However, decrease in dense forest from 12.16% to 10.77%, agriculture from 66.15% to 59.64% and waterbody from 0.72 to 0.01% could also takes place from the years 2020 to 2100 as shown in Figures 4.6 and 4.7.

Table 4.5a: Area (%) under predicted future land use/land cover

LU/LC class	Area (%) under future land use/land cover				
	2020	2040	2060	2080	2100
Dense forest	12.16	11.26	11.01	10.59	10.77
Degraded/Open forest	14.82	16.26	17.35	18.62	18.82
Agriculture area	66.15	64.12	61.96	60.30	59.74
Barren land	5.80	7.65	9.14	9.86	10.03
Waterbody	0.72	0.25	0.06	0.01	0.01
Settlement	0.36	0.47	0.49	0.62	0.64
Total area (%)	100.00	100.00	100.00	100.00	100.00

Table 4.5b: Percent change between future time-periods

	Area (%) under future land use/land cover			
LU/LC class	**2020-2040**	**2040-2080**	**2060-2080**	**2080-20100**
Dense forest	-0.90	-0.25	-0.42	0.18
Degraded/Open forest	1.44	1.09	1.27	0.20
Agriculture area	-2.03	-2.16	-1.66	-0.56
Barren land	1.85	1.49	0.72	0.17
Waterbody	-0.47	-0.19	-0.05	0.00
Settlement	0.11	0.02	0.13	0.02

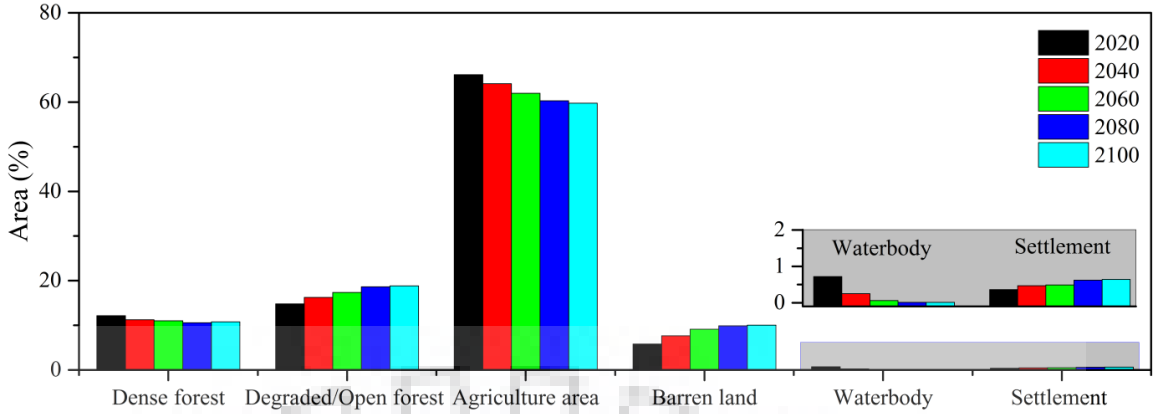

Figure 4.6: Graphical representation of future land use/land cover

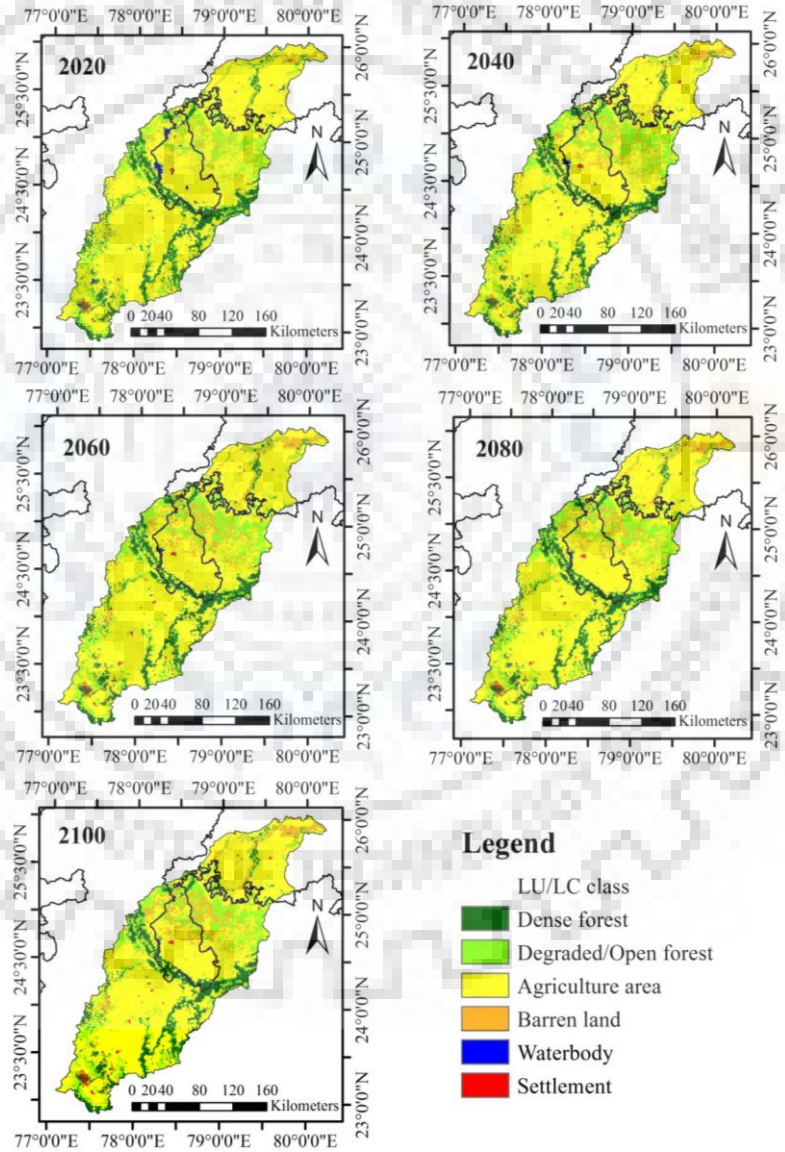

Figure 4.7: Future LU/LC maps for the years 2020, 2040, 2060, 2080 and 2100

In this analysis, future LU/LC pattern has been also discriminated for two geographical contexts covered within the BRB area (Figures 4.7 and 4.8). Analysis show that dense forest, agriculture area and waterbody could decrease by 1.13%, 3.36% and 0.28% for Madhya

Pradesh, and 0.26%, 3.05% and 0.43% for Uttar Pradesh. However, increase in degraded forest, barren land and settlement area by 2.97%, 1.72% and 0.08% for Madhya Pradesh, and 1.02%, 2.51% and 0.20% for Uttar Pradesh could take place during the years 2020 to 2100 (Figures 4.7 and 4.8). Result depicts that, future LU/LC may also change similarly in both the States covered within the study area. This simulation demonstrated that total decrease in waterbody (0.71%) could decline agriculture area by 6.41%, hence may affect food production in the future scenario. Therefore, sustainable development of water resources is necessitated to maintain agriculture productivity in the BRB. This would be possible when both states can jointly work for trans-boundary management and development of land resources at basin level.

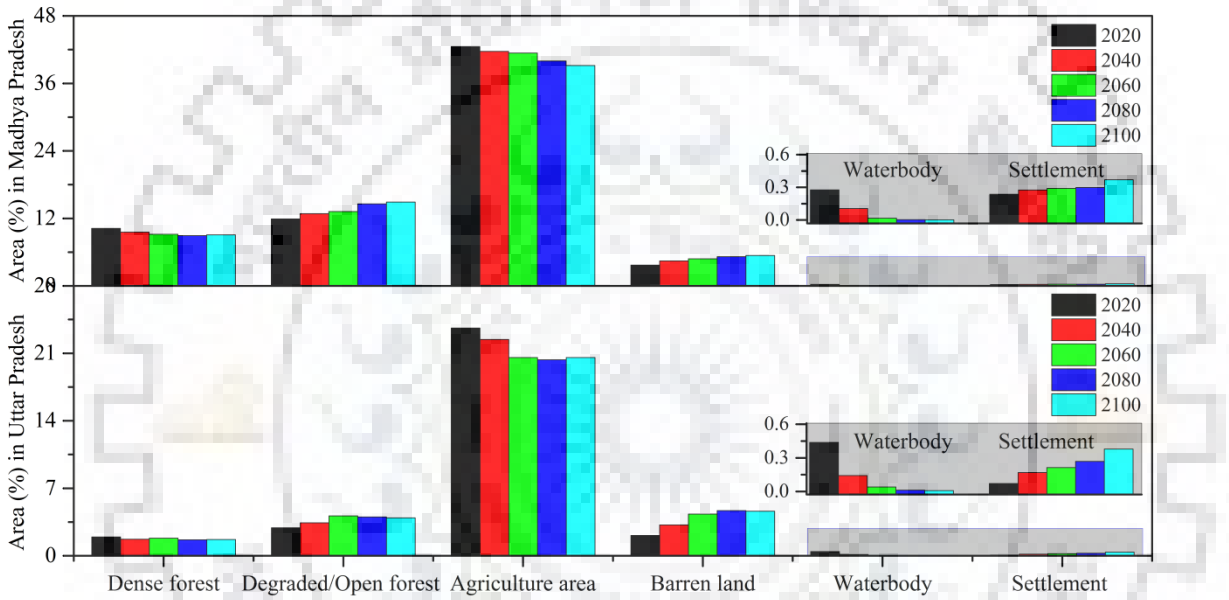

Figure 4.8: Area (%) wise distribution of future LU/LC in Madhya Pradesh and Uttar Pradesh

4.4 DISCUSSION

In the present study, different spatiotemporal resolution of satellite data has been used, and therefore, it may cause uncertainty and errors in the LU/LC modelling. These errors were somewhat removed by rescaling satellite-derived LU/LC maps into same spatial resolution, and then utilized for future simulation. The historical LU/LC analysis showed increase in agriculture area by 4.16% due to increased irrigation water availability from waterbody area (1.62%). However, decrease in dense forest area (9.08%) cease to increase in degraded forest area by 4.83%. This change in forest area was occurred due to increased anthropogenic activities, such as deforestation. Therefore, vegetation cover in BRB has been reduced during the years 1972 to 2013. Further, analysis showed that similar variations in the LU/LC classes for the two geographical areas. Thus, understanding of these historical changes may be helpful for integrated planning and management of natural resources, and policy interventions in a trans-boundary region. [better u check land use statics of MP/UP for population scenario]

Spatiotemporal analysis shows that, agriculture area was altered with respect to changes in waterbody area. In the BRB, surface waterbody is the main source of irrigation which depends on monsoon rainfall, and therefore changes in monsoonal rainfall could have significant impact on irrigation water availability, thus on agriculture production (Singh et al., 2014). For initial years (1972 and 1976), analysis showed less agriculture area due to drought effect (Pandey et al., 2008). However, surface water availability from reservoir, lake and pond is mainly responsible for positive changes in the agriculture area. After 2007, accrued in agriculture area (1.75%) has been observed due to increase in irrigation water availability mainly from Rajghat reservoir (Chaube et al., 2011). This reservoir is newly accomplished in the middle part of BRB, and was put in operation from 2006. It has a large water storage capacity (Trivedi et al., 2006) which facilitated more irrigation water supply to the agriculture area. Moreover, this inter-state project provides irrigation to both Madhya Pradesh (1210 km^2) and Uttar Pradesh (1380 km^2) States. Rajghat reservoir is used not only for irrigation but also for drinking purpose. Therefore, it serves great significance to supply not only irrigation water but also drinking water in the trans-boundary region of the BRB. Hence, the trans-boundary projects are helpful in rural development and to improve socio-economic status of the peoples. Therefore, this study demonstrated that sustainable agriculture productivity can be further continued with integrated planning, management and development of water resources (Singh et al., 2014) in trans-boundary river basin.

For future LU/LC prediction, the CA-MC model has been previously implemented, and accomplished by Arsanjani et al. (2011 and 2013), and their results were satisfactorily validated. Thus, this model helps to interactively predict different LU/LC scenarios by furnishing some solutions to the land resource problems such as food security (Santé et al., 2010). From future analysis, it has been observed that small amount of increase in dense forest could facilitate to maintain vegetation cover in the BRB, but this increase is negligible. Moreover, future agriculture area could reduce and exert pressure on food supply. Therefore, surface water resources such as reservoirs, lakes and ponds need to be developed for irrigation water availability. For Madhya Pradesh and Uttar Pradesh, present study reveals that dense forest and degraded forest area may also alter in the future decades. Decline in dense forest (1.39%) and agriculture area (6.41%) could significantly affect vegetation cover. This depicts that conservation measures are essential to preserve the vegetative area of the BRB.

The results of future LU/LC pattern are significantly related to environmental and socioeconomic implications for sustainable planning and management in two geographical contexts of the BRB. Both Madhya Pradesh and Uttar Pradesh could face same problem of

increasing pressure on food productivity area due to decline in agriculture while increase in barren land and settlement area. For instance, the continuing decline in agriculture area on one hand and increase in barren land and settlement areas on the other hand imply severe decrease in cultivable area, which could potentially threaten rural livelihoods of the BRB area. Therefore, this study discovered these future hot-spots, which would be useful to prioritize the BRB area and to implement the immediate policy interventions for sustainable development of land resources. This study will be devoted to evaluate planning and management scenarios for present land resources.

The focal objective of spatiotemporal LU/LC modeling is to understand possible land resources problems in a trans-boundary river basin. The simulated maps can serve as an early-warning information to the land resource planners, managers and policy makers. Therefore, integrated CA-MC modeling approach is capable to interactively predict future paths as well as allocating quantity of change in the most probable LU/LC area such as agriculture and waterbody.

4.5 CONCLUSIONS

The present study significantly identified trans-boundary issues and problems of land for the Betwa river basin. This study represents an important contribution to spatiotemporal LU/LC modelling by an integrated CA-MC model for a trans-boundary region. The model applied in this study has been successfully incorporated satellite-derived LU/LC maps through GIS-based MCE and MOLA methods. The CA-MC model was validated twice using automated map comparison method and visual inspection analysis. In this study, Kappa statistics shows strong agreement between satellite-derived and simulated LU/LC maps. Followings are some general conclusions of the present study:

1. Two States, namely Madhya Pradesh and Uttar Pradesh, have undergone similar historical LU/LC changes, and could have parallel changing pattern in the future years.
2. From the year 2007, newly accomplished Rajghat reservoir has played an important role to provide sufficient water for irrigation and drinking purpose. Therefore, this study revealed that inter-state water resource projects are necessitated for a trans-boundary development.
3. Future problems such as food security and surface water resources availability are successfully discovered by employing CA-MC model.
4. The model validation revealed that degraded forest, agriculture and settlement are relatively well simulated and the barren land class was poorly simulated due to less

classification accuracy. The model's validation provides confidence in the future LU/LC modelling employing satellite-derived LU/LC maps.

5. Future LU/LC simulation up to 2100 indicated that if, current trends continue without development policies for the trans-boundary region then severe land degradation in agriculture and waterbody area threatens rural livelihood.
6. Different spatiotemporal satellite images have been used and rescaled for LU/LC modelling. Thus, as part of future research it is suggested to use high spatial resolution and same temporal resolution satellite data in the forthcoming studies.

The approach used in this study will also encourage research community to predict future LU/LC for food security problems of trans-boundary basins. Moreover, further comparative studies are required to clarify whether the predicted LU/LC patterns are particular and empirically replicated in trans-boundary area. Thus, the present study demonstrated CA-MC modelling approach that interactively offered an enhanced understanding of future LU/LC trends which is essential to discover natural resource problems of river basin area.

CHAPTER 5

RELATIONSHIP BETWEEN HYDRO-CLIMATIC VARIABLES AND LAND COVER DYNAMICS UNDER DRY AND WET SPELLS

In this chapter, the MODIS NDVI and land cover time-series datasets have been used for assessing the hydro-climatic greening and degradation response under the effect of dry and wet spells over the Betwa River Basin (BRB), Central India. A conceptual framework representing climatic greening, climatic degradation, non-climatic greening and non-climatic degradation has been employed to provide the results on monthly, seasonal and annual time-scale for the years 2001 to 2013. Further, effect of the dry and wet spells have been significantly studied using the MODIS time-series datasets for sustainable planning and management of land resources over the Betwa River Basin.

5.1 BACKGROUND OF THE STUDY

Land degradation is related to changes in the vegetation cover due to the key role of plants in the Earth system to control the hydrological, erosional and biological cycles (Bodí et al., 2011; Cassinari et al., 2015; Keesstra et al., 2017; Muñoz-Rojas et al., 2016). Therefore, it is necessary to carry out scientific studies to assess the changes in land cover to determine the impacts of human cause in the Earth system (Abbasi et al., 2015; Beyene, 2015; Caúla et al., 2016). Regional variation in vegetation and land cover dynamics shows climate change impact on ecosystems with time and space (Jacob et al., 2015). Thus, changing vegetation response as a consequence of climate is relevant to understand the Earth Surface processes, such as changes in discharge, forest fires or biota (Keesstra et al., 2007; Pereira et al., 2016; Russell & Ward, 2016). Vegetation is an important component of the land cover, and has a response to climate variables (Kiunsi & Meadows, 2006; Chen et al., 2014). Vegetation determines the infiltration capacity of soils, runoff generation, soil erosion, and fauna and flora recovery after disturbances as fires, grazing, tillage, or agriculture land abandonment (Cerdà and Doerr, 2005; Zucca et al., 2016; Keesstra et al., 2017). Changes in land cover and vegetation succession have a significant impact on soil quality (van Hall et al., 2016), mainly on organic carbon and nitrogen capacities for re-vegetation (Yu & Jia, 2014). Therefore, it has become imperative to explore land components to analyze land greening and degradation response with different climatic and hydrologic variables using remotely sensed time series data sets (Funk & Brown, 2006; Tadesse et al., 2010; Symeonakis et al., 2014).

It is also important to assess the linkage between land surface and hydro-climatic variables to achieve the sustainability (Pilgrim et al., 1988). Dry and wet spells are relevant for the

sustainability of agriculture (Kessler & Stroosnijder, 2006; Lobell et al., 2011) and water resources (Singh & Ranade, 2010; Ouedraogo et al., 2015). Improvement in the regional environment is possible only when national policy would be used to combat land degradation issues (Akhtar-Schuster et al., 2011). Land degradation would not only be controlled by addressing climate and bio-diversity but also requires financial support to tackle the issues of poverty and food security (Gisladottir & Stocking, 2005).

In previous studies, the Normalized Difference Vegetation Index (NDVI) has been widely used as an effective indicator to perceive the information of vegetation response at a global and regional scale (Tucker, 1979; Li et al., 2013; Jiang et al., 2013; Gong et al., 2015; Aly et al., 2016; Van Eck et al., 2016). Nowadays, many NDVI data sets are available from remote sensors using spectral reflectance of near infrared (NIR) and red (RED) bands (Zhou et al., 2001; Piao et al., 2011; Wang et al., 2011; Chen et al., 2014). The Moderate Resolution Imaging Spectro-radiometer (MODIS) has an improved sensors NDVI and land cover data for vegetation monitoring. The MODIS NDVI spectral band includes an improvement in atmospheric, geometric and radiometric corrections (Huete et al., 2002). Therefore, it is used as an improvement over the previous NDVI data sets. The MODIS NDVI data without smoothing shows incorrect interpretation of result, therefore, quality assessment and noise removal has been carried out to smooth NDVI data for land greening and degradation response analysis. In a recent study, Zhang et al. (2017) detected sensor degradation for the MODIS Collection 5 (C5) data when compare to the newly released MODIS Collection 6 (C6) MOD13C2 NDVI data. But, the MOD13C2 NDVI data has very coarse spatial resolution (about 5600 m), and can be effective for global scale studies. For the regional scale study, high spatial resolution (about 250 m) MOD13Q1 NDVI data is required for precise vegetation change monitoring. Moreover, the global land cover products MCD12Q1 and MCD12Q2 have been improved from MODIS (Friedl et al., 2002; Hansen et al., 2002). The supervised classification method was employed to generate MODIS land cover products (Friedl et al., 2010). Also, more accurate land cover information can be obtained from this data for a large river basin area.

Dry and wet spells (Varikoden & Preethi, 2013) can influence vegetation growth and food production (Milesi et al., 2010), and thus the Indian economy (Webster et al., 1998). Hence, early-warning system is prerequisite to improve the sustainable management and development plans for current land dynamics. Further, river basins are most sensitive natural systems to the changes in land cover and hydrology (Mutiibwa et al., 2014). Indian River basins are the most sensitive environmental natural systems to the short and long-term changes in hydro-climate variables. Due to this, land characteristics of the Indian river basin can be gradually affected.

For large river basins, field-based investigations on land greening and/or degradation change are time-consuming and challenging, however its rate and extent of change can be significantly assessed using various remotely sensed data sets (Omuto et al., 2014; Belay et al., 2015; Mahyou et al., 2016). The literature suggests that both climatic and hydrologic (i.e. hydro-climatic) variables have been rarely used to investigate the response of land cover for the Indian River Basin in general and Betwa River Basin (BRB) in particular.

Looking to the aforementioned, this chapter was planned with the specific objective to study the hydro-climatic greening and degradation responses under dry and wet spells employing MODIS NDVI and land cover data sets over the BRB area of Central India.

5.2 MATERIALS AND METHODS

The detailed description of the study area and the satellite data pertaining to this study are briefly given in Chapter-3. The detailed methodology flowchart adopted in the present study is provided in Figure 5.1.

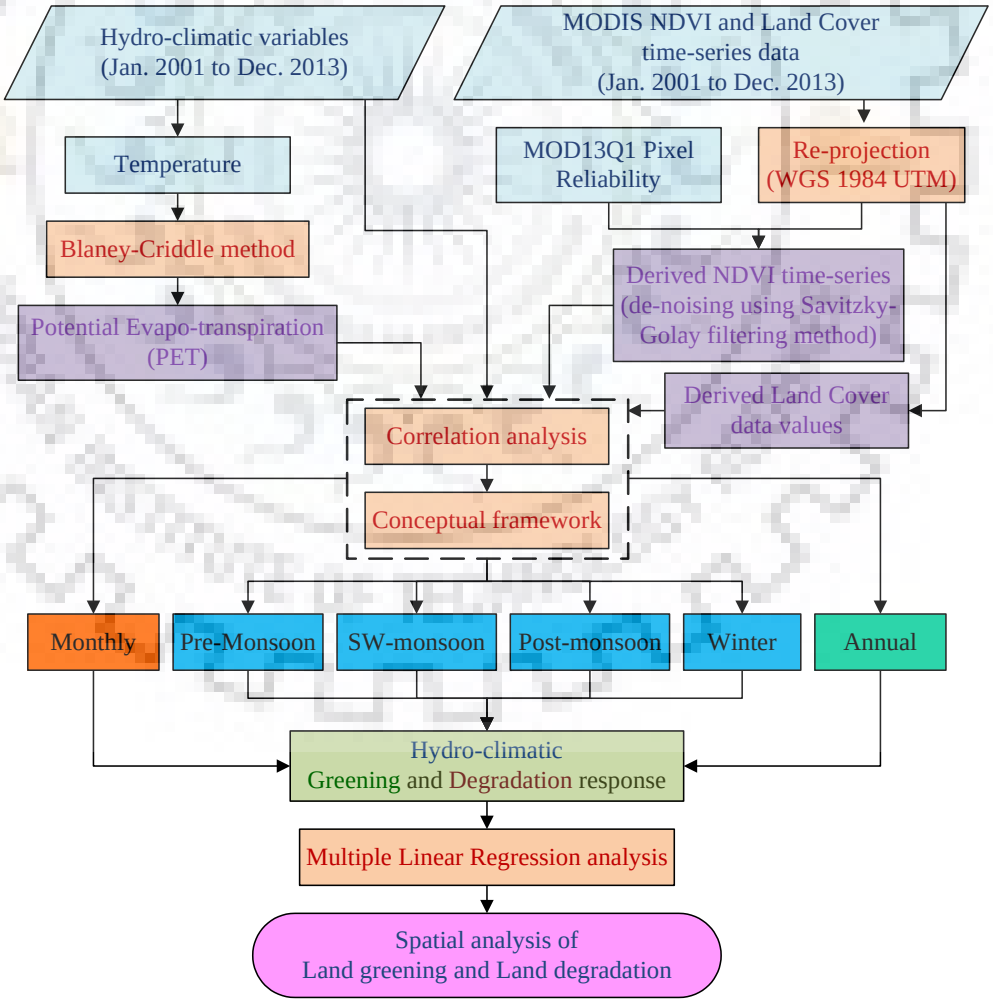

Figure 5.1: Methodology used in the present study

5.2.1 Inverse Distance Weighted (IDW) interpolation method

Inverse distance weighted (IDW) interpolation method uses the data of close stations which is more alike than those apart from each other. Thus, this method assumes that the measured data has local influence, and can diminish with an increase in the distance. It gives more weights to the stations closest to the prediction station, and weights diminish with increase in station distance, hence the name inverse distance weighted. Thus, in this study the missing values of climatic data were estimated by employing IDW interpolation method using the following equation:

$$P_i = \frac{\sum_n (P_n / D_n^{\,2})}{\sum_n (1.0 / D_n^{\,2})} \qquad \ldots(5.1)$$

where, P_i is the interpolated value at a rain-gauge station, P_n is the measured value of the n^{th} nearest neighbor, and D_n is the distance to the n^{th} nearest neighbor. When D = 0.0 for a particular P_n, then P_i is assigned the value of P_n, making IDW an exact interpolator.

In this study, pre-monsoon (March to May), SW-monsoon (June to September), post-monsoon (October and November) and winter (December to February) seasons (Kumar & Hingane, 1988) are considered to categorize hydro-climatic variables and MODIS data sets for the present study. In addition to this, monthly and annual analyses were also carried out. During a normal year, non-clear sky days were discovered in the July and August (SW-monsoon) and December (Winter Season).

5.2.2 Blaney-Criddle method

The potential evapo-transpiration (PET) is generally calculated by using the Penman–Monteith method which requires several meteorological parameters like mean temperature, wind speed, relative humidity and solar radiation etc. Due to unavailability of these meteorological parameters, this study uses the Blaney-Criddle method (Blaney and Criddle 1962), which requires only mean temperature parameter, for estimation of the PET employing the following equation:

$$PET = K \times p \times (0.46 \times T_{mean} + 8.13) \qquad \ldots(5.2)$$

where, PET is the daily potential evapotranspiration (mm/day); K is the monthly consumptive use coefficient which depends upon the vegetation type, location and season (Vangelis et al., 2013); p is the mean daily percentage of maximum possible annual day light hours; and T_{mean} is the calculated mean temperature (°C), based on the daily maximum and minimum temperature using the equation:

$$T_{mean} = \frac{(T_{max} + T_{min})}{2} \quad \ldots(5.3)$$

Using hydro-climatic variables, few variables have been developed for relationship analysis, i.e. P/PET (aridity index) and Tdiff (i.e. Tmax-Tmin). Depending on the temporal scale of satellite data, these hydro-climatic variables were calculated on monthly, seasonal and annual basis to study dry and wet spell effects over the BRB area.

5.2.3 Dry and wet spells

In this study, dry and wet spell effects are mainly focused on land greening and degradation response analysis. The 13 years of time-series data were categorized into dry and wet years employing standardized anomalies of the annual rainfall time-series (Figure 5.2). Negative and positive anomaly values were categorized as dry and wet years respectively. Thus, the total analysis period was categorized into nine dry years (2001, 2002, 2005, 2006, 2007, 2008, 2009, 2010 and 2012) and four wet years (2003, 2004, 2011 and 2013). It is inferred that annual rainfall is skewed towards dry years. However, based on standard deviations the 2007 and 2013 were found to be an extreme dry and wet years respectively.

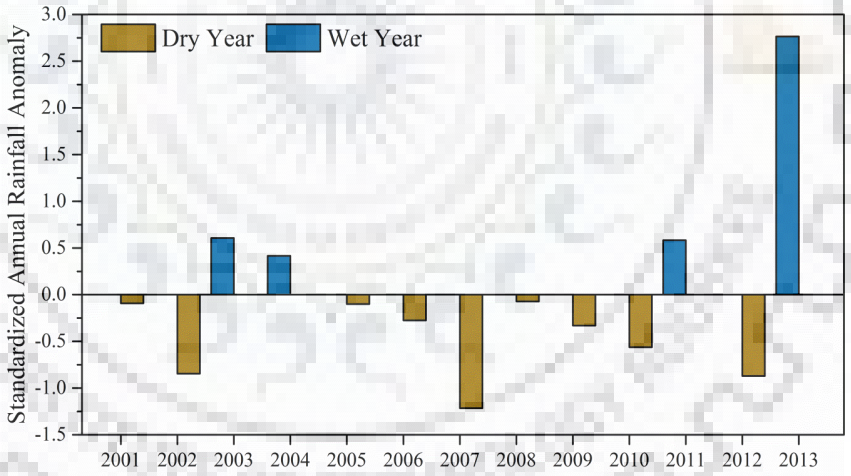

Figure 5.2: Standardized annual rainfall anomalies over the years 2001 to 2013

5.2.4 MODIS data products

In this study, remotely sensed time-series data sets of MODIS NDVI (collection 5) Terra (MOD13Q1) and MODIS Land Cover Type (MCD12Q1) products have been used to assess the relationship with hydro-climatic variables. These data sets were retrieved from the online Reverb tool (http://reverb.echo.nasa.gov/reverb/), courtesy of the NASA EOSDIS Land Processes Distributed Active Archive Center (LP DAAC). The present study area is covered within one MODIS tile of h25v06.

5.2.4.1 MODIS NDVI data

The MOD13Q1 Terra NDVI data is available from February-2000 to present on 16-days temporal resolution and 250 m spatial resolution. In this study, NDVI data sets were retrieved from January 2001 to December, 2013. Based on maximum number of days during start and end time of Terra spacecraft, one satellite imagery was selected for each month, and then the monthly NDVI values were obtained for relationship analysis. The MODIS NDVI composite products are developed by selecting the higher quality pixels of atmospherically corrected bi-directional surface reflectance (Huete et al., 2002). All NDVI tiles were re-projected from Sinusoidal to a standard World Geodetic System (WGS) 1984 Universal Transverse Mercator (UTM) coordinate system (Zone 44N) using batch processing utility of MODIS Reprojection Tool (MRT). Then, NDVI values were extracted for the study area within ArcGIS environment. The NDVI time-series for the BRB were calculated as mean value for 6×6 pixel (1.5 km ×1.5 km) area centered on each of the 18 IMD stations to avoid the land heterogeneity effect (Karlsen et al., 2008; Gong et al., 2015).

The NDVI data quality was also assessed using corresponding quality assessment (QA) information that describes the utility of NDVI values. Invalid data were eliminated and interpolated linearly. The Savitzky-Golay filtering method was employed to de-noise and to smooth the NDVI time-series data (Chen et al., 2004) as shown in Figure 5.3. This method uses local polynomial regression to determine the smoothed data values at each data point. Therefore, it performed best to de-noise the temporal NDVI data (Geng et al., 2014). The reliability band of MOD13Q1 data composite has been used to weight each data point in the NDVI time-series. For this, good data (value 0) had full weight (1), marginal data (values 1-2) had half weight (0.5), and cloudy data (value 3) had minimum weight (0.1). The function-fitting was carried out using TIMESAT software (Jönsson & Eklundh, 2004). For instance, the resultant smoothed NDVI value (Y^*) from the original NDVI value (Y) and the coefficient for the i^{th} NDVI is computed using the following formula:

$$Y_j^* = \frac{\sum_{i=-m}^{i=m} C_i Y_{j+i}}{N} \qquad \ldots(5.4)$$

where, j is running index of the ordinate data in the original data table, m is the half width of the smoothing window, and N represents the number of convoluting integers which is equal to the smoothing window size $2m+1$ (Savitzky and Golay, 1964).

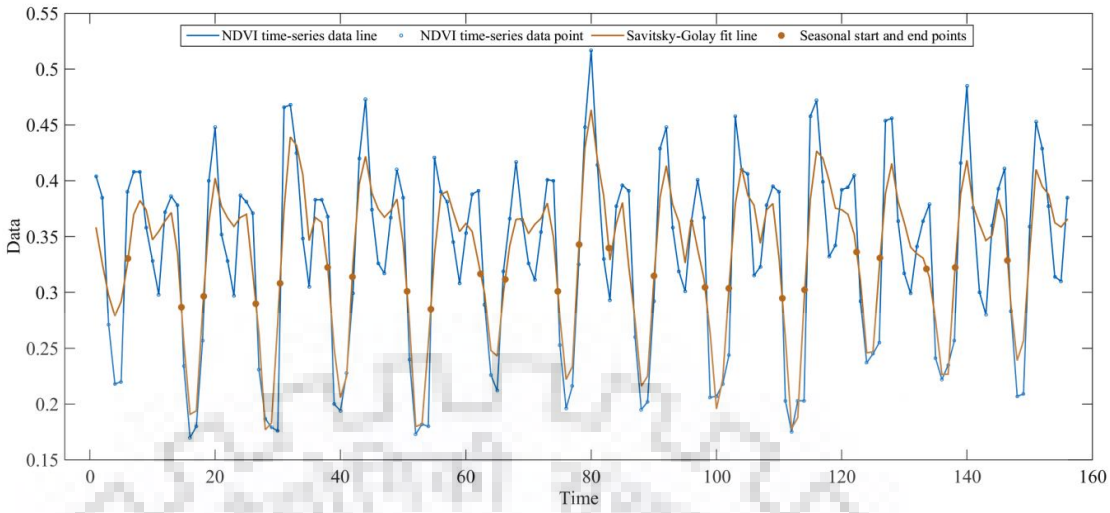

Figure 5.3: Smoothed NDVI time-series of the years 2001-2013 illustrating original MODIS NDVI values and de-noised temporally interpolated NDVI values

Further, phenological parameters were extracted for the Crop Land (CL) area of BRB (Table 5.1). Highest peak of the NDVI has been found for the 7th season, and maximum length of the season was found to be 8.71 months for the 4th season. The smoothed NDVI time-series data were then used to analyze land greening and degradation response and to develop linear regression models.

Table 5.1: Phenological parameters for the crop land area of the BRB during 2001-2013

Season	Start (in Month)	End (in Month)	Length (in Month)	Base value (NDVI)	Peak time (in Month)	Peak value (Maximum NDVI)	Amplitude (NDVI)
1	6.12	14.61	8.49	0.23	10.29	0.38	0.15
2	18.16	26.51	8.35	0.18	22.10	0.40	0.22
3	30.34	37.96	7.62	0.19	32.70	0.44	0.25
4	41.88	50.60	8.71	0.19	46.00	0.42	0.23
5	54.39	62.37	7.98	0.21	57.69	0.39	0.18
6	66.28	74.68	8.39	0.23	70.73	0.38	0.15
7	78.07	82.81	4.74	0.22	80.00	0.46	0.24
8	90.06	98.16	8.10	0.21	92.20	0.41	0.21
9	102.00	110.50	8.50	0.19	106.10	0.41	0.23
10	114.10	122.40	8.26	0.21	116.70	0.43	0.21
11	126.10	133.60	7.42	0.24	128.00	0.42	0.18
12	138.10	146.50	8.36	0.23	142.00	0.42	0.19

5.2.4.2 MODIS land cover data

The MCD12Q1 land cover data products are available on yearly time scale at a spatial resolution of 500 m. The MCD12Q1 (Friedl et al., 2002) product describes land cover

properties derived from input observation of MODIS NDVI data. The International Geosphere Biosphere Program (IGBP) defined MCD12Q1 land cover data into mainly 17 classes. Among these, 11 classes are of natural vegetation, 3 classes are of developed and mosaicked land, and 3 classes are non-vegetated land (Friedl et al., 2010). Among these classes, increase in the CL (81.32% to 87.54%) was the major contributor to the total area of the BRB. In the BRB, snow and ice (S&I) land cover is not available. Further, evergreen needle leaf forest (ENF), evergreen broadleaf forest (EBF) and deciduous needle leaf forest (DNF) were infrequently grown in the study area. Thus, these classes were excluded from the relationship analysis.

5.2.5 Multiple Linear Regression (MLR) analysis

In the present study, the MLR method was employed to establish the relationship of MODIS NDVI and land cover data to hydro-climatic variables. The MLR equation is expressed as:

$$y = c + (m_1 \times x_1) + (m_2 \times x_2) + ... + (m_n \times x_n) \quad \ldots(5.5)$$

where, y is the NDVI or land cover class; c is the intercept; and m_1, m_2 ..... m_n are the coefficients of the variables x_1, x_2 ..... x_n.

To understand the relative importance of each variable in MLR analysis, the standardized coefficient (β, beta coefficient) was estimated to measure the change in standard deviations of the dependent variables (NDVI and land cover) per changes in standard deviation of the predictor (hydro-climatic) variables. This coefficient standardizes all variables to have a variance equal to 1. It is very helpful to know the effect of independent variables on the dependent variables in a MLR analysis.

5.2.6 Conceptual framework

A conceptual framework proposed by Hoscilo et al. (2014) has been used to attribute the relationship among the hydro-climatic variables and MODIS (NDVI and land cover) data sets. The framework was attributed by four concepts of climatic greening, climatic degradation, non-climatic greening and non-climatic degradation for spatiotemporal relationship analysis between annual NDVI and rainfall (Figure 5.4). For instance, the relationship between rainfall and vegetation is attributed as: i) Climatic greening: area where green vegetation cover increases under increased rainfall over a time and space; ii) Climatic degradation: area having reduced green vegetation cover under decreased rainfall; iii) Non-climatic greening: area shows increase in green vegetation cover under low rainfall, which suggests that greening was caused by water availability from pond, lake, river or reservoir, i.e. hydrologic greening response; iv)

Non-climatic degradation: area shows a decrease in green vegetation cover despite the occurrence of more rainfall, and it may be caused due to anthropogenic activity or fire.

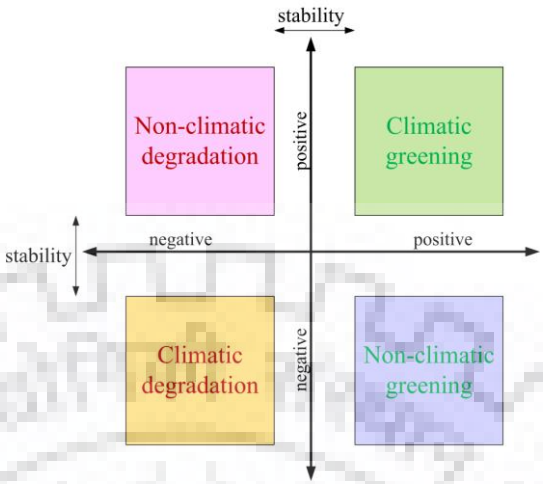

Figure 5.4: Interpretation of conceptual framework for relationship analysis (*Hoscilo et al., 2014*)

5.3 RESULTS AND DISCUSSION

5.3.1 Pattern analysis

Initially, the time-series pattern of hydro-climatic parameters and MODIS NDVI of the years 2001 to 2013 was analyzed on monthly, seasonal (winter, pre-monsoon, SW-monsoon and post-monsoon) and annual basis to understand their trend over the BRB (Figures 5.5a to 5.5d). Due to annual data scale, the MODIS land cover data was analyzed on annual basis only.

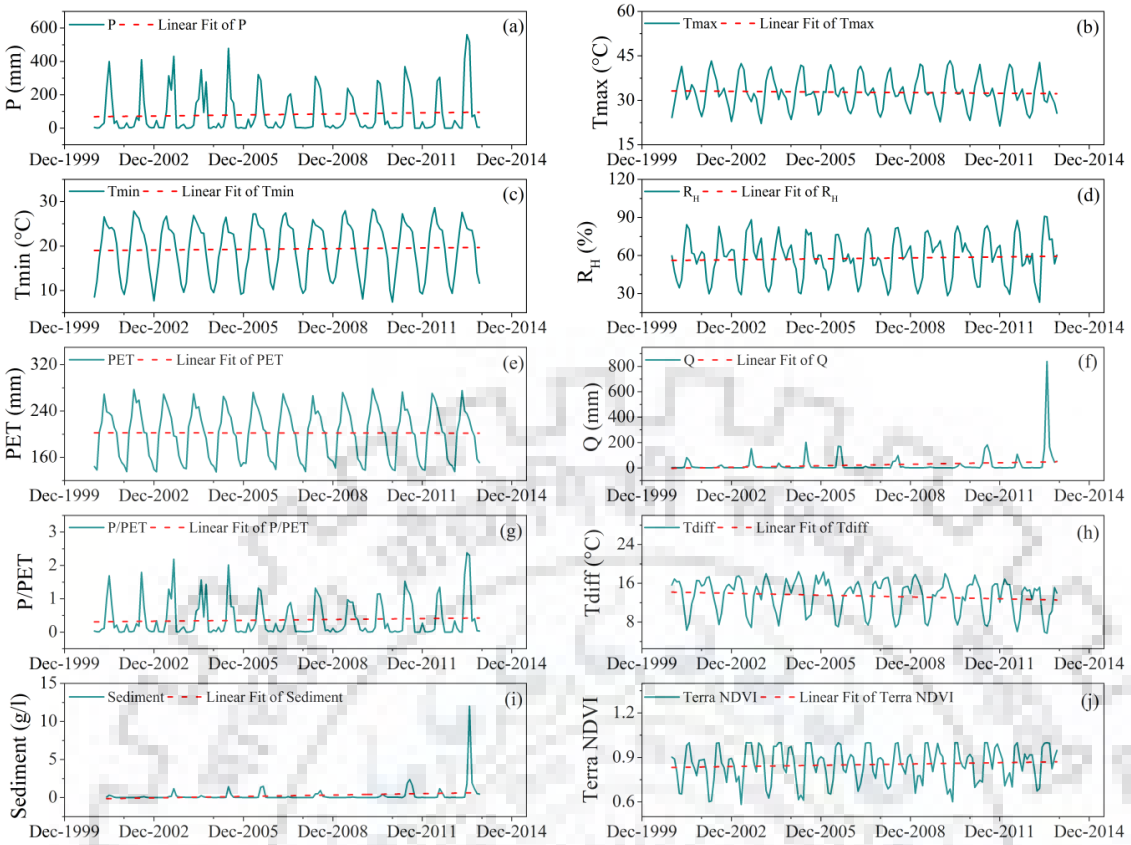

Figure 5.5a: Monthly time series graphs of hydro-climatic variables and MODIS NDVI values

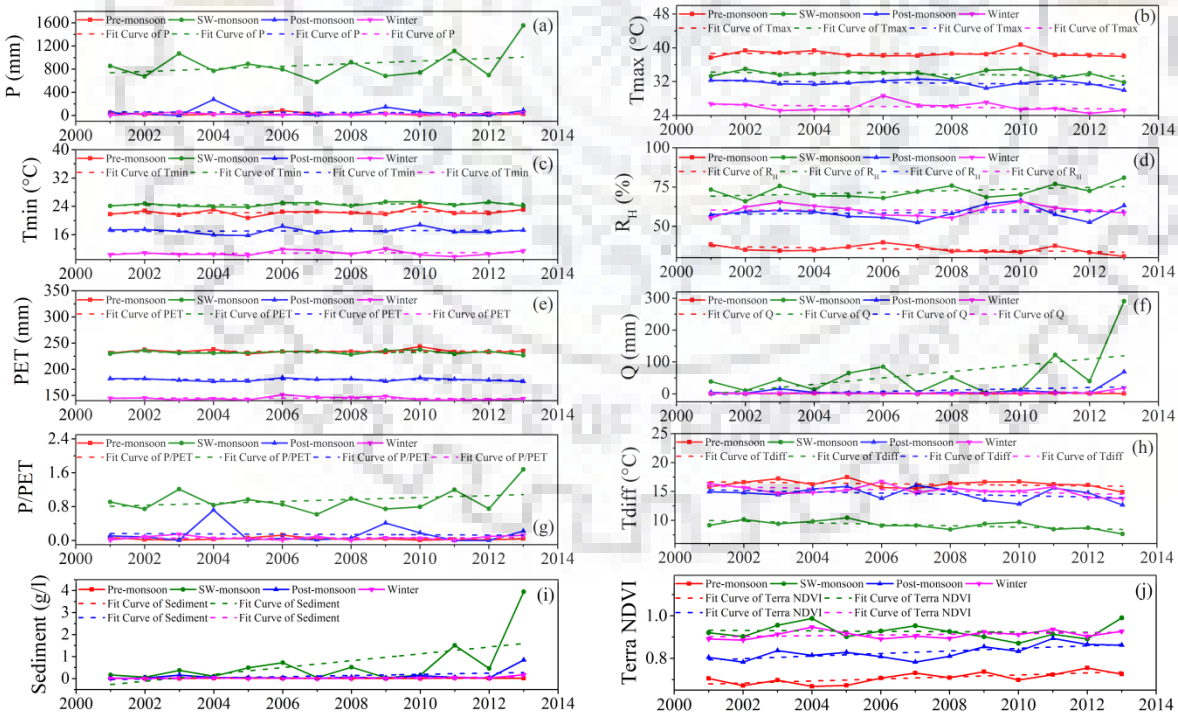

Figure 5.5b: Seasonal time series graphs of hydro-climatic variables and MODIS NDVI values

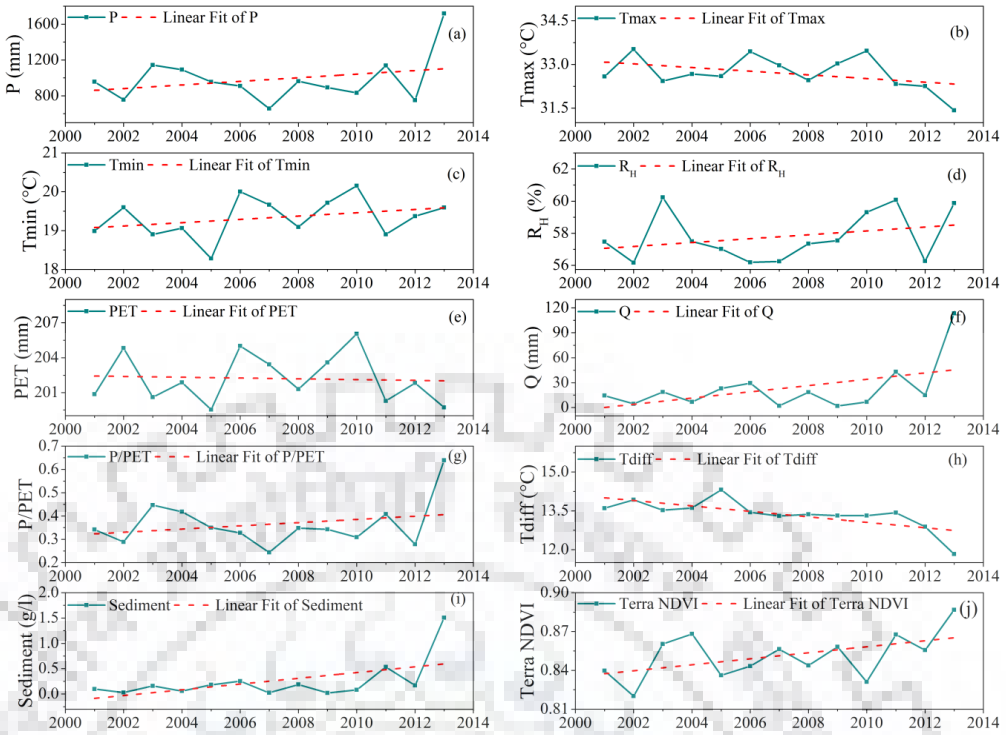

Figure 5.5c: Annual time series graphs of hydro-climatic variables and MODIS NDVI values

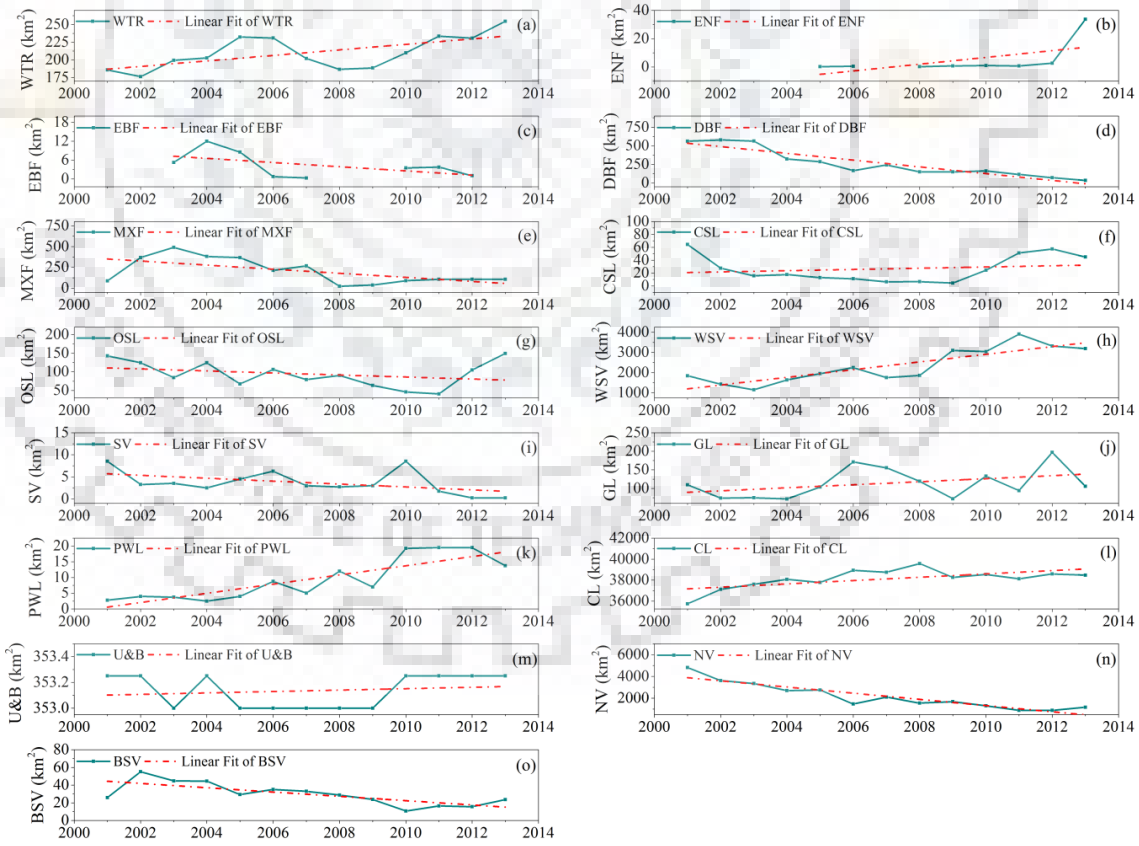

Figure 5.5d: Annual time series graphs of MODIS land cover classes

5.3.1.1 Pattern of hydro-climatic variables

The pattern of Hydro-climatic variables was studied, and is presented in Figures 5.5a, 5.5b and 5.5c. The highest annual rainfall of 1718 mm was recorded for the year 2013 (Figure 5.5c). It is observed that, precipitation has been increased for SW-monsoon, post-monsoon, winter seasons, and on annual basis by 699 mm, 42 mm, 45 mm and 762 mm respectively, over the years 2001-2013. Due to increase in precipitation, discharge was also increased by 252 mm, 64 mm, 17 mm and 99 mm for the SW-monsoon, post monsoon, winter and annual basis, respectively (Figures 5.5b and 5.5c). Similarly, sediment yield was also increased by 3.79 g/l, 0.83 g/l, 0.17 g/l and 1.41 g/l (Figure 5.5b). In the SW-monsoon season, changes in precipitation brought a significant rise in R_H and P/PET by 7.64% and 0.77, respectively (Figure 5.5b). These variations in the hydro-climatic variable can have strong association with changes in the vegetation and the land cover of the BRB area.

In this study, three temperature parameters, i.e. Tmax, Tmin and Tdiff, were used to understand their response with NDVI and land cover. Among these, Tmax and Tmin showed decreasing (1.16°C) and increasing (0.61°C) annual trends, respectively (Figures 5.5b and 5.5c). This opposite pattern has manifested to decrease the trend of temperature difference (Tdiff) over the BRB (Figure 5.5b). This may turn out to be an inadequate seasonal temperature condition for proper plant growth.

Further, the R_H parameter has significant increase in the SW-monsoon season (by 7.64%) and the value of R_H was decreased significantly in the pre-monsoon season (by 7.64%) during the years 2001-2013. The result shows that R_H has a complete reverse pattern for pre-monsoon (decreased by -7.64%) and SW-monsoon season (increased by +7.64%) as shown in Figure 5.5b. This R_H pattern may be induced due to opposite rainfall and temperature pattern in both the seasons. Furthermore, more PET losses were also found in pre-monsoon and SW-monsoon seasons as shown in Figure 5.5b. The slight increasing trend of PET (4 mm) has been observed in the pre-monsoon season due to increase in Tmin (1.30°C). However, due to varying vegetation pattern and temperature condition, the PET losses were decreased by 5.4 mm and 6.8 mm in the post-monsoon (Figure 5.5b) and monthly scale, respectively (Figures 5.5a & 5.5b). Further, the aridity index pattern showed slight decrease (0.03) in pre-monsoon season and increase (0.77) in the SW-monsoon season. Overall, the annual aridity index pattern was found to be increased by 0.30 (Figure 5.5c). As per the aridity index classification given by Kukal and Irmak (2016), the present analysis reveals that the BRB area had experienced semi-arid to dry sub-humid climatic condition over the recent years 2001-2013.

5.3.1.2 Pattern of MODIS NDVI and land cover

The significant positive trend of NDVI time-series were observed for pre-monsoon and winter seasons (Figure 5.5b). The BRB area has many small to large capacity water storage structures i.e. lakes and reservoirs. This might be a reason to show the non-climatic or hydrologic greening response during non-monsoon season. During SW-monsoon season, NDVI has slightly decreasing trend under the increase in SW-monsoon rainfall as shown in Figure 5.5b. This climatic degradation response might be due to wetland condition or flooding condition in the study area.

Further, different MODIS land cover (MCD12Q1) classes showed a significant trend during the years 2001 to 2013 (Figure 5.5d). Among them, significant increase in the areas of WSV (1342.50 km^2) and CL (2731.75 km^2) were observed. However, a large amount of land degradation of about 3652.25 km^2 was found for the NV. Also, slight decrease in the area of OSL (6.25 km^2) and slight increase in the area of CSL (19.50 km^2) were also detected in the present study. These changes in shrub land were took place due to the varying hydro-climatic response in the sub-tropical region. The area under ENF and EBF were changed during 2001 to 2013 (Figure 5.5d). These classes have limited data points, therefore, not considered in the present study. Further, the result shows that the increase in the area of WTR from 0.42% to 0.58% indicates increase in surface water availability in the BRB. In the last decade, a newly constructed interstate project Rajghat reservoir had the major contribution to increase WTR area and to provide water for irrigation, drinking and rehabilitation purpose. Figure 5.5d also shows a greening response to the areas of CSL, WSV, GL, PWL and CL and degradation response for the areas of DBF, OSL, SV, NV and BSV in the BRB.

5.3.2 Relationship analysis

In this study, the relationship of MODIS NDVI and land cover with the hydro-climatic variables has been analyzed at monthly, seasonal and annual time-scale. The climatic and non-climatic greening and degradation responses are also categorized based on the results of relationship analysis employing a conceptual framework. Furthermore, the MLR model development and the spatial change analysis has been carried out in this study.

5.3.2.1 Relationship with MODIS NDVI

From hydro-climatic variables, monthly rainfall exhibited moderate positive correlations with NDVI i.e. a climatic greening response for vegetation in dry, wet and all year analysis (Table 5.2). Moreover, annual rainfall has good correlation with the NDVI in wet year as compare to dry year. Among temperature parameters, monthly Tmax exhibited a moderate negative

correlations with NDVI i.e. a climatic degradation response in dry (r = -0.676), wet (r = -0.649) and all year (r = -0.669) analysis (Table 5.2). Similarly, the difference between maximum and minimum temperature (Tdiff) has moderate negative correlations to the monthly NDVI in dry (r = -0.653), wet (r = -0.642) and all year (r = -0.651) analysis (Table 5.2). This analysis also shows a climatic degradation response to the monthly NDVI. The result shows that, inadequate Tmax and Tdiff may be caused to have a climatic degradation response for monthly vegetative growth in the BRB. From Table 5.2, the Tmax parameter also exhibited significant negative correlation with dry year NDVI in post-monsoon season (r = -0.838) and on annual basis (r = -0.732), and with wet year NDVI in pre-monsoon season (r = -0.983). In wet year, Tmin also exhibited a significant negative correlation (r = -0.776) with NDVI in SW-monsoon season. These results show that increase in the value of Tmax and Tmin could degrade the wet year vegetation cover. The present analysis demonstrated the effect of dry and wet spells to have climatic greening response due to rainfall and a climatic degradation response due to temperature in the BRB.

In addition to this, monthly R_H has a significant positive correlation to the NDVI in dry (r = 0.864), wet (r = 0.854) and all year (r = 0.861) analysis (Table 5.2). Result depicts that, effect of dry and wet spells had not altered the positive response between R_H and vegetation cover. The PET parameter has few moderate negative correlations to the NDVI. Annual NDVI (r = -0.668) in dry year analysis, pre-monsoon NDVI (r = -0.704) in wet year analysis and SW-monsoon NDVI (-0.621) in all year analysis showed degradation response to the vegetation cover. During wet years, a positive moderate response (r = 0.653) was also exhibited during post-monsoon season. Thus, PET parameter has been undergone different responses to the vegetation under dry and wet spells effect.

According to the rainfall pattern analysis, the runoff (Q) and the sediment parameters also showed similar responses in the wet years (Table 5.2). On monthly basis, the vegetation cover showed a moderate positive response to both Q and sediment in dry, wet and all year analyses. However, a small negative correlation in pre-monsoon season had not changed under dry and wet spells. The result reveals that, small increase in the vegetation cover could decreases runoff and sediment losses, i.e. a negative response. It is also observed that, both Q and sediment have similar response to the vegetation under dry and wet spells (Table 5.2).

Table 5.2: Correlation between hydro-climatic parameters and MODIS NDVI for dry, wet and all (dry+wet) years

Spells	Analysis	P	Tmax	Tmin	RH	PET	Q	P/PET	Tdiff	Sediment
Dry	Monthly	0.544	-0.676	-0.232	**0.864**	-0.316	0.388	0.561	-0.653	0.382
	Pre-monsoon	-0.090	-0.330	0.023	-0.256	-0.167	-0.120	-0.120	-0.529	-0.192
	SW-monsoon	-0.063	-0.493	-0.237	0.282	-0.441	0.158	-0.087	-0.387	0.077
	Post-monsoon	0.368	-0.838	-0.096	0.244	-0.529	0.173	0.383	-0.424	0.252
	Winter	0.263	-0.333	0.081	0.507	-0.245	-0.123	0.225	-0.547	0.434
	Annual	0.259	-0.732	-0.633	0.332	-0.668	0.228	0.221	0.033	0.288
Wet	Monthly	0.459	-0.649	-0.208	**0.854**	-0.317	0.304	0.464	-0.642	0.277
	Pre-monsoon	0.130	-0.983	-0.188	-0.118	-0.704	-0.285	0.283	-0.454	-0.078
	SW-monsoon	0.115	-0.082	-0.776	-0.134	-0.285	0.186	0.117	0.066	0.214
	Post-monsoon	-0.712	0.262	0.557	-0.220	**0.653**	0.161	-0.712	-0.044	0.180
	Winter	-0.802	**0.651**	-0.173	-0.278	0.443	-0.112	-0.806	0.316	-0.079
	Annual	0.411	-0.264	**0.658**	-0.720	0.281	0.300	0.407	-0.424	0.336
Combined Dry+Wet	Monthly	0.510	-0.669	-0.226	**0.861**	-0.317	0.294	0.520	-0.651	0.243
	Pre-monsoon	-0.024	-0.446	-0.041	-0.173	-0.259	-0.206	-0.034	-0.464	-0.177
	SW-monsoon	0.490	-0.585	-0.511	0.447	-0.621	0.450	0.498	-0.350	0.459
	Post-monsoon	-0.023	-0.494	-0.096	0.240	-0.388	0.334	-0.012	-0.278	0.344
	Winter	0.125	-0.458	-0.165	0.469	-0.383	0.371	0.116	-0.448	0.455
	Annual	-0.054	-0.203	-0.144	-0.332	-0.150	0.017	-0.082	-0.078	0.028

During wet years, the aridity index, i.e. P/PET, parameter has significant correlation to the NDVI in post-monsoon (r = -0.712) and winter seasons (r = -0.806) as shown in Table 5.2. It means, the vegetation greening may be responded to deflect the aridity due to wet spell effect. The combined dry and wet spells showed none significant relationship between aridity index and vegetation cover of the BRB (Table 5.2).

In the present study, the most satisfactory correlation results are obtained on the monthly analyses. This study demonstrated that NDVI has a more significant relationship in wet years as compared to dry year analysis (Table 5.2). However, the combined dry and wet spells effect showed a moderate response between hydro-climatic variables and vegetation (Table 5.2). But, the R_H parameter is an exceptional parameter possesses significant positive correlations to the monthly NDVI in all year analysis. Under dry spell effect, three temperature parameters were negatively correlated to the NDVI, and hence strongly affected the vegetation cover. However, due to wet spell, the effect of temperature on vegetation cover was found to be moderate positive response in the BRB.

5.3.2.2 Relationship with MODIS land cover

In this study, annual MODIS land cover (MCD12Q1) time-series data set has been also correlated with hydro-climatic variables as shown in Table 5.3. The low annual rainfall in dry years showed none significant response to the vegetation. But in wet years, more annual rainfall showed many significant correlations with all MODIS land cover classes. Due to wet spell, the rainfall resulted to increase surface water availability, i.e. WTR area (r = 0.823). Thus, it induces a climatic greening response to OSL, GL and CL with correlation (r) value of 0.648, 0.812 and 0.730, respectively (Table 5.3). Further, the climatic degradation response was observed for the DBF, MXF and SV with correlation (r) value of -0.623, -0.569 and -0.842 respectively. The combined effect of dry and wet spells resulted a moderate rainfall response only with WTR (0.525) area as shown in Table 5.3. The result demonstrated that, the prolonged dry spell might suppress the effect of wet year rainfall on the land cover area.

In dry year analysis, the Tmax and Tmin parameters have none significant effect on land cover area (Table 5.3). Nevertheless, the difference between maximum and minimum temperature (Tdiff) showed several moderate relationships with DBF (0.602), MXF (0.704), WSV (-0.634), GL (-0.602), PWL (-0.677) and NV (0.606). But, in the wet years, the Tmax significantly affected the WTR and GL area with correlation values of r = -0.885 and -0.894, respectively. However, the SV area (r = 0.849) responded positively by the Tmax parameter as shown in Table 5.3. The Tmin parameter also showed few significant correlations with OSL, SV and CL under correlation (r) value of 0.815, -0.838 and 0.801 respectively. The result shows that, crop growth is very sensitive to the changes in the Tmin under the wet spell effect. Moreover, the developed temperature parameter Tdiff showed a significant positive correlation with SV (r = 0.870), i.e. climatic greening response. The Tdiff parameter also showed climatic degradation response to WTR, GL and CL under correlation (r) value of -0.852, -0.837 and -0.762, respectively. The result shows that the rise in temperature difference may induce climatic degradation response to the crop land. Hence, it could affect agriculture production in the BRB. From Table 5.3, the combined effect of dry and wet spells shows only moderate responses in the present study.

Among other hydro-climatic parameters, R_H has a moderate response to the MODIS land cover in dry and wet year analysis (Table 5.3). However, in all year analysis, R_H has none good response to land cover. During a wet spell, the PET parameter exhibited significant negative response with the areas of WTR (r = -0.790) and GL (r = -0.867). From Table 5.3, the PET and the aridity index have some moderate correlations with the land cover in the wet year analysis.

Table 5.3: Correlation between hydro-climatic parameters and MODIS land cover for dry, wet and all (dry+wet) years

Spells	LC class	P	Tmax	Tmin	RH	PET	Q	P/PET	Tdiff	Sediment
Dry	WTR	0.008	-0.163	-0.096	-0.144	-0.126	**0.609**	-0.046	-0.055	**0.656**
	DBF	0.040	0.201	-0.264	-0.148	-0.097	-0.172	0.027	**0.602**	-0.373
	MXF	-0.316	0.315	-0.242	-0.518	-0.005	0.085	-0.317	**0.704**	-0.056
	CSL	-0.037	-0.365	-0.168	-0.002	-0.241	0.038	-0.096	-0.190	0.030
	OSL	0.046	-0.159	-0.181	-0.538	-0.207	0.220	-0.031	0.068	0.124
	WSV	-0.054	-0.111	0.362	0.391	0.210	-0.109	0.013	-0.634	0.056
	SV	0.420	0.416	0.155	0.595	0.230	0.167	0.362	0.267	0.043
	GL	-0.340	-0.243	0.229	-0.262	0.053	0.379	-0.455	-0.602	0.515
	PWL	-0.171	-0.106	0.397	0.382	0.285	0.033	-0.171	-0.677	0.268
	CL	-0.156	0.007	0.330	-0.025	0.240	0.148	-0.153	-0.454	0.339
	U&B	-0.249	0.065	0.160	0.225	0.198	-0.267	-0.252	-0.147	-0.241
	NV	0.208	0.009	-0.426	-0.086	-0.307	-0.088	0.179	**0.606**	-0.306
	BSV	-0.157	0.384	-0.067	-0.635	0.113	-0.024	-0.140	0.539	-0.161
Wet	WTR	**0.823**	-0.885	**0.733**	0.406	-0.790	**0.939**	**0.736**	-0.852	**0.945**
	DBF	-0.623	**0.659**	-0.624	-0.076	0.496	-0.753	-0.514	**0.665**	-0.774
	MXF	-0.569	**0.652**	-0.501	-0.286	**0.627**	-0.748	-0.447	**0.612**	-0.761
	CSL	0.480	-0.602	0.352	0.464	-0.711	**0.696**	0.354	-0.523	**0.701**
	OSL	**0.648**	-0.484	**0.815**	-0.416	0.054	0.432	**0.715**	-0.627	0.446
	WSV	0.386	-0.503	0.285	0.359	-0.604	**0.610**	0.253	-0.433	**0.620**
	SV	-0.842	**0.849**	-0.838	-0.135	**0.600**	-0.907	-0.765	**0.870**	-0.922
	GL	**0.812**	-0.894	**0.682**	0.532	-0.867	**0.940**	**0.726**	-0.837	**0.940**
	PWL	0.349	-0.498	0.187	0.549	-0.709	0.591	0.220	-0.392	0.592
	CL	**0.730**	-0.704	**0.801**	-0.118	-0.374	**0.776**	**0.654**	-0.762	**0.801**
	U&B	0.290	-0.262	0.430	-0.418	0.017	0.374	0.193	-0.335	0.410
	NV	-0.490	0.585	-0.415	-0.297	**0.605**	-0.688	-0.363	0.536	-0.701
	BSV	-0.431	0.564	-0.290	-0.495	**0.711**	-0.658	-0.303	0.474	-0.662
Dry+Wet	WTR	0.525	-0.516	-0.042	0.295	-0.357	**0.728**	0.488	-0.489	**0.707**
	DBF	-0.211	0.300	-0.307	-0.089	0.007	-0.416	-0.173	0.584	-0.450
	MXF	-0.046	0.163	-0.344	-0.053	-0.075	-0.203	0.016	0.478	-0.240
	CSL	0.254	-0.449	-0.141	0.226	-0.343	0.357	0.211	-0.332	0.362
	OSL	0.341	-0.294	0.025	-0.247	-0.173	0.338	0.344	-0.323	0.326
	WSV	0.230	-0.285	0.251	0.327	-0.037	0.405	0.188	-0.518	0.446
	SV	-0.336	0.598	0.181	-0.063	0.426	-0.384	-0.36	0.448	-0.428
	GL	-0.363	0.052	0.358	-0.421	0.244	-0.008	-0.408	-0.271	-0.02
	PWL	0.114	-0.228	0.304	0.341	0.066	0.326	0.073	-0.507	0.363
	CL	-0.004	-0.035	0.352	-0.050	0.200	0.136	-0.009	-0.354	0.161
	U&B	0.223	-0.188	0.103	0.224	-0.009	0.235	0.209	-0.285	0.280
	NV	-0.140	0.190	-0.373	-0.164	-0.111	-0.340	-0.118	0.531	-0.378
	BSV	-0.072	0.273	-0.142	-0.292	0.089	-0.231	-0.017	0.408	-0.256

Moreover, two hydrologic parameters, Q and sediment, exhibited a moderate positive correlation to the WTR area in dry years as shown in Table 5.3. With respect to the rainfall, more Q and sediment losses were produced under the wet spell. In the present study, the Q parameter shows the significant positive response with WTR, GL and CL with a correlation (r) value of 0.939, 0.940 and 0.776, respectively. It means, these land cover classes helps to induce more runoff during wet years. Also, the Q parameter shows the negative response with DBF, MXF and SV areas with correlation (r) values of -0.753, -0.748 and -0.907, respectively (Table 5.3). The result reveals that the DBF, MXF and SV area have significant impact on minimizing surface runoff. Furthermore, the sediment parameter has a positive correlation to the increased areas of WTR, GL and CL with correlation (r) values of 0.945, 0.940 and 0.801, respectively (Table 5.3). Also, sediment was negatively correlated to decrease in the areas of DBF, MXF and SV with correlation (r) values of -0.774, -0.761 and -0.922, respectively. This shows that both Q and sediment parameters were responded similarly to all land cover classes. Among them, the DBF, MXF and SV classes helps to reduce Q and sediment losses during the wet years. On an annual basis, the combined dry and wet spell effect shows only moderate positive response of Q and sediment parameters to WTR area with correlation (r) values of 0.728 and 0.707 respectively (Table 5.3).

This study also reveals the more significant correlations in the wet year analysis as compare to the dry year analysis. It is observed that, the WTR class was the most sensitive land cover class to the hydro-climatic variables in dry, wet and all year analysis. In wet years, other land cover classes also well responded to the hydro-climatic variables due to the effect of wet spells.

5.3.3 Development of MLR models for land greening and degradation

In this study, MLR models were developed between hydro-climatic variables and MODIS (NDVI and land cover) datasets (2001-2008), and then validated for the years 2009 to 2013. Each MLR model was evaluated using coefficient of correlation (r) value and enables to be utilized for better prediction. Tables 5.4a & 5.4b shows satisfactory model performance in the validation.

Table 5.4a: Validation of MLR model for MODIS NDVI

NDVI analysis	Correlation coefficient (r)
Monthly	0.832
Pre-monsoon	0.508
SW-monsoon	0.728
Post-monsoon	0.375
Winter	0.550
Annual	0.828

Table 5.4b: Validation of MLR model for MODIS land cover

Land cover class	Correlation coefficient (r)
WTR	0.752
DBF	0.958
MXF	0.807
CSL	0.517
OSL	0.939
WSV	0.857
SV	0.608
GL	0.645
PWL	0.642
CL	0.705
U&B	0.833
NV	0.656
BSV	0.651

Furthermore, the relative dependency of different hydro-climatic variables was evaluated using standardized coefficient. The analysis shows that the rainfall (β = 0.62) and R_H (β = 0.32) have the most relative dependency to the vegetation area on monthly scale. In this study, seasonal and annual scale analysis showed multi-collinearity in the variables (Table 5.5a & 5.5b). Therefore, their relative dependency for MLR analysis cannot be easily interpreted due to multi-collinearity. The MLR models for the land greening and degradation response with hydro-climatic variables are given in the Appendix B.

Table 5.5a: Standardized coefficients between hydro-climatic variables and NDVI

Variable	Standardized coefficient					
	Monthly	Pre-monsoon	SW-monsoon	Post-monsoon	Winter	Annual
Rainfall	0.62	-23.32	-84.67	0.10	0.00	-9.69
Tmax	0.00	-3.92	-8.38	-15.42	0.00	-1.82
Tmin	-0.44	2.30	-3.21	0.00	1.14	0.00
RH	0.32	-1.47	-1.71	-0.54	0.05	-2.33
PET	-0.08	0.00	0.00	18.40	-1.24	0.00
Discharge	-0.07	1.47	14.72	0.74	0.46	4.85
AI	-0.74	22.72	75.52	0.00	-0.90	10.69
Tdiff	-0.74	0.00	0.00	11.84	-0.50	-1.36
Sediment	0.10	-1.12	-8.72	0.19	0.29	-3.97

Table 5.5b: Standardized coefficients between hydro-climatic variables and land cover

Variable	Standardized coefficient												
	WTR	**DBF**	**MXF**	**CSL**	**OSL**	**WSV**	**SV**	**GL**	**PWL**	**CL**	**U&B**	**NV**	**BSV**
Rainfall	-11.90	6.54	-8.94	9.91	10.13	-1.41	5.06	-4.86	3.79	-6.22	8.16	7.17	0.44
Tmax	-1.91	1.44	-0.63	1.23	1.71	-0.74	0.49	-0.93	0.55	-0.90	1.33	1.02	1.25
Tmin	0.00	0.00	0.00	0.00	0.00	0.00	0.00	0.00	0.00	0.00	0.00	0.00	0.00
RH	-2.87	2.30	-0.94	1.68	1.13	-1.65	0.63	-1.31	0.72	-1.43	0.80	1.80	0.79
PET	0.00	0.00	0.00	0.00	0.00	0.00	0.00	0.00	0.00	0.00	0.00	0.00	0.00
Discharge	6.82	-0.89	3.28	0.34	-1.56	2.54	3.57	3.72	-5.11	-1.57	-1.70	0.39	-2.72
AI	12.42	-6.86	9.35	-9.92	-9.29	1.70	-5.20	4.39	-4.30	6.30	-7.29	-7.36	-0.01
Tdiff	-0.85	0.60	-0.11	0.25	0.11	-0.48	-0.30	-0.98	0.28	-0.35	0.40	0.47	0.47
Sediment	-4.77	-0.35	-2.57	-1.75	-0.09	-1.75	-3.71	-2.51	5.33	2.66	-0.03	-1.69	2.09

5.3.4 Spatial interpretation of changes in NDVI and land cover

Figures 5.6a to 5.6c illustrates the spatial land greening and degradation during the years 2001-2013. The maximum land greening has been produced for the CL class (2731.75 km^2). However, maximum land degradation was resulted for the NV class (3652.25 km^2). In BRB, the CL class is a dominant land cover of the BRB area. Some inter-transitions between CL and NV were also took place during the years 2001 to 2013. Hence, the NV-CL legend shows degradation of NV class into greening of CL area. The unchanged CL and NV area has been also shown by CL-CL (greening) and NV-NV (degradation) category in Figures 5.6b & 5.6c. These classes showed more land cover dynamics in the upper-most and the middle part of BRB area.

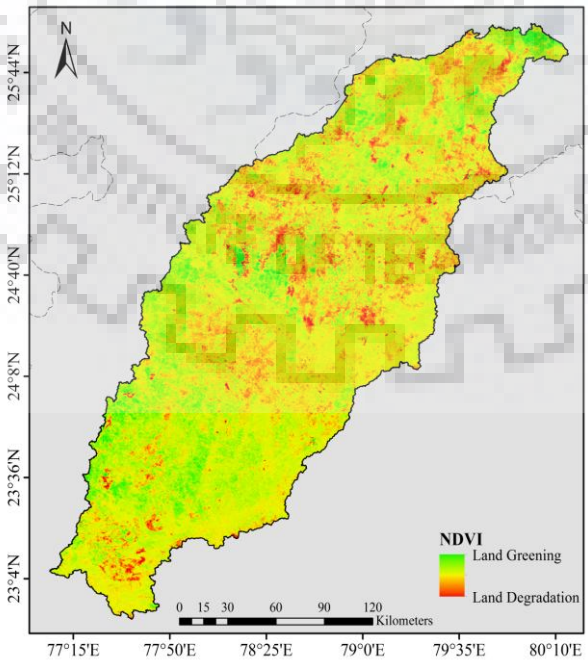

Figure 5.6a: Spatial representation of land greening and degradation using NDVI change analysis during 2001 to 2013

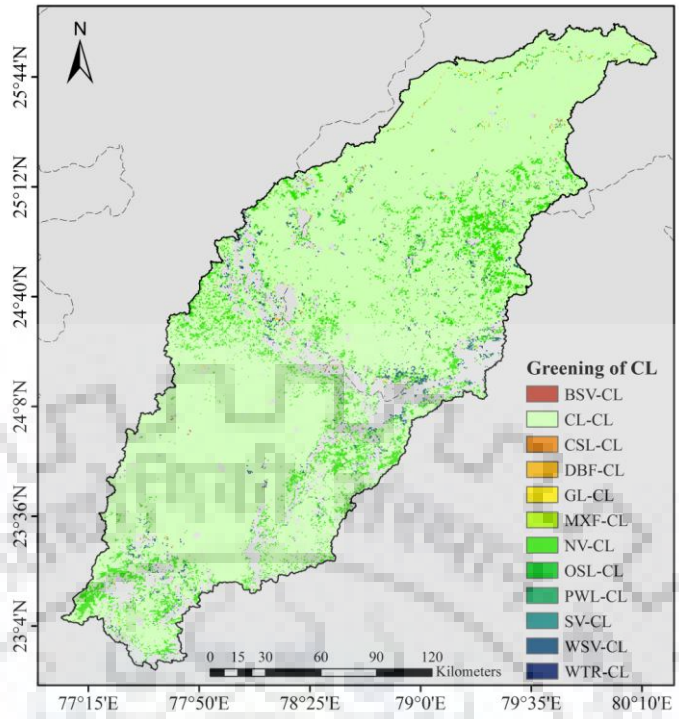

Figure 5.6b: Spatial representation of land greening for Crop Land (CL) during 2001-2013 [*In legend,* Land Cover class− CL: Represents greening of a land cover class into CL, and CL−CL represents no change in CL area]

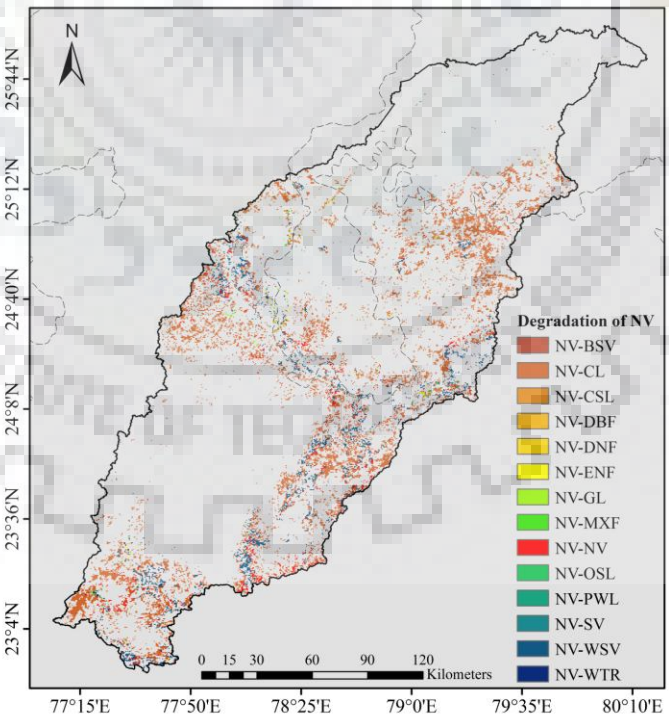

Figure 5.6c: Spatial representation of land degradation for Natural Vegetation (NV) during 2001-2013 [*In legend,* NV−Land Cover class: Represents degradation of NV into a land cover class, and NV-NV represents no change in NV area]

Moreover, four different patterns of the conceptual framework have been spatially represented in Figure 5.7. It helps to address the driving forces behind the climatic and non-climatic effects on land greening and degradation. The greening and degradation areas are variedly distributed from upper to lower part of the BRB. Figure 5.7 shows that most of the upper basin had experienced climatic greening response due to high rainfall; however, the lower basin had experienced non-climatic greening i.e. hydrologic response during the years 2001 to 2013. The non-climatic greening area is distributed on the downstream river network, where most of the large reservoirs, mainly Rajghat and Matatila reservoirs, provide water for rehabilitation and irrigation purpose in monsoon and non-monsoon seasons.

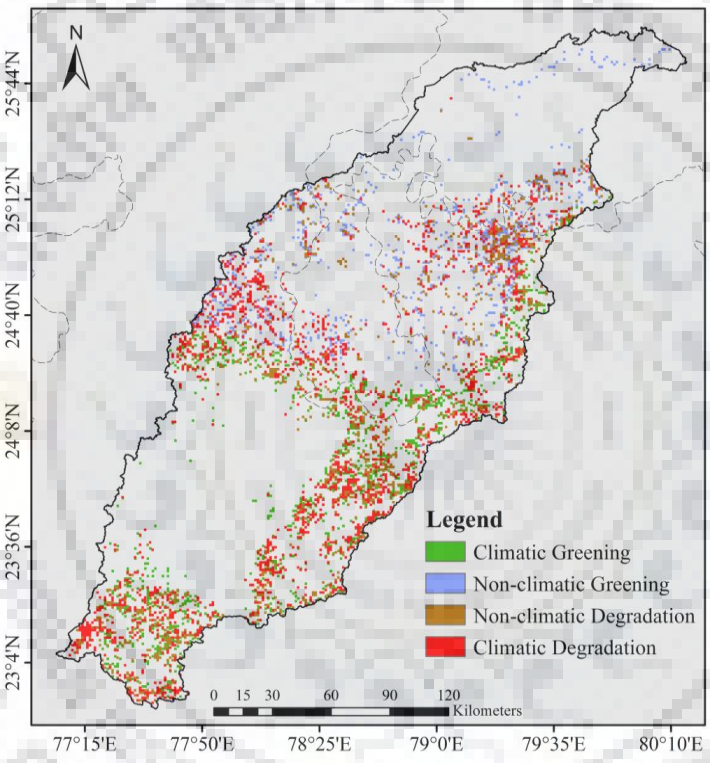

Figure 5.7: Spatial representation of climatic greening, climatic degradation, non-climatic greening and non-climatic degradation in Betwa River basin

The land degradation due to the climatic and non-climatic response has been also illustrated in Figure 5.7. The spatial analysis represents that the upper-most, middle and middle-East, and lower-East basin areas had experienced the land degradation during 2001-2013. The results show that more climatic degradation has been also observed for upper basin area, where maximum rainfall induces flooding during the monsoon season. However, the non-climatic degradation might be caused due to anthropogenic disturbances. In this spatial change analysis, the hydro-climatic impact on land greening and degradation is detected for the upper BRB area. Therefore, sustainable planning and management are required to be implemented for conservation and protection of land resources.

5.3.5 Effects of dry, wet and all year analysis

The effect of dry and wet spells on hydro-climatic greening and degradation response has been also observed in the present study.

5.3.5.1 Dry spell effects

In dry years, vegetation has different responses (i.e. positive or negative) to the monthly hydro-climatic variables (Table 5.2). Mainly, the Tmax and Tdiff parameters have a climatic degradation response to the monthly and seasonal NDVI that declines the vegetation cover under prolonged dry spell effect. However, on annual scale Tmax and Tmin have significantly degraded vegetation cover. The aridity index has a moderate response to the monthly NDVI which shows the inadequate soil moisture condition under dry spells. It might be caused due to deficient and uneven distribution of rainfall in the Madhya Pradesh (Duhan & Pandey, 2013) which is adversely affecting the crop growth (Lal et al., 1999). In BRB, forest growth was limited by low SW-monsoon rainfall (Shah et al., 2007) and less moist climate condition (Chauhan & Quamar, 2010). Overall, study depicted that Tmax and Tdiff are the most affecting climate variables in dry years.

The effect of dry spell also showed degradation and greening response to different land cover areas. The WSV, GL and PWL classes have experienced the land degradation due to the Tdiff. Also, the Tdiff parameter has a climatic greening response for DBF, MXF and NV in dry years (Table 5.3). This might be due to adequate temperature for the growth of these vegetative areas. Thus, the Tdiff parameter is the most responsive parameter in dry years. Two hydrologic parameters, Q and sediment showed a moderate positive response to the WTR class. It demonstrated that changes in the surface discharge can have direct effect on WTR area of the BRB.

5.3.5.2 Wet spell effects

In wet years, monthly correlation analysis between NDVI and few hydro-climatic variables (Tmax, R_H and Tdiff) showed the similar response with the vegetation cover as compare to the dry year analysis (Table 5.2). The increase in the wet year rainfall has resulted a significant climatic degradation response to the vegetation during post-monsoon and winter seasons. This may be due to the degradation of saturated cereal-based agriculture land (Chauhan & Quamar, 2012; Quamar & Chauhan, 2014). Similar results were observed by Chauhan & Quamar (2012) for the South-West forest area of Madhya Pradesh with respect to the increase of rainfall. The vegetative land shows a significant climatic greening response to the monthly R_H ($r = 0.854$), and a climatic degradation response to the annual R_H ($r = -0.720$). This analysis also depicts

that the significant land degradation response of Tmax in the pre-monsoon season was decreased from SW-monsoon to winter season. Hence, the effect of wet spell helps to reduce land degradation and raised climatic-greening response to vegetation of the BRB.

In wet year analysis, nearly all land cover classes showed good correlations to the hydro-climatic variables (Table 5.3). Here, the DBF and MXF showed similar positive response for Tmax, PET and Tdiff parameters; however the negative response to rainfall, Q and sediment (Table 5.3). The prominent CL area has been significantly degraded due to Tmax and Tdiff; as well as positively responded to rainfall, Tmin, Q, aridity index and sediment during wet years (Table 5.3). The result shows that WTR, DBF, MXF, SV, GL and CL were the most influenced land cover areas under wet spell effect.

5.3.5.3 Combined dry and wet spell effects

In this study, the combined dry and wet spells effect has been analyzed for the full analysis period, i.e. dry plus wet years (2001 to 2013). Very few good correlations were observed between hydro-climatic variables and NDVI as shown in Table 5.2. It is clearly observed that vegetation have well responded to the hydro-climatic variables in monthly and SW-monsoon season analysis. It is observed that, monthly and SW-monsoon rainfall showed moderate climatic greening response to vegetation. The vegetation has degradation response with the Tmax and Tdiff parameters. It means, these temperature parameters have unaltered response with the NDVI. In this analysis, good correlation results were estimated in the monthly and SW-monsoon season analysis; however, other scale analysis showed very less response. This analysis demonstrated that the combined effects of dry and wet spells have induced variation in vegetation response over the BRB area.

In all year analysis, MODIS land cover classes have moderate correlations with hydro-climatic variables as shown in Table 5.3. The WTR class shows more and better response with hydro-climatic variables. The degradation response of Tmax and Tdiff to the land cover has been lowered in all year analysis. The result also shows that positive response of Q and sediment were not altered for the WTR area during 2001 to 2013. On annual basis, the ENF, CSL, WSV, GL, PWL and CL land cover had experienced climatic greening response due to increased annual rainfall (762 mm) and WTR area of the BRB. However, the non-climatic degradation response for DBF, CSL, SV, GL, NV and BSV area were mainly caused owing to increased anthropogenic activities within the study area.

Further, the unequal data set values used for dry and wet year analysis is one of the major limitation of the present study. Principally, the occurrence of dry and wet spells never equal in

numbers during the analysis period. Thus, the unequal data points exhibited somewhat differed relationship and response analysis. However, the study on the combined effect of dry and wet spells may be helpful to implement sustainable development plans under hydro-climatic land greening and degradation response in the BRB area and the river basins with similar land use/cover areas.

5.4 CONCLUSIONS

In the present study, effect of dry and wet spells over large BRB area has been successfully analyzed employing the MODIS time-series data sets. The conceptual framework immensely helps to furnish the climatic and non-climatic greening and degradation response over the BRB area. The statistical MLR models have been developed for each multi-temporal analysis of hydro-climatic variables with NDVI and land cover areas. The relative dependency of all the hydro-climatic variables in the MLR model was tested by using the standardized coefficient value. Result showed that rainfall (β = 0.62) and R_H (β = 0.32) are the most relative dependent variables to the vegetation cover. Following conclusions are drawn from this study:

1. In this study, the aridity index analysis shows that the BRB area had experienced semi-arid to dry-sub humid climatic condition during the years 2001 to 2013.
2. In this study, discharge and sediment of the outlet of the Betwa basin has been used. Therefore, correlation between these two variables and NDVI has not been focused particularly on water area or non-water area of the basin. Overall basin response for NDVI change has been studied. However, in non-water area the monsoon rainfall could have significant impact on NDVI variations.
3. The spatial analysis of land greening and degradation showed that the changes are variedly distributed from upper to lower part of the BRB area. Due to high rainfall region, the upper basin area had experienced climatic greening; however, the lower basin had experienced non-climatic greening owing to the less rainfall.
4. In the lower basin, the non-climatic or hydrologic land greening was happened due to water availability from the Rajghat and Matatila reservoirs, for rehabilitation and irrigation purpose.
5. The climatic and non-climatic land degradation were observed for the upper-most, the middle and middle-East, and the lower-East region. The non-climatic land degradation has been encountered due to the anthropogenic disturbances in these regions.
6. In case of the upper BRB part, the climatic land degradation was observed because of the maximum rainfall region which induces flood during the monsoon season. The

prolonged dry spells effect may also accelerates climatic degradation due to the changes in temperature parameters on monthly, seasonal and annual scale.

7. Therefore, the study depicted that the impact of hydro-climatic variables on land cover has been mostly encountered in the upper basin area. Therefore, sustainable management and development plans are crucial to conserve and protect land resources of the BRB.

CHAPTER 6

HYDROLOGICAL MODELLING OF WATER STORAGES USING SOIL AND WATER ASSESSMENT TOOL (SWAT)

This chapter encompasses description of the Soil and Water Assessment Tool (SWAT) model, basin attributes, model setup, sensitivity and uncertainty analysis, calibration, validation, and the model performance evaluation. This chapter also includes the modelling of different water storages (7 reservoirs and 2 weirs) located on main channel as well as tributary channel of the Betwa River Basin. Required spatial information of these water storages has been extracted from remote sensing data, and information on storage volume and outflow have been estimated using gauge data obtained from the authorities. Further, these water storages are successfully implemented and managed for reliable hydrological simulation using the SWAT model.

6.1 BACKGROUND OF THE STUDY

Several types of water storage structures are being constructed for rain water storage, and to fulfill the water requirement for agriculture and urban sectors in present and future scenarios. Different types of water storages, including small-sized ponds to large-sized reservoirs, are used for flow regulation and water utilization (Gross & Moglen, 2007; Lopez-Moreno et al., 2009). These water storages are also the main human interference in a natural system affecting hydrological processes. Hydrological modelling in a region having human interferences can affect the results of a model simulation; therefore, the interference is required for implementation of a reliable hydrological simulation. To account water storage interference, several approaches have been developed to optimize the limited water resources in small-sized river basin (Jayatilaka et al., 2003). For a large river basin, the effect of water storages on hydrological process has not been well addressed due to insufficient data and information of water storages required for hydrological modelling purpose. Thus, the study has been planned to model the numerous water storages by employing the remote sensing data, empirical methods, and estimation of water storage and outflows.

The Soil and Water Assessment Tool (SWAT) can be explicitly used to model the water storages by approximate parameterization of the pond or reservoir modules (Wagner et al., 2011; Zhang et al., 2012b). Payan et al. (2008) proposed an approach to implement the reservoir in a lumped hydrological model using measured volume variations which may not reflect the various reservoir processes in France, the United States and Brazil. Güntner et al. (2004) used a deterministic water balance scheme to represent thousands of reservoirs in a distributed model in Brazil. The scheme includes water storages classification into 6 categories

based on storage capacity of the reservoirs. This scheme also followed one assumption that the small-sized reservoirs located upstream of large-sized reservoirs contribute all flows into the large-sized reservoirs located downstream. Wang & Xia (2010) modelled 61 water storages to assess their impact on streamflow using SWAT2000 in China. Due to lack of sufficient information for numerous water storages, the model was turn out to be less feasible to account their impacts. Moreover, Zhang et al. (2012b) modelled the small- to medium-sized water storages for Fengman reservoir located in the Second Songhua River basin, China using SWAT2005. Their analysis was enhanced by incorporating the water balance and transport network combining both sequential and parallel streams and storage links. Hence, these studies show that basin hydrology can be accurately simulated using available water storages information in the SWAT model. Therefore, in this study an improved version of SWAT2012 has been used for water storages modelling in a large agricultural river basin of central India, which has not been reported yet in the literature.

Indian River basins need to be well developed and managed for the scarce water resources in an integrated and environmentally sound basis. The Betwa River Basin, with number of small- to large-sized water storages, is least discovered region. Various water storages either on the main channel or tributary channel are crucial to manage for sustainable agriculture production in the Central India. In this context, the main water storages regulating river flows in the Betwa River Basin have been studied with certain degree of reliability by a hydrological modelling approach using SWAT.

6.2 MATERIALS AND METHODS

6.2.1 Data acquisition

The details of the study area, hydro-meteorological data, and spatial datasets are provided in Chapter-3. The input information needs to provide in ArcGIS compatible raster datasets (GRIDS), vector datasets (shapefiles), and SWAT database formats. After all data formatting, the model setup was carried out for hydrologic simulation.

6.2.2 Assumptions and limitations

In India, the Central Water Commission (CWC) presently regulates hydrologic measurement in river basins. Change in magnitude and frequency of stream flow could affect target water storages. Also, presently available reservoir could change in future due to ongoing litigation and boundary conditions which may possibly affect SWAT simulation.

In this study, water storages of the Betwa river basin have been modeled using the SWAT model. The curve number approach and Modified Universal Soil Loss Equation (MUSLE) are

particular weaknesses of the SWAT model (Benaman et al., 2005). Thus, the watershed model selection could be a limitation of this study. The elevation levels and soil zones are assumed to be remained constant during analysis period.

The water storages of the Betwa River basin are implemented in the SWAT model for reliable hydrological simulation. Reservoir module of the SWAT model has been used to implement the weirs located on main river channel, considering weir parameter has same functionality as the reservoir parameter. This study assumes that the effect of upstream small water storages, such as ponds and lakes, is minimal at the downstream of reservoir. Also, these small water storages are also not interconnected between the reservoirs considered in this study and the gauges. Hence, outflow of small water storages is contributed into the reservoirs located within a sub-watershed. Therefore, the small water storages having negligible effect on the streamflow are excluded in this study.

6.2.3 SWAT model

The SWAT is a physically based semi-distributed hydrologic model that operates at different time-steps, daily or sub-daily (Arnold et al., 1998; Arnold and Fohrer, 2005; Arnold et al., 2012a). Daily, monthly, and annual model outputs can be obtained at sub-watershed or hydrologic response unit (HRU) level. USDA's Agricultural Research Service (ARS) developed the SWAT model to predict the impact of land management practices on water balance, sediment loads and water contaminant in complex and large watersheds (Borah and Bera, 2003; Arnold and Fohrer, 2005; Neitsch et al., 2005; Miller et al., 2007). The SWAT model underlies the ArcSWAT and QSWAT interface, where GIS software is used to provide geographic analyses for data preparation and model simulation. In this study, the ArcSWAT interface for the modelling purpose has been applied. Bian et al. (1996) described that SWAT model is a semi-empirical and semi-physically based model. For the representation of physical mechanism of hydrologic system, mathematical equations are used in the SWAT model. The model also uses discrete area units for the analysis, hence it is feasible to use the SWAT with the integration of GIS. The detailed documentation about the SWAT model and the related software or interface can be found at SWAT website (http://swat.tamu.edu). Several statistical tools have been also developed and employed for evaluation of the SWAT simulation.

Following major steps are generally used for the model setup and run:

1. Data preparation
2. Watershed delineation
3. HRU definition

4. Sensitivity and uncertainty analysis
5. Model calibration and validation

SWAT model setup includes elevation data (DEM), land use map, soil map, slope information and climatic parameters (rainfall, minimum and maximum temperature, radiation, wind speed, relative humidity). From literature, it is observed that feeble outputs may cause due to insufficient rainfall representation in the model. This might be due to inadequate rain-gauge network or watershed configuration covering spatial details of precipitation (Cao et al., 2006). In addition, an imprecise model simulation (Harmel et al., 2006) and the relatively short periods of calibration and validation (Chanasyk et al., 2003) are some reasons that affect SWAT model performance evaluation. Empirical and semi-empirical models, MUSLE and SCS-CN, adopted in SWAT model simulate less accurate stream-flow and sediment loads (Qiu et al., 2012). Therefore, in this study reasonable monthly stream-flow values and monthly sediment values, majorly peak simulations, were underestimated.

The study area can be divided into several sub-watersheds preserving natural channel and flow paths in the river basin. Each sub-watershed consists of Hydrological Response Units (HRU's) based on land use, soil and elevation data is defined to have a regulated flow in a more or less homogenous way. The final results of all the HRUs are aggregated per sub-watershed and averaged at the basin outlet.

From the relevant review literature, it is observed that SWAT model can be used as a robust and flexible tool for management of land and conservation interventions. Limited studies have been carried out on the model suitability for mixed vegetated and large agricultural Indian River basins in general, and Betwa River basin in particular. River channel having erosion/degradation problem needs adequate protection and conservation measures. Thus, there is a scope for water resources planning and management employing SWAT model in the Betwa river basin, as there are many water resources structure that have controlled and/or uncontrolled influence on river flows.

Detailed methodology used for SWAT model set-up and run is presented in Figure 6.1.

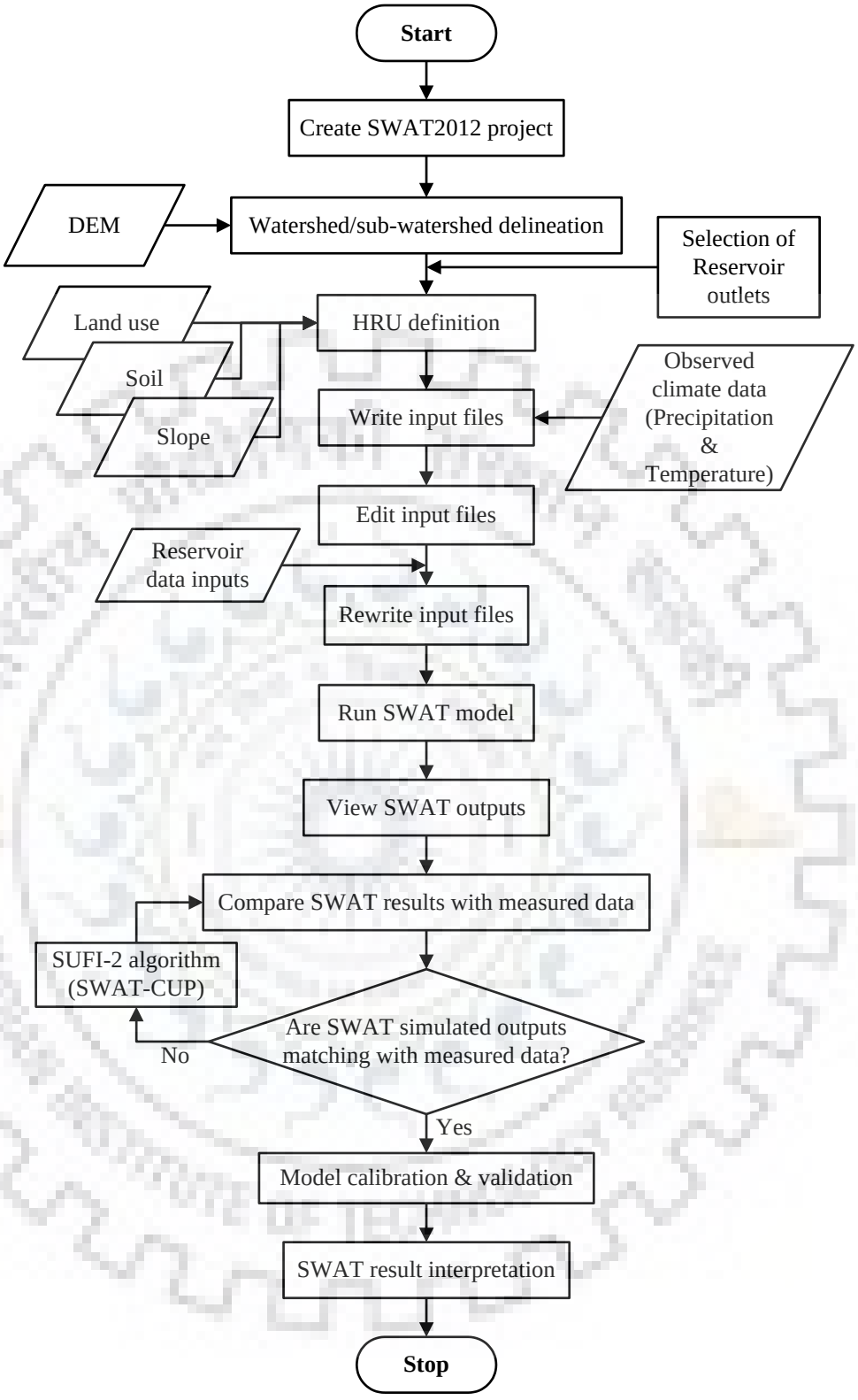

Figure 6.1: Methodology flowchart used for SWAT model simulation

6.2.3.1 Model setup

(a) Data preparation

Spatial datasets (DEM, land use map, soil map etc.) required for the SWAT model were projected into the same co-ordinate system (WGS 1984) using the ArcGIS interface. Satellite

imagery derived land use maps were reclassified into the SWAT land use data type. User look-up table was provided to identify the SWAT code for all land use classes. The soil map of the study area was prepared and enlisted in the look-up table, which is not available in the U.S. soil database.

(b) Watershed delineation

Delineation of the study area comprises the entire boundary of Betwa river basin. Shuttle Radar Topography Mission (SRTM) DEM was used to delineate the study watershed, and to prepare the river drainage network. Confluence of the Betwa river with the Yamuna River near Hamirpur gives geographical coverage of about 43936.59 km^2. This area fairly matches with the area reported in National Water Development Agency (NWDA, 1993) technical report of the Betwa basin (43895 km^2). The marginal variation in the drainage area of the Betwa River Basin used in this study and reported by NWDA may be due to fixing of the outlet point or confluence point in the watershed delineation process.

In this study, Betwa river basin was further divided into 57 sub-watersheds based on the defined threshold value (50000 ha) by trial and error, the four hydrologic gauging sites (Basoda, Garrauli, Mohana and Shahijina), and the outlet points provided for nine reservoir outlets to facilitate precise hydrologic simulation of the model (Figure 3.8, Chapter 3). The selection of threshold value was based on the desired stream network density and connectivity of the drainage network with reservoirs, available in the study area. Furthermore, each sub-watershed should be smaller than the area of precipitation recording to minimize the uncertainty in capturing spatial information in the watershed.

(c) HRU definition

The SWAT model uses other physical layers to determine unique hydrological response units (HRUs). The Betwa basin was divided into many HRUs (3874) representing homogenous hydrological regions defined with unique land use (threshold value = 0), soil type (threshold value = 1) and slope (threshold value = 0). Sub-watershed wise HRU distribution and land use and soil characteristics are presented in Appendix D.

Further, the sub-watersheds generated by points given for reservoirs were selected to demonstrate the reservoir outlets (Figure 6.2). In this study, nine water storage structures, including 7 reservoirs and 2 weirs, located on the main and tributary river channel were used in the SWAT modelling. The details of reservoir management in the SWAT are provided in Section *6.2.3.6*.

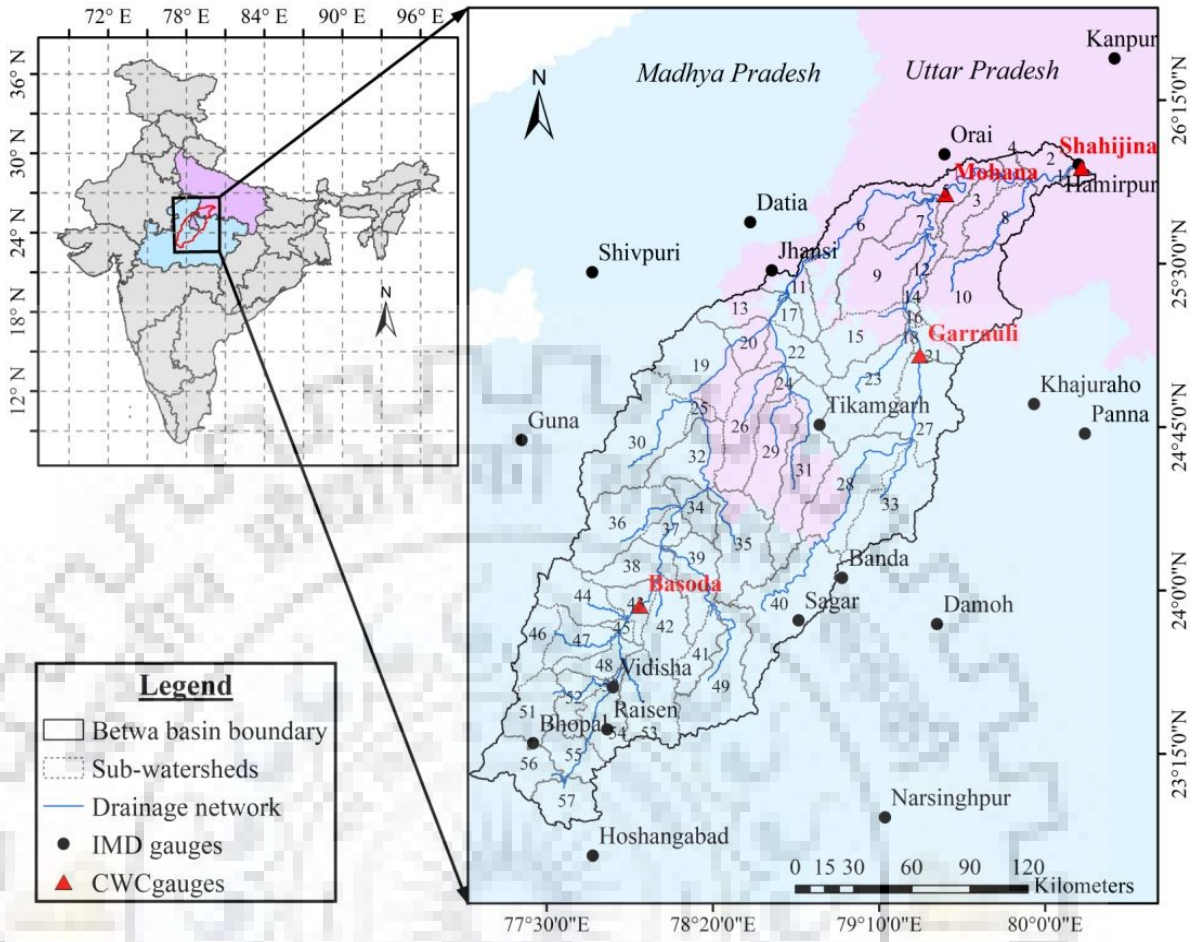

Figure 6.2: Sub-watershed division map with IMD and CWC gauges in the Betwa river basin

6.2.3.2 Basin attributes

The attributes of sub-watersheds, tributary channels and main channels are determined in the ArcSWAT interface as follows (Neitsch et al., 2004):

(a) Sub-watershed

The first level of basin/catchment division is the sub-watershed. Sub-watersheds possess a geographic position, and spatially connected to each other. Its delineation can be defined by surface topography so that the entire area accumulates flow to the sub-watershed outlet.

(b) Hydrologic Response Units (HRU)

Area in a sub-watershed may be divided into Hydrologic Response Units (HRUs). HRU possess unique land use/ slope/ soil attributes.

(c) Main channels / reach

Main channel is associated with each sub-watershed and carries flow loadings in the channel segment. Outflow from the upstream channel segment(s) enters in the main segment.

(d) Tributary channels

Tributary channel differentiates surface runoff input for channelized flow in a sub-watershed. This channel can be used to estimate the time of concentration of runoff generated, and transmission losses from runoff, as it flows to the main channel.

(e) Reservoirs / ponds / wetlands

In SWAT model, surface water bodies within a study area can be modeled as ponds, wetlands or reservoirs.

6.2.3.3 Theoretical considerations in SWAT

SWAT is a theoretical continuous model operates on daily time steps. This study uses monthly simulation outputs for the analysis purpose. The hydrologic components simulated on a HRU level is routed from HRU to sub-watershed, and then subsequently to the whole study basin outlet. Two hydrology component systems, namely land hydrology and channel hydrology, controls the movement of water, sediment fluxes and nutrient loads from overland to watershed outlet through the river channel network.

Water balance is the driving basis of watershed simulation using SWAT model (Neitsch et al., 2005; 2011) and is given by the equation 6.1.

$$SW_t = SW + \sum_{i-1}^{n}(R - Q - ET - P - QR) \quad \ldots (6.1)$$

where, SW_t is the final soil water content (mm), SW is the initial soil water content (mm), t is the time (days), R is the amount of precipitation (mm), Q is the amount of surface runoff (mm), ET is the amount of evapotranspiration (mm), P is percolation (mm), and QR is the amount of return flow (mm) on i^{th} day.

(a) Surface runoff

Surface runoff can be estimated using one of the available option, which includes the modified SCS curve number method (USDA Soil Conservation Service, 1972) and the Green & Ampt infiltration method (Green and Ampt, 1911).

In the present study, the SCS curve number method has been used for estimation of runoff. It is an empirical model that estimates the amounts of runoff depth under varying land use and soil types. Curve number varies non-linearly with the moisture content in soil. Curve number drops

when soil approaches to wilting point, and increases up to 100 when approaches to saturation. The SCS curve number equation (6.2) used in the model is as follows (USDA Soil Conservation Service, 1972):

$$Q = \frac{(R - 0.2s)^2}{(R + 0.8s)}, \qquad \text{for R>0.2s} \qquad \ldots (6.2)$$

$$Q = 0.0, \qquad \text{for R} \leq 0.2\text{s} \qquad \ldots (6.3)$$

where, Q is the daily runoff (mm), R is the daily rainfall (mm), and s is a retention parameter (mm). The retention parameter, s, varies (a) among sub-basins because of the variation in soils, land use, management and slope with time because of changes in soil water content. The parameter s is related to curve number (CN) by the SCS equation 6.4 (USDA Soil Conservation Service, 1972):

$$s = 254\left(\frac{100}{CN} - 1\right) \qquad \ldots (6.4)$$

The constant, 254, in the above equation gives s in mm. Thus, R and Q are also expressed in mm. CN is the curve number for antecedent moisture condition (AMC) II, i.e. for average condition, under different land use and hydrologic soil groups.

Modified rational method is used to estimate peak runoff rate. It is based on an assumption that if rainfall intensity falls for long period more than the time of concentration, then runoff will increase until t_c. When maximum runoff occurs, all sub-watersheds contribute to peak flow at the watershed outlet. It is expressed by following equation (6.5):

$$q_{peak} = \frac{\alpha_{tc} \times Q \times A}{3.6 \times t_c} \qquad \ldots (6.5)$$

where, q_{peak} is the peak runoff rate (m^3/s), α_{tc} is the fraction of daily rainfall occurs during the time of concentration, A is the sub-watershed area (km^2) and t_c is the time of concentration for a sub-watershed (hr).

The sub-watershed time of concentration is generally a sum of two types of concentrations (Equation 6.6).

$$t_c = t_{ov} + t_{ch} \qquad \ldots (6.6)$$

where, t_{ov} is the time of concentration for overland flow (hr), and t_{ch} is the time of concentration for channel flow (hr). These can be expressed as follows (Equations 6.7 and 6.8):

$$t_{ov} = \frac{L_{slp}^{0.6} \times n^{0.6}}{18 \times slp_{ov}^{0.3}} \quad \ldots (6.7)$$

$$t_{ch} = \frac{0.62 \times L \times n^{0.75}}{A^{0.125} \times slp_{ch}^{0.375}} \quad \ldots (6.8)$$

where, *Lslp* is the sub-watershed slope length (m), *n* is the manning's roughness coefficient, slp_{ov} is the average slope in the sub-watershed, *L* is the channel length from the most distant point to the sub-watershed outlet (km), slp_{ch} is the average slope for river channel.

(b) Evapotranspiration

Evapotranspiration (*ET*) is one of the most basic components of the hydrologic cycle. It is a combination of evaporation (from open water surface body) and transpiration (from vegetation) processes that converts Earth's surface water into water vapour. In the SWAT model, three methods are incorporated for estimation of potential evapotranspiration (PET), namely (1) Penman-Monteith method (Monteith, 1965; Allen, 1986; Allen et al., 1989), (2) Priestley-Taylor method (Priestley and Taylor, 1972), and (3) Hargreaves method (Hargreaves et al., 1985). The Penman-Monteith method requires several meteorological parameters such as solar radiation, air temperature, relative humidity and wind speed. Moreover, the Priestley-Taylor method also requires solar radiation, air temperature and relative humidity for estimation of evapotranspiration. If wind speed, relative humidity, and solar radiation data are not available, the Hargreaves methods provide options that give realistic results in most cases (Arnold et al., 1998; Williams et al., 2008). Due to non-availability of the other data set, Hargreaves method that requires air temperature only has been used in this study.

Based on extraterrestrial radiation and air temperature, the Hargreaves method estimates potential evapotranspiration using following modified equation (6.9):

$$\lambda E_o = 0.0023 \times H_o \times (T_{\max} - T_{\min})^{0.5} (T_{avg} + 17.8) \quad \ldots (6.9)$$

where, λE_o is the potential evapotranspiration (mm/day); H_o is the extraterrestrial radiation (MJ/m^2/day); and $T_{\max}$, $T_{\min}$ and T_{avg} are the maximum, minimum and average air temperatures (°C)

The actual evapotranspiration can be calculated by using values obtained by Hargreaves method. In the process, rainfall intercepted by the plant canopy is initially evaporated. Then, actual amount of sublimation and evaporation are calculated after computation of corresponding maximum values. After rainfall, the canopy storage is filled before any water

allowed to reach the ground. When evaporation is computed, then firstly water is removed from canopy storage.

Canopy storage is directly considered when the curve number method is used to compute surface runoff. Otherwise, if Green-Ampt method is used for runoff computation, SWAT models the canopy storage separately using maximum amount of water that can be stored at maximum leaf area index. It can be presented by equation (6.10) as follows:

$$Can_{day} = Can_{\max} \times \frac{LAI}{LAI_{\max}} \quad \ldots (6.10)$$

where, Can_{day} is the maximum amount of water trapped in the canopy on a particular day (mm); $Can_{\max}$ is the maximum amount of water trapped in the canopy when canopy is at fully developed stage (mm); LAI is the leaf area index for a given day; and $LAI_{\max}$ is the maximum leaf area index for the plant.

(c) Percolation

Percolation can be calculated for each soil layer, as it occurs when water content in the soil exceeds the field capacity. The water percolated below root zone becomes lost from the watershed, due to groundwater contribution or as a return flow at the downstream. In SWAT model, the flow through each soil layer uses storage routing technique combined with a crack-flow. The storage routing technique is based on the following equation (6.11):

$$SW_i = SW_{oi} \times \exp\left(\frac{-\Delta t}{TT_i}\right) \quad \ldots (6.11)$$

where, SW_i is the soil water contents at the beginning of day (mm); SW_{oi} is the soil water contents at the end of day (mm); Δt is the time interval (24 h); and TT_i is the travel time through layer *i*. Thus, subtracting SW_{oi} from SW_i can compute the percolation (Equation 6.12):

$$O_i = SW_{oi} \times \left[1 - \exp\left(\frac{-\Delta t}{TT_i}\right)\right] \quad \ldots (6.12)$$

where, O_i is the percolation rate in mm/day.

The travel time for soil layer *i* (TT_i) can be computed following linear storage equation (6.13):

$$TT_i = \frac{\left(SW_i - FC_i\right)}{H_i} \quad \ldots (6.13)$$

where, H_i is the hydraulic conductivity (mm/hr); and FC_i is the field capacity minus wilting point water content for layer i in mm. The hydraulic conductivity value varies from the saturation capacity to field capacity as presented in Equation (6.14).

$$H_i = SC_i \times \left(\frac{SW_i}{UL_i} \right)^{\beta_i} \quad \ldots (6.14)$$

where, SC_i is the saturated conductivity for layer i (mm/hr); UL_i is the soil water content at saturation in (mm/mm); β_i is the parameter that causes H_i to approach zero as SW_i approaches FC_i. The β can be estimated using equation (6.15) as below:

$$\beta_i = \frac{-2.655}{\log_{10}\left(\frac{FC_i}{UL_i} \right)} \quad \ldots (6.15)$$

The constant (-2.655) in the above equation was set to assure $H_i = 0.002SC_i$ at field capacity. Flow may occur upward when a lower layer exceeds its field capacity. The ratio of two layers, soil water to field capacity, regulates water movement from one lower layer to another upper layer. Soil temperature can affect the percolation, as temperature in a particular soil layer goes at 0°C or below, no percolation is allowed.

(d) Lateral subsurface flow

For soil profile up to 2 m depth, the lateral subsurface flow is also calculated with percolation. In the SWAT model, the kinematic storage model developed by Sloan and Moore (1984) is used to calculate lateral flow movement in each soil layer. It is expressed as below (Equation 6.16):

$$q_{lat} = 0.024 \times \frac{\lfloor 2S \times SC \times \sin(\alpha) \rfloor}{\theta_d \times L} \quad \ldots (6.16)$$

where, q_{lat} is lateral flow (mm/day), S is drainable volume of soil water (m/hr), α is slope (m/m), θ_d is drainable porosity (per mm), and L is flow length (m).

(e) Ground water flow

SWAT model differentiate groundwater into two aquifer systems which contribute return flow to streams, i.e. a shallow unconfined aquifer (within the watershed), and a deep confined aquifer (outside the watershed). Ground water flow contribution to total stream flow is simulated by creating shallow aquifer storage. The water balance equation (6.17) for the shallow aquifer is as follows:

$$Vs_{sh,i} = Vs_{sh,i-1} + Rc - revap - rf - perc_{gw} - WU_{sh} \quad \text{... (6.17)}$$

where, $Vs_{sh,i}$ is the shallow aquifer storage on day *i* (mm); $Vs_{sh,i-1}$ is the shallow aquifer storage on day *i-1* (mm); *Rc* is the recharge percolates from bottom of the soil profile (mm); *revap* is the root uptake from the shallow aquifer (mm); *rf* is the return flow (mm); $perc_{gw}$ is the percolation to the deep aquifer (mm); and WU_{sh} is the water use (withdrawal) from the shallow aquifer (mm).

The water balance equation (6.18) for the deep aquifer is as follows:

$$Vs_{dp,i} = Vs_{dp,i-1} + perc_{dp} - WU_{dp} \quad \text{… (6.18)}$$

where, $Vs_{dp,i}$ is the amount of water stored in deep aquifer on i^{th} day (mm); $Vs_{dp,i-1}$ is the amount of water stored in deep aquifer on day *i-1* (mm); per_{dp} is the amount of water percolating from shallow aquifer into deep aquifer (mm); and WU_{dp} is the amount of water removed from deep aquifer by pumping (mm).

(f) Routing method

River channel flow can be routed by using variable storage coefficient method or Muskingum routing method, developed by Williams (1969). User can define width and depth of the channel when it fills up to the top of the river bank. Also, channel length and channel slope with its roughness coefficient (Manning's 'n') values are required in the model. It is used to calculate the rate and velocity of flow in a given time. Following continuity equation (6.19) can be used to represent the routing method:

$$V_{in} - V_{out} = \Delta V_{stored} \quad \text{… (6.19)}$$

where, V_{in} is the volume of inflow (m^3); V_{out} is the volume of outflow (m^3); and ΔV_{stored} is the change in volume of storage (m^3) during the time step.

This equation (6.20) can also be expressed as:

$$\Delta t \times \left(\frac{q_{in,1} + q_{in,2}}{2} \right) - \Delta t \times \left(\frac{q_{out,1} + q_{out,2}}{2} \right) = V_{stored,2} - V_{stored,1} \quad \text{… (6.20)}$$

where, Δt is the length of the time step (s); $q_{in,1}$ and $q_{in,2}$ are the inflow rates at the beginning and end of the time step (m^3/s); $q_{out,1}$ and $q_{out,2}$ are the outflow rates at the beginning and end

of the time step (m^3/s); $V_{stored,1}$ and $V_{stored,2}$ are the storage volumes at the beginning and end of the time step (m^3/s), respectively.

The travel time (*TT*) is the ratio of volume of water stored in channel and outflow rate and is given as equation 6.21.

$$TT = \frac{V_{stored}}{q_{out}} = \frac{V_{stored,1}}{q_{out,1}} = \frac{V_{stored,2}}{q_{out,2}} \quad \ldots (6.21)$$

Equation (6.22) representing relationship between travel time and storage coefficient is as follows:

$$q_{out,2} = \left(\frac{2\times\Delta t}{2\times TT + \Delta t}\right)\times q_{in,avg} + \left(1 - \frac{2\times\Delta t}{2\times TT + \Delta t}\right)\times q_{out,1} \quad \ldots (6.22)$$

The storage coefficient (*SC*) can be calculated as equation (6.23):

$$SC = \frac{2\times\Delta t}{2\times TT + \Delta t} \quad \ldots (6.23)$$

The volume of outflow is calculated by using the following equation (6.24):

$$V_{out,2} = SC\times\left(V_{in} + V_{stored,1}\right) \quad \ldots (6.24)$$

In main channel, the bank storage, channel water balance, transpiration and evaporation losses at the end of time step are estimated using suitable equations.

(g) Other processes

- *Erosion*

In the SWAT model, the Modified Universal Soil Loss Equation (MUSLE) is used to estimate the soil erosion and the sediment yield at HRU level. MUSLE represented as follows (Equation 6.25):

$$Y = [a\times(Q\times q_p)^b]\times RKLSCP \quad \ldots (6.25)$$

where, Y is the sediment yield (tones); Q is the streamflow rate (m^3/s); qp is the peak flow rate (m^3/s); R is the rainfall erosivity factor (MJ mm/ha/hr/year); K is the soil erodibility factor (t ha hr /ha/Mj/mm); LS is the topographic factor (dimensionless); C is the crp management factor (dimensionless); P is the conservation practice factor (dimensionless); and a, b are the coefficients.

- *Management practices*

Ongoing land and water management practices in the study area have incorporated in the SWAT model. This model facilitates the user defined land management practices, such as begin and end of the growing season, timing and amounts of fertilizer, pesticides and irrigation applications, tillage operations, crop rotation and multiple cropping practices. These land management practices can be defined at HRU level in each sub-watershed. Further, water management option includes irrigation water, tile drainage, depression areas, water transfer, consumptive use and loading from point sources. Moreover, available water resources structures such as reservoir, lake, weir, can be managed well within the SWAT model.

6.2.3.4 Model input files

The SWAT model incorporates various input files/information at watershed level, sub-watershed level and HRU level. In case of point source or reservoirs, the input data is provided for each feature. Watershed/ river basin level inputs are provided to model the same process for all sub-watersheds of the study area. Sub-watershed/ sub-basin level input provides the same value to all HRUs covered within a sub-watershed. To set a unique value for each HRU, the HRU level inputs must be provided.

(a) Watershed level inputs

- *Master watershed file (file.cio)*

  This file is assessed by the model to perform database management for the inputs of sub-basin, climate, watershed level inputs and outputs.

- *Watershed configuration file (.fig)*

  Data of this file is used to simulate process within sub-watershed or to route in drainage network of watershed.

- *Basin input file (.bsn)*

  This file is used to define general basin attributes such as drainage area, base flow and initial soil water content, which control physical processes in entire watershed.

- *Precipitation input file (.pcp)*

  This is an optional file and contains daily measured precipitation data, which can be generated or can read from the observed data. This file can hold precipitation data of up to 300 gauging stations.

- *Temperature input file (.tmp)*

  This is also an optional file contains daily measured minimum and maximum temperature data. This file can hold data records up to 150 gauging stations.

- *Solar radiation input file (.slr)*

  This optional file contains daily solar radiation data. This file can hold data of up to 300 stations.

- *Wind Speed input file (.wnd)*

  This optional file contains daily average wind speed, and holds data record up to 300 stations.

- *Relative humidity input file (.hmd)*

  This optional file contains daily relative humidity values, and holds data record up to 300 stations.

- *Potential evapotranspiration input file (.pet)*

  This optional file contains daily potential evapotranspiration values for watershed.

- *Land cover/plant growth database file (crop.dat)*

  This database file contains information of specific parameters required to simulate plant growth by the plant species. Parameters for the crop specified in management file (.mgt) taken from crop.dat file.

- *Tillage database file (till.dat)*

  This file contains tillage mixing efficiency, reference number and name of the operation. Traditional tillage operations having mixing efficiencies of over 70% are selected in the management file (Arnold et al., 1998).

- *Fertilizer database file (fert.dat)*

  This file summarizes the fertilizer fractions in terms of nitrogen (N) and phosphorous (P). It can also store the information of bacteria levels in the manure.

- *Pesticide database file (pest.dat)*

  This database file contains information of degradation and mobility of pesticides in watershed.

- *Urban database file (urban.dat)*

  This file contains information of urban/built-up/wash-off areas in the watershed.

- *Septic database file (septic.dat)*

  This database file contains information about septic systems.

(b) Sub-watershed level inputs

- *Sub-basin level file (.sub)*

  This input file contains sub-basin information related to a diversity of features. It includes properties of tributary channels, amount of topographic relief, and variables related to number/name of HRUs.

- *Weather generator file (.wgn)*

  This file contains sub-basin wise statistical information of climate variables.

- *Main channel file (.rte)*

  This file contains physical properties of main channel, as well as transport of sediments, nutrients and pesticides with the main channel flow.

(c) HRU level inputs

- *Hydrologic response unit file (.hru)*

  This input file contains HRU level data, which represents unique combination of land use, soil and slope.

- *Management file (.mgt)*

  Management file contains details of land and water management practices used in the watershed, such as planting, harvesting, and tillage operations; and fertilizer, pesticide and irrigation application.

- *Soil file (.sol)*

  This input file contains soil texture and its physicochemical properties. Also, information about available soil water content, hydraulic conductivity, bulk density and organic carbon content in different soil layers are included in the soil file.

- *Groundwater file (.gw)*

  The groundwater file contains sub-basin wise information about deep and shallow aquifers in the watershed.

6.2.3.5 Model output files

The SWAT model can provide the outputs for reaches (output.rch), sub-basins (output.sub), HRUs (output.hru) and reservoirs (output.res). While running the model, output information stores in these files which can be later used for analysis purpose. Two types of SWAT model results can be obtained. (1) Outputs with the information collected and formatted to use in SWAT model, as well as the additional data representing background information. (2) Other type of results obtained by calibration, validation and sensitivity analysis of the SWAT model for simulation of runoff and sediment loads.

6.2.3.6 Reservoir management in SWAT

Distributed extensive water storages within a large river basin can significantly impact the basin hydrologic processes. The impacts may be further integrated in the parameterization and calibration process of a large-scale hydrological model such as SWAT. In addition, it is not feasible to individually evaluate the number of water storages available in the Betwa basin. Thus, this study has planned to implement and manage water storages located on river channel using SWAT model. This may facilitate the reasonable behavior and simulation of water storage system in the study area.

Detailed information of water storage design and operation is unknown for all reservoirs located in the Betwa River basin. For Indian water storages, limited information is available on the India-WRIS (Water Resources Information System) website (http://india-wris.nrsc.gov.in/), and the WRIS publications (http://www.india-wris.nrsc.gov.in/wrpinfo/index.php?title=WRIS_Publications). The total drainage area and storage volumes of reservoirs and weirs can be obtained at the sub-watershed level. During watershed delineation, the outlet locations of these reservoirs are given on drainage network so that sub-watersheds could be separated for the model simulation (Figure 6.2). Therefore, the water storages located on main channel and tributary channel are considered for adequate water system management in the SWAT model.

The SWAT model includes a reservoir module that can simulate water storages with detailed design and running information. Thus, it can be used to assess the impact of water storage at the basin level. In this study, seven reservoirs and two weirs are added to SWAT2012, and then simulated by the reservoir module. It is assumed that the effect of small water storages, such as small ponds and lakes, is minimal in such a large river basin. This accounts that the upstream small water storages have none effect on the downstream of the reservoir. Also, small water storages are not interconnected between the downstream of reservoir and the gauging station.

Hence, outflow of small water storage is attributed to the reservoirs located within a sub-watershed. Therefore, these small water storages are excluded in this study. The similar approach was also adopted by Güntner et al. (2004). The water storages available in the Betwa River Basin are provided in Table 6.1.

Table 6.1: Water storages located in main and tributary channels of the Betwa basin

Water storages	India-WRIS number	River	Years of commencement to completion
Bah Dam	D01630	Bah	-
Devri Dam*	-	Dhasan	-
Dhukwan Weir	W00106	Betwa	1900-1905
Lachura Dam	D00525	Dhasan	1910**
Matatila Dam	D00590	Betwa	1958**
Maudaha (Swami Brahmanand) Dam	D00127	Virma	2003**
Pariccha Weir	W00267	Betwa	1881-1886
Rajghat (Rani Laxmi Bai Sagar) Dam	D02674	Betwa	1977-2000
Samrat Ashok Sagar (Halali) Dam	D04471	Halali	1997**

*Information about the Devri dam is not available from India-WRIS website. This information was acquired during the field visit.
**Only the year of completion.

All these nine water storage structures are implemented in the reservoir module of SWAT2012, given that (1) they largely affect the hydrology of the study area, (2) they represent the most important water supplies in the study area, and (3) detailed information of these reservoirs is available for modelling purpose. Available information of water storages is limited to the year of completion, maximum target storage and storage volume. Nevertheless, remotely sensed surface area, and outflow regulations were obtained for successful reservoir management in the SWAT model. In the literature, Wagner et al. (2011) derived these parameters for six reservoirs located in the Western Ghats of India. Also, Zhang et al. (2012b) estimated reservoir parameters for small to large water storages of China. The same methodology has been adopted in this study for estimation of the surface area, and outflow regulations. On this basis, the reservoir management can be successfully incorporated.

(a) Surface area estimation

In SWAT model, surface area of water storage is essential to estimate the amount of precipitation falling, and the amount of losses (evaporation and seepage) with respect to the

water storages in the SWAT model. In general, water surface area varies with the storage volume. As the water surface area and the storage volume depends on drainage area and available storage, their relationship varies with different types of water storages. Thus, it is not feasible to use explicit relationship for the estimation of surface area and storage volume as done previously in the literature. Güntner et al. (2004) estimated surface area as a function of the actual storage volume using following equation (6.26):

$$A_{res} = C_{res} \times (V_{res})^{D_{res}} \quad \ldots (6.26)$$

where, A_{res} is the surface area of reservoir (m^2); V_{res} is the volume of water storage (m^3); and C_{res} and D_{res} are the reservoir specific constants depending on the geometry.

Liebe et al. (2005) calculated storage volume as a function of the surface area using following equation (6.27):

$$V_{res} = 0.00857 \times (A_{res})^{1.4367} \quad \ldots (6.27)$$

Recently, Zhang et al. (2012b) proposed routing scheme, combining both sequential and parallel streams and storages links, to describe the position of upstream-downstream water storages. The sequential and parallel routing scheme is based on the inflow and outflow from the water storage. Also, they presented calibration steps to include both physical and human interferences such as water storages and water consumption. SWAT model allows the input of water withdrawn within any sub-watersheds, which can be modelled as a water loss from the system. The water consumption information varies for each month, different years and different locations. However, it is difficult to measure and collect the water-use data in such a large river basin.

Several literature studies have estimated the surface area of reservoir using satellite imagery data (Frazier & Page, 2000; Pandey et al., 2016a). In India, the water storage volumes of reservoirs were calculated using Landsat images (Mialhe et al., 2008), which are presently available at spatial resolution of 30 m and 15 m. Numerous remote sensing based methodologies/approaches, the single band threshold method, the difference of spectrum relationship method, the Normalized Difference Vegetation Index (NDVI) method and the Normalized Difference Water Index (NDWI) method, are available for the extraction of water surface area.

In this study, the NDWI method developed by McFeeters (1996) to estimate the reservoir surface area extracted from Landsat 8 OLI (Operational Land Imager) imagery data (22nd and 29th Oct, 2013) has been used. The equation (6.28) of NDWI method is as follow:

$$NDWI = \frac{(G - NIR)}{(G + NIR)} \quad \ldots (6.28)$$

where, *NIR* is the near-infrared band, and *G* is the green band of Landsat 8 OLI.

The Landsat 8 OLI data is available for every 16 days temporal resolution and at 30 m high spatial resolution. Imagery data of late flooding period in a wet year (2013) has been used to extract the surface area of the reservoirs, when all reservoirs within the study area are completely filled with water. Here, it is assumed that, the extracted surface area is valid and accurately estimated along with the regular storage volumes collected from the India-WRIS.

(b) Target storage and outflow regulations

Due to lack of information regarding the reservoir outflows, the outflow simulation code number 2 which represents the simulated controlled outflow-target release in the SWAT model has been used. This SWAT option needs minimal inputs of the monthly target reservoir storage (STARG), beginning month of non-flood season (IFLOD1R), ending month of non-flood season (IFLOD2R), and number of days required to achieve a target storage from the current reservoir storage (NDTARGR). In India, different outflow regulations are used along with seasonal changes, i.e. monsoon (June to October) and non-monsoon (November to May) with respect to Indian water-year from June to May. Also, measurements of outflow release and target storages are unavailable from the available sources. Therefore, the monthly storage volume and regulated outflows for feasible implementation of reservoirs in the SWAT model was fixed.

In this study, a methodology proposed by Wagner et al. (2011) for the Indian River basin has been adopted to manage the monthly target storage volume and the required days to reach target storage during monsoon and non-monsoon periods. The parameters derived for each reservoir is presented in Table 6.2. The monthly target storage of the reservoir is kept equal to the maximum target storage obtained from India-WRIS, during June to October. From November onwards, the target storages are set as decreased for every month. During this period, water is released at a linear rate, and is limited by the maximum flow rate in dry season (Table 6.2). This reservoir management can secure the water supply until a possible late monsoon in mid-June.

Also, the same input of minimum water flow rate is specified for monsoon season as given in Table 6.2. This allows the reservoir filling up to the maximum target storage with the mean annual precipitation. If the water goes beyond the target storage, it is assumed as flood storage. This study accounted that 10% of the maximum target storage is the flood storage. Hence, the flood storage varies with the dam-specific maximum outflow rate. The storage information, available online at the India-WRIS, provides evidence of the adequate reservoir management in this study.

In addition, the average daily principle spillway release rate (RES_RR) for all the water storages, based on the respective downstream gauge measurements were also estimated and incorporated, and is presented in Table 6.2. For instance, the CWC gauging station Basoda is located at the downstream of the Bah dam and Halali dam in upper Betwa basin. Therefore, average daily principle spillway outflows for these two reservoirs are estimated based on the daily observed data of the Basoda station. This allows the daily outflow regulation from the reservoir to match the measurements at Basoda station. Similarly, the measured data of Mohana, Garruli and Shahijina station were also used to estimate the average daily principle spillway outflows for the upstream water storages or the nearby downstream water storages.

Table 6.2: Characteristics of reservoirs estimated by general management rules using measured river discharge at the downstream gauges

Reservoir name	Surface area (ha)	Maximum target storage (MCM)	Number of days to reach target storage	Average daily principle spillway outflow (m^3/s)	Monsoon minimum outflow (m^3/s)	Non-monsoon maximum outflow (m^3/s)
Bah Dam	195.6	76.5	2	41	12.2	24.3
Devri Dam	266.7	21.0	3	40	4.6	26.6
Dhukwan Weir	1396.9	95.0	1	118	30.8	118.4
Halali Dam	6240.0	226.1	3	41	12.2	24.3
Lachura Dam	116.0	20.6	2	40	4.6	26.6
Matatila Dam	13885.0	1019.4	2	118	30.8	118.4
Maudaha Dam	5939.0	179.0	3	75	48.6	220.0
Paricha Weir	802.0	77.2	2	118	30.8	118.4
Rajghat Dam	24210.0	1975.0	3	118	30.8	118.4

6.2.4 SWAT model calibration and validation

The successful application of the hydrologic model depends on how well a model is performing. For calibration, few parameters are considered based on the literature studies carried out for the Betwa river basin, the regions located nearby the study area as well as in

India (Narsimlu et al., 2013; Kumar et al., 2017; Anand et al., 2018). The range of parameters was also chosen from the studies carried out by Murty et al. (2014) and Suryavanshi et al. (2017). The identified sensitive parameters were further used as an input to the initial simulation of streamflow and sediment loads. Model calibration was carried out at the four Central Water Commission (CWC) gauging stations located in the Betwa basin, i.e. Basoda (HO 676), Garrauli (HO 693), Mohana (HO 714) and Shahijina (HO 737). The sub-watershed outlets at SW-45, SW-27, SW-6 and SW-2 represent the Basoda, Garrauli, Mohana and Shahijina gauges, respectively (Table 6.3). Therefore, the simulations of these outlets were used for calibration and validation of the SWAT model during the years 2001 to 2013. First two years (2001 and 2002) of the simulation were reserved as "warm-up period" in order to realistically setup the states of its internal hydrological components, e.g. groundwater store, soil moisture content etc. The measured streamflow and sediment data of initial seven years (2003-2009) and last four years (2010-2013) were taken into consideration respectively for calibration and validation of the SWAT model by comparing its outputs.

Table 6.3: Details of the gauging sites in the Betwa basin

Name of CWC gauge	India-WRIS number	Hydrologic Observation (HO)	Sub-watershed outlet
Basoda	HO 676	GD	SW-45
Garrauli	HO 693	GDS	SW-27
Mohana	HO 714	GD	SW-6
Shahijina	HO 737	GDS	SW-2

Note: G = gauge; D = discharge; S = sediment load

In this study, the SWAT- Calibration and Uncertainty Programs (CUP) Sequential Uncertainty Fitting version 2 (SUFI-2) algorithm (Abbaspour et al., 2007; 2015) has been used for calibration, and validation of the model on monthly time scale. In addition, the SWAT-CUP has been used for sensitivity and uncertainty analysis. The calibration parameters are regionalized as per the guidelines provided by Abbaspour et al., (2015). The main benefit of SUFI-2 application over other algorithms is that the SUFI-2 accounts for all sources of uncertainty such as model input uncertainty, model conception uncertainty, model parameter uncertainty, and uncertainty in the measured data. Also, SUFI-2 was found quite efficient algorithm for time-consuming large-scale models (Yang et al., 2008). In this study, five iterations each with 1000 simulations were performed with multiple set of parameters.

In hydrological model, the over-parameterization is often reported the simulation problem (Beven, 1989). More number of parameters in the SWAT model can cause difficulty in the selection of parameter as well as the model response. Sensitivity analysis is used to identify the order of parameters having a significant influence on model simulations for a specific watershed (van Griensven et al., 2006). During calibration process, the sensitive parameters are significantly used to reduce the model calibration uncertainty and the run time to match the measured values of streamflow and sediment load.

6.2.4.1 Sensitivity analysis

The parameter sensitivity was assessed initially for streamflow, and then for sediment.

(a) One-At-a-Time (OAT) sensitivity analysis

In this method, sensitivity of a variable (streamflow and sediment) to the change in a parameter is analyzed while keeping other parameters constant at some specified value. Change in objective function (statistical parameter) represents OAT sensitivity of a parameter to the hydrological simulation. The OAT sensitive parameters were further selected as inputs in calibration process.

(b) Global sensitivity analysis

After selection of sensitive parameters, a global sensitivity analysis was performed to identify the relative sensitivity, following multiple linear approximations, of all parameters. It regress the Latin hypercube generated parameters against the objective function values (Khalid et al., 2016). This method estimates the change in objective function resulting from change in each parameter while all other parameters are changing. Hence, global sensitivity analysis provides some information about sensitivity between objective function and model parameters.

6.2.4.2 Uncertainty analysis

SWAT-CUP estimates degree of uncertainties in terms of two statistical measures referred to as *p-factor* and the *r-factor*. The *p-factor* measures the 95 percentile prediction uncertainty (95PPU) calculated at the 2.5% and 97.5% levels of cumulative distribution of the output, which can be obtained through Latin-Hypercube sampling. The *r-factor* shows the average thickness of ratio between the 95PPU band and the standard deviation of measured data. The SUFI-2 algorithm seeks to categories the measured data with the large *p-factor* (100%) and the small *r-factor* (minimum 0).

In this study, total 23 sensitive parameters were considered for streamflow (9 parameters) and sediment (14 parameters) based on sensitivity order obtained in SWAT-CUP. The

regionalization of the parameters has done by replacement (v__), by addition (a__) and by multiplication (r__) of a relative change depending on the nature of parameter. However, a parameter has never been allowed to go beyond the predefined absolute parameter range during the calibration process.

Further, the model performance was evaluated by statistical parameters and the hydrographs between measured data and simulated outputs.

6.2.4.3 Model evaluation criteria

After successful model run, the output variable needs to be evaluate by comparing the measured/observed variable. The continuous time series of the observed data and the simulated outputs were used for evaluation of streamflow and sediment loads. Moriasi et al. (2007) provided the model performance evaluation guidelines for monthly simulations based on quantitative statistics of coefficient of determination (R^2), Nash-Sutcliffe efficiency (NSE), percent bias (PBIAS), and ratio of the root mean square error to the standard deviation of measured data (RSR). In this study, following statistical parameters are used for the model evaluation.

(a) Coefficient of determination (R^2)

Coefficient of determination generally used to describe the proportion of total variance in the measured data that can be simulated by the model. It is given by following equation (6.29):

$$R^2 = \left[\frac{\sum_{i=1}^{n} (x_i - \bar{x})(y_i - \bar{y})}{\sqrt{\sum_{i=1}^{n} (x_i - \bar{x})^2} \sqrt{\sum_{i=1}^{n} (y_i - \bar{y})^2}} \right]^2 \quad \ldots(6.29)$$

where, X_i^{obs} is the i^{th} measured data; $\bar{x}$ is mean of measured data; X_i^{sim} is the i^{th} simulated value; $\bar{y}$ is the mean of model simulated value; and n is the total number of events.

The correlation or correlation based measurement (R^2) has been widely used to evaluate the goodness of fit of hydrologic models. The value of coefficient of determination varies from 0 to 1, with higher values indicating better agreement, while lower values indicating more error variance. These measures are over sensitive to extreme values, and are insensitive to additive and proportional difference between the model simulations and observations (Willmott, 1984; Legates & McCabe, 1999).

(b) Nash-Sutcliffe Efficiency (NSE)

The NSE is the normalized statistic, used to provide relative magnitude of the residual variance compared to measured data variance (Nash and Sutcliffe, 1970). This also indicates the fit of plot between measured and simulated data with respect to the 1:1 line. Thus, the NSE has been widely used to evaluate the performance of hydrologic models (Wilcox et al., 1990). It can be calculated using the following equation (6.30):

$$NSE = 1 - \frac{\sum_{i=1}^{n}(x_i - y_i)^2}{\sum_{i=1}^{n}(x_i - \bar{x})^2} \quad \text{... (6.30)}$$

where, X_i^{obs} is the i^{th} measurement for the constituent being evaluated, X_i^{sim} is the i^{th} simulated value for the constituent being evaluated, $\bar{x}$ is the mean of measured data for the constituent being evaluated, and n is the total number of measurements.

In general, the NSE value varies from 0 to 1, where 1 indicating a perfect fit. If the daily measured data approaches an average value, the denominator of the NSE equation goes to zero. If the NSE approaches minus infinity, then it indicates that the model has some minor miss predictions. The NSE statistics represents an improvement over R^2 for model evaluation, as it is sensitive to the difference in measured and simulated means and variance.

(c) Percent bias (PBIAS)

Percent bias (PBIAS) statistics is mainly used to measure the average tendency of simulated data with respect to the measured data (Gupta et al., 1999). The value of PBIAS is acceptable when it closes to zero, indicating accurate model simulation. A positive PBIAS indicates underestimation, while a negative PBIAS value indicates overestimation of the model (Gupta et al., 1999). It is calculated using the following equation (6.31):

$$PBIAS = \left[\frac{\sum_{i=1}^{n}(x_i - y_i)\times 100}{\sum_{i=1}^{n}(x_i)}\right] \quad \text{… (6.31)}$$

where, *PBIAS* is the expressed as a percentage.

According to Luo et al. (2008), NSE values between 0.0 and 1.0 are generally accepted based on the model performance, whereas a NSE value less than 0.0 indicates that the mean measured value is a better predictor than the simulated value, which indicates unacceptable performance.

(d) RMSE-Observations Standard Deviation Ratio (RSR)

The RSR statistics is a ratio of the RMSE value and the standard deviation (STDEV) of measured data. It used to combine both error (RMSE) index and standardized RMSE value (Legates & McCabe, 1999; Singh et al., 2005). RMSE is commonly accepted error statistics with lower value (Chu and Shirmohammadi, 2004; Singh et al., 2005; Vasquez-Amábile and Engel, 2005). The RSR statistics is calculated as follows (Equation 6.32):

$$RSR = \frac{RMSE}{STDEV} = \frac{\sqrt{\sum_{i=1}^{n}(x_i - y_i)^2}}{\sqrt{\sum_{i=1}^{n}(x_i - \bar{x})^2}} \quad \ldots (6.32)$$

Optimal RSR value is zero, indicates perfect model simulation. It varies from the lowest zero value to a large positive value. Hence, the lower RSR, due to low RMSE, shows better model performance (Moriasi et al., 2007).

In this study, model evaluation criteria suggested by Moriasi et al. (2007) has been used to quantify the accuracy in SWAT simulation (Table 6.4).

Table 6.4: Model evaluation criteria for monthly SWAT simulation

Performance rating	NSE	PBIAS (%)		RSR
		Streamflow	Sediment	
Very good	0.75 < NSE < 1.00	PBIAS < ± 10	PBIAS < ± 15	0.00 < RSR < 0.50
Good	0.65 < NSE < 0.75	± 10 < PBIAS < ± 15	± 15 < PBIAS < ± 30	0.50 < RSR < 0.60
Satisfactory	0.50 < NSE < 0.65	± 15 < PBIAS < ± 25	± 30 < PBIAS < ± 55	0.60 < RSR < 0.70
Unsatisfactory	NSE < 0.50	PBIAS > ± 25	PBIAS > ± 55	RSR > 0.70

Source: Moriasi et al. (2007)

6.3 RESULTS AND DISCUSSION

6.3.1 Sensitivity and uncertainty analysis

A set of model parameters have been selected for sensitivity and uncertainty analysis by referring the SWAT and SWAT-CUP documentation (Arnold et al., 2012a; Abbaspour et al., 2013), as well as relevant literatures (Narsimlu et al., 2013; Murty et al., 2014; Kumar et al., 2017; Suryavanshi et al., 2017; Anand et al., 2018). The parameters with high sensitivity value have been used for calibration and validation of the model. The selected parameters with their fitted values and sensitivity order for streamflow and sediment loads are presented in Table 6.5. Sensitivity analysis shows that streamflow is most sensitive to the curve number (CN2) followed by SURLAG (surface runoff lag coefficient) to SOL_AWC (available water capacity

of the soil layer) as shown in Table 6.5. Among sediment parameters, the channel erodibility factor (CH_ERODMO) is the most sensitive parameter followed by USLE_K (soil erodibility factor for USLE equation) to USLE_C (minimum value of USLE_C factor applicable to the forest area) as shown in Table 6.5. The sensitivity analysis results were considered for the model calibration process employing the SWAT-CUP.

Uncertainty analysis has been used to determine the reliability of model simulations, considering various sources of uncertainty. For selective sensitive parameters, the uncertainty analysis and calibration of the streamflow and sediment load were performed at monthly time-step using SUFI-2 algorithm. In this study, the measured data and the simulation outputs were analysed for the river gauges given in Table 6.3. The optimal value of p-factor is equal to one (100%), and r-factor equal to zero (0.0) for an ideal condition. This is because of the stochastic procedure of SUFI-2 algorithm, it provides range of parameter value rather than a single value after the calibration (Khalid et al., 2016). Results show the percent observations bracketed by the 95% prediction uncertainty (95PPU) were more than 70% (*p-factor*). The *r-factor* values, the average thickness of 95 PPU band divided by standard deviation of measure data, were also satisfactory for all the gauges in Betwa basin. The fitted values of the selected parameters found by SUFI-2 uncertainty algorithm were considered as final calibration values in the SWAT model. The calibrated parameter values were further used in the model validation process.

Table 6.5: Calibrated parameters with their fitted values and sensitivity order for streamflow and sediment

Sensitivity order	Parameters	Calibration range	Fitted value
	Streamflow		
1	CN2.mgt	-0.2 to 0.2	-0.17
2	SURLAG.bsn	0.05 to 10	1.64
3	ALPHA_BF.gw	0.3 to 0.9	0.41
4	GDRAIN.mgt	0 to 1	0.63
5	RCHRG_DP.gw	0 to 0.8	0.36
6	ESCO.hru	0.01 to 1	0.58
7	GWQMN.gw	0 to 30	0.07
8	GW_DELAY.gw	0 to 150	31.70
9	SOL_AWC().sol	0 to 0.5	0.08
	Sediment load		
1	CH_ERODMO().rte	0 to 0.5	0.03
2	USLE_K().sol	0 to 0.5	0.13
3	RES_STLR_CO.bsn	0.2 to 0.9	0.76
4	PRF.bsn	0.5 to 2	1.90
5	CH_COV1.rte	0.01 to 0.3	0.08
6	ADJ_PKR.bsn	0.8 to 1.5	0.85
7	RES_SED.res	400 to 1600	1133.79
8	CH_COV2.rte	0.1 to 0.8	0.50
9	USLE_P.mgt	0.3 to 0.8	0.65
10	LAT_SED.hru	0 to 100	7.54
11	USLE_C{1}.plant.dat_____AGRL	0.05 to 0.2	0.15
12	RES_NSED.res	10 to 200	19.48
13	SPEXP.bsn	0.5 to 1.5	0.76
14	USLE_C{7,8}.plant.dat_____FRSD,FRSE	0.1 to 0.4	0.23

Streamflow parameter description: *CN2.mgt = Initial SCS runoff curve number for moisture condition II; GDRAIN.mgt = Drain tile lag time (hr); ALPHA_BF.gw = Baseflow alpha factor (1/days); GW_DELAY.gw = Groundwater delay time (days); GWQMN.gw = Threshold depth of water in the shallow aquifer required for return flow to occur (mm H_2O); RCHRG_DP.gw = Deep aquifer percolation fraction; SOL_AWC().sol = Available water capacity of the soil layer (mm H2O/ mm soil); SURLAG.bsn = Surface runoff lag coefficient; ESCO.hru = Soil evaporation compensation factor.*

Sediment load parameter description: *USLE_P.mgt = USLE equation support practice factor; USLE_K().sol = USLE equation soil erodibility (K) factor; USLE_C{1}.plant.dat_____AGRL = Minimum value of USLE C factor applicable to the agriculture land; USLE_C{7,8}.plant.dat_____FRSD,FRSE = Minimum value of USLE C factor applicable to the forest area; PRF.bsn = Peak rate adjustment factor for sediment routing in the main channel; SPEXP.bsn = Exponent parameter for calculating sediment re-entrained in channel sediment routing; ADJ_PKR.bsn = Peak rate adjustment factor for sediment routing in the sub-watershed (tributary channels); RES_STLR_CO.bsn = Reservoir sediment settling coefficient; CH_ERODMO().rte = Jan. channel erodability factor; CH_COV1.rte = Channel erodibility factor; CH_COV2.rte = Channel cover factor; LAT_SED.hru = Sediment concentration in lateral flow and groundwater flow (mg/l); RES_SED.res = Initial sediment concentration in the reservoir (mg/l); RES_NSED.res = Equilibrium sediment concentration in the reservoir (mg/l).*

6.3.2 Model calibration and validation

In order to utilize the calibrated model for estimating the effect of different scenarios on water balancing of the Betwa River basin, the model was tested against an independent set of measured data. Calibration and validation of streamflow and sediment were performed using the SUFI-2 algorithm in the SWAT-CUP. The NSE with threshold value of 0.5 was used as the objective function for calibration using SWAT-CUP. The model performance was assessed at four CWC gauging stations, namely Basoda, Garrauli, Mohana and Shahijina. The goodness-of-fit of the monthly SWAT simulation was evaluated by comparison with the measured monthly data using visual interpretation of time-series plots, and statistical measures discussed in methodology section. The model was calibrated for the years 2003-2013, and then validated for independent validation period (2010-2013). Ideally, for a large river basin, the validation process has to be multi-gauge and based on sensitivity analyses performed in advance. This is especially important when the model has to be further applied at the regional scale analysis.

6.3.2.1 Streamflow

Initially, the SWAT model was calibrated and validated for streamflow simulation. Results show the satisfactory to good performance of the SWAT model during calibration and validation on the monthly time scale (Table 6.6) at all four gauging sites (Figure 6.3). Also, time-series of the monthly streamflow were plotted to visualize and to check the model simulation accuracy (Figure 6.4). In calibration, the high values of the R^2 (0.90, 0.94, 0.91 and 0.92), NSE (0.88, 0.91, 0.91 and 0.92), the low values of PBIAS (-14.20, -11.10, -7.70 and -16.30) and RSR (0.34, 0.30, 0.31 and 0.29) indicates satisfactory to very good model performance for streamflow simulation at Basoda, Garrauli, Mohana and Shahijina gauges, respectively (Moriasi et al., 2007). For validation, the model performance also indicates satisfactory to very good simulation of the streamflow, with the high values of the R^2 (0.90, 0.92, 0.90 and 0.88), NSE (0.84, 0.91, 0.89 and 0.86), the low values of PBIAS (-13.60, -16.50, -3.90 and -7.50) and RSR (0.41, 0.30, 0.33 and 0.38) at Basoda, Garrauli, Mohana and Shahijina gauges, respectively (Moriasi et al., 2007). Result reveals that SWAT model can be used satisfactorily to simulate the streamflow on monthly time-scale.

In this study, the graphical and statistical evaluation showed satisfactory streamflow simulation. However, the SWAT model results were underestimated during high-flow periods (Figures 6.3 and 6.4). It may be partly due to the curve number method, which is not able to generate accurate streamflow prediction for the storm periods (Kim and Lee, 2008). This method defines rainfall event is the sum of all rainfall occurred during a day, and this might lead to underestimation of the surface runoff (Choi et al., 2002).

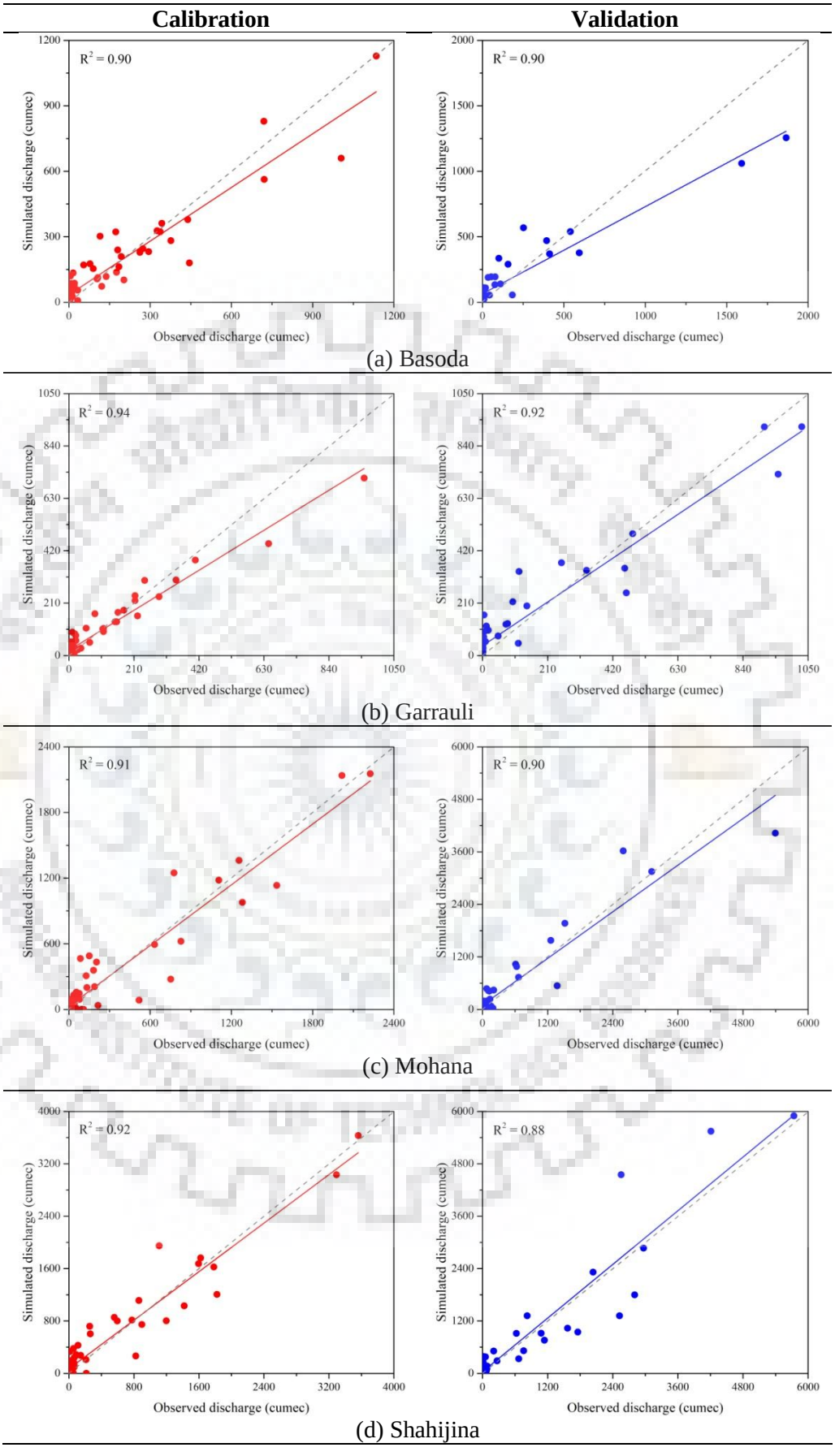

Figure 6.3: Linear regression between measured and simulated streamflow during calibration (2003-2009) and validation (2010-2013) for comparison with 1:1 trendline

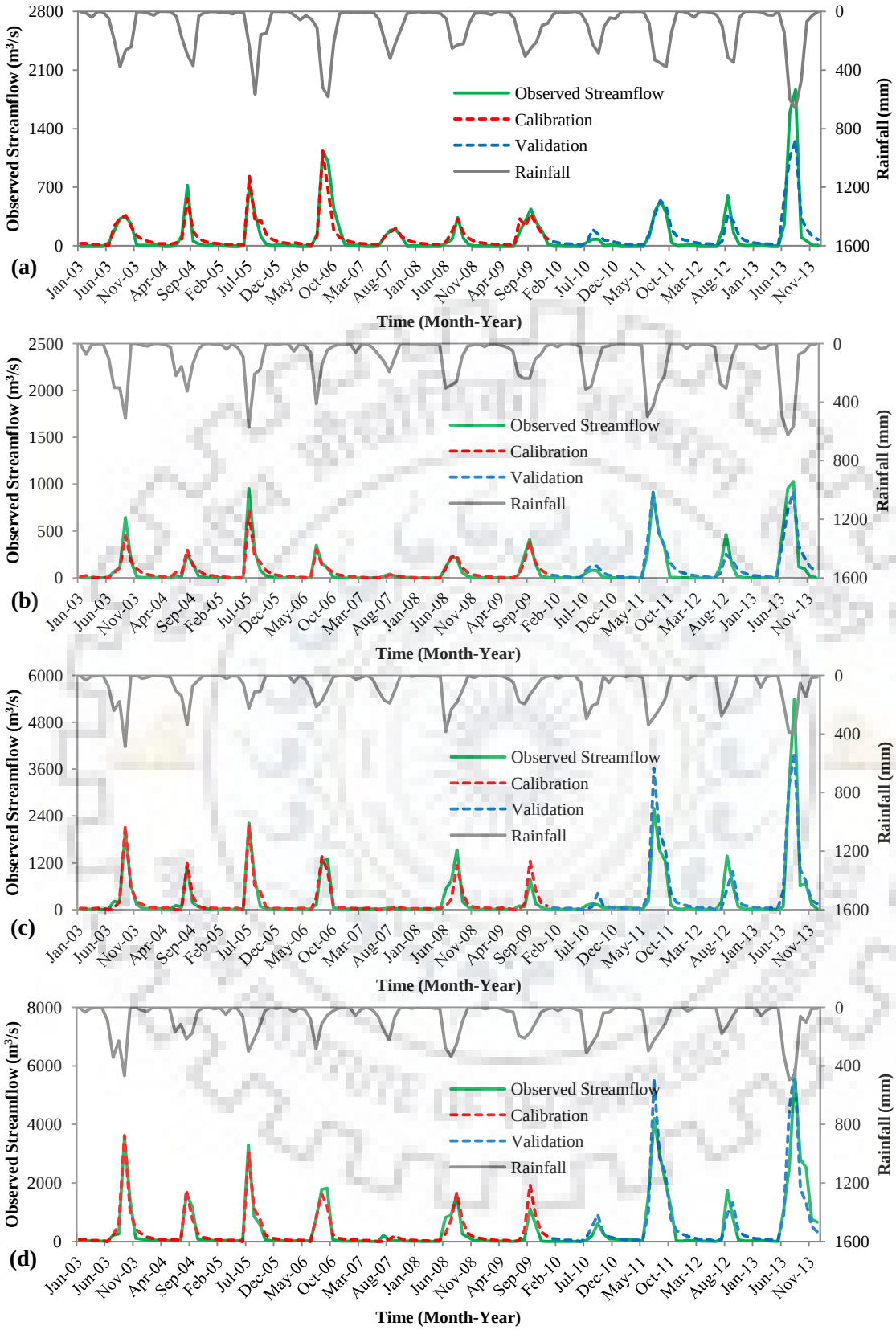

Figure 6.4: Comparison of measured and SWAT simulated streamflow at (a) Basoda, (b) Garrauli, (c) Mohana, and (d) Shahijina for monthly calibration (2003-2009) and validation (2010-2013)

Table 6.6: Performance evaluation of the SWAT model for monthly streamflow simulation

Gauging station	Calibration				Validation			
	R^2	NSE	PBIAS	RSR	R^2	NSE	PBIAS	RSR
Basoda	0.90	0.88	-14.20	0.34	0.90	0.84	-13.60	0.41
Garrauli	0.94	0.91	-11.10	0.30	0.92	0.91	-16.50	0.30
Mohana	0.91	0.91	-7.70	0.31	0.90	0.89	-3.90	0.33
Shahijina	0.92	0.92	-16.30	0.29	0.88	0.86	-7.50	0.38

Table 6.7: Statistical analysis of streamflow during calibration (2003-2009) and validation (2010-2013)

Statistic	Basoda		Garrauli		Mohana		Shahijina	
	Measured	Simulated	Measured	Simulated	Measured	Simulated	Measured	Simulated
				Calibration				
Max	1135.28	1128.00	953.86	711.20	2225.34	2154.00	3561.53	3630.00
Avg	105.78	120.81	59.89	66.52	188.09	202.51	296.12	344.30
SD	213.85	185.09	145.55	114.38	434.39	421.94	661.82	638.59
Count	84	84	84	84	84	84	84	84
				Validation				
Max	1864.97	1256.00	1029.66	917.00	5395.39	4026.00	5737.65	5899.00
Avg	137.61	156.32	117.60	136.97	397.19	452.39	681.88	733.02
SD	364.40	255.67	254.42	221.59	980.63	918.74	1240.84	1354.94
Count	48	48	48	48	48	48	48	48

Note: *Max = maximum value; Avg = average value; SD = standard deviation; and Count = number of samples*

In this analysis, the peak flows for the year 2013 do not match due to the weakness of curve number methodology used in the SWAT model. Moreover, during calibration and validation the peaks for the Basoda, Garrauli, and Mohana sites have under-simulation as compared to the measured peak streamflow value (Figure 6.4). Only the Shahijina site has overestimated the streamflow simulation for maximum values (Figure 6.4 and Table 6.7). Also, the statistical analysis for monthly streamflow simulation shows satisfactory performance for maximum, average and standard deviation values (Table 6.7).

6.3.2.2 Sediment load

The calibration and validation of the SWAT model was further carried out for simulation of monthly sediment load of the Betwa River basin. During calibration, the high values of R^2 (0.89 and 0.78), NSE (0.89 and 0.77), the low values of PBIAS (-9.30 and -4.10) and RSR (0.33 and 0.48) indicates satisfactory to very good simulation of sediment load at the Garrauli and Shahijina gauges, respectively (Moriasi et al., 2007). During validation, the SWAT model performance also shows satisfactory to good simulation of the sediment load, with the high values of R^2 (0.90 and 0.81), NSE (0.90 and 0.81), the low values of PBIAS (0.70 and 1.60) and RSR (0.32 and 0.44) at the Garrauli and Shahijina gauges, respectively (Table 6.8 and

Figure 6.5). Simulated hydrographs are more or less following the measured hydrographs pattern. Result shows that this model is satisfactorily performing the sediment load simulation on monthly time-scale.

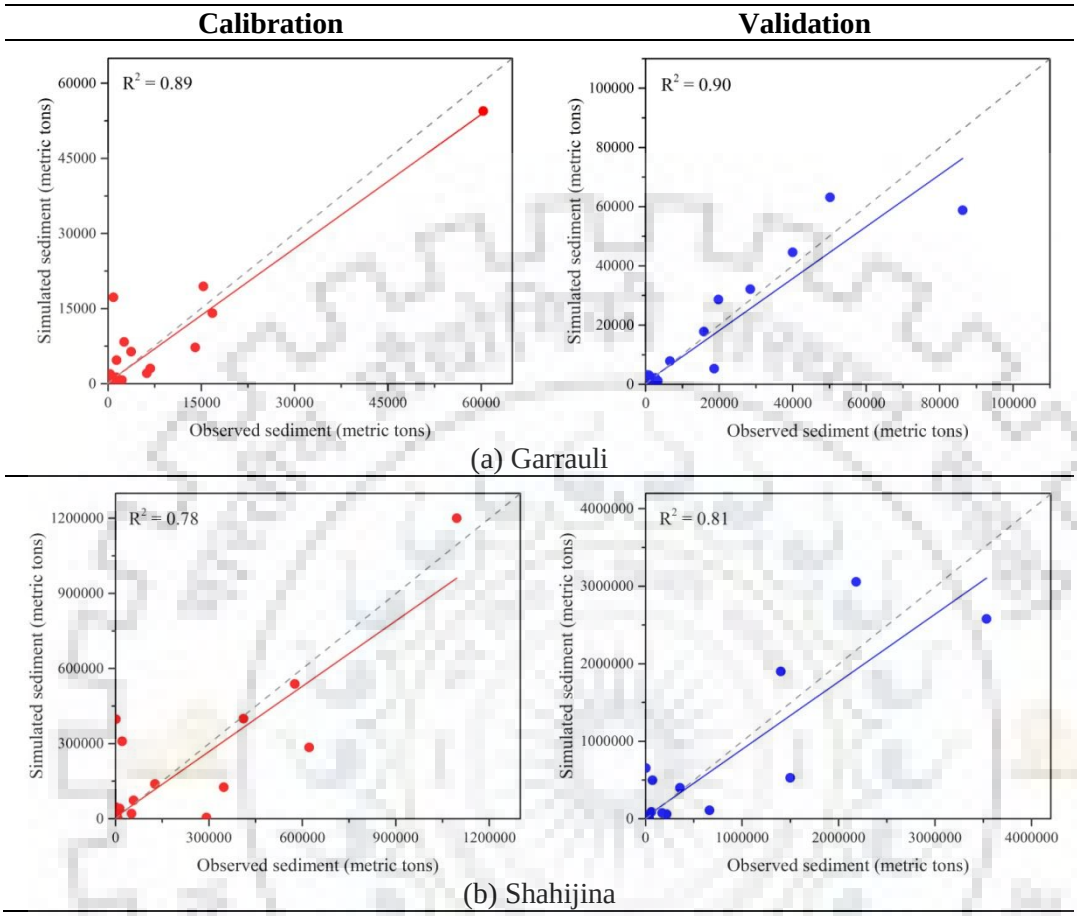

Figure 6.5: Linear regression between measured and simulated sediment load during calibration (2003-2009) and validation (2010-2013) for comparison with 1:1 trendline

Table 6.8: Performance evaluation of SWAT model for monthly sediment simulation

Gauging station	Calibration				Validation			
	R^2	NSE	PBIAS	RSR	R^2	NSE	PBIAS	RSR
Garrauli	0.89	0.89	-9.30	0.33	0.90	0.90	0.70	0.32
Shahijina	0.78	0.77	-4.10	0.48	0.81	0.81	1.60	0.44

In this analysis also, the peak sediment loads for the year 2013 do not perfectly match due to the weakness of MUSLE methodology used for simulation of the sediment in the SWAT model. Moreover, during calibration and validation the peaks for the Garrauli and Shahijina sites have low sediment simulation as compared to the measured values (Figure 6.6). Also, the monthly statistical analysis for sediment simulation shows satisfactory performance for maximum, average and standard deviation values (Table 6.9).

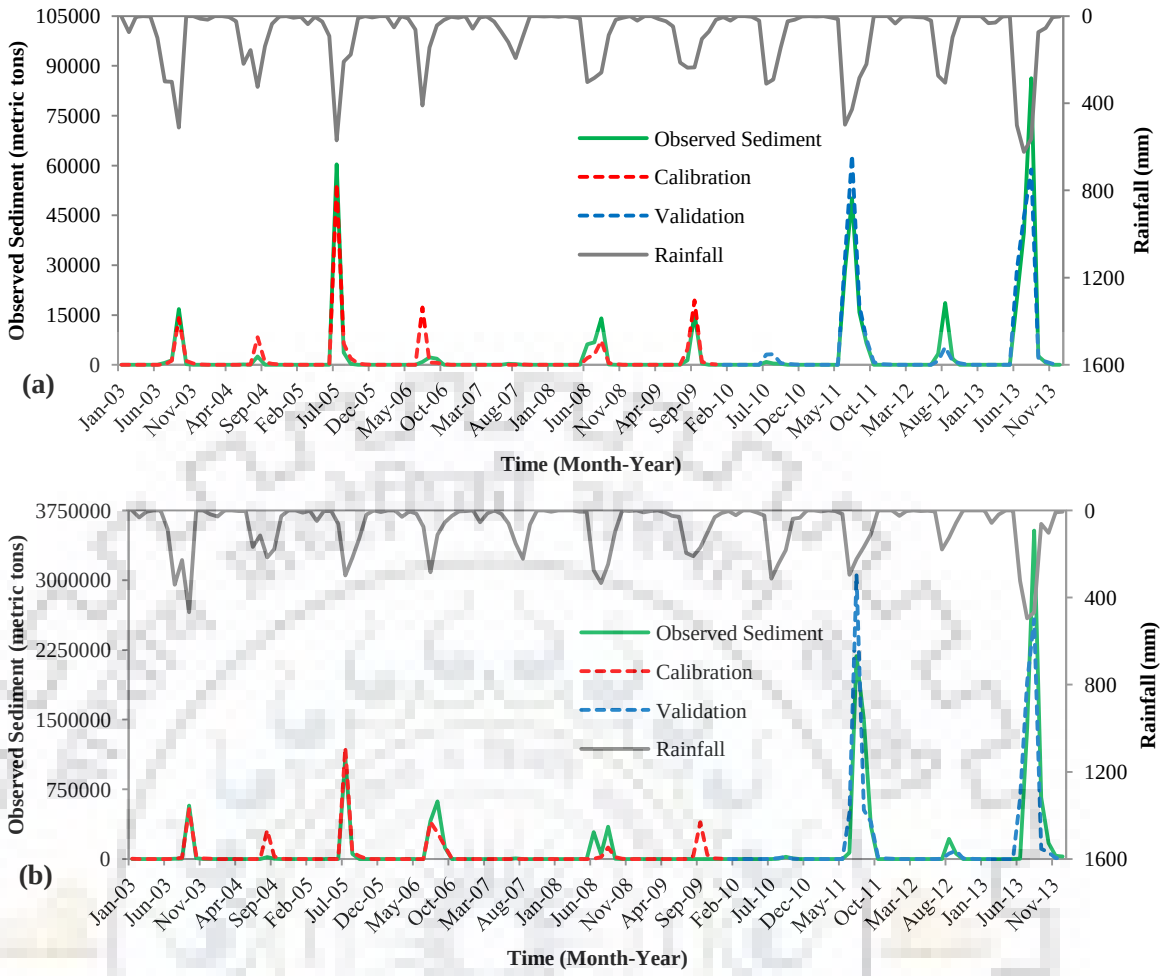

Figure 6.6: Comparison of measured and the SWAT simulated sediment load at (a) Garrauli and (b) Shahijina for monthly calibration (2003-2009) and validation (2010-2013)

Table 6.9: Statistical analysis of sediment during calibration (2003-2009) and validation (2010-2013)

Statistic	Garrauli		Shahijina	
	Measured	Simulated	Measured	Simulated
		Calibration		
Max	60322.51	54450.00	1096018.50	1200000.00
Avg	1620.63	1771.12	43420.49	45221.55
SD	7154.96	6753.48	161270.16	159157.50
Count	84	84	84	84
		Validation		
Max	86243.33	63170.00	3532665.25	3057000.00
Avg	5745.49	5702.41	213838.41	210392.64
SD	15865.13	14704.85	650904.10	629690.76
Count	48	48	48	48

Note: *Max = maximum value; Avg = average value; SD = standard deviation; and Count = number of samples*

The high R^2 value of streamflow at the Garrauli gauge (Tables 6.6 and 6.7) show that the model simulation performance is very good. Other gauging sites have the low R^2 values, which

might be due to the effect of water storage (reservoirs and weirs) structures in the SWAT model. In case of simulation of the sediment load also, the analysis shows the high R^2 value (0.89) at the Garrauli site as compared to the Shahijina (R^2 = 0.78) site. Similar model performance was also observed during the validation period (Tables 6.8 and 6.9). In addition, the low PBIAS values (about -8% to -4%) for the Mohana gauge (Table 6.6) indicate that the streamflow is well controlled and regulated owing to upstream water storage implementation and their management in the SWAT. Because of this, the sediment load is well simulated with low PBIAS values at the downstream Shahijina site (about -4% to 1.6%) as shown in Table 6.8. Overall, the model performance shows satisfactorily simulations of the streamflow and sediment load on monthly time-scale, and can be further used for water balance study, water resources assessment, and land use and climate change impact analysis.

The graphical results of the simulated streamflow and sediment load with measured data are presented in Figures 6.3, 6.4, 6.5 and 6.6. Analysis shows that model simulation is closely matching at the most of part, except during the year 2013 with high flow events which are underestimated by the model. The decrease in the model performance for simulation of the sediment may be attributed to the weakness of the SWAT, i.e. high-flow event simulation is based on many empirical and semi-empirical models, such as SCS-CN and MUSLE, which may be the cause for less accurate simulation of the streamflow and sediment load (Qiu et al., 2012).

The calibrated SWAT model is conditioned at various steps of the analysis, which includes the procedure, boundary conditions, objective function, and on the type and length of measured data used in the calibration, etc. (Abbaspour, 2011). SWAT model always performs better for a long term simulation as compared to the short term or single storm simulation (Borah et al., 2007). Also, the range of calibrated parameters for the streamflow and sediment load will not be identical, i.e. within the possible physically meaningful range of parameters, at different time-scale. Furthermore, if the model set-up changes because of the inputs obtained from different sources, then the calibration parameters can be different for each model set-up producing significant simulation results.

6.4 CONCLUSIONS

This study integrates satellite-derived products, gauge measurements, field based data and water storage information in the hydrological modelling of the BRB employing the ArcSWAT model. It is built-up in the ArcGIS modelling environment for simulation of the streamflow and sediment load in a large agricultural Betwa river basin of central India. The basin area was divided into 57 sub-watersheds comprising 3874 HRUs on the basis of unique soil, land use

and slope classes used in the modelling. Different water storage structures were implemented and managed for reliable hydrologic simulation. It is recommended to use spatial information obtained from remote sensing data for data scare regions of India. Initially, the SUFI-2 algorithm in the SWAT-CUP was used for sensitivity and uncertainty analysis. Then, based on sensitivity order, total 23 sensitive parameters were used for calibration and validation of the SWAT model for simulation of the streamflow and sediment load. In this study, the monthly calibration (2003-2009) and validation (2010-2013) of the SWAT model was carried out. Based on the SWAT modeling, following conclusions are drawn from this study:

1. Nine water storages of the Betwa basin, including 7 reservoirs and 2 weirs, located in main channel as well as tributary channel having significant effect on the river channel flow were successfully implemented and managed for reliable hydrological prediction using the SWAT model.
2. Sensitivity analysis reveals that the curve number (CN2) is the most sensitive parameter for streamflow, followed by SURLAG (surface runoff lag coefficient) to SOL_AWC (available water capacity of the soil layer). Whereas, the channel erodibility factor (CH_ERODMO) is the most sensitive parameter for sediment load, followed by USLE_K (soil erodibility factor for USLE equation) to USLE_C (minimum value of USLE C factor applicable to the forest area).
3. For calibration of the SWAT model, high value of R^2 in the range of 0.90 to 0.94; NSE of 0.88 to 0.92; PBIAS of -16.3 to -7.7; and RSR of 0.29 to 0.34, whereas for validation, high R^2 value in the range of 0.88 to 0.92; NSE of 0.84 to 0.91; PBIAS of -16.50 to -3.9; and RSR of 0.30 to 0.41 indicate accurate simulation of the monthly streamflow for the Betwa River basin.
4. The model performance for the monthly sediment load simulation at Garrauli and Shahijana gauges was also good during calibration with R^2 value ranges from 0.78 to 0.89; NSE value ranges from 0.77 to 0.89; PBIAS value ranges from -9.3 to -4.1; and RSR value ranges from 0.33 to 0.48, whereas validation with R^2 value ranges from 0.81 to 0.90; NSE value ranges from 0.81 to 0.90; PBIAS value ranges from 0.7 to 1.6; and RSR value ranges from 0.32 to 0.44.
5. The model simulation at Garrauli gauging site without any upstream water storage structure (no structure is available), showed high model performance as compare to the model simulation with upstream water storage (reservoirs and weirs) structure using SWAT.

6. This study reveals that the better information of the water storage structures promise a significantly improved hydrological simulation using the SWAT model.

CHAPTER 7

INDIVIDUAL AND COMBINED IMPACT OF LAND USE AND CLIMATE CHANGES ON HYDROLOGY OF BETWA BASIN

In this chapter, previously calibrated and validated Soil and Water Assessment Tool (SWAT) model has been used to simulate the water balance and sediment yield components under consideration of land use and climate change in the Betwa River basin. The model simulation has been initially used to assess the individual as well as combined impact of both land use change and climate change. For model simulation, the bias-corrected and downscaled CMIP5 GCM data has been utilized for the baseline 1986 period (1986-2005), and for four future climate periods, i.e. horizon 2020 (2020-2039), horizon 2040 (2040-2059), horizon 2060 (2060-2079), and horizon 2080 (2080-2099).

7.1 BACKGROUND OF THE STUDY

Land use and climate are the intrinsic drivers of hydrological processes (Blöschl et al., 2007; Juckem et al., 2008; Li et al., 2009). Human activities (such as reservoir construction, urbanization, and natural resource utilization) as well as climate change (mainly in temperature and precipitation variables) are widely acknowledged to be the main reasons of change in hydrological response of a river basin (Gao et al., 2010; Hovenga et al., 2016; Grum et al., 2017). Recent studies have demonstrated that land use and climate changes have significant impacts on water balance (Morán-Tejeda et al., 2010; Mango et al., 2011; Cornelissen et al., 2013) and sediment (Gebremicael et al., 2013; Khoi and Suetsugi, 2014; Julian and Ward, 2014). Thus, the surface water and sediment loads have significantly affected due to the World-wide land use and climate changes from last few decades (Gao et al., 2010; Miao et al., 2010; Zhao et al., 2014).

Land use change is observed progressively and abruptly by human-environment interaction, and due to the result of socio-economic and biophysical drivers (Lambin et al., 2001). The deforestation, urbanization and agricultural changes have pronounced their impact on soil erosion, flooding, drought and agricultural productivity which may cause the land degradation problems (Lørup et al., 1998). In addition to land use change, the climate change is generally characterized by shift in temperature and precipitation parameters. Temperature change induces more evapotranspiration, and affects the regional weather circulation pattern. This can leads to alter frequency and intensity of precipitation occurrence in the hydrological system which in turn can increase the frequency of flash flooding and potential risk to the environment. Soil erosion, a process of detachment, transportation and deposition of soil particles, is primarily the

result of extreme precipitation events. Climate change has an influence on soil erosion processes in terms of amount, concentration and distribution of the fluvial sediments in watersheds (Lal and Pimentel, 2008; Routschek et al., 2014). Thus, it is important to investigate to what extent climate change would impair the current conditions and hinder the future management.

In the past, various researchers have investigated the individual or combined impact of land use and climate change on hydrology (Niehoff et al., 2002; Juckem et al., 2008; Li et al., 2009; Setegn et al., 2011; Santos et al., 2014) and sediment or nutrients (Huang et al., 2009; Tu, 2009; Li et al., 2011; Bieger et al., 2015) in dissimilar watersheds under considerably different conditions (Gassman et al., 2007). Generally, a simple statistical method or the process-based models were used to study the runoff and sediment fluxes (including soil erosion and sediment transport). However, the process-based models are reliable for precise simulations under changing land use/climate conditions. Statistical or the non-modelling methods lack a physical mechanism which brings attention towards the use of physically based models for hydrological simulation at different scales. Among available hydrologic models, the Soil and Water Assessment Tool (SWAT) has been widely used across the globe to assess the land use and climate change impacts on water resources (Conradt et al., 2012; Kim et al., 2013; Khoi and Suetsugi, 2014; Hyandye et al., 2018). The SWAT model can incorporate climate projections from downscaled global climate models (GCMs) and regional climate models (RCMs) (Phan et al., 2011; Narsimlu et al., 2013; Shrestha et al., 2013; Jha and Gassman, 2014). In addition, some hydrological modelling studies have coupled land use and climate change using SWAT (Chen et al., 2005; Schilling et al., 2008; Semadeni-Davies et al., 2008; Park et al., 2011; Yan et al., 2013). Effect of land use and climate change is complex phenomenon, and can be disentangled by using the modelling framework with several scenarios. The scenario based simulations can provide potential effects of future changes which can be a basis for sustainability of available natural resources. Therefore, assessment of land use and climate change impacts on hydrological processes and sediment loads has great importance for sustainable management of water resources and land use planning. Thus, this study employed a modelling framework to investigate consecutive impacts of land use and climate change on water balance and sediment loads.

In this context, this study has been planned to investigate the isolated and coupled land use and climate change impacts on water balance and associated sediment loads in a large river basin, Betwa River basin, located in Central part of India. Apparently, maximum potential climate change can be used to inform and guide future management strategies based on water balance

and sediment yield response. This combined as well as individual study on land use and climate change shall be valuable for policymakers and Government agencies for efficient natural resources management.

7.2 MATERIALS AND METHODS

7.2.1 Data acquisition

Details of the study area, hydro-meteorological data, GCM data and spatial datasets (DEM, land use and soil data) used in the SWAT model set-up and run are provided in Chapters 3 and 6. The downscaled and bias-corrected CMIP5 MPI-ESM-MR model datasets have been used to prepare the future climate inputs. Calibrated and validated SWAT model with different land use maps and climate variables has been used to simulate the water balance and sediment yield components. All the required input information were provided in ArcGIS compatible raster datasets (GRIDS), vector datasets (shapefiles), and SWAT database formats. After all data formatting, the model inputs were used to assess individual as well as combined impacts of land use and climate change in future horizons.

In this study, land use data of the years 2013 and 2040 has been used for land use change analysis. Furthermore, numerous climate scenarios have been considered for the SWAT simulation based on GCM-derived climate inputs: baseline 1986: historical time-period 1986-2005; horizon 2020: future time-period 2020-2039; horizon 2040: future time-period 2040-2059; horizon 2060: future time-period 2060-2079; and horizon 2080: future time-period 2080-2099.

7.2.2 Assumptions and limitations

In this study, the individual as well as combined impacts of land use change and climate change on hydrological simulation has been assessed using the SWAT model. The curve number approach and the MUSLE are particular weaknesses of the SWAT model (Benaman et al., 2005). Thus, the selection of watershed model for hydrological simulation could be limitation of this study. The elevation levels and soil zones are assumed to be remained constant during analysis period.

To assess an individual impact of land use and climate change, the SWAT model is simulated by assuming one data type (land use or climate) changing while another data type is constant. For instance, the climate data was kept constant while assessing land use change impact, and the land use data was also kept constant while assessing climate change impact on water balance and sediment yield. The land use and climate change can produce individual as well as combined impacts on hydrologic simulations (Bronstert et al., 2002; Pervez and Henebry,

2015; Feng et al., 2016; Zuo et al., 2016). Therefore, this study assesses the individual as well as combined impacts of land use and climate changes on hydrology of a river basin employing a conceptual framework.

Present climate model dataset includes different CO_2 concentrations (such as RCP2.6, RCP4.5, RCP6 and RCP8.5). In this study, the use of such different RCPs can produce variation in the SWAT model simulation. Therefore, to avoid the effect of several RCPs on the model outputs, study is limited to use only one climate scenario (RCP8.5) which can induce maximum possible impact of CO_2 concentration in future. This may help in sustainable water resources planning and management considering maximum possible climate change impact.

7.2.3 Methodology

In this study, land use data of the year 2013 and 2040 has been used for land use change impact analysis. In addition, the station-wise observed historical climate data and the future climate data derived from CMIP5 GCM (MPI-ESM-MR model) datasets of RCP8.5 scenario were initially compared by some statistical measures (maximum, minimum, average values, standard deviation and root-mean-square error). After satisfactory evaluation, the GCM-derived climate data from historical to future periods has been used as an input to the calibrated and validated SWAT model. Detailed methodology flowchart used in this study is provided in Figure 7.1.

This study accomplishes analysis of individual as well as combined impact of land use and climate change on the hydrologic simulation, with respect to the baseline simulations obtained from the SWAT model. In baseline simulation, the land use map of the year 2013 and climate data of the years 1986-2005 were used as an input to the SWAT model. To study an individual land use change impact, the land use map of the year 2040 has been used while climate data (1986-2005) was same. To study individual climate change impact, the climate data of the future years 2020-2099 has been used with the same land use map (2013) of the baseline simulation. In the combined impact assessment study, the land use map of year 2040 and the climate data of years 2020-2099 have been utilized as changed inputs to the SWAT model. In this study, the model simulation was obtained using climate data of the years 2020-2099 which is divided into four future climate horizons (horizon 2020, horizon 2040, horizon 2060 and horizon 2080). Further, a conceptual framework has been employed to provide the model results on individual as well as combined impact study of the land use change and climate change on the basin hydrology.

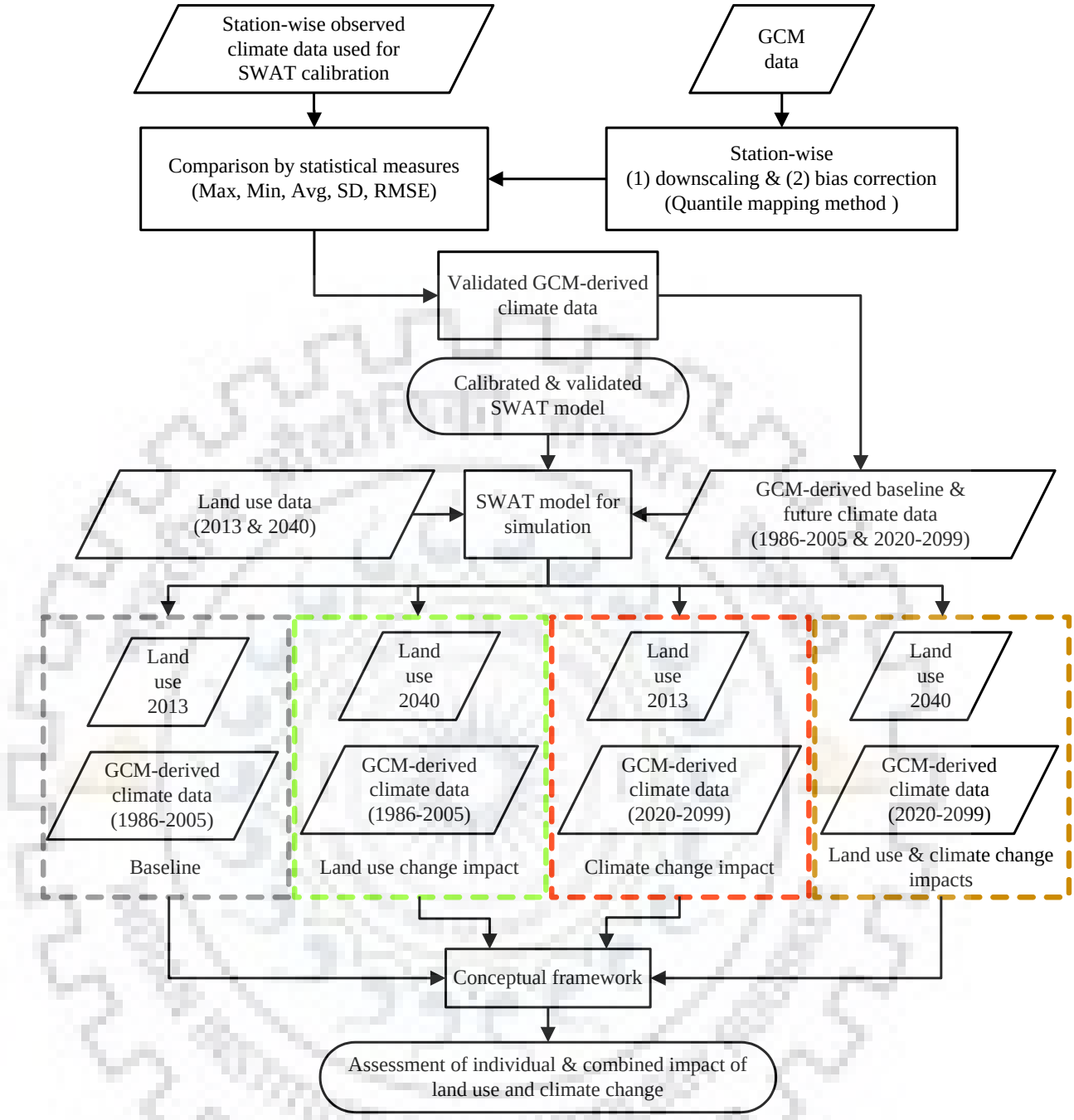

Figure 7.1: Methodology flowchart used for assessment of individual and combined impacts of land use and climate change

7.2.4 Scenarios for land use and climate change impact assessment

As discussed earlier, the present study aims to assess individual as well as combined impacts of land use and climate change on the model simulation. For this purpose, study considers four scenarios based on the input(s) used for model simulation (Table 7.1).

Table 7.1: Model simulation scenarios considered in the present study

Scenario	Land use data year	Climate data period	Remark
Scenario-1 (S1)	2013	1986-2005	Baseline
Scenario-2 (S2)	2040	1986-2005	Change in land use data
Scenario-3 (S3)	2013	2020-2099	Change in climate data
Scenario-4 (S4)	2040	2020-2099	Change in both land use and climate data

The SWAT model results for scenarios S1 and S4 represents actual simulation conditions during historical period and future period, respectively. Here, S1 indicates baseline simulation of the present study. The analysis of S2-S1 represents individual land use change impact, and the analysis of S3-S1 represents individual climate change impact on the model simulation. For combined impact assessment, the analysis of S4-S1 has been performed in the study. Based on the analyses, a conceptual framework has been further employed to furnish the model simulation results.

7.2.5 Conceptual framework

The conceptual framework represents an individual as well as the combined impacts of land use change and climate change (RCP8.5 scenario) with respect to the baseline simulation (Figure 7.2).

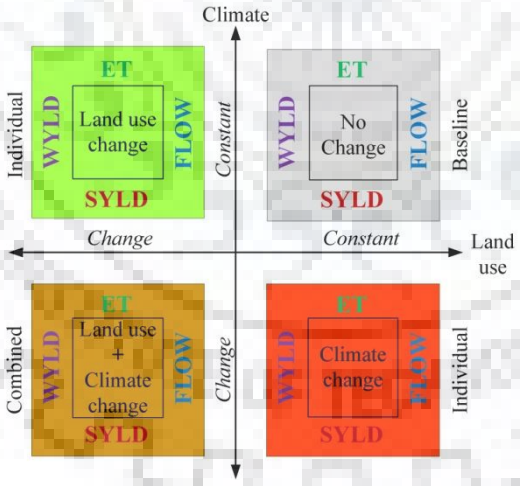

Figure 7.2: A conceptual framework to compare the individual as well as combined impacts of land use and climate change on hydrology

In this conceptual framework, two-dimensional Cartesian system has been used to divide it into four regions, known as quadrants, each limited by two half-axes of land use and climate. Here, the first quadrant represents the result of baseline simulation, second quadrant represents the results of individual land use change impact, third quadrant represents the result of combined land use and climate change, and fourth quadrant represents the result of individual climate

change impact. Within each quadrant, the four hydrology components streamflow (FLOW), sediment yield (SYLD), evapotranspiration (ET), and water yield (WYLD) are represented to study the impacts analysis. For the first time, this conceptual framework has been developed to study an individual as well as the combined impact of land use and climate change on the SWAT model simulation.

7.3 RESULTS AND DISCUSSION

7.3.1 Evaluation of GCM-derived climate data

In this study, the GCM-derived climate variables have been evaluated prior to use in the future simulation employing the SWAT model. This study uses numerous statistical measures, such as maximum, minimum, average, standard deviation and root-mean-square-error values, to compare the observed and the GCM-derived precipitation and temperature variables on daily, monthly and annual time-scales (Table 7.2).

Table 7.2: Statistical evaluation of observed and GCM-derived climate data

Statistic	Daily		Monthly		Annual	
	Observed	Downscaled	Observed	Downscaled	Observed	Downscaled
			Precipitation (mm)			
Max	103	159	560	707	1718	1757
Min	0	0	0	0	658	688
Avg	3	3	80	91	962	980
SD	7	10	125	151	267	286
RMSE	0.432		0.315		0.295	
			Maximum temperature (°C)			
Max	46.27	45.86	43.39	43.15	33.54	33.52
Min	13.48	17.44	21.33	22.96	31.44	31.52
Avg	32.71	32.40	32.70	32.39	32.71	32.40
SD	5.85	5.69	5.38	5.34	0.58	0.52
RMSE	0.091		0.088		0.087	
			Minimum temperature (°C)			
Max	31.07	32.42	28.62	29.24	20.18	20.30
Min	3.33	2.78	7.41	7.34	18.31	19.03
Avg	19.36	19.44	19.33	19.41	19.36	19.44
SD	6.32	6.56	6.07	6.30	0.52	0.39
RMSE	0.027		0.023		0.022	

Note: Max = maximum value; Min = minimum value; Avg = average value; SD = standard deviation; and RMSE = root-mean-square-error.

Result shows that minimum and maximum temperature variables have acceptable range of statistical measures. Average value of the observed and GCM-derived precipitation data has acceptable difference in maximum, minimum and mean value. However, the range of standard

deviation and RMSE values of GCM-derived precipitation differs little bit higher than the observed precipitation, but in acceptable range for RCP8.5 climate outputs. This may be due to the influence of downscaling and bias-correction methods used in the GCM-derived precipitation (Teutschbein & Seibert, 2012; Shrestha et al., 2016). Thus, the evaluation of downscaled and bias-corrected climate variables showed suitability of climate model outputs for the application in hydrological modelling. In this study, the GCM-derived climate variables (precipitation and temperature) have been further utilized as an input to the SWAT model for future hydrological simulation.

7.3.2 Changes in GCM-derived climatic variables

The climatic variables were categorized into the baseline period and four future climate horizons have been studied to understand the effect of future climatic variability with respect to the historic climate. This would also help to discuss the result of climate change impact analysis.

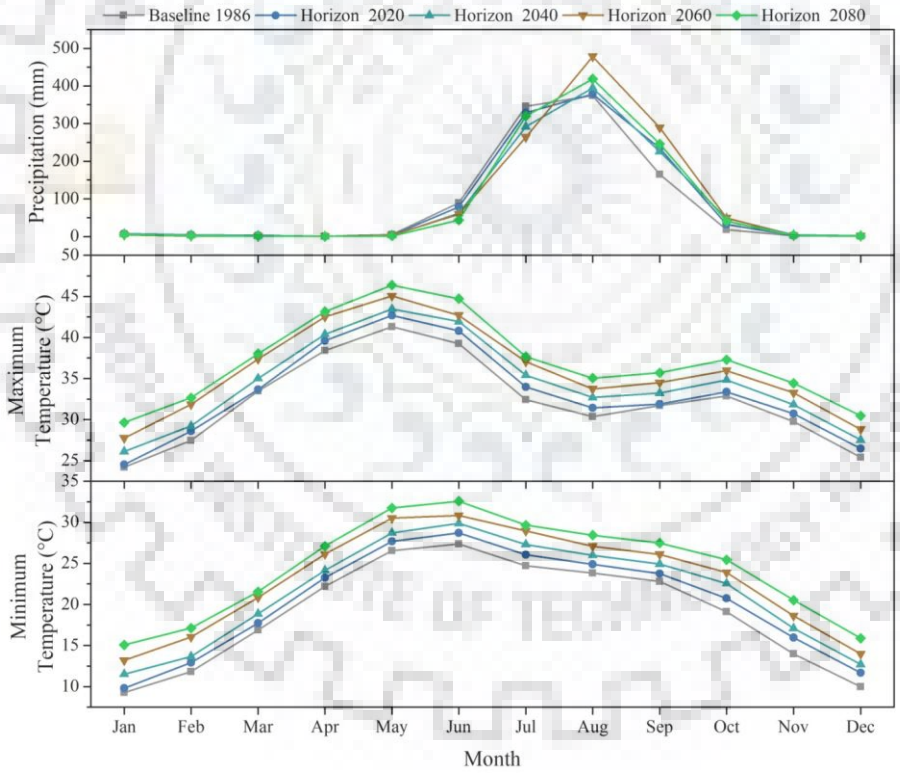

Figure 7.3: Monthly variations in GCM-derived climate variables

7.3.2.1 Precipitation

Figure 7.3 shows the monthly precipitation variations in four future horizons (i.e. horizon 2020, horizon 2040, horizon 2060 and horizon 2080) with respect to the baseline 1986 (1986-2005). Monthly plots show that the monsoon precipitation gradually increases from June to August,

and then decreases up to October month. However, in non-monsoon period the precipitation changes are non-significant as compared to the monsoon changes.

Amount of precipitation change in future has been estimated by calculating the difference between future horizon precipitation and baseline precipitation (Table 7.3). In horizon 2020, maximum decrease (17 mm) and increase (69 mm) in precipitation was obtained for July and September months, respectively. Similarly, during horizon 2040, maximum decrease (55 mm) and maximum increase (60 mm) in precipitation was obtained for July and September months, respectively. In horizon 2060, the highest decrease (82 mm) and maximum increase (124 mm) in precipitation was observed for July and September, respectively. Subsequently, in horizon 2080, maximum reduction (45 mm) and maximum increase (80 mm) in precipitation was observed in the months of June and September, respectively. Furthermore, maximum average annual precipitation change was observed for the horizon 2060, i.e. 140 mm, followed by horizon 2080 (69 mm), horizon 2020 (61 mm) and horizon 2040 (28 mm) (Table 7.3).

The result shows that horizon 2060 has a great monsoon precipitation variation, followed by horizon 2080, horizon 2020 and horizon 2040 as compared to the precipitation in baseline 1986 period. During monsoon period, more amount of precipitation decrease is observed in June and July; however substantial precipitation increase is observed in August and September. Similar findings were also observed in the literature studies by Guhathakurta and Rajeevan (2008), and Jayshankar et al. (2015) for Indian regions.

Table 7.3: Change in future precipitation (mm) with respect to baseline period

Month	Horizon 2020	Horizon 2040	Horizon 2060	Horizon 2080
Jan	0.55	-0.36	-2.84	-1.48
Feb	0.59	-0.12	-2.29	-1.29
Mar	0.88	-0.20	-1.28	-1.21
Apr	0.06	0.22	-0.04	0.11
May	-1.32	-2.02	-1.33	-3.70
Jun	-10.24	-27.60	-29.56	-45.35
Jul	-17.18	-54.61	-81.94	-26.36
Aug	3.28	19.88	103.40	44.00
Sep	68.93	60.07	123.99	80.52
Oct	13.88	29.51	30.65	22.45
Nov	0.60	1.99	0.34	0.56
Dec	0.62	1.49	0.57	0.54
Annual change	60.64	28.26	139.67	68.78

7.3.2.2 Maximum temperature

Figure 7.3 presents the variation of maximum temperature during four future climate horizons with respect to the baseline period (1986-2005). Analysis shows a clear distinct variation of maximum temperature from baseline 1986 to the future horizon 2080.

From Table 7.4, the maximum temperature of horizon 2020 increases from 0.19 °C (September, and March) to 1.57 °C (June). During horizon 2040, maximum temperature increase of 1.51°C to 2.97 °C was observed in September and July, respectively. Furthermore, in horizon 2060 the maximum temperature increases from 2.79 °C to 4.63 °C was observed in September and July, respectively. Also, the maximum temperature increase of 3.99 °C (September) to 5.47 °C (June) was observed in future horizon 2080. It is clearly observed that there is a gradual rise of maximum temperature in each future climate horizon with respect to the baseline. Thus, highest rise in maximum temperature (3.99 °C to 5.47 °C) was observed in the last future horizon 2080. The average annual maximum temperature also increases from 0.92 °C to 4.87 °C in future horizons (Table 7.4).

This analysis shows that increase in maximum temperature may be possible at the beginning month of monsoon season (June and July), and lowered at the end of monsoon season (September month). Similar results were obtained in the previous studies carried out by Revadekar et al. (2012), and Das et al. (2018) for India and the Western Himalayan region.

Table 7.4: Change in future maximum temperature (°C) with respect to baseline period

Month	Horizon 2020	Horizon 2040	Horizon 2060	Horizon 2080
Jan	0.32	1.90	3.56	5.45
Feb	1.12	1.75	4.37	5.17
Mar	0.19	1.54	3.92	4.55
Apr	1.21	2.00	4.10	4.75
May	1.36	2.15	3.74	5.06
Jun	1.57	2.70	3.45	5.47
Jul	1.54	2.97	4.63	5.23
Aug	1.05	2.31	3.36	4.67
Sep	0.19	1.51	2.79	3.99
Oct	0.48	1.95	3.08	4.41
Nov	0.97	2.08	3.51	4.69
Dec	1.05	2.11	3.40	5.05
Annual change	0.92	2.08	3.66	4.87

7.3.2.3 Minimum temperature

Changes in minimum temperature in future horizon with respect to the baseline are illustrated in Figure 7.3. It shows that changes in the minimum temperature are nearly similar to the

changes observed for maximum temperature, i.e. significantly rises from baseline 1986 to the last future horizon 2080.

The minimum temperature in horizon 2020 increases from 0.54 °C to 1.99 °C in January and November, respectively (Table 7.5). During horizon 2040, change in minimum temperature varies from 1.82°C to 3.44°C in February and October, respectively. In horizon 2060, this change again increases from 3.27 °C to 4.77 C in August and October, respectively. Highest rise in minimum temperature is observed for horizon 2080, i.e. increases from 4.62 °C (August) to 6.53 °C (November). Furthermore, annual change in minimum temperature may gradually increases from horizon 2020 (1.22 °C) to horizon 2080 (5.34 °C) as shown in Table 7.5.

The results of present analysis show that minimum temperature increases significantly in future period (2020-2099). In this analysis also, increase in minimum temperature (from 4.62°C to 6.53°C) has been observed for the last horizon 2080. High changes in minimum temperature are mainly observed for post-monsoon months (October and November) in all future horizons. However, low changes vary with climate horizons, i.e. for first two horizons 2020 and 2040 the low changes are observed for winter months (January and February), and for last two horizons 2060 and 2080 the low change has been observed for monsoon month (August). Thus, the pattern of change in annual minimum temperature varies seasonally in future horizons. Similar results were also reported in the studies carried out by Revadekar et al. (2012), and Das et al. (2018) for India and the Western Himalayan region.

Table 7.5: Change in future minimum temperature (°C) with respect to baseline period

Month	Horizon 2020	Horizon 2040	Horizon 2060	Horizon 2080
Jan	0.54	2.23	3.93	5.81
Feb	1.09	1.82	4.19	5.28
Mar	0.84	1.98	3.95	4.67
Apr	1.08	1.96	3.91	4.90
May	1.11	2.17	3.96	5.19
Jun	1.37	2.52	3.47	5.22
Jul	1.32	2.57	4.22	4.93
Aug	1.07	2.18	3.27	4.62
Sep	0.95	2.11	3.31	4.68
Oct	1.61	3.44	4.77	6.31
Nov	1.99	3.10	4.62	6.53
Dec	1.71	2.73	4.01	5.92
Annual change	1.22	2.40	3.97	5.34

7.3.2.4 Overview of GCM-derived climate variables

Based on the standardized annual rainfall anomaly, the dry and wet years have been categorized for baseline and four future climate horizon periods (Figure 7.4). It is observed

that, horizon 2060 has more effects of dry and wet spells. During horizon 2060 period (2060-2079), the year 2075 and 2078 would be the wettest and driest year, respectively, in future. Simultaneous occurrence of frequent dry and wet years in the same climate horizon (2060) reflects requisite of proper planning and management under changing climatic condition (Singh et al., 2014; Vinnarasi & Dhanya, 2016). The analysis of dry and wet year categorization has been further used to discuss the simulation results.

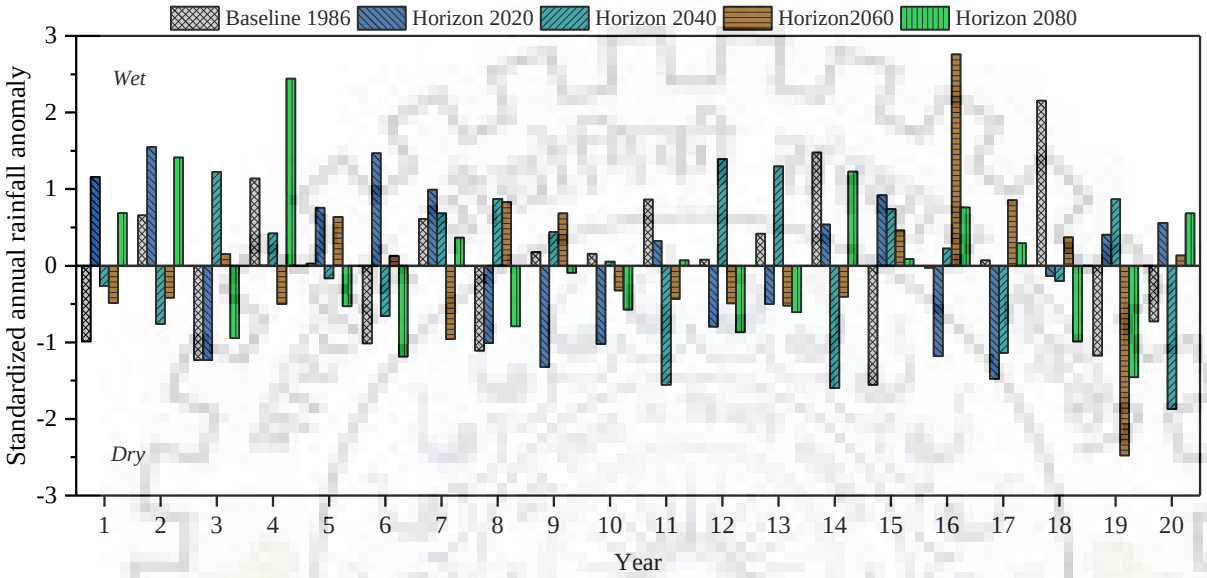

Figure 7.4: Standardized annual rainfall anomaly for categorization of dry and wet years during baseline 1986 (1986-2005), horizon 2020 (2020-2039), horizon 2040 (2050-2059), horizon 2060 (2060-2079), and horizon 2080 (2080-2099)

Table 7.6: Statistical summary of GCM-derived annual climate variables for baseline (1986-2005) and four future horizons (2020-2099)

Statistic	GCM-derived annual climate variables				
	Baseline 1986	Horizon 2020	Horizon 2040	Horizon 2060	Horizon 2080
	Precipitation (mm)				
Max	1657	1494	1449	1964	2097
Min	548	673	492	424	476
Avg	1013	1074	1041	1152	1082
SD	299	271	293	294	416
	Maximum temperature (°C)				
Max	32.93	33.97	35.92	36.87	39.12
Min	30.99	32.19	33.10	34.52	35.68
Avg	32.22	33.14	34.30	35.88	37.10
SD	0.42	0.63	0.76	0.61	0.78
	Minimum temperature (°C)				
Max	19.67	20.98	22.71	24.05	26.16
Min	18.35	19.56	20.57	21.70	23.20
Avg	19.04	20.27	21.45	23.01	24.38
SD	0.42	0.42	0.63	0.63	0.76

Note: Max = maximum annual value; Min = minimum annual value; Avg = average annual value; and SD = standard deviation of annual climate data.

After analysis of changes in the GCM-derived climate variables, their statistical summary was also studied for the baseline and future climate horizons. Table 7.6 shows maximum, minimum, average and standard deviations values for precipitation, and maximum and minimum temperature variables. Results show that the low precipitation about 424 mm and the high precipitation about 1964 mm have been observed for horizon 2060. Hence, during this period (2060-2079) pronounced effect of extreme dry and wet spells may induce hydrologic changes. Also, both maximum and minimum temperature variables are significantly increases in the future years (Revadekar et al., 2012). These changes need to be account for climate change impact study.

7.3.3 SWAT simulations using land use maps and GCM-derived climate data

After evaluation, the GCM-derived climate variables have been used as an input to the SWAT model to simulate streamflow, sediment yield (SYLD), evapotranspiration (ET) and water yield (WYLD). In this study, sub-watershed level analysis has been performed for each climate period, i.e. from baseline 1986 to horizon 2080, under varying land use maps of the years 2013 and 2040.

7.3.3.1 Streamflow (FLOW)

The sub-watershed outputs using land use map of the year 2013 show that baseline streamflow is high (>250 cumec) in sub-watersheds SW-1, SW-2, SW-4 and SW-5 located near to the outlet of the study area (Figure 7.5a). Furthermore, few sub-watersheds namely SW-6, SW-11, SW-17 and SW-32 have streamflow variation from 151 cumec to 250 cumec. These sub-watersheds can be considered as critical areas under high streamflow (more than 150 cumec). Furthermore, the SW-34 in horizon 2020 (Figure 7.5c); the SW-19, SW-20, SW-34 and SW-37 in horizon 2040 (Figure 7.5e); the SW-19, SW-20, SW-25, SW-34 and SW-37 in horizon 2060 (Figure 7.5g); and the SW-19, SW-20, SW-34 and SW-37 in horizon 2080 (Figure 7.5i) could produce more than 150 cumec streamflow. Thus, these sub-watersheds would be critical areas in upcoming decades. Due to high precipitation events in horizon 2060, the critical sub-watershed especially SW-6, SW-11 and SW-17 may have more than 250 cumec streamflow (Figure 7.5g). Also, during this period a high streamflow (201-250 cumec) may also be possible in SW-19, SW-20, SW-32 and SW-34 under changing climate. Thus, precipitation change can significantly affect the sub-watershed level future streamflow contribution in Betwa River basin area.

Similarly, the model simulation using land use map of the year 2040 show that the sub-watershed wise future streamflow is nearly similar to the outputs obtained under historical land

use map of the year 2013 in all climate periods. Only for the SW-6, the streamflow may increase in future horizons 2020 (Figure 7.5c&d) and 2040 (Figure 7.5e&f) under varying land use. It may be due to the decreased forest area which consequently increase non-vegetative land use, and generates more water flows in the SW-6. Bonell et al. (2010) observed such impacts of change in forest area on surface and sub-surface water flows in Western Ghats of India.

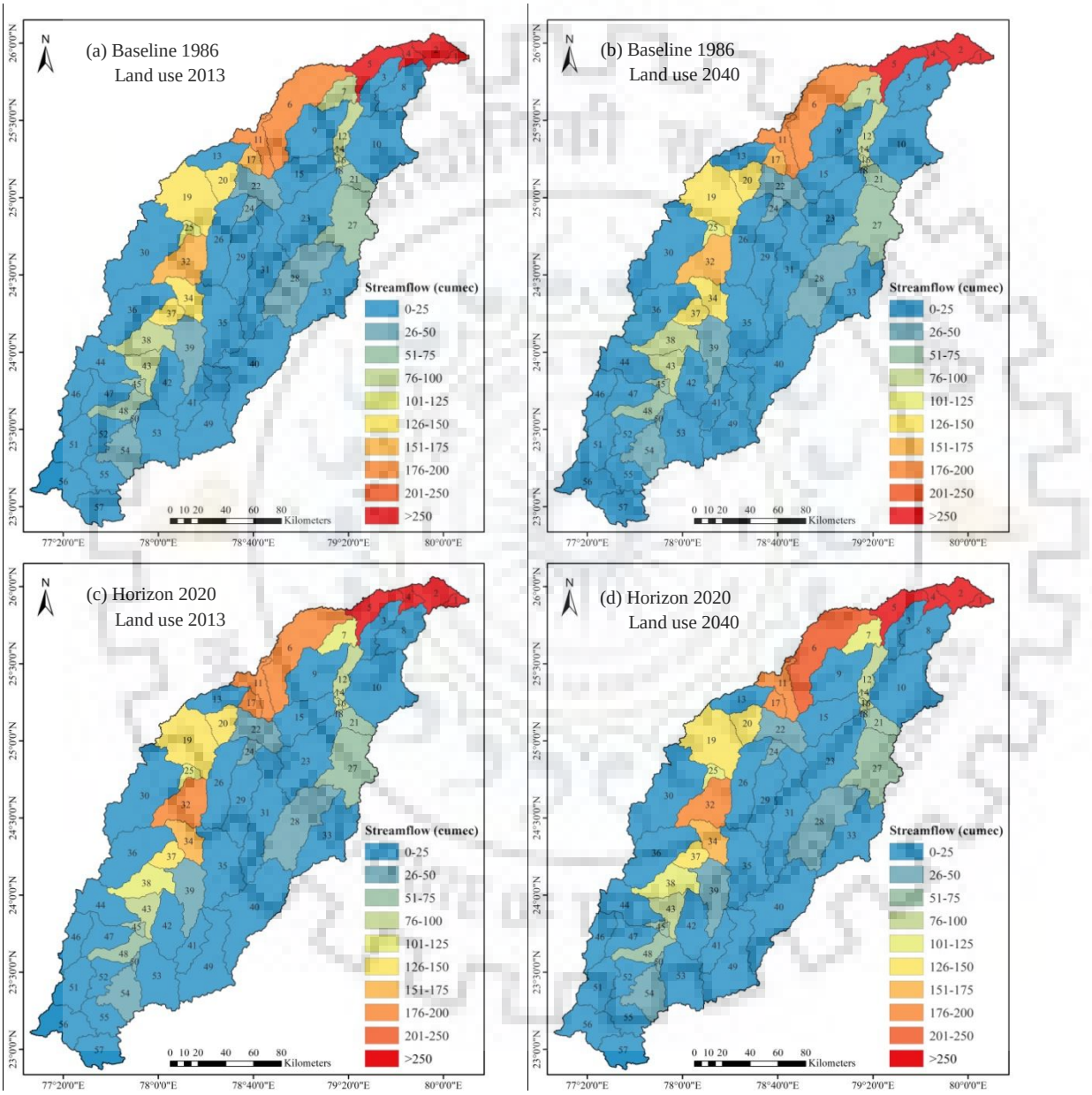

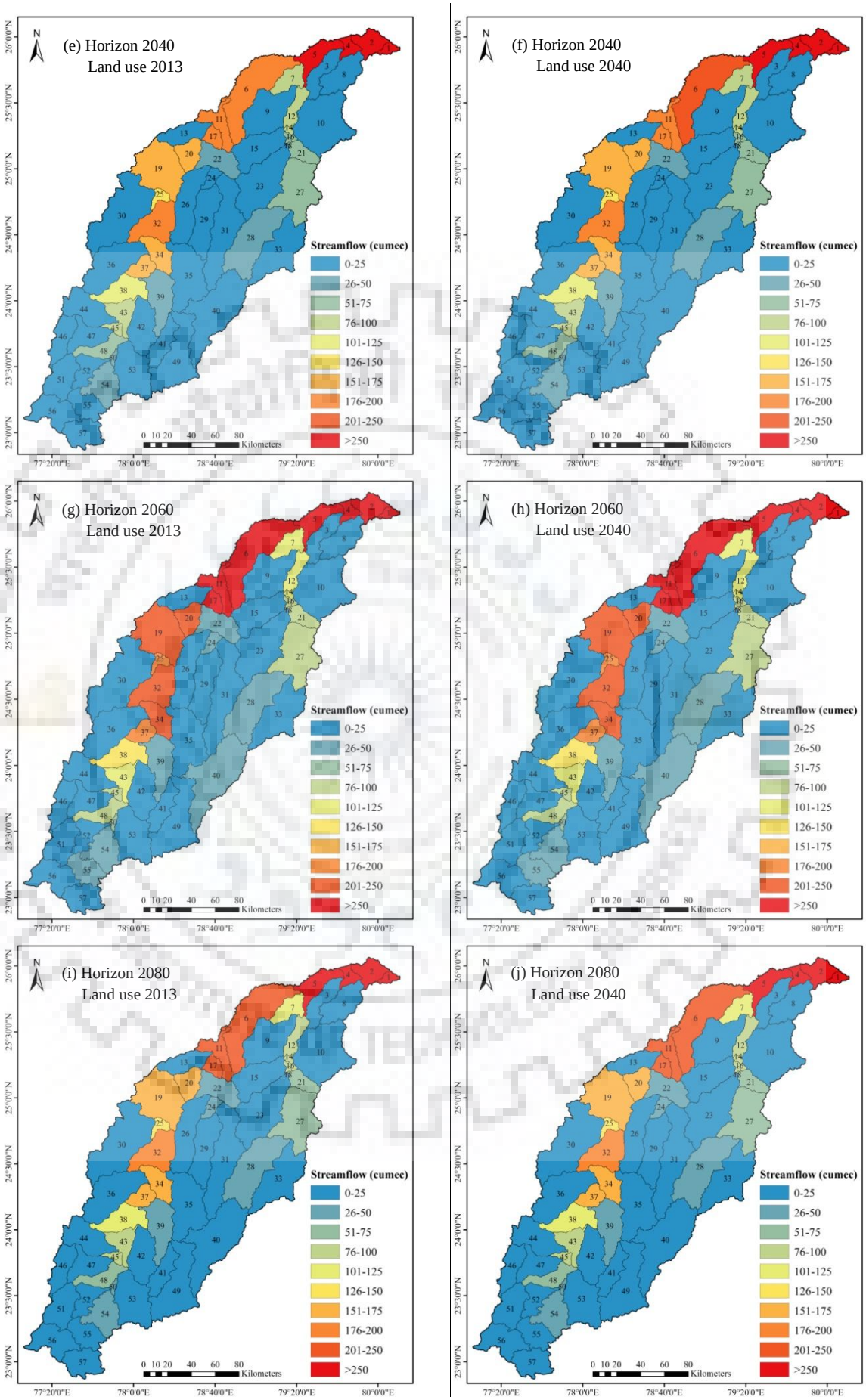

Figure 7.5: Streamflow (mm) variation under future land use and climate change

7.3.3.2 Sediment yield (SYLD)

During baseline 1986, the model simulation under land use map of the year 2013 shows that few sub-watersheds, namely SW-1, SW-4, SW-14 and SW-16, located near the outlet of the study area have high (about >150 t ha^{-1}) sediment yield (Figure 7.6a). These sub-watersheds can be considered as very severe soil erosion prone areas of the Betwa river basin. In these sub-watersheds, more soil erosion may be due to loose and fine soil surface with unfeasible field practices and less vegetation cover which eroded easily due to high velocity of upstream flows, and resulted more sediment loads (Maina et al., 2013). Furthermore, two sub-watersheds SW-2 and SW-17 having sediment yield between 40-80 t ha^{-1}, five sub-watersheds SW-5, SW-11, SW-12, SW-18 and SW-20 having sediment yield between 20-40 t ha^{-1}, the SW-7 has sediment yield between 10-20 t ha^{-1} can also be considered as the very high to medium class soil erosion areas. These sub-watersheds can be treated as critical areas under large amount of sediment yields (more than 10 t ha^{-1}). In future, the SW-34 may have more sediment yield, and thus can be considered as critical area for the treatment of management practices in the Betwa basin. It is observed that, the rate of sediment yield for these critical sub-watersheds varies under changing future climate condition from horizon 2020 to horizon 2080 (Figures 7.6c,e,g&i).

Similarly, the SWAT simulation using land use map of the year 2040 show that in all climate periods the sub-watershed wise sediment yield could be very similar to the sediment yield obtained under historical land use map 2013. Here also, only the SW-6 has increased sediment yield in future horizon 2040 under varying land use, i.e. decrease in vegetative cover (Figures 7.6e&f).

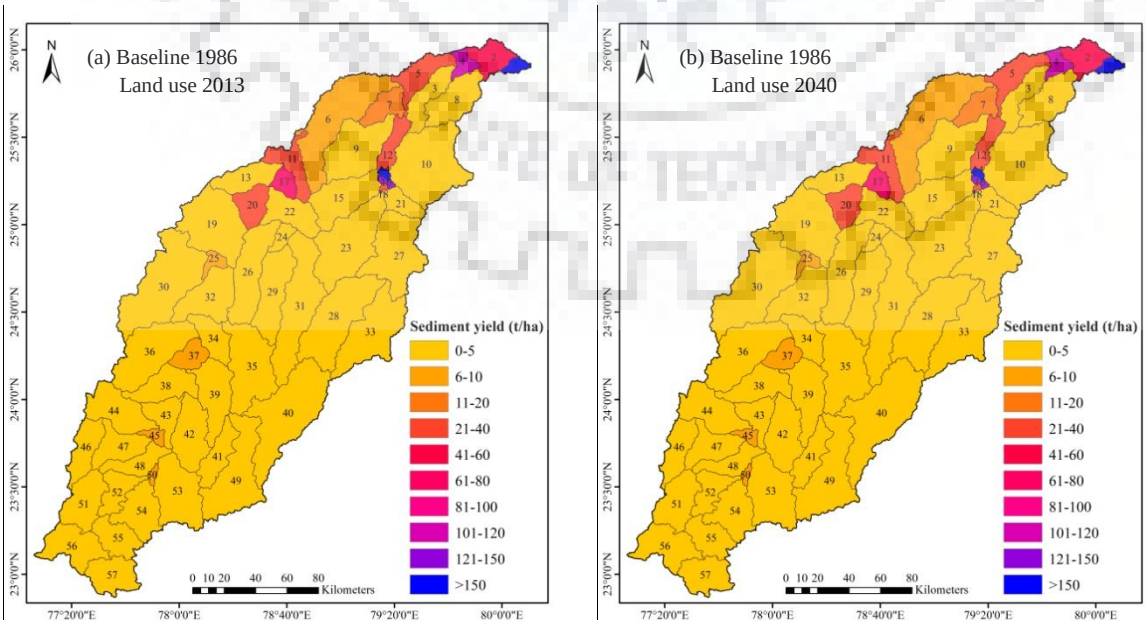

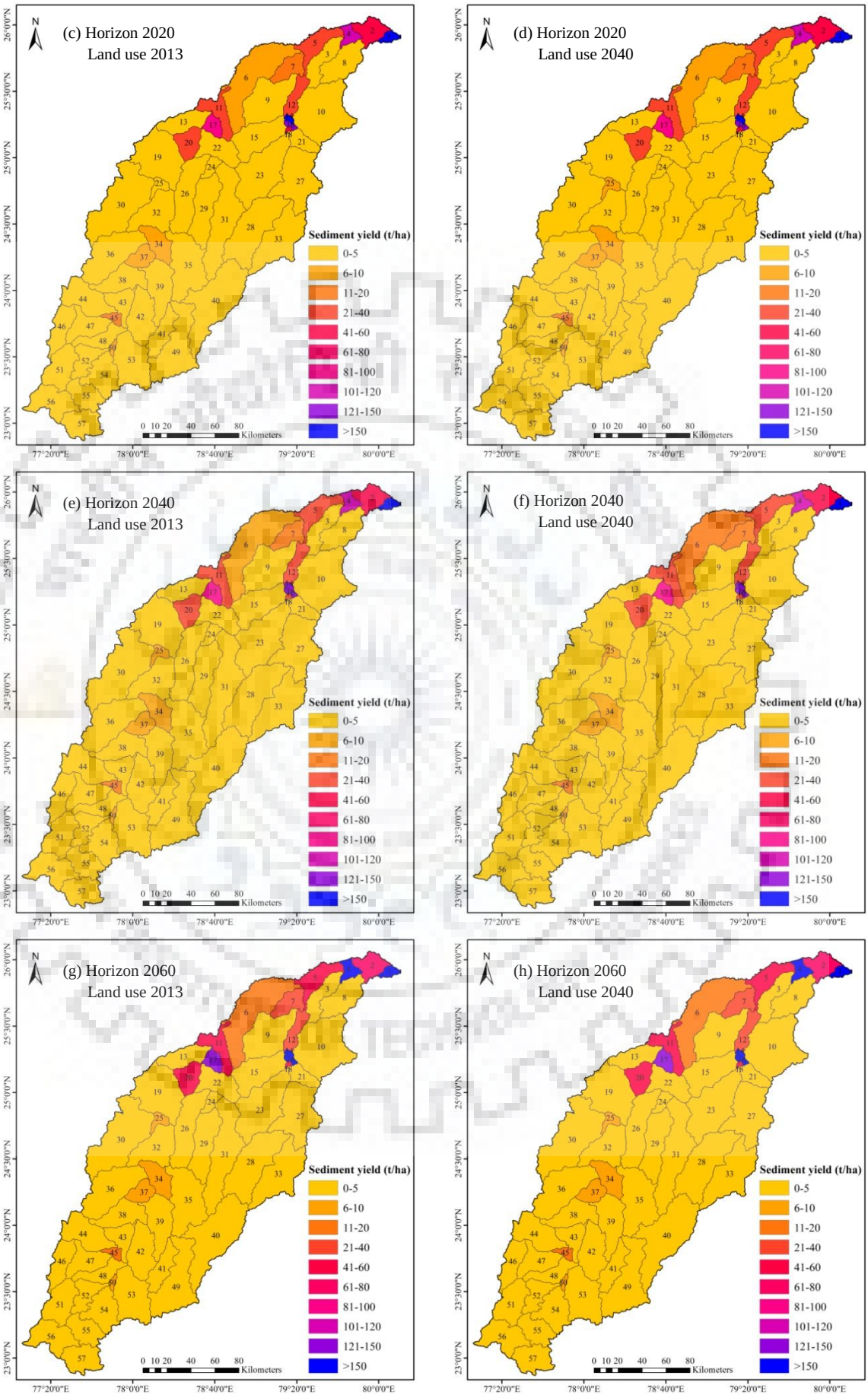
(c) Horizon 2020
Land use 2013
(d) Horizon 2020
Land use 2040
(e) Horizon 2040
Land use 2013
(f) Horizon 2040
Land use 2040
(g) Horizon 2060
Land use 2013
(h) Horizon 2060
Land use 2040
N
Sediment yield (t/ha)
0-5
6-10
11-20
21-40
41-60
61-80
81-100
101-120
121-150
>150
0 10 20 40 60 80
Kilometers
77°20'0"E
78°0'0"E
78°40'0"E
79°20'0"E
80°0'0"E
26°0'0"N
25°30'0"N
25°0'0"N
24°30'0"N
24°0'0"N
23°30'0"N
23°0'0"N

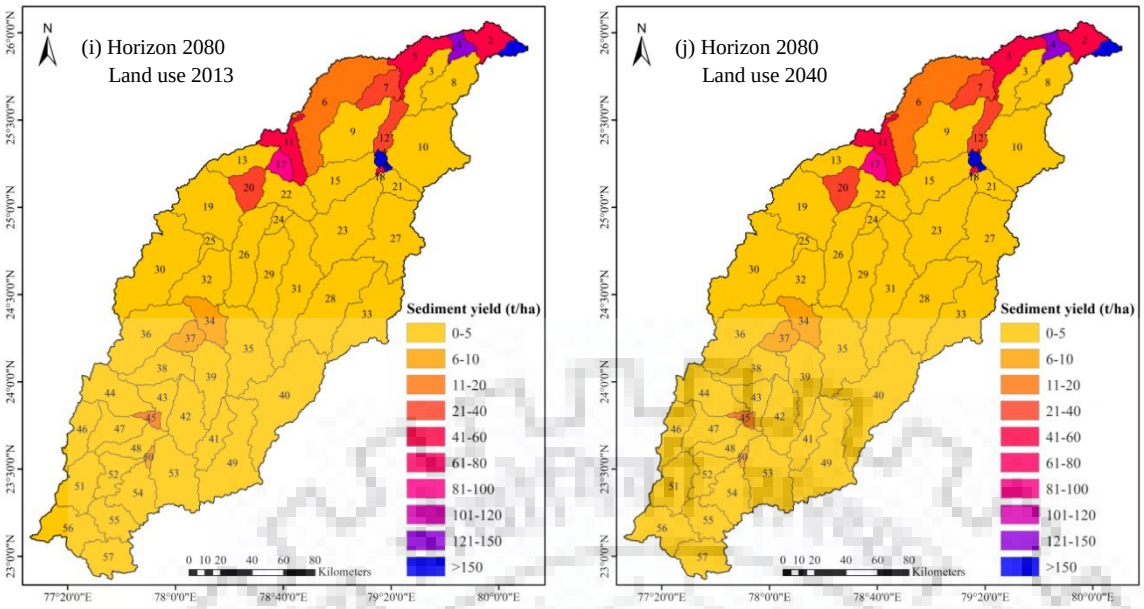

Figure 7.6: Sediment yield (t ha^{-1}) variation under future land use and climate change

7.3.3.3 Evapotranspiration (ET)

Results of ET simulation under land use map of the year 2013 show that the sub-watersheds namely SW-18, SW-19, SW-32 and SW-51 located in the middle and upper part of the study basin have more ET losses, i.e. more than 560 mm, during baseline period (Figure 7.7a). In these sub-watersheds, evaporation losses are mainly contributed from open surface of the large water storages (like reservoirs/weirs/lakes), mainly Rajghat and Matatila reservoirs. Several sub-watersheds are having ET loss in the range of 501 mm to 560 mm which is also contributed from surface evaporation of small to medium sized open water storages. Here, the rate of ET change varies with the future climatic condition from the horizon 2020 to horizon 2080. The sub-watersheds having more ET values can be considered as water loosing areas under vaporization (more than 500 mm). Also, it is observed that more ET losses could be possible in future horizons 2020 and 2040, because of rise in temperature during these horizons.

Nevertheless, the ET simulation has a significant changing pattern under land use of the year 2040. During baseline as well as future horizons, only SW-32 has high ET losses, i.e. more than 560 mm. Very few sub-watersheds have ET value in the range of 500-560 mm in baseline period (1986-2005) as shown in Figure 7.7b. But, in several sub-watersheds the ET value could be decreased due to changes in land use pattern in the future years (Figures 7.7d,f,h&j). Also, some sub-watersheds have increased ET losses. Especially, the SW-34, SW-39, SW-40, SW-41 and SW-49 may have high water losses during horizon 2020 and horizon 2040 under varying land use and a rise in temperature.

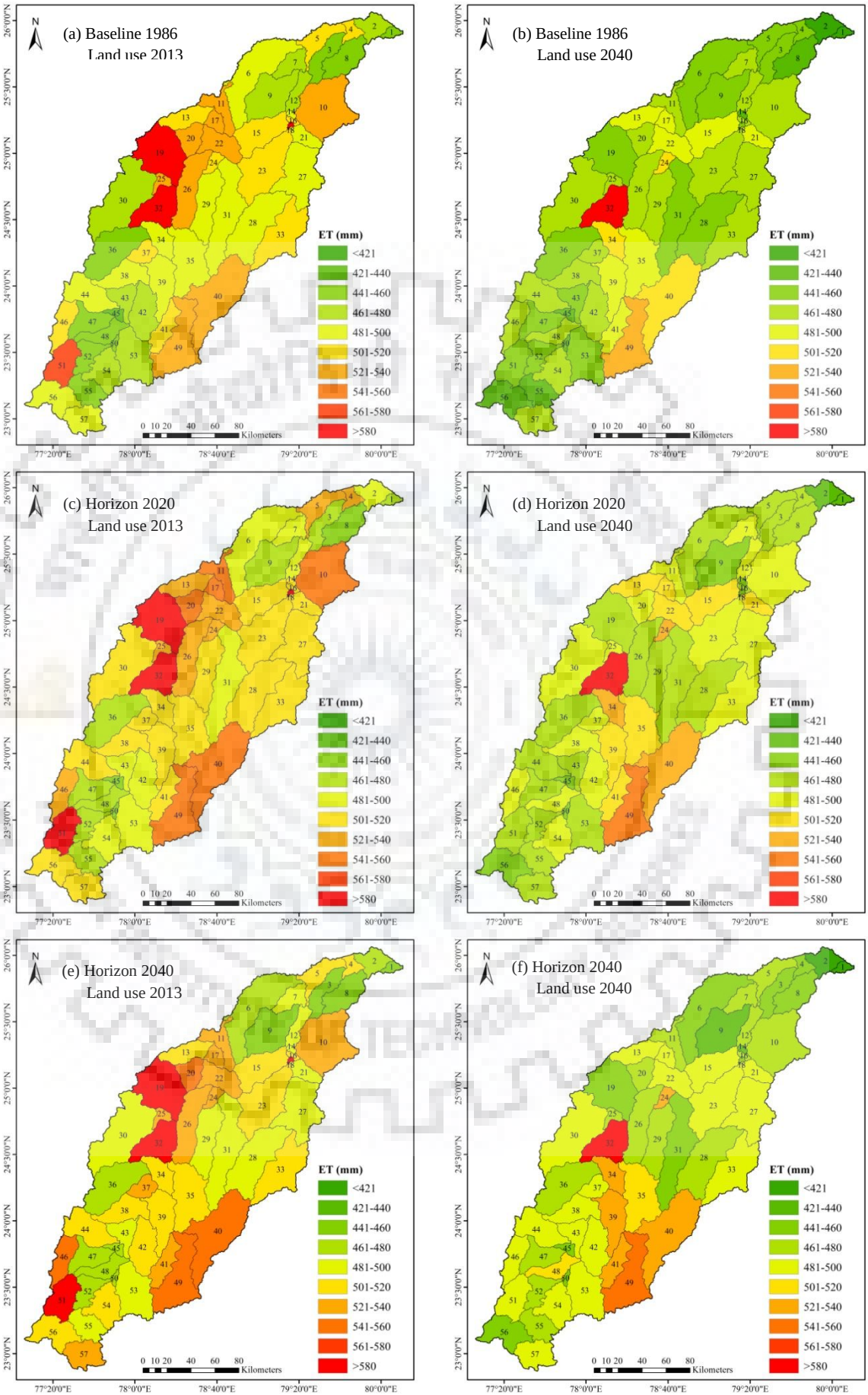
(a) Baseline 1986
Land use 2013
(b) Baseline 1986
Land use 2040
(c) Horizon 2020
Land use 2013
(d) Horizon 2020
Land use 2040
(e) Horizon 2040
Land use 2013
(f) Horizon 2040
Land use 2040
N
ET (mm)
<421
421-440
441-460
461-480
481-500
501-520
521-540
541-560
561-580
>580
0 10 20 40 60 80
Kilometers
77°20'0"E
78°0'0"E
78°40'0"E
79°20'0"E
80°0'0"E
26°0'0"N
25°30'0"N
25°0'0"N
24°30'0"N
24°0'0"N
23°30'0"N
23°0'0"N

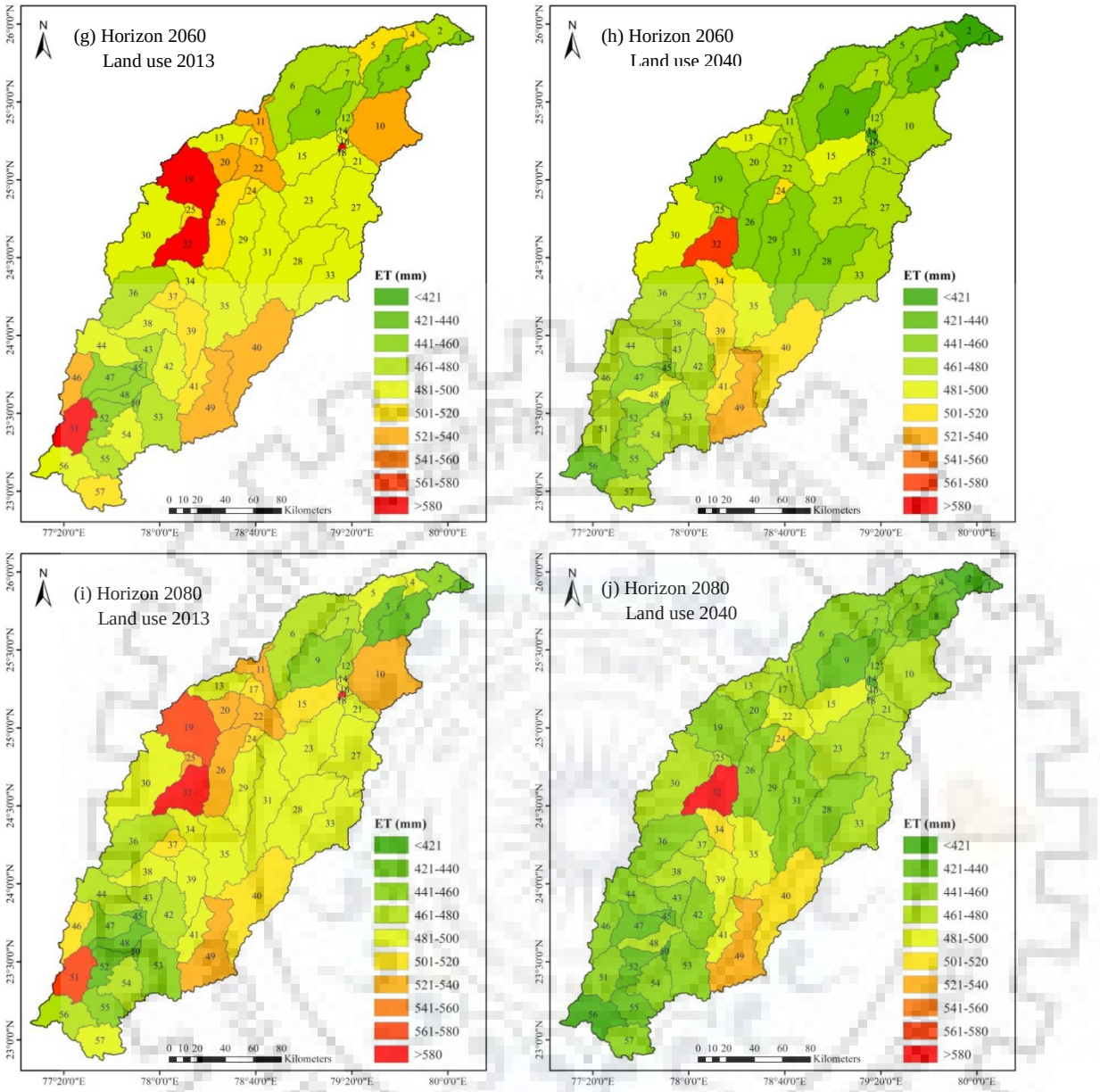

Figure 7.7: Evapotranspiration (mm) variation under future land use and climate change

7.3.3.4 Water yield (WYLD)

Water yield simulation using land use map of the year 2013 shows that sub-watersheds namely SW-35, SW-37, SW-38, SW-43, SW-44, SW-45, SW-47, SW-48, SW-50, SW-52, SW-54 and SW-57 located in the middle and upper part of the study basin have more water yields, i.e. more than 600 mm, during baseline period (Figure 7.8a). Result demonstrates that, in these sub-watersheds, the net amount of water contributed to reach is more than the other sub-watersheds of the Betwa basin. It may be because of high water utility for agriculture purpose in these areas. Also, dense (forest) vegetation cover is more in upper basin area which tends to store more amount of water in the field than losing it (Bosch & Hewlett, 1982). Furthermore, the sub-watersheds located in middle and lower basin area have a large amount of water yield (more than 600 mm). Rate of change in water yield varies with the future climatic variation

from horizon 2020 to horizon 2080. In horizon 2060, having high precipitation events, a significant amount of water yield (more than 550 mm) induces in all sub-watersheds, except for few sub-watersheds of the lower basin (Figure 7.8g). These sub-watersheds can be considered as more water affording areas of the Betwa basin. However, during horizon 2040, water yield contributing in lower basin area is less due to the effects of frequent dry spells. Similarly, the future water yield simulated using land use map of the year 2040 shows that the sub-watershed wise water yield would be similar to the water yield obtained under historical land use map of the year 2013 (Figures 7.8).

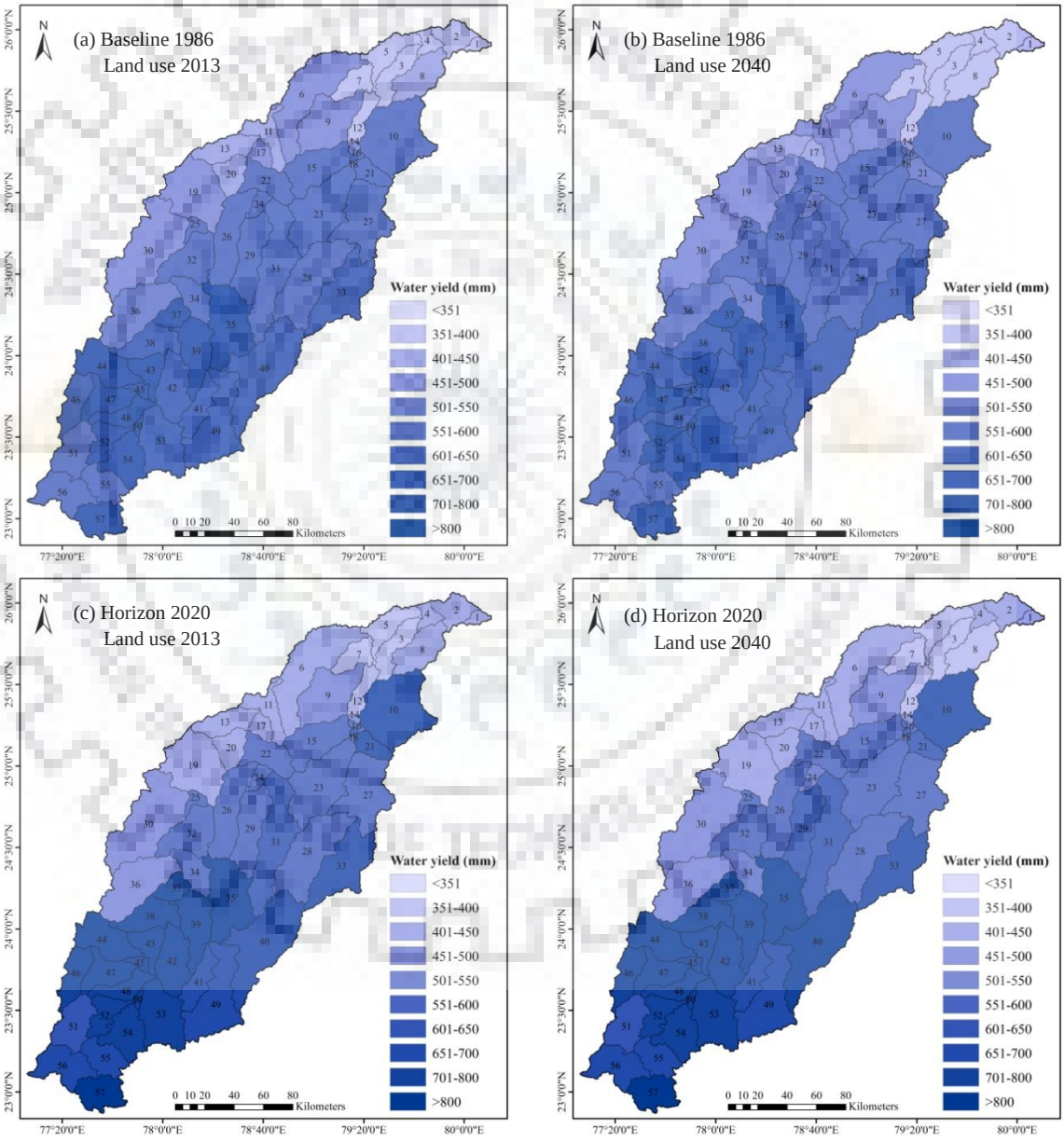

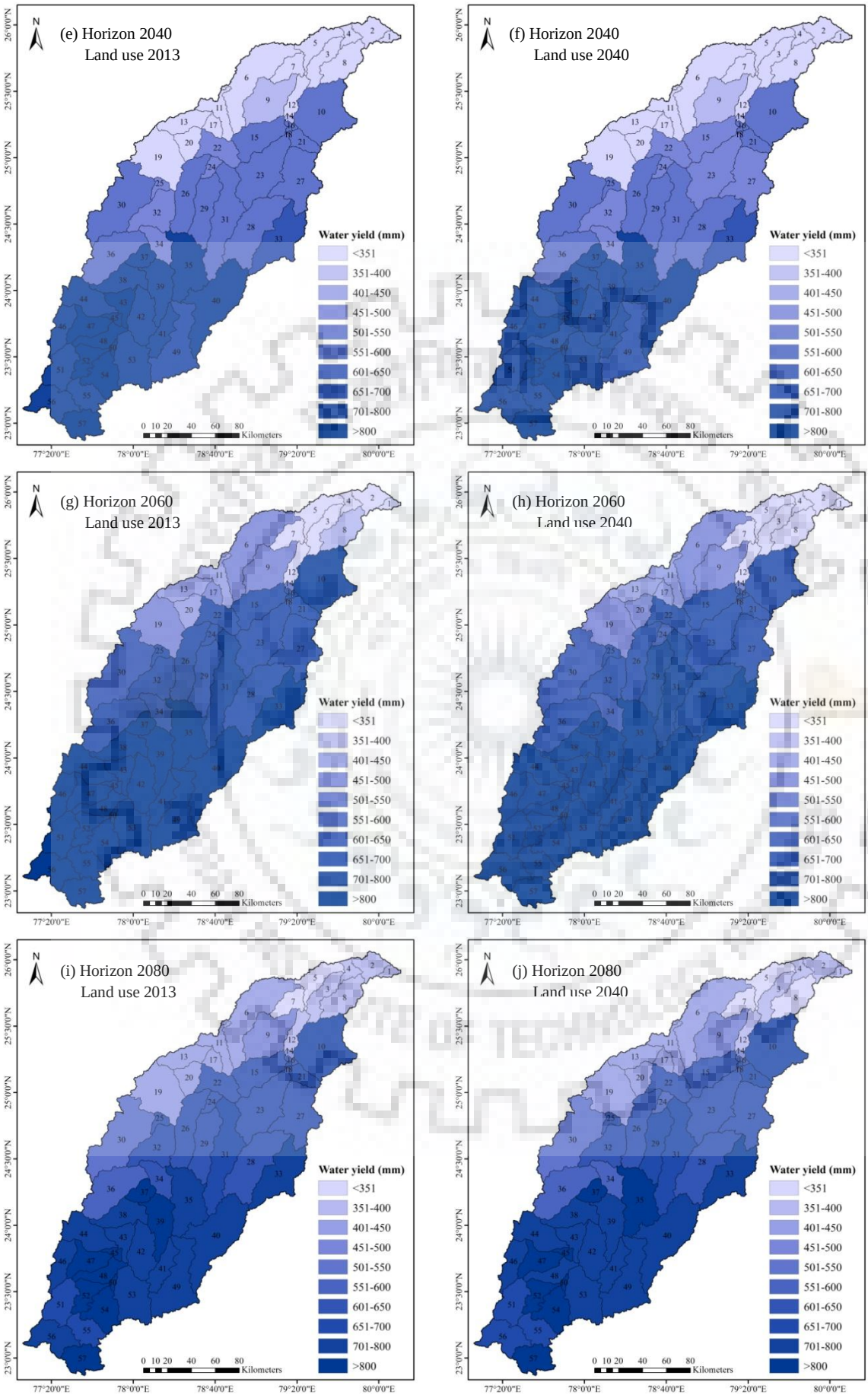

Figure 7.8: Water yield (mm) variation under future land use and climate change

7.3.4 Land use change impact assessment

As discussed earlier, the land use change impact has been assessed by subtracting scenario-2 and scenario-1 (S2-S1). In this study, scenario-1 is for a baseline simulation, and scenario-2 is for a simulation under change in land use map of the year 2013 by 2040, while keeping the same climate data (1986-2005) of the baseline.

7.3.4.1 Land use changes during 2013-2040

Initially, the study on land use changes has been carried out for the six historical land use classes, i.e. dense forest, degraded forest, agriculture, barren land, waterbody and settlement.

Results show that area under the dense forest rapidly changes in the range of 10-18% in SW-11, SW-13, SW-14, SW-19, SW-20, SW-23 and SW-27 (Figure 7.9a). Mostly, all the sub-watersheds have 1-9% changes or none significant change in dense forest area. Further, numerous sub-watersheds have increased the degraded forest area in future. Also, few sub-watersheds have decrease in degraded forest area, especially the SW-25, SW-33 and SW-40 have decrease of about 10-18%, and the SW-28, SW-28, SW-32, SW-34, SW-35, SW-41, SW-44 and SW-52 have decrease of about 1-9% (Figure 7.9b). The sub-watersheds with decrease in degraded area also have increase in agriculture area. It means several sub-watersheds of the Betwa basin may undergo inter-transitions between degraded forest and agriculture area. Among them, the SW-25, SW-32, SW-33 and SW-40 have 10-18% increase, and the SW-28, SW-35 and SW-41 have 1-9% increase in agriculture area (Figure 7.9c). Moreover, the SW-1, SW-2, SW-4, SW-22 and SW-24 also have decrease in agriculture area from the years 2013 to 2040. Overall, the upper-West, middle and lower parts of the Betwa basin would undergo decrease in agriculture area; hence the less food productivity problem may rise in future.

Furthermore, among non-vegetative area the barren land in SW-10, SW-21, SW-56 and SW-57 by 1-9% may decreases; however in other sub-watersheds the barren land may increases by 1-29% (Figure 7.9d). In most of the sub-watersheds, waterbody may decrease by 1-9%; except the SW-18 and SW-32 where siltation in reservoirs may result in low storage capacity, hence low water availability (Figure 7.9d). The settlement area in future may alter in numerous sub-watersheds which includes the SW-1, SW-3, SW-7, SW-8, SW-11, SW-14, SW-15, SW-16, SW-20, SW-21, SW-26, SW-37, SW-38, SW-39, SW-50, SW-51 and SW-56 having increased settlement area by 1-9% during 2013-2040 (Figure 7.9f).

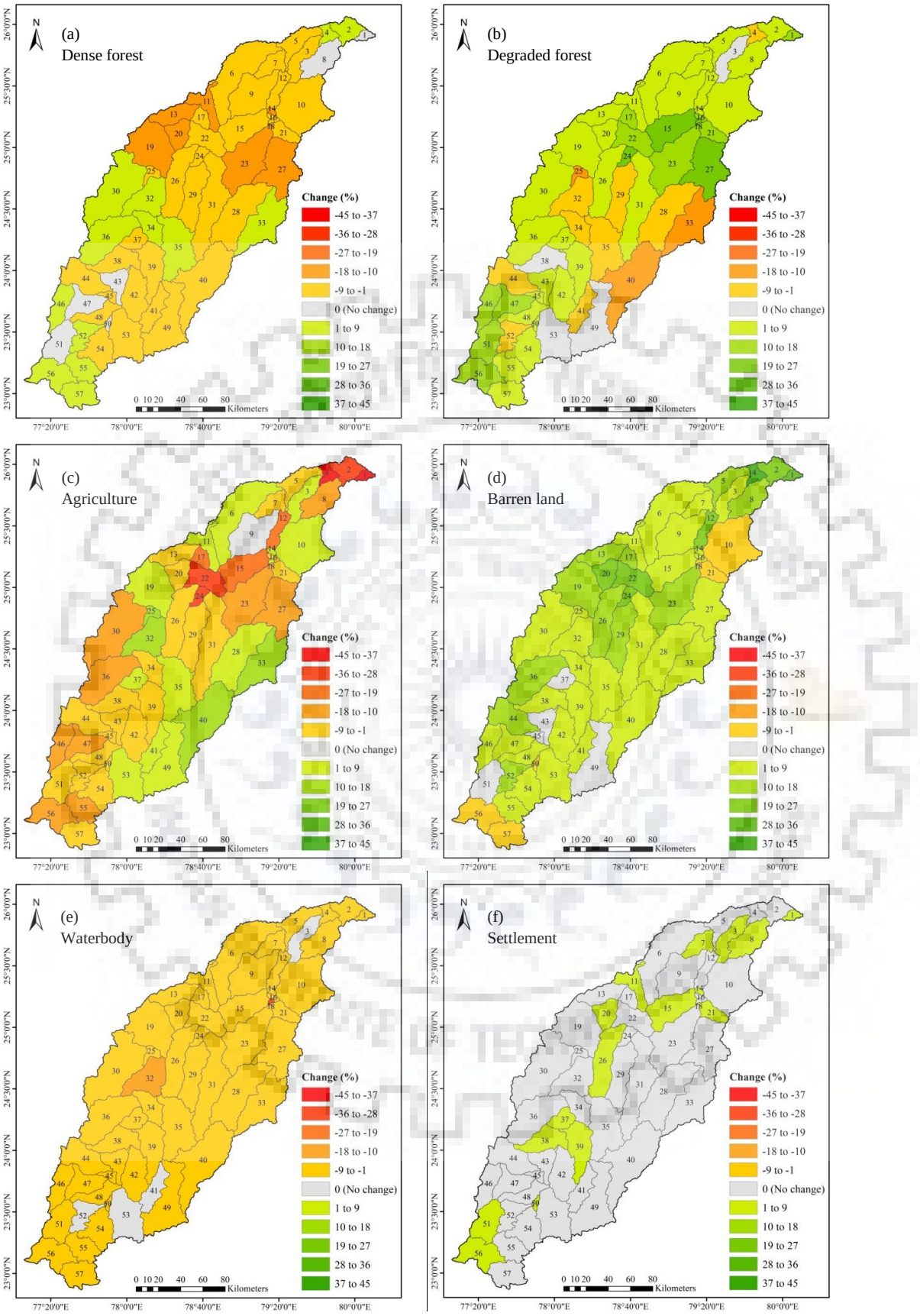

Figure 7.9: Spatial representation of percent land use (a) dense forest, (b) degraded forest, (c) agriculture, (d) barren land, (e) waterbody, and (f) settlement change during 2013-2040

Overall, dense forest and agriculture are the most rapidly decreasing vegetative areas, and the settlement and waterbody are the rapidly changing non-vegetative areas of the Betwa River basin.

7.3.4.2 Changes in SWAT simulation under varying land use

The SWAT model simulation at sub-watershed level has been analyzed using varying land use maps for the historical year 2013 and the future year 2040. Difference between baseline simulation (S1) and land use change simulation (S2) has been estimated to analyze their impacts on changes in streamflow, sediment yield, ET and water yield.

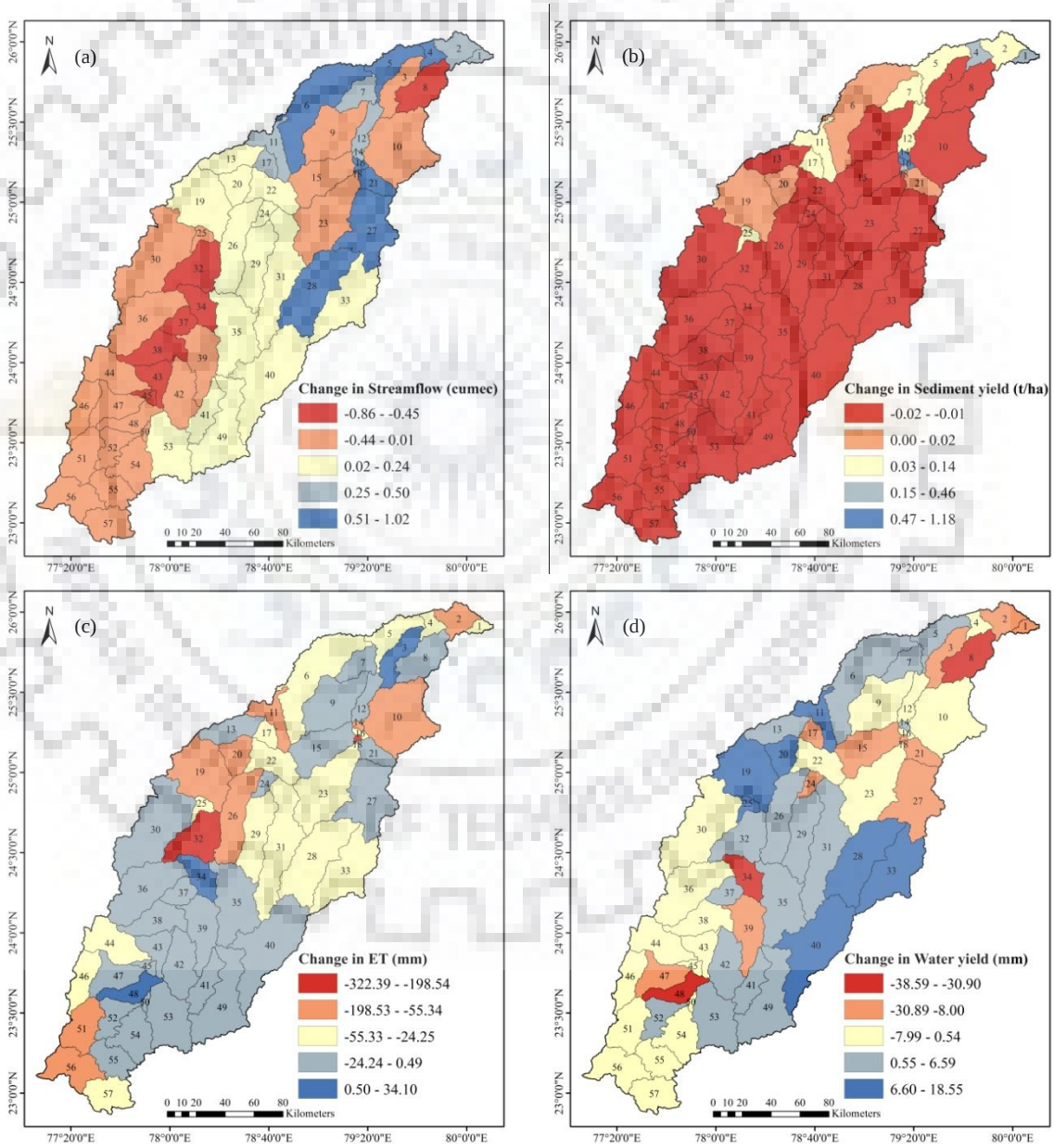

Figure 7.10: Spatial representation of individual land use change impact on SWAT simulations: (a) streamflow (cumec), (b) sediment yield (t ha^{-1}), (c) evapotranspiration (mm), and (d) water yield (mm)

Land use change simulation result shows that streamflow has decreased in upper part of the study area. Mainly, the SW-32, SW-34, SW-37, SW-38, SW-43 and SW-45 have decreased streamflow in the range of 0.45-0.86 cumec, and other sub-watersheds have streamflow reduction in the range of 0 to 0.44 cumec (Figure 7.10a). In lower basin, several sub-watersheds SW-4, SW-5, SW-6, SW-16, SW-18, SW-21, SW-27 and SW-28 have increased streamflow in the range of 0.51 to 1.20 cumec under land use change analysis. In these sub-watersheds, change in vegetative area, as resulted in previous analysis, may induce streamflow variations. Results of sediment yield simulation show that all the sub-watersheds have reduced sediment yields with decrease in water flow. Nevertheless, very few areas have increase sediment yield with increasing streamflow as shown in Figure 7.10b. Among them, the SW-6, SW-19, SW-20 and SW-21 have increase in sediment yield of about 0-0.02 t ha^{-1}; the SW-2, SW-5, SW-7, SW-11, SW-12, SW-17 and SW-25 have increase in sediment yield of about 0.03-0.14 t ha^{-1}; the SW-1, SW-4 and SW-18 have increase in sediment yield of about 0.15-0.46 t ha^{-1}; and the SW-14 and SW-16 have increase in sediment yield more than 1 t ha^{-1}. These changes in sediment yield are associated with the streamflow changes generated under varying vegetation areas at sub-watershed level.

Furthermore, the ET change is mostly negative in numerous sub-watersheds, where SW-18 and SW-32 have highest ET decrease of about 198-322 mm (Figure 7.10c). Increase in ET value of about 0.05-34 mm is observed for SW-3, SW-34 and SW-48 because of more evaporation under land use change. The water yield at sub-watershed level shows highest decrease of about 31 to 39 mm in SW-8, SW-34 and SW-48, and highest increase of about 7 to 18 mm in SW-11, SW-19, SW-20, SW-28, SW-33 and SW-40 as shown in Figure 7.10d. These changes in water yield are associated with the changes in vegetation and waterbody area of the Betwa basin.

7.3.4.3 Relationship between land use and the model outputs

In this analysis, a correlation method has been used to investigate the significance impact (at *p* value < 0.0.5) of land use change on model simulation at sub-watershed level. In this analysis, percent change in model simulations and percent change in each land use class was used to correlate the value of coefficient of determination (R^2).

Results show that changes in streamflow and sediment yields exhibited none significant relationship with the changes in land use classes as shown in Figures 7.11 and 7.12. In this analysis, the ET change has significant positive relationship (R^2 = 0.842, $p<0.05$) with the change in waterbody class (Figure 7.13). It demonstrates that ET is highly dependent on surface water evaporation than the vegetative water vaporization (transpiration). Figure 7.14 shows that water yield exhibited significant relationships with the change in dense forest (R^2 =

0.076, p<0.05), degraded forest (R^2 = 0.2, p<0.05) and agriculture (R^2 = 0.245, p<0.05). Here, the changes in both the forest areas are negatively correlated; however, the changes in agriculture are positively correlated to the changes in water yield of the Betwa basin. Thus, water yield is the most sensitive water balance component under land use change, mainly due to changes in dominant vegetation areas, i.e. dense forest, degraded forest and agriculture.

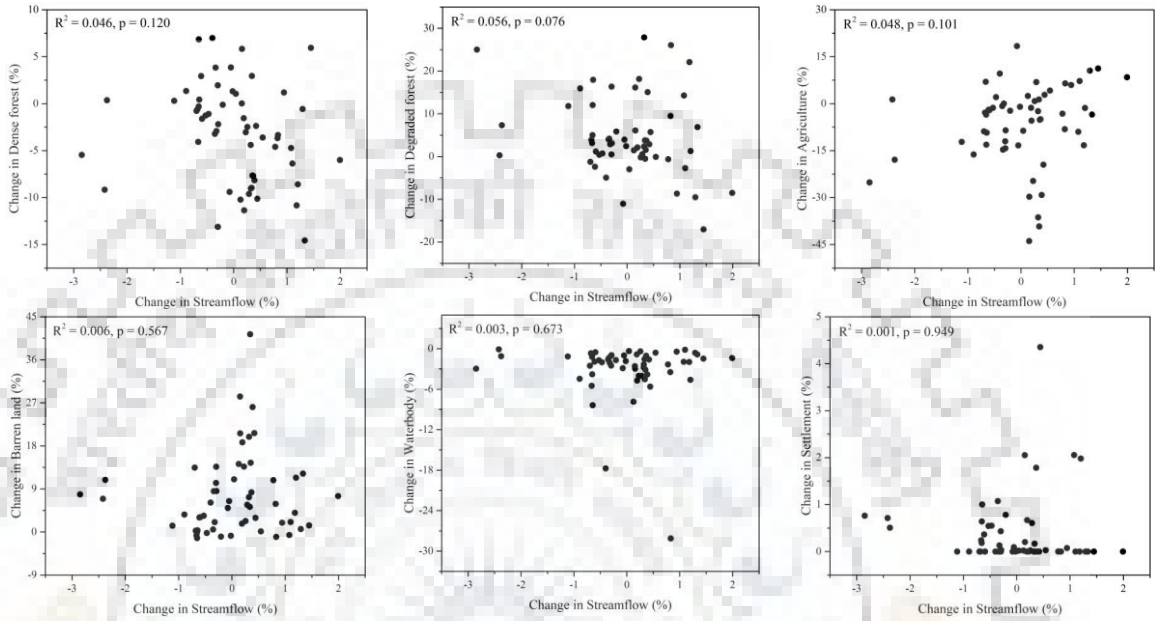

Figure 7.11: Change in streamflow (%) and its relation to the percentage of changed land use at sub-watershed level

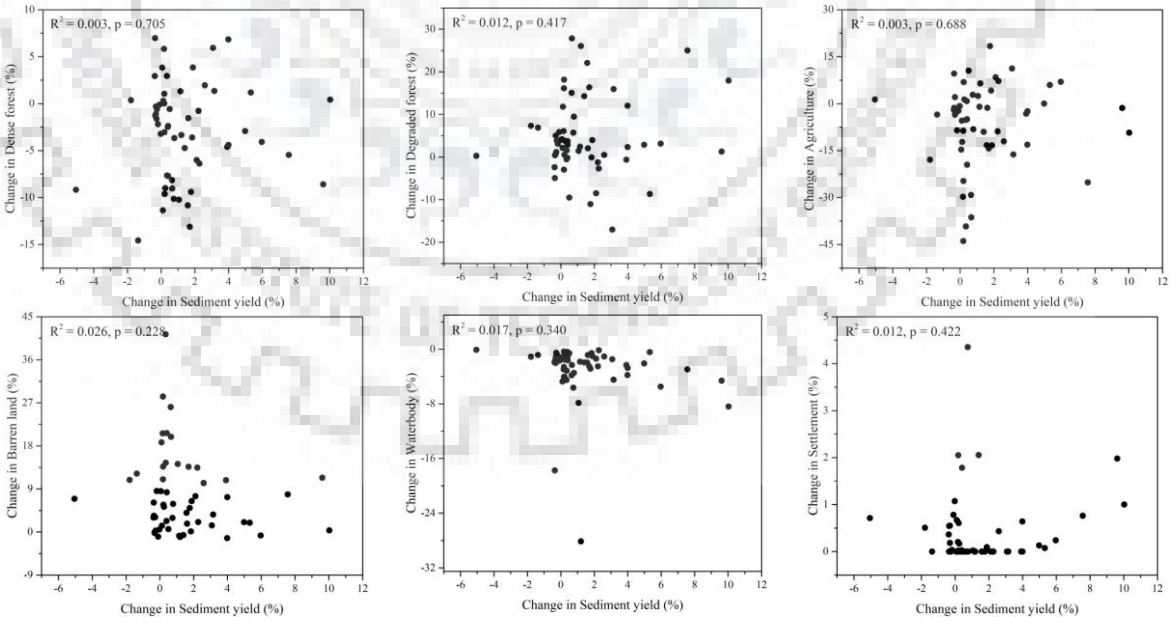

Figure 7.12: Change in sediment yield (%) and its relation to the percentage of changed land use at sub-watershed level

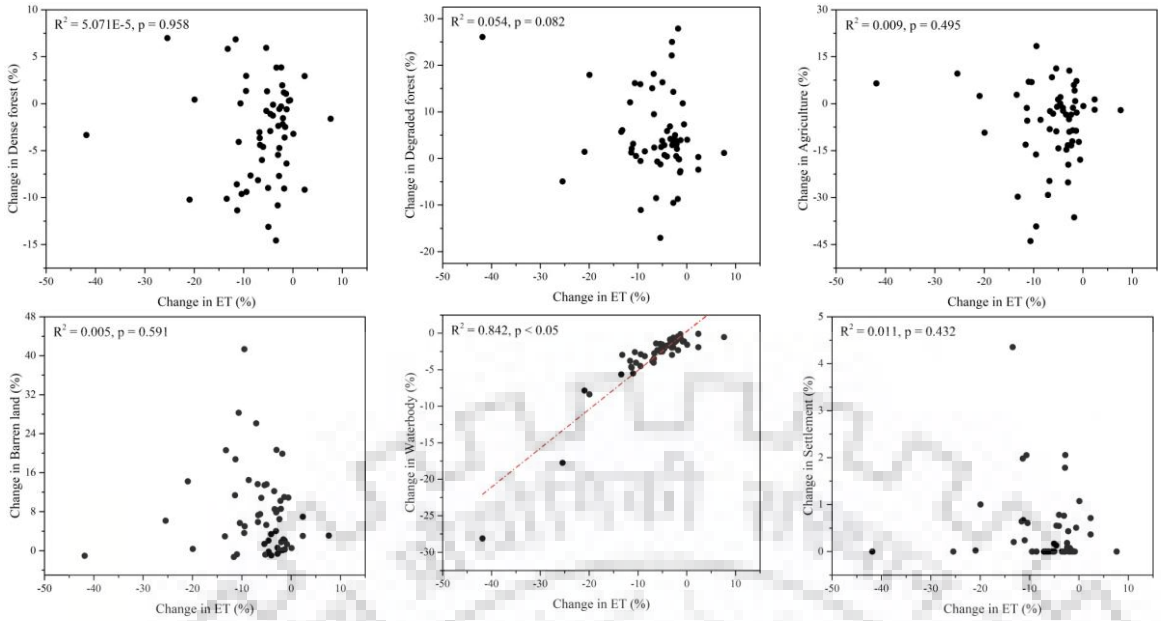

Figure 7.13: Change in evapotranspiration (%) and its relation to the percentage of changed land use at sub-watershed level

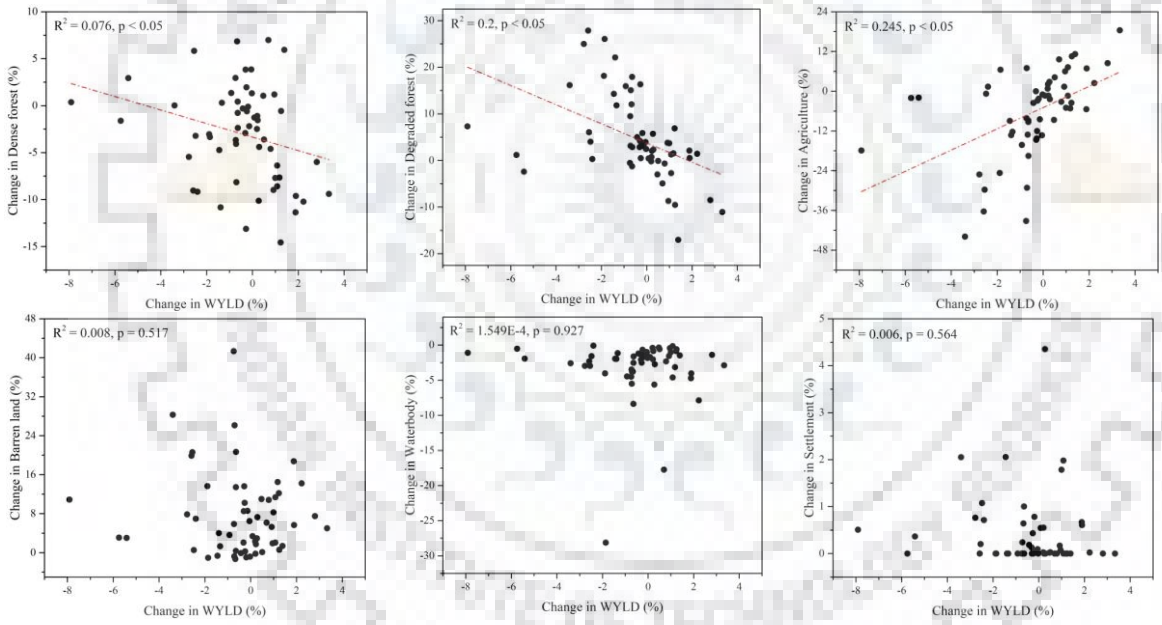

Figure 7.14: Change in water yield (%) and its relation to the percentage of changed land use at sub-watershed level

Overall, analysis reveals that the two water balance components, ET and water yield, are significantly influencing under land use change during the years 2013-2040. Three vegetation areas namely dense forest, degraded forest and agriculture, and the waterbody could have possible impact on these water balance components. Thus, vegetation planting and water conservation practices are essential to reduce and avert these land use change impacts on hydrology of the Betwa basin.

7.3.5 Climate change impact assessment

To assess the climate change impact on the model simulation, difference between scenario-3 and scenario-1 simulation (S3-S1) has been analyzed in the present study. Here, scenario-1 is for a baseline simulation, and scenario-3 is for a simulation under change in climate data of the period 1986-2005 by 2020-2099, while keeping the same land use data of the year 2013. In this study, impact of precipitation change has been mainly assessed at sub-watershed level.

7.3.5.1 Changes in future precipitation at sub-watershed level

At sub-watershed level, the analysis was performed to estimate the precipitation variation with respect to the baseline precipitation which shows remarked changes in future horizons as shown in Figure 7.15. Mostly, the upper part of the study basin receives increased precipitation amount in the range of about 71 mm to 140 mm during horizons 2020, 141 mm to 280 mm during horizon 2040, 281 mm to 363 mm during horizon 2060, and 71 mm to 210 mm during horizon 2080. Nevertheless, in middle and lower parts of the basin, the precipitation amount decreases in all future horizons. During horizon 2040, precipitation decrease (127 mm) and increase (280 mm) were observed for lower and upper basin area, respectively (Figure 7.15). Furthermore, a large variation in precipitation distribution in horizon 2060 may induce dry and wet spells in the study area. Hence, the future precipitation changes can influence hydrology of the Betwa basin.

Therefore, the future precipitation pattern with respect to the baseline precipitation shows significant changes, thus, their impact on the hydrologic components needs to be quantified for adaptation and mitigation strategies in the study area.

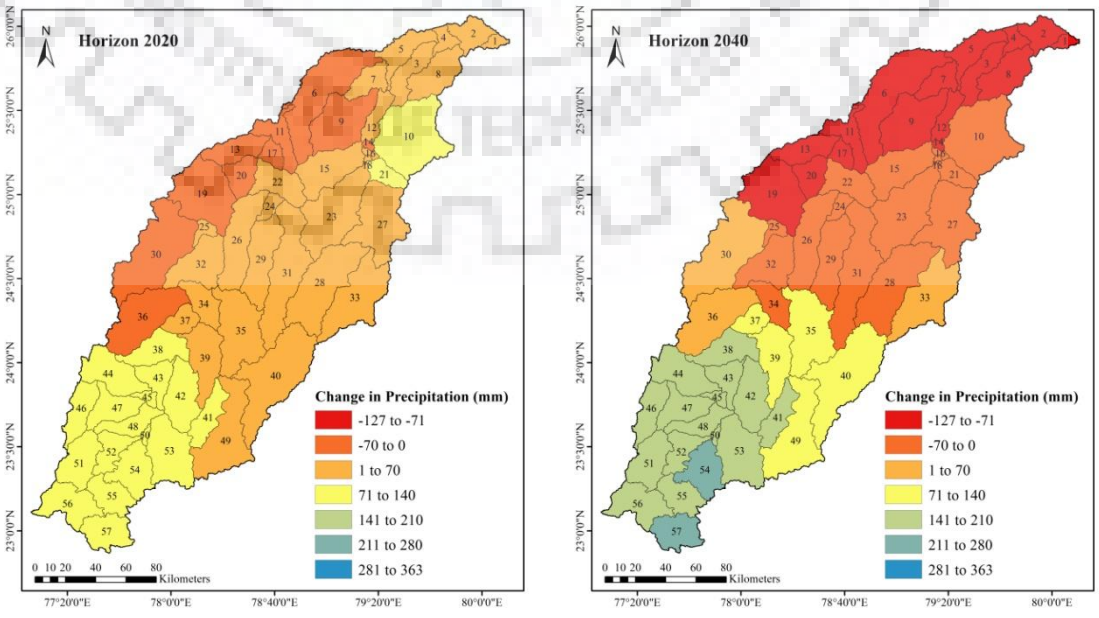

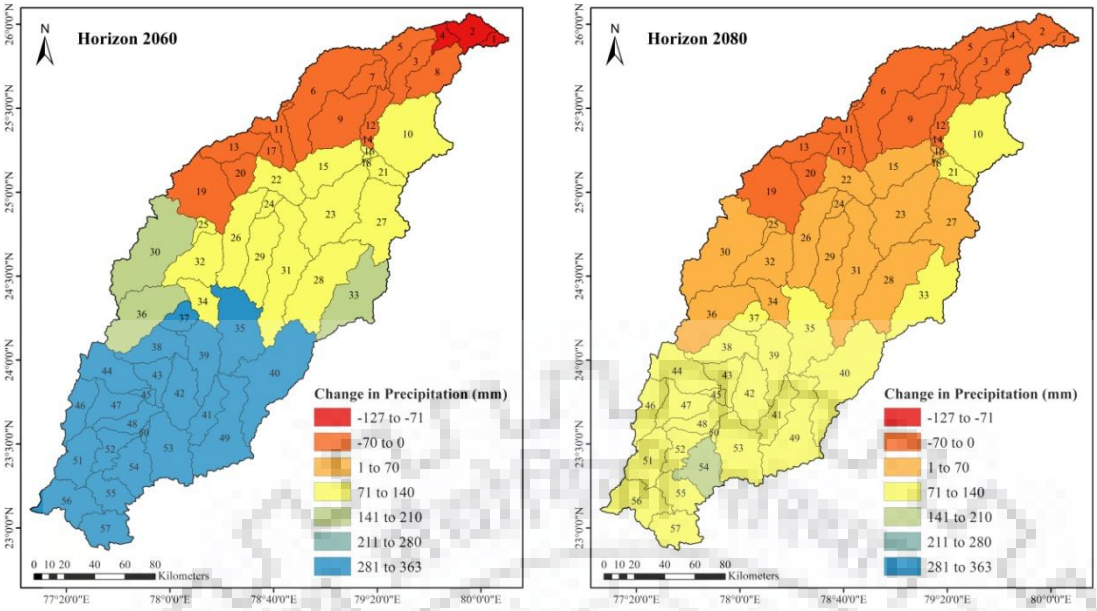

Figure 7.15: Spatial representation of change in average annual precipitation in horizon 2020, horizon 2040, horizon 2060, and horizon 2080 at sub-watershed level

7.3.5.2 Changes in SWAT simulation under varying precipitation pattern

In this study, impact of climate (here precipitation) change on the model simulation has been assessed at sub-watershed level, as well as on monthly time-scale. However, only sub-watershed level analysis has been continued to study the significance level of climate change impact on the hydrology of Betwa basin.

(a) Future simulation at sub-watershed level

i. Streamflow

Effect of future climate change on streamflow analysis is provided in Figure 7.16. Results show that in horizon 2020 most of the sub-watersheds have 1-20 cumec increment in streamflow, except the SW-9, SW-13, SW-30 and SW-36 where a low amount of streamflow reduction (0-8 cumec) was observed (Figure 7.16). In horizon 2040, the area of streamflow reduction could be more with less precipitation occurrence in lower part of the Betwa basin. However, during horizon 2060, more precipitation change in several sub-watersheds induces an increased streamflow up to 109 cumec, because of accumulated river flow from upper to lower basin area. Thus, high streamflow change has been observed during horizon 2060 near the basin outlet (Figure 7.16). During horizon 2080, the SW-1, SW-2, SW-4, SW-5, SW-11 and SW-17 have streamflow changes of about 41-60 cumec. Similar streamflow changes in lower amount have been also observed for the horizon 2080 owing to similar high precipitation changes in future.

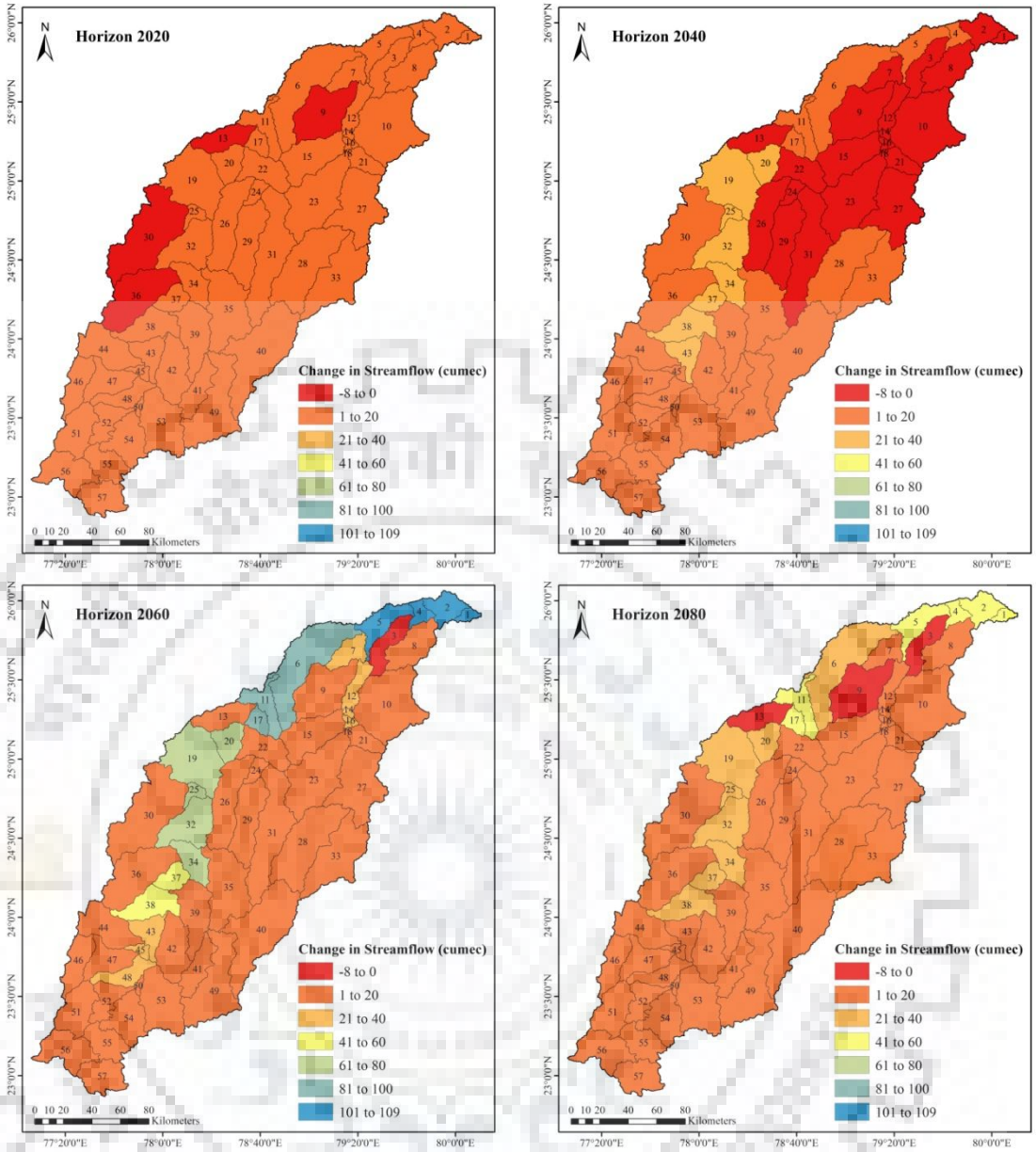

Figure 7.16: Spatial representation of individual climate change impact on streamflow in horizon 2020, horizon 2040, horizon 2060, and horizon 2080 at sub-watershed level

ii. Sediment yield

The sub-watershed level analysis shows that low changes in sediment yield has been induced under low precipitation, and hence with the low streamflow change. In most of the sub-watersheds, sediment yield change of about 1-10 t ha^{-1} was observed; except the SW-25 in horizon 2020, and SW-1, SW-2, SW-7, SW-12, SW-14, SW-16, SW-18, SW-21, SW-22 and SW-24 in the horizon 2040 having sediment yield reduction of about 0-9 t ha^{-1}. In horizon 2060, high sediment yield (51-80 t ha^{-1}) change has been observed in the SW-1, SW-4 and SW-16; about 41-50 t ha^{-1}in the SW-16 and SW-17; and about 11-30 t ha^{-1} in the SW-2, SW-5, SW-11 and SW-20 (Figure 7.17). Very small amount of sediment yield reduction (0-9 t ha^{-1}) could induce in SW-25, which may be due to sediment deposition in upstream water storage (Rajghat

reservoir located in SW-32) in future horizon 2020 and horizon 2080. Thus, high impact of climate change on sediment yield has been resulted from the analysis. The similar impact of climate change on sediment was found by Maina et al. (2013) for Madagascar's major coral reef areas.

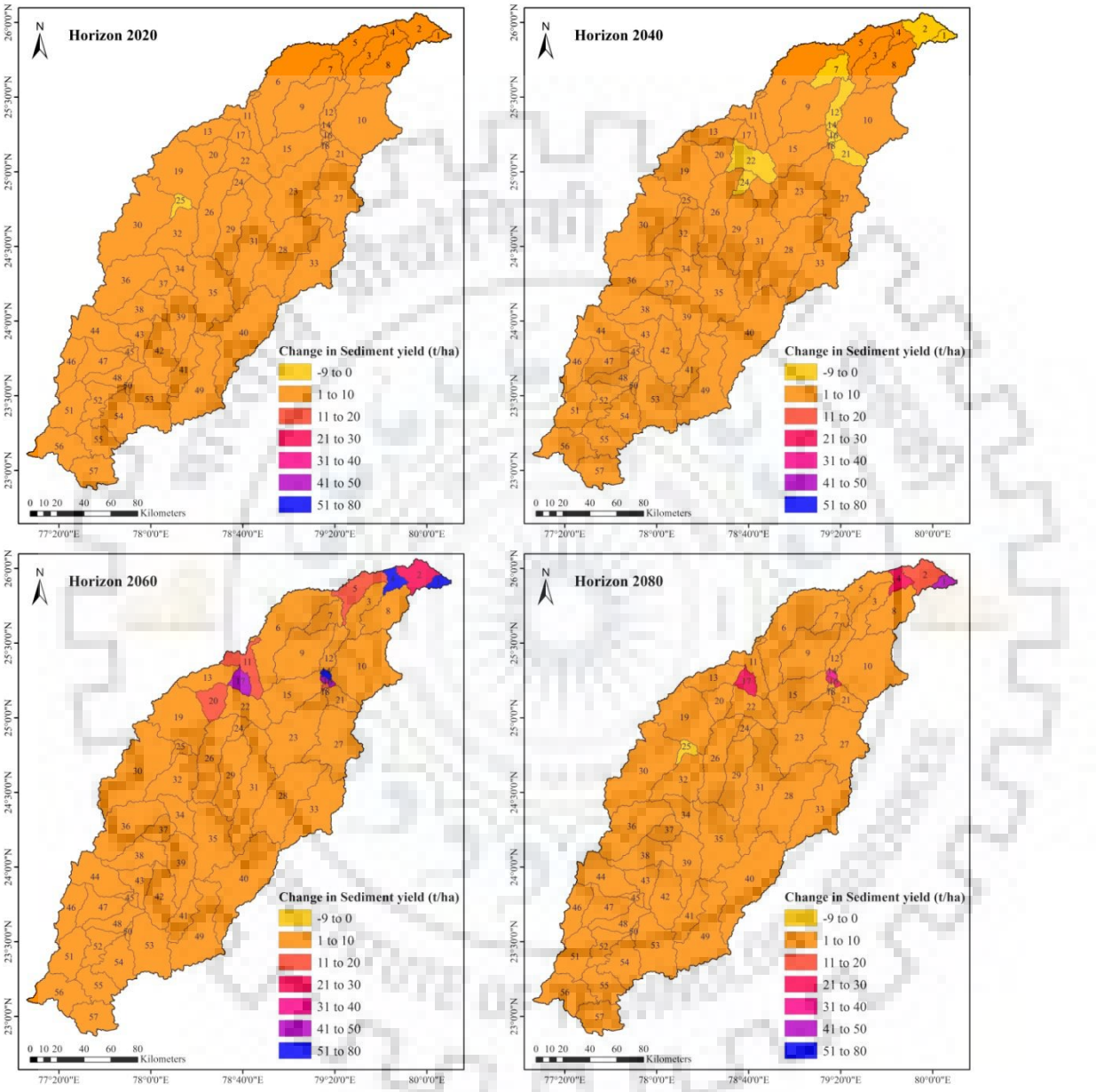

Figure 7.17: Spatial representation of individual climate change impact on sediment yield in horizon 2020, horizon 2040, horizon 2060, and horizon 2080 at sub-watershed level

iii. Evapotranspiration

The change in ET at sub-watershed level has been also studied under future climatic changes. Results show an increase in ET loss of 0-35 mm during horizon 2020 for all the sub-watersheds of the study area. During horizon 2040, only two sub-watersheds (SW-6 and SW-9) located in lower basin area has decrease of ET (1-9 mm), whereas remaining area has an

increase in ET losses under future climate change. In horizon 2060, the future ET changes occurred mainly in the upper basin area where ET increases (10-18 mm), and in lower basin area the ET decreases (1-9 mm) (Figure 7.18). In horizon 2080, the ET loss may also lower (1-27 mm) under future climatic changes. Although the precipitation is high during the horizon 2080, the increased temperature in this horizon 2080 may induce more water vaporization with the increased precipitation, and hence high ET losses could be possible at the end of the 21st century. The result reveals that the impact of future climate change on ET is possible in the Betwa basin. Thus, there is need to assess the future climate change impact in the Betwa basin.

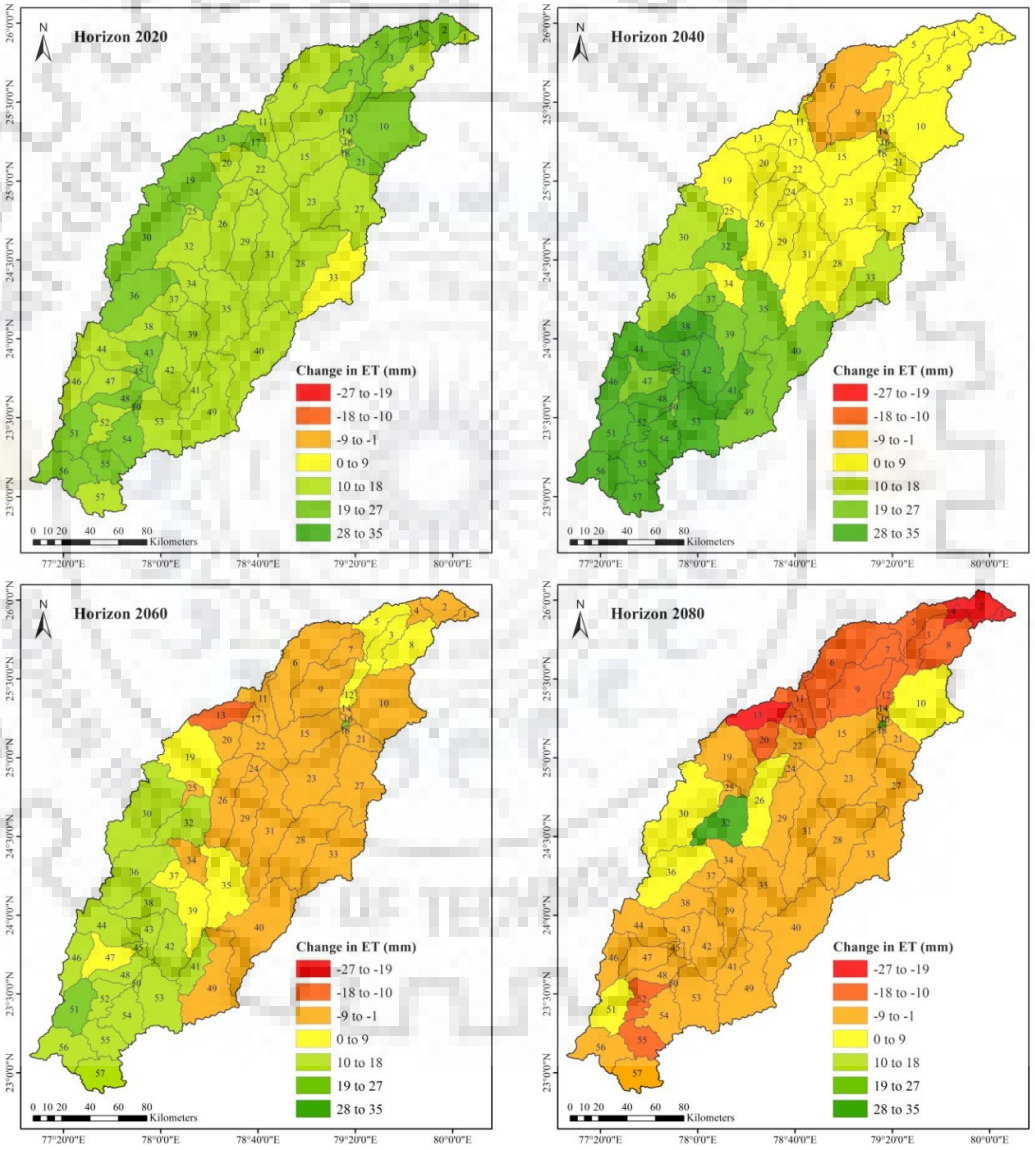

Figure 7.18: Spatial representation of individual climate change impact on evapotranspiration in horizon 2020, horizon 2040, horizon 2060, and horizon 2080 at sub-watershed level

iv. Water yield

In this study, impact of climate change on water yield corresponds to baseline simulation has been analyzed at sub-watershed level. Result shows the maximum decrease in water yield

about 127 mm, and the maximum increase in water yield about 346 mm in future (Figure 7.19). Water yield has been majorly increases up to 346 mm during horizon 2060; due to more precipitation. However, decrease in water yield up to 127 mm has been observed for horizon 2040 due to less precipitation. Few sub-watersheds namely SW-1, SW-2 and SW-4 have large reductions in water yield of about 71-127 mm in horizons 2060. Thus, effect of dry and wet spells during horizons 2060 could induces high impact on water yield. In horizon 2080, the effect of precipitation change also observed which is mainly in sub-watersheds of upper basin area (Figure 7.19). Overall, future precipitation change can significantly impact on water yield of the Betwa basin.

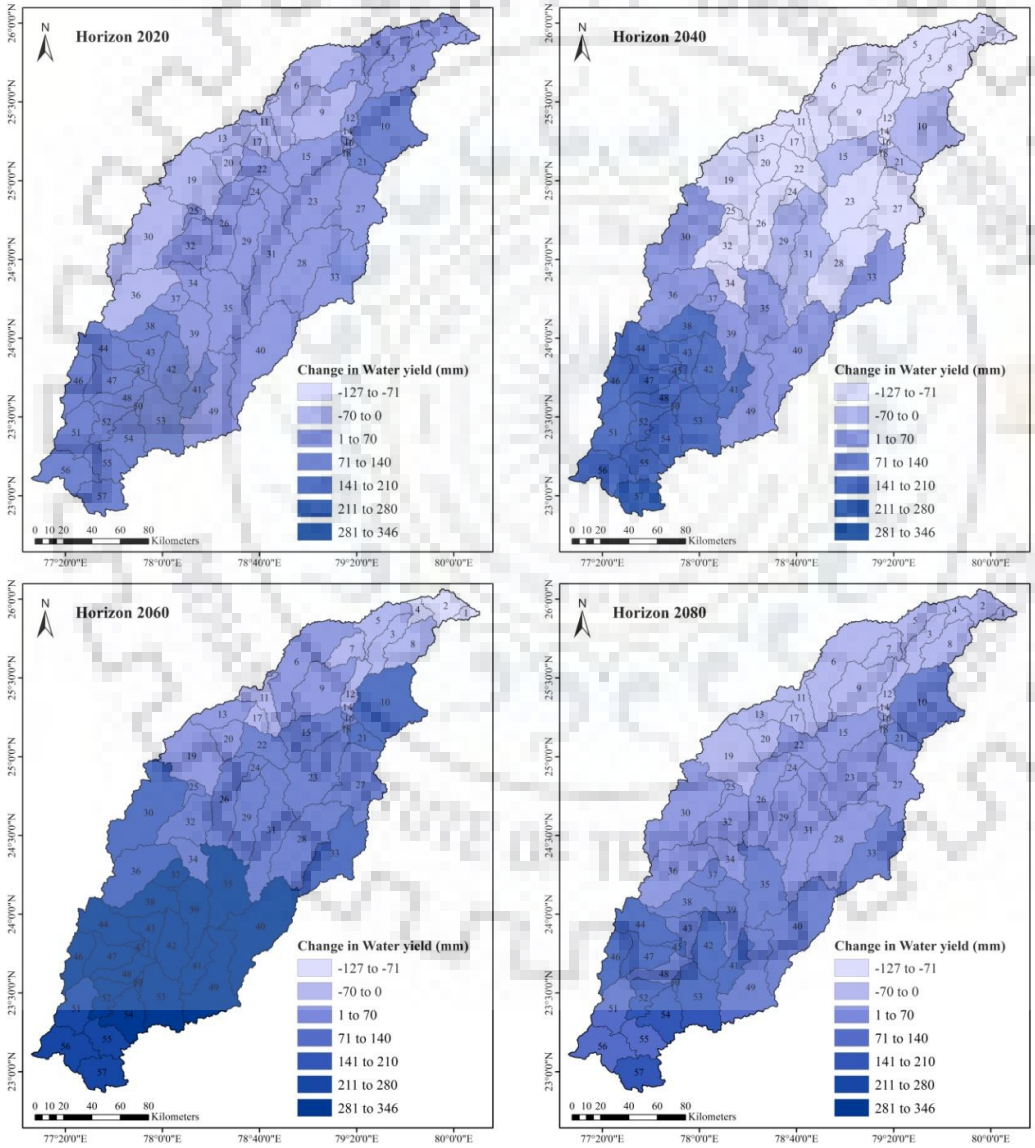

Figure 7.19: Spatial representation of individual climate change impact on water yield in horizon 2020, horizon 2040, horizon 2060, and horizon 2080 at sub-watershed level

(b) Future simulation on monthly time-scale

In addition, the monthly change analysis has been carried out to estimate the climate change impact on the monthly streamflow, sediment yield, ET and water yield of the Betwa basin. Monthly changes in hydrologic components during baseline and four future climate horizons are illustrated in Figure 7.20.

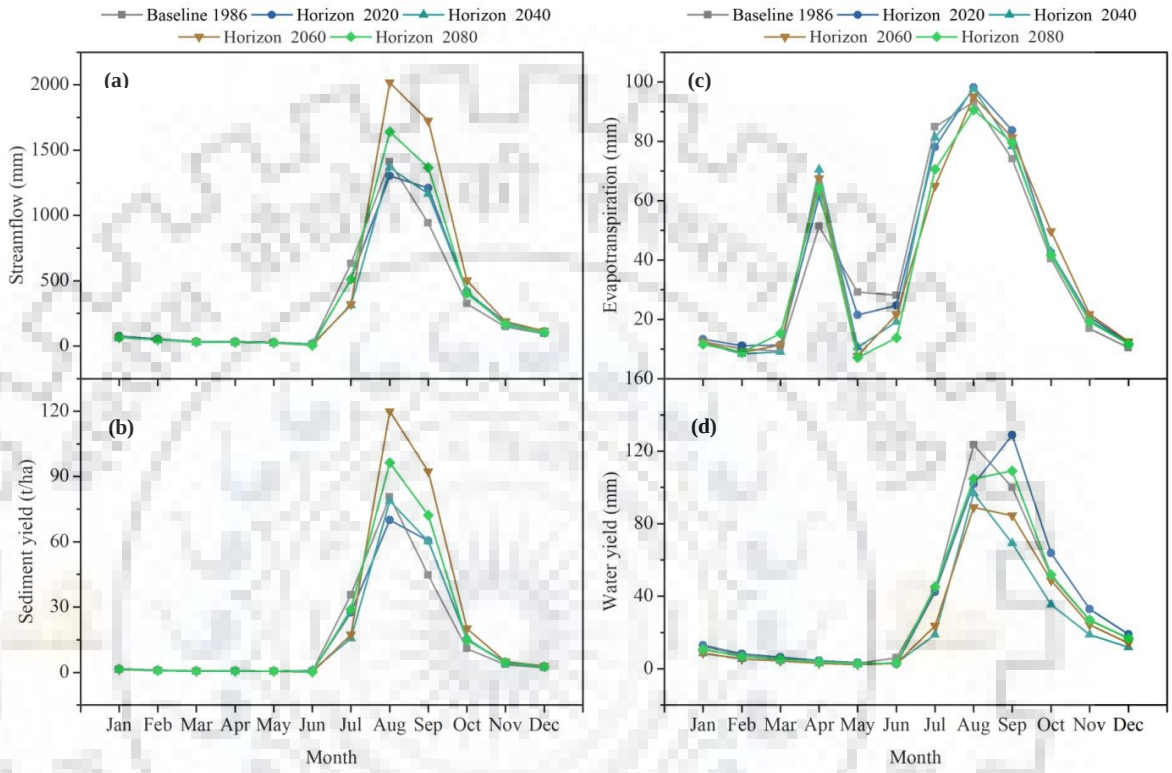

Figure 7.20: Monthly variations in streamflow, sediment yield, ET and water yield

i. Streamflow

Based on the monthly model simulation, maximum and minimum streamflow during baseline year 1986 were 1409.39 cumec in August (monsoon season) and 15.78 cumec in June month, respectively (Figure 7.20a). In future, the peak streamflow increases with time in August month, i.e. 1303.69 cumec streamflow in horizon 2020, 1367.34 cumec streamflow in horizon 2040, 2017.44 cumec streamflow in horizon 2060, and 1640.40 cumec streamflow in horizon 2080 (Figure 7.20a). However, the reverse pattern of low streamflow, i.e. decrease in streamflow about 14.79 cumec in horizon 2020, 17.05 cumec in horizon 2040, 4.07 cumec in horizon 2060, and 6.56 cumec in horizon 2080 has been observed in June month. Results show that, the low and high streamflows may induce in horizon 2060 period (2060-2079) due to future precipitation variability. Results demonstrated that the streamflow has been significantly increases in August, and decreases in June. Thus, the monsoon streamflow, in June and August months, may alter largely in future due to the precipitation changes.

ii. Sediment yield

Figure 7.20b represents monthly sediment yield in baseline 1986 and four future climatic horizons. Monthly sediment yield during baseline 1986 is high (80.65 t ha^{-1}) in August. In future climate periods, sediment yield is high (70.05 t ha^{-1}) during horizon 2020, 78.82 t ha^{-1} during horizon 2040, 119.92 t ha^{-1} during horizon 2060, and 96.28 t ha^{-1} during horizon 2080 in August month. In this analysis also, future sediment yield is higher during monsoon months, especially in horizon 2060. The pattern of sediment yield change is very similar to the changes in streamflow. Thus, both streamflow and sediment yield may possibly have exhibited a significant relationship under monthly climatic changes. In this analysis, changes in monthly sediment yield are mainly observed for monsoon season, similar to the observed streamflow changes, in the Betwa basin.

iii. Evapotranspiration

In this analysis, high monthly ET losses have been observed in summer as well as monsoon season (Figure 7.20c). During baseline 1986, monthly maximum ET losses are estimated to be 51 mm in April (summer), and 93 mm in August (monsoon). It is observed that the high ET induces during three months of monsoon season, i.e. July to September. In future, high ET losses, i.e. 98 mm in horizon 2020, 98 mm in horizon 2040, 95 mm in horizon 2060, and 91 mm in horizon 2080 are observed for August month. Although the temperature is high in summer than other seasons, the less availability of water during summer may induce low ET losses, as compared to monsoon ET losses. Nevertheless, due to more surface water evaporation by increased monsoon temperature, high ET loss has been observed in monsoon season. Therefore, seasonal changes in future may have significant impact on water evaporation loss.

iv. Water yield

Results show that high amount of water yield has been obtained in monsoon season, and it will continue in future also. Monthly simulated water yield is high (123 mm) in baseline 1986, (August), 129 mm in horizon 2020 (September), 97 mm in horizon 2040 (August), 89 mm in horizon 2060 (August), and 109.07 in horizon 2080 (September). Thus, August and September months in monsoon season have high water yields as shown in Figure 7.20d. It is observed that, high water yield in monsoon season was further lowered in winter, and then in summer goes nearly zero. Thus, water yield also changes with the seasonal climatic changes in the Betwa basin.

7.3.5.3 Relationship between future precipitation and the model outputs

In horizon 2020, the relationship analysis between changes in precipitation and the model simulation shows significant positive correlations for streamflow (R^2 = 0.554, p<0.05), sediment yield (R^2 = 0.074, p<0.05), ET (R^2 = 0.207, p<0.05), and water yield (R^2 = 0.985, p<0.05). In this analysis, all hydrology components exhibited the positive correlations as shown in Figure 7.21. Thus, the precipitation changes during horizon 2020 have significant impact on streamflow, sediment yield, ET and water yield of the Betwa basin.

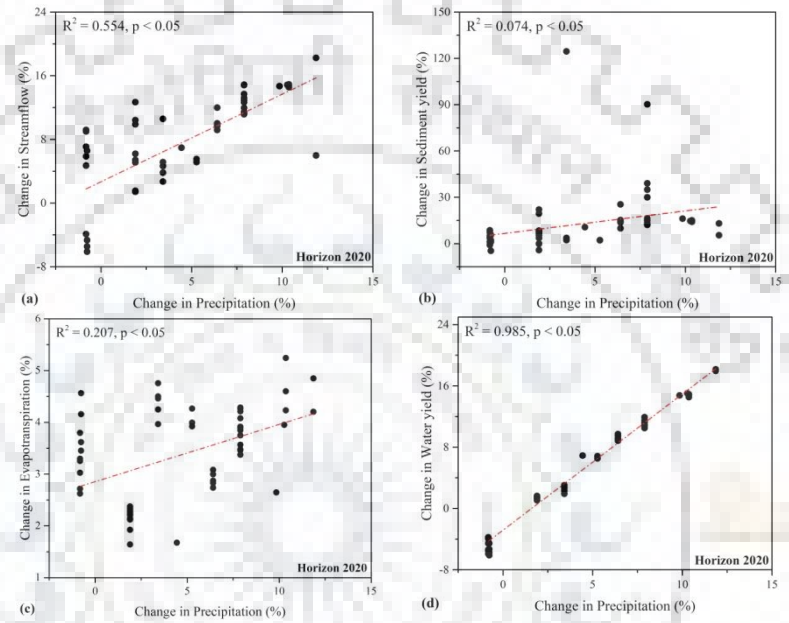

Figure 7.21: Change in future precipitation and its relation to the change in (a) streamflow, (b) sediment yield, (c) evapotranspiration, and (d) water yield during horizon 2020 (2020-2039) at sub-watershed level

Similarly, in horizon 2040, the relationship analysis between precipitation change and the model simulation change shows significant positive correlations for streamflow (R^2 = 0.156, p<0.05), sediment yield (R^2 = 0.089, p<0.05), ET (R^2 = 0.178, p<0.05), and water yield (R^2 = 0.946, p<0.05) as given in Figure 7.22. Thus, the precipitation changes in horizon 2040 also have significant impact on hydrology of the Betwa basin.

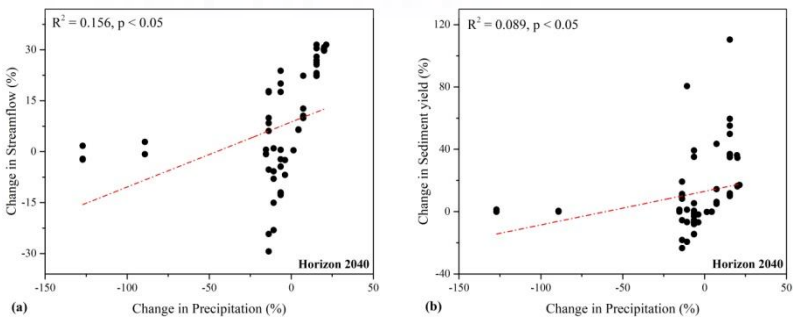

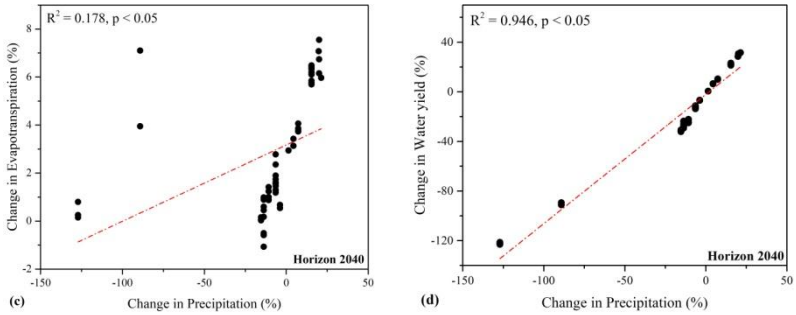

Figure 7.22: Change in future precipitation and its relation to the change in (a) streamflow, (b) sediment yield, (c) evapotranspiration, and (d) water yield during horizon 2040 (2040-2059) at sub-watershed level

In horizon 2060, the relationship analysis between precipitation change and the model simulation change shows significant positive correlations for streamflow (R^2 = 0.216, p<0.05), ET (R^2 = 0.472, p<0.05), and water yield (R^2 = 0.989, p<0.05). Here, the sediment yield analysis shows none response (p = 0.782) to the future precipitation changes (Figure 7.23b), might be due to an effect of frequent dry and wet spells or low intensity rainfall during horizon 2060. Thus, the precipitation changes during horizon 2060 have significant impact only on three hydrology components (streamflow, ET and water yield) of the Betwa basin.

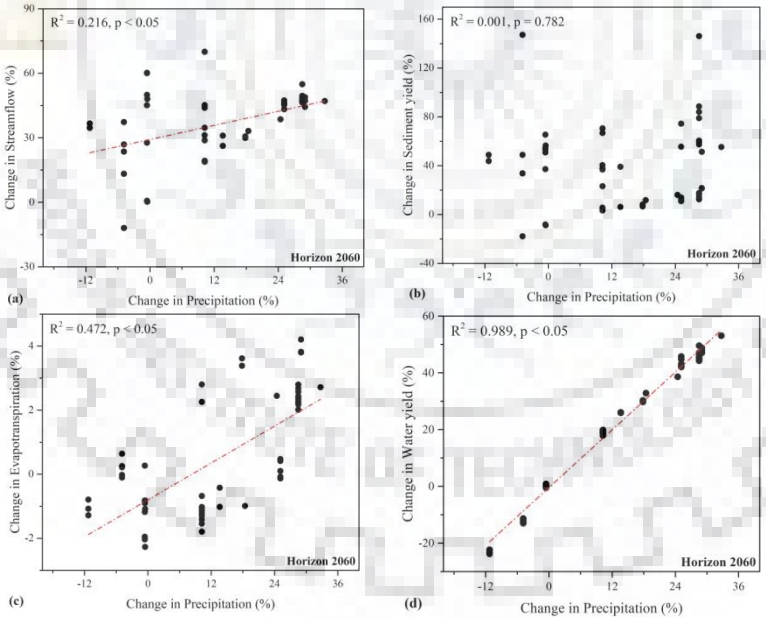

Figure 7.23: Change in future precipitation and its relation to the change in (a) streamflow, (b) sediment yield, (c) evapotranspiration, and (d) water yield during horizon 2060 (2060-2079) at sub-watershed level

Again, in horizon 2080, the relationship between precipitation change and the model simulation change shows significant positive correlations for streamflow (R^2 = 0.157, p<0.05), ET (R^2 = 0.168, p<0.05), and water yield (R^2 = 0.991, p<0.05). In this analysis also, sediment yield has none response (p = 0.766) to the future precipitation changes (Figure 7.24b). Thus, the

precipitation changes during horizon 2080 also have significant impact on three hydrologic components (streamflow, ET and water yield) of the Betwa river basin.

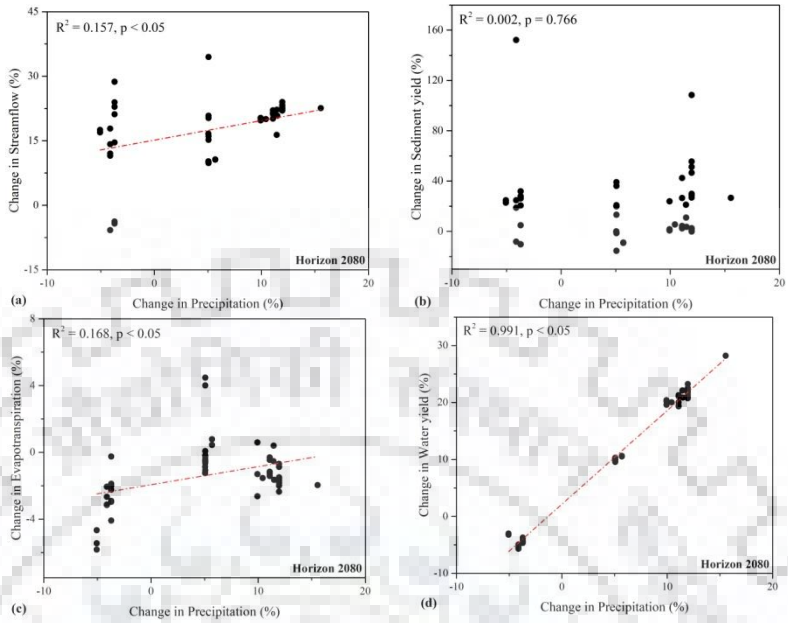

Figure 7.24: Change in future precipitation and its relation to the change in (a) streamflow, (b) sediment yield, (c) evapotranspiration, and (d) water yield during horizon 2080 (2080-2099) at sub-watershed level

7.3.6 Combined land use and climate change impact assessment

The combined impact of land use and climate change on the hydrology of the Betwa basin has been assessed by estimating simulation difference between scenario-4 and scenario-1 (S4-S1). Scenario-1 is for a baseline simulation, and scenario-4 is for a model simulation under changes in land use data of the years 2013 by 2040, and changes in climate data of the years 1986-2005 by four future horizons of the years 2020-2099. Furthermore, the relationship analysis has been performed to estimate the Pearson's correlation coefficient (r) value and the significance level (p value < 0.05) of their impact on hydrology.

7.3.6.1 Spatial analysis of change in future simulation at sub-watershed level

In this study, sub-watershed wise changes in the model simulation have been analyzed spatially for future climate horizons 2020, 2040, 2060 and 2080.

i. Streamflow

The changes in future streamflow at sub-watershed level are presented in Figure 7.25. It is observed that, results of combined land use and climate change have very similar changing pattern to the results obtained in an individual climate change analysis. Due to combination of land use change impact, some aggregated changes are also induced in the present study. Results

show that in horizon 2020 nearly all the sub-watersheds have increase in streamflow (1-20 cumec), except the SW-3, SW-9, SW-13, SW-15, SW-30 and SW-36 where a low amount of streamflow reduction (0-8 cumec) has been observed (Figure 7.25). This streamflow reduction could be more in horizon 2040 due to low precipitation in lower part of the study area. However, due to more precipitation during horizon 2060, the streamflow increases up to 110 cumec in few sub-watersheds due to flow contribution from upper to lower basin area. Thus, high streamflow change during horizon 2060 has been observed near the basin outlet (Figure 7.25). Similar type of streamflow changes in lower amount are also observed for horizon 2080 owing to high precipitation changes in future. Result shows that the SW-1, SW-2, SW-4, SW-5, SW-6, SW-11 and SW-17 have streamflow changes in the range of 41-60 cumec.

Overall, the combined impact of both land use and climate change induces more significant changes in the model simulation. Especially, streamflow increases in the SW-3 and SW-15 during horizon 2020 and in the SW-6 during horizon 2080 as compared to the results obtained from the individual climate change impact analysis. From this analysis, it is observed that impact of climate change is dominant over the impact of land use change in future years.

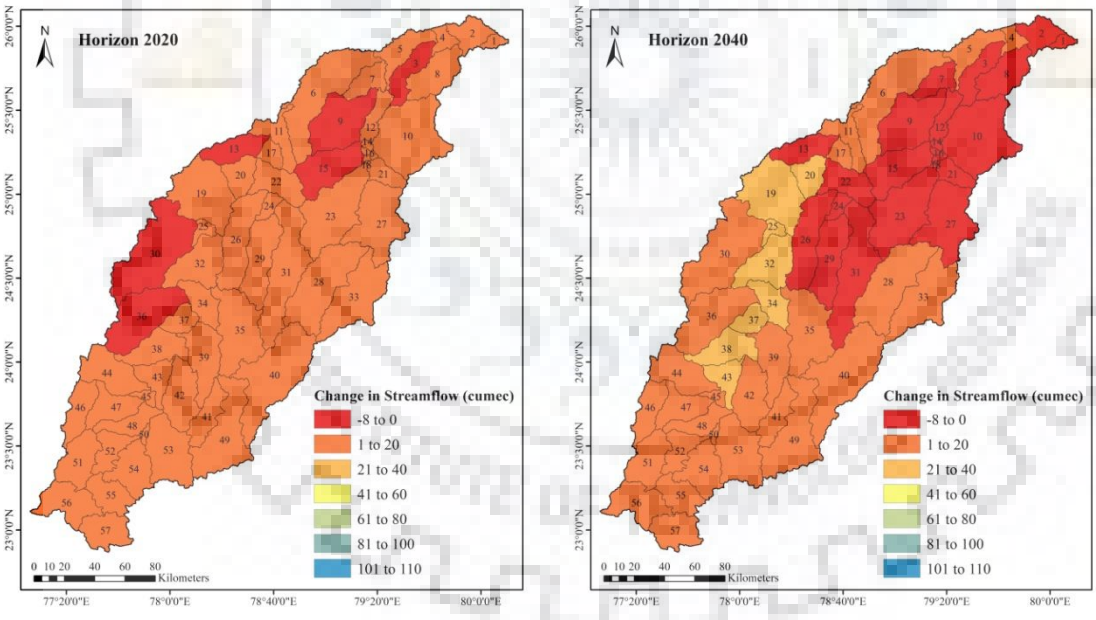

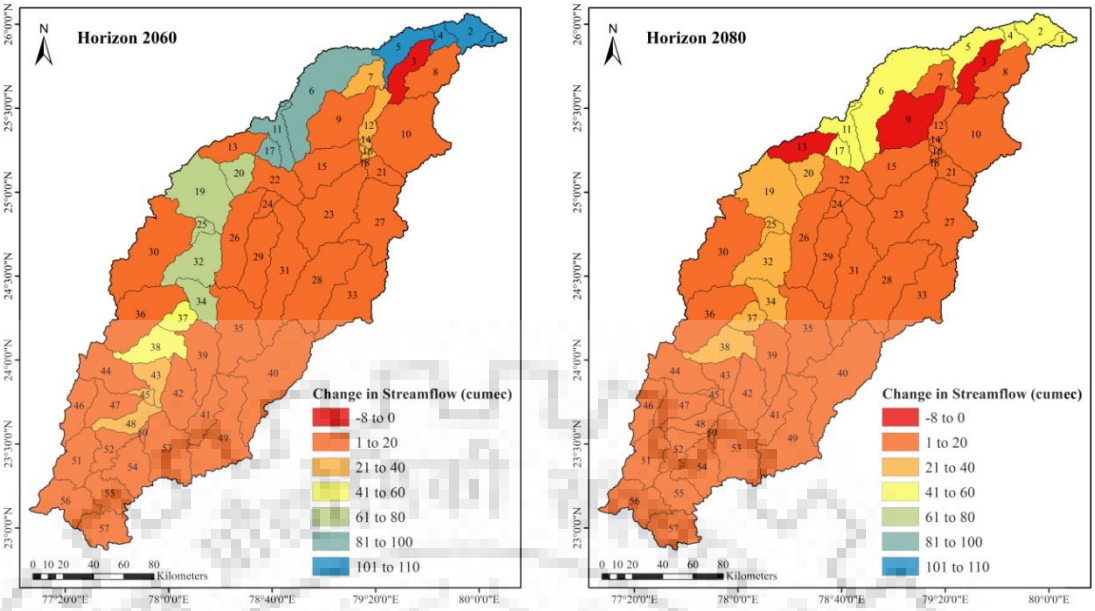

Figure 7.25: Spatial representation of combined land use and climate change impact on future streamflow at sub-watershed level

ii. Sediment yield

Similarly, the combined impact of land use and climate change also shows very similar effects on future sediment yield. Result shows that the small increase in sediment yield about 1-10 tha^{-1} has been induced in most of the sub-watersheds of study area. Several sub-watersheds, namely SW-25 in horizon 2020 and 2080; and the SW-7, SW-12, SW-14, SW-16, SW-18, SW-22 and SW-24 in horizon 2040 have sediment yield reduction of about 0-9 t ha^{-1}. In horizon 2060, sediment yield may increase (about 51-80 tha^{-1}) in SW-1, SW-4 and SW-16; about 41-50 t/ha in SW-16 and SW-17; and about 11-30 tha^{-1} in SW-2, SW-5, SW-11 and SW-20 (Figure 7.26). Similarly, few sub-watersheds SW-1, SW-2, SW-4, SW-14 and SW-16 have increased sediment yield (11-50 t/ha) during horizon 2080. This analysis reveals that combined impact of land use and climate change increases sediment yield in SW-1, SW-2 and SW-21 as compared to the sediment yield obtained under individual climate change analysis.

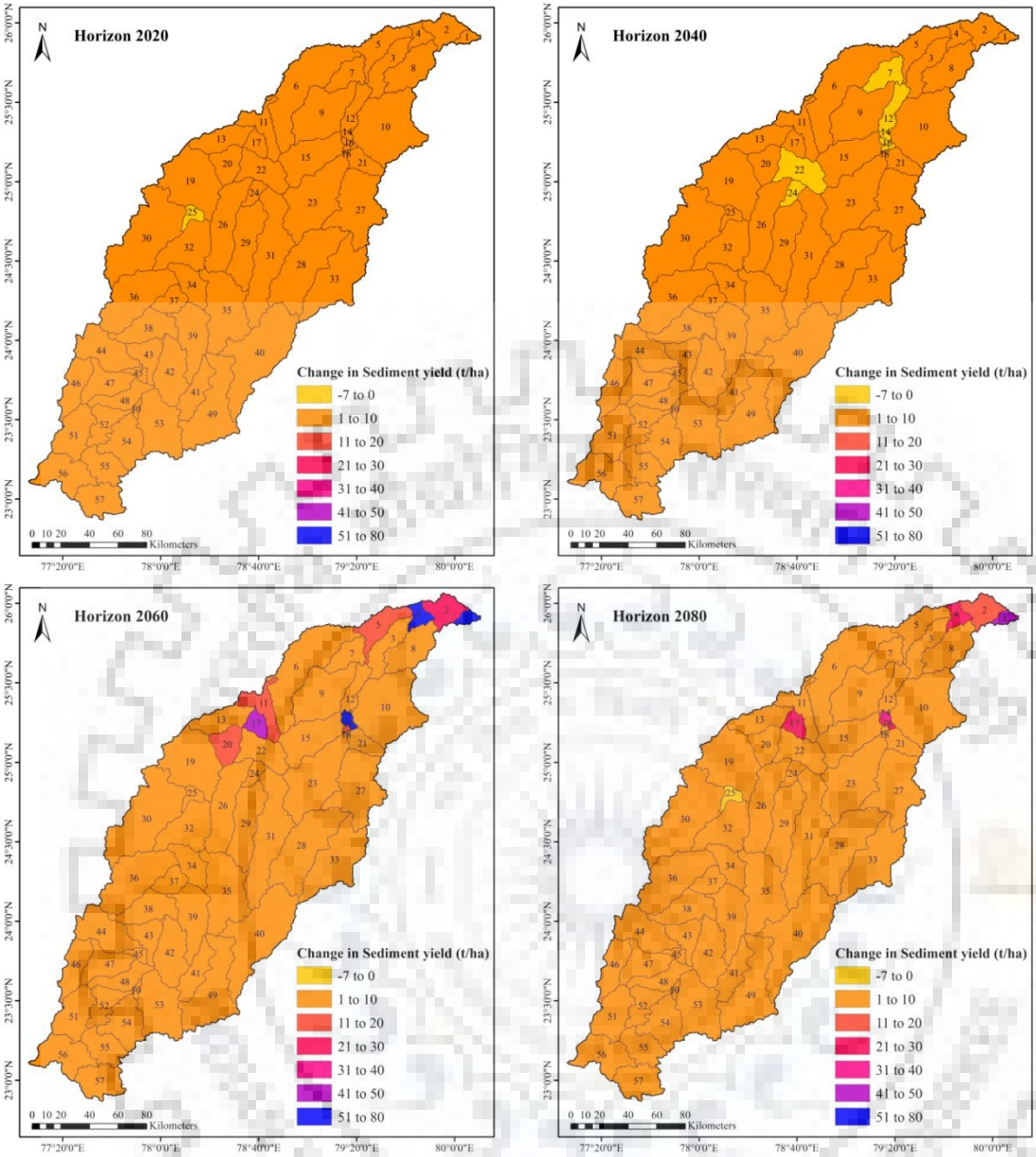

Figure 7.26: Spatial representation of combined land use and climate change impact on future sediment yield at sub-watershed level

iii. Evapotranspiration

In this analysis, all the sub-watersheds located in the upper basin area have increased ET loss (69 mm) during horizon 2020, 2040 and 2060. Only two sub-watersheds (SW-34 and SW-48) located in upper basin area has increased ET loss (0-69 mm) during horizon 2080 (Figure 7.27). Also, in this analysis, most of the ET group values indicate decrease in future ET under combined impact of land use and climate change. The SW-32 and SW-18 have decrease in ET values from 181 to 240 mm and from 301 to 329 mm, respectively in all future horizons. Although, the precipitation change is high during horizons 2060 and 2080, the increased temperature in horizon 2080 may induce more water evaporation, and hence high ET losses at

sub-watershed level. Thus, this combined impact analysis reveals that the impact of increased temperature on ET loss is dominant over the impact of increased precipitation in future.

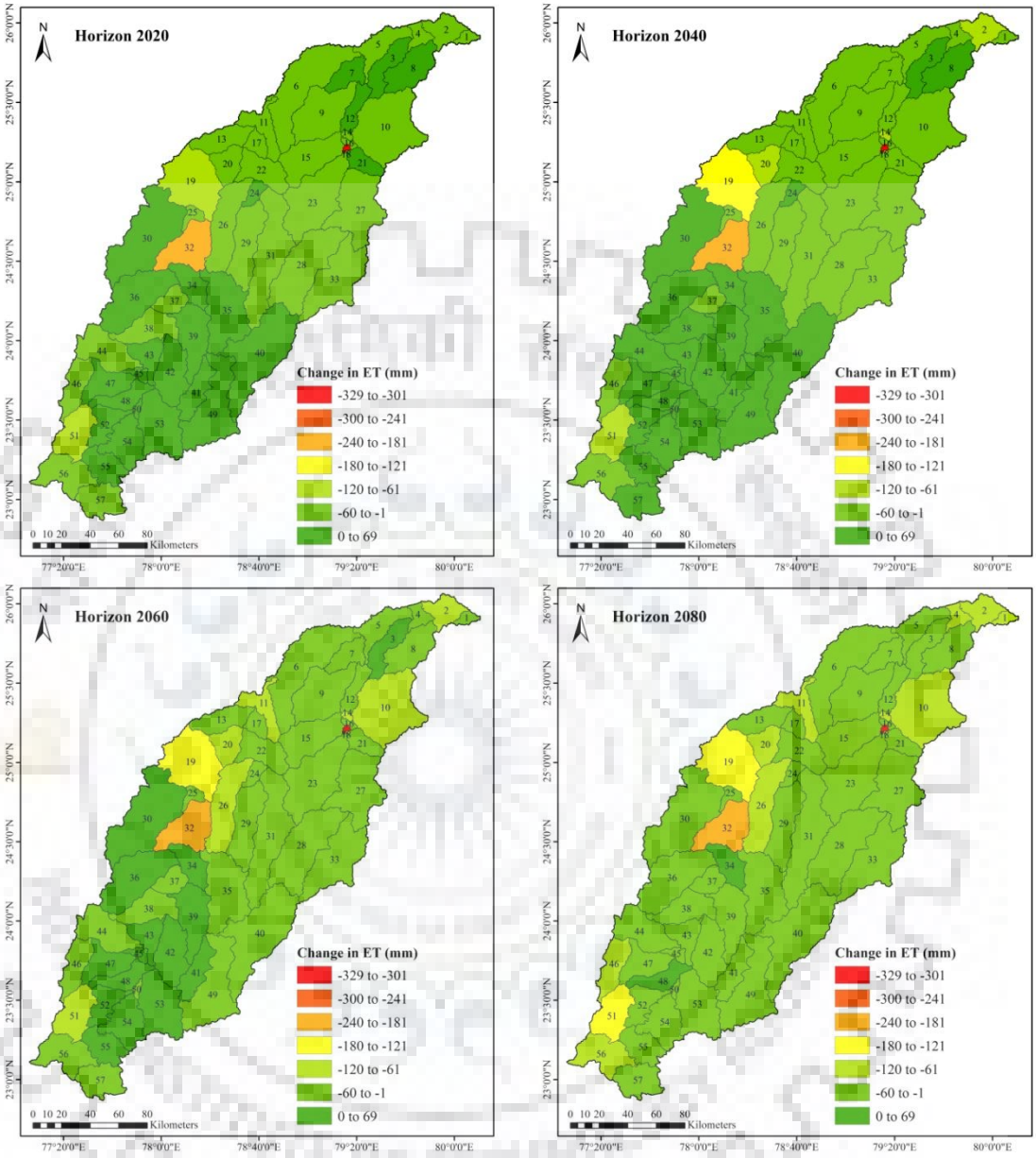

Figure 7.27: Spatial representation of combined land use and climate change impact on future evapotranspiration at sub-watershed level

iv. Water yield

The sub-watershed level analysis shows a decrease in future water yield under combined land use and climate change impact analysis (Figure 7.28). In upper basin area, the high water yield (71-140 mm) in few sub-watersheds (SW-43 to SW-48) has been decreased to 1-70 mm, under combined impact analysis during horizon 2020. Also, in horizon 2040, the SW-46, SW-47 and SW-48 have decreased water yield from 141-210 mm to 41-140 mm. The combined impact of land use and climate change decreases the water yields in SW-39 and SW-48 during horizon

2060; and in SW-46 and SW-47 during horizon 2080 (Figure 7.28). Furthermore, in the lower basin area few sub-watersheds show decrease in water yield under combined land use and climate change impact analysis as compare to the individual climate change analysis. Thus, the sub-watershed having decrease in water yield may have impacted due to dominant impact of land use change over climate change.

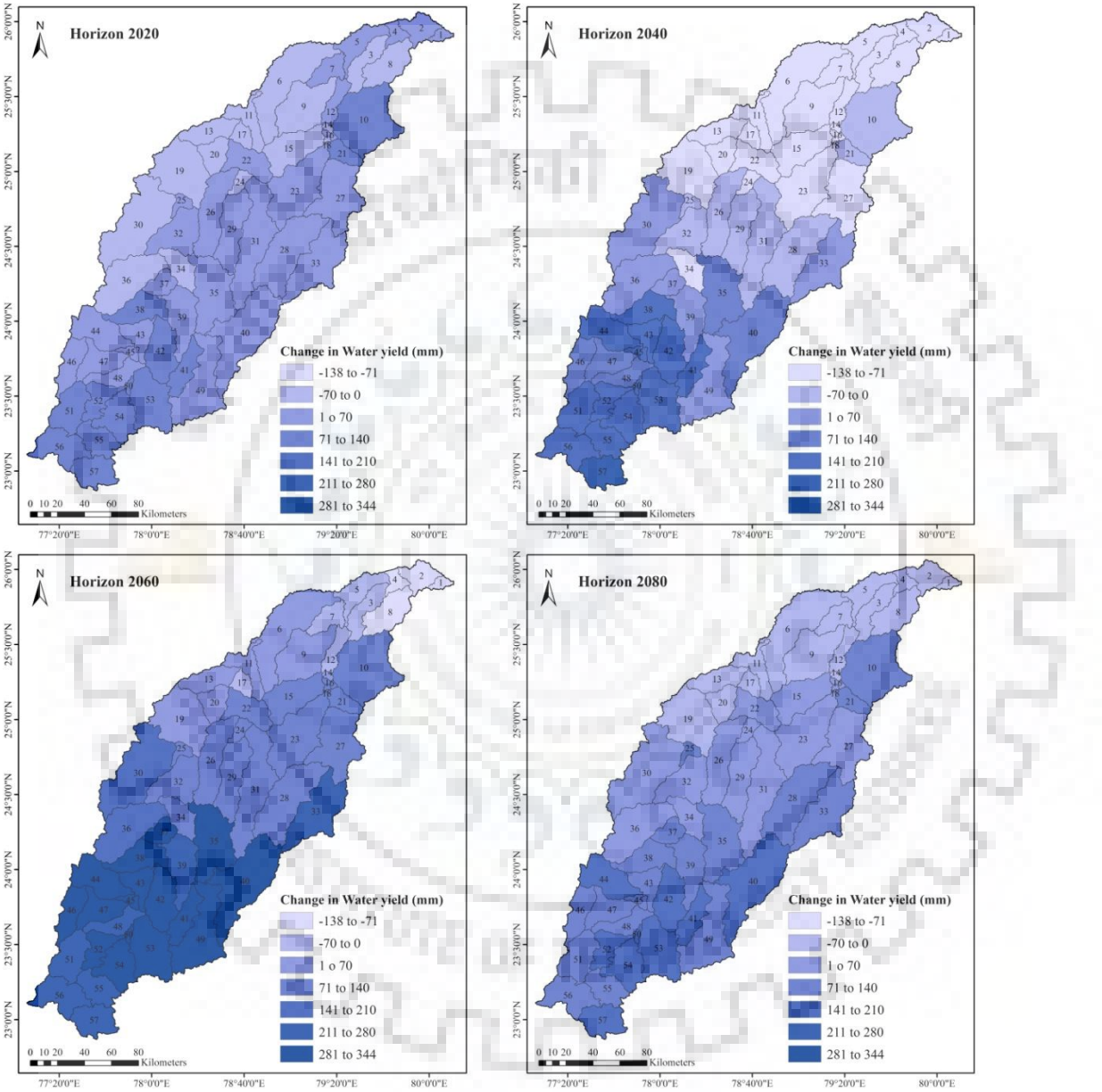

Figure 7.28: Spatial representation of combined land use and climate change impact on future water yield at sub-watershed level

7.3.6.2 Relationship analysis of combined land use and climate changes

To assess the significance level of combined impact of land use and climate change, the Pearson's correlation analysis has been carried out to correlate the change in model simulation to the changes in land use and climate (here precipitation) at sub-watershed level.

i. Streamflow

Analysis shows that the effect of dense forest exhibited significant positive correlation to the future streamflow change in first two climate horizons 2020 (r = 0.327) and 2040 (r = 0.457). However, the degraded forest change has significant negative relationship in last two future climate horizons 2060 (r = -0.271) and 2080 (r = -0.275). The effect of barren land on streamflow also exhibited a negative correlation in horizon 2020 (r = -0.371) and horizon 2040 (r = -0.342). Thus, decrease in dense forest and increase in degraded forest has varying response to the future streamflow. Bonell et al. (2010) observed similar impacts of change in forest area on surface and sub-surface water flows in Western Ghats of India. The agriculture area has significant positive response (r = 0.299) with streamflow increment during horizon 2020 only, which further reduces under future land use change from horizon 2040 to horizon 2080 (Table 7.7).

The effect of climate change, precipitation only, shows significant positive impact on the future streamflow under combined impact of land use and climate change analysis. With an increase in future precipitation, the streamflow also increases significantly in future years. Thus, the results of streamflow revealed that climate change impact is dominant over the land use change in all future climate horizons.

Table 7.7: Relationship of future land use and climate change to the change in future streamflow at sub-watershed level

Pearson's 'r' value		**Streamflow**			
		Horizon 2020	Horizon 2040	Horizon 2060	Horizon 2080
Land use	Dense forest	**0.327**	**0.457**	0.260	0.215
	Degraded forest	-0.241	-0.248	**-0.271**	**-0.275**
	Agriculture	**0.299**	0.218	0.233	0.255
	Barren land	**-0.371**	**-0.342**	-0.186	-0.176
	Waterbody	-0.004	0.054	-0.027	-0.062
	Settlement	-0.111	-0.181	-0.152	-0.129
Climate	Precipitation	**0.727**	**0.760**	**0.456**	**0.387**

Note: Bold values (green colour for direct response, and red colour for indirect response) represents relationship at the 0.05 significance level

ii. Sediment yield

The results of combined impact analysis show a significant positive response of change in dense forest area to the change in sediment yield at sub-watershed level during horizon 2020 (r = 0.310) and horizon 2040 (r = 0.439). Barren land exhibited a significant negative relationship (r = -0.297) only in horizon 2040. Change in precipitation pattern also have significant impact on sediment yield in horizon 2020 (r = 0.290), and horizon 2060 (r = 0.526) at sub-watershed

level (Table 7.8). During horizon 2060 and horizon 2080, the precipitation change has non-significant response to the sediment loss. It may be due to the wet weather condition causing prolonged soil moisture availability and results a less soil erodibility (Fitzjohn et al., 1998; Ziadat & Taimeh, 2013). Overall, the combined impact of land use and climate induces several significant changes in sediment yield of the Betwa basin.

Table 7.8: Relationship of future land use and climate change to the change in future sediment yield at sub-watershed level

Pearson's 'r' value		Sediment yield			
		Horizon 2020	Horizon 2040	Horizon 2060	Horizon 2080
Land use	Dense forest	**0.310**	**0.439**	0.229	0.220
	Degraded forest	0.018	-0.085	0.046	0.113
	Agriculture	-0.007	0.064	-0.098	-0.163
	Barren land	-0.237	**-0.297**	-0.021	-0.014
	Waterbody	0.091	0.077	-0.046	-0.003
	Settlement	-0.054	-0.117	0.020	0.048
Climate	Precipitation	**0.290**	**0.526**	0.056	-0.020

Note: Bold values (green colour for direct response, and red colour for indirect response) represents relationship at the 0.05 significance level

iii. Evapotranspiration

In future, the combined impacts of land use and climate change on ET losses have significant relationships mainly with waterbody and precipitation. The waterbody class has positive significant correlations with ET in all future climate horizons (Table 7.9). Changes in precipitation also have significant correlation in horizon 2040 (r = 0.528), horizon 2060 (r = 0.405), and horizon 2080 (r = 0.338). In horizon 2020, low temperature, as compared to other horizons, may induce insignificant relationship with precipitation change. Thus, results reveal that change in ET largely deals with the changes in waterbody vaporization. Thus, the future ET losses of the Betwa basin are considerably dependent on vaporization from the surface water, i.e. land use change impact is prominent here. Kundu et al. (2017a) reported that individual impact of land use change is prominent for more ET losses in Narmada river basin of central India.

Table 7.9: Relationship of future land use and climate change to the change in future evapotranspiration at sub-watershed level

Pearson's 'r' value		Evapotranspiration			
		Horizon 2020	Horizon 2040	Horizon 2060	Horizon 2080
Land use	Dense forest	0.032	0.139	0.116	-0.013
	Degraded forest	-0.210	-0.221	-0.232	-0.235
	Agriculture	-0.130	-0.050	-0.070	0.003
	Barren land	-0.063	-0.197	-0.158	-0.182
	Waterbody	**0.916**	**0.857**	**0.882**	**0.865**
	Settlement	-0.089	-0.172	-0.138	-0.135
Climate	Precipitation	0.247	**0.528**	**0.405**	**0.338**

Note: Bold values (green colour for direct response, and red colour for indirect response) represents relationship at the 0.05 significance level

iv. Water yield

Furthermore, the water yield in the present study area has significant relationship with changes in the dense forest, agriculture, barren land and precipitation in future (Table 7.10). The relationship of dense forest, agriculture and precipitation changes with the water yield exhibited positive correlations; however, the barren land has negative correlation as shown in Table 7.10. It shows that, the effect of agriculture area change on water yield is only responsive during high precipitation periods (horizon 2060 and horizon 2080) when an intensive agriculture would be possible. High water utility for agriculture purpose may store more water in the watershed than losing it (Bosch & Hewlett, 1982). Nevertheless, barren land may lose the water yield due to changes in the barren land at sub-watershed level pronounce a negative impact on the future water yield. In this analysis, change in water yield is highly correlated to the precipitation changes (Table 7.10). Thus, climate change impact is major on water yield than the land use change impact. Kundu et al. (2017a) reported that individual impact of climate change is prominent on the water yield of the Narmada river basin of central India.

Table 7.10: Relationship of future land use and climate change to the change in future water yield at sub-watershed level

Pearson's 'r' value		Water yield			
		Horizon 2020	Horizon 2040	Horizon 2060	Horizon 2080
Land use	Dense forest	**0.384**	**0.442**	**0.312**	**0.360**
	Degraded forest	-0.201	-0.158	-0.162	-0.192
	Agriculture	0.192	0.256	**0.379**	**0.331**
	Barren land	**-0.371**	**-0.555**	**-0.630**	**-0.551**
	Waterbody	0.159	0.194	0.136	0.125
	Settlement	-0.088	-0.213	-0.239	-0.232
Climate	Precipitation	**0.939**	**0.990**	**0.988**	**0.980**

Note: Bold values (green colour for direct response, and red colour for indirect response) represents relationship at the 0.05 significance level

7.3.7 A conceptual framework for individual and combined impact assessment

In this study, a conceptual framework representing four types of the model simulation results of baseline (no change), individual land use change, individual climate change, and combined land use and climate change analysis are limited by two half-axes of land use and climate change/constant for all quadrants. In each quadrant, four hydrology components (FLOW, SYLD, ET and WYLD) are considerably represented to compare the individual as well as combined impacts of land use and climate change on the future model simulations in comparison to the baseline simulation.

The conceptual framework representing the impact of land use and climate change on hydrologic components of the Betwa basin is shown in Figure 7.29. Result shows that FLOW variable increases from 67.77 cumec to 67.86 cumec due to land use change, from 67.77 cumec to 80.46 cumec due to climate change, and from 67.77 cumec to 80.56 cumec due to combined impact of land use and climate changes (Figure 7.29). Similarly, the SYLD variable increases from 16.51 t ha^{-1} to 16.58 t ha^{-1} due to land use change, from 16.51 t ha^{-1} to 19.61 t ha^{-1} due to climate change, and from 16.51 t ha^{-1} to 16.69 t ha^{-1} combined impact of land use and climate changes. Thus, both the FLOW and SYLD have positive impact of individual as well as combined changes in land use and climate of the Betwa basin.

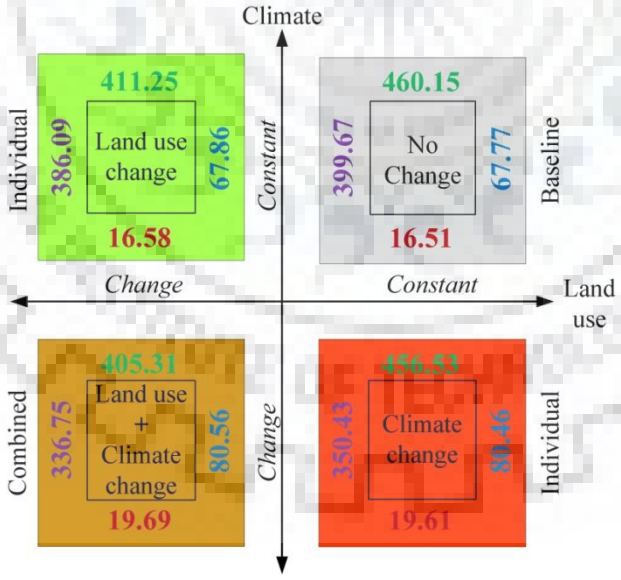

Figure 7.29: Comparison of individual and combined impacts of land use and climate change using a conceptual framework

[Blue colour value at right side represents streamflow (cumec), dark-red colour value at bottom side represents sediment yield (t/ha), green colour value at top side represents ET (mm), and purple colour value at left side represents water yield (mm)]

Furthermore, the results show that ET has negative impact of land use change (reduced from 460 mm to 411 mm), climate change (reduced from 460 mm to 456 mm), and combined land use and climate changes (reduced from 460 mm to 405 mm) with respect to the baseline ET value 460 mm (Figure 7.29). Similarly, the WYLD also has negative impact of land use change (reduced 400 mm to 386 mm), climate change (reduced from 400 mm to 350 mm), and combined land use and climate changes (reduced from 400 mm to 337 mm) with respect to the baseline WYLD value 400 mm. Thus, both ET and WYLD have negative impacts of individual as well as combined changes in land use and climate of the Betwa basin.

Overall, the climate change impact is higher than the land use change impact on the hydrology of the Betwa River basin. Kundu et al. (2017a) reported that an individual impact of climate change is prominent for water yield, and land use change impact is prominent for the more ET losses. Due to the land use and climate changes in Betwa basin, the FLOW and SYLD may increase, while the ET and WYLD may decrease in future. Thus, sustainable management practices are crucial to maintain the changes in hydrology components in future. In general, the proposed conceptual framework helps to interpret the results of model simulation under changing land use and climate conditions. Also, their individual as well as combined impact on hydrologic components can be easily analyzed, and substantially compared in the present study. It is recommended to adopt such methodology for future research studies not only in India, but also in other parts of the world facing rapid changes in regional land use and climate.

7.3.7.1 Limitations of the conceptual framework

- The conceptual framework proposed in this study is limited to few hydrology components only, i.e. FLOW, SYLD, ET and WYLD etc.
- This conceptual framework can represent the impact of land use and climate change only on hydrology of a river basin. It does not represent the impact in each sub-watershed of the study area. Separate analysis is required for each sub-watershed level impact assessment.
- Also, the conceptual framework is limited to represent only the changes in hydrology, not the changes in land use classes or the changes in climate parameters.

7.4 CONCLUSIONS

The SWAT model was employed to simulate the impacts of individual land use change, and climate change, and the impacts of combined land use and climate changes on hydrology of the Betwa basin. Further, a conceptual framework has been developed and employed to compare

these impacts on streamflow, sediment yield, ET and water yield. Based on the results, following conclusions are drawn from the present research study:

1. The GCM-derived future climate change analysis shows increase in precipitation (140 mm) during horizon 2060.
2. Analysis also shows significant increase in annual minimum temperature (from 1.22 °C to 5.34 °C) and annual maximum temperature (from 0.92 °C to 4.87 °C) during future years (2020-2099).
3. Spatial analysis of SWAT simulations under varying land use maps and GCM-derived climate datasets show remarkable impact of climate change as compare to the land use change impact on streamflow, sediment yield, ET and water yield at sub-watershed level.
4. Individual land use change impact assessment at sub-watershed level shows that ET change has significant positive response (R^2 = 0.842, P<0.05) to the vaporization from waterbody. Furthermore, the water yield exhibited significant response to the dense forest (R^2 = 0.076, P<0.05), degraded forest (R^2 = 0.2, P<0.05) and agriculture (R^2 = 0.245, P<0.05). Thus, land use change impact is found to be prominent on water balance of the Betwa basin.
5. Individual climate change impact assessment shows that precipitation has significant (p<0.05) positive impact on streamflow (R^2 = 0.554 and 0.156), sediment yield (R^2 = 0.074 and 0.089), ET (R^2 = 0.207 and 0.178), and water yield (R^2 = 0.985 and 0.946) during horizon 2020 and horizon 2040, respectively. In the last two horizons 2060 and 2080, only streamflow (R^2 = 0.216 and 0.157), ET (R^2 = 0.472 and 0.168), and water yield (R^2 = 0.989 and 0.991) have positive response to the precipitation change. In this analysis, the sediment yield has none significant response (p = 0.782 and 0.766) to the precipitation changes during horizons 2060 and 2080. Thus, climate change impact is found to be prominent on water yield of the Betwa basin.
6. In future, the impact of climate change is dominant over the land use change impact. Increase in precipitation under future climatic change may increases the losses of hydrologic components. Changes in dense forest, agriculture and waterbody induce positive impact; nevertheless the changes in degraded forest and barren land induce negative impact on hydrology of the Betwa basin.
7. The developed conceptual framework can successfully separate the individual as well as combined impacts of land use change and climate change on hydrology components i.e. FLOW, SYLD, ET and WYLD, of a river basin.

CHAPTER 8

EVALUATION OF BEST MANAGEMENT PRACTICES FOR SUSTAINABLE RIVER BASIN MANAGEMENT

This chapter deals with the evaluation of Best Management Practices (BMPs) and their recommendations for sustainable management of a large river basin. For this, a calibrated and validated SWAT model has been used to simulate the effective BMP intervention. This study is focused on evaluation of the four over-land BMPs namely tillage management, contour farming, residue management and strip cropping; and five in-stream BMPs namely grassed waterways, streambank/channel stabilization, grade stabilization structures, porous gully plugs and recharge structures in the Betwa River basin.

8.1 BACKGROUND OF THE STUDY

Development and utilization of natural resources in a river basin has focused the application of hydrological models considering all physical processes. Many watershed management programs suggested modelling strategies to investigate effective management practices at the watershed level (Pandey et al., 2009b; Lam et al., 2011; Jang et al., 2017). Modelling strategies for a watershed includes intervention of suitable and practicable Best Management Practices (BMPs) in critical soil erosion prone areas (Tripathi et al., 2005). Therefore, BMPs are generally accepted as an effective measure to control and protect the non-point sources of streamflow and sediment. The Soil and Water Assessment Tool (SWAT) is a world-wide used hydrologic model to predict the impact of BMPs on streamflow and sediment yields in a complex watershed (Ullrich and Volk, 2009; Arnold and Fohrer, 2005, Murty et al., 2014). In a river basin, priority of sub-watersheds is mainly depends on intensity of sediment/ nutrient losses produce from various natural resources, and can be taken as a basis for prioritization of the critical areas (Tripathi et al., 2005; Niraula et al., 2013). Ranking needs to assign before prioritization of critical sub-watershed based on the susceptibility to erosion (Singh et al., 1992; Pandey et al., 2009a, 2011). The approach of sub-watershed prioritization based on sediment yield can be applied for the BMPs intervention.

Soil, a productive component of land, is degrading under changing climate and land use; hence, land productivity reduces with soil erosion (Pender et al., 2004; Zhang et al., 2008, Gao et al., 2013; Wu, et al., 2018). The erosion process includes detachment, transportation and deposition of soil particles from one location to another through the natural agents like water (Foster and Meyer, 1972). Soil erosion is affected by natural factors such as climate, soil, topography, vegetation and anthropogenic activities (Kuznetsov et al., 1998). Information of

erosion pattern and trend can be obtained by modelling the water-induced soil erosion in relation to current and potential future changes in climate and land use (Millington, 1986). Therefore, the erosion caused by water needs to be managed for conservation of soil, and sustain the land productivity.

River channel is the primary element of a drainage basin carries flow and sediment load. Channel processes are quantitatively studied from last few decades, in terms of the impact of human activity and climate change on streamflow and sediment (Arnell, 1992; Rumsby and Macklin, 1994; Lake et al., 2000; Jiongxin, 2005; Zhang et al., 2018a; Gao et al., 2013; Wu et al., 2018). Channel segment reflects the interaction of streamflow and sediment loads with local factors including slope and cover (Froehlich et al., 1990; Bridge, 1993). The channel conveyance capacity can alter with time and magnitude of streamflow, and sediment loads by erosion and deposition. Thus, a river channel management requires understanding of channel process including streamflow and sediment transport. Moreover, an interaction between channel process and form of river channel should be known both physically and from management perspectives (Habersack et al., 2016; Narasimhan et al., 2017). For sustainability of river channel, feasible future management practices must be studied. The structural and non-structural measures viable for potential management approach are usually made to maximize the advantage of natural resource conservation, and to reflect the environmental issues (Kundzewicz, 2002; Mishra et al., 2007). It should be well managed within the dynamic context and with an understanding of past channel changes under contemporary conditions. The legal and political context of a river channels may influence the environment management in a watershed, particularly in a trans-boundary river basin (Cheng et al., 2003; Armitage, 2005; Giordano and Shah, 2014). Therefore, many countries have adopted legislation based river basin management plans for conservation and protection of channel segment.

In this study, an effective management for land and river channel has been envisioned in the context of Betwa River basin, India. This is a trans-boundary/inter-state river basin between Madhya Pradesh and Uttar Pradesh State plays an important role in water supply for agriculture and urban sectors. Extreme climatic event, like heavy rainfall occurred in 2013, causes flood and rapid erosion processes in the Indian River basin (Joseph et al., 2015; Arora et al., 2016; Agnihotri et al., 2017). It may have great impact on river channel segment disturbing environmental flow and waterway. The Betwa River basin has undergone on channel geometry changes due to extreme rainfall events, like in the year 2013. The river bank and channel bed were eroded with large streamflow and overland flows. To reduce erosions within river

channel, channel protection plans and conservation measures are important to introduce in an effective way.

Thus, this study is focused to evaluate the effective management practices for land, and protection of river channel by implementing over-land as well as in-stream BMPs at sub-watershed level. In this study, firstly soil erosion status of the study area has been accomplished by identification and prioritization of the critical sub-watersheds. After the calibration and validation, the SWAT model has been used for evaluation of BMPs. Initial evaluation of the SWAT model has been already carried out in Chapter-6. In this chapter, identification of critical soil erosion prone areas and evaluation of best management practices has been carried out for recommendation of suitable management interventions using the SWAT model.

8.2 MATERIALS AND METHODS

8.2.1 Data acquisition

The details of data pertaining to meteorological, hydrological, GCM and spatial data are briefly discussed in Chapter-3. All the required input information were provided in ArcGIS compatible raster (GRIDS), vector (shapefiles), and SWAT database formats. After data formatting, the SWAT model setup was carried out for hydrologic simulation. In this study, the calibrated and validated SWAT model was further used to evaluate the effectiveness of BMP implementation for sustainable river basin management. The methodology flowchart adopted in this study is provided in Figure 8.1.

8.2.2 Baseline simulation

The baseline values for the input parameters (pre-BMP) were selected by model calibration process, suggested values from the literature, and prior experience of the analyst. The baseline simulation was carried out for historical baseline period 1986 (1986-2005), and it was compared to the future climate horizon 2020 (2020-2039), horizon 2040 (2040-2059), horizon 2060 (2060-2079) and horizon 2080 (2080-2099). In this analysis, the existing river basin management practices have been included for the baseline simulations. It includes existing conventional tillage practice, land cover practice, water storages located on main channel and tributary channel of the Betwa River Basin and their management. Thus, this study is focused mainly on the evaluation of BMPs and their implementation and effectiveness in the Betwa River basin.

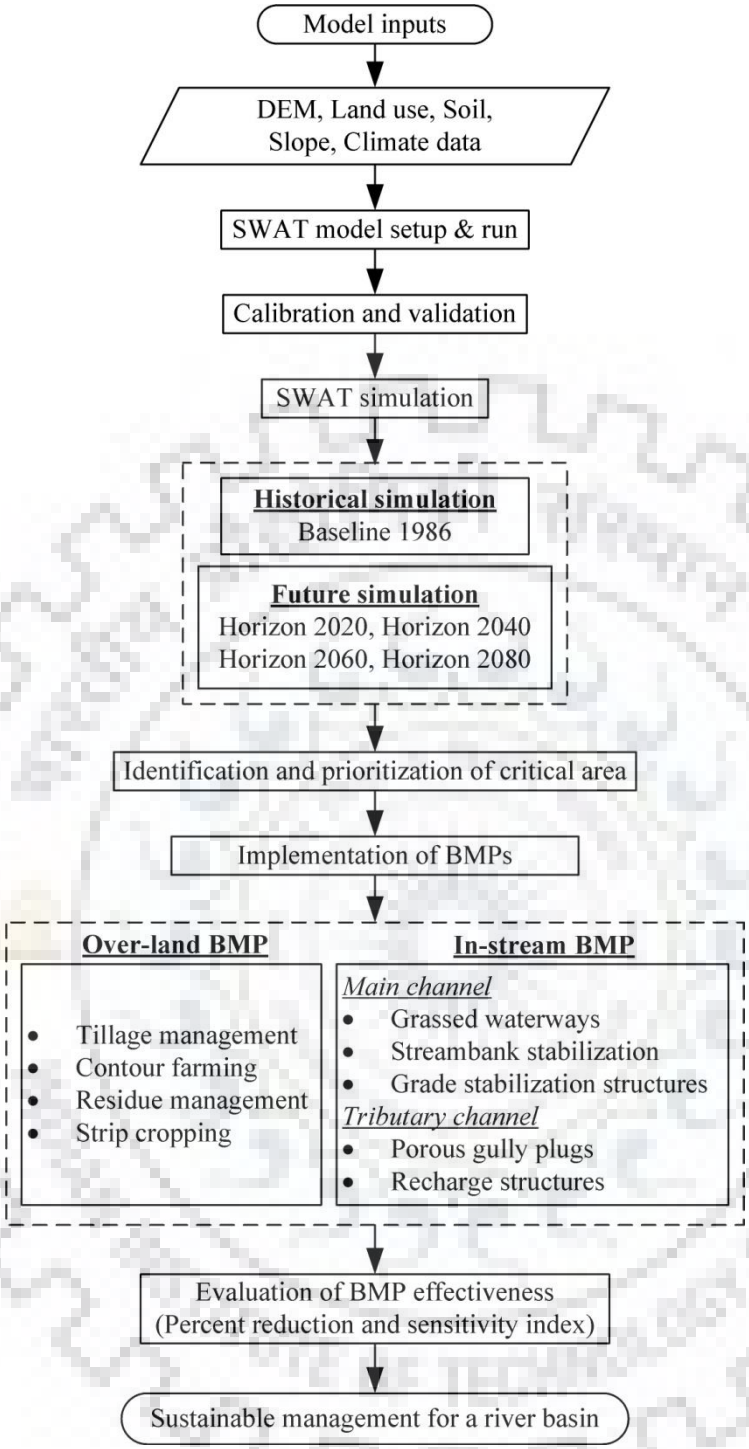

Figure 8.1: Methodology flowchart for evaluation of over-land and in-stream BMPs for sustainable river basin management

8.2.3 Assumptions and limitations

Central Water Commission (CWC) regulates the hydrologic measurement in Indian River basins. Change in magnitude and frequency of stream flow could affect target water storages. Also, presently available water storages could change in future due to ongoing litigation and boundary conditions which may possibly affect the sediment loads in the study basin. Thus, it

is considered that future boundary conditions of streamflow and sediment loads will remain unchanged from baseline period to future period.

From the literature, the land use and climate changes have individual and combined impacts on hydrologic simulations (Bronstert et al., 2002; Pervez and Henebry, 2015; Feng et al., 2016; Zuo et al., 2016). Thus, it is presumed that land use (of the year 2001) will remain constant from baseline period to future horizons, while assessing climate change impact. The climate models with several CO_2 concentrations (such as RCP2.6, RCP4.5, RCP6 and RCP8.5) could produce varying climate change response in the analysis. To avoid the effect of CO_2 concentration, this study is limited to use only one climate scenario (RCP8.5) having maximum possible impact of the CO_2 concentrations in future.

While implementing BMPs, only parameter (s) representing a BMP has been adjusted keeping the constant calibrated/default SWAT values of other parameters. However, the changes in land as well as river channel could be possible in future due to human disturbances. This could be a limitation of the present study.

8.2.4 Identification and prioritization of critical sub-watersheds

This study uses average annual sediment simulation to identify and prioritize the critical sub-watersheds of the Betwa River basin for future scenarios. Annual sediment yield was estimated for each sub-watershed of the study area using the SWAT model. The simulated sediment yield is in close agreement with the measured values, thus an average value of model outputs from different sub-watersheds can be quite appropriate to use for identification and prioritization of critical sub-watersheds. Initially, the sub-watershed wise average annual sediment yield was arranged in descending order, and then rank was assigned to each sub-watershed according to range of soil erosion classes (Table 8.1) adopted from Singh et al. (1992). Critical sub-watersheds were further prioritized from very severe (priority class-I) to slight (priority class-VI) erosion classes to apply BMPs as a soil and water conservation measure. In this study, over-land as well as in-stream BMPs implementations are focused for priority Class-I (very severe soil erosion class) to priority Class-V (moderate soil erosion class) under changing climate conditions. Impact of each BMP has been evaluated at both the sub-watershed and the river basin level, expressed by percent reduction and sensitivity index.

Table 8.1: Priority wise classification for sediment yield and soil erosion rates (Singh et al., 1992)

Sediment yield (t ha−1 year−1)	Soil erosion class	Priority class
0–5	Slight	VI
5–10	Moderate	V
10–20	High	IV
20–40	Very high	III
40–80	Severe	II
>80	Very severe	I

8.2.5 BMP representation in the SWAT model

The impact of BMP implementation has been assessed to establish the soil and water conservation as well as river channel protection/restoration plans for the Betwa basin. The SWAT model has been used to represent and analyze the feasible BMPs in critical sub-watersheds over historical baseline period (1986-2005) and future horizon period (2020-2099) under changing climate. The BMPs are considered based on the information available in the literature, and collected by the personal communication with the farmers, scientists and agricultural development officers. Based on the results of identification and prioritization of critical sub-watersheds, the watershed treatments are implemented in the study area.

In order to evolve an appropriate conservation and protection strategy for land as well as main/tributary channel of the Betwa River basin, nine BMPs have been implemented and evaluated in the present study as given in Table 8.2.

Table 8.2: Best management practices (BMPs) evaluated in the study

Over-land BMPs	In-stream-BMPs
1. Tillage management	1. Grassed waterways
2. Contour farming	2. Streambank stabilization
3. Residue management	3. Grade stabilization structures
4. Strip cropping	4. Porous gully plugs
	5. Recharge Structures

These BMPs are implemented based on the function of a conservation practice suggested to represent a BMP in SWAT. Definition and purpose of BMPs were obtained from the Natural Resources Conservation Service (NRCS) standard practice code (USDA-NRCS, 2008). Considering hydrologic processes simulated by the SWAT model and watershed subdivision relevant to this study, BMP parameters and their values were chosen based on published literature and expert opinion. The model parameters and their values used to simulate pre-BMP and post-BMP conditions are presented in Tables 8.3a&b.

Table 8.3a: Parameters and their values used to represent pre-BMP and post-BMP conditions in the SWAT model (**over-land BMP**)

BMP	Function	Selection	Variable name (input file)	Pre-BMP value (from calibration)	Post-BMP value	Reference
Tillage management (Conservation tillage, field cultivator, and zero tillage)	Reduce velocity of flow Facilitate sediment settling Reduce soil erosion	Agriculture land	DEPTIL (.til) EFFMIX (.til)*e CN2 (.mgt)	150 0.95 varies	100, 100, 25 0.25, 0.30, 0.05 CN2-2&3*a	Tripathi et al. (2005), Pandey et al. (2009b) and Tuppad et al. (2010)
Contour farming	Reduce sheet erosion	Agriculture land	CN2 (.mgt) USLE_P (.mgt)	varies 0.65	CN2-3*a slope dependent*b	Arabi et al. (2008) and Tuppad et al. (2010)
Residue management	Reduce overland flow Increase infiltration Reduce sheet and rill erosion	Agriculture land	CN2 (.mgt) USLE_C (.plant.dat) OV_N (.hru)	varies 0.15 0.14*d	CN2-2*a weighted*c 0.3	Arabi et al. (2008) and Jang et al. (2017)
Strip cropping	Reduce flow in small depressions Increase surface roughness Reduce sheet and rill erosion	Agriculture land	CN2 (.mgt) USLE_C (.plant.dat) USLE_P (.mgt) OV_N (.hru)	varies 0.15 0.65 0.14*d	CN2-3*a weighted*c slope dependent*b 0.19	Arabi et al. (2008)

**a CN2 reduced by 2 (CN2-2) and 3 (CN2-3) from the calibration values.*
**b USLE support practice factor (value given in bracket) varies with the land slopes-*
*For **contour farming**: 1-2% (0.60), 3-5% (0.50), 6-8% (0.50), 9-12% (0.60), 13-16% (0.70), 17-20% (0.80), and 21-25% (0.90).*
*For **strip cropping**: 1-2% (0.30), 3-5% (0.25), 6-8% (0.25), 9-12% (0.30), 13-16% (0.35), 17-20% (0.40), and 21-25% (0.40).*
**c Weighted average values for the residue management and strip cropping.*
**d Value assigned by the SWAT model based on hydrologic condition.*
**e Three post-BMP values are given for the three tillage treatments.*

Table 8.3b: Parameters and their values used to represent pre-BMP and post-BMP conditions in the SWAT model (**in-stream BMP**)

BMP	Function	Selection	Variable name (input file)	Pre-BMP value (from calibration)	Post-BMP value	Reference
Grassed waterways	Increase channel cover Reduce channel erodibility Increasing channel roughness	Main channel	CH_COV (.rte) CH_EROD (.rte) CH_N2 (.rte)	0.5 0.03 0.014*a	0.001 0.001 0.03	Bracmort et al. (2006) and Arabi et al. (2008)
Streambank stabilization	Reduce sediment load in main channel Maintain streamflow capacity	Main channel	CH_EROD (.rte) CH_N2 (.rte)	0.03 0.014*a	0.001 0.03	Narasimhan et al. (2017), Chow (1959) and Tuppad et al. (2010)
Grade stabilization structures	Reduce gully erosion Reduce slope steepness	Main channel	CH_EROD (.rte) CH_S2 (.rte)	0.03 assigned by SWAT*b	0.001 estimated*c	Bracmort et al. (2006) and Tuppad et al. (2010)
Porous gully plugs	Reduce gully erosion Reduce flow velocity Trap sediment	Tributary channel	CH_N1 (.sub)	0.014*a	0.05	Chow (1959), Srinivasan (2008) and Tuppad et al. (2010)
Recharge Structures	Increase ground water recharge	Tributary channel	CH_N1 (.sub) CH_K1 (.sub)	0.014*a 0.0	0.08 25	Lane (1983) and Tuppad et al. (2010)

**a Assigned by SWAT model based on hydrologic condition.*
**b Assigned by SWAT based on Digital Elevation Model (DEM) used in this study.*
**c Estimated for grade stabilization structure as given in methodology section.*

Description of each BMP and its representation in the SWAT model at pre-BMP and post-BMP condition is given below:

8.2.5.1 Tillage management

In this study, conservation tillage, field cultivator and zero tillage have been used to test against the existing/conventional tillage practice mould board plough (Table 8.4). Tillage management includes various practices that cause less soil disturbance than the conventional tillage. In SWAT, tillage practices are differing in terms of mixing efficiency, tillage depth, and the SCS runoff curve number (CN2). Mixing efficiency (EFFMIX) represents the fraction of materials (residue, nutrient and pesticides) on the soil surface that are mixed uniformly throughout the soil depth. The tillage depth (DEPTIL) represents the depth of mixing caused by tillage operation. Tillage treatments with their respective mixing efficiencies and tillage depth suggested by Tripathi et al. (2005), Neitsch et al. (2011) are provided in Table 8.4.

Table 8.4: Tillage management considered in the study

Tillage treatments	Tillage code	Tillage depth (DEPTIL)	Mixing efficiency (EFFMIX)
Mould board plough	MLDBOARD	150	0.95
Conservation tillage	CONSTILL	100	0.25
Field cultivator	FLDCULT	100	0.30
Zero tillage	ZEROTILL	25	0.05

In the study region, farmers do not use advanced tillage implements due to financial constraints, and poor knowledge towards improved agricultural implements. Thus, the conservation tillage treatment was selected based on the previous literature studies undertaken in different watersheds of India for evaluation of the tillage practices (Triphati et al., 2005; Behera and Panda, 2006; Pandey et al., 2009b).

8.2.5.2 Contour farming (NRCS practice code-330)

Contour farming consists of several field operations including plowing, planting, cultivating and harvesting the crops along the contour of the field. This practice is specially implemented to reduce surface runoff by impounding water in small depressions, to reduce sheet and rill erosion by reducing erosive power of surface runoff, and preventing or minimizing development of rills. The curve number (CN2) and USLE support practice factor (USLE_P) have been used to represent the contour farming practice in the SWAT model (Arabi et al., 2008; Tuppad et al., 2010).

8.2.5.3 Residue management (NRCS practice code-345)

Implementation of residue management practice helps to lower the surface runoff and peak runoff, to increase infiltration, and to reduce sheet and rill erosion by reducing surface flow volume, overland flow rate, raindrop impact, providing more surface cover and preventing

development of rills. In this study, curve number (CN2), Manning's roughness coefficient for overland flow (OV_N) and USLE cover factor (USLE_C) have been utilized for representation of the residue management practice in the SWAT model (Arabi et al., 2008; Jang et al., 2017).

8.2.5.4 Strip Cropping (NRCS Practice Code-585)

In strip cropping practice, crops are grown in a systematic arrangement of strips to reduce sheet and rill erosion as well as wind erosion from the field, reduce particulate emissions into the air and to improve the water quality. In this study, the curve number (CN2), the Manning's roughness coefficient for overland flow (OV_N), the USLE cover factor (USLE_C), and the USLE support practice factor (USLE_P) have been used to represent the strip cropping practice in the SWAT model (Arabi et al., 2008).

8.2.5.5 Grassed waterways (NRCS practice code-412)

Grassed waterway treatment uses to reduce erosion in the channel segment by establishing suitable vegetation cover to convey streamflow at a non-erosive velocity. It helps to increase sediment trapping in the main channel segment by resisting streamflow velocity. Then, increase in flow roughness reduces peak streamflow in the channel segment.

In the SWAT model, the channel cover factor (CH_COV), channel erodibility factor (CH_EROD), and Manning's roughness coefficient 'n' (CH_N2) have been used for representation of grassed waterways. The default Manning's 'n' value of 0.014 is increased to 0.03 considering excavated channel with earthen bottom (Chow, 1959). Both calibrated channel cover factor value of 0.5 and channel erodibility value of 0.03 used in pre-BMP simulation are decreased to 0.001 (fully covered) in the post-BMP simulation. Here, the CH_COV value of 0.001 is used instead of zero to avert the use of default value. This study does not focus on changes in channel width and depth, which can be assigned by SWAT model, to maintain the streamflow capacity in the study area. The approach of grassed waterways representation in SWAT was adopted from the previous studies (Bracmort et al., 2006; Arabi et al., 2008).

8.2.5.6 Streambank stabilization/lined waterways (NRCS practice code-580)

The main purpose of streambank stabilization is to prevent bank erosion or damage, occurring due to high streamflow, by maintaining streamflow capacity of river. This treatment uses vegetation or structural practices to stabilize and protect the banks of a natural river or the shoreline of constructed waterbodies against scour and erosion. Hence, it refers to lined waterways with erosion resistant material in channel segment.

In the SWAT model, the streambank stabilization can be represented by channel erodibility factor (CH_EROD) and channel roughness (CH_N2). The approach adopted by Narasimhan et al. (2007), Arabi et al. (2008) and Tuppad et al. (2010) has been used to implement the streambank stabilization in SWAT. The channel erodibility factor was adjusted to a value of 0.001 (non-erodible). If the CH_EROD value is set to zero, the default value will be used in SWAT simulation. Moreover, the Manning's 'n' value of 0.03 was replaced in post-BMP simulation instead of 0.014 (default SWAT value).

8.2.5.7 Grade stabilization structures (NRCS practice code-410)

This practice is used to stabilize the grades and the head cutting of natural or artificial channels in a watershed. This practice increases sediment trapping, decrease peak streamflow rate/velocity, and reduces channel erosion.

The channel erodibility factor (CH_EROD) and slope of the channel segment (CH_S2) are adjusted to represent the grade stabilization structures. These parameters are adopted from the previous studies carried out by Santhi et al. (2003), Bracmort et al. (2006), Arabi et al. (2008) and Tuppad et al. (2010) to evaluate the grade stabilization structures using SWAT model. Again, in this analysis also the channel erodibility factor (CH_EROD) was adjusted to 0.001 to represent non-erodible channel condition in post-BMP simulation. In this study, the main channel slope and the channel length assigned by SWAT were used to estimate the slope of channel segment in post-BMP condition, as follows:

$$CH\_S2 = CH\_S2_{SWATassigned} - \frac{h}{CH\_L2_{SWATassigned}} \quad \ldots (8.1)$$

where, *CH_S2* is the possible slope of main channel segment after implementation of grade stabilization structure; $CH\_S2_{SWATassigned}$ is the slope of channel, and $CH\_L2_{SWATassigned}$ is the length of channel before implementation of structure; and *h* is the height of structure, here considered as 1.2 m (Bracmort et al., 2006; Arabi et al., 2008).

8.2.5.8 Porous gully plugs

The porous gully plugs are used to reduce the erosive power as well as velocity of concentrated streamflow in a tributary channel. This treatment was generally implemented on the ephemeral gullies to facilitate the sediment settling. It can be represented by modifying Manning's roughness coefficient (CH_N1) of tributary channel (Srinivasan, 2008). The default value of Manning's 'n' (0.014) used for simulation at pre-BMP condition has been increased to 0.05 in post-BMP simulation assuming minor natural streams with more stones (Chow, 1959).

Previously, Tuppad et al. (2010) simulated porous gully plugs by modifying the CH_N1 parameter in the SWAT model, and similar approach has been employed in the present study.

8.2.5.9 Recharge Structures

The recharge structures are small dams applied to lower the streamflow energy and to retain streamflow through a channel segment for facilitating infiltration and percolation to ground water. In turn, it minimizes the sediment carrying capacity of streamflow. In this study, this intervention was represented by changing hydraulic conductivity (CH_K1) and Manning's roughness coefficient (CH_N1) of the tributary channels in all the critical sub-watersheds (Srinivasan, 2008). In this treatment, the CH_K1 controls infiltration and turn out to be a recharge function of the watershed. Increase in channel roughness reduces sediment transport by lowering the peak streamflow. The default Manning's 'n' value of 0.014 used in the pre-BMP simulation has been increased to 0.08 in the post-BMP simulation for a tributary channel assuming sluggish reaches with deep pools (Chow, 1959). Also, the default value of hydraulic conductivity (zero mm/hr) used in the pre-BMP simulation, represents insignificant to low loss rate, was increased to 25 mm/hr in the post-BMP simulation assuming increase in loss rate up to moderate level through tributary channel with sand and gravel mixture (Lane, 1983). An approach used by Tuppad et al. (2010) and Giri et al. (2012) has been adopted to implement recharge structures in the study area.

8.2.6 Evaluation of BMP effectiveness

8.2.6.1 Percent reduction

The output of SWAT simulation for the pre-BMP and post-BMP conditions has been used to estimate the percent reduction in average sediment yield at each sub-watershed. Pre-BMP simulation represents the baseline condition, and the post-BMP simulation represents the effect of adjusted parameters representing a BMP. All the proposed BMPs are simulated individually for soil and water conservation as well as river channel protection using the SWAT model. The result of the model simulation comprises of the watershed as well as sub-watershed level analysis for the percent sediment yield reduction. It can be calculated as:

$$\%reduction = \frac{100 \times (BMPpre - BMPpost)}{BMPpre} \quad \ldots (8.2)$$

This analysis has been performed for the baseline simulation and the future climate horizons to evaluate the effect of BMPs implementation under changing climate. In addition, a paired t-test was conducted on simulation time series at the watershed outlet, before and after BMP realization to test the significance level of change.

8.2.6.2 Sensitivity analysis of BMP parameters

Based on the SWAT simulation at watershed outlet, the sensitivity analysis of the BMP representative parameters has been carried out to understand the influence of change in BMP parameter values. This study uses a sensitivity index (*SI*) based on nominal/baseline range of a BMP parameter. This sensitivity analysis helps to evaluate the change in model outputs simulated by varying each BMP parameter across its specified range, and at the same simulation time and all other BMP parameters kept at their baseline values (Cullen and Frey, 1999; Tuppad et al., 2010).

$$SI = \frac{(X_2 - X_1)}{X_{preBMP}} \quad \ldots (8.3)$$

where, X_2 and X_1 are the model output values corresponding to minimum and maximum values of a BMP parameter, and X_{preBMP} is the pre-BMP model output at nominal or baseline value.

In this analysis, a positive *SI* value represents direct response of change in BMP parameter value to the model output, i.e. increase in the parameter value increases the model outputs, and vice versa. However, a negative *SI* value indicates indirect response between change in parameter value and model outputs, i.e. increase in parameter value decreases the model outputs, and vice versa. Hence, a negative value of SI represents that the BMP parameter and the model output (here streamflow and/or sediment yield) are inversely related to each other.

8.3 RESULTS AND DISCUSSION

In this section, the effect of BMP implementation at pre- and post-BMP conditions, and the sensitivity and uncertainty analysis of BMP effectiveness on model simulations are analyzed and evaluated for streamflow and sediment yield in the critical sub-watersheds of the Betwa river basin.

8.3.1 Critical sub-watersheds

The average annual sediment yield of all fifty-seven sub-watersheds of the Betwa River basin has been simulated for baseline and the four future horizons, as presented in Table 8.5. Ranking is given to all sub-watersheds based on the sediment yield obtained for the baseline period (1986-2005) as well as for the future horizon period (2020-2099) as shown in Table 8.6. According to the guidelines provided by Singh (1995) for Indian conditions, the average annual sediment yield was further regrouped into six soil erosion classes as shown in Table 8.7.

Table 8.5: Average annual sediment yield for sub-watersheds of Betwa basin

Sub-watershed	Area (ha)	Average annual Sediment yield (t ha^{-1} year^{-1})				
		Baseline 1986	Horizon 2020	Horizon 2040	Horizon 2060	Horizon 2080
SW-1	11253.78	182.03	186.01	181.79	262.26	223.51
SW-2	43520.13	46.79	47.80	46.74	67.38	57.45
SW-3	52576.11	0.00	0.00	0.00	0.00	0.00
SW-4	19452.24	110.92	113.41	112.22	164.85	138.20
SW-5	55177.92	39.00	39.86	39.46	57.97	48.60
SW-6	176287.41	9.69	10.17	10.48	14.86	12.22
SW-7	40620.06	18.37	19.03	17.14	24.53	21.76
SW-8	76524.30	0.11	0.24	0.19	0.26	0.27
SW-9	119800.98	0.00	0.00	0.00	0.00	0.00
SW-10	179577.09	0.00	0.00	0.00	0.00	0.00
SW-11	48750.66	33.01	34.86	36.53	51.65	42.24
SW-12	33527.34	22.18	22.99	20.73	29.64	26.29
SW-13	55269.09	0.00	0.00	0.00	0.00	0.00
SW-14	4012.83	157.14	162.95	148.75	215.55	189.17
SW-15	94267.53	0.00	0.00	0.00	0.00	0.00
SW-16	4704.93	132.45	137.26	125.38	182.05	159.66
SW-17	21368.52	78.95	84.73	87.93	122.07	100.09
SW-18	2070.63	38.85	40.88	37.76	53.17	46.58
SW-19	141855.21	0.88	0.95	0.97	1.32	0.91
SW-20	43248.69	29.02	31.53	34.65	48.10	38.33
SW-21	30941.64	1.70	1.79	1.67	2.36	2.06
SW-22	64202.58	0.38	0.38	0.33	0.47	0.43
SW-23	153413.46	0.00	0.00	0.00	0.00	0.00
SW-24	16729.02	0.56	0.56	0.48	0.69	0.63
SW-25	14033.16	5.28	5.78	5.50	7.35	4.41
SW-26	109016.91	0.00	0.00	0.00	0.00	0.00
SW-27	136146.33	0.26	0.28	0.26	0.36	0.31
SW-28	159767.28	0.08	0.09	0.08	0.12	0.10
SW-29	98769.60	0.00	0.00	0.00	0.00	0.00
SW-30	197607.15	0.00	0.00	0.00	0.00	0.00
SW-31	161891.37	0.00	0.00	0.00	0.00	0.00
SW-32	90014.94	2.99	3.57	4.02	4.98	4.07
SW-33	134213.76	0.00	0.00	0.00	0.00	0.00
SW-34	47748.51	4.58	5.58	6.35	7.80	6.36
SW-35	135564.39	0.00	0.00	0.00	0.00	0.00
SW-36	135404.55	0.00	0.00	0.00	0.00	0.00
SW-37	32159.52	5.52	6.90	7.87	9.59	7.83
SW-38	68338.44	2.01	2.61	2.99	3.59	2.94
SW-39	86532.03	0.12	0.13	0.14	0.18	0.15
SW-40	196250.58	0.00	0.00	0.00	0.00	0.00
SW-41	52138.35	0.00	0.00	0.00	0.00	0.00

SW-42	84435.48	0.00	0.00	0.00	0.00	0.00
SW-43	43345.89	2.55	3.44	3.93	4.68	3.84
SW-44	85231.17	0.00	0.00	0.00	0.01	0.00
SW-45	10735.56	9.06	12.56	14.32	16.97	14.00
SW-46	56537.46	0.00	0.00	0.00	0.00	0.00
SW-47	59029.74	0.57	1.06	1.16	1.36	1.15
SW-48	44285.76	1.02	1.17	1.38	1.63	1.32
SW-49	143310.15	0.00	0.00	0.00	0.00	0.00
SW-50	4810.50	6.05	6.97	8.28	9.67	7.82
SW-51	73755.72	0.00	0.00	0.00	0.00	0.00
SW-52	45707.85	0.15	0.18	0.20	0.24	0.19
SW-53	110209.14	0.00	0.00	0.00	0.00	0.00
SW-54	74063.25	0.16	0.18	0.22	0.25	0.20
SW-55	54460.62	0.11	0.12	0.14	0.16	0.13
SW-56	78435.63	0.00	0.00	0.00	0.00	0.00
SW-57	63491.31	0.00	0.01	0.01	0.01	0.00

Table 8.6: Ranking of critical sub-watersheds for baseline period and future horizon period

Sub-watershed	Area (ha)	Average annual Sediment yield (t ha^{-1} $year^{-1}$)		Ranking for Baseline period	Ranking for Future periods	Average Slope
		Baseline (1986-2005)	Horizon (2020-2099)			
SW-1	11253.78	182.03	213.39	1	1	3.08
SW-2	43520.13	46.79	54.84	6	6	3.91
SW-3	52576.11	0.00	0.00	56	56	3.89
SW-4	19452.24	110.92	132.17	4	4	4.52
SW-5	55177.92	**39.00**	**46.47**	7	7	4.62
SW-6	176287.41	**9.69**	**11.93**	13	14	6.04
SW-7	40620.06	**18.37**	**20.61**	12	12	5.05
SW-8	76524.30	0.11	0.24	32	29	5.17
SW-9	119800.98	0.00	0.00	55	55	5.38
SW-10	179577.09	0.00	0.00	52	50	5.40
SW-11	48750.66	**33.01**	**41.32**	9	9	5.89
SW-12	33527.34	22.18	24.91	11	11	5.07
SW-13	55269.09	0.00	0.00	57	57	4.89
SW-14	4012.83	157.14	179.10	2	2	6.12
SW-15	94267.53	0.00	0.00	46	48	5.53
SW-16	4704.93	132.45	151.09	3	3	5.58
SW-17	21368.52	**78.95**	**98.70**	5	5	5.37
SW-18	2070.63	**38.85**	**44.60**	8	8	4.54
SW-19	141855.21	0.88	1.04	24	25	4.96
SW-20	43248.69	29.02	38.15	10	10	4.96
SW-21	30941.64	1.70	1.97	22	22	5.99
SW-22	64202.58	0.38	0.40	27	27	4.56
SW-23	153413.46	0.00	0.00	45	47	5.93
SW-24	16729.02	0.56	0.59	26	26	5.56

SW-25	14033.16	5.28	5.76	17	18	5.56
SW-26	109016.91	0.00	0.00	51	52	4.41
SW-27	136146.33	0.26	0.30	28	28	5.94
SW-28	159767.28	0.08	0.10	34	34	5.24
SW-29	98769.60	0.00	0.00	50	51	4.01
SW-30	197607.15	0.00	0.00	54	54	5.07
SW-31	161891.37	0.00	0.00	48	49	4.05
SW-32	90014.94	2.99	4.16	19	19	4.73
SW-33	134213.76	0.00	0.00	39	41	6.69
SW-34	47748.51	**4.58**	**6.52**	18	17	3.99
SW-35	135564.39	0.00	0.00	42	43	4.14
SW-36	135404.55	0.00	0.00	53	53	4.35
SW-37	32159.52	5.52	8.05	16	16	3.46
SW-38	68338.44	2.01	3.03	21	21	3.52
SW-39	86532.03	0.12	0.15	31	32	3.36
SW-40	196250.58	0.00	0.00	44	44	5.47
SW-41	52138.35	0.00	0.00	47	45	5.65
SW-42	84435.48	0.00	0.00	41	40	4.23
SW-43	43345.89	2.55	3.97	20	20	3.86
SW-44	85231.17	0.00	0.00	36	36	4.45
SW-45	10735.56	**9.06**	**14.46**	14	13	3.63
SW-46	56537.46	0.00	0.00	37	37	4.07
SW-47	59029.74	0.57	1.18	25	24	3.43
SW-48	44285.76	1.02	1.38	23	23	3.36
SW-49	143310.15	0.00	0.00	49	46	4.98
SW-50	4810.50	6.05	8.19	15	15	3.15
SW-51	73755.72	0.00	0.00	43	42	3.51
SW-52	45707.85	0.15	0.20	30	31	5.34
SW-53	110209.14	0.00	0.00	38	39	4.39
SW-54	74063.25	0.16	0.21	29	30	6.30
SW-55	54460.62	0.11	0.14	33	33	4.97
SW-56	78435.63	0.00	0.00	40	38	4.74
SW-57	63491.31	0.00	0.01	35	35	5.91

Table 8.7: Prioritization of critical sub-watersheds under different soil erosion classes

Sediment yield (t ha-1year-1)	**Sub-watershed**	**Area (%)**	**Soil erosion class**	**Priority class**
0–5	3,8,9,10,13,15,19,21,22,23,24,26,27,28,29, 30,31,32,33,35,36,38,39,40,42,42,43,44, 46,47,48,49,51,52,53,54,55,56,57	80.63	Slight	VI
5–10	25,34,37,50	8.60	Moderate	V
10–20	6,45	3.15	High	IV
20–40	7,12,20	3.18	Very high	III
40–80	2,5,11,18	2.44	Severe	II
>80	1,4,14,16,17	2.00	Very severe	I

Based on the SWAT model output, sediment yield in the few sub-watersheds has increased in the future horizon simulation as compared to the baseline simulation. For instance, the SW-34 has low average sediment yield of 4.58 t ha^{-1} $year^{-1}$ during baseline period which further increases to 6.52 t ha^{-1} $year^{-1}$ in future horizon (Table 8.6). Hence, the sub-watershed (SW-34) changes from slight soil erosion class to moderate soil erosion class. Therefore, the SW-34 was considered for prioritization and BMP treatment under future climatic changes (Table 8.7).

Table 8.7 shows that about 80.63% sub-watershed area of the Betwa River basin falls under the slight erosion class (0-5 t $ha^{-1}yr^{-1}$). About 8.60% of the sub-watershed area falls under the moderate soil erosion class (5 to 10 t $ha^{-1}y^{-1}$). Two sub-watersheds (SW-6 and SW-45), one individually from upper and lower basin part, falling under high soil erosion rate (10-20 t $ha^{-1}yr^{-1}$) cover about 3.15% of the total basin area. Three sub-watersheds (SW-7, SW-12 and SW-20) falling under very high soil erosion class (20-40 t $ha^{-1}yr^{-1}$) cover 3.18% area of the Betwa river basin. The sub-watersheds with severe soil erosion class (40-80 t $ha^{-1}yr^{-1}$) covers about 2.44% of the total basin area, however only 2% of the total basin area comes under very severe soil erosion class (>80 t $ha^{-1}yr^{-1}$). In this class, more than 80 t $ha^{-1}year^{-1}$ sediment yields were obtained from the most critical sub-watersheds of the Betwa basin. Therefore, proper management practices are crucial to reduce sediment yield in future. The sub-watershed wise soil erosion map of the Betwa river basin is presented in Figure 8.2.

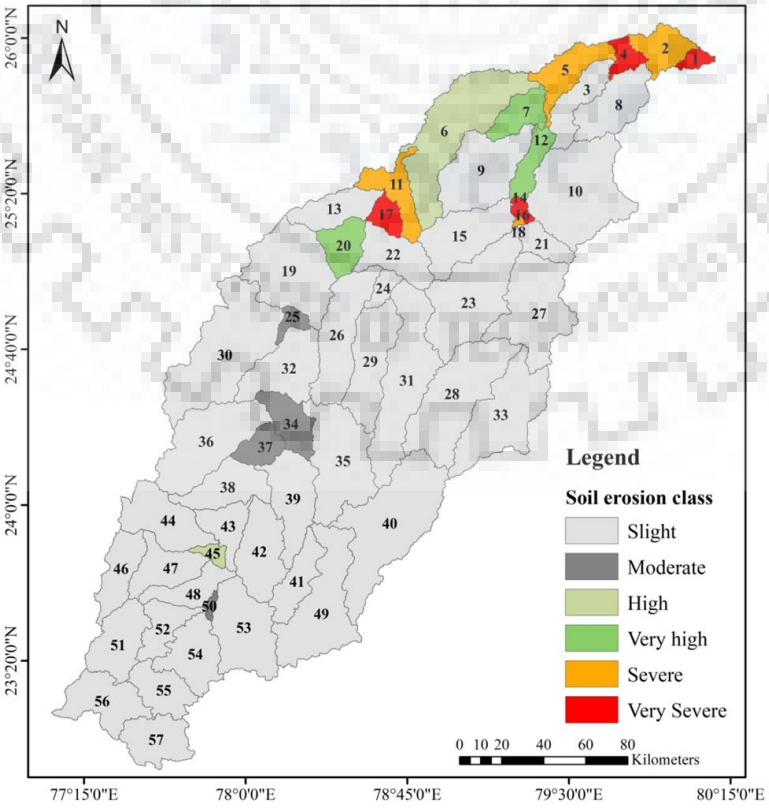

Figure 8.2: Critical sub-watersheds under different soil erosion classes in the Betwa basin

Among the identified critical sub-watersheds, the SW-34, SW-37, SW-45 and SW-50 are located in upper part, whereas other critical sub-watersheds located in the lower part of the basin (Figure 8.2). The result shows that highest sediment yield of about 213.39 t $ha^{-1}year^{-1}$ was simulated at the basin outlet (SW-1). High sediment yield (very high to very severe) was obtained mostly in the sub-watersheds located at downstream of the Betwa river basin. Area under maximum runoff experiences high sediment yield generation at sub-watershed level. The area covered by agriculture and forest have least rate of soil loss apart from the more slope gradient. Moreover, the main channel erosion due to flooding in monsoon season causes significant detachment and transportation of sediment particles from channel segment. Thus, high rate of sediment yield may be attributed to the sub-watershed level land erosion as well as stream bank or river channel erosion. In addition, none or a faulty method/practice of over-land and/or in-stream contributing more sediment yield which is prevalent in a large river basin. The results of this analysis can be used as a framework to develop soil and water conservation programs, as well as to protect and restore the river channel segment by evaluating feasible management practices.

Based on the average annual sediment yield, all sub-watersheds of the Betwa River basin were prioritized into six categories for conservation and protection treatments (Table 8.7). Five sub-watersheds (SW-1, SW-4, SW-14, SW-16 and SW-17) having sediment yields more than 80 t ha^{-1} $year^{-1}$ were assigned as first priority, four sub-watersheds (SW-2, SW-5, SW-11 and SW-18) having sediment yield in a range of 40–80 t ha^{-1} $year^{-1}$ were assigned as second priority, three sub-watersheds (SW-7, SW-12 and SW-20) having sediment yield in a range of 20–40 t ha^{-1} $year^{-1}$ were assigned as third priority, two sub-watersheds (SW-6 and SW-45) having sediment yield in a range of 10–20 t ha^{-1} $year^{-1}$ were assigned as fourth priority, and four sub-watersheds (SW-25, SW-34, SW-37 and SW-50) having sediment yield in the range of 5–10 t ha^{-1} $year^{-1}$ was assigned as fifth priority. These priorities are further used for application and evaluation of the BMPs in the Bewta River basin. In the past, Tripathi et al. (2003), Behera and Panda (2006), Pandey et al. (2007), and Agrawal et al. (2009) employed average annual sediment yields for the identification of critical areas in Indian watersheds. Moreover, Giri et al. (2012) and Rocha et al. (2012) also utilized average annual estimates of the sediment, runoff and nutrient loads for BMP treatments in USA and Brazil.

8.3.2 Effective management of BMPs

This study evaluated the effect of over-land as well as in-stream BMP implementation on the streamflow and sediment yield reductions by comparing the pre-BMP and post-BMP simulations obtained from the SWAT model at sub-watershed level. BMP effectiveness has

been evaluated by the percent reduction of model outputs and the sensitivity index (SI) values of corresponding model parameters representing a BMP within a critical sub-watershed of the study area.

8.3.2.1 Sensitivity of BMP parameters

(a) Sensitivity analysis for streamflow

The sensitivity of BMP parameters for streamflow in the critical sub-watersheds of the Betwa river basin is presented in Table 8.8. Among the over-land BMP parameters, the depth of tillage operation (DEPTIL), mixing efficiency of tillage operation (EFFMIX), curve number (CN2), USLE support practice factor (USLE_P) and cover factor (USLE_C) have positive SI values representing direct response to the streamflow. Only Manning's roughness coefficient overland flow (OV_N) parameter has negative sensitivity to the streamflow. Furthermore, among the in-stream BMP parameters, the channel cover (CH_COV), channel erodibility (CH_EROD) and average slope of main channel (CH_S2) have positive SI values which shows direct response to the change in streamflow at sub-watershed level. Nevertheless, negative sensitivity of other three in-stream BMP parameters namely Manning's roughness coefficients for main channel (CH_N2) as well as tributary channel (CH_N1) and the hydraulic conductivity in tributary channel (CH_K1) shows indirect response to the streamflow output in critical sub-watersheds of the Betwa basin.

Table 8.8: Sensitivity of BMP parameters for streamflow in critical sub-watersheds

Sub-watershed	Sensitivity index (SI) values for streamflow											
	Over-land BMP parameters						In-stream BMP parameters					
	DEPTIL	EFFMIX	CN2	USLE_P	USLE_C	OV_N	CH_COV	CH_EROD	CH_S2	CH_N2	CH_N1	CH_K1
SW-1	0.01	0.00	0.15	0.05	0.03	-0.01	0.01	0.11	0.25	-0.08	-0.06	-0.03
SW-2	0.01	0.00	0.16	0.05	0.03	-0.01	0.01	0.11	0.21	-0.13	-0.05	-0.02
SW-4	0.01	0.00	0.17	0.05	0.03	-0.01	0.02	0.11	0.21	-0.12	-0.05	-0.03
SW-5	0.01	0.00	0.17	0.05	0.03	-0.01	0.01	0.11	0.25	-0.08	-0.06	-0.02
SW-6	0.02	0.01	0.18	0.06	0.03	-0.01	0.01	0.11	0.21	-0.10	-0.07	-0.04
SW-7	0.00	0.00	0.17	0.00	0.02	-0.01	0.00	0.07	0.23	-0.06	0.00	0.00
SW-11	0.02	0.01	0.17	0.06	0.04	-0.01	0.01	0.08	0.21	-0.10	-0.04	-0.04
SW-12	0.00	0.00	0.18	0.03	0.02	-0.01	0.01	0.06	0.17	-0.04	0.00	0.00
SW-14	0.00	0.00	0.15	0.02	0.02	-0.01	0.01	0.07	0.04	-0.05	0.00	0.00
SW-16	0.00	0.00	0.15	0.04	0.03	-0.01	0.01	0.04	0.01	-0.02	-0.01	0.00
SW-17	0.02	0.01	0.16	0.06	0.04	-0.01	0.01	0.11	0.11	-0.08	-0.03	-0.04
SW-18	0.00	0.00	0.18	0.00	0.03	-0.01	0.00	0.09	0.07	-0.04	-0.01	0.00
SW-20	0.03	0.01	0.17	0.07	0.05	0.00	0.02	0.08	0.10	-0.10	-0.02	-0.03
SW-25	0.04	0.02	0.18	0.08	0.06	0.00	0.02	0.11	0.05	-0.11	-0.02	-0.04
SW-34	0.03	0.01	0.15	0.06	0.05	-0.02	0.01	0.10	0.03	-0.05	-0.02	0.00
SW-37	0.03	0.02	0.15	0.05	0.05	-0.02	0.01	0.04	0.02	-0.09	-0.03	0.00
SW-45	0.03	0.02	0.16	0.04	0.06	-0.02	0.02	0.05	0.02	-0.07	-0.03	0.00
SW-50	0.03	0.01	0.17	0.06	0.06	-0.02	0.02	0.07	0.00	-0.09	-0.02	0.00

Note: *DEPTIL = Depth of tillage operation; EFFMIX = Mixing efficiency of tillage operation; CN2 = SCS runoff curve number for moisture condition II; USLE_P = USLE support practice factor; USLE_C = USLE cover factor; OV_N = Manning's roughness coefficient for overland flow; CH_COV = Channel cover factor; CH_EROD = Channel erodibility factor; CH_S2 = Average slope of the main channel calculated with respect to structural height (1.2 m); CH_N2 = Main channel roughness (Manning's 'n') coefficient; CH_N1 = Tributary channel roughness (Manning's 'n') coefficient; and CH_K1 = Hydraulic conductivity (mm/hr) in the tributary channel.*

(b) Sensitivity analysis for sediment yield

The sensitivity of BMP parameters for sediment yield in critical sub-watersheds of the study area is presented in Table 8.9. Among the over-land BMP parameters, the depth of tillage operation (DEPTIL), mixing efficiency of tillage operation (EFFMIX), curve number (CN2), USLE support practice factor (USLE_P) and cover factor (USLE_C) have positive SI values representing direct response to the sediment yield. Only Manning's roughness coefficient overland flow (OV_N) parameter has negative sensitivity to the sediment yield. Furthermore, among the in-stream BMP parameters, the channel cover (CH_COV), channel erodibility (CH_EROD) and average slope of main channel (CH_S2) have positive SI values which show the direct response to the change in sediment yield at sub-watershed level. Nevertheless, negative sensitivity of other three in-stream BMP parameters namely Manning's roughness coefficients for main channel (CH_N2) as well as tributary channel (CH_N1) and the hydraulic

conductivity in tributary channel (CH_K1) shows indirect response to the sediment output in critical sub-watersheds of the study area.

Table 8.9: Sensitivity of BMP parameters for sediment yield in critical sub-watersheds

Sub-watershed	Sensitivity index (SI) values for sediment yield											
	Over-land BMP parameters						In-stream BMP parameters					
	DEPTIL	EFFMIX	CN2	USLE_P	USLE_C	OV_N	CH_COV	CH_EROD	CH_S2	CH_N2	CH_N1	CH_K1
SW-1	0.06	0.04	0.20	0.05	0.06	-0.01	0.12	0.24	0.13	-0.22	-0.07	-0.06
SW-2	0.06	0.04	0.20	0.03	0.06	-0.01	0.15	0.30	0.13	-0.22	-0.07	-0.06
SW-4	0.07	0.03	0.16	0.04	0.06	-0.01	0.15	0.27	0.17	-0.20	-0.07	-0.07
SW-5	0.07	0.04	0.19	0.03	0.06	-0.01	0.12	0.30	0.17	-0.20	-0.08	-0.07
SW-6	0.05	0.03	0.15	0.05	0.04	-0.01	0.10	0.30	0.25	-0.16	-0.02	-0.05
SW-7	0.03	0.01	0.17	0.01	0.06	-0.02	0.15	0.27	0.35	-0.17	-0.05	-0.03
SW-11	0.05	0.02	0.19	0.03	0.03	-0.01	0.11	0.30	0.29	-0.16	-0.03	-0.05
SW-12	0.03	0.01	0.16	0.01	0.06	-0.02	0.07	0.30	0.35	-0.17	-0.02	-0.03
SW-14	0.04	0.02	0.20	0.01	0.06	-0.02	0.06	0.18	0.34	-0.18	-0.01	-0.04
SW-16	0.04	0.02	0.21	0.01	0.06	-0.02	0.07	0.30	0.34	-0.18	-0.01	-0.04
SW-17	0.03	0.01	0.12	0.04	0.05	-0.01	0.15	0.30	0.33	-0.10	-0.03	-0.03
SW-18	0.02	0.01	0.16	0.03	0.04	-0.02	0.09	0.43	0.18	-0.16	-0.01	-0.02
SW-20	0.04	0.01	0.16	0.05	0.03	-0.02	0.11	0.29	0.32	-0.12	-0.04	-0.07
SW-25	0.02	0.03	0.10	0.05	0.03	0.00	0.15	0.56	0.13	-0.10	-0.02	0.00
SW-34	0.03	0.01	0.13	0.05	0.04	-0.01	0.23	0.55	0.21	-0.17	-0.03	-0.03
SW-37	0.02	0.01	0.11	0.04	0.03	-0.01	0.22	0.58	0.19	-0.17	-0.03	-0.02
SW-45	0.02	0.01	0.10	0.05	0.03	-0.01	0.18	0.55	0.20	-0.13	-0.01	0.00
SW-50	0.03	0.01	0.14	0.01	0.03	-0.01	0.24	0.42	0.23	-0.18	-0.01	-0.03

Note: *DEPTIL = Depth of tillage operation; EFFMIX = Mixing efficiency of tillage operation; CN2 = SCS runoff curve number for moisture condition II; USLE_P = USLE support practice factor; USLE_C = USLE cover factor; OV_N = Manning's roughness coefficient for overland flow; CH_COV = Channel cover factor; CH_EROD = Channel erodibility factor; CH_S2 = Average slope of the main channel calculated with respect to structural height (1.2 m); CH_N2 = Main channel roughness (Manning's 'n') coefficient; CH_N1 = Tributary channel roughness (Manning's 'n') coefficient; and CH_K1 = Hydraulic conductivity (mm/hr) in the tributary channel.*

Overall, the BMP parameters having positive SI value indicated that the increase in BMP parameter values can increase the model outputs; however, the negative SI value represents that an increase in the BMP parameter value can decrease the model outputs (Tuppad et al., 2010) in terms of streamflow and sediment yield outputs. It is observed that, the critical sub-watersheds covers within the lower basin area have large negative SI values as compared to the critical sub-watersheds lies within the upper basin area.

8.3.2.2 Evaluation of over-land BMPs

In this study, the tillage management, contour farming, residue management and strip cropping practices are evaluated for soil and water conservation treatment in the Betwa river basin.

(a) Evaluation of tillage operation

In the present analysis, effect of the three tillage operations, i.e. conservation tillage, field cultivator and zero tillage, in agriculture land has been evaluated for the critical sub-watersheds of the Betwa River basin. This practice include decrease in depth (DEPTIL) and mixing efficiency (EFFMIX) of the tillage operation as well as decrease in the curve number (CN2) to lower the surface flow and soil erosion, and reducing the sediment loads. Result of conservation tillage operation shows that reduction in the sediment yield (6.84% to 24.27%) is higher as compared to reduction in the streamflow (5.38% to 9.53%) for baseline as well as future horizons (Table 8.10a). Furthermore, the result of field cultivator operation shows high sediment yield reduction (4.15% to 22.73%) as compared to the streamflow reduction (6.30% to 11.20%) as shown in Table 8.10b. Also, the result of zero tillage operation shows high sediment yield reduction (12.66% to 31.46%) as compared to the streamflow reduction (1.05% to 5.08%) as shown in Table 8.10c. Although the streamflow reduction in the critical sub-watersheds (SW-25, SW-34, SW-37, SW-45 and SW-50) located at upper basin part is high, the tillage operations employed in this study can effectively reduce the soil erosion to some extent by decreasing depth and mixing efficiency of tillage operation. Sensitivity of the tillage parameters, i.e. DEPTIL, EFFMIX and CN2, is low for streamflow (Table 8.8) and high for sediment yield (Table 8.9). The sub-watersheds located in lower basin part of the basin have high sensitivity of DEPTIL, EFFMIX and CN2 resulting high (about 10% to 31%) sediment yield reduction (Tables 8.9 & 8.10a,b,c). These BMP parameters also reduces the flow but in lower extent (about 1% to 11%). In this study, the zero tillage operation reduces sediment yield in larger amount (up to 31%); however the field cultivator operation reduces streamflow in larger amount (up to 11%). Thus, the field cultivator operation is an effective tillage management practice for streamflow reduction, and the zero tillage is an effective tillage management practice for sediment yield reduction in the Betwa river basin.

Table 8.10a: Percent reduction in post-BMP simulation after implementation of conservation tillage

Sub-watershed	Streamflow (% reduction)					Sediment yield(% reduction)				
	Baseline 1986	Horizon 2020	Horizon 2040	Horizon 2060	Horizon 2080	Baseline 1986	Horizon 2020	Horizon 2040	Horizon 2060	Horizon 2080
SW-1	6.07	5.38	6.07	5.91	6.59	13.33	23.69	22.88	21.52	24.27
SW-2	6.77	6.03	5.38	5.91	5.98	13.32	23.74	22.92	22.32	23.44
SW-4	5.38	6.08	6.11	5.94	6.67	23.58	22.29	21.41	21.76	16.31
SW-5	6.89	6.09	6.12	5.94	6.03	23.60	23.29	22.42	21.78	17.13
SW-6	7.68	6.45	6.46	6.20	6.35	20.54	21.43	20.16	19.74	20.62
SW-7	7.14	6.49	6.48	6.64	6.88	20.02	20.33	19.64	18.94	18.01
SW-11	6.60	6.52	6.51	7.09	7.42	19.51	19.24	19.13	18.14	7.67
SW-12	7.14	6.49	6.48	6.64	6.88	16.94	22.56	21.52	20.63	22.44
SW-14	6.14	6.09	6.12	5.94	6.35	16.67	22.04	21.28	12.87	15.48
SW-16	7.29	6.27	6.29	6.07	6.19	19.01	20.77	20.27	19.95	18.46
SW-17	6.65	6.56	6.54	6.26	6.43	18.04	17.85	16.63	17.20	6.84
SW-18	6.87	6.50	6.50	6.86	7.15	15.48	15.48	15.48	15.48	15.48
SW-20	7.06	6.91	6.82	6.47	6.72	18.92	18.60	16.93	17.63	18.15
SW-25	9.53	7.22	7.08	6.65	8.56	18.41	16.00	12.03	7.87	19.29
SW-34	6.71	6.18	6.20	6.01	6.27	11.37	9.98	10.81	11.17	12.24
SW-37	6.97	6.42	6.41	6.16	6.31	13.79	7.33	7.37	7.87	10.03
SW-45	6.76	6.53	6.52	6.56	6.79	13.11	10.65	11.65	12.61	15.17
SW-50	6.96	6.70	6.66	6.67	6.94	16.75	16.00	14.33	16.00	16.60

Table 8.10b: Percent reduction in post-BMP simulation after implementation of field cultivator tillage

Sub-watershed	Streamflow (% reduction)					Sediment yield(% reduction)				
	Baseline 1986	Horizon 2020	Horizon 2040	Horizon 2060	Horizon 2080	Baseline 1986	Horizon 2020	Horizon 2040	Horizon 2060	Horizon 2080
SW-1	7.00	6.30	6.99	6.83	7.51	11.79	22.15	21.34	19.98	22.73
SW-2	7.94	7.21	6.55	7.08	7.16	11.37	21.79	20.97	20.36	21.48
SW-4	6.74	7.44	7.47	7.30	8.03	21.32	20.03	19.15	19.50	14.05
SW-5	8.28	7.48	7.51	7.33	7.42	21.29	20.98	20.11	19.47	14.82
SW-6	9.49	8.27	8.27	8.01	8.16	17.52	18.41	17.14	16.72	17.60
SW-7	8.66	8.00	8.00	8.16	8.40	17.50	17.81	17.12	16.42	15.48
SW-11	8.37	8.28	8.27	8.85	9.18	16.56	16.30	16.18	15.20	4.73
SW-12	8.66	8.01	8.00	8.16	8.40	14.40	20.02	18.98	18.10	19.91
SW-14	7.97	7.92	7.95	7.78	8.19	13.61	18.98	18.22	9.81	12.42
SW-16	8.96	7.95	7.96	7.74	7.87	16.22	17.98	17.48	17.16	15.67
SW-17	8.27	8.17	8.15	7.87	8.04	15.36	15.16	13.95	14.51	4.15
SW-18	8.23	7.86	7.86	8.23	8.51	13.21	13.21	13.21	13.21	13.21
SW-20	8.55	8.40	8.31	7.96	8.21	16.44	16.12	14.45	15.15	15.67
SW-25	11.20	8.88	8.74	8.32	10.23	15.63	13.22	9.25	5.09	16.51
SW-34	7.91	7.38	7.40	7.20	7.47	9.38	7.99	8.81	9.18	10.25
SW-37	8.01	7.45	7.45	7.20	7.35	12.06	5.60	5.64	6.14	8.30
SW-45	7.85	7.62	7.61	7.65	7.88	11.29	8.83	9.83	10.80	13.36
SW-50	7.91	7.65	7.60	7.61	7.88	15.17	14.43	12.75	14.43	15.02

Table 8.10c: Percent reduction in post-BMP simulation after implementation of zero tillage

Sub-watershed	Streamflow (% reduction)					Sediment yield(% reduction)				
	Baseline 1986	Horizon 2020	Horizon 2040	Horizon 2060	Horizon 2080	Baseline 1986	Horizon 2020	Horizon 2040	Horizon 2060	Horizon 2080
SW-1	3.61	2.92	3.61	3.44	4.12	18.08	28.44	27.62	26.26	29.01
SW-2	3.64	2.90	2.25	2.78	2.86	19.34	29.76	28.95	28.34	29.46
SW-4	1.76	2.47	2.50	2.32	3.06	30.54	29.25	28.37	28.72	23.27
SW-5	3.20	2.40	2.42	2.25	2.34	30.71	30.40	29.54	28.89	24.25
SW-6	2.85	1.62	1.63	1.36	1.52	29.84	30.73	29.46	29.04	29.92
SW-7	3.10	2.45	2.44	2.60	2.84	27.80	28.11	27.42	26.72	25.79
SW-11	1.89	1.81	1.80	2.37	2.71	28.58	28.31	28.20	27.21	16.74
SW-12	3.09	2.43	2.43	2.59	2.83	24.74	30.37	29.33	28.44	30.25
SW-14	1.24	1.19	1.22	1.05	1.46	26.10	31.46	30.71	22.29	24.90
SW-16	2.82	1.81	1.83	1.61	1.73	27.61	29.36	28.86	28.55	27.05
SW-17	2.36	2.26	2.24	1.96	2.14	26.31	26.12	24.90	25.47	15.10
SW-18	3.24	2.87	2.86	3.23	3.52	22.47	22.47	22.47	22.47	22.47
SW-20	3.09	2.94	2.85	2.50	2.75	26.56	26.23	24.57	25.27	25.79
SW-25	5.08	2.77	2.63	2.20	4.11	26.97	24.56	20.59	16.43	27.85
SW-34	3.52	2.99	3.01	2.81	3.08	17.52	16.13	16.95	17.32	18.39
SW-37	4.20	3.65	3.65	3.40	3.54	19.12	12.66	12.69	13.19	15.35
SW-45	3.86	3.63	3.61	3.66	3.89	18.70	16.24	17.24	18.20	20.77
SW-50	4.44	4.18	4.14	4.15	4.42	21.60	20.85	19.18	20.85	21.45

In addition, the effect of future climate change has been also studied using post-BMP simulation compared to the pre-BMP simulation. Results show horizon 2080 has high reduction in streamflow as compare to the other climate horizons (Figures 8.3a, 8.3b and 8.3c). In case of the sediment yield reduction, few sub-watersheds followed the similar pattern of streamflow reduction at sub-watershed level, but in larger percentages. In this analysis, the streamflow has nearly similar response in all the critical sub-watersheds during future climate horizons, while the sediment yield has varying response, especially under conservation tillage and field cultivator operations. In this analysis, zero tillage operation resulted a high streamflow reduction in the critical sub-watersheds having low land slopes. Hence, the effectiveness of zero tillage operation reduces with an increase in agriculture land slope of the Betwa basin. Thus, the climate change impact induces some variations in the streamflow and sediment yield reduction under the similar tillage management practice. It may be due to varying soil erosivity under the future climatic changes.

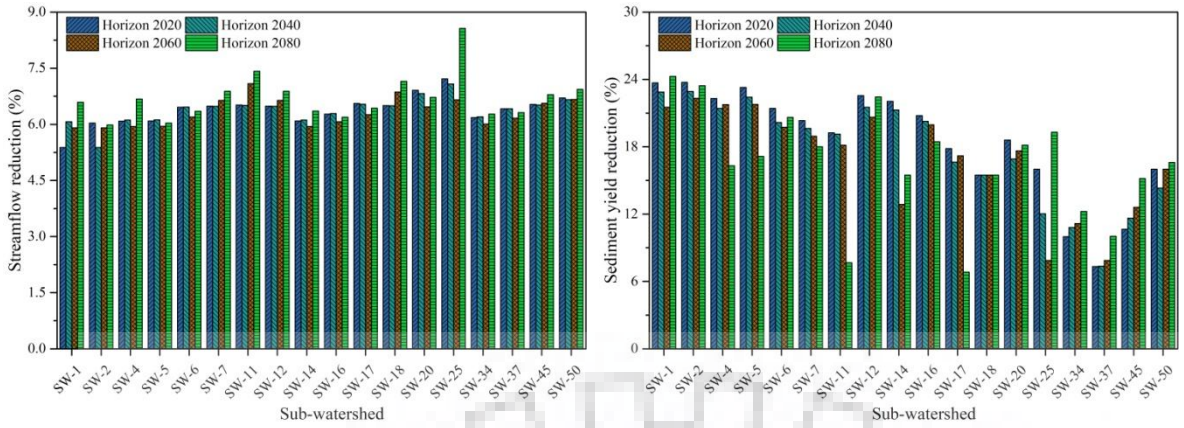

Figure 8.3a: Effect of conservation tillage on future streamflow and sediment yield

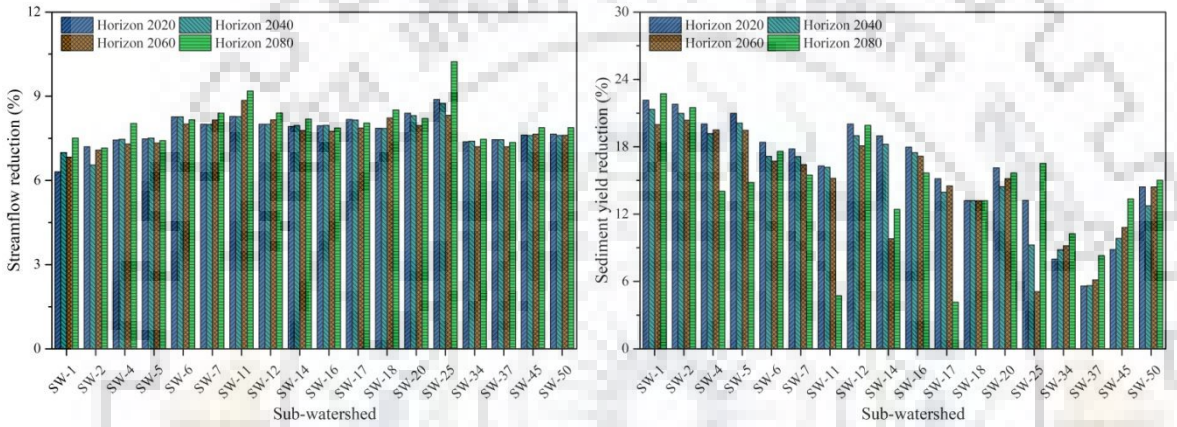

Figure 8.3b: Effect of field cultivator tillage on future streamflow and sediment yield

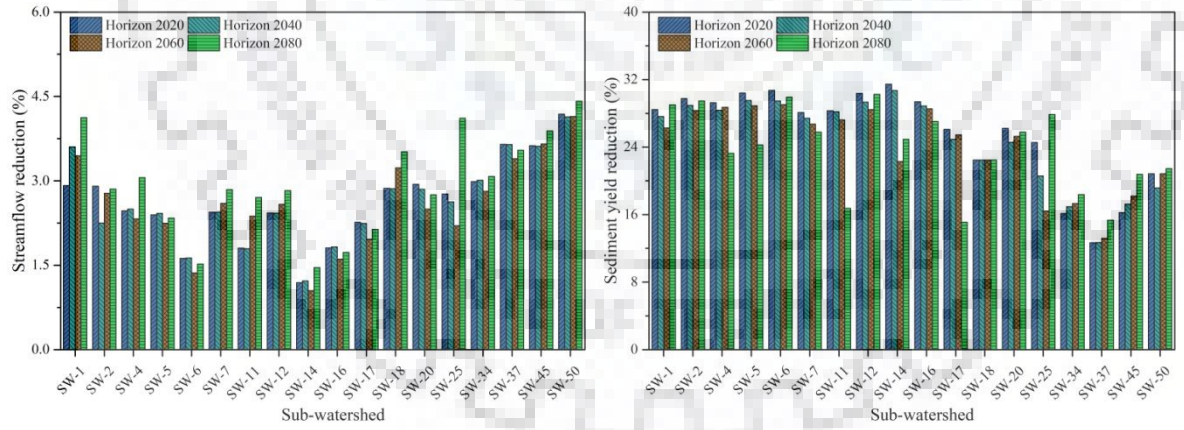

Figure 8.3c: Effect of zero tillage on future streamflow and sediment yield

The effective management of tillage operations was also analyzed for each priority class given to critical sub-watersheds. Result of conservation tillage shows the high percent of streamflow reduction in class-III followed by class V, class IV, class-II and class-I (Table 8.11a). Nevertheless, the high sediment yield reductions are observed for priority class-III, followed by class-I, class-II, class-IV and class-V. The result of field cultivator shows high streamflow reduction in order of class III, IV, V, II and I; and high sediment yield reduction in order of

class III, I, II, IV and V (Table 8.11b). Also, the result of zero tillage resulted high streamflow reduction in order of class V, III, IV, II and I; and high sediment yield reduction in order of class III, I, II, IV and V (Table 8.11c). It is because of varying sensitivity of BMP parameters in critical sub-watersheds of a priority class. Thus, priority class wise these tillage operations have varying response to the streamflow and sediment yield reduction.

Table 8.11a: Priority class wise average reduction (%) in streamflow and sediment yield under effective conservation tillage

Priority class	Streamflow (% reduction)					Sediment yield (% reduction)				
	Baseline 1986	Horizon 2020	Horizon 2040	Horizon 2060	Horizon 2080	Baseline 1986	Horizon 2020	Horizon 2040	Horizon 2060	Horizon 2080
I	6.31	6.08	6.23	6.02	6.45	18.13	21.33	20.50	18.66	16.27
II	6.78	6.29	6.13	6.45	6.65	17.98	20.44	19.99	19.43	15.93
III	7.11	6.63	6.60	6.58	6.83	18.63	20.50	19.36	19.07	19.53
IV	7.22	6.49	6.49	6.38	6.57	16.82	16.04	15.90	16.18	17.90
V	7.54	6.63	6.59	6.37	7.02	15.08	12.33	11.13	10.73	14.54

Table 8.11b: Priority class wise average reduction (%) in streamflow and sediment yield under effective field cultivator tillage

Priority class	Streamflow (% reduction)					Sediment yield (% reduction)				
	Baseline 1986	Horizon 2020	Horizon 2040	Horizon 2060	Horizon 2080	Baseline 1986	Horizon 2020	Horizon 2040	Horizon 2060	Horizon 2080
I	7.79	7.56	7.71	7.50	7.93	15.66	18.86	18.03	16.19	13.80
II	8.21	7.71	7.55	7.87	8.07	15.61	18.07	17.62	17.06	13.56
III	8.62	8.13	8.10	8.09	8.34	16.11	17.98	16.85	16.55	17.02
IV	8.67	7.94	7.94	7.83	8.02	14.40	13.62	13.48	13.76	15.48
V	8.76	7.84	7.80	7.58	8.23	13.06	10.31	9.11	8.71	12.52

Table 8.11c: Priority class wise average reduction (%) in streamflow and sediment yield under effective zero tillage

Priority class	Streamflow (% reduction)					Sediment yield (% reduction)				
	Baseline 1986	Horizon 2020	Horizon 2040	Horizon 2060	Horizon 2080	Baseline 1986	Horizon 2020	Horizon 2040	Horizon 2060	Horizon 2080
I	2.36	2.13	2.28	2.08	2.50	25.73	28.93	28.09	26.26	23.87
II	2.99	2.49	2.33	2.66	2.85	25.28	27.74	27.29	26.73	23.23
III	3.09	2.61	2.57	2.56	2.81	26.37	28.24	27.10	26.81	27.27
IV	3.35	2.62	2.62	2.51	2.70	24.27	23.48	23.35	23.62	25.34
V	4.31	3.40	3.36	3.14	3.79	21.30	18.55	17.35	16.95	20.76

(b) Evaluation of contour farming

The contour farming practice has been implemented by adjusting curve number (CN2) and USLE support practice factor (USLE_P), and then evaluated for critical sub-watersheds of the Betwa river basin. In this practice, the USLE_P and CN2 values are decreased to reduce sheet

erosion from the agriculture land. Results show that reduction in sediment yield (6.38% to 34.41%) is higher than the reduction in streamflow (9.78% to 13.25%) for baseline as well as future horizons (Table 8.12). It is observed that, percentage reduction in sediment yield has great variation due to varying response of BMP parameters as compare to the response of streamflow reduction. Although the streamflow reduction in critical sub-watersheds (SW-25, SW-34, SW-37, SW-45 and SW-50) located at upper basin part is high, the contour farming can effectively reduce the sheet erosion by decreasing flow velocity and support practice factor. In this analysis, the BMP parameters, i.e. the CN2 and the USLE_P, have low sensitivity for streamflow (Table 8.8) and high sensitivity for sediment yield (Table 8.9). The sub-watersheds located in the lower basin part have high sensitivity of CN2 and USLE_P resulting high (more than 25%) sediment yield reduction (Tables 8.9 & 8.12) than the upper basin part. Sensitivity of these BMP parameters also reduces the flow in some percent (about 10%), which is lesser than the sediment yield reduction. Result shows that the USLE_P parameter increases the effect of contour farming on streamflow and sediment yield reduction. Therefore, the contour farming is an effective management practice in the Betwa River basin.

Table 8.12: Percent reduction in post-BMP simulation after implementation of contour farming

Sub-watershed	Streamflow (% reduction)					Sediment yield(% reduction)				
	Baseline 1986	Horizon 2020	Horizon 2040	Horizon 2060	Horizon 2080	Baseline 1986	Horizon 2020	Horizon 2040	Horizon 2060	Horizon 2080
SW-1	10.56	10.43	10.55	10.59	10.89	23.59	32.68	31.99	31.68	34.41
SW-2	10.56	9.78	10.55	10.59	10.89	22.16	33.78	32.05	31.75	33.61
SW-4	10.72	10.59	10.68	10.72	11.06	32.14	32.04	31.23	30.83	26.14
SW-5	10.75	9.90	9.96	10.74	11.09	32.18	33.05	31.26	30.16	26.98
SW-6	11.93	10.63	10.64	10.93	12.35	30.11	29.87	28.55	27.18	29.60
SW-7	11.02	10.36	10.64	10.86	11.62	32.14	23.19	31.23	22.63	22.90
SW-11	10.93	10.75	10.73	10.18	11.53	26.71	26.64	25.23	24.80	23.52
SW-12	10.77	10.89	10.54	11.09	10.74	26.14	23.20	30.30	22.64	31.60
SW-14	11.02	10.72	10.68	11.21	11.54	32.14	27.61	23.98	26.73	24.52
SW-16	10.93	10.60	10.50	11.20	11.58	29.44	29.84	28.25	27.48	25.25
SW-17	12.30	10.84	10.80	11.11	10.58	23.84	23.92	22.68	22.94	6.38
SW-18	11.26	10.80	10.85	11.25	10.66	32.14	25.40	27.61	24.68	23.71
SW-20	11.83	11.53	11.36	10.65	12.49	25.15	25.04	24.71	24.67	27.03
SW-25	12.63	12.15	11.87	11.02	13.25	24.82	20.37	16.41	10.75	23.65
SW-34	11.91	11.28	11.30	10.93	11.91	14.06	14.37	14.98	15.66	18.01
SW-37	11.57	11.15	10.94	11.56	11.29	12.37	7.01	8.11	9.12	11.60
SW-45	11.85	11.52	11.11	11.82	11.89	23.42	19.30	20.56	20.85	27.06
SW-50	11.92	11.66	11.30	11.59	12.57	23.10	20.37	18.70	20.37	20.37

Furthermore, the impact of future climate change on post-BMP simulation shows that the horizon 2080 has high reduction in streamflow and sediment yield as compare to the other

climate horizons (Figure 8.4). Similar to the previous analysis, the sediment yield reduction in few sub-watersheds followed the similar pattern of streamflow reduction in lower part of the study area. In this analysis, the streamflow has nearly similar response in all critical sub-watersheds during future climate horizons, while the sediment yield has varying response to the contour farming practice. Thus, the climate change also has small impact on model simulation reductions under the same management practice.

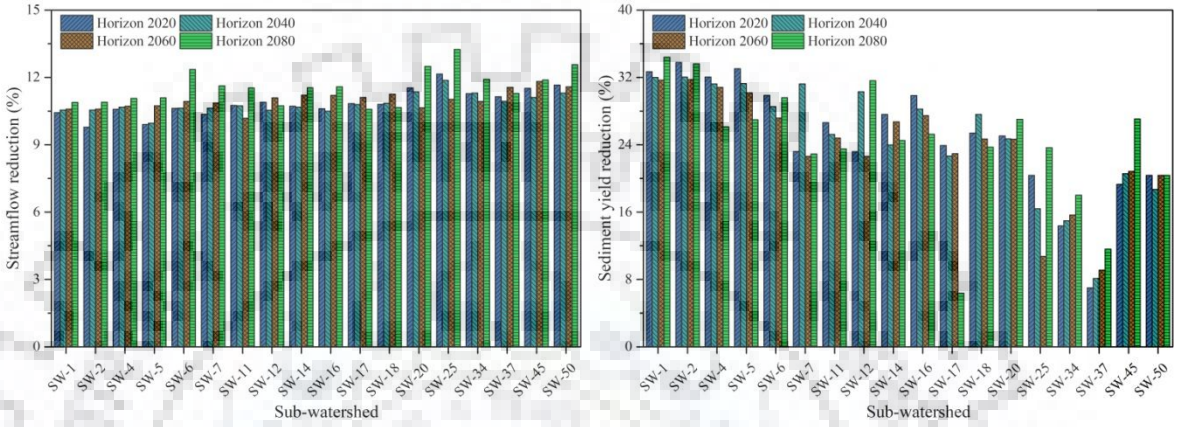

Figure 8.4: Effect of contour farming on future streamflow and sediment yield

Effective management of contour farming was also analyzed for each priority class given to critical sub-watersheds (Table 8.13). Results show that the high percent of streamflow reduction in class-V followed by class IV, class III, class-I and class-II. Nevertheless, the high sediment yield reductions are observed for priority class-II, followed by class-I, class-III, class-IV and class-V. Thus, the contour farming has varying response to the streamflow and sediment yield reduction for different priority classes.

Table 8.13: Priority class wise average reduction (%) in streamflow and sediment yield under effective contour farming

Priority class	Streamflow (% reduction)					Sediment yield(% reduction)				
	Baseline 1986	Horizon 2020	Horizon 2040	Horizon 2060	Horizon 2080	Baseline 1986	Horizon 2020	Horizon 2040	Horizon 2060	Horizon 2080
I	11.11	10.64	10.64	10.97	11.13	28.23	29.22	27.62	27.93	23.34
II	10.87	10.31	10.52	10.69	11.04	28.30	29.72	29.04	27.85	26.95
III	11.21	10.93	10.84	10.87	11.62	27.81	23.81	28.75	23.31	27.18
IV	11.89	11.07	10.87	11.37	12.12	26.77	24.59	24.55	24.01	28.33
V	12.01	11.56	11.35	11.27	12.25	18.59	15.53	14.55	13.97	18.41

(c) Evaluation of residue management

In this study, residue management has been implemented by considering changes in curve number (CN2), USLE cover factor (USLE_C), and Manning's roughness coefficient for

overland flow (OV_N) in critical sub-watersheds of the Betwa river basin. In this analysis, the CN2 and USLE_C values were decreased to reduce overland flow, sheet and rill erosion, while the OV_N was increased to get more surface roughness. Results show that reduction in sediment yield (6.04% to 20.53%) is higher than the reduction in streamflow (6.44% to 9.08%) for baseline as well as future horizons (Table 8.14). Although the streamflow reduction in critical sub-watersheds (SW-25, SW-34, SW-37, SW-45 and SW-50) located at the upper basin part is high, the residue management practices can effectively reduce the sheet and rill erosion by decreasing flow velocity and land cover factor with more surface roughness. The BMP parameters, i.e. the CN2, USLE_C and OV_N, have low sensitivity for the streamflow (Table 8.8) and high sensitivity for the sediment yield (Table 8.9). Thus, in the present analysis the sediment yield reduction is higher than the streamflow reduction. Mainly, the sub-watersheds located in lower basin area have high sensitivity of BMP parameters resulting high (about 18%) sediment yield reduction (Tables 8.9 & 8.14). Analysis shows that residue management practice has low effect on streamflow and sediment yield reduction, as compared to the contour farming.

Table 8.14: Percent reduction in post-BMP simulation after implementation of residue management

Sub-watershed	Streamflow (% reduction)					Sediment yield(% reduction)				
	Baseline 1986	Horizon 2020	Horizon 2040	Horizon 2060	Horizon 2080	Baseline 1986	Horizon 2020	Horizon 2040	Horizon 2060	Horizon 2080
SW-1	7.12	7.03	7.11	7.31	7.54	8.93	18.21	19.50	18.30	20.53
SW-2	7.12	7.03	7.11	7.31	7.54	8.92	20.32	18.50	18.35	19.71
SW-4	7.22	7.13	7.19	7.41	7.67	19.10	18.75	17.90	17.67	18.24
SW-5	7.24	6.44	6.47	7.42	7.69	19.13	18.78	17.92	16.99	19.09
SW-6	8.03	7.88	6.81	7.36	8.63	16.32	15.94	15.84	14.25	16.15
SW-7	7.49	7.37	6.83	7.40	8.20	16.12	12.82	18.58	12.26	12.53
SW-11	6.95	6.87	6.86	7.43	7.76	14.03	15.01	13.64	13.55	19.40
SW-12	7.12	8.14	7.21	7.42	7.60	18.07	12.83	16.91	12.27	17.20
SW-14	7.16	6.89	7.00	7.47	7.61	17.06	15.81	16.92	15.14	15.81
SW-16	7.23	7.16	7.14	7.49	8.15	14.39	16.51	13.91	13.44	17.78
SW-17	7.00	8.09	6.89	7.48	7.83	12.56	12.36	11.15	11.71	14.86
SW-18	7.45	7.19	7.02	7.66	8.20	14.64	15.91	14.28	15.29	17.60
SW-20	9.08	7.26	7.17	7.90	8.41	15.15	13.11	12.90	13.22	13.99
SW-25	7.80	7.56	7.42	8.27	8.91	12.41	7.85	6.04	14.88	10.00
SW-34	7.08	7.43	7.27	7.51	7.88	13.80	14.53	13.30	14.53	17.69
SW-37	7.11	7.37	7.12	7.70	7.72	14.54	13.25	13.11	14.18	14.43
SW-45	7.59	7.08	7.22	7.66	8.18	13.39	12.22	11.18	14.72	13.80
SW-50	7.76	7.45	7.24	7.86	8.12	10.00	10.00	8.33	10.00	10.00

The analysis of future climate change impact on post-BMP simulation shows that horizon 2080 has high reduction in streamflow and sediment yield (Figure 8.5). Sediment yield reduction in few critical sub-watersheds located at lower basin area is in similar pattern to the streamflow reduction. In this analysis, the streamflow has increased in all the critical sub-watersheds during future years, while the sediment yield has varying response to the residue management practice. Thus, the climate change also has an impact on future streamflow and sediment yield reduction in the present study.

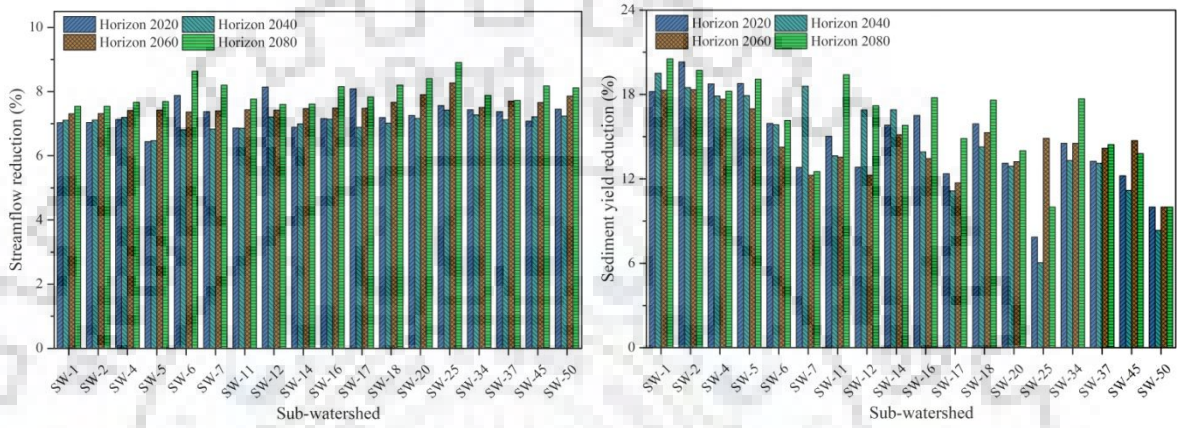

Figure 8.5: Effect of residue management on future streamflow and sediment yield

The effective management of residue management was also analyzed for each priority class given to the critical sub-watersheds (Table 8.15). Results show that the high percent of streamflow reduction in class-V followed by class IV, class III, class-I and class-II. Nevertheless, the high sediment yield reductions are observed for priority class-II, followed by class-I, class-IV, class-III and class-V. Thus, the residue management has varying response to the streamflow and sediment yield reduction for the different priority classes.

Table 8.15: Priority class wise average reduction (%) in streamflow and sediment yield under effective residue management

Priority class	Streamflow (% reduction)					Sediment yield(% reduction)				
	Baseline 1986	Horizon 2020	Horizon 2040	Horizon 2060	Horizon 2080	Baseline 1986	Horizon 2020	Horizon 2040	Horizon 2060	Horizon 2080
I	7.15	7.26	7.07	7.43	7.76	14.41	16.33	15.88	15.25	17.44
II	7.19	6.88	6.86	7.46	7.80	14.18	17.50	16.08	16.04	18.95
III	7.90	7.59	7.07	7.57	8.07	16.45	12.92	16.13	12.58	14.57
IV	7.81	7.48	7.01	7.51	8.40	14.85	14.08	13.51	14.49	14.98
V	7.44	7.46	7.27	7.84	8.16	12.69	11.41	10.19	13.40	13.03

(d) Evaluation of strip cropping

In this study, strip cropping has been implemented by adjusting the curve number (CN2), USLE cover factor (USLE_C), USLE support practice factor (USLE_P) and Manning's

roughness coefficient for overland flow (OV_N) in critical sub-watersheds of the Betwa basin. In this analysis, the CN2, USLE_C and USLE_P decreased to reduce flow in small depressions, sheet and rill erosion, while the OV_N increased to get more surface roughness. Results show that reduction in sediment yield (21.04% to 37.28%) is higher than the reduction in streamflow (11.07% to 13.97%) for baseline as well as future horizons (Table 8.16). Although, the streamflow reduction in critical sub-watersheds (SW-25, SW-34, SW-37, SW-45 and SW-50) located at the upper basin part is high, the strip cropping practice can effectively reduce the sheet and rill erosion by decreasing flow velocity in depressions and cover factor, and more surface roughness. The BMP parameters, i.e. the CN2, USLE_P, USLE_C and OV_N, have low sensitivity for streamflow (Table 8.8) and high sensitivity for sediment yield (Table 8.9). Thus, in the present analysis also the sediment yield reduction is higher than the streamflow reduction. Mainly, the sub-watersheds located in the lower basin area have high sensitivity of the BMP parameters resulting high (more than 30%) sediment yield reduction (Tables 8.9 & 8.16). This analysis shows that residue management practice is highly effective on streamflow and sediment yield reduction, as compared to the previous over-land BMP treatments. Thus, the strip cropping is the most effective over-land management practice in the Betwa basin.

Table 8.16: Percent reduction in post-BMP simulation after implementation of strip cropping

Sub-watershed	Streamflow (% reduction)					Sediment yield(% reduction)				
	Baseline 1986	Horizon 2020	Horizon 2040	Horizon 2060	Horizon 2080	Baseline 1986	Horizon 2020	Horizon 2040	Horizon 2060	Horizon 2080
SW-1	11.73	11.63	11.72	11.85	12.11	26.07	35.26	35.56	34.80	37.28
SW-2	11.74	11.30	11.73	11.85	12.11	25.54	36.87	35.09	34.86	36.47
SW-4	11.86	11.75	11.83	11.96	12.26	35.62	35.21	34.38	34.06	32.00
SW-5	11.89	11.07	11.11	11.97	12.28	35.65	35.73	34.41	33.39	32.85
SW-6	12.87	12.15	11.62	12.04	13.39	33.22	32.72	32.01	30.53	32.69
SW-7	11.63	11.70	11.80	11.97	12.18	32.85	27.82	34.94	27.26	27.53
SW-11	11.83	11.70	11.69	11.70	12.54	30.37	30.64	29.25	28.99	34.66
SW-12	11.93	12.41	11.81	12.09	11.13	34.86	27.83	33.26	27.27	32.35
SW-14	11.89	11.46	11.65	12.45	12.23	33.74	31.85	26.81	31.11	30.19
SW-16	12.14	11.88	11.76	11.98	12.97	30.47	32.77	29.51	29.01	33.68
SW-17	12.55	12.36	11.74	12.19	12.10	28.20	27.95	26.73	27.14	29.94
SW-18	12.05	11.66	11.81	11.76	12.39	30.65	31.92	27.77	30.82	32.42
SW-20	13.35	12.29	12.16	12.17	13.34	30.15	28.89	28.62	28.76	30.33
SW-25	13.11	12.75	12.54	12.54	13.97	28.61	23.93	21.04	30.64	26.64
SW-34	12.18	11.76	11.92	11.95	12.68	29.69	30.47	28.14	29.92	33.05
SW-37	12.52	12.15	11.88	12.25	12.72	30.09	28.21	28.72	29.44	30.13
SW-45	12.48	12.19	12.18	12.55	13.18	29.38	28.15	25.86	30.60	29.53
SW-50	12.76	12.20	12.21	12.70	13.01	25.00	25.00	23.33	25.00	25.00

Future climate change impact analysis shows that the horizon 2080 has high reduction in streamflow and sediment yield (Figure 8.6). Sediment yield in critical sub-watersheds located at lower basin area reduces in similar pattern to the streamflow reduction. In this analysis also, streamflow response increases in all critical sub-watersheds during future horizons, while the sediment yield has varying response to the residue management practice. Thus, the climate change also has an impact on streamflow and sediment reduction under strip cropping treatment.

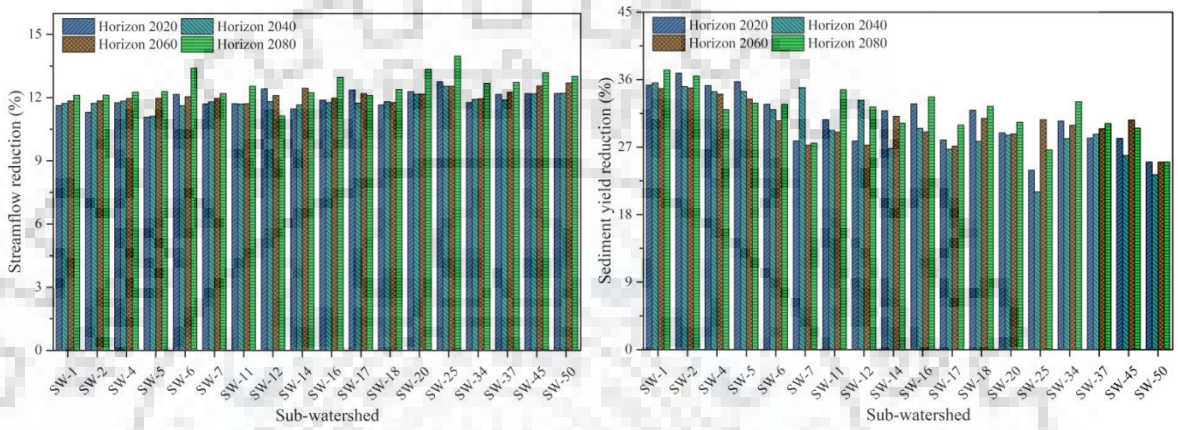

Figure 8.6: Effect of strip cropping on future streamflow and sediment yield

The effective management of strip cropping was also analyzed for the each priority class given to critical sub-watersheds (Table 8.17). Results show the high percent of streamflow reduction in class-V followed by class IV, class III, class-I and class-II. Nevertheless, the high sediment yield reductions are observed for priority class-II, followed by class-I, class-IV, class-III and class-V. Thus, the residue management has varying response to streamflow and sediment yield reduction for different priority classes.

Table 8.17: Priority class wise average reduction (%) in streamflow and sediment yield under effective strip cropping

Priority class	Streamflow (% reduction)					Sediment yield(% reduction)				
	Baseline 1986	Horizon 2020	Horizon 2040	Horizon 2060	Horizon 2080	Baseline 1986	Horizon 2020	Horizon 2040	Horizon 2060	Horizon 2080
I	12.03	11.82	11.74	12.08	12.33	30.82	32.61	30.60	31.23	32.62
II	11.88	11.43	11.58	11.82	12.33	30.55	33.79	31.63	32.02	34.10
III	12.31	12.13	11.92	12.08	12.22	32.62	28.18	32.27	27.76	30.07
IV	12.68	12.17	11.90	12.29	13.28	31.30	30.44	28.93	30.56	31.11
V	12.64	12.22	12.14	12.36	13.10	28.35	26.90	25.31	28.75	28.71

Sensitivity of the BMP parameters usually vary in each critical area, hence, the BMP effectiveness also varied in this study. Among the over-land BMP parameters, decrease in the

DEPTIL, EFFMIX, CN2, USLE_C and USLE_P values, due to positive sensitivity, can induce the low streamflow and sediment yield outputs. Only the OV_N parameter was increased to have more resistance to the overland flow, due to negative sensitivity. In agriculture area, the contour farming and the strip cropping can be used as the most effective over-land BMPs treatments. Both the agriculture treatments can significantly reduces streamflow and sediment yield in the Betwa basin. Effectiveness of the BMP treatments can vary under future climatic changes, and hence induces varying response for each priority class as well as the critical areas. In the past, Tripathi et al. (2005) employed these three tillage treatments for Nagwan watershed, and recommended that the field cultivator can replace conventional tillage treatment. Furthermore, in Indian regions, Behera and Panda (2006) recommended conservation tillage for Kapgari watershed, Pandey et al. (2005) recommended zero tillage and conservation tillage treatments for Banikdih watershed, and Pandey et al. (2009a) recommended field cultivator as tillage treatment for the Karso watershed over the conventional tillage practice.

8.3.2.3 Evaluation of in-stream BMPs

In this study, the grassed waterways, streambank stabilization, grade stabilization structures, porous gully plugs and recharge structures have been evaluated for protection and restoration of river channels of the Betwa river basin.

(a) Evaluation of grassed waterways

In this study, the grassed waterway has been implemented on main river channel, and then evaluated for critical sub-watersheds of the Betwa basin. This practice increases channel cover (CH_COV) and channel roughness (CH_N2), as well as reduces the main channel erodibility (CH_EROD) to facilitate low flow velocity for sediment settling. Result shows that sediment yields of SW-45 reduce in the range of 50.54% to 56.42% for baseline (1986-2005) and future climate horizons (2020-2099), respectively (Table 8.18). Although the low amount of streamflow (about 1.77%) reduces in SW-45, this protection practice effectively reduces the erosion in main channel due to high sensitivity of CH_COV, CH_EROD and CH_N2 (Tables 8.8 & 8.9). Similarly, the SW-18 and SW-37 with high sensitivity of CH_COV, CH_EROD and CH_N2 resulting a large percent reduction in sediment yield (more than 45%). High sensitivity of CH_N2 at downstream river basin simulates more sediment yield reduction in SW-1, SW-2, SW-4 and SW-5 (Table 8.9). The sensitivity of main channel roughness also reduces small percentages of streamflow (more than 3%) in lower basin sub-watersheds as compared to the upper basin sub-watersheds.

Furthermore, the sediment yield reduction is less in SW-14 and SW-25 as compared to the sediment yields from other critical sub-watersheds. It may be due to low sensitivity of CH_COV (SI = 0.06) and CH_EROD (SI = 0.18) in SW-14, and low negative sensitivity of CH_N2 (SI = -0.10) in SW-25. Sensitivity of the BMP parameters in SW-25 may reduce in future and thus, resulting decrease in sediment yield from horizon 2020 to horizon 2080. For all critical sub-watersheds, present study shows high percent sediment reduction in the range of 7.86% to 56.42%, and low streamflow reduction in the range of 1.62% to 3.62%. Thus, the grassed waterways in main channel can significantly reduce the sediment yield and protect the main river channel in the critical sub-watersheds located in upper as well as lower part of the Betwa River basin.

Table 8.18: Percent reduction in post-BMP simulation after implementation of grassed waterways

Sub-watershed	Streamflow (% reduction)					Sediment yield (% reduction)				
	Baseline 1986	Horizon 2020	Horizon 2040	Horizon 2060	Horizon 2080	Baseline 1986	Horizon 2020	Horizon 2040	Horizon 2060	Horizon 2080
SW-1	3.57	3.51	3.62	3.21	3.36	38.81	38.94	40.42	42.35	40.43
SW-2	3.58	3.53	3.62	3.21	3.36	39.16	39.31	40.76	42.75	40.79
SW-4	3.51	3.46	3.53	3.14	3.29	35.45	35.09	35.94	36.75	35.77
SW-5	3.41	3.37	3.45	3.06	3.21	35.60	35.24	36.08	36.89	35.91
SW-6	3.43	3.39	3.39	3.02	3.18	31.83	30.60	30.99	32.58	31.95
SW-7	2.20	2.20	2.22	2.16	2.16	21.67	19.85	20.02	24.36	22.96
SW-11	2.70	2.69	2.67	2.50	2.57	28.83	27.59	28.86	30.56	29.93
SW-12	1.98	1.98	1.98	1.99	1.98	21.76	19.90	20.04	24.44	23.02
SW-14	1.65	1.66	1.62	1.71	1.67	21.32	19.71	19.94	23.72	22.41
SW-16	1.74	1.76	1.73	1.79	1.77	21.76	20.15	20.36	24.10	22.82
SW-17	2.46	2.46	2.44	2.33	2.36	26.55	24.66	26.30	28.85	28.00
SW-18	1.86	1.85	1.84	1.88	1.86	46.08	46.15	46.68	47.00	46.59
SW-20	2.39	2.40	2.36	2.27	2.30	25.96	24.55	26.49	28.93	27.96
SW-25	2.21	2.21	2.19	2.13	2.17	29.96	24.77	18.70	13.36	7.86
SW-34	2.15	2.15	2.15	2.11	2.12	35.75	40.40	40.11	38.93	39.39
SW-37	1.99	2.00	2.00	2.00	1.99	48.41	52.24	51.77	50.95	51.41
SW-45	1.74	1.77	1.79	1.81	1.77	50.54	56.42	55.40	54.77	55.45
SW-50	1.77	1.79	1.83	1.84	1.79	44.61	44.58	44.04	43.19	43.52

In addition, the effect of future climate change on post-BMP simulation has also been analyzed in the study. Results show the SW-25 has sediment yield reduction variation from horizon 2020 (about 24.77%) to horizon 2080 (about 7.86%) as shown in Figure 8.7. It means SW-25 is most affected critical sub-watershed under climatic changes. Figure 8.7 illustrates that the critical sub-watersheds located at downstream of the Betwa River basin have similar pattern between streamflow reduction and sediment yield reduction. However, four sub-watersheds (SW-34, SW-37, SW-45 and SW-50) located at upper part of the basin have high sensitivity to the

sediment yield reduction. Result demonstrated that sensitivity of grassed waterways parameter is not very effective to reduce the streamflow in a river channel.

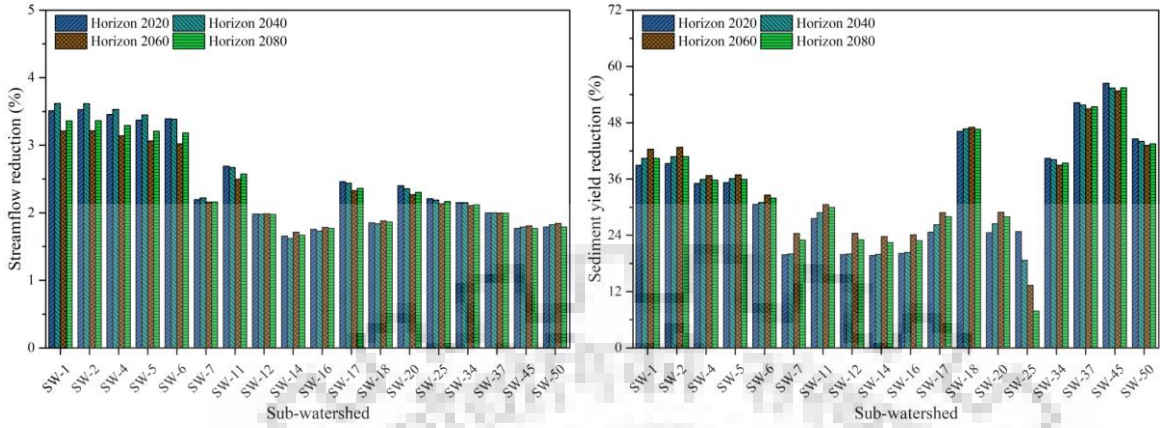

Figure 8.7: Effect of grassed waterways on future streamflow and sediment yield

Effective management of grassed waterway was also analyzed for each priority class (Table 8.19). Results show the high percent reductions of streamflow for class-II followed by class-I, class-IV, class-III and class-V. Nevertheless, the high sediment yield reductions are observed for priority class-IV, followed by class-V, class-II, class-I and class-III. Thus, in the present study the grassed waterway implementation has varied response to the streamflow and sediment yield under different priority classes.

Table 8.19: Priority class wise average reduction (%) in the streamflow and sediment yield under effective grassed waterways

Priority class	Streamflow (% reduction)					Sediment yield (% reduction)				
	Baseline 1986	Horizon 2020	Horizon 2040	Horizon 2060	Horizon 2080	Baseline 1986	Horizon 2020	Horizon 2040	Horizon 2060	Horizon 2080
I	2.59	2.57	2.59	2.44	2.49	28.78	27.71	28.59	31.15	29.89
II	2.89	2.86	2.89	2.66	2.75	37.42	37.07	38.10	39.30	38.31
III	2.19	2.19	2.19	2.14	2.15	23.13	21.43	22.18	25.91	24.65
IV	2.59	2.58	2.59	2.41	2.47	41.18	43.51	43.20	43.68	43.70
V	2.03	2.04	2.04	2.02	2.02	39.69	40.50	38.65	36.61	35.55

(b) Evaluation of streambank stabilization

Streambank stabilization, also called lined waterways, is used to reduce sediment loads while maintaining streamflow capacity in the main channel segment. This practice was implemented by lowering channel erodibility (CH_EROD) and channel roughness (CH_N2) which shows a high percent reduction of sediment yield in the SW-12 and SW-14 during all periods, i.e. from historical baseline to future horizons (Table 8.20). Streambank stabilization practice responds well to the critical sub-watersheds located in upper and lower part of the study area. More sediment yield reductions with low streamflow changes are observed in upper basin sub-

watersheds, mainly SW-37 and SW-45, where as a negative sensitivity of CH_N2 is dominant over the sensitivity of CH_EROD (Tables 8.8 & 8.9). Thus, streambank stabilization is an effective treatment to reduce large percent of sediment yields in the upper basin area. In case of lower basin, the SW-1, SW-2, SW-4 and SW-5 have high sediment yield reductions (more than 35%) and small streamflow reductions (about 3%) as compared to the upper basin streamflow reductions. In lower basin area also, the sensitivity of CH_N2 is dominant over the low sensitivity of CH_EROD. Thus, in streambank stabilization practice, the lined channel reduces a significant amount of sediment yield in the critical sub-watersheds. Nevertheless, the lower sediment yield reduction in SW-12 (about 20%) and SW-14 (about 22%) shows that the negative sensitivity of CH_N2 in SW-12 (SI = -0.17) and SW-14 (SI = -0.18) is less effective in these critical areas (Table 8.9).

In this analysis, the percent reductions in the sediment yield and streamflow by the streambank stabilization are nearly similar to the percent reductions obtained by the grassed waterways. The grassed waterway parameter (mainly CH_COV) reduces more streamflow as compare to the streamflow reductions obtained by streambank stabilization practice. Contrary, the sediment yield reductions are higher in case of the streambank stabilization treatment. It means the streambank stabilization is optimal in-stream BMP for river channel protection.

Table 8.20: Percent reduction in post-BMP simulation after implementation of streambank stabilization

Sub-watershed	Streamflow (% reduction)					Sediment yield (% reduction)				
	Baseline 1986	Horizon 2020	Horizon 2040	Horizon 2060	Horizon 2080	Baseline 1986	Horizon 2020	Horizon 2040	Horizon 2060	Horizon 2080
SW-1	3.37	3.31	3.42	3.01	3.16	41.08	41.51	42.55	44.12	42.49
SW-2	3.38	3.33	3.42	3.01	3.16	40.79	41.18	42.32	44.03	42.30
SW-4	3.31	3.26	3.33	2.94	3.09	36.36	36.14	36.82	37.46	36.62
SW-5	3.21	3.17	3.25	2.86	3.01	36.09	35.80	36.56	37.27	36.36
SW-6	3.23	3.19	3.19	2.82	2.98	31.83	30.60	30.99	32.58	31.95
SW-7	2.00	2.00	2.02	1.96	1.96	21.98	20.12	20.25	24.60	23.20
SW-11	2.50	2.49	2.47	2.30	2.37	28.92	27.69	28.93	30.62	30.00
SW-12	1.78	1.78	1.78	1.79	1.78	21.76	19.90	20.04	24.44	23.02
SW-14	1.45	1.46	1.42	1.51	1.47	21.60	19.96	20.18	23.98	22.69
SW-16	1.54	1.56	1.53	1.59	1.57	21.76	20.15	20.36	24.10	22.82
SW-17	2.26	2.26	2.24	2.13	2.16	26.55	24.66	26.30	28.85	28.00
SW-18	1.66	1.65	1.64	1.68	1.66	57.34	56.54	57.10	59.11	58.21
SW-20	2.19	2.20	2.16	2.07	2.10	25.96	24.55	26.49	28.93	27.96
SW-25	2.01	2.01	1.99	1.93	1.97	54.83	52.15	49.60	48.21	37.94
SW-34	1.95	1.95	1.95	1.91	1.92	54.30	56.06	56.71	57.08	56.91
SW-37	1.79	1.80	1.80	1.80	1.79	61.54	63.04	63.44	63.84	63.63
SW-45	1.54	1.57	1.59	1.61	1.57	60.06	63.36	63.41	63.74	63.70
SW-50	1.57	1.59	1.63	1.64	1.59	56.65	56.41	57.03	57.23	56.94

In future, the streambank stabilization can significantly decrease sediment yield from the critical sub-watersheds with a lower amount of streamflow reductions (Figure 8.8). Based on the post-BMP simulation, the analysis reveals that the impacts of climate change on the percent reductions in sediment yield and streamflow under varying responses of BMP parameters in future. Mainly, in horizon 2060 the higher sediment yield reductions in all the sub-watersheds were observed with low changes in streamflow (Figure 8.8). Except in SW-25, where a low sediment yield reduction is observed for the horizon 2020 (about 52.15%) to horizon 2080 (about 37.94%). The result reveals that in SW-25 the effect of streambank stabilization deceases in future under changing climate. Thus, the effect of streambank stabilization practice in main channel varies under changing future climate.

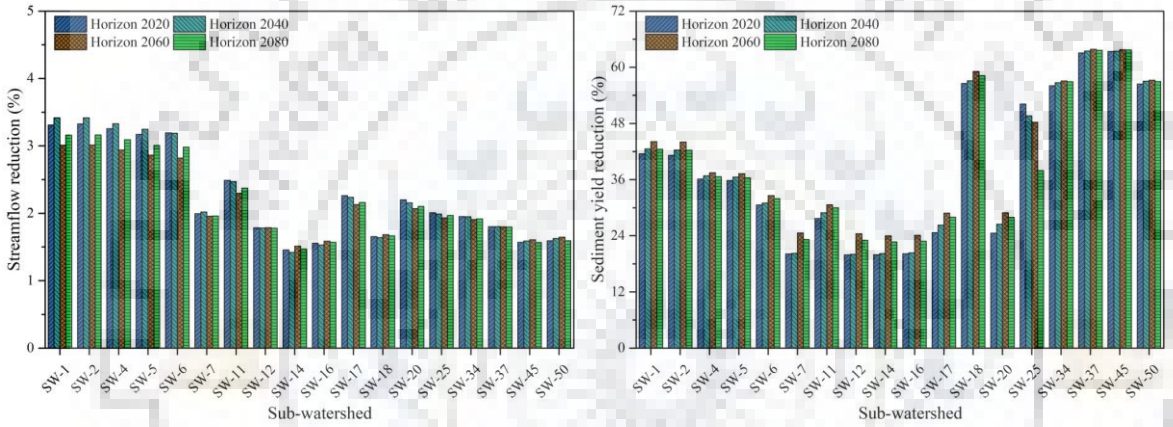

Figure 8.8: Effect of streambank stabilization on future streamflow and sediment yield

In this analysis, the streambank stabilization significantly reduces sediment yield in all the priority classes as compared to the streamflow (Table 8.21). Results show that the high streamflow reductions are observed for class-II followed by class-I, class-IV, class-III and class-V. However, the higher sediment yield reductions are observed for priority class-V, followed by class-IV, class-II, class-I and class-III. Thus, the streambank stabilization practice also has varying response in each priority classes.

Table 8.21: Priority class wise average reduction (%) in streamflow and sediment yield under effective streambank stabilization

Priority class	Streamflow (% reduction)					Sediment yield (% reduction)				
	Baseline 1986	Horizon 2020	Horizon 2040	Horizon 2060	Horizon 2080	Baseline 1986	Horizon 2020	Horizon 2040	Horizon 2060	Horizon 2080
I	2.39	2.37	2.39	2.24	2.29	29.47	28.48	29.24	31.70	30.52
II	2.69	2.66	2.69	2.46	2.55	40.79	40.30	41.22	42.76	41.72
III	1.99	1.99	1.99	1.94	1.95	23.23	21.52	22.26	25.99	24.73
IV	2.39	2.38	2.39	2.21	2.27	45.94	46.98	47.20	48.16	47.83
V	1.83	1.84	1.84	1.82	1.82	56.83	56.91	56.70	56.59	53.85

(c) Evaluation of grade stabilization structures

In this study, grade stabilization structures have also been implemented and evaluated for the main channel protection employing the SWAT model. This structural practice lowered the main channel erosion by decreasing the main channel erodibility (CH_EROD) and slope steepness (CH_S2). The results show a high percent sediment yield reduction (about 36%) from SW-12 as compared to other critical sub-watersheds (Table 8.22). Due to structural intervention, the CH_S2 parameter in SW-12 has a large sensitivity to the high sediment yield reduction (35-37%) and low streamflow reductions (about 7-8%) as shown in Tables 8.8 & 8.9. In this analysis, low sediment reductions are observed for SW-37, located at downstream of the Basoda gauging site, where main CH_S2 has a low sensitivity index value (SI = 0.19) affecting the model outputs (Table 8.9). Further, the changes in streamflow increased from upper to lower basin (SW-50 to SW-1) due to varying CH_S2 sensitivity at sub-watershed level (Table 8.8). Thus, the grade stabilization structure can be used as a sustainable management practice to protect the main channel segment by reducing streamflow velocity.

Table 8.22: Percent reduction in post-BMP simulation after implementation of grade stabilization structures

Sub-watershed	Streamflow (% reduction)					Sediment yield (% reduction)				
	Baseline 1986	Horizon 2020	Horizon 2040	Horizon 2060	Horizon 2080	Baseline 1986	Horizon 2020	Horizon 2040	Horizon 2060	Horizon 2080
SW-1	8.77	9.14	7.60	8.84	8.61	12.56	11.71	10.15	9.43	11.06
SW-2	8.06	6.97	7.27	9.07	9.29	12.83	11.91	10.31	9.51	11.23
SW-4	7.97	8.91	7.96	9.58	9.17	18.88	18.53	17.74	18.51	18.91
SW-5	7.56	7.88	7.81	10.43	8.91	19.17	18.74	17.97	18.72	19.17
SW-6	7.97	7.58	8.21	10.03	7.50	26.66	28.61	27.68	25.63	26.31
SW-7	7.66	7.35	8.65	8.74	8.11	36.09	35.47	36.76	35.96	35.73
SW-11	7.38	6.89	7.53	8.78	7.12	29.92	31.29	29.88	28.24	29.01
SW-12	7.90	7.23	7.72	7.19	7.12	36.33	35.72	37.04	36.15	35.96
SW-14	6.12	6.11	6.45	6.06	5.86	35.27	34.34	35.36	35.60	35.29
SW-16	5.83	5.83	5.83	6.59	5.83	34.93	33.95	34.98	35.35	35.00
SW-17	7.16	7.20	7.04	8.18	7.16	33.29	35.62	33.63	30.83	31.75
SW-18	5.83	5.83	5.83	5.83	6.12	15.57	15.42	15.52	14.58	14.92
SW-20	7.62	6.74	7.82	7.65	7.54	33.22	35.39	33.76	31.08	32.02
SW-25	6.82	6.13	6.63	7.81	6.58	13.53	14.42	16.72	18.23	23.00
SW-34	5.83	5.99	6.42	7.06	7.16	13.58	12.39	12.42	12.70	12.74
SW-37	6.23	6.01	6.50	6.37	6.16	9.12	8.25	8.29	8.53	8.62
SW-45	5.91	5.90	6.43	6.60	6.48	11.73	9.82	10.03	10.27	10.21
SW-50	6.10	6.01	6.35	6.01	6.16	13.04	13.22	13.14	13.78	13.88

High sediment yield reduces in the SW-12 during horizon 2060 (about 36.15%), and in SW-45 during horizon 2020 (about 8.25%) as illustrated in Figure 8.9. The SW-25 increases the sediment yield reduction under changing climate, i.e. from horizon 2020 (about 14.42%) to horizon 2080 (about 23%), because of the low sensitivity of CH_S2 (SI = 0.13) and high sensitivity of CH_EROD (SI = 0.56) in main river channel. Result shows that present sediment loads in the lower basin area can be minimized by implementation of the grade stabilization structures, especially in SW-7, SW-12, SW-14, SW-16, SW-17 and SW-20 where a high sensitivities of CH_S2 (SI value more than 0.32; Table 8.9) plays an important role to settling down the sediment flow in main river channel.

Streamflow reductions are more in future horizon 2060, when a flooding may be possible owing to maximum rainfall events. Thus, this practice would be an optimal solution to minimize flooding impact on river channel segment. It is clearly observed that the grade stabilization structures are more sensitive to the sediment yield reduction mainly in critical sub-watersheds located in the lower part of Betwa basin (Figure 8.9). In main channel, the CH_EROD parameter is less sensitive and the CH_S2 parameter is more sensitive for lower basin area (Table 8.8), which represents feasibility of structural practice to reduce the streamflow. Therefore, the present in-stream BMP intervention can be valuable for the reductions in sediment yield as well as streamflow of the Betwa basin in future years.

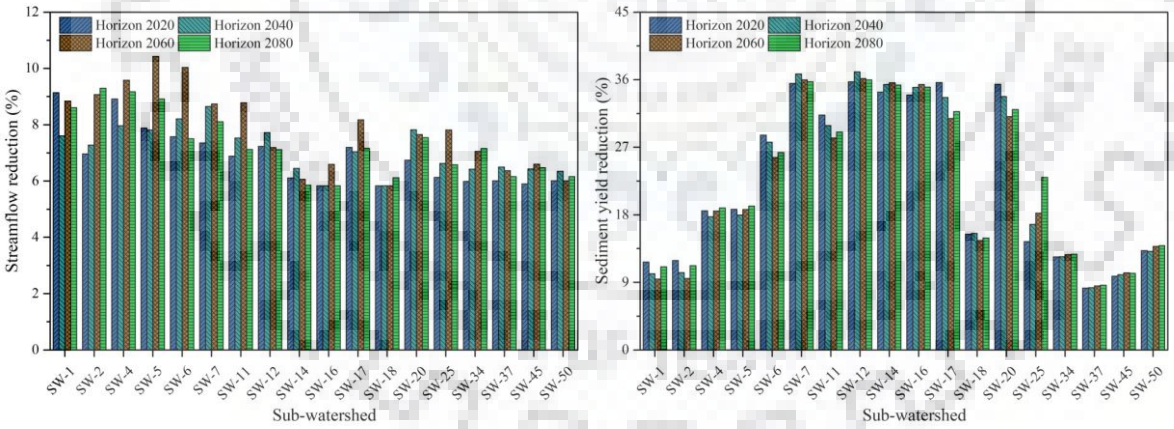

Figure 8.9: Effect of grade stabilization structures on future streamflow and sediment yield

As per the priority class, effect of grade stabilization structure is also analyzed in the present study. Table 8.23 shows the higher streamflow reductions for class-III followed by class-I, class-II, class IV and class-V. Similarly, the higher sediment yield reductions are observed for priority class-III, followed by class-I, class-II, class IV and class-V. Here, for all priority classes both streamflow and sediment yield reduces in same amount after intervention of the grade stabilization structures in main river channel.

Table 8.23: Priority class wise average reduction (%) in streamflow and sediment yield under effective grade stabilization structures

Priority class	Streamflow (% reduction)					Sediment yield (% reduction)				
	Baseline 1986	Horizon 2020	Horizon 2040	Horizon 2060	Horizon 2080	Baseline 1986	Horizon 2020	Horizon 2040	Horizon 2060	Horizon 2080
I	7.17	7.44	6.98	7.85	7.33	26.99	26.83	26.37	25.94	26.40
II	7.21	6.89	7.11	8.53	7.86	19.37	19.34	18.42	17.76	18.58
III	7.73	7.11	8.06	7.86	7.59	35.21	35.53	35.85	34.40	34.57
IV	6.94	6.74	7.32	8.32	6.99	19.19	19.22	18.85	17.95	18.26
V	6.24	6.03	6.47	6.81	6.51	12.32	12.07	12.64	13.31	14.56

(d) Evaluation of porous gully plugs

Porous gully plugs has been implemented by increasing the tributary channel roughness (CH_N1) to reduce the gully erosion by lowering streamflow velocity, and for sediment trapping. Result shows a high sediment yield reductions (more than 10%) in SW-6 during all analysis periods (Table 8.24). Similarly, the streamflow reductions are also around 10% in all climate periods, where the CH_N1 parameter has main role to reduce the streamflow of tributary channel with a sensitivity SI = -0.07 (Table 8.8). Moreover, the critical sub-watersheds SW-1, SW-2, SW-4 and SW-5 located at downstream of the SW-6 reduces large amount of sediment and streamflow with maximum sensitivity of CH_N1 (Tables 8.8 & 8.9). Thus, porous gully plugs in a tributary channel can reduce both streamflow as well as sediment yields in the similar way in critical sub-watersheds of the study area. Nevertheless, porous gully plugs has very low response in sub-watersheds located in the upper Betwa basin with lowered sensitivity of CH_N1. The study demonstrated that, the BMP effectiveness in tributary channels is very low as compared to the effect of BMPs implemented in main channel. It is because of large difference between Manning's roughness coefficients ('n' value) in main channel and tributary channel of the Betwa basin.

The porous gully plugs can significantly reduce sediment yields under varying climatic condition in all the critical sub-watersheds. Present BMP is observed to be more effective in horizon 2020, as compare to next future horizons (Figure 8.10). This practice performs gradually from upper to lower basin sub-watersheds of the Betwa River basin. This might be due to high negative sensitivity of CH_N1 from upper to lower basin area. In this analysis, both streamflow and sediment yields reduce in similar way in all future climate horizons. Therefore, an intervention of porous gully plugs could be an effective practice for protection of tributary channel segment.

Table 8.24: Percent reduction in post-BMP simulation after implementation of porous gully plugs

Sub-watershed	Streamflow (% reduction)					Sediment yield (% reduction)				
	Baseline 1986	Horizon 2020	Horizon 2040	Horizon 2060	Horizon 2080	Baseline 1986	Horizon 2020	Horizon 2040	Horizon 2060	Horizon 2080
SW-1	9.05	8.44	7.34	7.68	7.72	10.88	10.75	9.33	9.17	9.89
SW-2	9.06	8.45	7.35	7.69	7.73	10.88	10.74	9.33	9.19	9.89
SW-4	9.18	8.55	7.47	7.86	7.82	11.20	10.82	9.26	9.40	10.10
SW-5	9.23	8.57	7.50	7.90	7.84	11.19	10.81	9.26	9.42	10.11
SW-6	12.31	11.33	9.66	10.21	10.41	13.82	13.15	10.96	11.20	11.68
SW-7	1.84	1.72	1.78	1.74	1.40	0.82	0.71	1.08	1.08	0.60
SW-11	6.87	6.46	5.97	6.38	6.18	7.79	7.58	6.76	7.02	6.95
SW-12	0.33	0.25	0.56	0.69	0.18	0.72	0.63	0.97	1.04	0.52
SW-14	1.00	1.06	0.49	0.23	0.82	0.83	0.88	0.34	0.08	0.58
SW-16	0.81	0.83	0.39	0.16	0.61	0.82	0.87	0.33	0.08	0.58
SW-17	5.64	5.39	5.14	5.50	5.25	6.11	5.89	5.51	5.83	5.62
SW-18	0.71	0.71	0.46	0.35	0.57	0.28	0.29	0.17	0.12	0.22
SW-20	6.90	6.56	6.04	6.41	6.31	7.13	6.94	6.23	6.60	6.57
SW-25	6.26	5.99	5.75	6.04	5.88	5.43	19.24	5.79	5.41	5.80
SW-34	4.71	4.52	4.52	5.03	4.77	1.98	1.68	1.94	2.20	1.89
SW-37	2.37	2.37	2.83	3.06	2.65	0.84	0.66	1.06	1.22	0.89
SW-45	0.31	0.39	1.20	1.31	0.74	0.01	0.03	0.32	0.42	0.17
SW-50	0.61	0.50	0.22	0.30	0.19	0.24	0.23	0.09	0.22	0.06

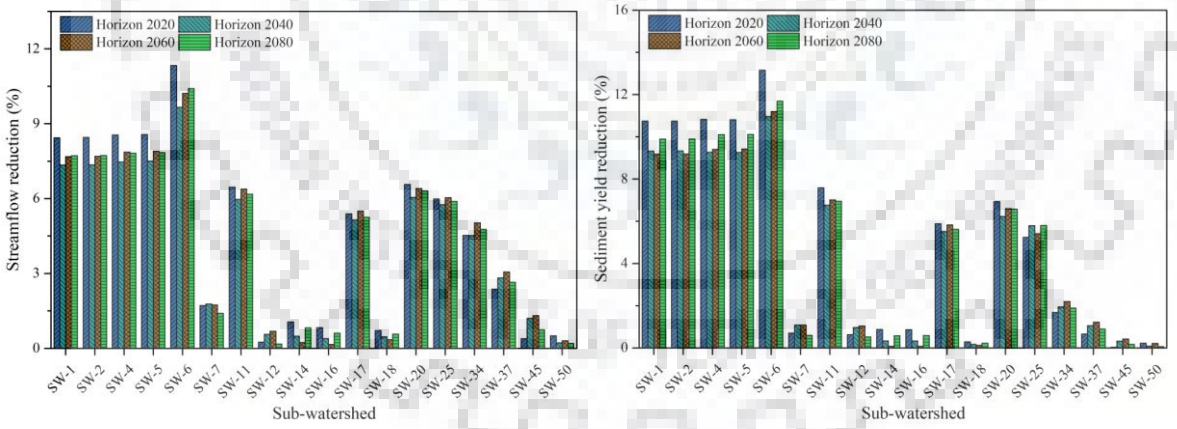

Figure 8.10: Effect of porous gully plugs on future streamflow and sediment yield

From Table 8.25, results show the higher streamflow reductions for class-II followed by class-IV, class-I, class V and class-III. Similarly, the higher sediment yield reductions are observed for priority class-II, followed by class-IV, class-I, class-III and class-V. Thus, the intervention of porous gully plugs in tributary channel can effectively reduce sediment yield and streamflow in the similar order of priority classes.

Table 8.25: Priority class wise average reduction (%) in streamflow and sediment yield under effective porous gully plugs

Priority class	Streamflow (% reduction)					Sediment yield (% reduction)				
	Baseline 1986	Horizon 2020	Horizon 2040	Horizon 2060	Horizon 2080	Baseline 1986	Horizon 2020	Horizon 2040	Horizon 2060	Horizon 2080
I	5.13	4.85	4.17	4.29	4.44	5.97	5.84	4.95	4.91	5.35
II	6.47	6.05	5.32	5.58	5.58	7.53	7.36	6.38	6.44	6.79
III	3.02	2.84	2.79	2.94	2.63	2.89	2.76	2.76	2.91	2.57
IV	6.31	5.86	5.43	5.76	5.58	6.91	6.59	5.64	5.81	5.92
V	3.49	3.35	3.33	3.61	3.37	2.12	1.20	2.22	2.26	2.16

(e) Evaluation of recharge structures

The practice of recharge structure has been implemented to trap sediment and to increase the ground water recharge by adjusting channel roughness (CH_N1) and hydraulic conductivity (CH_K1) in the tributary channels. Results show a high sediment yield reduction in the sub-watersheds near the outlet of basin. Mainly, the SW-6 has high reductions in the sediment yield (about 11% to 14%) and streamflow (about 10% to 12%) in future (Table 8.26). Also, the SW-1, SW-2, SW-4 and SW-5 have high reductions in sediment yield (about 9% to 11%) and streamflow (about 7% to 10%) due to maximum negative sensitivity of the CH_N1 and CH_K1 in tributary channel (Table 8.9). In this analysis, the sensitivity of CH_K1 induces a very small impact on sediment and streamflow. This is similar to the results obtained from the porous gully structure treatment in the tributary channels.

In lower basin area, a large amount of sediment load reduction has been induced in horizon 2020, followed by horizon 2080, horizon 2060 and horizon 2040 (Figure 8.11). It means that the effectiveness of BMP parameters (CH_N1 and CH_K1) varies with climatic changes. Increase in hydraulic conductivity, i.e. up to 25 mm/hr, has moderate loss rate, and resulting a very low impact on the model output as compared to the impact of channel roughness. From this analysis, it is observed that the recharge structures can effectively protect the tributary channel under changing future climate.

Higher streamflow reductions are obtained for class-II followed by class-IV, class-I, class V and class-III. And, the higher sediment yield reductions are obtained for priority class-II, followed by class-IV, class-I, class-III and class-V (Table 8.27). Thus, the implementation of recharge structures can effectively reduces the sediment yield and streamflow in all the priority classes.

Table 8.26: Percent reduction in post-BMP simulation after implementation of recharge structures

Sub-watershed	Streamflow (% reduction)					Sediment yield (% reduction)				
	Baseline 1986	Horizon 2020	Horizon 2040	Horizon 2060	Horizon 2080	Baseline 1986	Horizon 2020	Horizon 2040	Horizon 2060	Horizon 2080
SW-1	9.08	8.46	7.36	7.69	7.75	11.08	10.93	9.46	9.30	9.85
SW-2	9.09	8.46	7.37	7.71	7.75	11.08	10.92	9.46	9.31	9.86
SW-4	9.22	8.58	7.48	7.88	7.85	11.36	10.97	9.36	9.50	10.24
SW-5	9.27	8.59	7.52	7.92	7.87	11.36	10.96	9.36	9.52	10.25
SW-6	12.38	11.37	9.68	10.24	10.45	13.96	13.26	11.03	11.26	11.77
SW-7	1.83	1.71	1.77	1.74	1.40	0.88	0.76	1.11	1.10	0.64
SW-11	6.94	6.51	6.00	6.42	6.21	7.93	7.69	6.83	7.08	7.04
SW-12	0.33	0.25	0.57	0.69	0.18	0.78	0.67	0.99	1.08	0.56
SW-14	1.00	1.06	0.49	0.24	0.82	0.79	0.84	0.31	0.06	0.55
SW-16	0.81	0.84	0.40	0.16	0.61	0.78	0.83	0.30	0.05	0.54
SW-17	5.71	5.43	5.17	5.53	5.29	6.19	5.96	5.56	5.87	5.67
SW-18	0.71	0.72	0.47	0.35	0.56	0.28	0.28	0.16	0.12	0.22
SW-20	6.99	6.62	6.08	6.44	6.37	7.27	7.04	6.30	6.65	6.65
SW-25	6.36	6.06	5.79	6.08	5.95	4.99	19.25	5.74	5.29	5.91
SW-34	4.71	4.52	4.52	5.03	4.77	2.04	1.74	1.97	2.23	1.92
SW-37	2.37	2.37	2.82	3.06	2.65	0.89	0.71	1.08	1.26	0.92
SW-45	0.31	0.39	1.20	1.31	0.75	0.03	0.05	0.33	0.44	0.19
SW-50	0.60	0.50	0.22	0.30	0.20	0.24	0.21	0.09	0.22	0.05

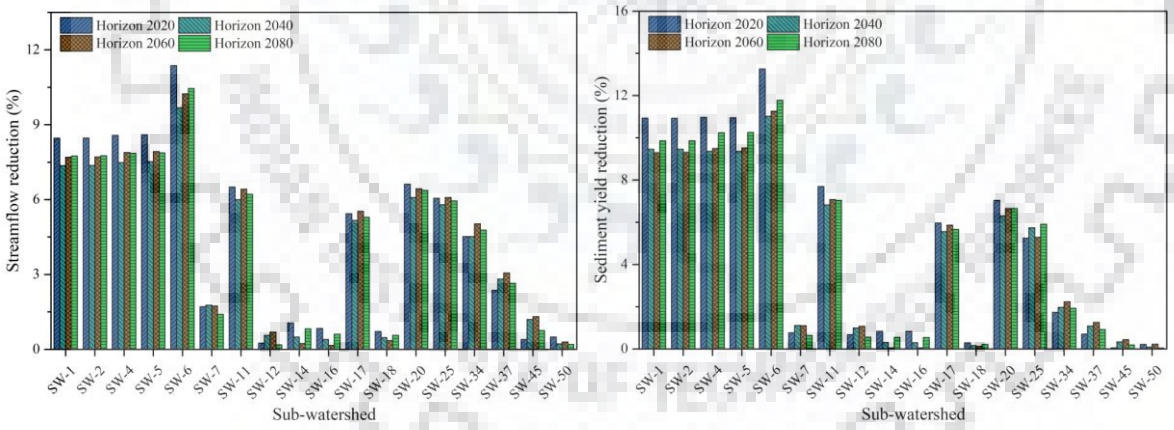

Figure 8.11: Effect of recharge structures on future streamflow and sediment yield

Table 8.27: Priority class wise average reduction (%) in streamflow and sediment yield under effective recharge structures

Priority class	Streamflow (% reduction)					Sediment yield (% reduction)				
	Baseline 1986	Horizon 2020	Horizon 2040	Horizon 2060	Horizon 2080	Baseline 1986	Horizon 2020	Horizon 2040	Horizon 2060	Horizon 2080
I	5.16	4.87	4.18	4.30	4.46	6.04	5.91	5.00	4.95	5.37
II	6.50	6.07	5.34	5.60	5.60	7.66	7.46	6.45	6.51	6.84
III	3.05	2.86	2.81	2.96	2.65	2.97	2.83	2.80	2.94	2.62
IV	6.34	5.88	5.44	5.78	5.60	6.99	6.65	5.68	5.85	5.98
V	3.51	3.36	3.34	3.62	3.39	2.04	1.98	2.22	2.25	2.20

Based on sensitivity of the BMP parameters, an increase in the CH_N2 value and the decrease in CH_COV, CH_EROD and CH_S2 values induced low sediment flow in main channel. Thus, these BMP parameters (CH_N2, CH_COV, CH_EROD and CH_S2) can effectively reduce the model output, i.e. sediment yield, at sub-watershed level. In tributary channel, both CH_N1 and CH_K1 have negative sensitivity, which reveals that increase in their values can induce reduction in the model outputs for protection and restoration of tributary channels. Two main channel stabilization treatments, namely grassed waterways and streambank stabilization, are adequate interventions for protection of main river channel from eroding. Their effect on sediment yield reduction is quite higher than the effect of grade stabilization structures. In horizon 2060, possible flood situation due to high rainfall events can be minimized by treatment of grade stabilization structures. Thus, this can be an optimal solution to reduce streamflow in the Betwa River basin. In this study, both grassed waterways and streambank stabilization produces maximum reductions in the critical sub-watersheds of the upper basin (SW-34, SW-37, SW-45 and SW-50) and lower basin areas (SW-1, SW-2, SW-4, SW-5, SW-6, SW-11, SW-18 and SW-25). Grade stabilization structures are the most effective in critical sub-watersheds (SW-7, SW-12, SW-14, SW-16, SW-17 and SW-20) where first two treatments are less effective. Therefore, these BMPs can be individually implemented to the respective sensitive areas for their effectiveness in streamflow and sediment yield reduction. Thus, the present study demonstrates a guideline for effective management for protection and restoration of river channels under changing climate. Bracmort et al. (2006) evaluated the grassed waterways and grade stabilization structuress for the Black Creek watershed, USA, and found that these BMPs can be implemented under high sediment yield conditions. Arabi et al. (2008) evaluated the river channel BMPs for the Smith Fry watershed of USA, and recommended that the grassed waterways, lined waterways/streambank stabilization and grade stabilization structures for sediment reductions in different orders of the river channels. From the study, BMP implementation, parameter selection and parameter sensitivity have altogether effective functioning on the river channel treatments, and their reasonableness in the SWAT model.

Overall, this study represents an effectiveness of over-land BMP treatments in agriculture land as well as in-stream BMP interventions in main and tributary channels of the Betwa River basin. Sub-watershed wise BMP effectiveness shows significant reduction in sediment yield; however, very low streamflow reductions are obtained. The sub-watersheds located in the upper and lower basin area have varied impact on hydrologic component due to different sensitivity of the BMP parameters for agriculture land and river channels. From over-land BMP analysis, the streamflow reductions has very similar effect in all the critical areas, while the

BMP effect on sediment reduction increases from upper to lower basin. From in-stream BMP analysis, the main channel interventions are highly effective in few sub-watersheds of the upper basin (SW34, SW-37, SW-45 and SW-50) and the lower basin (SW-1, SW-2, SW-4 and SW-5), whereas only SW-6 is the most sensitive area under tributary channel intervention.

8.3.3 Priority class wise BMP effectiveness

In addition, the BMP effectiveness on streamflow and sediment yield reduction has been studied for each priority class (from class-I to class-V) considered to implement the feasible management practices for agriculture land and river channels.

8.3.3.1 Over-land BMP effectiveness

In this analysis, contour farming and strip cropping were effective in minimizing the streamflow (Table 8.28) due to high sensitivity of CN2 (Table 8.29) for streamflow. Moreover, the sensitive USLE_C and UCLE_P parameters can induce an impact on streamflow reductions contributed in each priority class. Highest streamflow reductions were observed for priority class-V where CN2 (SI = 0.16), USLE_C (SI = 0.06) and USLE_P (SI = 0.06) parameters pronounces dominant effect on streamflow (Table 8.29). Due to an over-land BMP treatment, sediment yield reduction is more than the streamflow reduction in all priority classes. In this analysis also, both contour farming and strip cropping contributes high reduction in sediment yield due to more SI values of BMP parameters. Highest reduction in the sediment yield was observed for priority class-II. Here, the sensitivity of CN2 (SI = 0.18), USLE_C (SI = 0.03) and USLE_P (SI = 0.06) facilitates flow resistant and erosion settling in agriculture land. Results revealed that the strip cropping is the most effective over-land BMP treatment for soil and water conservation in critical sub-watersheds of the Betwa basin.

Table 8.28: Priority class wise average reduction (%) under effective over-land BMP implementation

Priority class	Average reduction (%) in future					
	Tillage management			Contour farming	Residue management	Strip cropping
	CT	FC	ZT			
	Streamflow reduction (%)					
I	6.19	7.67	2.25	10.84	7.38	11.99
II	6.38	7.80	2.59	10.64	7.25	11.79
III	6.66	8.17	2.64	11.06	7.58	12.09
IV	6.48	7.93	2.61	11.36	7.60	12.41
V	6.65	7.86	3.42	11.61	7.68	12.45
	Sediment reduction (%)					
I	19.19	16.72	26.79	27.03	16.23	31.76
II	18.95	16.58	26.25	28.39	17.15	32.88
III	19.62	17.10	27.36	25.76	14.05	29.57
IV	16.50	14.08	23.95	25.37	14.26	30.26
V	12.18	10.16	18.40	15.62	12.01	27.42

Note: CT = Conservation tillage; FC = Field cultivator; ZT = Zero tillage

Table 8.29: Priority class wise average sensitivity of over-land BMP parameters

Priority class	Sensitivity Index (SI) values					
	DEPTIL	EFFMIX	CN2	USLE_C	USLE_P	OV_N
	Streamflow					
I	0.01	0.00	0.16	0.04	0.03	-0.01
II	0.01	0.00	0.17	0.04	0.03	-0.01
III	0.01	0.00	0.17	0.03	0.03	-0.01
IV	0.02	0.02	0.17	0.05	0.04	-0.02
V	0.03	0.01	0.16	0.06	0.06	-0.02
	Sediment yield					
I	0.02	0.02	0.18	0.03	0.05	-0.01
II	0.01	0.03	0.18	0.03	0.06	-0.01
III	0.03	0.01	0.16	0.02	0.05	-0.02
IV	0.03	0.02	0.12	0.05	0.03	-0.01
V	0.02	0.02	0.12	0.04	0.03	-0.01

8.3.3.2 In-stream BMP effectiveness

Results show that the in-stream BMP effect on streamflow is less as compare to the impact on sediment yield. The grade stabilization structures can reduce the streamflow in large amount (Table 8.30) due to high sensitivity of CH_S2 parameter for streamflow (Table 8.31). Two main channel BMPs (grassed waterways and streambank stabilization) reduces a large amount of sediment yield in all the priority classes; except class-III where the grade stabilization structure is more effective due to high sensitivity of CH_S2 (SI = 0.34) for sediment yield

(Table 8.31). In tributary channel, priority class-IV has high streamflow reductions, and class-II has high sediment yield reductions in tributary channel. Both porous gully plugs and recharge structures have a similar effect on streamflow and sediment yield. However, a very small amount of additional percent reduction is observed by recharge structure over porous gully plugs, because of very low sensitivity of CH_K1 parameter in recharge structure treatment. The effect of hydraulic conductivity on model simulation is clearly visible when results were compared for the priority classes as shown in Table 8.30. The results of in-stream BMP analysis show that main channel BMP intervention is the most effective than the tributary channels for river channel protection from erodibility.

Table 8.30: Priority class wise average reduction (%) under effective in-stream BMP implementation

Priority class	Average reduction (%) in future				
	Grassed waterways	Streambank stabilization	Grade stabilization structures	Porous gully plugs	Recharge structures
	Streamflow reduction (%)				
I	2.52	2.32	7.40	4.44	4.45
II	2.79	2.59	7.60	5.63	5.65
III	2.17	1.97	7.65	2.80	2.82
IV	2.51	2.31	7.34	5.66	5.67
V	2.03	1.83	6.46	3.41	3.43
	Sediment yield reduction (%)				
I	29.33	29.99	26.39	5.27	5.31
II	38.19	41.50	18.53	6.74	6.82
III	23.54	23.62	35.09	2.75	2.80
IV	43.52	47.54	18.57	5.99	6.04
V	37.83	56.01	13.15	3.02	3.04

Table 8.31: Priority class wise average sensitivity of in-stream BMP parameters

Priority class	Sensitivity Index (SI) values					
	CH_COV	CH_EROD	CH_S2	CH_N2	CH_N1	CH_K1
	Streamflow					
I	0.01	0.09	0.13	-0.07	-0.03	-0.02
II	0.01	0.07	0.17	-0.09	-0.04	-0.02
III	0.01	0.10	0.18	-0.07	-0.01	-0.01
IV	0.01	0.08	0.11	-0.08	-0.05	-0.02
V	0.02	0.08	0.03	-0.08	-0.02	-0.01
	Sediment yield					
I	0.11	0.26	0.26	-0.18	-0.04	-0.05
II	0.12	0.33	0.19	-0.18	-0.05	-0.05
III	0.11	0.29	0.34	-0.16	-0.03	-0.05
IV	0.21	0.42	0.23	-0.14	-0.01	-0.02
V	0.14	0.53	0.19	-0.15	-0.02	-0.02

8.3.4 Uncertainty in BMP effectiveness

Uncertainty associated with an effective BMP simulation is considerably lower than that associated with the absolute prediction (Arabi et al., 2007). In addition, response of each BMP parameter varies with their minimum and maximum values used for an effective BMP treatment. The minimum and maximum values that may be the calibration (pre-BMP) value and/or post-BMP value can influence evaluation of the BMP effectiveness. In this study, various SWAT model parameters were used to implement the over-land and in-stream BMPs for sustainable management of the Betwa river basin. Therefore, uncertainty associated with the changes in BMP parameter value is needed to evaluate for an effective BMP implementation.

In the study, depth of tillage (DEPTIL), mixing efficiency of tillage operation (EFFMIX), curve number (CN2), USLE factors (USLE_C and USLE_P) and channel roughness coefficient for overland flow (OV_N) were adjusted to implement the over-land BMPs, namely conservation tillage, contour farming, residue management and strip cropping in the agriculture land. For tillage management, this study uses conservation tillage, field cultivator and zero-tillage practice. Change in tillage operations having DEPTIL value up to 25 mm can reduce more sediment loads (Figure 8.12a) with changes in EFFMIX and CN2 values (Figure 8.12b). Thus, these changes can simulate different sediment reductions, and may result uncertainty in the tillage management. Any small change in two USLE factors can also have different response to the sediment reduction (Figures 8.12c&d), which may affect the output of the post-BMP simulation. The OV_N has small impact on changes in model output (Figure 8.12f), thus it can lead to a small uncertainty in BMPs implementation. In this study, only agriculture land, a dominant area of the Betwa basin, was considered for the over-land BMPs evaluation. Thus, the USLE_C factor of agriculture was only considered for the BMP treatment. However, while considering the other vegetative area, such as forest land, the change in USLE_C factor may also affect the model outputs (Figure 8.12e).

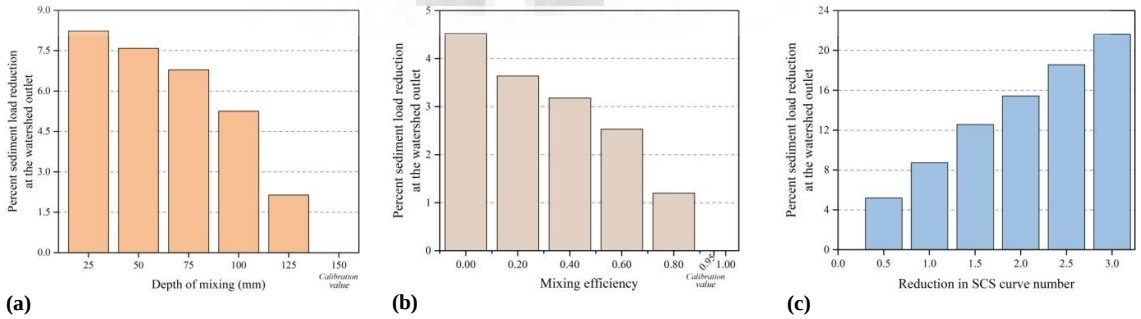

(a) **(b)** **(c)**

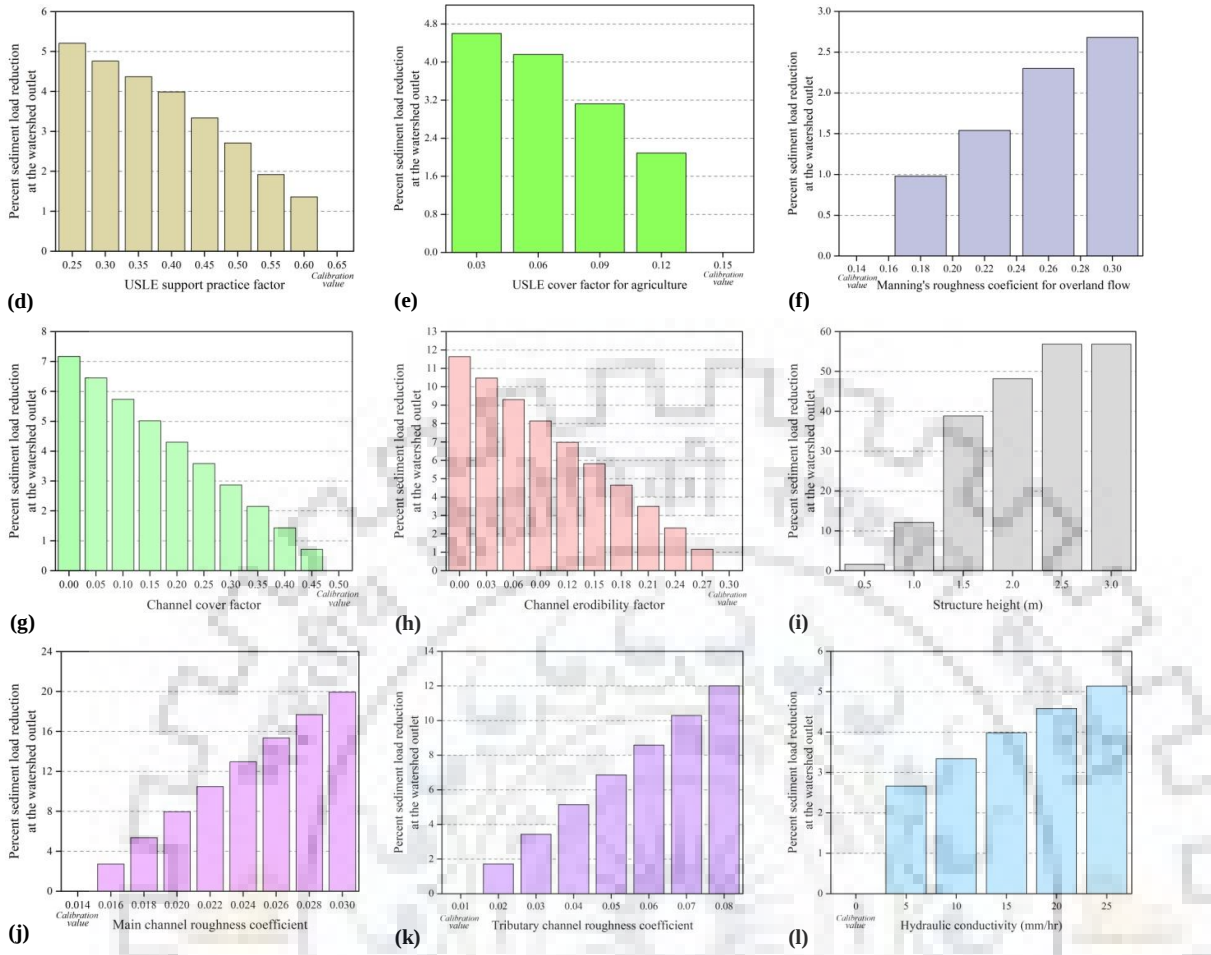

Figure 8.12: Variations in percent sediment load reduction at the watershed outlet with respect to changing BMP parameters

(a) Depth of tillage operation, (b) Mixing efficiency of tillage operation, (c) SCS runoff curve number for moisture condition II, (d) USLE support practice factor, (e) USLE cover factor, (f) OV_N = Manning's roughness coefficient for overland flow, (g) channel cover factor, (h) channel erodibility factor, (i) structure height used to estimate average slope of the main channel, (j) main channel roughness coefficient, (k) tributary channel roughness coefficient, and (l) hydraulic conductivity

In case of in-stream BMPs, the channel cover factor (CH_COV), channel erodibility factor (CH_EROD), average channel slope (CH_S2) and channel roughness coefficient (CH_N2) were considered for implementation of the grassed waterways, streambank stabilization and grade stabilization structures in the main channel. The protection of tributary channel was also done by an implementation of porous gully plugs and recharge structures considering channel roughness (CH_N1) and hydraulic conductivity (CH_K1). Results of post-BMP simulation showed that sub-watershed wise sensitivity of these BMP parameters varied for streamflow and sediment (Tables 8.8 & 8.9). In Figure 8.12, effect of different parameter values on percent reduction in sediment yield has been assessed at the watershed outlet. It is observed that sediment load increases with decrease in parameter value of both CH_COV and CH_EROD with respect to the calibration value. This study uses nearly zero (0.001) value of these BMP

parameters for the implementation of grassed waterways. The CH_COV and CH_EROD reduces sediment yield by 7% and 11.5%, respectively (Figure 8.12g&h). Implementation of grade stabilization structure with different height from 0.5 m to 3 m affects the sediment outputs as shown in Figure 8.12i. Thus, the CH_S2 value estimated using the user-defined structure height and the SWAT assigned channel dimensions may cause high uncertainties in in-stream BMP implementation, i.e. the effectiveness of grade stabilization structure treatment in particular. This study used 1.2 m height of the grade stabilization structure showing significant decrease in sediment load. The streambank stabilization provided with increase in CH_N2 value of 0.03, resulted more sediment load reduction (about 20%) in main channel (Figure 8.12j). Impact of CH_N1 parameter also showed significant sediment reduction, i.e. Manning's 'n' value of 0.05 (for porous gully plugs) reduces sediment loads about 7% and a value of 0.08 (for recharge structures) reduces sediment loads about 12% (Figure 8.12k). From this analysis, the response of Manning's 'n' vary spatially as well as type/order of river channel, i.e. main channel and tributary channel, considered for in-stream BMP intervention. Moreover, the changes in CH_K1, from insignificant loss rate (0 mm/hr) to moderate loss rate (25 mm/hr), were tested which simulated the maximum sediment load reduction of about 5% (Figure 8.12l). The analysis for recharge structure shows that the tributary channel roughness is more sensitive than the hydraulic conductivity. Thus, any change in the value of a BMP parameter can also induce uncertainty in in-stream BMP effectiveness.

8.4 CONCLUSIONS

Based on the SWAT simulation, critical areas were identified and prioritized for the BMP treatments at sub-watershed level. The post-BMP simulations and the pre-BMP simulation were used to estimate the percent yield reductions and the sensitivity index values. Change in the model outputs with respect to the BMP parameter (minimum and maximum value) range was also investigated to assess the uncertainties of BMP implementation and their evaluation for soil and water conservation and river channel protection/restoration interventions. Based on the results, following conclusions are drawn:

1. The SWAT model was successfully utilized for identification and prioritization of the critical sub-watersheds of the Betwa river basin for effective BMP treatments in agriculture land and river channels.
2. About 2% of the total basin area was categorized as priority class-I; followed by 2.44% area under priority class-II, 3.18% area under priority class-III, 3.15% are under priority class-IV and 8.60% area under priority class-V, i.e. from very severe (more than 80 t $ha^{-1}year^{-1}$) to moderate (5-10 t ha^{-1} $year^{-1}$) soil erosion class.

3. Sensitivity of all BMP parameters varies across the study area from upper to lower basin, and thus BMP effectiveness varies for each critical sub-watershed and the prioritized classes.
4. Over-land BMP analysis showed that strip cropping can be the most effective treatment of agriculture land reducing streamflow about 11.07% to 13.97% and sediment yield about 21.04% to 37.28% for soil and water conservation. However, among three tillage operations, the field cultivator can be the most effective treatment for streamflow reduction (up to 11%), and the zero tillage is the most effective treatment for sediment yield reduction (up to 31%) in the agriculture area of Betwa basin.
5. Analysis of the in-stream BMPs shows that both grassed waterways and streambank stabilization practices can be an effective river channel treatments for sediment yield reduction (about 20% to 60%) in critical areas of the upper basin (SW-34, SW-37, SW-45 and SW-50) and the lower basin (SW-1, SW-2, SW-4, SW-5, SW-6, SW-11, SW-18 and SW-25). The grade stabilization structure can be the most effective treatments for streamflow reduction (about 6% to 10%) in critical areas of the lower basin (SW-7, SW-12, SW-14, SW-16, SW-17 and SW-20).
6. The grade stabilization structures can effectively reduce the streamflow in main river channel during future horizon 2060, when flooding may occur due to large precipitation events in future.
7. Uncertainty analysis reveals that the dependency of structure height may affect CH_S2, and hence induce high uncertainty in the model in-stream BMP simulation while employing grade stabilization structure.

Overall, an approach used in this study can be useful to prioritize the critical areas for intervention of the effective BMPs for sustainable river basin management in future. It is recommended to employ feasible BMPs initially for over-land critical areas, and then for in-stream areas. The sequence of such BMP implementation may help to lower the surface erosion as well as to maintain the natural flow in river. The approach used in this study can be adopted for the regions having not only the land erosion but also the river channel erosion problems due to excessive flooding.

CHAPTER 9
SUMMARY AND CONCLUSIONS

9.1 SUMMARY

In order to manage the increasing pressure on the world's natural resources, new planning methodologies/processes for sustainable development of river basin are evolved (Hedelin, 2008). The efficient management and proper use of land resources is a prime concern to required development all over the world. In a river basin, development of agriculture food production and water resources requires comprehensive knowledge of numerous variables including climate, Land Use/Land Cover (LU/LC), water availability, water distribution networks and management practices (Todorovic and Steduto, 2003). Therefore, the judicious management and conservation of land and water resources is a prerequisite to secure future food productivity.

India is one of the major agriculture food producing country in the world. The variations in topography, climate, land and soil of the India are entirely different from those in other parts of the world. There are many challenging issues in the agriculture and water resources due to meteorological reasons like different climatic variations (Kumar et al., 2005; Mall et al., 2006). The climatic variations caused dry and wet spells (Singh & Ranade, 2010; Varikoden & Preethi, 2013) that affects food production (Milesi et al., 2010), and thus the Indian economy (Webster et al., 1998). Nevertheless, climate change impact studies in small/large catchments using hydrological modelling can be help to the policy and decision makers to prevent the future food problems.

For large river basins, field-based investigations are time-consuming and challenging. Nowadays, its rate and extent can be significantly assessed using remotely sensed data (Omuto et al., 2014; Belay et al., 2015; Mahyou et al., 2016). Therefore, advanced geo-spatial technologies have been widely used for agriculture and water resources management to explore human interactions and to illustrate the importance of natural resource development (Hoalst-Pullen & Patterson, 2010). River basins are most sensitive to the changes in LU/LC and hydrology (Mutiibwa et al., 2014; Wagner et al., 2016). Indian River basins are also sensitive natural systems to the short and long-term changes in the climate that affects the land resources. Improvement in the local and regional resources is enabling when the national policy used to combat these issues (Akhtar-Schuster et al., 2011). Natural resource problems can be controlled not only by addressing climate but financial support is also required to tackle the

issues of poverty and food security (Gisladottir & Stocking, 2005). Hence, early-warning system is the prerequisite to improve sustainable management and development plans.

The spatial and temporal variability of hydrological responses to LU/LC changes are vital for land and water resources management (Fang et al., 2013; Wagner et al., 2013). LU/LC change can significantly influence the hydrological cycle by affecting surface runoff, sediment and water quality (Fohrer et al., 2001; Badar et al., 2013; Niu and Sivakumar, 2013), hence affect catchment water balance which in turn results in resource problems such as land degradation. Therefore, it is important to understand and predict the potential hydrological consequences of existing land use practices (Du et al., 2013).

In the past decades, different hydrological models were used for evaluation and selection of alternative land use and management practices for sustainability productivity of agricultural land (Dixon et al., 1994; Rosenthal et al., 1995; Mummey et al., 1998; Hudak et al., 2004; Anand et al., 2007; Butler and Srivastava, 2007; Cau and Paniconi, 2007; Ullrich and Volk, 2009; Meghdadi, 2013). Among them, Soil and Water Assessment Tool (SWAT) is one of the most popular model which is used to study of small and large catchments worldwide, and turned out to be an effective tool to predict the consequences of LU/LC change (Du et al., 2013). In the past studies, calibration and validation was carried out using SWAT model (Ndomba et al., 2008; Pandey et al., 2009b; Dhar and Mazumdar, 2009; Lam et al., 2010; Kushwaha and Jain, 2013; Maharjan et al., 2013; Bieger et al., 2014). Recently, many researchers applied the SWAT model for runoff, sediment and water quality simulation (Bannwarth et al., 2014; Jajarmizadeh et al., 2014; Ji et al., 2014; Memarian et al., 2014; Rahman et al., 2014; Tessema et al., 2014; Murty et al., 2014). Some studies on Best Management Practices (BMP) were also carried out for the river basin development (Arabi et al., 2006; Chang et al., 2007; Lemke et al., 2011; Jia et al., 2013; Yu et al., 2013). SWAT model was employed to quantify the effectiveness of BMP applications under climate change scenario (Lam et al., 2011; Van Liew et al., 2012; Woznicki and Nejadhashemi, 2014). In these studies SWAT model performed satisfactorily in small and large catchments. Looking to the aforementioned, SWAT model has been selected as an effective and precise tool for the development of a river basin area.

The advanced remote sensing and GIS techniques could enable to address water demand, and LU/LC change and climate change impacts. Climate change affects the availability of water resources, hence the agriculture food production (Arnell, 1999; Arnell, 2004, Krysanova et al., 2005). Many studies evaluated local climate change impacts using different climate models, i.e. Global Climate Models (GCM) and Regional Climate Models (RCM). GCM data were mostly

used to downscale the global climate parameters at local scale (Wilby et al., 2002; Chu et al., 2010; Weiland et al., 2010), and projected to predict the future climate scenarios using climate data (Immerzeel, 2008; Golmohammadi et al., 2013; Duhan and Pandey, 2014). The future climate outputs can be useful for hydrological modelling to underpin the hydrology of a river basin (Vaze and Teng, 2011; Wagner et al., 2015). Therefore, climate change consideration in SWAT model simulation may ensure the need of management and development for future agriculture water.

Looking to the aforesaid, this research work has been planned with the following specific objectives:

1. To study the spatiotemporal land use/land cover (LU/LC) changes of the Betwa river basin and its modelling for future analysis.
2. To study the relationship between hydro-climatic variables and land cover dynamics under dry and wet spells over Betwa Basin.
3. Hydrological modelling of water storages in the Betwa River basin using Soil and Water Assessment Tool (SWAT).
4. To study the individual as well as combined impact of land use and climate change on hydrology of the Betwa river basin.
5. Evaluation of the best management practices (BMPs) for sustainable development of the Betwa river basin

9.1.1 Data acquisition and analysis

The daily observed climate data and hydrologic (discharge and sediment) time-series data for the years 2001-2013 were used in this study. Observed climate data of 18 rain-gauges were obtained from India Meteorological Department (IMD), Pune. Hydrologic time-series data of four gauging sites were obtained from the Yamuna Basin Organization (YBO), Central Water Commission (CWC), New Delhi. Soil data was procured from the National Bureau of Soil Survey and Land Use Planning (NBSS&LUP), Nagpur. For elevation data, the DEM of Shuttle Radar Topography Mission (SRTM) data of 30 m spatial resolution were utilized for the study area delineation and slope map preparation. Various satellite imageries were obtained from the USGS GloVis and NRSC to prepare the LU/LC maps. The satellite-derived LU/LC maps were further utilized in future LU/LC prediction employing an integrated Cellular Automata (CA) – Markov Chain (MC) model. The remotely sensed MODIS (collection 5) time-series datasets of NDVI Terra (MOD13Q1) and Land Cover (MCD12Q1) products, obtained from the NASA's Earth Observing System (EOS) Clearing House (ECHO), were used in relationship analysis with numerous hydro-climatic variables over the years 2001-2013. A conceptual framework

was developed and used to furnish the relationship analysis results, i.e. the change in response of NDVI and land cover to the changes in hydro-climatic variables of the Betwa river basin.

In this study, the SWAT, a semi-distributed physical model was used to set-up and run the hydrological process of the Betwa river basin considering numerous water storages, i.e. 7 reservoirs and 2 weirs. The land use of the years 2013 and 2040 were used to assess the land use change impact on hydrology of the Betwa river basin. Further, the downscaled and bias-corrected CMIP5 GCM (MPI-ESM-MR model) dataset of RCP8.5 climate scenario was used as an input to the SWAT model for climate change impact assessment. A newly developed conceptual framework was further employed to assess the individual as well as combined impact of land use and climate changes on streamflow (FLOW), sediment yield (SYLD), evapotranspiration (ET) and water yield (WYLD). For identified and prioritized critical area of the Betwa river basin, the effective over-land as well as in-stream BMPs were implemented and evaluated in agriculture land and river channels for soil and water conservation and sustainable river basin management in future.

9.1.2 Land use/land cover (LU/LC) changes and its future modelling

In this analysis, remote sensing and GIS techniques were used to extract the spatial information of LU/LC changes using spatiotemporal satellite imageries. It includes the imageries of the Landsat-1 Multispectral Scanner (MSS), Landsat-2 MSS, Landsat-5 Thematic Mapper (TM), Landsat-7 Enhanced Thematic Mapper Plus (ETM+), Landsat-8 Operational Land Imager (OLI), and Indian Remote-sensing Satellite (IRS-P6) Linear Imaging and Self Scanning (LISS) III. Maximum likelihood supervised image classification was carried out to prepare the land use maps of the years 1972, 1976, 1991, 2001, 2007, 2010 and 2013. Image pre-processing, classification of satellite data, and accuracy assessment of satellite-derived LU/LC maps were carried out using ERDAS Imagine 2014 and ArcGIS 10.2.2 version software. The LU/LC change analysis was further distinguished into two areas i.e. Madhya Pradesh and Uttar Pradesh. Further, an integrated Cellular Automata (CA) – Markov Chain (MC) model was employed to predict the future LU/LC maps for the years 2020, 2040, 2060, 2080 and 2100.

9.1.2.1 Historical LU/LC changes

In the historical LU/LC classification, overall classification accuracy and Kappa coefficient varies from 77% to 87% and 0.709 to 0.836, respectively. Analysis showed that dense forest declined from 23.39% to 14.31% during the years 1972 to 2013, respectively. However, the area under degraded forest, agriculture area, barren land, waterbody and settlement has increased from 8.54% to 13.37%, 63.75% to 67.91%, 2.98% to 1.27%, 1.22% to 2.84%, 0.12%

to 0.39%, respectively. The LU/LC change analysis for Madhya Pradesh showed decrease in dense forest and barren land by 7.67 % and 1.17 % during 1972 to 2013. However, degraded forest, agriculture, waterbody and settlement were increased by 4.1%, 3.37 %, 0.85% and 0.16%, respectively. Similarly, decrease in dense forest (1.41%) and barren land (0.54%), and increase in degraded forest (0.73%), agriculture area (0.43%), waterbody (0.77%) and settlement (0.03%) were also observed in the basin area covered under Uttar Pradesh.

9.1.2.2 LU/LC modelling using CA-MC model

In this study, the satellite-derived historical LU/LC maps of the years 2001 and 2007 were utilized as an input to the CA-MC model for prediction of future LU/LC. Initially, the model was validated for the predictions of LU/LC maps of the years 2010 and 2013. The LU/LC modelling resulted satisfactory unbiased summary statistics in terms of Kappa indices, i.e. Kno values 0.850 and 0.867, Klocation values 0.788 and 0.812, KlocationStrata values 0.788 and 0.812 and Kstandard values 0.768 and 0.793 for the simulation years 2010 and 2013, respectively. Also, the visual inspection analysis showed strong agreement for the area of simulated and satellite-derived LU/LC maps.

9.1.2.3 Future LU/LC changes

Future analysis showed an increase in the area of degraded forest from 14.82% to 18.82%, barren land from 5.80% to 10.03% and settlement from 0.36% to 0.64%; the decrease in dense forest from 12.16% to 10.77%, agriculture from 66.15% to 59.64% and waterbody from 0.72 to 0.01% could also takes place in Betwa basin during the years 2020 to 2100. Analysis for interstate LU/LC change showed that dense forest, agriculture area and waterbody could decrease by 1.13%, 3.36% and 0.28% in Madhya Pradesh, and 0.26%, 3.05% and 0.43% in Uttar Pradesh. However, increase in degraded forest, barren land and settlement area by 2.97%, 1.72% and 0.08% for Madhya Pradesh, and 1.02%, 2.51% and 0.20% for Uttar Pradesh could take place during the years 2020 to 2100.

The methodology adopted in this study can be extended to the other parts of the world to predict future LU/LC pattern, and its usefulness for future water and food security purpose. The results obtained from this study will be helpful for inter-state planning and management of land resources in the Betwa basin.

9.1.3 Relationship analysis using conceptual framework

In this analysis, MODIS NDVI and Land Cover time-series datasets were used to establish a relationship with numerous hydro-climatic variables, namely precipitation, Tmin, Tmax, Tdiff, R_H, PET, P/PET, discharge and sediment etc. Further, a conceptual framework was used to

furnish the results of relationship analysis for dry years, wet years, and combined dry and wet year analyses.

9.1.3.1 Dry year analysis

In dry year analysis, temperature parameters, especially Tmax and Tdiff, showed climatic degradation response ($r > -0.6$) to the monthly and seasonal NDVI that declined the vegetation cover under prolonged dry spell effect. On annual basis, the Tmax and Tmin parameters were significantly degraded the vegetation area ($r > -0.6$), hence climatic degradation response. Monthly RH shows a significant positive response to the vegetation ($r = 0.864$). Monthly relationship between aridity index and NDVI showed a moderate correlation value of $r = 0.561$, which indicate an inadequate soil moisture condition for crop growth and development. Thus, deficient and uneven rainfall distribution in dry year may adversely affect crop production in the Betwa river basin.

Among the land cover classes, the forest growth was limited by the low monsoon rainfall and the less moist climate condition. The woody savannas, grass land and permanent wet land growth were affected due to the Tdiff variable having high negative correlation value ($r > -0.6$). The dry year analysis showed more number of responses to the numerous land cover classes, hence depicted that Tdiff is the most affecting climate variable for land cover area of the Betwa basin.

9.1.3.2 Wet year analysis

During wet years, the correlation analysis between NDVI and hydro-climatic variables (especially rainfall, Tmax, Tmin, R_H, PET, aridity index and Tdiff) showed significant response (positive or negative) at monthly, seasonal and annual time-scale. Changes in the rainfall induces a significant climatic degradation response to the NDVI during post-monsoon ($r = -0.712$) and winter ($r = -0.802$). The correlation analysis shows significant climatic greening response of the monthly R_H ($r = 0.854$), however climatic degradation response of the annual R_H ($r = -0.332$). In this analysis, the land degradation response of Tmax in the pre-monsoon season ($r = -0.983$) was further decreased in SW-monsoon, and later again upraised the significant climatic-greening response to NDVI in winter ($r = 0.651$).

The wet year analysis showed large number of good correlations ($r > \pm 0.5$) between all the land cover classes and hydro-climatic variables at annual time-scale. Among them, the DBF and MXF showed positive response to the Tmax, PET and Tdiff parameters ($r > 0.5$); however, a negative response to the rainfall, Q and sediment ($r = -0.6$ to -0.8). The dominant crop land exhibited a significant negative correlation with Tmax and Tdiff ($r > -0.7$); as well as positive

correlation with rainfall, Tmin, Q, aridity index and sediment (r > 0.65) in wet years. This analysis revealed that the WTR, DBF, MXF, SV, GL and CL were the most influenced land cover areas under wet spell effects over the Betwa basin.

9.1.3.3 Combined effects of dry and wet years

The combined, dry and wet years, analysis showed very few good correlations between hydro-climatic variables and vegetation. On monthly basis, NDVI exhibited significant response to few climate parameters Tmax (r = -0.669), R_H (r = 0.861) and Tdiff (r = -0.651). The monthly rainfall showed moderate response (r = 0.51) i.e. climatic greening response to NDVI. Analysis showed more good correlations (r >= 0.5) for monthly and SW-monsoon analyses. Thus, the monthly and monsoon season rainfall has a very important role for vegetative growth in the Betwa river basin. This analysis demonstrated that the combined effect of dry and wet years reduces the NDVI response to the hydro-climatic variables. The MODIS land cover exhibited moderate correlations with hydro-climatic variables. The WTR class has significant positive response to Q (r = 0.728) and sediment (r = 0.707). Overall, this analysis showed reduced hydro-climatic response to the land cover area of the Betwa river basin.

Thus, the land cover dynamics can be easily analyzed using remote sensing time-series datasets for large river basins. Analysis pertaining to the crop-land can be applied to secure the food productivity considering the climatic and non-climatic land greening and degradation responses.

9.1.4 Hydrological modelling using SWAT

In the study, different water storages (7 reservoirs and 2 weirs) located on main as well as tributary channels of the Betwa river basin were considered to successfully implement and manage the hydrological process of Betwa basin in the SWAT model. Sensitivity and uncertainty analysis were carried out to select the parameters for calibration and validation of the SWAT model.

9.1.4.1 Water storages management in SWAT modelling

The reservoir module in SWAT was used to adequately manage the water storages of Betwa basin. The surface area was extracted by Normalized Difference Water Index (NDWI) method using Landsat 8 OLI imagery of the flooding year 2013. Due to lack of water storage outflow data, the monthly target storage volume (STARG), beginning month of non-flood season (IFLOD1R), ending month of non-flood season (IFLOD2R), average daily principle spillway release rate (RES_RR) and the required days to reach target storage during monsoon and non-

monsoon periods (NDTARGR) were managed in the study. This allows the daily outflow regulation from the reservoir to precisely simulate outflow using the SWAT model.

9.1.4.2 Sensitivity and uncertainty analysis

In this study, the sensitivity and uncertainty analysis were carried out using the SUFI-2 algorithm in SWAT-CUP. Firstly, One-At-a-Time (OAT) sensitivity analysis was carried out to select the most sensitive parameters for calibration process. Then, global sensitivity analysis was performed to identify the relative sensitivity among the selected parameters for streamflow and sediment. Based on sensitivity analysis, total 23 sensitive parameters were considered for calibration of the streamflow (9 parameters) and sediment (14 parameters) using the SWAT model. Streamflow is the most sensitive to the curve number (CN2) followed by SURLAG (surface runoff lag coefficient) to SOL_AWC (available water capacity of the soil layer). Sediment is most sensitive to the channel erodibility factor (CH_ERODMO) followed by USLE_K (soil erodibility factor for USLE equation) to USLE_C (minimum value of USLE C factor applicable to the forest area). The uncertainty analysis was also carried out in terms of *p-factor* and *r-factor* obtained through Latin-Hypercube sampling. The analysis shows that the percent observations bracketed by the 95% prediction uncertainty (95PPU) were more than 70% (*p-factor*). Also, the average thickness of 95PPU band divided by standard deviation of measure data, i.e. *r-factor*, were also satisfactory for all gauging sites of the Betwa basin.

9.1.4.3 SWAT model calibration and validation

The SUFI-2 algorithm of the SWAT-CUP was used to calibrate and validate the SWAT model for streamflow and sediment at four gauging stations, namely Basoda, Garrauli, Mohana and Shahijina. During calibration process, high values of the R^2 (0.90, 0.94, 0.91 and 0.92), NSE (0.88, 0.91, 0.91 and 0.92), and the low values of PBIAS (-14.20, -11.10, -7.70 and -16.30) and RSR (0.34, 0.30, 0.31 and 0.29) indicates satisfactory model performance. In validation, the high values of R^2 (0.90, 0.92, 0.90 and 0.88), NSE (0.84, 0.91, 0.89 and 0.86), and the low values of PBIAS (-13.60, -16.50, -3.90 and -7.50) and RSR (0.41, 0.30, 0.33 and 0.38) also showed satisfactory model performance for streamflow simulation at Basoda, Garrauli, Mohana and Shahijina sites, respectively.

Furthermore, performance of the SWAT model was also evaluated for sediment yield. During calibration process, high values of the R^2 (0.89 and 0.78), NSE (0.89 and 0.77), the low values of PBIAS (-9.30 and -4.10) and RSR (0.33 and 0.48) indicates satisfactory calibration performance. Also, in validation, the high values of R^2 (0.90 and 0.81), NSE (0.90 and 0.81),

and the low values of PBIAS (0.70 and 1.60) and RSR (0.32 and 0.44) indicates satisfactory to good simulation of sediment at Garrauli and Shahijina sites, respectively.

9.1.5 Modelling hydrological response under future changes

In this study, future land use and climate change impact on hydrology of the Betwa basin was assessed using the output of SWAT model. Also, a conceptual framework was developed to assess the individual as well as the combined impacts considering the land use and climatic changes in the study area.

9.1.5.1 Individual land use change impact

This analysis showed that change in land use class exhibited none significant impact (*p* value<0.05) on two hydrologic components i.e. streamflow and sediment yield. Among water balance components, the ET has significant positive relationship (R^2 = 0.842, p<0.05) with the changes in waterbody class. The water yield exhibited significant relationships with the changes in dense forest (R^2 = 0.076, p<0.05), degraded forest (R^2 = 0.2, p<0.05) and agriculture (R^2 = 0.245, p<0.05).

9.1.5.2 Individual climate change impact

In this analysis, future precipitation change showed significant impact (at *p* value < 0.05) on streamflow (R^2 = 0.554, 0.156, 0.216, 0.157), ET (R^2 = 0.207, 0.178, 0.472, 0.168), and water yield (R^2 = 0.985, 0.946, 0.989, 0.991) during horizon 2020, horizon 2040, horizon 2060 and horizon 2080, respectively. The sediment yield is the exceptional hydrologic component having significant impact of precipitation change during horizon 2020 (R^2 = 0.074, p<0.05) and horizon 2040 (R^2 = 0.089, p<0.05). However, the future climate change impact is insignificant in horizon 2060 (*p* value = 0.782) and in horizon 2080 (*p* value = 0.766).

9.1.5.3 Combined impact of land use and climate changes

The combined land use and climate change analysis showed significant impact on streamflow with the changes in land use classes, mainly dense forest (r = 0.327 in horizon 2020, r = 0.457 in horizon 2040), degraded forest (r = -0.271 in horizon 2060, r = -0.275 in horizon 2080), agriculture (r = 0.299 in horizon 2020) and barren land (r = -0.371 in horizon 2020, r = -0.342 in horizon 2040); and the changes in precipitation (r = 0.727, 0.760, 0.456 and 0.387) in future climate horizons 2020, 2040, 2060 and 2080, respectively. Sediment yield has significant impact of dense forest (r = 0.310 in horizon 2020, r = 0.439 in horizon 2040), barren land (r = -0.297 in horizon 2040), and precipitation (r = 0.290 in horizon 2020, r = 0.526 in horizon 2040).

Among the water balance components, the ET has significant positive impact of changes in the waterbody (r = 0.916, 0.857, 0.882, 0.865), and the precipitation (r = 0.247 at *p* value > 0.05, 0.528, 0.405, 0.338) during horizons 2020, 2040, 2060 and 2080, respectively. Also, the water yield has significant positive impact (at *p* value < 0.05) for changes in the dense forest (r = 0.384, 0.442, 0.312, 0.360) and the precipitation (r = 0.939, 0.990, 0.988, 0.980); and the negative impact of changes in the barren land (r = -0.371, -0.555, -0.630, -0.551) during horizons 2020, 2040, 2060 and 2080, respectively.

9.1.5.4 Development of conceptual framework for individual and combined impact assessment

In this study, a conceptual framework has been developed. This framework has four quadrants representing baseline (no change), individual land use change, individual climate change, and combined land use and climate change impact. The framework quadrants are limited by two half-axes of land use and climate change/constant. In each quadrant, the model outputs in terms of four hydrology components (FLOW, SYLD, ET and WYLD) are considerably represented to assess the individual as well as the combined impacts of land use and climate changes.

The analysis showed that FLOW variable increases from 67.77 cumec to 67.86 cumec due to land use change, from 67.77 cumec to 80.46 cumec due to climate change, and from 67.77 cumec to 80.56 cumec due to combined impact of land use and climate changes. Similarly, the SYLD variable increases from 16.51 t ha^{-1} to 16.58 t ha^{-1} due to land use change, from 16.51 t ha^{-1} to 19.61 t ha^{-1} due to climate change, and from 16.51 t ha^{-1} to 16.69 t ha^{-1} due to combined impact of land use and climate changes. Thus, both the FLOW and SYLD have positive impact of land use and climate changes in all quadrants of the conceptual framework.

Further, the ET has negative impact of land use change (reduced from 460 mm to 411 mm), climate change (reduced from 460 mm to 456 mm), and combined land use and climate changes (reduced from 460 mm to 405 mm). Similarly, the WYLD also has negative impact of land use change (reduced 400 mm to 386 mm), climate change (reduced from 400 mm to 350 mm), and combined land use and climate changes (reduced from 400 mm to 337 mm). Thus, both ET and WYLD have negative impact of land use and climate changes in the Betwa basin.

9.1.6 Evaluation of the best management practices (BMP)

In this study, the non-structural and structural BMPs including four over-land BMPs namely tillage management, contour farming, residue management and strip cropping for agriculture area; and the five in-stream BMPs namely grassed waterways, streambank/channel stabilization, grade stabilization structures, porous gully plugs and recharge structures for river

channel were implemented in the SWAT model, and then evaluated for soil and water conservation as well as river bank protection in future.

9.1.6.1 Critical area identification and prioritization

Initially, the SWAT simulation showed that most of the sub-watersheds (about 80.63% of the total Betwa basin area) falls under the slight erosion class (0-5 t ha^{-1} $year^{-1}$). About 8.60% area has moderate soil erosion (5-10 t ha^{-1} $year^{-1}$); about 3.15% area has high soil erosion (10-20 t ha^{-1} $year^{-1}$); about 3.18% area has very high soil erosion (20-40 t ha^{-1} $year^{-1}$); about 2.44% area has severe soil erosion (40-80 t ha^{-1} $year^{-1}$); and about 2% area has very severe soil erosion (80 t ha^{-1} $year^{-1}$) in the Betwa river basin. These identified critical sub-watersheds were further prioritized to implement and evaluate the over-land as well as in-stream BMPs to reduce the soil erosion in future.

9.1.6.2 Effectiveness of over-land BMP

The analysis of tillage management showed that conservation tillage operation can effectively reduce the streamflow and sediment yield in the range of 5.38% to 9.53% and 6.84% to 24.27%, respectively. The field cultivator operation reduces the streamflow and sediment yield in the range of 6.30% to 11.20% and 4.15% to 22.73%, respectively. The zero tillage operation reduces the streamflow and sediment yield in the range of 1.05% to 5.08% and 12.66% to 31.46% respectively. The contour farming practice also effectively reduced the streamflow (9.78% to 13.25%) and sediment yield (6.38% to 34.41%). The residue management effectively reduces the streamflow and sediment yield in the range of 6.44% to 9.08% and 6.04% to 20.53%, respectively. Also, strip cropping practice effectively reduced the streamflow (11.07% to 13.97%) and sediment yield (21.04% to 37.28%) for baseline and future horizons.

9.1.6.3 Effectiveness of in-stream BMP

In this analysis, the grassed waterways effectively reduced streamflow (1.62% to 3.62%) and sediment yield (7.86% to 56.42%), the streambank stabilization effectively reduced streamflow (1.42% to 3.42%) and sediment yield (19.90% to 63.84%), and the grade stabilization structure effectively reduced streamflow (5.83% to 10.43%) and sediment yield (8.25% to 37.04%) in the main channel of the Betwa river basin. Furthermore, the porous gully plugs effectively reduced streamflow (0.16% to 12.31%) and sediment yield (0.01% to 13.82%), and the recharge structures effectively reduced streamflow (0.16% to 12.38%) and sediment yield (0.03% to 13.96%) in tributary channel of the Betwa river basin.

In-stream BMP analysis showed that both the grassed waterways and streambank stabilization can be the most effective treatments for sediment yield reduction (about 20% to 60%) in the

critical areas of the upper basin (SW-34, SW-37, SW-45 and SW-50) and the lower basin (SW-1, SW-2, SW-4, SW-5, SW-6, SW-11, SW-18 and SW-25). The grade stabilization structure is the most effective treatment for streamflow reduction (about 6% to 10%) in lower sub-watersheds (SW-7, SW-12, SW-14, SW-16, SW-17 and SW-20) of the Betwa basin.

9.1.6.4 Sensitivity and uncertainty analysis of BMP parameters

Among the over-land BMP parameters, the depth of tillage operation (DEPTIL), mixing efficiency of tillage operation (EFFMIX), curve number (CN2), USLE support practice factor (USLE_P) and cover factor (USLE_C) have positive sensitivity, while the Manning's roughness coefficient overland flow (OV_N) has negative sensitivity to the change in streamflow and sediment yield. Furthermore, among the in-stream BMP parameters the channel cover (CH_COV), channel erodibility (CH_EROD) and average slope of main channel (CH_S2) have positive sensitivity, while the Manning's roughness coefficients for main channel (CH_N2) as well as tributary channel (CH_N1) and the hydraulic conductivity in tributary channel (CH_K1) have negative sensitivity to the change in model outputs.

The changes in BMP parameter across its minimum and maximum value showed uncertainty in the BMP implementation and their effectiveness on sediment load reduction. Change in tillage operations having DEPTIL values from 150 mm to 25 mm can reduce sediment loads up to 8 t ha^{-1}. Any small change in two USLE factors can also have different response to the sediment reduction at post-BMP condition. In this study, the USLE_C factor has been only considered for agriculture dominant area of the Betwa basin. However, while considering the other vegetative area, such as forest land, the changes in USLE_C factor can uncertain the sediment reduction. Among in-stream BMP parameters, the CH_S2 value, estimated using the user-defined structure height (1.2 m) and the SWAT assigned channel dimensions, may cause high uncertainty in BMP effectiveness, i.e. the implementation of grade stabilization structure in particular. Moreover, in the study the Manning's roughness coefficient 'n' vary spatially as well as with the type/order of river channel, i.e. main channel and tributary channel, considered for in-stream BMP intervention.

Mainly the over-land interventions will be useful for sustainability of the agriculture food productivity as well as the land productivity. In addition, in-stream interventions will be helpful to protect the eroding river channels in future flooding situation.

9.2 GENERAL CONCLUSIONS

1. Historical spatiotemporal LU/LC change analysis showed the accrued in agriculture area by 8.55% with increase in irrigation water availability from waterbody (1.62%)

during the year 1972-2013. In 20th century, about 1.75% agriculture area has increased due to newly constructed Rajghat reservoir located at central part of the Betwa basin.

2. Future analysis showed decline in the major dense forest (1.39%) and agriculture (6.41%) areas which can significantly affect the vegetation cover in Betwa basin.
3. Monthly rainfall exhibited a climatic greening response to vegetation (NDVI) in dry, wet and all year analyses. However, Tmax and Tdiff exhibited a climatic degradation response to the NDVI. The positive response between monthly R_H and vegetation were not altered under dry and wet spells.
4. The dominant CL area showed significantly positive response with rainfall, Tmin, Q, aridity index and sediment by correlation (r) values 0.730, 0.801, 0.776, 0.654 and 0.801, respectively. The crop land was affected by the Tmax (-0.704) and Tdiff (-0.762) in the wet year analysis. However, in dry and all year analysis, none good correlation has been observed for CL area during the years 2001-2013.
5. In the SWAT model, nine water storages of the Betwa basin, including 7 reservoirs and 2 weirs, located in main channel as well as tributary channel having significant effect on the river channel flow were successfully implemented and managed for reliable hydrological prediction. Garrauli gauging site with none upstream water storage structure showed better model simulations than other gauging sites (Basoda, Mohana, and Shihijina) having upstream water storage structures.
6. In future, the impact of climate change is dominant over the land use change impact. Increase in precipitation under future climatic change showed major impact on hydrology. Changes in dense forest, agriculture and waterbody induce positive impact; nevertheless the changes in degraded forest and barren land induce negative impact on hydrology of the Betwa basin.
7. The developed conceptual framework can considerably separate the individual as well as combined impacts of land use change and climate change on hydrology components i.e. FLOW, SYLD, ET and WYLD, of a river basin.
8. In future, GCM-derived temperature parameters have annual increasing trend i.e. minimum temperature increases from 1.22 °C to 5.34 °C and maximum temperature increases from 0.92 °C to 4.87 °C during 2020-2099. However, the GCM-derived precipitation has decreasing trend in future except during the horizon 2060. In this horizon 2060, increase in precipitation (140 mm) was observed due to high average annual precipitation about 1153 mm during 2060-2079.

9. Strip cropping can be the most effective over-land BMP treatment for agriculture land reducing streamflow (11.07% to 13.97%) and sediment yield (21.04% to 37.28%) for soil and water conservation under changing future climate..
10. The grassed waterways and streambank stabilization practices can be the most effective in-stream BMP treatments reducing sediment yield (about 20% to 60%) for protection of river channel segment. Also, the grade stabilization structure can effectively reduce the streamflow in main river channel during future horizon 2060, when flooding would be possible due to large precipitation events under future climatic changes.
11. Study demonstrates the application of remote sensing datasets in land use change modelling, land cover dynamics, and their response analysis to hydrologic and climatic variables for sustainable land and water resources management of a large river basin.
12. Future policies should be formulated on the basis of climate change impact than the land use change impact. This may be helpful to secure the water and food productivity in an agricultural dominant river basin of central India. However, similar approach can be adopted in the other parts of the world for sustainable river basin management.
13. Overall, it is advised to employ modelling approach for sustainable water management strategies, and to implement government policies especially in critical erosion prone areas of an inter-state river basin for soil and water conservation, and protection of existing natural resources.

9.3 OVERALL CONCLUSIONS AND RECOMMENDATIONS

1. Increasing trend in pre-monsoon season rainfall may affect the harvesting of Rabi season crops. Therefore, the early-growing crop variety should be introduced in the Betwa basin.
2. Increase in the minimum and maximum temperature may lead to a significant change in the growing season, growth stages and crop water use that subsequently affects the yield. Therefore, the crop varieties, which can sustain the high temperature, should be introduced in future.
3. Strip cropping is recommended as the most effective over-land BMP treatment in agriculture land for soil and water conservation under changing future climate.
4. Both grassed waterways and streambank stabilization practices are recommended as the most effective in-stream BMP treatments protecting the river channels from future flood erosion.

5. The grade stabilization structure can effectively reduce the streamflow in main river channel during future horizon 2060, due to large precipitation events under future climatic changes.

9.4 MAJOR RESEARCH CONTRIBUTIONS

1. Integrated CA-MC model was employed to analyze the LU/LC changes for a trans-boundary/inter-state river basin of central India. As per the land use model simulation, the future LU/LC change analysis has been carried out for the whole duration of 21st century.
2. A conceptual framework was employed to study the dry and wet spells effect on NDVI and land cover changes in the Betwa river basin.
3. The required data/information to implement and manage the reservoirs and weirs in the SWAT model was estimated using remote sensing and measured data for the Betwa river basin.
4. A conceptual framework has been developed to assess the individual and combined impacts of land use and climatic changes on the hydrology of the Betwa river basin for future years.
5. Effectiveness of over-land as well as in-stream best management practices (BMP) were evaluated for soil and water conservation, and for river channel protection and restoration in the Betwa river basin.

9.5 LIMITATIONS AND FUTURE RESEARCH SCOPE

- Remote sensing data used in this study has different spatial and temporal resolutions, which may affect the change analysis and modelling, and may be one of the limitation of the present research study.
- In this study, monthly streamflow and sediment yield simulations were carried out at sub-watershed level analysis. However, the SWAT model simulation at daily time-scale and at HRU level can provide more detailed hydrologic study.
- Small ponds and lakes have not been considered in hydrological modelling using the SWAT, due to non-availability of data, this could be the limitation of this study. For HRU level analysis, small water storages information will be help to adequately simulate and model the complex hydrological processes of a river basin.
- The water quality modelling can be also carried out for environmental management in the Betwa basin.

- Cost-effectiveness of the combined (over-land plus in-stream) BMP implementation is needed to evaluate for recommendation of optimal sustainable solutions for a river basin.
- In this study, only one GCM model (RCP 8.5 scenario) for future climate change analysis has been employed. However, use of different RCP scenarios (other than RCP 8.5 such as RCP 2.6, RCP4.5, RCP6.0 etc.) for future climate change impact assessment can be a scope for future research work.

REFERENCES

Abbasi, M. K., Mahmood Tahir, M., Sabir, N., & Khurshid, M. (2015). Impact of the addition of different plant residues on nitrogen mineralization–immobilization turnover and carbon content of a soil incubated under laboratory conditions. Solid Earth, 6(1), 197-205.

Abbaspour, K. C. (2007). User manual for SWAT-CUP, SWAT calibration and uncertainty analysis programs. Swiss Federal Institute of Aquatic Science and Technology, Eawag, Duebendorf, Switzerland.

Abbaspour, K. C. (2011). User manual for SWAT-CUP4. SWAT calibration and uncertainty Programs, Swiss Federal Institute of Aquatic Science and Technology, Eawag, Duebendorf, Switzerland.

Abbaspour, K. C. (2013). SWAT-CUP 2012. SWAT Calibration and Uncertainty Program—A User Manual.

Abbaspour, K. C., Faramarzi, M., Ghasemi, S. S., & Yang, H. (2009). Assessing the impact of climate change on water resources in Iran. Water Resources Research, 45(10).

Abbaspour, K. C., Rouholahnejad, E., Vaghefi, S., Srinivasan, R., Yang, H., & Kløve, B. (2015). A continental-scale hydrology and water quality model for Europe: Calibration and uncertainty of a high-resolution large-scale SWAT model. Journal of Hydrology, 524, 733-752.

Abbaspour, K. C., Yang, J., Maximov, I., Siber, R., Bogner, K., Mieleitner, J., Zobrist, J., & Srinivasan, R. (2007). Modelling hydrology and water quality in the pre-alpine/alpine Thur watershed using SWAT. Journal of Hydrology, 333(2-4), 413-430.

Abbott, M. B., Bathurst, J. C., Cunge, J. A., O'Connell, P. E., & Rasmussen, J. (1986a). An introduction to the European Hydrological System—Systeme Hydrologique Europeen,"SHE", 1: History and philosophy of a physically-based, distributed modelling system. Journal of Hydrology, 87(1-2), 45-59.

Abbott, M. B., Bathurst, J. C., Cunge, J. A., O'connell, P. E., & Rasmussen, J. (1986b). An introduction to the European Hydrological System—Systeme Hydrologique Europeen,"SHE", 2: Structure of a physically-based, distributed modelling system. Journal of Hydrology, 87(1-2), 61-77.

Abu-Zreig, M., Rudra, R. P., Lalonde, M. N., Whiteley, H. R., & Kaushik, N. K. (2004). Experimental investigation of runoff reduction and sediment removal by vegetated filter strips. Hydrological Processes, 18(11), 2029-2037.

Adams, D. M., Alig, R. J., Callaway, J. M., Winnett, S. M., & McCarl, B. A. (1996). The forest and agricultural sector optimization model (FASOM): model structure and policy applications. Diane Publishing.

Agarwal, C., Green, G. M., Grove, J. M., Evans, T. P., & Schweik, C. M. (2002). A review and assessment of land-use change models: dynamics of space, time, and human choice. Gen. Tech. Rep. NE-297. Newton Square, PA: US Department of Agriculture, Forest Service, Northeastern Research Station. 61 p., 297. DOI: https://doi.org/10.2737/NE-GTR-297.

Agnihotri, R., Dimri, A. P., Joshi, H. M., Verma, N. K., Sharma, C., Singh, J., & Sundriyal, Y. P. (2017). Assessing operative natural and anthropogenic forcing factors from long-

term climate time series of Uttarakhand (India) in the backdrop of recurring extreme rainfall events over northwest Himalaya. Geomorphology, 284, 31-40.

Agrawal, A. (2000). Adaptive management in transboundary protected areas: The Bialowieza National Park and Biosphere Reserve as a case study. Environmental Conservation, 27(04), 326-333.

Agrawal, N., Verma, M. K., & Tripathi, M. P. (2009). Effective Management of Critical Sub-watersheds Using SWAT Model, Remote Sensing and GIS. Agricultural Engineering Today, 33(4), 15-20.

Akhtar-Schuster, M., Thomas, R. J., Stringer, L. C., Chasek, P., & Seely, M. (2011). Improving the enabling environment to combat land degradation: Institutional, financial, legal and science-policy challenges and solutions. Land Degradation & Development, 22(2), 299-312.

Ale, S., Bowling, L. C., Owens, P. R., Brouder, S. M., & Frankenberger, J. R. (2012). Development and application of a distributed modeling approach to assess the watershed-scale impact of drainage water management. Agricultural Water Management, 107, 23-33.

Allen, R. G., Jensen, M. E., Wright, J. L., & Burman, R. D. (1989). Operational estimates of reference evapotranspiration. Agronomy Journal, 81(4), 650-662.

Aly, A. A., Al-Omran, A. M., Sallam, A. S., Al-Wabel, M. I., & Al-Shayaa, M. S. (2016). Vegetation cover change detection and assessment in arid environment using multi-temporal remote sensing images and ecosystem management approach. Solid Earth, 7(2), 713-725.

Anand, J., Gosain, A. K., Khosa, R., & Srinivasan, R. (2018). Regional scale hydrologic modeling for prediction of water balance, analysis of trends in streamflow and variations in streamflow: The case study of the Ganga River basin. Journal of Hydrology: Regional Studies, 16, 32-53.

Anand, S., Mankin, K. R., McVay, K. A., Janssen, K. A., Barnes, P. L., & Pierzynski, G. M. (2007). Calibration and Validation of ADAPT and SWAT for Field-Scale Runoff Prediction. JAWRA Journal of the American Water Resources Association, 43(4), 899-910.

Anderson, J. R. (1971). Land-use classification schemes. Photogrammetric Engineering, 37(4), 379-387.

Aouissi, J., Benabdallah, S., Chabaâne, Z. L., & Cudennec, C. (2016). Evaluation of potential evapotranspiration assessment methods for hydrological modelling with SWAT—Application in data-scarce rural Tunisia. Agricultural Water Management, 174, 39-51.

Arabi, M., Frankenberger, J. R., Engel, B. A., & Arnold, J. G. (2008). Representation of agricultural conservation practices with SWAT. Hydrological Processes, 22(16), 3042-3055.

Arabi, M., Govindaraju, R. S., & Hantush, M. M. (2007). A probabilistic approach for analysis of uncertainty in the evaluation of watershed management practices. Journal of Hydrology, 333(2-4), 459-471.

Arabi, M., Govindaraju, R. S., Hantush, M. M., & Engel, B. A. (2006). Role of Watershed Subdivision on Modeling the Effectiveness of Best Management Practices with SWAT 1. JAWRA Journal of the American Water Resources Association, 42(2), 513-528.

Armitage, D. (2005). Adaptive capacity and community-based natural resource management. Environmental Management, 35(6), 703-715.

Arnell, N. W. (1992). Impacts of climatic change on river flow regimes in the UK. Water and Environment Journal, 6(5), 432-442.

Arnell, N. W. (1999). Climate change and global water resources. Global Environmental Change, 9, S31-S49.

Arnell, N. W. (2004). Climate change and global water resources: SRES emissions and socio-economic scenarios. Global Environmental Change, 14(1), 31-52.

Arnold, J. G., & Fohrer, N. (2005). SWAT 2000: current capabilities and research opportunities in applied watershed modelling. Hydrological Processes, 19(3), 563-572.

Arnold, J. G., Kiniry, J. R., Srinivasan, R., Williams, J. R., Haney, E. B., & Neitsch, S. L. (2012a). Soil and Water Assessment Tool input/output file documentation: Version 2012. Texas Water Resources Institute, technical report TR-439.

Arnold, J. G., Moriasi, D. N., Gassman, P. W., Abbaspour, K. C., White, M. J., Srinivasan, R., ... & Kannan, N. (2012b). SWAT: Model use, calibration, and validation. Transactions of the ASABE, 55(4), 1491-1508.

Arnold, J. G., Srinivasan, R., Muttiah, R. S., & Williams, J. R. (1998). Large area hydrologic modeling and assessment part I: model development. JAWRA Journal of the American Water Resources Association, 34(1), 73-89.

Arnold, J., Bieger, K., White, M., Srinivasan, R., Dunbar, J., & Allen, P. (2018). Use of decision tables to simulate management in SWAT+. Water, 10(6), 713. https://doi.org/10.3390/w10060713.

Arora, M., Kumar, R., Singh, R. D., Malhotra, J., & Kumar, N. (2016). Analysis of unusual meteorological conditions that led to recent floods in Bhagirathi Basin (Uttarakhand Himalayas). Hydrological Sciences Journal, 61(7), 1238-1243.

Arsanjani, J. J., Helbich, M., Kainz, W., & Boloorani, A. D. (2013). Integration of logistic regression, Markov chain and cellular automata models to simulate urban expansion. International Journal of Applied Earth Observation and Geoinformation, 21, 265-275.

Arsanjani, J. J., Kainz, W., & Mousivand, A. J. (2011). Tracking dynamic land-use change using spatially explicit Markov Chain based on cellular automata: the case of Tehran. International Journal of Image and Data Fusion, 2(4), 329-345.

Badar, B., Romshoo, S. A., & Khan, M. A. (2013). Modelling catchment hydrological responses in a Himalayan Lake as a function of changing land use and land cover. Journal of Earth System Science, 122(2), 433-449.

Bagan, H., & Yamagata, Y. (2012). Landsat analysis of urban growth: How Tokyo became the world's largest megacity during the last 40years. Remote Sensing of Environment, 127, 210-222.

Bakker, M., & Matsuno, Y. (2001). A framework for valuing ecological services of irrigation water–A case of an irrigation-wetland system in Sri Lanka. Irrigation and Drainage Systems, 15(2), 99-115.

Bannwarth, M. A., Hugenschmidt, C., Sangchan, W., Lamers, M., Ingwersen, J., Ziegler, A. D., & Streck, T. (2014). Simulation of stream flow components in a mountainous catchment in northern Thailand with SWAT, using the ANSELM calibration approach. Hydrological Processes, 29(6), 1340-1352.

Barfield, B. J., Hayes, J. C., Stevens, E., Harp, S. L., & Fogle, A. (1996). SEDIMOT III model. Watershed Models, 381-398.

Barfield, J. B., Hayes, J. C., Harp, S. L., Holbrook, K. F., & Gillespie, J. (2006b). Chapter 15: IDEAL: Integrated Design and Evaluation of loading Models. Watershed models, Singh, V. P., and Donald, K. F., Taylor and Francis, Colo. 361–379.

Barron, J., Enfors, E., Cambridge, H., & Moustapha, A. M. (2010). Coping with rainfall variability: Dry spell mitigation and implication on landscape water balances in small-scale farming systems in semi-arid Niger. International Journal of Water Resources Development, 26(4), 543-559.

Beasley, D. B., Huggins, L. F., & Monke, A. (1980). ANSWERS: A model for watershed planning. Transactions of the ASAE, 23(4), 938-0944.

Beck, M. B. (1987). Water quality modeling: a review of the analysis of uncertainty. Water Resources Research, 23(8), 1393-1442.

Behera, S., & Panda, R. K. (2006). Evaluation of management alternatives for an agricultural watershed in a sub-humid subtropical region using a physical process based model. Agriculture, Ecosystems & Environment, 113(1-4), 62-72.

Belay, K. T., Van Rompaey, A., Poesen, J., Van Bruyssel, S., Deckers, J., & Amare, K. (2015). Spatial analysis of land cover changes in eastern Tigray (Ethiopia) from 1965 to 2007: are there signs of a forest transition?. Land Degradation & Development, 26(7), 680-689.

Benaman, J., Shoemaker, C. A., & Haith, D. A. (2005). Calibration and validation of soil and water assessment tool on an agricultural watershed in upstate New York. Journal of Hydrologic Engineering, 10(5), 363-374.

Bergström, S., & Forsman, A. (1973). Development of a conceptual deterministic rainfall-runoff mode. Nord. Hydrol, 4, 240-253.

Berry, M. W., Hazen, B. C., MacIntyre, R. L., & Flamm, R. O. (1996). LUCAS: a system for modeling land-use change. IEEE Computational Science and Engineering, 3(1), 24-35.

Besalatpour, A., Hajabbasi, M. A., Ayoubi, S., & Jalalian, A. (2012). Identification and prioritization of critical sub-basins in a highly mountainous watershed using SWAT model. Eurasian Journal of Soil Science (EJSS), 1(1), 58-63.

Betrie, G. D., Mohamed, Y. A., Griensven, A. V., & Srinivasan, R. (2011). Sediment management modelling in the Blue Nile Basin using SWAT model. Hydrology and Earth System Sciences, 15(3), 807-818.

Beven, K. (1989). Changing ideas in hydrology—the case of physically-based models. Journal of Hydrology, 105(1-2), 157-172.

Beyene, S. T. (2015). Rangeland Degradation in a Semi-Arid Communal Savannah of Swaziland: Long–Term DIP-Tank Use Effects on Woody Plant Structure, Cover and their Indigenous Use in Three Soil Types. Land Degradation & Development, 26(4), 311-323.

Bhave, A. G., Mittal, N., Mishra, A., & Raghuwanshi, N. S. (2016). Integrated assessment of no-regret climate change adaptation options for reservoir catchment and command areas. Water Resources Management, 30(3), 1001-1018.

Bian, L., Sun, H., Blodgett, C., Egbert, S., Li, W., Ran, L., & Koussis, A. (1996). An integrated interface system to couple the SWAT model and ARC/INFO. In Proceedings of the 3rd

International Conference on Integrating GIS and Environmental Modeling. US National Center for Geographic Information and Analysis, Santa Fe, New Mexico, CD-ROM.

Bičík, I., Jeleček, L., & Štěpánek, V. (2001). Land-use changes and their social driving forces in Czechia in the 19th and 20th centuries. Land Use Policy, 18(1), 65-73.

Bicknell, B. R., Imhoff, J. C., Kittle, J. L., Donigan, A. S., & Johanson, R. C. (1993). Hydrologic Simulation Program: Fortran User's Manual for Release 10. US Environmental Protection Agency, Athens, Georgia. Report EPA/600/R-93/174.

Bieger, K., Arnold, J. G., Rathjens, H., White, M. J., Bosch, D. D., Allen, P. M., ... & Srinivasan, R. (2017). Introduction to SWAT+, a completely restructured version of the soil and water assessment tool. JAWRA Journal of the American Water Resources Association, 53(1), 115-130.

Bieger, K., Hörmann, G., & Fohrer, N. (2014). Simulation of streamflow and sediment with the soil and water assessment tool in a data scarce catchment in the three Gorges region, China. Journal of Environmental Quality, 43(1), 37-45.

Bingner, R. L. (1996). Runoff simulated from Goodwin Creek watershed using SWAT. Transactions of the ASAE, 39(1), 85-90.

Bingner, R. L., Theurer, F. D., & Yuan, Y. (2011). AnnAGNPS technical processes. USDA-ARS. Version 5.2. USDA–ARC, National Sedimentation Laboratory and USDA–NRCS National Water and Climate Center.

Blöschl, G., Ardoin-Bardin, S., Bonell, M., Dorninger, M., Goodrich, D., Gutknecht, D., Matamoros, D., Merz, B., Shand, P., & Szolgay, J. (2007). At what scales do climate variability and land cover change impact on flooding and low flows?. Hydrological Processes, 21(9), 1241-1247.

Bodí, M. B., Mataix-Solera, J., Doerr, S. H., & Cerdà, A. (2011). The wettability of ash from burned vegetation and its relationship to Mediterranean plant species type, burn severity and total organic carbon content. Geoderma, 160(3-4), 599-607.

Bonell, M., Purandara, B. K., Venkatesh, B., Krishnaswamy, J., Acharya, H. A. K., Singh, U. V., ... & Chappell, N. (2010). The impact of forest use and reforestation on soil hydraulic conductivity in the Western Ghats of India: implications for surface and sub-surface hydrology. Journal of Hydrology, 391(1-2), 47-62.

Bonilla, C. A., Norman, J. M., Molling, C. C., Karthikeyan, K. G., & Miller, P. S. (2008). Testing a grid-based soil erosion model across topographically complex landscapes. Soil Science Society of America Journal, 72(6), 1745-1755.

Bookhagen, B., & Burbank, D. W. (2010). Toward a complete Himalayan hydrological budget: Spatiotemporal distribution of snowmelt and rainfall and their impact on river discharge. Journal of Geophysical Research: Earth Surface, 115(F3).

Boongaling, C. G. K., Faustino-Eslava, D. V., & Lansigan, F. P. (2018). Modeling land use change impacts on hydrology and the use of landscape metrics as tools for watershed management: The case of an ungauged catchment in the Philippines. Land Use Policy, 72, 116-128.

Borah, D. K. (1989). Runoff simulation model for small watersheds. Transactions of the ASAE, 32(3), 881-0886.

Borah, D. K., & Bera, M. (2003). Watershed-scale hydrologic and nonpoint-source pollution models: Review of mathematical bases. Transactions of the ASAE, 46(6), 1553.

Borah, D. K., Arnold, J. G., Bera, M., Krug, E. C., & Liang, X. Z. (2007). Storm event and continuous hydrologic modeling for comprehensive and efficient watershed simulations. Journal of Hydrologic Engineering, 12(6), 605-616.

Borah, D. K., Bera, M., Shaw, S., & Keefer, L. (1999). Dynamic Modeling and Monitoring of Water, Sediment, Nutrients, and Pesticides in Agricultural Watersheds during Storm Events. Contract Report 655, Illinois State Water Survey Watershed Science Section Champaign, Illinois.

Bosch, J. M., & Hewlett, J. D. (1982). A review of catchment experiments to determine the effect of vegetation changes on water yield and evapotranspiration. Journal of Hydrology, 55(1-4), 3-23.

Bossa, A. Y., Diekkrüger, B., Giertz, S., Steup, G., Sintondji, L. O., Agbossou, E. K., & Hiepe, C. (2012). Modeling the effects of crop patterns and management scenarios on N and P loads to surface water and groundwater in a semi-humid catchment (West Africa). Agricultural water management, 115, 20-37.

Bouraoui, F., & Dillaha, T. A. (1996). ANSWERS-2000: Runoff and sediment transport model. Journal of Environmental Engineering, 122(6), 493-502.

Bracmort, K. S., Arabi, M., Frankenberger, J. R., Engel, B. A., & Arnold, J. G. (2006). Modeling long-term water quality impact of structural BMPs. Transactions of the ASABE, 49(2), 367-374.

Bridge, J. S. (1993). The interaction between channel geometry, water flow, sediment transport and deposition in braided rivers. Geological Society, London, Special Publications, 75(1), 13-71.

Bronstert, A., Niehoff, D., & Bürger, G. (2002). Effects of climate and land-use change on storm runoff generation: present knowledge and modelling capabilities. Hydrological Processes, 16(2), 509-529.

Broxton, P. D., Zeng, X., Sulla-Menashe, D., & Troch, P. A. (2014). A global land cover climatology using MODIS data. Journal of Applied Meteorology and Climatology, 53(6), 1593-1605.Liang, D., Zuo, Y., Huang, L., Zhao, J., Teng, L., & Yang, F. (2015). Evaluation of the consistency of MODIS Land Cover Product (MCD12Q1) based on Chinese 30 m GlobeLand30 datasets: A case study in Anhui Province, China. ISPRS International Journal of Geo-Information, 4(4), 2519-2541.

Bulygina, N., Ballard, C., McIntyre, N., O'Donnell, G., & Wheater, H. (2012). Integrating different types of information into hydrological model parameter estimation: application to ungauged catchments and land use scenario analysis. Water Resources Research, 48(6). doi: 10.1029/2011WR011207

Butler, G. B., & Srivastava, P. (2007). An Alabama BMP database for evaluating water quality impacts of alternative management practices. Applied Engineering in Agriculture, 23(6), 727-736.

Byrne, G. F., Crapper, P. F., & Mayo, K. K. (1980). Monitoring land-cover change by principal component analysis of multitemporal Landsat data. Remote Sensing of Environment, 10(3), 175-184.

Cai, T., Li, Q., Yu, M., Lu, G., Cheng, L., & Wei, X. (2012). Investigation into the impacts of land-use change on sediment yield characteristics in the upper Huaihe River basin, China. Physics and Chemistry of the Earth, Parts A/B/C, 53, 1-9.

Cao, W., Bowden, W. B., Davie, T., & Fenemor, A. (2006). Multi-variable and multi-site calibration and validation of SWAT in a large mountainous catchment with high spatial variability. Hydrological Processes, 20(5), 1057-1073.

Carlson, D. H., Thurow, T. L., & Wright, J. R. (1995). SPUR91: simulation of production and utilization of rangelands. Computer Models of Watershed Hydrology. Singh, V. P. (Ed.), Water Resources Publishers, Highland s Ranch, Colorado; 1021–1068.

Čarni, A., Jarnjak, M., & Oštir-Sedej, K. (1998). Past and present forest vegetation in NE Slovenia derived from old maps. Applied Vegetation Science,1(2), 253-258.

Carvalho-Santos, C., Monteiro, A. T., Azevedo, J. C., Honrado, J. P., & Nunes, J. P. (2017). Climate change impacts on water resources and reservoir management: uncertainty and adaptation for a mountain catchment in northeast Portugal. Water Resources Management, 31(11), 3355-3370.

Cassinari, C. H. I. A. R. A., Manfredi, P., Giupponi, L. U. C. A., Trevisan, M. A. R. C. O., & Piccini, C. (2015). Relationship between hydraulic properties and plant coverage of the closed-landfill soils in Piacenza (Po Valley, Italy). Solid Earth, 6(3), 929-943.

Cau, P., & Paniconi, C. (2007). Assessment of alternative land management practices using hydrological simulation and a decision support tool: Arborea agricultural region, Sardinia. Hydrology and Earth System Sciences Discussions, 11(6), 1811-1823.

Caúla, R. H., de Oliveira-Júnior, J. F., de Gois, G., Delgado, R. C., Pimentel, L. C. G., & Teodoro, P. E. (2017). Nonparametric Statistics Applied to Fire Foci Obtained by Meteorological Satellites and Their Relationship to the MCD12Q1 Product in the State of Rio de Janeiro, Southeast Brazil. Land Degradation & Development, 28(3), 1056-1067.

Cerdà, A., & Doerr, S. H. (2005). Influence of vegetation recovery on soil hydrology and erodibility following fire: an 11-year investigation. International Journal of Wildland Fire, 14(4), 423-437.

Čerkasova, N., Umgiesser, G., & Ertürk, A. (2018). Development of a hydrology and water quality model for a large transboundary river watershed to investigate the impacts of climate change–A SWAT application. Ecological Engineering, 124, 99-115.

Chanasyk, D. S., Mapfumo, E., & Willms, W. (2003). Quantification and simulation of surface runoff from fescue grassland watersheds. Agricultural Water Management, 59(2), 137-153.

Chandramouli, C., & Sinha, S. (2014). Census of India 2011: District Census Handbook Bhopal. Directorate of Census Operations, Madhya Pradesh, Government of India, Series-24, Part XII-B.

Chang, C. L., Chiueh, P. T., & Lo, S. L. (2007). Effect of spatial variability of storm on the optimal placement of best management practices (BMPs). Environmental Monitoring and Assessment, 135(1-3), 383-389.

Chaube, U. C., Suryavanshi, S., Nurzaman, L., & Pandey, A. (2011). Synthesis of flow series of tributaries in Upper Betwa basin. International Journal of Environmental Sciences, 1(7), 1466-1482.

Chaube, U.C. (1988). Model study of water use and water balance in Betwa Basin. Journal of Institution of Engineers (India), 69:169–173.

Chauhan, M. S., & Quamar, M. F. (2010). Vegetation and climate change in southeastern Madhya Pradesh during Late Holocene, based on pollen evidence. Journal of the Geological Society of India, 76(2), 143-150.

Chauhan, M. S., & Quamar, M. F. (2012). Pollen records of vegetation and inferred climate change in southwestern Madhya Pradesh during the last ca. 3800 years. Journal of the Geological Society of India, 80(4), 470-480.

Chen, B., Xu, G., Coops, N. C., Ciais, P., Innes, J. L., Wang, G., ... & Cao, L. (2014). Changes in vegetation photosynthetic activity trends across the Asia–Pacific region over the last three decades. Remote Sensing of Environment, 144, 28-41.

Chen, J., Jönsson, P., Tamura, M., Gu, Z., Matsushita, B., & Eklundh, L. (2004). A simple method for reconstructing a high-quality NDVI time-series data set based on the Savitzky–Golay filter. Remote sSensing of Environment, 91(3-4), 332-344.

Chen, J., Li, X., & Zhang, M. (2005). Simulating the impacts of climate variation and land-cover changes on basin hydrology: A case study of the Suomo basin. Science in China Series D: Earth Sciences, 48(9), 1501-1509.

Chen, L., Qian, X., & Shi, Y. (2011b). Critical area identification of potential soil loss in a typical watershed of the three Gorges reservoir region. Water Resources Management, 25(13), 3445.

Chen, Y., Ale, S., Rajan, N., & Munster, C. (2017). Assessing the hydrologic and water quality impacts of biofuel-induced changes in land use and management. Gcb Bioenergy, 9(9), 1461-1475.

Cheng, A. S., Kruger, L. E., & Daniels, S. E. (2003). "Place" as an integrating concept in natural resource politics: Propositions for a social science research Agenda. Society & Natural Resources, 16(2), 87-104.

Chiang, L. C., Chaubey, I., Gitau, M. W., & Arnold, J. G. (2010). Differentiating impacts of land use changes from pasture management in a CEAP watershed using the SWAT model. Transactions of the ASABE, 53(5), 1569-1584.

Chien, H., Yeh, P. J. F., & Knouft, J. H. (2013). Modeling the potential impacts of climate change on streamflow in agricultural watersheds of the Midwestern United States. Journal of Hydrology, 491, 73-88.

Chiew, F. H. S., Teng, J., Vaze, J., Post, D. A., Perraud, J. M., Kirono, D. G. C., & Viney, N. R. (2009). Estimating climate change impact on runoff across southeast Australia: Method, results, and implications of the modeling method. Water Resources Research, 45(10). doi:10.1029/2008WR007338

Choi, J. Y., Engel, B. A., & Chung, H. W. (2002). Daily streamflow modelling and assessment based on the curve-number technique. Hydrological Processes, 16(16), 3131-3150.

Chomitz, K., & Gray, D. A. (1999). Roads, lands, markets, and deforestation: a spatial model of land use in Belize. The World Bank Economic Review, 10, 487-512.

Chow, V. T. (1959). Open-channel hydraulics. McGraw-Hill, New York, p 112.

Chowdary, V. M., Chakraborthy, D., Jeyaram, A., Murthy, Y. K., Sharma, J. R., & Dadhwal, V. K. (2013). Multi-criteria decision making approach for watershed prioritization using analytic hierarchy process technique and GIS. Water Resources Management, 27(10), 3555-3571.

Chowdary, V. M., Ramakrishnan, D., Srivastava, Y. K., Chandran, V., & Jeyaram, A. (2009). Integrated water resource development plan for sustainable management of Mayurakshi

watershed, India using remote sensing and GIS. Water Resources Management, 23(8), 1581-1602.

Christianson, R. D., Powell, G. M., Hutchinson, S. L., & Presley, D. (2008). Stormwater Best Management Practice Maintenance. Agricultural Experiment Station and Cooperative Extension Service, Kansas State University.

Christopher, S. F., Tank, J. L., Mahl, U. H., Yen, H., Arnold, J. G., Trentman, M. T., ... & Royer, T. V. (2017). Modeling nutrient removal using watershed-scale implementation of the two-stage ditch. Ecological Engineering, 108, 358-369.

Chu, J. T., Xia, J., Xu, C. Y., & Singh, V. P. (2010). Statistical downscaling of daily mean temperature, pan evaporation and precipitation for climate change scenarios in Haihe River, China. Theoretical and Applied Climatology, 99(1-2), 149-161.

Chu, T. W., & Shirmohammadi, A. (2004). Evaluation of the SWAT model's hydrology component in the piedmont physiographic region of Maryland. Transactions of the American Society of Agricultural Engineers, 47(4): 1057-1073.

Cibin, R., Chaubey, I., Muenich, R. L., Cherkauer, K. A., Gassman, P. W., Kling, C. L., & Panagopoulos, Y. (2017). Influence of Bioenergy Crop Production and Climate Change on Ecosystem Services. JAWRA Journal of the American Water Resources Association, 53(6), 1323-1335.

Clarke, K. C., Brass, J. A., & Riggan, P. J. (1994). A cellular automation model of wildfire propagation and extinction. Photogrammetric Engineering and Remote Sensing, 60(11), 1355-1367.

Clarke, K. C., Hoppen, S., & Gaydos, L. (1997). A self-modifying cellular automaton model of historical urbanization in the San Francisco Bay area. Environment and planning B: Planning and design, 24(2), 247-261.

Colwell J. E., & Weber F. P. (1981). Forest change detection. In Proceeding of 15th International Symposium of Remote Sensing of Environment, 839-852.

Conradt, T., Koch, H., Hattermann, F. F., & Wechsung, F. (2012). Spatially differentiated management-revised discharge scenarios for an integrated analysis of multi-realisation climate and land use scenarios for the Elbe River basin. Regional Environmental Change, 12(3), 633-648.

Cornelissen, T., Diekkrüger, B., & Giertz, S. (2013). A comparison of hydrological models for assessing the impact of land use and climate change on discharge in a tropical catchment. Journal of Hydrology, 498, 221-236.

Costanza, R., & Ruth, M. (1998). Using dynamic modeling to scope environmental problems and build consensus. Environmental Management, 22(2), 183-195.

Craine, J. M., Nippert, J. B., Elmore, A. J., Skibbe, A. M., Hutchinson, S. L., & Brunsell, N. A. (2012). Timing of climate variability and grassland productivity. Proceedings of the National Academy of Sciences, 109(9), 3401-3405.

Crawford, N. H., & Linsley, R. K. (1966). Digital Simulation in Hydrology'Stanford Watershed Model 4.

Cullen, A. C., & Frey, H. C. (1999). Probabilistic techniques in exposure assessment: a handbook for dealing with variability and uncertainty in models and inputs. Springer Science & Business Media, Plenum, New York.

Da Silva, R. M., Montenegro, S. M. G. L., & Santos, C. A. G. (2012). Integration of GIS and remote sensing for estimation of soil loss and prioritization of critical sub-catchments: a case study of Tapacurá catchment. Natural Hazards, 62(3), 953-970.

da Silva, V. D. P. R., Silva, M. T., Singh, V. P., de Souza, E. P., Braga, C. C., de Holanda, R. M., ... & Braga, A. C. R. (2018). Simulation of stream flow and hydrological response to land-cover changes in a tropical river basin. Catena, 162, 166-176.

Dabral, P. P., Baithuri, N., & Pandey, A. (2008). Soil erosion assessment in a hilly catchment of North Eastern India using USLE, GIS and remote sensing. Water Resources Management, 22(12), 1783-1798.

Daggupati, P., Pai, N., Ale, S., Douglas-Mankin, K. R., Zeckoski, R. W., Jeong, J., ... & Youssef, M. A. (2015). A recommended calibration and validation strategy for hydrologic and water quality models. Transactions of the ASABE, 58(6), 1705-1719.

Das, L., Dutta, M., Mezghani, A., & Benestad, R. E. (2018). Use of observed temperature statistics in ranking CMIP5 model performance over the Western Himalayan Region of India. International Journal of Climatology, 38(2), 554-570.

Dawson, C. W., & Wilby, R. L. (2001). Hydrological modelling using artificial neural networks. Progress in Physical Geography, 25(1), 80-108.

Dedina, S. (1995). The political ecology of transboundary development: land use, flood control and politics in the Tijuana River Valley. Journal of Borderlands Studies, 10(1), 89-110.

Devia, G. K., Ganasri, B. P., & Dwarakish, G. S. (2015). A review on hydrological models. Aquatic Procedia, 4, 1001-1007.

Dewan, A. M., & Yamaguchi, Y. (2009). Land use and land cover change in Greater Dhaka, Bangladesh: Using remote sensing to promote sustainable urbanization. Applied Geography, 29(3), 390-401.

Dey, P., & Mishra, A. (2017). Separating the impacts of climate change and human activities on streamflow: A review of methodologies and critical assumptions. Journal of Hydrology, 548, 278-290.

Dhar, S., & Mazumdar, A. (2009). Hydrological modelling of the Kangsabati river under changed climate scenario: case study in India. Hydrological Processes: An International Journal, 23(16), 2394-2406.

Dhliwayo, M. (2002). Legal Aspects of Trans-Boundary Natural Resources Management in Southern Africa. In “Commons in an Age of Globalisation", the Ninth Conference of the International Association for the Study of Common Property.

Di Piazza, A., Conti, F. L., Noto, L. V., Viola, F., & La Loggia, G. (2011). Comparative analysis of different techniques for spatial interpolation of rainfall data to create a serially complete monthly time series of precipitation for Sicily, Italy. International Journal of Applied Earth Observation and Geoinformation, 13(3), 396-408.

Dixon, B., & Earls, J. (2012). Effects of urbanization on streamflow using SWAT with real and simulated meteorological data. Applied Geography, 35(1-2), 174-190.

Dixon, R. K., Winjum, J. K., Andrasko, K. J., Lee, J. J., & Schroeder, P. E. (1994). Integrated land-use systems: assessment of promising agroforest and alternative land-use practices to enhance carbon conservation and sequestration. Climatic Change, 27(1), 71-92.

Downer, C. W., & Ogden, F. L. (2004). GSSHA: Model to simulate diverse stream flow producing processes. Journal of Hydrologic Engineering, 9(3), 161-174.

Du, J., Rui, H., Zuo, T., Li, Q., Zheng, D., Chen, A., ... & Xu, C. Y. (2013). Hydrological simulation by SWAT model with fixed and varied parameterization approaches under land use change. Water Resources Management, 27(8), 2823-2838.

Duan, W., He, B., Takara, K., Luo, P., Nover, D., & Hu, M. (2017). Impacts of climate change on the hydro-climatology of the upper Ishikari river basin, Japan. Environmental Earth Sciences, 76(14), 490.

Duhan D., & Pandey A. (2013). Statistical analysis of long term spatial and temporal trends of precipitation during 1901–2002 at Madhya Pradesh, India. Atmospheric Research 122: 136-149. DOI: 10.1016/j.atmosres.2012.10.010

Duhan, D., & Pandey, A. (2015). Statistical downscaling of temperature using three techniques in the Tons River basin in Central India. Theoretical and Applied Climatology, 121(3-4), 605-622.

Eckhardt, K., & Arnold, J. G. (2001). Automatic calibration of a distributed catchment model. Journal of Hydrology, 251(1-2), 103-109.

Eckhardt, K., Haverkamp, S., Fohrer, N., & Frede, H. G. (2002). SWAT-G, a version of SWAT99. 2 modified for application to low mountain range catchments. Physics and Chemistry of the Earth, Parts A/B/C, 27(9-10), 641-644.

Ewen, J., Parkin, G., & O'Connell, P. E. (2000). SHETRAN: distributed river basin flow and transport modeling system. Journal of Hydrologic Engineering, 5(3), 250-258.

Falcucci, A., Maiorano, L., & Boitani, L. (2007). Changes in land-use/land-cover patterns in Italy and their implications for biodiversity conservation. Landscape Ecology, 22(4), 617-631.

Fang, X., Ren, L., Li, Q., Zhu, Q., Shi, P., & Zhu, Y. (2013). Hydrologic response to land use and land cover changes within the context of catchment-scale spatial information. Journal of Hydrologic Engineering, 18(11), 1539-1548.

Favis-Mortlock, D. T. (1996). An evolutionary approach to the simulation of rill initiation and development. In Proceedings of the first international conference on GeoComputation, Abrahart RJ. (ed.), (Volume 1). School of Geography, University of Leeds: Leeds, 248-281.

Feng, X., Cheng, W., Fu, B., & Lü, Y. (2016). The role of climatic and anthropogenic stresses on long-term runoff reduction from the Loess Plateau, China. Science of the Total Environment, 571, 688-698.

Fitz, H. C., DeBellevue, E. B., Costanza, R., Boumans, R., Maxwell, T., Wainger, L., & Sklar, F. H. (1996). Development of a general ecosystem model for a range of scales and ecosystems. Ecological Modelling, 88(1-3), 263-295.

Fitzjohn, C., Ternan, J. L., & Williams, A. G. (1998). Soil moisture variability in a semi-arid gully catchment: implications for runoff and erosion control. Catena, 32(1), 55-70.

Fohrer, N., Haverkamp, S., Eckhardt, K., & Frede, H. G. (2001). Hydrologic response to land use changes on the catchment scale. Physics and Chemistry of the Earth, Part B: Hydrology, Oceans and Atmosphere, 26(7-8), 577-582.

Fontaine, T. A., Klassen, J. F., Cruickshank, T. S., & Hotchkiss, R. H. (2001). Hydrological response to climate change in the Black Hills of South Dakota, USA. Hydrological Sciences Journal, 46(1), 27-40.

Foster, G. R., and Meyer, L. D. (1972). A closed-form soil erosion equation for upland areas. Sedimentation Symposium in Honor Prof. H.A. Einstein. Shen HW (Ed.), Colorado State University, Fort Collins, CO; 12.1–12.19.

Frazier, P. S., & Page, K. J. (2000). Water body detection and delineation with Landsat TM data. Photogrammetric Engineering and Remote Sensing, 66(12), 1461-1468.

Frederick, K. D., & Major, D. C. (1997). Climate change and water resources. Climatic Change, 37(1), 7-23.

Frere, M. H., Onstad, C. A., & Holtan, H. N. (1975). Agricultural Research Service. Classic reprint series. ACTMO an Agricultural Chemical Transport Model. Reprint. London: Forgotten Books, 2013.

Friedl, M. A., McIver, D. K., Hodges, J. C., Zhang, X. Y., Muchoney, D., Strahler, A. H., ... & Baccini, A. (2002). Global land cover mapping from MODIS: algorithms and early results. Remote Sensing of Environment, 83(1-2), 287-302.

Friedl, M. A., Sulla-Menashe, D., Tan, B., Schneider, A., Ramankutty, N., Sibley, A., & Huang, X. (2010). MODIS Collection 5 global land cover: Algorithm refinements and characterization of new datasets. Remote Sensing of Environment, 114(1), 168-182.

Fritz, S., & See, L. (2004, April). Improving quality and minimising uncertainty of land cover maps using fuzzy logic. In Proceedings of the 12th Annual Conference on GIS Research (GISRUK 2004), University of East Anglia, Norwich, UK (pp. 28-30).

Froehlich, W., Gil, E., Kasza, I., & Starkel, L. (1990). Thresholds in the transformation of slopes and river channels in the Darjeeling Himalaya, India. Mountain Research and Development, 301-312.

Fu, C., James, A. L., & Yao, H. (2014). SWAT-CS: Revision and testing of SWAT for Canadian Shield catchments. Journal of Hydrology, 511, 719-735.

Fuchs, R., Herold, M., Verburg, P. H., Clevers, J. G., & Eberle, J. (2015). Gross changes in reconstructions of historic land cover/use for Europe between 1900 and 2010. Global Change Biology, 21(1), 299-313.

Funk, C. C., & Brown, M. E. (2006). Intra-seasonal NDVI change projections in semi-arid Africa. Remote Sensing of Environment, 101(2), 249-256.

Gao, P., Geissen, V., Ritsema, C. J., Mu, X. M., & Wang, F. (2013). Impact of climate change and anthropogenic activities on stream flow and sediment discharge in the Wei River basin, China. Hydrology and Earth System Sciences, 17, 961-972.

Gao, P., Zhang, X., Mu, X., Wang, F., Li, R., & Zhang, X. (2010). Trend and change-point analyses of streamflow and sediment discharge in the Yellow River during 1950–2005. Hydrological Sciences Journal, 55(2), 275-285.

Gashaw, T., Tulu, T., Argaw, M., & Worqlul, A. W. (2018). Modeling the hydrological impacts of land use/land cover changes in the Andassa watershed, Blue Nile Basin, Ethiopia. Science of the Total Environment, 619, 1394-1408.

Gassman, P. W., Reyes, M. R., Green, C. H., & Arnold, J. G. (2007). The soil and water assessment tool: historical development, applications, and future research directions. Transactions of the ASABE, 50(4), 1211-1250.

Gebremicael, T. G., Mohamed, Y. A., Betrie, G. D., van der Zaag, P., & Teferi, E. (2013). Trend analysis of runoff and sediment fluxes in the Upper Blue Nile basin: A combined analysis of statistical tests, physically-based models and landuse maps. Journal of Hydrology, 482, 57-68.

Geng, L., Ma, M., Wang, X., Yu, W., Jia, S., & Wang, H. (2014). Comparison of eight techniques for reconstructing multi-satellite sensor time-series NDVI data sets in the Heihe river basin, China. Remote Sensing, 6(3), 2024-2049.

Geoghegan, J., Villar, S. C., Klepeis, P., Mendoza, P. M., Ogneva-Himmelberger, Y., Chowdhury, R. R., Turner II, B.L. & Vance, C. (2001). Modeling tropical deforestation in the southern Yucatan peninsular region: comparing survey and satellite data. Agriculture, Ecosystems & Environment, 85(1), 25-46.

Ghaffari, G., Keesstra, S., Ghodousi, J., & Ahmadi, H. (2010). SWAT-simulated hydrological impact of land-use change in the Zanjanrood basin, Northwest Iran. Hydrological Processes: An International Journal, 24(7), 892-903.

Gilruth, P. T., Marsh, S. E., & Itami, R. (1995). A dynamic spatial model of shifting cultivation in the highlands of Guinea, West Africa. Ecological modelling, 79(1-3), 179-197.

Giordano, M., & Shah, T. (2014). From IWRM back to integrated water resources management. International Journal of Water Resources Development, 30(3), 364-376.

Giri, S., Nejadhashemi, A. P., & Woznicki, S. A. (2012). Evaluation of targeting methods for implementation of best management practices in the Saginaw River Watershed. Journal of Environmental Management, 103, 24-40.

Gisladottir, G., & Stocking, M. (2005). Land degradation control and its global environmental benefits. Land Degradation & Development, 16(2), 99-112.

Gitau, M. W., Chaubey, I., Gbur, E., Pennington, J. H., & Gorham, B. (2010). Impacts of land-use change and best management practice implementation in a Conservation Effects Assessment Project watershed: Northwest Arkansas. Journal of Soil and Water Conservation, 65(6), 353-368.

Goldshleger, N., Maor, A., Garzuzi, J., & Asaf, L. (2015). Influence of land use on the quality of runoff along Israel′ s coastal strip (demonstrated in the cities of Herzliya and Ra′ anana). Hydrological Processes, 29(6), 1289-1300.

Golmohammadi, G., Prasher, S. O., Madani, A., & Rudra, R. (2013). Using SWAT to Evaluate Climate Change Impact on Water Resources: Case Study in Canagagigue Creek Watershed, Canada. EIC Climate Change Technology Conference (CCTC) 2013 Paper Number 1569694805.

Golmohammadi, G., Rudra, R., Prasher, S., Madani, A., Mohammadi, K., Goel, P., & Daggupatti, P. (2017a). Water Budget in a Tile Drained Watershed under Future Climate Change Using SWATDRAIN Model. Climate, 5(2), 39.

Golmohammadi, G., Rudra, R., Prasher, S., Madani, A., Youssef, M., Goel, P., & Mohammadi, K. (2017b). Impact of tile drainage on water budget and spatial distribution of sediment generating areas in an agricultural watershed. Agricultural Water Management, 184, 124-134.

Gong, P. (1993). Change detection using principal component analysis and fuzzy set theory. Canadian Journal of Remote Sensing, 19(1), 22-29.

Gong, Z., Kawamura, K., Ishikawa, N., Goto, M., Wulan, T., Alateng, D., ... & Ito, Y. (2015). MODIS normalized difference vegetation index (NDVI) and vegetation phenology dynamics in the Inner Mongolia grassland. Solid Earth, 6(4), 1185-1194.

Gosain, A. K., & Rao, S. A. N. D. H. Y. A. (2007). Impact assessment of climate change on water resources of two river systems in India. Jalvigyan Sameeksha, 22(1), 1-20.

Goswami, B. N., Venugopal, V., Sengupta, D., Madhusoodanan, M. S., & Xavier, P. K. (2006). Increasing trend of extreme rain events over India in a warming environment. Science, 314(5804), 1442-1445.

Govers, G. (2011). Misapplications and misconceptions of erosion models. In: Morgan, R.P.C. and Nearing, M.A. (Editors), Handbook of erosion modelling, Blackwell Publishing Ltd., 117-134.

Green, W. H., & Ampt, G. A. (1911). Studies on Soil Phyics. The Journal of Agricultural Science, 4(1), 1-24.

Griffin, C. B. (1999). Watershed Councils: An Emerging Form of Public Participation in Natural Resource Management 1. JAWRA Journal of the American Water Resources Association, 35(3), 505-518.

Gross, E. J., & Moglen, G. E. (2007). Estimating the hydrological influence of Maryland state dams using GIS and the HEC-1 model. Journal of Hydrologic Engineering, 12(6), 690-693.

Grum, B., Woldearegay, K., Hessel, R., Baartman, J. E., Abdulkadir, M., Yazew, E., ... & Geissen, V. (2017). Assessing the effect of water harvesting techniques on event-based hydrological responses and sediment yield at a catchment scale in northern Ethiopia using the Limburg Soil Erosion Model (LISEM). Catena, 159, 20-34.

Guan, D., Li, H., Inohae, T., Su, W., Nagaie, T., & Hokao, K. (2011). Modeling urban land use change by the integration of cellular automaton and Markov model. Ecological Modelling, 222(20), 3761-3772.

Guhathakurta, P., & Rajeevan, M. (2008). Trends in the rainfall pattern over India. International Journal of Climatology, 28(11), 1453-1469.

Güntner, A., Krol, M. S., Araújo, J. C. D., & Bronstert, A. (2004). Simple water balance modelling of surface reservoir systems in a large data-scarce semiarid region. Hydrological Sciences Journal, 49(5), 901-918.

Guo, Y., Cao, J., Li, H., Wang, J., & Ding, Y. (2016). Simulation of the interface between the Indian summer monsoon and the East Asian summer monsoon: Intercomparison between MPI-ESM and ECHAM5/MPI-OM. Advances in Atmospheric Sciences, 33(3), 294-308.

Gupta, H. V., Sorooshian, S., & Yapo, P. O. (1999). Status of automatic calibration for hydrologic models: Comparison with multilevel expert calibration. Journal of Hydrologic Engineering, 4(2), 135-143.

Gupta, V. K., Waymire, E., & Wang, C. T. (1980). A representation of an instantaneous unit hydrograph from geomorphology. Water Resources Research, 16(5), 855-862.

Guzha, A. C., Rufino, M. C., Okoth, S., Jacobs, S., & Nóbrega, R. L. B. (2018). Impacts of land use and land cover change on surface runoff, discharge and low flows: Evidence from East Africa. Journal of Hydrology: Regional Studies, 15, 49-67.

Habersack, H., Hein, T., Stanica, A., Liska, I., Mair, R., Jäger, E., Hauer, C., & Bradley, C. (2016). Challenges of river basin management: Current status of, and prospects for, the River Danube from a river engineering perspective. Science of the Total Environment, 543, 828-845.

Hammouri, N., Adamowski, J., Freiwan, M., & Prasher, S. (2017). Climate change impacts on surface water resources in arid and semi-arid regions: a case study in northern Jordan. Acta Geodaetica et Geophysica, 52(1), 141-156.

Han, J., Hayashi, Y., Cao, X., & Imura, H. (2009). Application of an integrated system dynamics and cellular automata model for urban growth assessment: A case study of Shanghai, China. Landscape and Urban Planning, 91(3), 133-141.

Hansen, M. C., DeFries, R. S., Townshend, J. R. G., Sohlberg, R., Dimiceli, C., & Carroll, M. (2002). Towards an operational MODIS continuous field of percent tree cover algorithm: examples using AVHRR and MODIS data. Remote Sensing of Environment, 83(1-2), 303-319.

Hardie, I. W., & Parks, P. J. (1997). Land use with heterogeneous land quality: an application of an area base model. American Journal of Agricultural Economics, 79(2), 299-310.

Hargreaves, G. L., Hargreaves, G. H., & Riley, J. P. (1985). Agricultural benefits for Senegal River basin. Journal of Irrigation and Drainage Engineering, 111(2), 113-124.

Harlin, J. (1991). Development of a process oriented calibration scheme for the HBV hydrological model. Hydrology Research, 22(1), 15-36.

Harmel, R. D., Cooper, R. J., Slade, R. M., Haney, R. L., & Arnold, J. G. (2006). Cumulative uncertainty in measured streamflow and water quality data for small watersheds. Transactions of the ASABE, 49(3), 689-701.

Havnø, K., Madsen, M. N., & Dørge, J. (1995). MIKE 11–a generalized river modelling package. Computer Models of Watershed Hydrology, 733-782.

He, J., Liu, Y., Yu, Y., Tang, W., Xiang, W., & Liu, D. (2013). A counterfactual scenario simulation approach for assessing the impact of farmland preservation policies on urban sprawl and food security in a major grain-producing area of China. Applied Geography, 37, 127-138.

Hedelin, B. (2008). Criteria for the assessment of processes for sustainable river basin management and their congruence with the EU Water Framework Directive. European Environment, 18(4), 228-242.

Her, Y., Chaubey, I., Frankenberger, J., & Jeong, J. (2017). Implications of spatial and temporal variations in effects of conservation practices on water management strategies. Agricultural Water Management, 180, 252-266.

Herold, M., Mayaux, P., Woodcock, C. E., Baccini, A., & Schmullius, C. (2008). Some challenges in global land cover mapping: An assessment of agreement and accuracy in existing 1 km datasets. Remote Sensing of Environment, 112(5), 2538-2556.

Hoalst-Pullen, N., & Patterson, M. W. (2011). Applications and trends of remote sensing in professional urban planning. Geography Compass, 5(5), 249-261.

Hoalst-Pullen, N., & Patterson, M. W. (Eds.). (2010). Geospatial technologies in environmental management (Vol. 3). Springer Science & Business Media.

Holy, M., Vaska, J., & Vrana, K. (1988). SMODERP: A Simulation Model for Determination of Surface Runoff and Prediction of Erosion Processes. Technical Papers of the Faculty of Civil Engineering, CTU Prague, Series, 8, 5-42.

Hoscilo, A., Balzter, H., Bartholomé, E., Boschetti, M., Brivio, P. A., Brink, A., ... & Pekel, J. F. (2014). A conceptual model for assessing rainfall and vegetation trends in sub-Saharan Africa from satellite data. International Journal of Climatology, 35(12), 3582-3592.

Hovenga, P. A., Wang, D., Medeiros, S. C., Hagen, S. C., & Alizad, K. (2016). The response of runoff and sediment loading in the Apalachicola River, Florida to climate and land use land cover change. Earth's Future, 4(5), 124-142.

Howarth, P. J., & Wickware, G. M. (1981). Procedures for change detection using Landsat digital data. International Journal of Remote Sensing, 2(3), 277-291.

Hu, Z., & Lo, C. P. (2007). Modeling urban growth in Atlanta using logistic regression. Computers, Environment and Urban Systems, 31(6), 667-688.

Huang, G. B., Ding, X., & Zhou, H. (2010). Optimization method based extreme learning machine for classification. Neurocomputing, 74(1), 155-163.

Huang, J., Pontius, R. G., Li, Q., & Zhang, Y. (2012). Use of intensity analysis to link patterns with processes of land change from 1986 to 2007 in a coastal watershed of southeast China. Applied Geography, 34, 371-384.

Huang, S., Hesse, C., Krysanova, V., & Hattermann, F. (2009). From meso-to macro-scale dynamic water quality modelling for the assessment of land use change scenarios. Ecological Modelling, 220(19), 2543-2558.

Hudak, A. T., Fairbanks, D. H., & Brockett, B. H. (2004). Trends in fire patterns in a southern African savanna under alternative land use practices. Agriculture, Ecosystems & Environment, 101(2-3), 307-325.

Huete, A., Didan, K., Miura, T., Rodriguez, E. P., Gao, X., & Ferreira, L. G. (2002). Overview of the radiometric and biophysical performance of the MODIS vegetation indices. Remote sensing of environment, 83(1-2), 195-213.

Hutchinson, S. L., Keane, T., Christianson, R. D., Skabeland, L., Moore, T. L., Greene, A. M., & Kingery-Page, K. (2011). Management practices for the amelioration of urban stormwater. Procedia Environmental Sciences, 9, 83-89.

Hyandye, C. B., Worqul, A., Martz, L. W., & Muzuka, A. N. (2018). The impact of future climate and land use/cover change on water resources in the Ndembera watershed and their mitigation and adaptation strategies. Environmental Systems Research, 7(1), 7.

Iizumi, T., Sakurai, G., & Yokozawa, M. (2013). An ensemble approach to the representation of subgrid-scale heterogeneity of crop phenology and yield in coarse-resolution large-area crop models. Journal of Agricultural Meteorology, 69(4), 243-254.

Immerzeel, W. (2008). Historical trends and future predictions of climate variability in the Brahmaputra basin. International Journal of Climatology, 28(2), 243-254.

Immerzeel, W. W., & Droogers, P. (2008). Calibration of a distributed hydrological model based on satellite evapotranspiration. Journal of Hydrology, 349(3-4), 411-424.

Immerzeel, W. W., Van Beek, L. P., & Bierkens, M. F. (2010). Climate change will affect the Asian water towers. Science, 328(5984), 1382-1385.

Islam, A. K. M., Paul, S., Mohammed, K., Billah, M., Fahad, M., Rabbani, G., ... & Bala, S. K. (2018). Hydrological response to climate change of the Brahmaputra basin using CMIP5 general circulation model ensemble. Journal of Water and Climate Change, 9(3), 434-448.

Jackson, B. M., Browne, C. A., Butler, A. P., Peach, D., Wade, A. J., & Wheater, H. S. (2008). Nitrate transport in Chalk catchments: monitoring, modelling and policy implications. Environmental Science & Policy, 11(2), 125-135.

Jacob, M., Romeyns, L., Frankl, A., Asfaha, T., Beeckman, H., & Nyssen, J. (2015). Land Use and Cover Dynamics Since 1964 in the Afro-Alpine Vegetation Belt: Lib Amba Mountain in North Ethiopia. Land Degradation & Development, 27(3), 641-653.

Jain, S. K., & Goel, M. K. (2002). Assessing the vulnerability to soil erosion of the Ukai Dam catchments using remote sensing and GIS. Hydrological Sciences Journal, 47(1), 31-40.

Jajarmizadeh, M., Lafdani, E. K., Harun, S., & Ahmadi, A. (2015). Application of SVM and SWAT models for monthly streamflow prediction, a case study in South of Iran. KSCE Journal of Civil Engineering, 19(1), 345-357.

Jakeman, A. J., Green, T. R., Beavis, S. G., Zhang, L., Dietrich, C. R., & Crapper, P. F. (1999). Modelling upland and instream erosion, sediment and phosphorus transport in a large catchment. Hydrological Processes, 13(5), 745-752.

Jakeman, A. J., Littlewood, I. G., & Whitehead, P. G. (1990). Computation of the instantaneous unit hydrograph and identifiable component flows with application to two small upland catchments. Journal of Hydrology, 117(1-4), 275-300.

Jang, S. S., Ahn, S. R., & Kim, S. J. (2017). Evaluation of executable best management practices in Haean highland agricultural catchment of South Korea using SWAT. Agricultural Water Management, 180, 224-234.

Jayasankar, C. B., Surendran, S., & Rajendran, K. (2015). Robust signals of future projections of Indian summer monsoon rainfall by IPCC AR5 climate models: Role of seasonal cycle and interannual variability. Geophysical Research Letters, 42(9), 3513-3520.

Jayatilaka, C. J., Sakthivadivel, R., Shinogi, Y., Makin, I. W., & Witharana, P. (2003). A simple water balance modelling approach for determining water availability in an irrigation tank cascade system. Journal of Hydrology, 273(1-4), 81-102.

Jetten, V., Govers, G., & Hessel, R. (2003). Erosion models: quality of spatial predictions. Hydrological Processes, 17(5), 887-900.

Jha, M. K., & Gassman, P. W. (2014). Changes in hydrology and streamflow as predicted by a modelling experiment forced with climate models. Hydrological Processes, 28(5), 2772-2781.

Ji, U., Kim, T. G., Lee, E. J., Ryoo, K. S., Hwang, M. H., & Jang, E. K. (2014). Analysis of sediment discharge by long-term runoff in Nakdong River Watershed using SWAT model. Journal of Environmental Science International, 23(4), 723-735.

Jia, H., Yao, H., Tang, Y., Shaw, L. Y., Zhen, J. X., & Lu, Y. (2013). Development of a multi-criteria index ranking system for urban runoff best management practices (BMPs) selection. Environmental Monitoring and Assessment, 185(9), 7915-7933.

Jiang, D., Fu, X., & Wang, K. (2013). Vegetation dynamics and their response to freshwater inflow and climate variables in the Yellow River Delta, China. Quaternary International, 304, 75-84.

Jiongxin, X. (2005). The water fluxes of the Yellow River to the sea in the past 50 years, in response to climate change and human activities. Environmental Management, 35(5), 620-631.

Jönsson, P., & Eklundh, L. (2004). TIMESAT—a program for analyzing time-series of satellite sensor data. Computers & Geosciences, 30(8), 833-845.

Joseph, S., Sahai, A. K., Sharmila, S., Abhilash, S., Borah, N., Chattopadhyay, R., Pillai, P. A., Rajeevan, M., & Kumar, A. (2015). North Indian heavy rainfall event during June 2013: diagnostics and extended range prediction. Climate Dynamics, 44(7-8), 2049-2065.

Juckem, P. F., Hunt, R. J., Anderson, M. P., & Robertson, D. M. (2008). Effects of climate and land management change on streamflow in the driftless area of Wisconsin. Journal of Hydrology, 355(1-4), 123-130.

Julian, M. M., & Ward, P. J. (2014). Assessment of the effects of climate and land cover changes on river discharge and sediment yield, and an adaptive spatial planning in the Jakarta region. Natural Hazards, 73(2), 507-530.

Julien, P. Y., & Saghafian, B. (1991). CASC2D User's Manual. Civil Engineering Report, Department of Civil Engineering, Colorado State University, Fort Collins, CO 80523.

Kalcic, M., Crumpton, W., Liu, X., D'Ambrosio, J., Ward, A., & Witter, J. (2018). Assessment of beyond-the-field nutrient management practices for agricultural crop systems with subsurface drainage. Journal of Soil and Water Conservation, 73(1), 62-74.

Kamusoko, C., Aniya, M., Adi, B., & Manjoro, M. (2009). Rural sustainability under threat in Zimbabwe–simulation of future land use/cover changes in the Bindura district based on the Markov-cellular automata model. Applied Geography, 29(3), 435-447.

Kandel, D. D., Western, A. W., Grayson, R. B., & Turral, H. N. (2004). Process parameterization and temporal scaling in surface runoff and erosion modelling. Hydrological Processes, 18(8), 1423-1446.

Karlsen, S. R., Tolvanen, A., Kubin, E., Poikolainen, J., Høgda, K. A., Johansen, B., ... & Makarova, O. (2008). MODIS-NDVI-based mapping of the length of the growing season in northern Fennoscandia. International Journal of Applied Earth Observation and Geoinformation, 10(3), 253-266.

Karydas, C. G., Panagos, P., & Gitas, I. Z. (2014). A classification of water erosion models according to their geospatial characteristics. International Journal of Digital Earth, 7(3), 229-250.

Keesstra, S. D. (2007). Impact of natural reforestation on floodplain sedimentation in the Dragonja basin, SW Slovenia. Earth Surface Processes and Landforms: The Journal of the British Geomorphological Research Group, 32(1), 49-65.

Keesstra, S., Wittenberg, L., Maroulis, J., Sambalino, F., Malkinson, D., Cerdà, A., & Pereira, P. (2017). The influence of fire history, plant species and post-fire management on soil water repellency in a Mediterranean catchment: The Mount Carmel range, Israel. Catena, 149, 857-866.

Kessler, C. A., & Stroosnijder, L. (2006). Land degradation assessment by farmers in Bolivian mountain valleys. Land Degradation & Development, 17(3), 235-248.

Khalid, K., Ali, M. F., Rahman, N. F. A., Mispan, M. R., Haron, S. H., Othman, Z., & Bachok, M. F. (2016). Sensitivity Analysis in Watershed Model Using SUFI-2 Algorithm. Procedia Engineering, 162, 441-447.

Khoi, D. N., & Suetsugi, T. (2014). Impact of climate and land-use changes on hydrological processes and sediment yield—a case study of the Be River catchment, Vietnam. Hydrological Sciences Journal, 59(5), 1095-1108.

Kim, J., Choi, J., Choi, C., & Park, S. (2013). Impacts of changes in climate and land use/land cover under IPCC RCP scenarios on streamflow in the Hoeya River Basin, Korea. Science of the Total Environment, 452, 181-195.

Kim, N. W., & Lee, J. (2008). Temporally weighted average curve number method for daily runoff simulation. Hydrological Processes, 22(25), 4936-4948.

Kindt, J. W. (1986). International environmental law and policy: an overview of transboundary pollution. San Diego Law Review., 23, 583.

Kingston, D. G., & Taylor, R. G. (2010). Sources of uncertainty in climate change impacts on river discharge and groundwater in a headwater catchment of the Upper Nile Basin, Uganda. Hydrology and Earth System Sciences, 14(7), 1297-1308.

Kirkby, M. J. (1998). Across scales: the MEDALUS family of models. Modelling Soil Erosion by Water, Boardmand, J., and Favis-Mortlock, D. (Eds.). NATO ASI Series. Series I: Global Environmental Change 55, 161-174.

Kirkby, M. J., & Beven, K. J. (1979). A physically based, variable contributing area model of basin hydrology. Hydrological Sciences Journal, 24(1), 43-69.

Kirkby, M. J., Baird, A. J., Lockwood, J. G., McMahon, M. D., Mitchell, P. J., Shao, J., ... & Woodward, F. I. (1993). MEDALUS Project A1: Physically Based Soil Erosion Models for Process Modes: Final Report. (Part of MEDALUS I final report, Ed. by ThornesJ.B.).

Kirkby, M. J., Jones, R. J. A., Irvine, B., Gobin, A., Govers, G., Cerdan, O., … & Huting, J. (2004). Pan-European Soil Erosion Risk Assessment: The PESERA Map, Version 1 October 2003. Explanation of Special Publication Ispra 2004 No.73 (S.P.I.04.73). European Soil Bureau Research Report No.16, EUR 21176, 18pp. and 1 map in ISO B1 format. Office for Official Publications of the European Communities, Luxembourg.

Kirtland, D., DeCola, L., Gaydos, L., Acevedo, W., Clarke, K., & Bell, C. (1994). An analysis of human-induced land transformations in the San Francisco Bay/Sacramento area. World Resource Review; (United States), 6(CONF-940422--).

Kiunsi, R. B., & Meadows, M. E. (2006). Assessing land degradation in the Monduli District, northern Tanzania. Land Degradation & Development, 17(5), 509-525.

Knisel, W. G. (1980). CREAMS: A field-scale model for chemicals, runoff and erosion for agricultural management systems. US Department of Agriculture, Conservation Research Report 26.

Knisel, W. G., Davis, F. M., Leonard, R. A., & Nicks, A. D. (1993). GLEAMS version 2.10, Part III: user's manual. Conservation Research Rep., USDA, Washington, D.C.

Krysanova, V., Hattermann, F., & Habeck, A. (2005). Expected changes in water resources availability and water quality with respect to climate change in the Elbe River basin (Germany). Hydrology Research, 36(4-5), 321-333.

Krysanova, V., Müller-Wohlfeil, D. I., & Becker, A. (1998). Development and test of a spatially distributed hydrological/water quality model for mesoscale watersheds. Ecological Modelling, 106(2-3), 261-289.

Kuemmerle, T., Radeloff, V. C., Perzanowski, K., & Hostert, P. (2006). Cross-border comparison of land cover and landscape pattern in Eastern Europe using a hybrid classification technique. Remote Sensing of Environment, 103(4), 449-464.

Kukal, M., & Irmak, S. (2016). Long-term patterns of air temperatures, daily temperature range, precipitation, grass-reference evapotranspiration and aridity index in the USA Great Plains: Part II. Temporal trends. Journal of Hydrology, 542, 978-1001.

Kulkarni, A. V., & Karyakarte, Y. (2014). Observed changes in Himalayan glaciers. Current Science, 237-244.

Kumar, K. R., & Hingane, L. S. (1988). Long-term variations of surface air temperature at major industrial cities of India. Climatic Change, 13(3), 287-307.

Kumar, M., & Warsi, A. S. (1998). Role of Soil and Water Conservation Measures on Crop Yields and Ground Water Recharge in a Yamuna Ravine Watershed–A Field Experience. Indian Journal of Soil Conservation, 26(3), 264-268.

Kumar, N., Singh, S. K., Srivastava, P. K., & Narsimlu, B. (2017). SWAT Model calibration and uncertainty analysis for streamflow prediction of the Tons River Basin, India, using Sequential Uncertainty Fitting (SUFI-2) algorithm. Modeling Earth Systems and Environment, 3(1), 30.

Kumar, R., Singh, R. D., & Sharma, K. D. (2005). Water resources of India. Current Science, 794-811.

Kumar, S., Mishra, A., & Raghuwanshi, N. S. (2014). Identification of critical erosion watersheds for control management in data scarce condition using the SWAT model. Journal of Hydrologic Engineering, 20(6), C4014008.

Kumari, N., Chowdary, V. M., Waghaye, A. M., & Tiwari, K. N. (2016). Assessment of Surface Runoff and Sediment Yield using WEPP Model. Nature Environment and Pollution Technology, 15(2), 491.

Kundu, S., Khare, D., & Mondal, A. (2017a). Individual and combined impacts of future climate and land use changes on the water balance. Ecological Engineering, 105, 42-57.

Kundu, S., Khare, D., & Mondal, A. (2017b). Past, present and future land use changes and their impact on water balance. Journal of Environmental Management, 197, 582-596.

Kundzewicz, Z. W. (2002). Non-structural flood protection and sustainability. Water International, 27(1), 3-13.

Kushwaha, A., & Jain, M. K. (2013). Hydrological simulation in a forest dominated watershed in Himalayan region using SWAT model. Water Resources Management, 27(8), 3005-3023.

Kuznetsov, M. S., Gendugov, V. M., Khalilov, M. S., and Ivanuta, A. A. (1998). An equation of soil detachment by flow. Soil and Tillage Research, 46 (1), 97–102.

Laflen, J. M., Lane, L. J., & Foster, G. R. (1991). WEPP: A new generation of erosion prediction technology. Journal of Soil and Water Conservation, 46(1), 34-38.

Lake, P. S., Palmer, M. A., Biro, P., Cole, J., Covich, A. P., Dahm, C., Gibert, J., Goedkoop, W., Martens, K., & Verhoeven, J. (2000). Global Change and the Biodiversity of Freshwater Ecosystems: Impacts on Linkages between Above-Sediment and Sediment Biota: All forms of anthropogenic disturbance—changes in land use, biogeochemical processes, or biotic addition or loss—not only damage the biota of freshwater sediments but also disrupt the linkages between above-sediment and sediment-dwelling biota. AIBS Bulletin, 50(12), 1099-1107. DOI: 10.1641/0006-3568(2000)050[1099:GCATBO]2.0.CO;2

Lakshmanan, A., Geethalakshmi, V., Rajalakshmi, D., Bhuvaneswari, K., Srinivasan, R., Sridhar, G., ... & Annamalai, H. (2011). Climate change adaptation strategies in the Bhavani basin using the SWAT model. Applied Engineering in Agriculture, 27(6), 887-893.

Lal, M., Singh, K. K., Srinivasan, G., Rathore, L. S., Naidu, D., & Tripathi, C. N. (1999). Growth and yield responses of soybean in Madhya Pradesh, India to climate variability and change. Agricultural and Forest Meteorology, 93(1), 53-70.

Lal, R., & Pimentel, D. (2008). Soil erosion: a carbon sink or source?. Science, 319(5866), 1040-1042.

Lam, Q. D., Schmalz, B., & Fohrer, N. (2010). Modelling point and diffuse source pollution of nitrate in a rural lowland catchment using the SWAT model. Agricultural Water Management, 97(2), 317-325.

Lam, Q. D., Schmalz, B., & Fohrer, N. (2011). The impact of agricultural Best Management Practices on water quality in a North German lowland catchment. Environmental Monitoring and Assessment, 183(1-4), 351-379.

Lambin, E. F., Turner, B. L., Geist, H. J., Agbola, S. B., Angelsen, A., Bruce, J. W., ... & George, P. (2001). The causes of land-use and land-cover change: moving beyond the myths. Global Environmental Change, 11(4), 261-269.

Lampurlanés, J., Plaza-Bonilla, D., Álvaro-Fuentes, J., & Cantero-Martínez, C. (2016). Long-term analysis of soil water conservation and crop yield under different tillage systems in Mediterranean rainfed conditions. Field Crops Research, 189, 59-67.

Landis, J. D. (1994). The California urban futures model: a new generation of metropolitan simulation models. Environment and Planning B: Planning and Design, 21(4), 399-420.

Landis, J. D., Monzon, J. P., Reilly, M., & Cogan, C. (1998). Development and pilot application of the California urban and biodiversity analysis (CURBA) Model. (Berkeley, CA: Institute of Urban and Regional Development), Monograph, 1-98.

Landis, J. R., & Koch, G. G. (1977). The measurement of observer agreement for categorical data. Biometrics, 159-174.

Landis, J., & Zhang, M. (1998). The second generation of the California urban futures model. Part 1: Model logic and theory. Environment and Planning B: Planning and Design, 25(5), 657-666.

Lane, L. J. (1983). Chapter 19: Transmission Losses, Soil Conservation Service (SCS)–National Engineering Handbook, Section 4, Hydrology. U.S. Government Printing Office, Washington, DC, 19.

Lane, L. J., Nichols, M. H., Levick, L. R., & Kidwell, M. R. (2001). A simulation model for erosion and sediment yield at the hillslope scale. In Landscape Erosion and Evolution Modeling (pp. 201-237). Springer, Boston, MA.

Leavesley, G. H., Lichty, R. W., Troutman, B. M., & Saindon, L. G. (1983). Precipitation-runoff modeling system: User's manual (p. 207). Washington, DC: USGS, Water Resour. Invest. Rep. 83-4238.

Lee, M., Park, G., Park, M., Park, J., Lee, J., & Kim, S. (2010). Evaluation of non-point source pollution reduction by applying Best Management Practices using a SWAT model and QuickBird high resolution satellite imagery. Journal of Environmental Sciences, 22(6), 826-833.

Legates, D. R. & McCabe, G. J. (1999). Evaluating the use of goodness-of-fit measures in hydrologic and hydroclimatic model validation. Water Resources Research, 35(1): 233-241.

Lemann, T., Zeleke, G., Amsler, C., Giovanoli, L., Suter, H., & Roth, V. (2016). Modelling the effect of soil and water conservation on discharge and sediment yield in the upper Blue Nile basin, Ethiopia. Applied Geography, 73, 89-101.

Lemke, A. M., Kirkham, K. G., Lindenbaum, T. T., Herbert, M. E., Tear, T. H., Perry, W. L., & Herkert, J. R. (2011). Evaluating agricultural best management practices in tile-drained subwatersheds of the Mackinaw River, Illinois. Journal of Environmental Quality, 40(4), 1215-1228.

Leonard, R. A., Knisel, W. G., & Still, D. A. (1987). GLEAMS: Groundwater loading effects of agricultural management systems. Transactions of the ASAE, 30(5), 1403-1418.

Leta, O., El-Kadi, A., & Dulai, H. (2018). Impact of Climate Change on Daily Streamflow and Its Extreme Values in Pacific Island Watersheds. Sustainability, 10(6), 2057.

Li, X., & Gar-On Yeh, A. (2004). Data mining of cellular automata's transition rules. International Journal of Geographical Information Science, 18(8), 723-744.

Li, Y., Chen, B. M., Wang, Z. G., & Peng, S. L. (2011). Effects of temperature change on water discharge, and sediment and nutrient loading in the lower Pearl River basin based on SWAT modelling. Hydrological Sciences Journal, 56(1), 68-83.

Li, Z., Huffman, T., McConkey, B., & Townley-Smith, L. (2013). Monitoring and modeling spatial and temporal patterns of grassland dynamics using time-series MODIS NDVI with climate and stocking data. Remote Sensing of Environment, 138, 232-244.

Li, Z., Liu, W. Z., Zhang, X. C., & Zheng, F. L. (2009). Impacts of land use change and climate variability on hydrology in an agricultural catchment on the Loess Plateau of China. Journal of Hydrology, 377(1-2), 35-42.

Licciardello, F., Rossi, C. G., Srinivasan, R., Zimbone, S. M., & Barbagallo, S. (2011). Hydrologic evaluation of a Mediterranean watershed using the SWAT model with multiple PET estimation methods. Transactions of the ASABE, 54(5), 1615-1625.

Liebe, J., Van De Giesen, N., & Andreini, M. (2005). Estimation of small reservoir storage capacities in a semi-arid environment: A case study in the Upper East Region of Ghana. Physics and Chemistry of the Earth, Parts A/B/C, 30(6-7), 448-454.

Lindström, G., Pers, C., Rosberg, J., Strömqvist, J., & Arheimer, B. (2010). Development and testing of the HYPE (Hydrological Predictions for the Environment) water quality model for different spatial scales. Hydrology Research, 41(3), 295-319.

Littleboy, M., Silburn, D. M., Freebairn, D. M., Woodruff, D. R., Hammer, G. L., & Leslie, J. K. (1992). Impact of soil erosion on production in cropping systems. I. Development and validation of a simulation model. Australian Journal of Soil Research, 30(5), 757-774.

Liu, S., Yu, X., Li, Q., Li, H., & Lei, F. (2010). Land use change in loess hilly region based on CA-Markov model. Transactions of the Chinese Society of Agricultural Engineering, 26(11), 297-303.

Liu, X., Li, X., Shi, X., Wu, S., & Liu, T. (2008). Simulating complex urban development using kernel-based non-linear cellular automata. Ecological Modelling, 211(1), 169-181.

Lobell, D. B., Torney, A., & Field, C. B. (2011). Climate extremes in California agriculture. Climatic Change, 109(1), 355-363.

Lopes, V. L. (1987). A numerical model of watershed erosion and sediment yield. Dissertation of Doctoral Degree. University of Arizona, graduate college.

López, E., Bocco, G., Mendoza, M., & Duhau, E. (2001). Predicting land-cover and land-use change in the urban fringe: a case in Morelia city, Mexico. Landscape and Urban Planning, 55(4), 271-285.

López-Moreno, J. I., Vicente-Serrano, S. M., Beguería, S., García-Ruiz, J. M., Portela, M. M., & Almeida, A. B. (2009). Dam effects on droughts magnitude and duration in a transboundary basin: The Lower River Tagus, Spain and Portugal. Water Resources Research, 45(2), W02405, DOI: 10.1029/2008WR007198.

Lørup, J. K., Refsgaard, J. C., & Mazvimavi, D. (1998). Assessing the effect of land use change on catchment runoff by combined use of statistical tests and hydrological modelling: case studies from Zimbabwe. Journal of Hydrology, 205(3-4), 147-163.

Luo, Y., He, C., Sophocleous, M., Yin, Z., Hongrui, R., & Ouyang, Z. (2008). Assessment of crop growth and soil water modules in SWAT2000 using extensive field experiment data in an irrigation district of the Yellow River Basin. Journal of Hydrology, 352(1-2), 139-156.

MacPhail, D. D., & Campbell, L. F. (1970). The El-Paso (Texas-New Mexico) study area: A comprehensive analysis of Gemini 4 and Apollo 6 and 9 space photography. AAG commission on Graphic Applications of Remote Sensing, East Tennessee State Univeristy, Johnson City.

Maharjan, G. R., Park, Y. S., Kim, N. W., Shin, D. S., Choi, J. W., Hyun, G. W., ... & Lim, K. J. (2013). Evaluation of SWAT sub-daily runoff estimation at small agricultural watershed in Korea. Frontiers of Environmental Science & Engineering, 7(1), 109-119.

Maharjan, G. R., Ruidisch, M., Shope, C. L., Choi, K., Huwe, B., Kim, S. J., ... & Arnhold, S. (2016). Assessing the effectiveness of split fertilization and cover crop cultivation in order to conserve soil and water resources and improve crop productivity. Agricultural Water Management, 163, 305-318.

Mahyou, H., Tychon, B., Balaghi, R., Louhaichi, M., & Mimouni, J. (2016). A Knowledge-Based Approach for Mapping Land Degradation in the Arid Rangelands of North Africa. Land Degradation & Development, 27(6), 1574-1585.

Maina, J., De Moel, H., Zinke, J., Madin, J., McClanahan, T., & Vermaat, J. E. (2013). Human deforestation outweighs future climate change impacts of sedimentation on coral reefs. Nature Communications, 4, 1986.

Makalle, A. M., Obando, J., & Bamutaze, Y. (2008). Effects of land use practices on livelihoods in the transboundary sub-catchments of the Lake Victoria Basin. African Journal of Environmental Science and Technology, 2(10), 309-317.

Malagó, A., Bouraoui, F., Vigiak, O., Grizzetti, B., & Pastori, M. (2017). Modelling water and nutrient fluxes in the Danube River Basin with SWAT. Science of the Total Environment, 603, 196-218.

Malekian, A., & Azarnivand, A. (2016). Application of integrated Shannon's entropy and VIKOR techniques in prioritization of flood risk in the Shemshak watershed, Iran. Water Resources Management, 30(1), 409-425.

Malila, W. A. (1980, January). Change vector analysis: an approach for detecting forest changes with Landsat. In LARS symposia (p. 385).

Mall, R. K., Gupta, A., Singh, R., Singh, R. S., & Rathore, L. S. (2006). Water resources and climate change: An Indian perspective. Current Science, 1610-1626.

Mango, L. M., Melesse, A. M., McClain, M. E., Gann, D., & Setegn, S. G. (2011). Land use and climate change impacts on the hydrology of the upper Mara River Basin, Kenya: results of a modeling study to support better resource management. Hydrology and Earth System Sciences, 15(7), 2245-2258.

Mas, J. F. (1999). Monitoring land-cover changes: a comparison of change detection techniques. International Journal of Remote Sensing, 20(1), 139-152.

Mati, B. M., Mutie, S., Gadain, H., Home, P., & Mtalo, F. (2008). Impacts of land-use/cover changes on the hydrology of the transboundary Mara River, Kenya/Tanzania. Lakes & Reservoirs: Research & Management, 13(2), 169-177.

Matsuno, Y., Giardano, M., & Barker, R. (2007). Transfer of water from irrigation to other uses: lessons from case studies. Paddy and Water Environment, 5(4), 211-211.

Matsuno, Y., Horino, H., & Hatcho, N. (2013). On-farm irrigation development and management in lower Myanmar: factors for sustainable rice production and collective action. Paddy and Water Environment, 11(1-4), 455-462.

Mauget, S. A., Adhikari, P., Leiker, G., Baumhardt, R. L., Thorp, K. R., & Ale, S. (2017). Modeling the effects of management and elevation on West Texas dryland cotton production. Agricultural and Forest Meteorology, 247, 385-398.

McDonough, K., Moore, T., & Hutchinson, S. L. (2017). Understanding the relationship between stormwater control measures and ecosystem services in an urban watershed. Journal of Water Resources Planning and Management, 143(5), 04017008.

McFeeters, S. K. (1996). The use of the Normalized Difference Water Index (NDWI) in the delineation of open water features. International Journal of Remote Sensing, 17(7), 1425-1432.

Meghdadi, A. R. (2013). Identification of effective best management practices in sediment yield diminution using GeoWEPP: the Kasilian watershed case study. Environmental Monitoring and Assessment, 185(12), 9803-9817.

Mehrotra, D., & Mehrotra, R. (1995). Climate change and hydrology with emphasis on the Indian subcontinent. Hydrological Sciences Journal, 40(2), 231-242.

Melching, C. S., & Wenzel, H. G. (1985). Calibration Procedure and Improvement in MULTSED. Civil Engineering Studies, Hydraulic Engineering Series No. 38. University of Illinois.

Memarian, H., Balasundram, S. K., Abbaspour, K. C., Talib, J. B., Boon Sung, C. T., & Sood, A. M. (2014). SWAT-based hydrological modelling of tropical land-use scenarios. Hydrological Sciences Journal, 59(10), 1808-1829.

Mertens, B., & Lambin, E. F. (1997). Spatial modelling of deforestation in southern Cameroon: spatial disaggregation of diverse deforestation processes. Applied Geography, 17(2), 143-162.

Mialhe, F., Gunnell, Y., & Mering, C. (2008). Synoptic assessment of water resource variability in reservoirs by remote sensing: General approach and application to the runoff harvesting systems of south India. Water Resources Research, 44(5), W05411, 1-14.

Miao, C., Ni, J., & Borthwick, A. G. (2010). Recent changes of water discharge and sediment load in the Yellow River basin, China. Progress in Physical Geography, 34(4), 541-561.

MIKE 11. (1995). A computer based modeling system for rivers and channels: Reference manual. DHI Water and Environment.

Milesi, C., Samanta, A., Hashimoto, H., Kumar, K. K., Ganguly, S., Thenkabail, P. S., ... & Myneni, R. B. (2010). Decadal variations in NDVI and food production in India. Remote Sensing, 2(3), 758-776.

Miller, J. D., Immerzeel, W. W., & Rees, G. (2012). Climate change impacts on glacier hydrology and river discharge in the Hindu Kush–Himalayas: a synthesis of the scientific basis. Mountain Research and Development, 32(4), 461-467.

Miller, S. N., Semmens, D. J., Goodrich, D. C., Hernandez, M., Miller, R. C., Kepner, W. G., & Guertin, D. P. (2007). The automated geospatial watershed assessment tool. Environmental Modelling & Software, 22(3), 365-377.

Millington, A. C. (1986). Reconnaissance scale soil erosion mapping using a simple geographic information system in the humid tropics. Land evaluation for land-use planning and conservation in sloping areas, Siderius, W. ed. ILRI; 64-81.

Minns, A. W., & Hall, M. J. (1996). Artificial neural networks as rainfall-runoff models. Hydrological Sciences Journal, 41(3), 399-417.

Mishra, A., Froebrich, J., & Gassman, P. W. (2007a). Evaluation of the SWAT model for assessing sediment control structures in a small watershed in India. Transactions of the ASABE, 50(2), 469-477.

Mishra, A., Kar, S., & Singh, V. P. (2007b). Prioritizing structural management by quantifying the effect of land use and land cover on watershed runoff and sediment yield. Water Resources Management, 21(11), 1899-1913.

Misra, R. K., & Rose, C. W. (1996). Application and sensitivity analysis of process-based erosion model GUEST. European Journal of Soil Science, 47(4), 593-604.

Mitsova, D., Shuster, W., & Wang, X. (2011). A cellular automata model of land cover change to integrate urban growth with open space conservation. Landscape and Urban Planning, 99(2), 141-153.

Molina-Navarro, E., Andersen, H. E., Nielsen, A., Thodsen, H., & Trolle, D. (2018). Quantifying the combined effects of land use and climate changes on stream flow and nutrient loads: A modelling approach in the Odense Fjord catchment (Denmark). Science of the Total Environment, 621, 253-264.

Mondal, P., & Southworth, J. (2010). Evaluation of conservation interventions using a cellular automata-Markov model. Forest Ecology and Management,260(10), 1716-1725.

Monteith, J.L. (1965). Evaporation and the environment. p. 205-234. In The state and movement of water in living organisms. 19th Symposia of the Society for Experimental Biology. Cambridge Univ. Press, London, U.K.

Moore, I. D., & Grayson, R. B. (1991). Terrain-based catchment partitioning and runoff prediction using vector elevation data. Water Resources Research, 27(6), 1177-1191. Refsgaard, J. C. (1987, August). A methodology for distinguishing between the effects of human influence and climate variability on the hydrologic cycle. In Proceedings of the Vancouver Symposium 'The Influence of Climate Change Variability on the Hydrologic Regime and Water Resources (pp. 557-570).

Morán-Tejeda, E., Ceballos-Barbancho, A., & Llorente-Pinto, J. M. (2010). Hydrological response of Mediterranean headwaters to climate oscillations and land-cover changes: The mountains of Duero River basin (Central Spain). Global and Planetary Change, 72(1-2), 39-49.

Morgan, R. P. C., Quinton, J. N., & Rickson, R. J. (1993). EUROSEM: A user guide. Silsoe College, Cranfield University, UK, 83.

Moriasi, D. N., Arnold, J. G., Van Liew, M. W., Bingner, R. L., Harmel, R. D., & Veith, T. L. (2007). Model evaluation guidelines for systematic quantification of accuracy in watershed simulations. Transactions of the ASABE, 50(3), 885-900.

Moriasi, D. N., Gowda, P. H., Arnold, J. G., Mulla, D. J., Ale, S., & Steiner, J. L. (2013). Modeling the impact of nitrogen fertilizer application and tile drain configuration on nitrate leaching using SWAT. Agricultural Water Management, 130, 36-43.

Mtibaa, S., Hotta, N., & Irie, M. (2018). Analysis of the efficacy and cost-effectiveness of best management practices for controlling sediment yield: A case study of the Joumine watershed, Tunisia. Science of the Total Environment, 616, 1-16.

Mummey, D. L., Smith, J. L., & Bluhm, G. (1998). Assessment of alternative soil management practices on N2O emissions from US agriculture. Agriculture, Ecosystems & Environment, 70(1), 79-87.

Muñoz-Rojas, M., Erickson, T. E., Martini, D. C., Dixon, K. W., & Merritt, D. J. (2016). Climate and soil factors influencing seedling recruitment of plant species used for dryland restoration. Soil, 2(2), 287-298.

Muro, M., & Jeffrey, P. (2008). A critical review of the theory and application of social learning in participatory natural resource management processes. Journal of Environmental Planning and Management, 51(3), 325-344.

Murty, P. S., Pandey, A., & Suryavanshi, S. (2014). Application of semi-distributed hydrological model for basin level water balance of the Ken basin of Central India. Hydrological Processes, 28(13), 4119-4129.

Mutiibwa, D., Kilic, A., & Irmak, S. (2014). The Effect of Land Cover/Land Use Changes on the Regional Climate of the USA High Plains. Climate, 2(3), 153-167.

Myint, S. W., & Wang, L. (2006). Multicriteria decision approach for land use land cover change using Markov chain analysis and a cellular automata approach. Canadian Journal of Remote Sensing, 32(6), 390-404.

Naik, M. G., Rao, E. P., & Eldho, T. I. (2009). Finite element method and GIS based distributed model for soil erosion and sediment yield in a watershed. Water Resources Management, 23(3), 553-579.

Napoli, M., Massetti, L., & Orlandini, S. (2017). Hydrological response to land use and climate changes in a rural hilly basin in Italy. Catena, 157, 1-11.

Narasimhan, B., Allen, P. M., Coffman, S. V., Arnold, J. G., & Srinivasan, R. (2017). Development and Testing of a Physically Based Model of Streambank Erosion for Coupling with a Basin-Scale Hydrologic Model SWAT. JAWRA Journal of the American Water Resources Association, 53(2), 344-364.

Narsimlu, B., Gosain, A. K., & Chahar, B. R. (2013). Assessment of future climate change impacts on water resources of upper sind river basin, India using SWAT model. Water Resources Management, 27(10), 3647-3662.

Nash, J. E., & Sutcliffe, J. V. (1970). River flow forecasting through conceptual models part I—A discussion of principles. Journal of Hydrology, 10(3), 282-290.

Ndomba, P., Mtalo, F., & Killingtveit, A. (2008). SWAT model application in a data scarce tropical complex catchment in Tanzania. Physics and Chemistry of the Earth, Parts A/B/C, 33(8-13), 626-632.

Nearing, M. A., Wei, H., Stone, J. J., Pierson, F. B., Spaeth, K. E., Weltz, M. A., ... & Hernandez, M. (2011). A rangeland hydrology and erosion model. Transactions of the ASABE, 54(3), 901-908.

Neitsch, S. L., Arnold, J. G., Kiniry, J. R., & Williams, J. R. (2011). Soil and water assessment tool theoretical documentation version 2009. Texas Water Resources Institute Technical Report No. 406, Texas Aand M University System, College Station, Texas.

Neitsch, S. L., Arnold, J. G., Kiniry, J. R., Srinivasan, R., & Williams, J. R. (2004). Soil and water assessment tool input/output file documentation, version 2005: Temple, TX. US Department of Agriculture, Agricultural Research Service, Grassland, Soil and Water Research Laboratory, available online at: ftp://ftp. brc. tamus. edu. pub/outgoing/sammons/swat2005 (accessed 11/28/06).

Neitsch, S. L., Arnold, J. G., Kiniry, J. R., Williams, J. R., & King, K. W. (2005). Soil and water assessment tool theoretical documentation. Grassland. Soil and Water Research Laboratory, Temple, TX.

Nelson, E., Mendoza, G., Regetz, J., Polasky, S., Tallis, H., Cameron, D., Chan, K.M.A., Daily, G.C., Goldstein, J., Kareiva, P.M., Lonsdorf, E., Naidoo, R., Ricketts, T.H. & Shaw, M. (2009). Modeling multiple ecosystem services, biodiversity conservation, commodity production, and tradeoffs at landscape scales. Frontiers in Ecology and the Environment, 7(1), 4-11.

Nelson, R. F. (1983). Detecting forest canopy change due to insect activity using Landsat MSS. Photogrammetric Engineering and Remote Sensing, 49(9), 1303-1314.

Nepal, S., & Shrestha, A. B. (2015). Impact of climate change on the hydrological regime of the Indus, Ganges and Brahmaputra river basins: a review of the literature. International Journal of Water Resources Development, 31(2), 201-218.

Newham, L. T., Letcher, R. A., Jakeman, A. J., & Kobayashi, T. (2004). A framework for integrated hydrologic, sediment and nutrient export modelling for catchment-scale management. Environmental Modelling & Software, 19(11), 1029-1038.

Niehoff, D., Fritsch, U., & Bronstert, A. (2002). Land-use impacts on storm-runoff generation: scenarios of land-use change and simulation of hydrological response in a meso-scale catchment in SW-Germany. Journal of Hydrology, 267(1-2), 80-93.

Niraula, R., Kalin, L., Srivastava, P., & Anderson, C. J. (2013). Identifying critical source areas of nonpoint source pollution with SWAT and GWLF. Ecological Modelling, 268, 123-133.

Niraula, R., Kalin, L., Wang, R., & Srivastava, P. (2011). Determining nutrient and sediment critical source areas with SWAT: effect of lumped calibration. Transactions of the ASABE, 55(1), 137-147.

Niu, J., & Sivakumar, B. (2014). Study of runoff response to land use change in the East River basin in South China. Stochastic Environmental Research and Risk Assessment, 28(4), 857-865.

Noor, H., Fazli, S., Rostami, M., & Kalat, A. B. (2017). Cost-effectiveness analysis of different watershed management scenarios developed by simulation–optimization model. Water Science and Technology: Water Supply, 17(5), 1316-1324.

Nunes, J. P., Vieira, G. N., & Seixas, J. (2005). MEFIDIS–A physicallybased, spatially-distributed runoff and erosion model for extreme rainfall events. Watershed Models. CRC press, Boca Raton, 291-314.

NWDA (1993). Technical study No. 70, Water Balance Study of lower Betwa Sub basin of Betwa Basin, National Water Development Agency, Government of India, pp 156.

O'Callaghan, J. R. (1995). NELUP: An Introduction. Journal of Environmental Planning and Management, 38 (1), 5-19.

Oglethorpe, D. R. (1995). Farm-level economic modelling within a river catchment decision support system. Journal of Environmental Planning and Management, 38(1), 93-106.

Omani, N., Srinivasan, R., Smith, P. K., & Karthikeyan, R. (2017). Glacier mass balance simulation using SWAT distributed snow algorithm. Hydrological Sciences Journal, 62(4), 546-560.

Omuto, C. T., Balint, Z., & Alim, M. S. (2014). A framework for national assessment of land degradation in the drylands: a case study of Somalia. Land Degradation & Development, 25(2), 105-119.

Ouedraogo, I., Barron, J., Tumbo, S. D., & Kahimba, F. C. (2015). Land cover transition in northern Tanzania. Land Degradation & Development, 27(3), 682-692.

Oxley, T., McIntosh, B. S., Winder, N., Mulligan, M., & Engelen, G. (2004). Integrated modelling and decision-support tools: a Mediterranean example. Environmental Modelling & Software, 19(11), 999-1010.

Paegelow, M., & Olmedo, M. T. C. (2005). Possibilities and limits of prospective GIS land cover modelling—a compared case study: Garrotxes (France) and Alta Alpujarra Granadina (Spain). International Journal of Geographical Information Science, 19(6), 697-722.

Palmate, S. S., Pandey, A., & Mishra, S. K. (2017). Modelling spatiotemporal land dynamics for a trans-boundary river basin using integrated cellular automata and markov chain approach. Applied Geography, 82, 11-23.

Pandey, A., & Palmate, S. S. (2018). Assessments of spatial land cover dynamic hotspots employing MODIS time-series datasets in the Ken River Basin of Central India. Arabian Journal of Geosciences, 11(17), 479.

Pandey, A., Chaube, U. C., Mishra, S. K., & Kumar, D. (2016a). Assessment of reservoir sedimentation using remote sensing and recommendations for desilting Patratu Reservoir, India. Hydrological Sciences Journal, 61(4), 711-718.

Pandey, A., Chowdary, V. M., & Mal, B. C. (2007). Identification of critical erosion prone areas in the small agricultural watershed using USLE, GIS and remote sensing. Water Resources Management, 21(4), 729-746.

Pandey, A., Chowdary, V. M., Mal, B. C., & Billib, M. (2009a). Application of the WEPP model for prioritization and evaluation of best management practices in an Indian watershed. Hydrological Processes, 23(21), 2997-3005.

Pandey, A., Chowdary, V. M., Mal, B. C., & Dabral, P. P. (2011). Remote sensing and GIS for identification of suitable sites for soil and water conservation structures. Land Degradation & Development, 22(3), 359-372.

Pandey, A., Himanshu, S. K., Mishra, S. K., & Singh, V. P. (2016b). Physically based soil erosion and sediment yield models revisited. Catena, 147, 595-620.

Pandey, A., Lalrempuia, D., & Jain, S. K. (2015). Assessment of hydropower potential using spatial technology and SWAT modelling in the Mat River, southern Mizoram, India. Hydrological Sciences Journal, 60(10), 1651-1665.

Pandey, R. P., Mishra, S. K., Singh, R., & Ramasastri, K. S. (2008). Streamflow drought severity analysis of Betwa river system (INDIA). Water Resources Management, 22(8), 1127-1141.

Pandey, V. K., Panda, S. N., & Sudhakar, S. (2005). Modelling of an agricultural watershed using remote sensing and a geographic information system. Biosystems Engineering, 90(3), 331-347.

Pandey, V. K., Panda, S. N., Pandey, A., & Sudhakar, S. (2009b). Evaluation of effective management plan for an agricultural watershed using AVSWAT model, remote sensing and GIS. Environmental Geology, 56(5), 993-1008.

Park, J. Y., Ale, S., Teague, W. R., & Dowhower, S. L. (2017). Simulating hydrologic responses to alternate grazing management practices at the ranch and watershed scales. Journal of Soil and Water Conservation, 72(2), 102-121.

Park, J. Y., Park, M. J., Ahn, S. R., Park, G. A., Yi, J. E., Kim, G. S., ... & Kim, S. J. (2011). Assessment of future climate change impacts on water quantity and quality for a mountainous dam watershed using SWAT. Transactions of the ASABE, 54(5), 1725-1737.

Payan, J. L., Perrin, C., Andréassian, V., & Michel, C. (2008). How can man-made water reservoirs be accounted for in a lumped rainfall-runoff model?. Water Resources Research, 44(3), DOI: 10.1029/2007WR005971.

Peel, M. C., & Blöschl, G. (2011). Hydrological modelling in a changing world. Progress in Physical Geography, 35(2), 249-261.

Pender, J., Nkonya, E., Jagger, P., Sserunkuuma, D., & Ssali, H. (2004). Strategies to increase agricultural productivity and reduce land degradation: evidence from Uganda. Agricultural Economics, 31(2-3), 181-195.

Pereira, P., Cerdà, A., Lopez, A. J., Zavala, L. M., Mataix-Solera, J., Arcenegui, V., ... & Novara, A. (2016). Short-term vegetation recovery after a grassland fire in Lithuania: The effects of fire severity, slope position and aspect. Land Degradation & Development, 27(5), 1523-1534.

Perrin, C., Michel, C., & Andréassian, V. (2001). Does a large number of parameters enhance model performance? Comparative assessment of common catchment model structures on 429 catchments. Journal of Hydrology, 242(3-4), 275-301.

Pervez, M. S., & Henebry, G. M. (2015). Assessing the impacts of climate and land use and land cover change on the freshwater availability in the Brahmaputra River basin. Journal of Hydrology: Regional Studies, 3, 285-311.

Petit, C. C., & Lambin, E. F. (2002). Long-term land-cover changes in the Belgian Ardennes (1775–1929): model-based reconstruction vs. historical maps. Global Change Biology, 8(7), 616-630.

Phan, D. B., Wu, C. C., & Hsieh, S. C. (2011). Impact of climate change on stream discharge and sediment yield in Northern Viet Nam. Water Resources, 38(6), 827-836.

Phomcha, P., Wirojanagud, P., Vangpaisal, T., & Thaveevouthti, T. (2012). Modeling the impacts of alternative soil conservation practices for an agricultural watershed with the SWAT model. Procedia Engineering, 32, 1205-1213.

Piao, S., Wang, X., Ciais, P., Zhu, B., Wang, T. A. O., & Liu, J. I. E. (2011). Changes in satellite-derived vegetation growth trend in temperate and boreal Eurasia from 1982 to 2006. Global Change Biology, 17(10), 3228-3239.

Pilgrim, D. H., Chapman, T. G., & Doran, D. G. (1988). Problems of rainfall-runoff modelling in arid and semiarid regions. Hydrological Sciences Journal, 33(4), 379-400.

Piman, T., Cochrane, T. A., Arias, M. E., Green, A., & Dat, N. D. (2012). Assessment of flow changes from hydropower development and operations in Sekong, Sesan, and Srepok rivers of the Mekong basin. Journal of Water Resources Planning and Management, 139(6), 723-732.

Ponce, R. D., Fernández, F., Stehr, A., Vásquez-Lavín, F., & Godoy-Faúndez, A. (2017). Distributional impacts of climate change on basin communities: an integrated modeling approach. Regional Environmental Change, 17(6), 1811-1821.

Prabhanjan, A., Rao, E. P., & Eldho, T. I. (2014). Application of SWAT model and geospatial techniques for sediment-yield modeling in ungauged watersheds. Journal of Hydrologic Engineering, 20(6), C6014005.

Prasanchum, H., & Kangrang, A. (2018). Optimal reservoir rule curves under climatic and land use changes for Lampao Dam using Genetic Algorithm. KSCE Journal of Civil Engineering, 22(1), 351-364.

Priestley, C. H. B., & Taylor, R. J. (1972). On the assessment of surface heat flux and evaporation using large-scale parameters. Monthly Weather Review, 100(2), 81-92.

Qiu, B., & Chen, C. (2008). Land use change simulation model based on MCDM and CA and its application. Acta Geographica Sinica-Chinese Edition, 63(2), 165.

Qiu, L. J., Zheng, F. L., & Yin, R. S. (2012). SWAT-based runoff and sediment simulation in a small watershed, the loessial hilly-gullied region of China: capabilities and challenges. International Journal of Sediment Research, 27(2), 226-234.

Quamar, M. F., & Chauhan, M. S. (2014). Signals of Medieval Warm Period and Little Ice Age from southwestern Madhya Pradesh (India): a pollen-inferred late-Holocene vegetation and climate change. Quaternary International, 325, 74-82.

Rahman, K., Etienne, C., Gago-Silva, A., Maringanti, C., Beniston, M., & Lehmann, A. (2014). Streamflow response to regional climate model output in the mountainous watershed: a case study from the Swiss Alps. Environmental Earth Sciences, 72(11), 4357-4369.

Rahman, K., Maringanti, C., Beniston, M., Widmer, F., Abbaspour, K., & Lehmann, A. (2013). Streamflow modeling in a highly managed mountainous glacier watershed using SWAT: the Upper Rhone River watershed case in Switzerland. Water Resources Management, 27(2), 323-339.

Rahmati, O., Haghizadeh, A., & Stefanidis, S. (2016). Assessing the accuracy of GIS-based analytical hierarchy process for watershed prioritization; Gorganrood River Basin, Iran. Water Resources Management, 30(3), 1131-1150.

Raneesh, K. Y., & Thampi Santosh, G. (2011). A study on the impact of climate change on streamflow at the watershed scale in the humid tropics. Hydrological Sciences Journal, 56(6), 946-965.

Records, R. M., Arabi, M., Fassnacht, S. R., Duffy, W. G., Ahmadi, M., & Hegewisch, K. C. (2014). Climate change and wetland loss impacts on a western river's water quality. Hydrology and Earth System Sciences, 18(11), 4509-4527.

Reddy, K. S., Kumar, M., Maruthi, V., Lakshminarayana, P., Vijayalakshmi, B., & Reddy, Y. V. K. (2016). Climate change impacts on crop water balance of maize (Zea mays L.) in lower Krishna River Basin of South India. Current Science, 111(3), 565.

Refsgaard, C. J. (1995). MIKE SHE. Computer models of catchment hydrology, 809-846.

Refsgaard, J. C., Seth, S. M., Bathurst, J. C., Erlich, M., Storm, B., & Chandra, S. (1992). Application of the SHE to catchments in India Part 1. General results. Journal of Hydrology, 140(1-4), 1-23.

Revadekar, J. V., Kothawale, D. R., Patwardhan, S. K., Pant, G. B., & Kumar, K. R. (2012). About the observed and future changes in temperature extremes over India. Natural Hazards, 60(3), 1133-1155.

Rocha, J., Roebeling, P., & Rial-Rivas, M. E. (2015). Assessing the impacts of sustainable agricultural practices for water quality improvements in the Vouga catchment (Portugal) using the SWAT model. Science of the Total Environment, 536, 48-58.

Rosenthal, W. D., Srinivasan, R., & Arnold, J. G. (1995). Alternative river management using a linked GIS-hydrology model. Transactions of the ASAE, 38(3), 783-790.

Routschek, A., Schmidt, J., & Kreienkamp, F. (2014). Impact of climate change on soil erosion—a high-resolution projection on catchment scale until 2100 in Saxony/Germany. Catena, 121, 99-109.

Roxy, M. K., Modi, A., Murtugudde, R., Valsala, V., Panickal, S., Prasanna Kumar, S., Ravichandran, M., Vichi, M., & Lévy, M. (2016). A reduction in marine primary productivity driven by rapid warming over the tropical Indian Ocean. Geophysical Research Letters, 43(2), 826-833.

Roy, P. S., & Tomar, S. (2001). Landscape cover dynamics pattern in Meghalaya. International Journal of Remote Sensing, 22(18), 3813-3825.

Roy, P. S., Giriraj, A., Agarwal, C., Green, G. M., Grove, J. M., Evans, T. P., ... & Britto, S. J. (2001). The development of a land cover change model for Southern Senegal. Journal of Applied Sciences, 8(8), 2903-2908.

Rumsby, B. T., & Macklin, M. G. (1994). Channel and floodplain response to recent abrupt climate change: the Tyne basin, northern England. Earth Surface Processes and Landforms, 19(6), 499-515.

Russell, J. M., & Ward, D. (2016). Historical Land-use and Vegetation Change in Northern Kwazulu-Natal, South Africa. Land Degradation & Development, 27(7), 1691-1699.

Sabbaghian, R. J., Zarghami, M., Nejadhashemi, A. P., Sharifi, M. B., Herman, M. R., & Daneshvar, F. (2016). Application of risk-based multiple criteria decision analysis for selection of the best agricultural scenario for effective watershed management. Journal of Environmental Management, 168, 260-272.

Sang, L., Zhang, C., Yang, J., Zhu, D., & Yun, W. (2011). Simulation of land use spatial pattern of towns and villages based on CA–Markov model. Mathematical and Computer Modelling, 54(3), 938-943.

Santé, I., García, A. M., Miranda, D., & Crecente, R. (2010). Cellular automata models for the simulation of real-world urban processes: A review and analysis. Landscape and Urban Planning, 96(2), 108-122.

Santhi, C., Srinivasan, R., Arnold, J. G., & Williams, J. R. (2006). A modeling approach to evaluate the impacts of water quality management plans implemented in a watershed in Texas. Environmental Modelling & Software, 21(8), 1141-1157.

Santos, R. M. B., Fernandes, L. S., Moura, J. P., Pereira, M. G., & Pacheco, F. A. L. (2014). The impact of climate change, human interference, scale and modeling uncertainties on the estimation of aquifer properties and river flow components. Journal of Hydrology, 519, 1297-1314.

Sardar, B., Singh, A. K., Raghuwanshi, N. S., & Chatterjee, C. (2012). Hydrological modeling to identify and manage critical erosion-prone areas for improving reservoir life: Case study of Barakar basin. Journal of Hydrologic Engineering, 19(1), 196-204.

Savitzky, A., & Golay, M. J. (1964). Smoothing and differentiation of data by simplified least squares procedures. Analytical Chemistry, 36(8), 1627-1639.

Schilling, K. E., Jha, M. K., Zhang, Y. K., Gassman, P. W., & Wolter, C. F. (2008). Impact of land use and land cover change on the water balance of a large agricultural watershed: Historical effects and future directions. Water Resources Research, 44(7).

Schmidt, J. (1991). A mathematical model to simulate rainfall erosion. Catena Supplement, 19(9), 101-109.

Schulze, R. E. (2000). Modelling hydrological responses to land use and climate change: a southern African perspective. AMBIO: A Journal of the Human Environment, 29(1), 12-22.

Schumann, A. H. (1993). Development of conceptual semi-distributed hydrological models and estimation of their parameters with the aid of GIS. Hydrological Sciences Journal, 38(6), 519-528.

Schuol, J., Abbaspour, K. C., Srinivasan, R., & Yang, H. (2008). Estimation of freshwater availability in the West African sub-continent using the SWAT hydrologic model. Journal of Hydrology, 352(1-2), 30-49.

Semadeni-Davies, A., Hernebring, C., Svensson, G., & Gustafsson, L. G. (2008). The impacts of climate change and urbanisation on drainage in Helsingborg, Sweden: Combined sewer system. Journal of Hydrology, 350(1-2), 100-113.

Seo, M., Jaber, F., Srinivasan, R., & Jeong, J. (2017). Evaluating the impact of Low Impact Development (LID) practices on water quantity and quality under different development designs using SWAT. Water, 9(3), 193.

Setegn, S. G., Rayner, D., Melesse, A. M., Dargahi, B., & Srinivasan, R. (2011). Impact of climate change on the hydroclimatology of Lake Tana Basin, Ethiopia. Water Resources Research, 47(4).

Setyorini, A., Khare, D., & Pingale, S. M. (2017). Simulating the impact of land use/land cover change and climate variability on watershed hydrology in the Upper Brantas basin, Indonesia. Applied Geomatics, 9(3), 191-204.

Shah, S. K., Bhattacharyya, A., & Chaudhary, V. (2007). Reconstruction of June–September precipitation based on tree-ring data of teak (Tectona grandis L.) from Hoshangabad, Madhya Pradesh, India. Dendrochronologia, 25(1), 57-64.

Sharmila, S., Joseph, S., Sahai, A. K., Abhilash, S., & Chattopadhyay, R. (2015). Future projection of Indian summer monsoon variability under climate change scenario: An assessment from CMIP5 climate models. Global and Planetary Change, 124, 62-78.

Shaw, S. B., Marrs, J., Bhattarai, N., & Quackenbush, L. (2014). Longitudinal study of the impacts of land cover change on hydrologic response in four mesoscale watersheds in New York State, USA. Journal of Hydrology, 519, 12-22.

Shen, W., Reynolds, J. F., & Hui, D. (2009). Responses of dryland soil respiration and soil carbon pool size to abrupt vs. gradual and individual vs. combined changes in soil temperature, precipitation, and atmospheric [CO2]: a simulation analysis. Global Change Biology, 15(9), 2274-2294.

Shrestha, B., Babel, M. S., Maskey, S., Griensven, A. V., Uhlenbrook, S., Green, A., & Akkharath, I. (2013). Impact of climate change on sediment yield in the Mekong River basin: a case study of the Nam Ou basin, Lao PDR. Hydrology and Earth System Sciences, 17(1), 1-20.

Shrestha, S., Shrestha, M., & Babel, M. S. (2016). Modelling the potential impacts of climate change on hydrology and water resources in the Indrawati River Basin, Nepal. Environmental Earth Sciences, 75(4), 280.

Simons, M., Podger, G., & Cooke, R. (1996). IQQM—a hydrologic modelling tool for water resource and salinity management. Environmental Software, 11(1-3), 185-192.

Singh, A. (1986). Change detection in the tropical forest environment of northeastern India using Landsat. Remote Sensing and Tropical Land Management, 237-254.

Singh, A., & Gosain, A. K. (2004). Resolving conflicts over transboundary watercourses: An Indian perspective. Land Use Water Resources Research, 4, 2-1.

Singh, D., Tsiang, M., Rajaratnam, B., & Diffenbaugh, N. S. (2014). Observed changes in extreme wet and dry spells during the South Asian summer monsoon season. Nature Climate Change, 4(6), 456.

Singh, G., Babu, R., Narain, P., Bhushan, L. S., & Abrol, I. P. (1992). Soil erosion rates in India. Journal of Soil and Water Conservation, 47(1), 97-99.

Singh, J., Knapp, H. V., Arnold, J. G., & Demissie, M. (2005). Hydrological modeling of the Iroquois River watershed using HSPF and SWAT. Journal of the American Water Resources Association, 41(2), 343-360.

Singh, N., & Ranade, A. (2010). The wet and dry spells across India during 1951–2007. Journal of Hydrometeorology, 11(1), 26-45.

Singh, R., Garg, K. K., Wani, S. P., Tewari, R. K., & Dhyani, S. K. (2014a). Impact of water management interventions on hydrology and ecosystem services in Garhkundar-Dabar watershed of Bundelkhand region, Central India. Journal of Hydrology, 509, 132-149.

Singh, R., Wagener, T., Crane, R., Mann, M. E., & Ning, L. (2014b). A vulnerability driven approach to identify adverse climate and land use change combinations for critical hydrologic indicator thresholds: Application to a watershed in Pennsylvania, USA. Water Resources Research, 50(4), 3409-3427.

Singh, V. P. (1988). Hydrologic systems. Volume I: Rainfall-runoff modeling. Prentice Hall, Englewood Cliffs, New Jersey.

Singh, V. P. (1989). Hydrologic systems, volume II: watershed modeling. Prentice-Hall, Inc., Englewood Cliffs, New Jersey.

Singh, V. P. (1995). Computer models of watershed hydrology. Chapter 1: Watershed Modelling. Water Resources Publications, Colorado.

Singh, V. P. (1996). Kinematic wave modeling in water resources, surface-water hydrology. John Wiley & Sons, New York.

Singh, V. P. (2002). Kinematic wave modeling in hydrology. In ASCE World Water and Environmental Resources Congress, 2003 (pp. 1-38).

Singh, V. P., & Frevert, D. K. (2006). Watershed Models. Taylor and Fransis, CRC Press, Boka Raton.

Singh, V. P., & Woolhiser, D. A. (2002). Mathematical modeling of watershed hydrology. Journal of Hydrologic Engineering, 7(4), 270-292.

Sinha, R. K., & Eldho, T. I. (2018). Effects of historical and projected land use/cover change on runoff and sediment yield in the Netravati river basin, Western Ghats, India. Environmental Earth Sciences, 77(3), 111.

Sinnathamby, S., Douglas-Mankin, K. R., & Craige, C. (2017). Field-scale calibration of crop-yield parameters in the Soil and Water Assessment Tool (SWAT). Agricultural Water Management, 180, 61-69.

Sloan, P.G., & Moore, I.D. (1984). Modeling subsurface stormflow on steeply sloping forested watersheds. Water Resources Research. 20(12): 1815-1822.

Smith, R. E. (1992). Opus, an integrated simulation model for transport of nonpoint source pollutants at the field scale: Volume I, Documentation. ARS-US, Washington: USDA Agricultural Research Service; 120.

Spadavecchia, L., & Williams, M. (2009). Can spatio-temporal geostatistical methods improve high resolution regionalisation of meteorological variables?. Agricultural and Forest Meteorology, 149(6-7), 1105-1117.

Sperna Weiland, F. C., Van Beek, L. P. H., Kwadijk, J. C. J., & Bierkens, M. F. P. (2010). The ability of a GCM-forced hydrological model to reproduce global discharge variability. Hydrology and Earth System Sciences, 14(8), 1595-1621.

Srinivasan, R. (2008). Bosque river environmental infrastructure improvement plan: Phase I final report. TR-312, Texas Water Resources Institute. Texas A & M University, College Station.

Srinivasan, R., Ramanarayanan, T. S., Arnold, J. G., & Bednarz, S. T. (1998). Large area hydrologic modeling and assessment part II: model application 1. JAWRA Journal of the American Water Resources Association, 34(1), 91-101.

Stang, C., Gharabaghi, B., Rudra, R. P., Golmohammadi, G., Mahboubi, A. A., & Ahmed, S. I. (2016). Conservation management practices: Success story of the hog creek and sturgeon river watersheds, Ontario, Canada. Journal of Soil and Water Conservation, 71(3), 237-248.

Stehr, A., Debels, P., ARUMI, J. L., Romero, F., & Alcayaga, H. (2009). Combining the Soil and Water Assessment Tool (SWAT) and MODIS imagery to estimate monthly flows in a data-scarce Chilean Andean basin. Hydrological Sciences Journal, 54(6), 1053-1067.

Strehmel, A., Schmalz, B., & Fohrer, N. (2016). Evaluation of land use, land management and soil conservation strategies to reduce non-point source pollution loads in the three gorges region, China. Environmental Management, 58(5), 906-921.

Sulla-Menashe, D., Friedl, M. A., Krankina, O. N., Baccini, A., Woodcock, C. E., Sibley, A., ... & Elsakov, V. (2011). Hierarchical mapping of Northern Eurasian land cover using MODIS data. Remote Sensing of Environment, 115(2), 392-403.

Sultan, M., Metwally, S., Milewski, A., Becker, D., Ahmed, M., Sauck, W., ... & Wagdy, A. (2011). Modern recharge to fossil aquifers: Geochemical, geophysical, and modeling constraints. Journal of Hydrology, 403(1-2), 14-24.

Sun, L., Seidou, O., Nistor, I., Goïta, K., & Magagi, R. (2016). Simultaneous assimilation of in situ soil moisture and streamflow in the SWAT model using the Extended Kalman Filter. Journal of Hydrology, 543, 671-685.

Sun, Z., Lotz, T., & Chang, N. B. (2017). Assessing the long-term effects of land use changes on runoff patterns and food production in a large lake watershed with policy implications. Journal of Environmental Management, 204, 92-101.

Suryavanshi, S., Pandey, A., & Chaube, U. C. (2017). Hydrological simulation of the Betwa River basin (India) using the SWAT model. Hydrological Sciences Journal, 62(6), 960-978.

Suryavanshi, S., Pandey, A., Chaube, U. C., & Joshi, N. (2014). Long-term historic changes in climatic variables of Betwa Basin, India. Theoretical and Applied Climatology, 117(3-4), 403-418.

Sutcliffe, J. V., Agrawal, R. P., & Tucker, J. M. (1981). The water balance of the Betwa basin, India/Le bilan hydrologique du bassin versant de Betwa en Inde. Hydrological Sciences Journal, 26(2), 149-158.

Swallow, S. K., Talukdar, P., & Wear, D. N. (1997). Spatial and temporal specialization in forest ecosystem management under sole ownership. American Journal of Agricultural Economics, 79(2), 311-326.

Symeonakis, E., Karathanasis, N., Koukoulas, S., & Panagopoulos, G. (2014). Monitoring sensitivity to land degradation and desertification with the environmentally sensitive area index: The case of lesvos island. Land Degradation & Development, 27(6), 1562-1573.

Szczypta, C., Gascoin, S., Houet, T., Hagolle, O., Dejoux, J. F., Vigneau, C., & Fanise, P. (2015). Impact of climate and land cover changes on snow cover in a small Pyrenean catchment. Journal of Hydrology, 521, 84-99.

Tadesse, T., Wardlow, B. D., Hayes, M. J., Svoboda, M. D., & Brown, J. F. (2010). The Vegetation Outlook (VegOut): A new method for predicting vegetation seasonal greenness. GIScience & Remote Sensing, 47(1), 25-52.

Tallis, H., & Polasky, S. (2009). Mapping and valuing ecosystem services as an approach for conservation and natural-resource management. Annals of the New York Academy of Sciences, 1162(1), 265-283.

Teague, W. R., & Foy, J. K. (2002). Validation of SPUR2. 4 rangeland simulation model using a cow-calf field experiment. Agricultural Systems, 74(2), 287-302.

Tessema, S. M., Lyon, S. W., Setegn, S. G., & Mörtberg, U. (2014). Effects of different retention parameter estimation methods on the prediction of surface runoff using the SCS curve number method. Water Resources Management, 28(10), 3241-3254.

Teutschbein, C., & Seibert, J. (2012). Bias correction of regional climate model simulations for hydrological climate-change impact studies: Review and evaluation of different methods. Journal of Hydrology, 456, 12-29.

Thai, T. H., Thao, N. P., & Dieu, B. T. (2017). Assessment and Simulation of Impacts of Climate Change on Erosion and Water Flow by Using the Soil and Water Assessment Tool and GIS: Case Study in Upper Cau River basin in Vietnam. Vietnam Journal of Earth Sciences, 39(4), 376-392.

Theobald, D. M., & Hobbs, N. T. (1998). Forecasting rural land-use change: a comparison of regression-and spatial transition-based models. Geographical and Environmental Modelling, 2, 65-82.

Thrasher, B., Maurer, E. P., Duffy, P. B., & McKellar, C. (2012). Technical Note: Bias correcting climate model simulated daily temperature extremes with quantile mapping. Hydrology and Earth System Sciences, 16(9), 3309-3314.

Tiwari, P. C. (2000). Land-use changes in Himalaya and their impact on the plains ecosystem: need for sustainable land use. Land Use Policy, 17(2), 101-111.

Todorovic, M., & Steduto, P. (2003). A GIS for irrigation management. Physics and Chemistry of the Earth, Parts A/B/C, 28(4-5), 163-174.

Torrens, P. M. (2006). Geosimulation and its application to urban growth modeling. In Complex artificial environments (pp. 119-136). Springer Berlin Heidelberg.

Tripathi, M. P., Panda, R. K., & Raghuwanshi, N. S. (2003). Identification and prioritisation of critical sub-watersheds for soil conservation management using the SWAT model. Biosystems Engineering, 85(3), 365-379.

Tripathi, M. P., Panda, R. K., & Raghuwanshi, N. S. (2005). Development of effective management plan for critical subwatersheds using SWAT model. Hydrological Processes: An International Journal, 19(3), 809-826.

Tripathi, M. P., Panda, R. K., Raghuwanshi, N. S., & Singh, R. (2004). Hydrological modelling of a small watershed using generated rainfall in the soil and water assessment tool model. Hydrological Processes, 18(10), 1811-1821.

Trivedi, R. K., Chourasia, L. P., & Singh, D. K. (2006). Application of remote sensing in the study of geoenvironmental aspects of Rajghat dam project. Journal of the Indian Society of Remote Sensing, 34(3), 309-317.

Tu, J. (2009). Combined impact of climate and land use changes on streamflow and water quality in eastern Massachusetts, USA. Journal of Hydrology, 379(3-4), 268-283.

Tucker, C. J. (1979). Red and photographic infrared linear combinations for monitoring vegetation. Remote Sensing of Environment, 8(2), 127-150.

Tuppad, P., Kannan, N., Srinivasan, R., Rossi, C. G., & Arnold, J. G. (2010). Simulation of agricultural management alternatives for watershed protection. Water Resources Management, 24(12), 3115-3144.

Turner, A. G., & Annamalai, H. (2012). Climate change and the South Asian summer monsoon. Nature Climate Change, 2(8), 587-595.

Turner, B. L., & Meyer, W. B. (1991). Land use and land cover in global environmental change: considerations for study. International Social Science Journal, 43(130), 669-679.

Udias, A., Malagò, A., Pastori, M., Vigiak, O., Reynaud, A., Elorza, F. J., & Bouraoui, F. (2016). Identifying efficient nitrate reduction strategies in the upper danube. Water, 8(9), 371.

Ullrich, A., & Volk, M. (2009). Application of the Soil and Water Assessment Tool (SWAT) to predict the impact of alternative management practices on water quality and quantity. Agricultural Water Management, 96(8), 1207-1217.

USDA Soil Conservation Service (1972). Section 4. Hydrology. In National Engineering Handbook, US. Department of Agriculture-Soil Conservation Service: Washington, DC.

USDA-NRCS (2008). National handbook of conservation practices. USDA-NRCS, Washington, DC. Available at: http://www.nrcs.usda.gov/technical/standards/nhcp.html. Accessed 18 May 2009.

Van Eck, C. M., Nunes, J. P., Vieira, D. C., Keesstra, S., & Keizer, J. J. (2016). Physically-Based Modelling of the Post-Fire Runoff Response of a Forest Catchment in Central Portugal: Using Field versus Remote Sensing Based Estimates of Vegetation Recovery. Land Degradation & Development, 27(5), 1535-1544.

van Griensven, A., Meixner, T., Grunwald, S., Bishop, T., Diluzio, M., and Srinivasan, R. (2006). A global sensitivity analysis tool for the parameters of multi-variable catchment models. Journal of Hydrology, 324(1), 10-23.

Van Hall, R. L., Cammeraat, L. H., Keesstra, S. D., & Zorn, M. (2016). Impact of secondary vegetation succession on soil quality in a humid Mediterranean landscape. Catena, 149, 836-843.

Van Liew, M. W., & Garbrecht, J. (2003). Hydrologic simulation of the little Washita river experimental watershed using SWAT 1. JAWRA Journal of the American Water Resources Association, 39(2), 413-426.

Van Liew, M. W., Feng, S., & Pathak, T. B. (2012). Climate change impacts on streamflow, water quality, and best management practices for the Shell and Logan Creek Watersheds in Nebraska, USA. International Journal of Agricultural and Biological Engineering, 5(1), 13-34.

Vangelis, H., Tigkas, D., & Tsakiris, G. (2013). The effect of PET method on Reconnaissance Drought Index (RDI) calculation. Journal of Arid Environments, 88, 130-140.

Varikoden, H., & Preethi, B. (2013). Wet and dry years of Indian summer monsoon and its relation with Indo-Pacific sea surface temperatures. International Journal of Climatology, 33(7), 1761-1771.

Vaze, J., & Teng, J. (2011). Future climate and runoff projections across New South Wales, Australia: results and practical applications. Hydrological Processes, 25(1), 18-35.

Vazquez- Amábile, G. G., & Engel, B. A. (2008). Fitting of time series models to forecast streamflow and groundwater using simulated data from SWAT. Journal of Hydrologic Engineering, 13(7), 554-562.

Vazquez-Amábile, G. G., & Engel, B. A. (2005). Use of SWAT to compute groundwater table depth and streamflow in the Muscatatuck River watershed. American Society of Agricultural Engineering, 48(3): 991-1003.

Veldkamp, A., & Fresco, L. O. (1996a). CLUE: a conceptual model to study the conversion of land use and its effects. Ecological Modelling, 85(2-3), 253-270.

Veldkamp, A., & Fresco, L. O. (1996b). CLUE-CR: an integrated multi-scale model to simulate land use change scenarios in Costa Rica. Ecological modelling, 91(1-3), 231-248.

Vertessy, R. A., Wilson, C. J., Silburn, D. M., Connolly, R. D., & Ciesiolka, C. A. (1990). Predicting erosion hazard areas using digital terrain analysis. Int. Assoc. Hydrol. Sci. Publ, 192, 298-308.

Viney, N. R., & Sivapalan, M. (1999). A conceptual model of sediment transport: application to the Avon River Basin in Western Australia. Hydrological Processes, 13(5), 727-743.

Vinnarasi, R., & Dhanya, C. T. (2016). Changing characteristics of extreme wet and dry spells of Indian monsoon rainfall. Journal of Geophysical Research: Atmospheres, 121(5), 2146-2160.

Vitousek, P. M. (1994). Beyond global warming: ecology and global change. Ecology, 75(7), 1861-1876.

Voinov, A., Costanza, R., Wainger, L., Boumans, R., Villa, F., Maxwell, T., & Voinov, H. (1999). Patuxent landscape model: integrated ecological economic modeling of a watershed. Environmental Modelling & Software, 14(5), 473-491.

Vörösmarty, C. J., Green, P., Salisbury, J., & Lammers, R. B. (2000). Global water resources: vulnerability from climate change and population growth. Science, 289(5477), 284-288.

Wagener, T. (2007). Can we model the hydrological impacts of environmental change?. Hydrological Processes, 21(23), 3233-3236.

Wagner, P. D., Bhallamudi, S. M., Narasimhan, B., Kantakumar, L. N., Sudheer, K. P., Kumar, S., ... & Fiener, P. (2016). Dynamic integration of land use changes in a hydrologic assessment of a rapidly developing Indian catchment. Science of the Total Environment, 539, 153-164.

Wagner, P. D., Fiener, P., Wilken, F., Kumar, S., & Schneider, K. (2012). Comparison and evaluation of spatial interpolation schemes for daily rainfall in data scarce regions. Journal of Hydrology, 464, 388-400.

Wagner, P. D., Kumar, S., & Schneider, K. (2013). An assessment of land use change impacts on the water resources of the Mula and Mutha Rivers catchment upstream of Pune, India. Hydrology and Earth System Sciences, 17(6), 2233-2246.

Wagner, P. D., Kumar, S., Fiener, P., & Schneider, K. (2011). Hydrological modeling with SWAT in a monsoon-driven environment: experience from the Western Ghats, India. Transactions of the ASABE, 54(5), 1783-1790.

Wagner, P. D., Reichenau, T. G., Kumar, S., & Schneider, K. (2015). Development of a new downscaling method for hydrologic assessment of climate change impacts in data scarce regions and its application in the Western Ghats, India. Regional Environmental Change, 15(3), 435-447.

Wang, G., & Xia, J. (2010). Improvement of SWAT2000 modelling to assess the impact of dams and sluices on streamflow in the Huai River basin of China. Hydrological Processes, 24(11), 1455-1471.

Wang, G., Xu, Z., & Zhang, S. (2014). The influence of land use patterns on water quality at multiple spatial scales in a river system. Hydrological Processes, 28(20), 5259-5272.

Wang, X., Piao, S., Ciais, P., Li, J., Friedlingstein, P., Koven, C., & Chen, A. (2011). Spring temperature change and its implication in the change of vegetation growth in North America from 1982 to 2006. Proceedings of the National Academy of Sciences, 108(4), 1240-1245.

Wear, D. N., Turner, M. G., & Flamm, R. O. (1996). Ecosystem management with multiple owners: landscape dynamics in a southern Appalachian watershed. Ecological Applications, 6(4), 1173-1188.

Wear, D. N., Turner, M. G., & Naiman, R. J. (1998). Land cover along an urban–rural gradient: implications for water quality. Ecological Applications, 8(3), 619-630.

Weber, A., Fohrer, N., & Möller, D. (2001). Long-term land use changes in a mesoscale watershed due to socio-economic factors—effects on landscape structures and functions. Ecological Modelling, 140(1-2), 125-140.

Webster, P. J., Magana, V. O., Palmer, T. N., Shukla, J., Tomas, R. A., Yanai, M. U., & Yasunari, T. (1998). Monsoons: Processes, predictability, and the prospects for prediction. Journal of Geophysical Research: Oceans, 103(C7), 14451-14510.

Wei, C., Chen, J., Song, X., Yao, Z., Kou, C., & Zhang, X. (2016). Effects of Land Use Change on Runoff in Qiaoyu River Basin. Journal of Residuals Science & Technology, 13(6), 117.1 to 117.6.

Weismiller, R. A., Kristof, S. J., Scholz, D. K., Anuta, P. E., & Momin, S. M. (1977). Evaluation of change detection techniques for monitoring coastal zone environments. LARS Technical Reports, 70.

Wheater, H. S., Jakeman, A. J., & Beven, K. J. (1993). Progress and directions in rainfall-runoff modelling. Chapter 5, Modelling Change in Environmental Systems. Jakeman, A. K., Beck, M. B., McAleer, M. J. (Eds.), John Wiley and Sons, Chichester; 101–132.

White, M. J., Harmel, R. D., Arnold, J. G., & Williams, J. R. (2014). SWAT check: A screening tool to assist users in the identification of potential model application problems. Journal of Environmental Quality, 43(1), 208-214.

Wilby, R. L., Dawson, C. W., & Barrow, E. M. (2002). SDSM—a decision support tool for the assessment of regional climate change impacts. Environmental Modelling & Software, 17(2), 145-157.

Wilcox, B.P., Rawls, W.J., Brakensiek, D.L. & Wright, J.R. (1990). Predicting runoff from rangeland catchments: a comparison of two models. Water Resource Research, 26:2401–2410.

Williams, J. R., & Izaurralde, R. C. (2006). The APEX model. Watershed Models, Singh, V. P., and Frevert, D. K. eds. Boca Raton, Fla.: CRC Press; 437-482.

Williams, J. R., Jones, C. A., & Dyke, P. T. (1984). A modeling approach to determining the relationship between erosion and soil productivity. Transactions of the ASAE, 27(1), 129-144.

Williams, J. R., Nicks, A. D., & Arnold, J. G. (1985). Simulator for water resources in rural basins. Journal of Hydraulic Engineering, 111(6), 970-986.

Williams, J.R. (1969). Flood routing with variable travel time or variable storage coefficients. Transactions of the ASAE, 12(1):100-103.

Williams, J.W., Izaurralde, R.C., & Steglich, E.M. (2008). Agricultural Policy/Environmental Extender Model: Theoretical Documentation Version 0604, Black Land Research and Extension Center, Texas, Joint Global Change Research Institute Pacific Northwest National Lab and University of Maryland.

Willmott, C. J. (1984). On the evaluation of model performance in physical geography. In Spatial statistics and models, edited by: Gaile, G. L. and Willmot, C. J., D. Reidel, Dordrecht, 443–460.

Wolf, A. T., & Hamner, J. H. (2000). Trends in transboundary water disputes and dispute resolution. In Environment and Security (pp. 123-148). Palgrave Macmillan UK.

Wolmer, W. (2003). Transboundary conservation: the politics of ecological integrity in the Great Limpopo Transfrontier Park*. Journal of Southern African Studies, 29(1), 261-278.

Woolhiser, D. A., Smith, R. E., & Goodrich, D. C. (1990). KINEROS—A kinematic runoff and erosion model: Documentation and user manual. Rep. No. ARS-77, USDA, Washington, D.C.

Woznicki, S. A., & Nejadhashemi, A. P. (2014). Assessing uncertainty in best management practice effectiveness under future climate scenarios. Hydrological Processes, 28(4), 2550-2566.

Wu, J., Miao, C., Yang, T., Duan, Q., & Zhang, X. (2018). Modeling streamflow and sediment responses to climate change and human activities in the Yanhe River, China. Hydrology Research, 49(1), 150-162.

Wu, J., Miao, C., Zhang, X., Yang, T., & Duan, Q. (2017). Detecting the quantitative hydrological response to changes in climate and human activities. Science of the Total Environment, 586, 328-337.

Xu, H., & Luo, Y. (2015). Climate change and its impacts on river discharge in two climate regions in China. Hydrology and Earth System Sciences, 19(11), 4609-4618.

Yan, B., Fang, N. F., Zhang, P. C., & Shi, Z. H. (2013). Impacts of land use change on watershed streamflow and sediment yield: an assessment using hydrologic modelling and partial least squares regression. Journal of Hydrology, 484, 26-37.

Yang, J., Reichert, P., Abbaspour, K. C., Xia, J., & Yang, H. (2008). Comparing uncertainty analysis techniques for a SWAT application to the Chaohe Basin in China. Journal of Hydrology, 358(1-2), 1-23.

Yeh, A. G. O., & Li, X. (1997). An integrated remote sensing and GIS approach in the monitoring and evaluation of rapid urban growth for sustainable development in the Pearl River Delta, China. International Planning Studies, 2(2), 193-210.

Young, R. A., Onstad, C. A., Bosch, D. D., & Anderson, W. P. (1989). AGNPS: A nonpoint-source pollution model for evaluating agricultural watersheds. Journal of Soil and Water Conservation, 44(2), 168-173.

Yu, J., Yu, H., & Xu, L. (2013). Performance evaluation of various stormwater best management practices. Environmental Science and Pollution Research, 20(9), 6160-6171.

Yu, Y., & Jia, Z. Q. (2014). Changes in soil organic carbon and nitrogen capacities of Salix cheilophila Schneid along a revegetation chronosequence in semi-arid degraded sandy land of the Gonghe Basin, Tibet Plateau. Solid Earth, 5(2), 1045-1054.

Zabaleta, A., Meaurio, M., Ruiz, E., & Antigüedad, I. (2014). Simulation climate change impact on runoff and sediment yield in a small watershed in the Basque Country, northern Spain. Journal of Environmental Quality, 43(1), 235-245.

Zeng, L., Song, K., Zhang, B., & Wang, Z. (2010, July). Spatial mapping of actual evapotranspiration and water deficit with MODIS products in the Songnen Plain, northeast China. In Geoscience and Remote Sensing Symposium (IGARSS), 2010 IEEE International (pp. 879-882). IEEE.

Zhang, A., Zhang, C., Fu, G., Wang, B., Bao, Z., & Zheng, H. (2012a). Assessments of impacts of climate change and human activities on runoff with SWAT for the Huifa River Basin, Northeast China. Water Resources Management, 26(8), 2199-2217.

Zhang, B., Shrestha, N., Daggupati, P., Rudra, R. P., Shukla, R., Kaur, B., & Hou, J. (2018a). Quantifying the Impacts of Climate Change on Streamflow Dynamics of Two Major Rivers of the Northern Lake Erie Basin in Canada. Sustainability, 10(8), 2897.

Zhang, C., Peng, Y., Chu, J., Shoemaker, C. A., & Zhang, A. (2012b). Integrated hydrological modelling of small-and medium-sized water storages with application to the upper Fengman Reservoir Basin of China. Hydrology and Earth System Sciences, 16(11), 4033-4047.

Zhang, L., Nan, Z., Yu, W., Zhao, Y., & Xu, Y. (2018b). Comparison of baseline period choices for separating climate and land use/land cover change impacts on watershed hydrology using distributed hydrological models. Science of the Total Environment, 622, 1016-1028.

Zhang, L., O'Neill, A. L., & Lacey, S. (1996). Modelling approaches to the prediction of soil erosion in catchments. Environmental Software, 11(1-3), 123-133.

Zhang, Q., Chen, G., Su, B., Disse, M., Jiang, T., & Xu, C. Y. (2008). Periodicity of sediment load and runoff in the Yangtze River basin and possible impacts of climatic changes and human activities. Hydrological Sciences Journal, 53(2), 457-465.

Zhang, S., Liu, Y., & Wang, T. (2014). How land use change contributes to reducing soil erosion in the Jialing River Basin, China. Agricultural Water Management, 133, 65-73.

Zhang, X., & Zhang, M. (2011). Modeling effectiveness of agricultural BMPs to reduce sediment load and organophosphate pesticides in surface runoff. Science of the Total Environment, 409(10), 1949-1958.

Zhang, Y., Song, C., Band, L. E., Sun, G., & Li, J. (2017). Reanalysis of global terrestrial vegetation trends from MODIS products: Browning or greening?. Remote Sensing of Environment, 191, 145-155.

Zhao, G., Mu, X., Strehmel, A., & Tian, P. (2014). Temporal variation of streamflow, sediment load and their relationship in the Yellow River Basin, China. PLoS One, 9(3), e91048.

Zheng, J., Yu, X., Deng, W., Wang, H., & Wang, Y. (2012). Sensitivity of Land-Use Change to Streamflow in Chaobai River Basin. Journal of Hydrologic Engineering, 18(4), 457-464.

Zhou, L., Tucker, C. J., Kaufmann, R. K., Slayback, D., Shabanov, N. V., & Myneni, R. B. (2001). Variations in northern vegetation activity inferred from satellite data of vegetation index during 1981 to 1999. Journal of Geophysical Research: Atmospheres, 106(D17), 20069-20083.

Ziadat, F. M., & Taimeh, A. Y. (2013). Effect of rainfall intensity, slope, land use and antecedent soil moisture on soil erosion in an arid environment. Land Degradation & Development, 24(6), 582-590.

Zucca, C., Arrieta Garcia, S., Deroma, M., & Madrau, S. (2016). Organic carbon and alkalinity increase in topsoil after rangeland restoration through Atriplex nummularia plantation. Land Degradation & Development, 27(3), 573-582.

Zuo, D., Xu, Z., Yao, W., Jin, S., Xiao, P., & Ran, D. (2016). Assessing the effects of changes in land use and climate on runoff and sediment yields from a watershed in the Loess Plateau of China. Science of the Total Environment, 544, 238-250.

APPENDIX-A

A1: Field Visit (August 2-3, 2013)

Place: Basoda-Ganj Village- near Rapta pul at right bank of Betwa River
Latitude: 23° 52' 41.0", **Longitude:** 77° 55' 05.6", **Elevation:** 400 m

Place: Basoda-Ganj Village- Farm near Rapta pul at right bank of the Betwa River
Latitude: 23° 52' 26.1", **Longitude:** 77° 55' 12.5", **Elevation:** 410 m

Place: Basoda-Ganj Village- river flow condition near Rapta pul, view from right bank of the Betwa River
Latitude: 23° 52' 41.0", **Longitude:** 77° 55' 05.6", **Elevation:** 400 m

Place: Basoda-Ganj Village- Sediment flow by Betwa River water near Rapta pul
Latitude: 23° 52' 41.0", **Longitude:** 77° 55' 05.6", **Elevation:** 400 m

Place: Basoda-Ganj Village- cutting of river bank by Betwa River water flow near Rapta pul
Latitude: 23° 52' 41.0", **Longitude:** 77° 55' 05.6", **Elevation:** 400 m

Place: Basoda- near Ambanagar pul water flow condition, view from right bank of the Betwa River
Latitude: 23° 53' 01.6", **Longitude:** 77° 55' 11.9", **Elevation:** 397 m

Place: Basoda- near Ambanagar pul, view from right bank of the Betwa River
Latitude: 23° 53' 01.6", **Longitude:** 77° 55' 11.9", **Elevation:** 397 m

Place: Basoda_Nandpura village- soyabeen farm at left bank of the Betwa River
Latitude: 23° 51' 08.6", **Longitude:** 77° 52' 45.6", **Elevation:** 414 m

Place: Basoda_Nandpura village- soyabeen farm observation by Prof. S.K. Sharma with farmer (after crossing Barighat pul) at left bank of the Betwa River- **Farmer:** Kushal Singh
Latitude: 23° 51' 08.6", **Longitude:** 77° 52' 45.6", **Elevation:** 414 m

Place: Vidisha - right bank view of the Betwa River before crossing the pul, near Mela ground
Latitude: 23° 32' 24.8", **Longitude:** 77° 48' 09.6", **Elevation:** 425 m

Place: Vidisha_ left bank view of the Betwa River after crossing the pul, near Mela ground
Latitude: 23° 32' 24.8", **Longitude:** 77° 48' 09.6", **Elevation:** 425 m

Place: Vidisha_ River divide in two way, view from right bank of the Betwa River, near Mela ground
Latitude: 23° 32' 24.8", **Longitude:** 77° 48' 09.6", **Elevation:** 425 m

A2: Field Visit (May 7-8, 2014)

Place: Nandpura Village near Basoda
Latitude: 23° 51' 8.6" N, **Longitude:** 77° 56' 45.6" E, **Elevation:** 420 m

Place: Ambanagar pul
Latitude: 23° 52' 59.1", **Longitude:** 77° 55’12.4", **Elevation** 400 m

Place: Barrighat pul
Latitude: 23° 51' 0.08", **Longitude**: 77° 53' 09.8", **Elevation:** 400 m

Place: Field2 (Basoda)
Latitude: 23° 52' 50.0", **Longitude:** 77° 55’10.0"

Place: Field 3 (Behind Manorma colony, Sagar)
Latitude: 23° 49' 54.5", **Longitude**: 78° 45' 52.6"

Place: Forest (Sagar)
Latitude: 23° 49' 27.1", **Longitude**: 78° 45' 7.09"

Place: Forest2 (Sagar)
Latitude: 23° 49' 37.6", **Longitude**: 78° 45' 6.25"

Place: Water Body Sagar (Pond)
Latitude: 23° 49' 59.0", **Longitude:** 78° 44' 48.5"

Place: Field (Sihora)
Latitude 23° 47' 57.0", **Longitude**: 78° 35' 01.8"

Place: Field (Rahatgadh)
Latitude: 23° 47' 37.6", **Longitude:** 78° 24' 28.0"

Place: Field (Begamganj)
Latitude: 23° 36' 13.0", **Longitude**: 78° 20' 53"

Place: Barren Land (Geratganj)
Latitude: 23° 25' 11.2", **Longitude:** 78° 14' 42.0"

Place: Field (Garhi)
Latitude: 23° 23' 20.4", **Longitude:** 78° 08' 59.3"

Place: Field (Dehgaon)
Latitude: 23° 19' 32.0", **Longitude:** 78° 06' 05.4"

Place: Field (Narwar)
Latitude: 23° 18' 30.4", **Longitude:** 77° 57' 58.0"

Place: Field (Raisen)
Latitude: 23° 19' 08.8", **Longitude:** 77° 47' 39.8"

Place: Field (Bhopal)
Latitude: 23° 14' 52.6", **Longitude:** 77° 32' 56.3"

Place: Field (Bhopal)
Latitude: 23° 15' 27.4", **Longitude:** 77° 30' 29.8"

Place: Bhopal (Waterbody)
Latitude: 23° 15' 12.3", **Longitude:** 77° 23' 26.8"

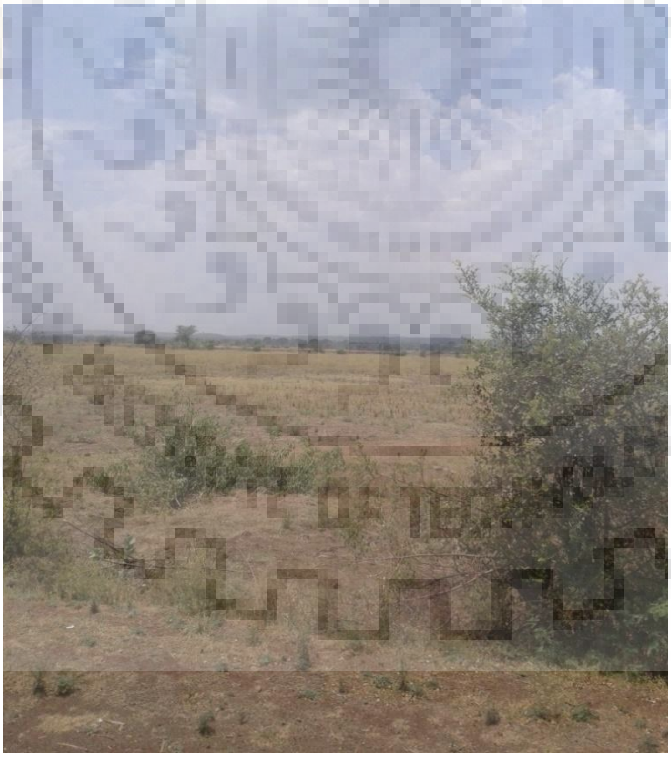

Place: Begamganj (Barren Land)
Latitude 23° 36' 38.2", **longitude** 77° 20' 58.0"

A3: Field Visit (November 19-22, 2014)

Place: Rajghat dam
Latitude: 24° 45.928' N, **Longitude**: 78° 14.264' E, **Elevation**: 345 m

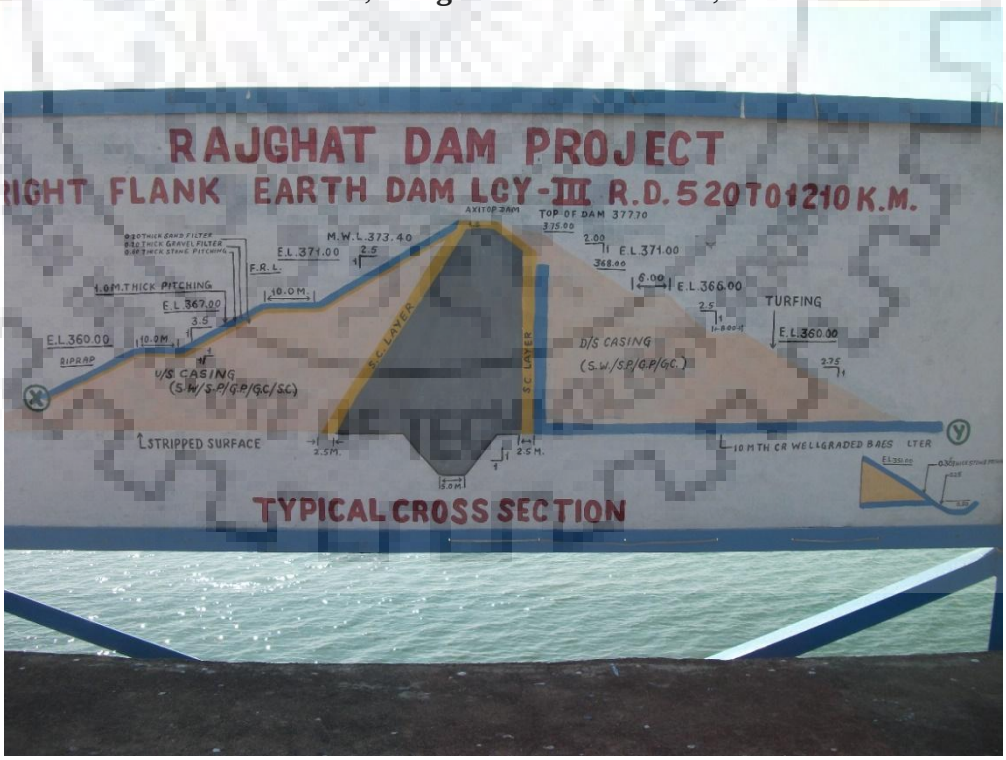

Place: Typical cross section board on Rajghat dam
Latitude: 24° 45.720' N, **Longitude**: 78° 14.198' E, **Elevation**: 380 m

Place: Side view from top-right side of the Rajghat dam
Latitude: 24° 45.720' N, **Longitude**: 78° 14.198' E, **Elevation**: 380 m

Place: Rajghat dam open gate
Latitude: 24° 45.720' N, **Longitude**: 78° 14.198' E, **Elevation**: 380 m

Place: Rajghat dam close gate
Latitude: 24° 45.720' N, **Longitude**: 78° 14.198' E, **Elevation**: 380 m

Place: Chanderi village view
Latitude: 24° 43.159' N, **Longitude**: 78° 08.372' E, **Elevation**: 437 m

Place: Fort near Chanderi village
Latitude: 24° 42.643' N, **Longitude**: 78° 08.417' E, **Elevation**: 501 m

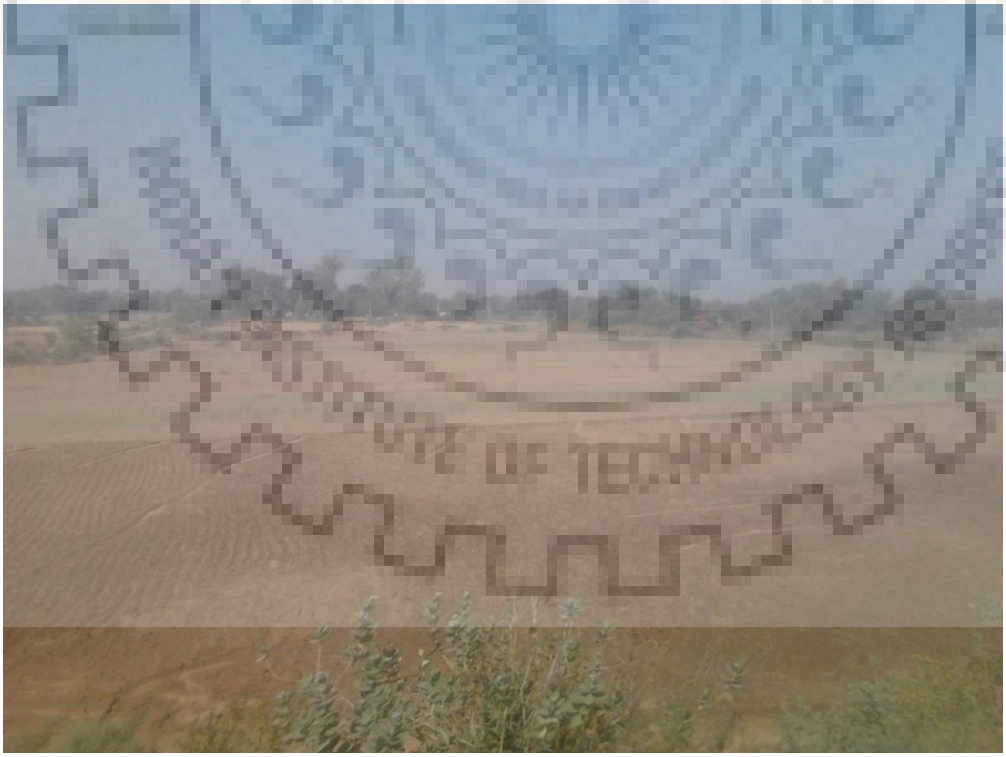

Place: Near Roda village
Latitude: 24° 44.701' N, **Longitude**: 78° 25.807' E, **Elevation**: 349 m

Place: Near Maharra village
Latitude: 24° 47.440' N, **Longitude**: 78° 26.843' E, **Elevation**: 340 m

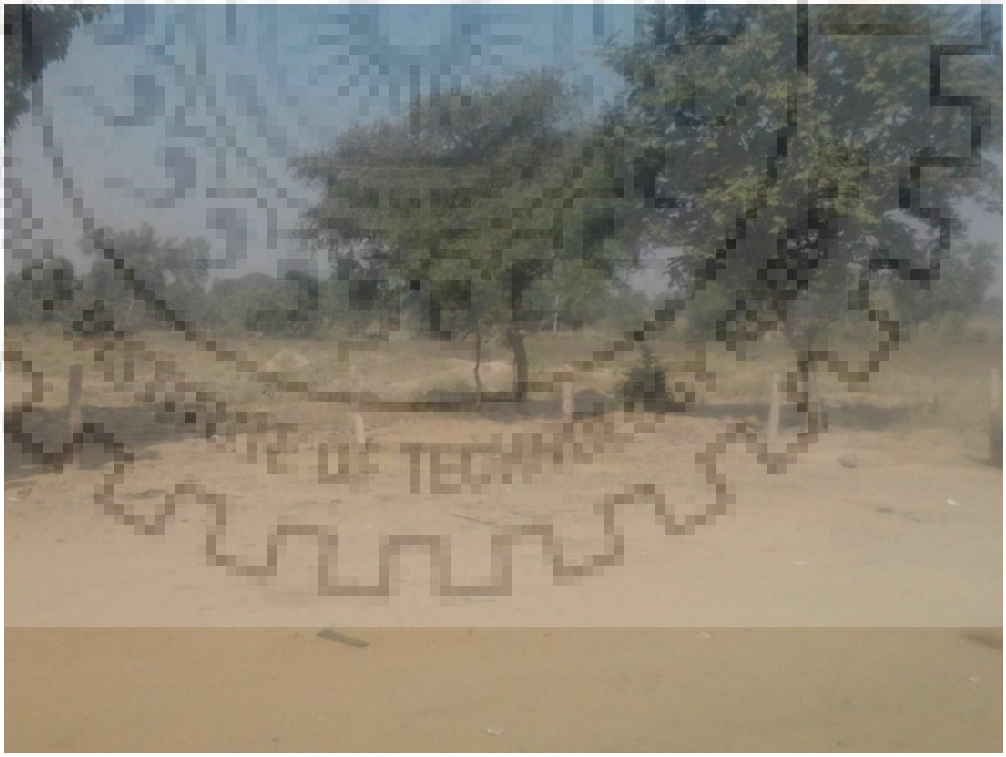

Place: Near Nadawara village
Latitude: 24° 47.711' N, **Longitude**: 78° 27.160' E, **Elevation**: 338 m

Place: Near Nadawara village
Latitude: 24° 48.322' N, **Longitude**: 78° 27.300' E, **Elevation**: 340 m

Place: Near Lakhanpura village
Latitude: 24° 50.360' N, **Longitude**: 78° 27.868' E, **Elevation**: 337 m

Place: Near Bansi village
Latitude: 24° 54.498' N, **Longitude**: 78° 28.069' E, **Elevation**: 337 m

Place: Shahjad reservoir
Latitude: 24° 56.761' N, **Longitude**: 78° 28.099' E, **Elevation**: 330 m

Place: Near Shahjad reservoir
Latitude: 24° 58.098' N, **Longitude**: 78° 27.987' E, **Elevation**: 329 m

Place: Near Matatila dam
Latitude: 25° 2.985' N, **Longitude**: 78° 23.040' E, **Elevation**: 306 m

Place: Matatila dam storage
Latitude: 25° 4.012' N, **Longitude**: 78° 22.778' E, **Elevation**: 305 m

Place: Downstream side of the Matatila dam
Latitude: 25° 5.887'N, **Longitude**: 78° 22.955' E, **Elevation**: 292 m

Place: Matatila dam
Latitude: 25° 5.887'N, **Longitude**: 78° 22.955' E, **Elevation**: 292 m

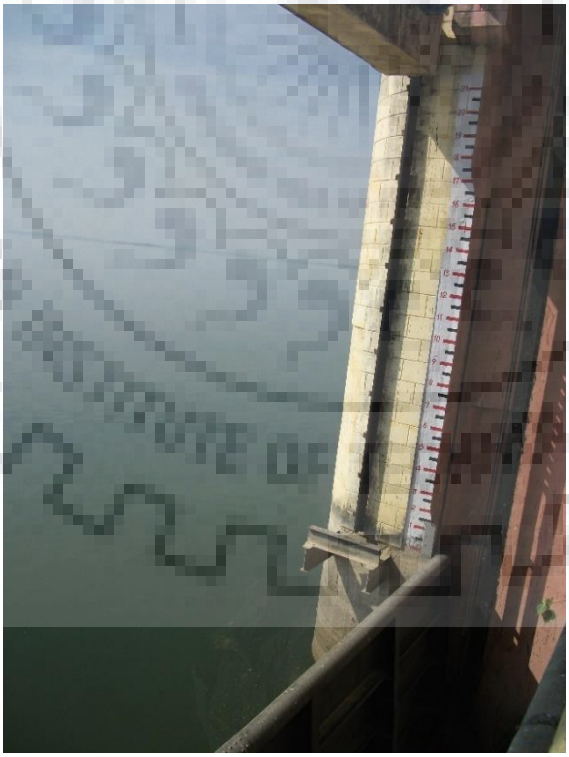

Place: Measure scale over gate
Latitude: 25° 5.705'N, **Longitude**: 78° 22.489' E, **Elevation**: 307 m

Place: Garden near Matatila dam
Latitude: 25° 5.887'N; **Longitude**: 78° 22.955' E; **Elevation**: 292m

Place: Near Khandi village
Latitude: 25° 4.128' N, **Longitude**: 78° 27.838' E, **Elevation**: 329 m

Place: Near Khandi village
Latitude: 25° 4.128' N, **Longitude:** 78° 27.838' E, **Elevation:** 329m

Place: Near Birdha village
Latitude: 25° 6.392' N, **Longitude**: 78° 31.395' E, **Elevation**: 302 m

A4: Field Visit (16-17 November 2016)

Place: Ch. Charan Singh Lahchura Dam (Dhasan River)
Latitude: 25°13’41.8597”N **Longitude**: 79°13’50”E **Elevation**: 169 m

Place: Energy dissipators in Lahchura Dam near Mau-Ranipur
Latitude: 25°13’41.8597”N **Longitude**: 79°13’50”E **Elevation**: 169 m

Place: Downstream view from Lahchura Dam in Dhasan river
Latitude: 25°13’41.8597”N **Longitude**: 79°13’50”E **Elevation**: 169 m

Place: Canal diverted from Lahchura Dam in Dhasan river
Latitude: 25°13’41.8597”N **Longitude**: 79°13’50”E **Elevation**: 169 m

Place: Agricultural land near Ghat Lahchura
Latitude: 25°15’39.0356”N **Longitude**: 79°14.37’ E **Elevation**: 153 m

Place: Forest near Lahchura Village
Latitude: 25°18’6.8292”N **Longitude**: 79°13’10.1”E **Elevation**: 366 m

Place: Saprar Dam near Mau-Ranipur
Latitude: 25.14°56’69.71”N **Longitude**: 79.8° 14. **Elevation**: 826 m

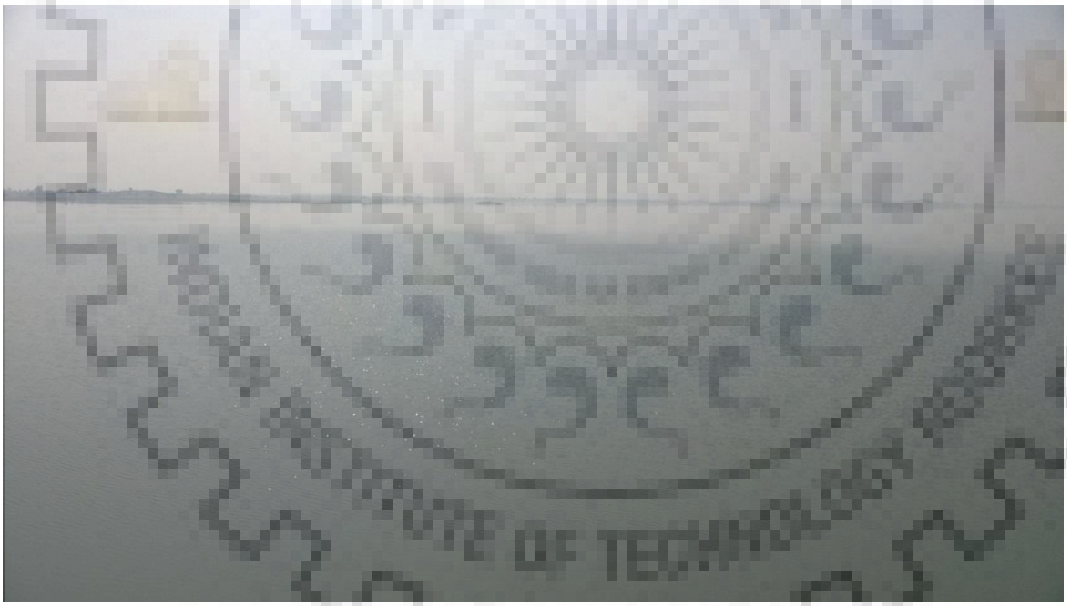

Place: Reservoir of Saprar Dam
Latitude: 25.14°56’69.71”N **Longitude**: 79.8° 14. **Elevation**: 826 m

Place: Downstream view of Saprar Dam
Latitude: 25.14°56’69.71”N **Longitude**: 79.8° 14. **Elevation**: 826 m

Place: Downstream view of Saprar Dam
Latitude: 25.14°56’69.71”N **Longitude**: 79.8° 14. **Elevation**: 826 m

Place: Shrub Land near Rath
Latitude: 25.35°19.9836'N **Longitude**: 79°42'22"E. **Elevation**: 703m

Place: Bramhanand Dam Near Rath
Latitude: 25.35°20.1552'N **Longitude**: 79°42'25.1" E. **Elevation**: 202m

Place: Downstream view of Bramhanand Dam Near Rath
Latitude: 25.35°20.1552'N **Longitude**: 79°42'25.1" E. **Elevation**: 202m

Place: Downstream view of Bramhanand Dam Near Rath
Latitude: 25.35°20.1552'N **Longitude**: 79°42'25.1" E. **Elevation**: 202m

Place: Agricultural Land
Latitude: 25.55° 4.4058’N **Longitude**: 79°47’29.0” E. **Elevation**: 843m

Place: Scrub Land
Latitude: 25.55° 48.866’N **Longitude**: 79°47’57.2” E. **Elevation**: 369m

Place: Scrub Land
Latitude: 25.55° 48.866’N **Longitude**: 79°47’57.2” E. **Elevation**: 369m

Place: Agricultural Land
Latitude: 25.58° **7**.8570’N **Longitude**: 79°49’13.4” E. **Elevation**: 270m

Place: Agricultural Land
Latitude: 25°59’19.0920’N **Longitude**: 79°51’43.5” E. **Elevation**: 277m

Place: Agricultural Land
Latitude: 25°59’19.0920’N **Longitude**: 79°52’54.8” E. **Elevation**: 216m

Place: Scrub land
Latitude: 25°57**’**20.2174’N **Longitude**: 80°5’52.7” E. **Elevation**: 984m

Place: Village Rameri Danda near Hamirpur
Latitude: 25°92**’**39.09”’N **Longitude**: 80°18’94.9” E. **Elevation**: 490m

Place: Agricultural land near confluence of Betwa and Yamuna River at Hamirpur
Latitude: 25°91’99.40” N **Longitude**: 80°20’15” E. **Elevation**: 590m

APPENDIX-B

The transition area matrix (TAM) and the transition probability matrix (TPM) generated in the CA-MC modelling are as follows:

B1: Model validation analysis

Table B1: Transition area matrix (TAM) among LU/LC categories in validation analysis

LU/LC class	Dense forest	Degraded forest	Agriculture area	Barren land	Waterbody	Settlement	Total area (km^2)
TAM for 2010 based on transition matrix of 2001-2007							
Dense forest	3160.69	793.22	1300.83	0.00	3.39	1.57	5259.70
Degraded forest	1070.31	2882.44	2112.82	262.25	2.19	21.33	6351.34
Agriculture area	701.49	2659.68	24171.26	1458.32	45.02	22.99	29058.76
Barren land	0.00	15.97	1069.39	1518.44	5.91	8.92	2618.63
Waterbody	16.37	11.49	112.73	7.20	367.86	0.00	515.65
Settlement	0.44	1.85	39.74	0.00	0.02	82.20	124.25
Total area (km^2)	4949.30	6364.65	28806.77	3246.21	424.39	137.01	43928.33
TAM for 2013 based on transition matrix of 2007-2010							
Dense forest	2954.27	848.98	1635.02	208.84	21.70	3.80	5672.61
Degraded forest	1428.13	1648.92	2740.43	269.04	7.86	7.61	6101.99
Agriculture area	1336.91	3007.38	24033.91	1043.78	98.50	54.60	29575.08
Barren land	42.08	436.02	1143.70	336.58	2.41	0.80	1961.59
Waterbody	58.16	35.95	44.82	9.96	336.82	0.21	485.92
Settlement	16.28	24.70	18.98	2.62	0.21	68.37	131.16
Total area (km^2)	5835.83	6001.95	29616.86	1870.82	467.50	135.39	43928.35

Table B2: Transition probability matrix (TPM) among LU/LC categories in validation analysis

LU/LC class	Dense forest	Degraded forest	Agriculture area	Barren land	Waterbody	Settlement
TPM for 2010 based on transition matrix of 2001-2007						
Dense forest	0.601	0.151	0.247	0.000	0.001	0.000
Degraded forest	0.169	0.454	0.333	0.041	0.000	0.003
Agriculture area	0.024	0.092	0.832	0.050	0.002	0.001
Barren land	0.000	0.006	0.408	0.580	0.002	0.003
Waterbody	0.032	0.022	0.219	0.014	0.713	0.000
Settlement	0.004	0.015	0.320	0.000	0.000	0.662
TPM for 2013 based on transition matrix of 2007-2010						
Dense forest	0.521	0.150	0.288	0.037	0.004	0.001
Degraded forest	0.234	0.270	0.449	0.044	0.001	0.001
Agriculture area	0.045	0.102	0.813	0.035	0.003	0.002
Barren land	0.022	0.222	0.583	0.172	0.001	0.000
Waterbody	0.120	0.074	0.092	0.021	0.693	0.000
Settlement	0.124	0.188	0.145	0.020	0.002	0.521

B2: Future LU/LC prediction

Table B3: Transition area matrix (TAM) among LU/LC categories in future prediction

LU/LC class	Dense forest	Degraded forest	Agriculture area	Barren land	Waterbody	Settlement	Total area (km^2)
TAM for 2020							
Dense forest	2053.41	700.77	2676.11	222.19	12.53	8.89	5673.9
Degraded forest	1524.33	1328.63	2878.31	337.47	5.53	29.4	6103.67
Agriculture area	1553.31	3833.26	22662.01	1400.89	72.62	57.84	29579.93
Barren land	128.45	561.6	684.96	559.83	14.6	12.5	1961.94
Waterbody	64.86	52.73	139.76	18.7	209.69	0.19	485.93
Settlement	20.8	36.02	18.11	6.34	0.14	49.81	131.22
Total area (km^2)	5345.16	6513.01	29059.26	2545.42	315.11	158.63	43936.59
TAM for 2040							
Dense forest	1833.54	583.12	2645.33	267.9	1.96	13.25	5345.1
Degraded forest	1684.36	1328.99	3008.02	459.55	1.42	31.28	6513.62
Agriculture area	1212.07	4334.45	21582.82	1839.29	15.45	75.28	29059.32
Barren land	138.27	803.5	810.14	770.97	3.05	19.51	2545.44
Waterbody	46.19	49.05	115.4	15.37	88.26	0.19	314.46
Settlement	35.72	43.49	8.27	4.98	0.05	66.1	158.61
Total area (km^2)	4950.15	7142.6	28169.94	3358.06	110.19	205.61	43936.59
TAM for 2060							
Dense forest	2481.97	213.16	2057.27	190.26	0.01	7.83	4950.5
Degraded forest	2127.87	2427.33	2007.57	563.72	0.01	16.06	7142.56
Agriculture area	174.46	3576.92	22745.92	1595.09	0.31	78.3	28171.02
Barren land	0	1335.03	344.61	1657.1	0	21.42	3358.16
Waterbody	13.18	27.17	37.66	5.36	25.57	0.01	108.95
Settlement	45.17	42.37	0	0	0	117.88	205.42
Total area (km^2)	14742.95	7621.98	27193.05	4011.53	25.9	241.5	43936.59
TAM for 2080							
Dense forest	1246.16	551.25	2804.57	331.93	0.03	16.55	4950.49
Degraded forest	1717.94	1401.72	3326.81	667.67	0.03	28.39	7142.56
Agriculture area	1309.84	4900.05	19422.21	2407.58	0.32	131.04	28171.02
Barren land	287.44	1256.23	873.9	910.74	0	29.83	3358.14
Waterbody	17.63	22.97	53.86	8.86	5.37	0.25	108.94
Settlement	76.64	46.54	12.66	4.85	0	64.73	205.42
Total area (km^2)	4655.65	8178.76	26493.99	4331.63	5.75	270.79	43936.59
TAM for 2100							
Dense forest	1011.54	671.36	2862.21	384.25	0.04	21.11	4950.51
Degraded forest	1441.38	1369.37	3611.41	686.49	0.04	33.87	7142.56
Agriculture area	1844.43	5088.08	18511.40	2577.52	0.3	149.27	28171.01
Barren land	355.2	1073.04	1163.74	737.5	0.01	28.67	3358.16
Waterbody	16.26	22.07	57.16	9.6	3.47	0.38	108.94
Settlement	66.39	43.13	40.05	8.59	0	47.26	205.42
Total area (km^2)	4735.2	8267.05	26245.98	4403.95	3.86	280.56	43936.59

Table B4: Transition probability matrix (TPM) among LU/LC categories in future prediction

LU/LC class	Dense forest	Degraded forest	Agriculture area	Barren land	Waterbody	Settlement
TPM for 2020						
Dense forest	0.362	0.124	0.472	0.039	0.002	0.002
Degraded forest	0.250	0.218	0.472	0.055	0.001	0.005
Agriculture area	0.053	0.130	0.766	0.047	0.003	0.002
Barren land	0.066	0.286	0.349	0.285	0.007	0.006
Waterbody	0.134	0.109	0.288	0.039	0.432	0.000
Settlement	0.159	0.275	0.138	0.048	0.001	0.380
TPM for 2040						
Dense forest	0.343	0.109	0.495	0.050	0.000	0.003
Degraded forest	0.259	0.204	0.462	0.071	0.000	0.005
Agriculture area	0.042	0.149	0.743	0.063	0.001	0.003
Barren land	0.054	0.316	0.318	0.303	0.001	0.008
Waterbody	0.147	0.156	0.367	0.049	0.281	0.001
Settlement	0.225	0.274	0.052	0.031	0.000	0.417
TPM for 2060						
Dense forest	0.501	0.043	0.416	0.038	0.000	0.002
Degraded forest	0.298	0.340	0.281	0.079	0.000	0.002
Agriculture area	0.006	0.127	0.807	0.057	0.000	0.003
Barren land	0.000	0.398	0.103	0.494	0.000	0.006
Waterbody	0.121	0.249	0.346	0.049	0.235	0.000
Settlement	0.220	0.206	0.000	0.000	0.000	0.574
TPM for 2080						
Dense forest	0.252	0.111	0.567	0.067	0.000	0.003
Degraded forest	0.241	0.196	0.466	0.094	0.000	0.004
Agriculture area	0.047	0.174	0.689	0.086	0.000	0.005
Barren land	0.086	0.374	0.260	0.271	0.000	0.009
Waterbody	0.162	0.211	0.494	0.081	0.049	0.002
Settlement	0.373	0.227	0.062	0.024	0.000	0.315
TPM for 2100						
Dense forest	0.204	0.136	0.578	0.078	0.000	0.004
Degraded forest	0.202	0.192	0.506	0.096	0.000	0.005
Agriculture area	0.066	0.181	0.657	0.092	0.000	0.005
Barren land	0.106	0.320	0.347	0.220	0.000	0.009
Waterbody	0.149	0.203	0.525	0.088	0.032	0.004
Settlement	0.323	0.210	0.195	0.042	0.000	0.230

APPENDIX-C

Multiple Linear Regression (MLR) models developed between hydro-climatic variables and MODIS NDVI and land cover data products are as follows:

C1: MLR models for NDVI

$$NDVI_{monthly} = 1.287 + (0.632\times10^{-3}\times V1) + (0.101\times10^{-3}\times V2) + (-0.879\times10^{-2}\times V3) + (0.246\times10^{-2}\times V4) + (-0.223\times10^{-3}\times V5) + (-0.239\times10^{-3}\times V6) + (-0.171\times V7) + (-0.026\times V8) + (0.043\times V9)$$

$$NDVI_{winter} = 0.315 + (-0.868\times10^{-3}\times V1) + (0.055\times V2) + (0.037\times V3) + (0.212\times10^{-3}\times V4) + (-0.826\times10^{-2}\times V5) + (0.968\times10^{-2}\times V6) + (-0.015\times V7) + (-0.013\times V8) + (0.465\times V9)$$

$$NDVI_{pre-monsoon} = -14.953 + (-0.019\times V1) + (-1.375\times V2) + (-0.832\times10^{-2}\times V3) + (-0.041\times V4) + (0.260\times V5) + (0.044\times V6) + (12.686\times V7) + (0.543\times V8) + (-1.053\times V9)$$

$$NDVI_{SW-monsoon} = 110.990 + (0.199\times10^{-2}\times V1) + (7.527\times V2) + (-0.011\times V3) + (-0.743\times10^{-2}\times V4) + (-1.425\times V5) + (-0.022\times V6) + (-0.663\times V7) + (-3.687\times V8) + (1.765\times V9)$$

$$NDVI_{post-monsoon} = -6.935 + (2.026\times10^{-5}\times V1) + (-0.644\times V2) + (-0.086\times V3) + (-0.816\times10^{-2}\times V4) + (0.141\times V5) + (0.302\times10^{-2}\times V6) + (0.062\times V7) + (0.304\times V8) + (0.074\times V9)$$

$$NDVI_{annual} = 8.474 + (-0.763\times10^{-3}\times V1) + (0.163\times V2) + (0.261\times10^{-4}\times V3) + (-0.025\times V4) + (-0.048\times V5) + (2.005\times10^{-4}\times V6) + (2.244\times V7) + (-0.141\times V8) + (-0.312\times10^{-3}\times V9)$$

where, $V1$=P, $V2$=Tmax, $V3$=Tmin, $V4$=RH, $V5$=PET, $V6$=Q, $V7$=P/PET, $V8$= Tdiff, and $V9$=sediment

C2: MLR models for land cover

$$WTR = 11507.874 + (-1.259\times V1) + (276\times V2) + (13.392\times V3) + (-41.492\times V4) + (-77.306\times V5) + (2.376\times V6) + (3476.170\times V7) + (-178.685\times V8) + (185.612\times V9)$$

$$DBF = -35761.686 + (7.636\times V1) + (845\times V2) + (16.547\times V3) + (317.650\times V4) + (-50.582\times V5) + (-24.771\times V6) + (-19627.450\times V7) + (246.937\times V8) + (-460.871\times V9)$$

$$MXF = 36847.059 + (-7.811\times V1) + (1310\times V2) + (50.715\times V3) + (-102.597\times V4) + (-325.337\times V5) + (3.418\times V6) + (21140.321\times V7) + (-588.630\times V8) + (-594.803\times V9)$$

$$CSL = -1605.085 + (1.270\times V1) + (180\times V2) + (16.051\times V3) + (24.966\times V4) + (-26.550\times V5) + (-3.441\times V6) + (-3065.313\times V7) + (-29.525\times V8) + (14.595\times V9)$$

$$OSL = -4760.006 + (1.676 \times V1) + (113 \times V2) + (13.017 \times V3) + (22.545 \times V4) + (-1.977 \times V5) + (-4.559 \times V6) + (-3788.459 \times V7) + (5.052 \times V8) + (10.991 \times V9)$$

$$WSV = 8.081 + (-1.404 \times V1) + (1633 \times V2) + (-373.379 \times V3) + (-398.541 \times V4) + (-4.645 \times V5) + (15.579 \times V6) + (6159.441 \times V7) + (-1246.464 \times V8) + (-1218.800 \times V9)$$

$$SV = 345.139 + (0.087 \times V1) + (32 \times V2) + (-1.763 \times V3) + (1.183 \times V4) + (-6.171 \times V5) + (-0.185 \times V6) + (-201.841 \times V7) + (-12.029 \times V8) + (2.479 \times V9)$$

$$GL = 11650.714 + (-0.894 \times V1) + (275 \times V2) + (13.38831 \times V3) + (-34.822 \times V4) + (-75.166 \times V5) + (2.842 \times V6) + (1213.185 \times V7) + (-233.603 \times V8) + (-128.883 \times V9)$$

$$PWL = -1025.608 + (0.032 \times V1) + (-62 \times V2) + (-8.810 \times V3) + (1.350 \times V4) + (14.053 \times V5) + (0.425 \times V6) + (-142.190 \times V7) + (25.919 \times V8) + (-13.021 \times V9)$$

$$CL = -58951.618 + (-54.844 \times V1) + (-14400 \times V2) + (4875.467 \times V3) + (-1366.348 \times V4) + (2522.247 \times V5) + (197.662 \times V6) + (130038.607 \times V7) + (2875.467 \times V8) + (-7532.667 \times V9)$$

$$U\ \&\ B = 333.014 + (0.661 \times 10^{-2} \times V1) + (0.180 \times V2) + (-0.136 \times V3) + (0.078 \times V4) + (-0.317 \times 10^{-2} \times V5) + (-0.023 \times V6) + (-84.572 \times V7) + (0.149 \times V8) + (18.980 \times V9)$$

$$NV = -11332460 + (55.742 \times V1) + (0.850 \times V2) + (612885 \times V3) + (1578.825 \times V4) + (-1515.232 \times V5) + (-189.166 \times V6) + (-136849.016 \times V7) + (-885.452 \times V8) + (-6.240 \times V9)$$

$$BSV = -2480 + (-0.028 \times V1) + (-51 \times V2) + (-5.2466 \times V3) + (5.483 \times V4) + (16.927 \times V5) + (-0.240 \times V6) + (92.424 \times V7) + (42.280 \times V8) + (1.881 \times V9)$$

where, $V1$=P, $V2$=Tmax, $V3$=Tmin, $V4$=RH, $V5$=PET, $V6$=Q, $V7$=P/PET, $V8$= Tdiff, and $V9$=sediment

APPENDIX-D

Table D1: Sub-watershed wise number of HRUS, area, elevation and slope distributions

Sub-watershed	Number of HRUs	Area of sub-watershed (ha)	Mean elevation (m)	Average slope (m/m)
SW-1	17	11253.78	113.92	3.08
SW-2	41	43520.13	122.17	3.91
SW-3	33	52576.11	147.41	3.89
SW-4	26	19452.24	122.25	4.52
SW-5	39	55177.92	134.09	4.62
SW-6	112	176287.41	188.77	6.04
SW-7	44	40620.06	155.89	5.05
SW-8	42	76524.30	139.09	5.17
SW-9	81	119800.98	197.31	5.38
SW-10	91	179577.09	194.51	5.4
SW-11	80	48750.66	242.84	5.89
SW-12	58	33527.34	170.01	5.07
SW-13	68	55269.09	292.19	4.89
SW-14	53	4012.83	198.81	6.12
SW-15	124	94267.53	253.94	5.53
SW-16	62	4704.93	203.90	5.58
SW-17	37	21368.52	268.13	5.37
SW-18	44	2070.63	199.73	4.54
SW-19	87	141855.21	353.55	4.96
SW-20	75	43248.69	296.60	4.96
SW-21	73	30941.64	227.18	5.99
SW-22	63	64202.58	307.03	4.56
SW-23	96	153413.46	289.71	5.93
SW-24	58	16729.02	318.70	5.56
SW-25	68	14033.16	363.74	5.56
SW-26	62	109016.91	360.67	4.41
SW-27	120	136146.33	279.29	5.94
SW-28	81	159767.28	368.00	5.24
SW-29	57	98769.60	366.34	4.01
SW-30	97	197607.15	456.75	5.07
SW-31	58	161891.37	386.17	4.05
SW-32	96	90014.94	398.44	4.73
SW-33	88	134213.76	402.85	6.69
SW-34	48	47748.51	403.31	3.99
SW-35	78	135564.39	439.39	4.14
SW-36	44	135404.55	455.96	4.35
SW-37	35	32159.52	399.10	3.46
SW-38	47	68338.44	422.51	3.52
SW-39	72	86532.03	424.74	3.36
SW-40	99	196250.58	504.96	5.47
SW-41	48	52138.35	476.31	5.65
SW-42	77	84435.48	429.70	4.23

SW-43	64	43345.89	413.98	3.86
SW-44	57	85231.17	473.86	4.45
SW-45	19	10735.56	415.13	3.63
SW-46	73	56537.46	483.13	4.07
SW-47	64	59029.74	443.65	3.43
SW-48	37	44285.76	432.19	3.36
SW-49	53	143310.15	526.05	4.98
SW-50	19	4810.50	419.79	3.15
SW-51	102	73755.72	489.86	3.51
SW-52	103	45707.85	458.73	5.34
SW-53	106	110209.14	451.01	4.39
SW-54	108	74063.25	456.40	6.3
SW-55	96	54460.62	467.11	4.97
SW-56	113	78435.63	507.21	4.74
SW-57	81	63491.31	475.91	5.91

APPENDIX-E

E1: SWAT simulations using different land use maps and GCM-derived climate data

Table E1: Streamflow simulation using land use 2013

Sub-watershed	Streamflow (cumec) using land use 2013				
	Baseline 1986	Horizon 2020	Horizon 2040	Horizon 2060	Horizon 2080
SW-1	315.30	332.71	312.95	424.20	368.72
SW-2	314.72	332.12	312.59	423.76	368.17
SW-3	3.23	3.32	2.48	2.84	3.04
SW-4	292.53	307.60	294.25	399.54	343.76
SW-5	288.63	303.48	291.48	396.29	340.05
SW-6	188.86	199.93	200.37	273.99	228.79
SW-7	97.87	101.61	90.03	120.90	109.62
SW-8	20.21	22.35	17.17	22.88	22.53
SW-9	9.26	8.90	7.02	9.32	8.87
SW-10	15.66	18.52	14.59	19.77	19.14
SW-11	177.34	189.01	192.24	262.45	217.91
SW-12	86.57	90.60	81.56	109.84	98.85
SW-13	3.73	3.50	2.64	3.74	3.59
SW-14	84.97	88.98	80.46	108.52	97.38
SW-15	8.56	8.69	7.51	10.21	9.42
SW-16	76.13	80.02	72.75	98.04	87.70
SW-17	170.64	182.73	187.61	255.76	211.50
SW-18	75.75	79.64	72.44	97.56	87.28
SW-19	129.24	141.12	152.24	206.85	166.37
SW-20	128.58	140.17	151.04	205.93	165.47
SW-21	61.77	65.46	60.25	80.88	71.87
SW-22	41.04	41.64	35.96	48.86	45.10
SW-23	13.82	14.01	12.05	16.48	15.23
SW-24	25.53	25.91	22.43	30.35	28.04
SW-25	104.45	117.69	129.29	177.48	140.43
SW-26	9.91	10.05	8.67	11.80	10.90
SW-27	59.16	62.36	57.83	77.58	68.67
SW-28	33.67	35.76	33.85	45.33	39.27
SW-29	9.11	9.25	8.02	10.83	10.01
SW-30	15.00	14.19	15.96	19.60	16.60
SW-31	15.00	15.23	13.20	17.82	16.48
SW-32	162.16	178.19	190.69	233.38	195.04
SW-33	13.33	14.25	13.38	17.74	16.00
SW-34	140.69	155.34	168.91	204.25	169.96
SW-35	14.18	15.48	15.58	20.31	17.04
SW-36	10.75	10.25	11.45	13.97	11.89
SW-37	125.83	140.93	153.93	185.37	153.58
SW-38	94.54	106.51	118.73	139.74	115.68
SW-39	28.11	30.93	31.67	41.00	34.07
SW-40	19.59	21.48	21.62	28.48	23.75

SW-41	5.04	5.64	6.21	7.53	6.21
SW-42	8.56	9.52	10.49	12.60	10.45
SW-43	79.14	89.36	99.84	117.05	96.91
SW-44	8.75	9.76	10.72	12.86	10.72
SW-45	66.13	74.86	83.89	97.89	81.00
SW-46	5.79	6.45	7.09	8.51	7.09
SW-47	11.97	13.31	14.65	17.54	14.61
SW-48	53.05	60.32	67.89	78.74	65.06
SW-49	14.02	15.40	15.50	20.51	17.03
SW-50	37.18	42.69	48.49	55.47	45.72
SW-51	6.53	7.50	8.54	9.72	7.85
SW-52	10.12	11.62	13.30	15.67	12.54
SW-53	11.28	12.54	13.79	16.56	13.77
SW-54	26.60	30.55	34.61	39.11	32.61
SW-55	19.12	21.93	24.96	27.60	23.00
SW-56	7.26	8.32	9.42	10.69	8.70
SW-57	7.01	8.04	9.22	9.72	8.47

Table E2: Streamflow simulation using land use 2040

Sub-watershed	Streamflow (cumec) using land use 2040				
	Baseline 1986	Horizon 2020	Horizon 2040	Horizon 2060	Horizon 2080
SW-1	315.78	333.31	313.52	424.66	369.18
SW-2	315.21	332.68	313.16	424.26	368.62
SW-3	3.15	3.22	2.39	2.75	2.95
SW-4	293.54	308.77	295.39	400.55	344.70
SW-5	289.65	304.79	292.69	397.40	341.08
SW-6	189.50	200.78	201.12	274.73	229.50
SW-7	98.23	101.99	90.45	121.21	109.90
SW-8	19.73	21.77	16.61	22.35	22.05
SW-9	9.23	8.87	6.98	9.28	8.83
SW-10	15.56	18.39	14.46	19.63	19.00
SW-11	177.85	189.73	192.85	263.07	218.51
SW-12	86.93	90.99	81.99	110.18	99.15
SW-13	3.78	3.56	2.69	3.79	3.63
SW-14	85.35	89.37	80.90	108.87	97.69
SW-15	8.32	8.43	7.21	9.94	9.16
SW-16	76.76	80.69	73.49	98.65	88.27
SW-17	171.02	183.30	188.08	256.28	212.02
SW-18	76.38	80.31	73.18	98.17	87.85
SW-19	129.41	141.43	152.49	207.14	166.69
SW-20	128.84	140.59	151.38	206.33	165.88
SW-21	62.44	66.17	61.05	81.56	72.52
SW-22	41.20	41.82	36.13	49.00	45.23
SW-23	13.78	13.97	11.99	16.41	15.15
SW-24	25.61	26.01	22.53	30.43	28.11
SW-25	104.37	117.74	129.26	177.52	140.53
SW-26	10.03	10.18	8.80	11.92	11.00

SW-27	59.86	63.12	58.67	78.30	69.36
SW-28	34.34	36.49	34.65	46.03	39.95
SW-29	9.18	9.34	8.11	10.91	10.09
SW-30	15.00	14.18	15.97	19.61	16.62
SW-31	15.05	15.28	13.25	17.86	16.51
SW-32	161.52	177.53	189.94	232.70	194.48
SW-33	13.52	14.46	13.63	17.96	16.22
SW-34	139.83	154.45	167.90	203.33	169.17
SW-35	14.31	15.63	15.75	20.46	17.17
SW-36	10.72	10.22	11.42	13.94	11.86
SW-37	125.24	140.33	153.21	184.73	153.04
SW-38	94.04	106.00	118.11	139.20	115.24
SW-39	28.01	30.83	31.57	40.89	33.97
SW-40	19.84	21.74	21.91	28.74	24.00
SW-41	5.10	5.70	6.28	7.59	6.27
SW-42	8.57	9.54	10.51	12.62	10.46
SW-43	78.62	88.82	99.21	116.49	96.44
SW-44	8.69	9.70	10.65	12.80	10.67
SW-45	65.68	74.39	83.33	97.39	80.59
SW-46	5.74	6.40	7.03	8.45	7.04
SW-47	11.84	13.17	14.48	17.39	14.48
SW-48	52.74	60.00	67.49	78.40	64.78
SW-49	14.10	15.48	15.58	20.58	17.09
SW-50	37.10	42.61	48.38	55.39	45.67
SW-51	6.49	7.45	8.46	9.65	7.81
SW-52	10.12	11.62	13.29	15.65	12.55
SW-53	11.31	12.57	13.82	16.59	13.79
SW-54	26.52	30.48	34.52	39.04	32.55
SW-55	19.06	21.87	24.89	27.54	22.96
SW-56	7.22	8.27	9.36	10.63	8.66
SW-57	7.01	8.04	9.22	9.72	8.48

Table E3: Sediment yield simulation using land use 2013

Sub-watershed	Sediment yield (t/ha) using land use 2013				
	Baseline 1986	Horizon 2020	Horizon 2040	Horizon 2060	Horizon 2080
SW-1	181.87	185.96	181.73	261.62	223.49
SW-2	46.75	47.78	46.73	67.21	57.44
SW-3	0.00	0.00	0.00	0.00	0.00
SW-4	110.80	113.33	112.12	164.88	138.12
SW-5	38.95	39.84	39.42	57.97	48.56
SW-6	9.70	10.19	10.50	14.88	12.24
SW-7	18.25	18.90	17.00	24.39	21.67
SW-8	0.11	0.25	0.20	0.27	0.28
SW-9	0.00	0.00	0.00	0.00	0.00
SW-10	0.00	0.00	0.00	0.00	0.00
SW-11	33.07	34.94	36.60	51.73	42.31

SW-12	22.03	22.84	20.56	29.47	26.17
SW-13	0.00	0.00	0.00	0.00	0.00
SW-14	156.31	162.08	147.67	214.47	188.46
SW-15	0.00	0.00	0.00	0.00	0.00
SW-16	131.74	136.54	124.46	181.14	159.06
SW-17	79.05	84.81	88.01	122.15	100.14
SW-18	38.79	40.84	37.65	53.09	46.57
SW-19	0.88	0.89	0.98	1.33	0.92
SW-20	29.18	31.70	34.80	48.26	38.48
SW-21	1.70	1.79	1.67	2.36	2.06
SW-22	0.38	0.38	0.33	0.47	0.43
SW-23	0.00	0.00	0.00	0.00	0.00
SW-24	0.56	0.56	0.48	0.69	0.63
SW-25	5.29	5.06	5.57	7.42	4.47
SW-26	0.00	0.00	0.00	0.00	0.00
SW-27	0.26	0.28	0.26	0.36	0.31
SW-28	0.08	0.09	0.08	0.12	0.10
SW-29	0.00	0.00	0.00	0.00	0.00
SW-30	0.00	0.00	0.00	0.00	0.00
SW-31	0.00	0.00	0.00	0.00	0.00
SW-32	3.00	3.59	4.06	5.01	4.09
SW-33	0.00	0.00	0.00	0.00	0.00
SW-34	4.60	5.61	6.40	7.84	6.40
SW-35	0.00	0.00	0.00	0.00	0.00
SW-36	0.00	0.00	0.00	0.00	0.00
SW-37	5.53	6.93	7.93	9.64	7.87
SW-38	2.01	2.62	3.02	3.60	2.95
SW-39	0.12	0.13	0.14	0.18	0.15
SW-40	0.00	0.00	0.00	0.00	0.00
SW-41	0.00	0.00	0.00	0.00	0.00
SW-42	0.00	0.00	0.00	0.00	0.00
SW-43	2.55	3.45	3.96	4.70	3.86
SW-44	0.00	0.00	0.00	0.01	0.00
SW-45	9.05	12.59	14.44	17.06	14.07
SW-46	0.00	0.00	0.00	0.00	0.00
SW-47	0.55	1.05	1.17	1.36	1.16
SW-48	1.03	1.18	1.40	1.65	1.33
SW-49	0.00	0.00	0.00	0.00	0.00
SW-50	6.12	7.06	8.38	9.75	7.88
SW-51	0.00	0.00	0.00	0.00	0.00
SW-52	0.15	0.18	0.21	0.24	0.19
SW-53	0.00	0.00	0.00	0.00	0.00
SW-54	0.16	0.19	0.22	0.25	0.21
SW-55	0.11	0.12	0.15	0.16	0.13
SW-56	0.00	0.00	0.00	0.00	0.00
SW-57	0.00	0.01	0.01	0.01	0.00

Table E4: Sediment yield simulation using land use 2040

Sub-watershed	Sediment yield (t/ha) using land use 2040				
	Baseline 1986	Horizon 2020	Horizon 2040	Horizon 2060	Horizon 2080
SW-1	182.21	186.34	182.08	261.93	223.87
SW-2	46.83	47.88	46.82	67.29	57.54
SW-3	0.00	0.00	0.00	0.00	0.00
SW-4	111.18	113.81	112.57	165.33	138.58
SW-5	39.09	40.01	39.58	58.14	48.73
SW-6	9.73	10.22	10.53	14.91	12.27
SW-7	18.32	18.99	17.10	24.46	21.73
SW-8	0.11	0.24	0.20	0.27	0.28
SW-9	0.00	0.00	0.00	0.00	0.00
SW-10	0.00	0.00	0.00	0.00	0.00
SW-11	33.14	35.04	36.68	51.81	42.40
SW-12	22.12	22.94	20.67	29.57	26.26
SW-13	0.00	0.00	0.00	0.00	0.00
SW-14	157.49	163.44	149.12	215.80	189.62
SW-15	0.00	0.00	0.00	0.00	0.00
SW-16	132.77	137.69	125.72	182.28	160.06
SW-17	79.21	85.05	88.20	122.34	100.38
SW-18	39.25	41.36	38.23	53.66	47.03
SW-19	0.89	0.90	0.98	1.33	0.92
SW-20	29.21	31.75	34.84	48.31	38.54
SW-21	1.72	1.82	1.70	2.39	2.08
SW-22	0.38	0.38	0.33	0.47	0.43
SW-23	0.00	0.00	0.00	0.00	0.00
SW-24	0.56	0.56	0.48	0.69	0.63
SW-25	5.38	5.20	5.57	7.47	4.47
SW-26	0.00	0.00	0.00	0.00	0.00
SW-27	0.27	0.28	0.26	0.37	0.32
SW-28	0.08	0.09	0.09	0.12	0.10
SW-29	0.00	0.00	0.00	0.00	0.00
SW-30	0.00	0.00	0.00	0.00	0.00
SW-31	0.00	0.00	0.00	0.00	0.00
SW-32	2.99	3.57	4.04	4.99	4.07
SW-33	0.00	0.00	0.00	0.00	0.00
SW-34	4.58	5.59	6.36	7.81	6.37
SW-35	0.00	0.00	0.00	0.00	0.00
SW-36	0.00	0.00	0.00	0.00	0.00
SW-37	5.51	6.91	7.89	9.61	7.85
SW-38	2.01	2.61	3.00	3.59	2.94
SW-39	0.12	0.13	0.14	0.18	0.15
SW-40	0.00	0.00	0.00	0.00	0.00
SW-41	0.00	0.00	0.00	0.00	0.00
SW-42	0.00	0.00	0.00	0.00	0.00
SW-43	2.55	3.43	3.94	4.68	3.85
SW-44	0.00	0.01	0.00	0.01	0.00

SW-45	9.03	12.55	14.35	17.00	14.02
SW-46	0.00	0.00	0.00	0.00	0.00
SW-47	0.55	1.05	1.16	1.36	1.15
SW-48	1.02	1.18	1.39	1.64	1.33
SW-49	0.00	0.00	0.00	0.00	0.00
SW-50	6.12	7.06	8.37	9.77	7.90
SW-51	0.00	0.00	0.00	0.00	0.00
SW-52	0.15	0.18	0.21	0.24	0.19
SW-53	0.00	0.00	0.00	0.00	0.00
SW-54	0.16	0.19	0.22	0.25	0.21
SW-55	0.11	0.12	0.15	0.16	0.13
SW-56	0.00	0.00	0.00	0.01	0.00
SW-57	0.00	0.01	0.01	0.01	0.00

Table E5: Evapotranspiration simulation using land use 2013

Sub-watershed	Evapotranspiration (mm) using land use 2013				
	Baseline 1986	Horizon 2020	Horizon 2040	Horizon 2060	Horizon 2080
SW-1	460.15	478.20	460.30	454.25	433.35
SW-2	477.25	497.60	477.50	472.10	451.25
SW-3	442.65	461.45	446.60	442.55	428.80
SW-4	504.55	524.70	505.35	500.55	481.00
SW-5	502.45	525.05	509.55	505.65	492.10
SW-6	481.15	495.70	478.35	471.75	466.90
SW-7	476.50	497.75	481.25	476.00	461.50
SW-8	441.30	458.80	445.15	442.25	429.55
SW-9	462.30	474.85	457.35	452.90	448.85
SW-10	535.40	557.90	539.00	533.15	537.55
SW-11	532.85	551.25	536.05	527.05	520.95
SW-12	475.45	498.05	481.35	476.65	460.45
SW-13	511.55	530.05	512.45	499.95	490.65
SW-14	497.35	510.40	494.85	491.50	488.00
SW-15	506.45	517.20	513.00	500.20	503.90
SW-16	501.05	511.80	507.50	495.45	499.05
SW-17	523.10	542.95	527.75	518.80	512.55
SW-18	770.55	783.20	788.70	792.10	805.00
SW-19	580.80	599.70	586.50	582.35	579.35
SW-20	538.70	556.45	541.15	533.85	528.10
SW-21	496.15	520.20	498.85	491.10	493.50
SW-22	526.45	538.75	535.60	521.05	525.55
SW-23	502.60	514.00	510.60	495.45	498.25
SW-24	520.25	532.60	529.25	512.90	516.90
SW-25	525.50	537.55	533.95	518.65	522.75
SW-26	522.70	534.25	530.90	519.15	523.10
SW-27	491.60	502.45	498.75	484.00	486.30
SW-28	491.05	502.45	498.65	482.25	484.95
SW-29	490.90	501.80	496.70	485.40	488.45

SW-30	479.05	500.90	495.45	496.35	482.80
SW-31	487.15	498.00	492.95	481.50	484.45
SW-32	780.25	795.25	801.90	797.85	811.50
SW-33	504.65	513.10	519.50	499.65	496.90
SW-34	499.00	510.30	508.45	493.65	497.80
SW-35	496.55	511.85	516.70	497.05	490.25
SW-36	458.45	477.50	472.80	473.95	460.50
SW-37	502.10	517.15	521.45	504.45	500.60
SW-38	486.55	503.90	516.25	499.55	483.20
SW-39	499.95	514.30	518.60	502.00	497.70
SW-40	526.65	541.55	546.60	525.95	519.20
SW-41	501.40	518.75	533.45	512.70	492.20
SW-42	477.85	495.75	507.50	489.00	470.60
SW-43	467.05	486.10	496.90	480.10	463.00
SW-44	489.30	506.30	517.45	499.15	480.40
SW-45	437.75	456.50	465.45	448.40	430.30
SW-46	519.10	536.60	548.65	531.65	514.55
SW-47	450.00	467.30	476.30	459.05	441.00
SW-48	445.60	464.60	474.50	457.05	438.95
SW-49	539.30	554.05	559.50	538.85	533.05
SW-50	441.80	460.40	468.85	452.30	434.85
SW-51	566.20	590.15	601.05	590.00	569.55
SW-52	449.75	467.25	478.75	459.55	439.15
SW-53	466.35	484.60	495.90	476.75	457.10
SW-54	472.25	490.90	505.65	485.05	463.00
SW-55	453.25	477.00	487.45	470.55	441.35
SW-56	480.65	502.75	513.05	498.90	474.40
SW-57	491.25	504.25	520.55	503.25	483.15

Table E6: Evapotranspiration simulation using land use 2040

Sub-watershed	Evapotranspiration (mm) using land use 2040				
	Baseline 1986	Horizon 2020	Horizon 2040	Horizon 2060	Horizon 2080
SW-1	411.25	430.40	409.05	402.10	379.70
SW-2	414.25	433.60	411.80	404.70	382.85
SW-3	453.15	474.10	459.15	454.85	440.70
SW-4	456.80	476.00	453.35	445.50	422.60
SW-5	459.25	480.25	464.15	459.75	445.10
SW-6	456.90	470.40	452.50	446.30	441.25
SW-7	463.05	483.65	467.20	462.00	447.50
SW-8	438.90	461.55	445.75	439.70	423.75
SW-9	441.15	453.50	434.80	429.55	424.40
SW-10	476.60	499.95	477.60	469.40	471.55
SW-11	477.50	494.20	477.05	467.80	460.55
SW-12	461.35	483.85	466.45	460.65	443.40
SW-13	493.95	511.20	493.45	481.55	472.85
SW-14	430.70	442.30	423.80	418.90	413.50
SW-15	491.15	503.00	499.25	481.90	484.55

SW-16	467.35	478.05	473.15	458.85	461.15
SW-17	487.60	508.30	491.35	480.00	470.90
SW-18	448.15	458.35	453.05	440.30	441.40
SW-19	459.25	475.60	457.20	449.95	443.45
SW-20	478.00	493.80	475.60	467.85	460.35
SW-21	482.50	508.35	485.00	476.80	478.50
SW-22	489.20	501.25	497.35	480.25	483.35
SW-23	477.65	488.55	484.85	468.60	470.75
SW-24	511.05	523.90	521.55	501.45	504.75
SW-25	476.10	486.35	479.75	466.65	469.30
SW-26	463.35	474.15	468.20	455.40	457.40
SW-27	476.50	487.65	484.55	467.95	470.15
SW-28	460.20	469.90	463.40	449.85	451.65
SW-29	461.20	470.90	464.25	452.65	455.00
SW-30	467.70	489.30	483.40	483.70	469.30
SW-31	454.65	465.15	459.05	446.45	448.40
SW-32	581.70	594.65	593.70	579.85	586.05
SW-33	477.30	485.00	489.05	469.85	466.05
SW-34	510.85	525.15	523.30	503.10	506.30
SW-35	487.40	502.15	506.30	486.80	480.45
SW-36	448.60	467.55	462.30	463.15	448.65
SW-37	479.20	494.15	497.65	479.70	474.75
SW-38	466.90	484.30	496.10	478.30	460.90
SW-39	500.45	515.05	520.60	501.45	495.05
SW-40	512.20	527.05	531.05	511.05	504.40
SW-41	494.90	511.65	525.50	505.35	485.65
SW-42	468.30	486.20	497.45	478.60	459.65
SW-43	455.80	474.70	485.65	467.75	449.50
SW-44	462.95	479.65	491.15	470.60	449.05
SW-45	432.20	451.25	460.20	442.50	423.80
SW-46	469.80	487.60	499.50	479.05	457.45
SW-47	446.35	464.40	474.35	455.45	435.55
SW-48	479.70	499.80	515.00	492.85	469.30
SW-49	530.15	545.20	550.25	529.55	523.75
SW-50	424.05	442.40	450.75	432.90	413.35
SW-51	453.30	478.75	489.35	472.30	442.25
SW-52	443.45	460.85	471.50	452.30	431.85
SW-53	459.00	477.35	488.40	469.05	449.25
SW-54	462.50	481.15	495.85	474.55	451.65
SW-55	438.15	461.40	471.65	453.50	422.55
SW-56	424.85	447.10	456.85	440.05	410.40
SW-57	465.45	477.90	494.10	475.60	454.20

Table E7: Water yield simulation using land use 2013

Sub-watershed	Water yield (mm) using land use 2013				
	Baseline 1986	Horizon 2020	Horizon 2040	Horizon 2060	Horizon 2080
SW-1	399.67	427.00	276.67	310.46	387.60
SW-2	386.41	411.70	264.16	296.71	374.02
SW-3	389.14	399.64	299.73	343.11	367.03
SW-4	377.28	402.50	255.87	287.75	365.14
SW-5	364.57	371.63	273.42	317.38	343.79
SW-6	465.57	444.40	345.05	467.58	444.59
SW-7	366.44	374.89	276.75	320.77	346.88
SW-8	402.46	414.63	313.45	357.00	380.06
SW-9	490.96	471.72	373.01	494.34	470.40
SW-10	555.60	656.50	518.41	700.55	678.40
SW-11	442.47	417.07	317.08	441.73	422.88
SW-12	374.02	381.17	282.79	328.15	355.53
SW-13	427.80	401.74	302.54	428.83	411.51
SW-14	498.68	479.88	380.93	502.86	480.08
SW-15	575.55	584.65	505.15	686.03	633.82
SW-16	586.75	595.70	516.05	696.96	644.68
SW-17	452.93	426.14	325.69	450.95	431.81
SW-18	612.80	622.80	544.25	722.71	671.33
SW-19	459.64	434.96	335.46	459.57	438.96
SW-20	445.11	420.62	321.11	445.02	425.24
SW-21	554.55	654.20	516.06	698.40	677.05
SW-22	565.65	572.90	492.85	674.91	622.18
SW-23	574.50	582.70	502.25	684.22	633.25
SW-24	554.45	561.60	481.05	664.03	610.89
SW-25	555.20	562.30	482.40	665.60	612.29
SW-26	579.65	587.80	507.95	689.37	637.32
SW-27	579.55	588.30	507.55	688.94	637.78
SW-28	573.55	581.40	500.85	683.59	631.94
SW-29	587.75	596.75	517.95	697.67	645.21
SW-30	485.80	459.98	516.75	633.04	537.34
SW-31	592.95	602.10	522.95	703.55	651.49
SW-32	550.53	556.49	475.05	659.89	606.74
SW-33	631.60	675.25	634.90	839.07	757.95
SW-34	570.90	578.80	497.10	679.21	625.78
SW-35	665.15	726.00	730.95	951.80	798.29
SW-36	507.12	484.10	540.38	658.10	560.45
SW-37	678.75	738.80	746.35	964.20	809.74
SW-38	644.70	718.10	790.40	946.70	784.60
SW-39	675.25	736.70	743.75	961.65	806.64
SW-40	637.85	698.40	703.10	923.91	772.15
SW-41	611.25	684.05	752.50	914.15	753.20
SW-42	643.20	715.45	787.80	945.95	784.55
SW-43	658.85	730.05	803.05	959.55	797.60
SW-44	652.25	727.35	798.75	956.80	799.30

SW-45	681.75	753.30	827.70	984.95	823.15
SW-46	647.10	720.70	792.20	950.35	791.85
SW-47	675.55	749.10	822.90	980.65	819.35
SW-48	671.85	742.45	816.60	974.00	812.35
SW-49	624.70	685.40	690.05	910.60	757.47
SW-50	689.75	762.35	838.30	995.00	833.00
SW-51	559.55	642.95	731.60	832.50	672.45
SW-52	665.80	738.55	810.10	968.95	810.35
SW-53	648.90	721.60	793.05	951.70	792.35
SW-54	651.05	748.90	836.75	996.75	834.60
SW-55	572.30	656.85	743.60	846.50	689.10
SW-56	586.05	671.25	759.55	861.80	700.85
SW-57	697.50	800.50	917.55	966.75	842.95

Table E8: Water yield simulation using land use 2040

Sub-watershed	Water yield (mm) using land use 2040				
	Baseline 1986	Horizon 2020	Horizon 2040	Horizon 2060	Horizon 2080
SW-1	386.09	410.40	263.44	297.31	375.86
SW-2	376.59	400.70	255.12	288.38	366.93
SW-3	379.82	388.09	287.94	331.48	355.80
SW-4	374.50	400.18	253.88	286.40	364.11
SW-5	368.89	376.93	278.14	321.33	346.72
SW-6	469.87	448.90	349.44	471.44	447.78
SW-7	370.10	378.97	280.43	323.77	348.93
SW-8	370.64	376.04	276.46	323.05	349.91
SW-9	489.44	470.34	371.14	492.48	468.72
SW-10	551.65	651.80	513.63	695.25	673.45
SW-11	450.87	426.33	326.53	450.41	429.16
SW-12	371.65	378.75	280.24	325.77	353.20
SW-13	433.07	408.26	309.02	434.59	416.03
SW-14	500.06	481.20	382.10	503.10	479.55
SW-15	559.60	566.35	485.55	668.71	616.47
SW-16	582.50	591.05	511.15	691.94	639.66
SW-17	444.40	416.13	315.17	440.85	422.80
SW-18	601.45	610.65	531.10	710.35	659.26
SW-19	469.90	446.20	346.96	469.60	447.90
SW-20	453.51	430.31	330.82	453.34	432.94
SW-21	546.55	644.25	506.96	688.60	667.65
SW-22	561.69	568.15	487.65	670.51	617.61
SW-23	572.90	581.25	499.70	681.79	629.97
SW-24	540.16	546.00	463.60	648.35	595.84
SW-25	573.75	582.45	504.50	684.54	631.11
SW-26	585.90	594.80	515.60	695.70	642.60
SW-27	571.50	579.70	497.95	680.07	627.72
SW-28	589.65	599.70	521.05	701.30	649.09
SW-29	592.40	602.05	524.00	703.09	650.80
SW-30	485.56	459.87	516.92	633.20	537.76

SW-31	594.70	604.05	524.90	704.91	652.84
SW-32	554.38	561.45	480.85	664.76	612.41
SW-33	640.40	684.80	646.55	850.45	768.14
SW-34	540.01	544.33	461.49	647.29	594.68
SW-35	671.55	732.95	738.90	958.05	805.30
SW-36	505.81	482.45	538.98	656.85	559.40
SW-37	680.20	740.50	747.20	965.30	811.04
SW-38	645.25	718.75	791.10	947.70	785.05
SW-39	658.50	720.10	724.55	944.00	789.73
SW-40	645.85	706.65	712.05	932.45	779.81
SW-41	617.85	691.25	760.70	921.11	760.40
SW-42	644.70	717.05	789.35	947.70	786.30
SW-43	656.10	728.25	801.35	958.15	796.15
SW-44	648.05	722.55	792.90	952.70	795.10
SW-45	680.10	751.80	826.15	984.40	822.20
SW-46	641.15	714.10	785.05	944.05	786.70
SW-47	666.55	739.10	812.45	970.15	809.85
SW-48	633.25	704.00	770.95	932.90	776.40
SW-49	627.85	688.85	692.90	913.99	761.07
SW-50	688.45	760.50	835.45	993.15	832.30
SW-51	555.95	638.20	725.05	826.95	669.38
SW-52	668.95	742.00	814.95	973.20	813.90
SW-53	650.20	722.95	795.45	953.55	793.70
SW-54	650.15	748.05	836.05	995.25	833.40
SW-55	570.60	655.40	741.90	845.05	688.65
SW-56	582.15	667.30	754.90	857.40	698.50
SW-57	697.35	800.60	917.55	967.30	843.30

E2: Land use change impact assessment

Table E9: Changes in land use classes during 2013-2040

Sub-watershed	Percent changes in each land use class during 2013-2040					
	Dense forest	Degraded forest	Agriculture	Barren land	Waterbody	Settlement
SW-1	0.02	16.14	-43.90	28.29	-2.60	2.05
SW-2	5.83	6.07	-29.73	20.60	-2.97	0.20
SW-3	-9.17	0.29	1.33	6.94	-0.10	0.71
SW-4	2.95	-0.55	-39.21	41.34	-4.53	0.00
SW-5	-7.66	1.52	-5.19	14.47	-3.15	0.00
SW-6	-8.98	3.79	1.32	5.26	-1.55	0.17
SW-7	-7.70	3.70	-5.00	8.27	-1.05	1.78
SW-8	0.37	7.31	-17.94	10.87	-1.11	0.51
SW-9	-2.92	2.85	-0.01	2.05	-2.10	0.13
SW-10	-4.08	3.14	6.95	-0.75	-5.50	0.24
SW-11	-9.63	0.52	6.86	5.67	-4.04	0.61
SW-12	-2.38	2.86	-19.53	20.67	-1.62	0.00
SW-13	-14.57	6.86	-3.50	12.19	-0.87	0.00

SW-14	-10.13	5.71	2.79	2.92	-5.64	4.35
SW-15	-5.47	24.99	-25.17	7.86	-2.97	0.76
SW-16	-3.68	9.47	-8.17	5.86	-3.48	0.00
SW-17	-3.04	18.15	-24.69	13.65	-4.05	0.00
SW-18	-3.35	26.06	6.46	-1.05	-28.13	0.00
SW-19	-10.22	1.43	2.44	14.20	-7.88	0.02
SW-20	-11.36	2.11	-5.44	18.75	-4.73	0.67
SW-21	-4.74	14.28	-8.99	-0.66	-1.95	2.05
SW-22	-8.16	15.05	-29.17	26.11	-3.83	0.00
SW-23	-13.12	16.35	-14.31	13.62	-2.51	0.00
SW-24	-9.05	27.84	-36.34	19.88	-2.34	0.00
SW-25	-9.40	-11.07	18.36	5.01	-2.89	0.00
SW-26	-8.58	1.27	-1.38	11.34	-4.62	1.98
SW-27	-10.83	22.08	-13.29	4.01	-1.97	0.00
SW-28	-6.00	-8.51	8.43	7.48	-1.41	0.00
SW-29	-4.61	-0.65	-3.22	10.82	-2.34	0.00
SW-30	3.84	3.95	-13.34	6.46	-1.01	0.09
SW-31	-4.40	2.33	-2.42	7.27	-2.75	0.00
SW-32	6.98	-4.94	9.58	6.14	-17.75	0.00
SW-33	5.94	-17.04	11.19	1.38	-1.47	0.00
SW-34	2.93	-2.42	-1.98	3.03	-1.93	0.36
SW-35	1.19	-8.69	5.95	1.92	-0.45	0.07
SW-36	1.94	0.50	-12.02	10.22	-1.07	0.43
SW-37	-1.11	0.72	2.07	-0.21	-2.03	0.55
SW-38	-1.27	0.41	-1.35	3.38	-1.71	0.54
SW-39	-3.23	4.02	-0.80	0.52	-1.59	1.07
SW-40	-0.58	-9.55	10.54	0.59	-0.61	0.00
SW-41	-6.38	-2.72	7.19	2.07	-0.17	0.00
SW-42	-1.56	2.03	-1.34	1.72	-0.86	0.00
SW-43	-0.32	4.99	-3.56	-0.09	-1.21	0.18
SW-44	-0.78	-1.26	-8.86	13.44	-2.53	0.00
SW-45	-0.61	3.90	-2.87	0.26	-0.68	0.00
SW-46	1.34	15.92	-16.25	3.62	-4.47	0.00
SW-47	0.29	11.81	-12.24	1.30	-1.16	0.00
SW-48	-1.62	1.17	-2.08	3.09	-0.54	0.00
SW-49	-3.61	-0.11	4.17	0.11	-0.59	0.03
SW-50	-0.13	5.86	-2.28	-0.97	-1.70	0.00
SW-51	0.42	17.93	-9.28	0.34	-8.39	0.00
SW-52	1.04	-3.00	-8.70	11.00	-0.37	0.02
SW-53	-2.48	-0.21	0.78	2.30	-0.41	0.02
SW-54	-2.19	3.08	-8.53	8.57	-0.97	0.03
SW-55	3.84	4.20	-14.70	8.52	-1.39	0.00
SW-56	6.84	12.03	-13.13	-1.30	-3.80	0.00
SW-57	1.31	2.43	-1.02	-0.81	-1.85	0.00

Table E10: Changes in SWAT simulation under varying land use (2013-2040)

Sub-watershed	Streamflow (cumec)	Sediment yield (t/ha)	ET (mm)	Water yield (mm)
SW-1	0.48	0.34	-48.90	-13.59
SW-2	0.49	0.08	-63.00	-9.82
SW-3	-0.08	0.00	10.50	-9.32
SW-4	1.00	0.38	-47.75	-2.78
SW-5	1.02	0.14	-43.20	4.32
SW-6	0.64	0.02	-24.25	4.30
SW-7	0.36	0.08	-13.45	3.66
SW-8	-0.48	0.00	-2.40	-31.82
SW-9	-0.03	0.00	-21.15	-1.52
SW-10	-0.10	0.00	-58.80	-3.95
SW-11	0.51	0.07	-55.35	8.39
SW-12	0.36	0.09	-14.10	-2.38
SW-13	0.05	0.00	-17.60	5.27
SW-14	0.38	1.18	-66.65	1.38
SW-15	-0.24	0.00	-15.30	-15.95
SW-16	0.63	1.03	-33.70	-4.25
SW-17	0.39	0.15	-35.50	-8.54
SW-18	0.63	0.47	-322.40	-11.35
SW-19	0.17	0.01	-121.55	10.26
SW-20	0.25	0.03	-60.70	8.40
SW-21	0.67	0.02	-13.65	-8.00
SW-22	0.16	0.00	-37.25	-3.96
SW-23	-0.04	0.00	-24.95	-1.60
SW-24	0.08	0.00	-9.20	-14.30
SW-25	-0.08	0.09	-49.40	18.55
SW-26	0.12	0.00	-59.35	6.25
SW-27	0.70	0.00	-15.10	-8.05
SW-28	0.67	0.00	-30.85	16.10
SW-29	0.07	0.00	-29.70	4.65
SW-30	-0.01	0.00	-11.35	-0.24
SW-31	0.05	0.00	-32.50	1.75
SW-32	-0.65	-0.01	-198.55	3.85
SW-33	0.19	0.00	-27.35	8.80
SW-34	-0.86	-0.02	11.85	-30.90
SW-35	0.13	0.00	-9.15	6.40
SW-36	-0.03	0.00	-9.85	-1.31
SW-37	-0.59	-0.02	-22.90	1.45
SW-38	-0.50	-0.01	-19.65	0.55
SW-39	-0.10	0.00	0.50	-16.75
SW-40	0.25	0.00	-14.45	8.00
SW-41	0.06	0.00	-6.50	6.60
SW-42	0.02	0.00	-9.55	1.50
SW-43	-0.52	-0.01	-11.25	-2.75
SW-44	-0.06	0.00	-26.35	-4.20
SW-45	-0.45	-0.02	-5.55	-1.65

SW-46	-0.05	0.00	-49.30	-5.95
SW-47	-0.13	0.00	-3.65	-9.00
SW-48	-0.31	0.00	34.10	-38.60
SW-49	0.08	0.00	-9.15	3.15
SW-50	-0.08	-0.01	-17.75	-1.30
SW-51	-0.04	0.00	-112.90	-3.60
SW-52	0.00	0.00	-6.30	3.15
SW-53	0.03	0.00	-7.35	1.30
SW-54	-0.08	0.00	-9.75	-0.90
SW-55	-0.06	0.00	-15.10	-1.70
SW-56	-0.05	0.00	-55.80	-3.90
SW-57	0.00	0.00	-25.80	-0.15

E3: Climate change impact assessment

Table E11: Changes in future precipitation at sub-watershed level

Sub-watershed	Horizon 2020	Horizon 2040	Horizon 2060	Horizon 2080
SW-1	43.60	-127.10	-93.15	-41.85
SW-2	43.60	-127.10	-93.15	-41.85
SW-3	28.35	-89.20	-40.45	-34.20
SW-4	43.60	-127.10	-93.15	-41.85
SW-5	28.35	-89.20	-40.45	-34.20
SW-6	-7.60	-127.35	-5.20	-34.35
SW-7	28.35	-89.20	-40.45	-34.20
SW-8	28.35	-89.20	-40.45	-34.20
SW-9	-7.60	-127.35	-5.20	-34.35
SW-10	121.95	-38.85	140.25	117.65
SW-11	-7.10	-126.80	-4.65	-34.30
SW-12	28.35	-89.20	-40.45	-34.20
SW-13	-7.10	-126.80	-4.65	-34.30
SW-14	-7.65	-127.35	-5.20	-34.40
SW-15	19.85	-66.90	107.00	52.90
SW-16	19.85	-66.90	107.05	52.95
SW-17	-7.65	-127.35	-5.20	-34.40
SW-18	19.85	-66.90	107.05	52.95
SW-19	-7.65	-127.35	-5.20	-34.40
SW-20	-7.65	-127.35	-5.20	-34.40
SW-21	121.90	-38.90	140.25	117.55
SW-22	19.85	-66.90	107.05	52.95
SW-23	19.85	-66.90	107.00	52.90
SW-24	19.85	-66.90	107.05	52.95
SW-25	19.85	-66.90	107.05	52.95
SW-26	19.85	-66.90	107.05	52.95
SW-27	19.85	-66.90	107.05	52.95
SW-28	19.85	-66.90	107.00	52.90
SW-29	19.85	-66.90	107.05	52.95

SW-30	-7.30	41.80	170.10	54.30
SW-31	19.85	-66.90	107.05	52.95
SW-32	19.85	-66.90	107.05	52.95
SW-33	49.70	15.75	206.05	116.65
SW-34	19.85	-66.90	107.05	52.95
SW-35	74.05	85.15	290.40	128.15
SW-36	-7.30	41.80	170.10	54.30
SW-37	74.05	85.15	290.40	128.15
SW-38	87.70	171.20	316.55	132.75
SW-39	74.05	85.15	290.40	128.15
SW-40	74.05	85.15	290.40	128.15
SW-41	87.70	171.20	316.55	132.75
SW-42	87.70	171.20	316.55	132.75
SW-43	87.70	171.20	316.55	132.75
SW-44	87.70	171.20	316.55	132.75
SW-45	87.70	171.20	316.55	132.75
SW-46	87.70	171.20	316.55	132.75
SW-47	87.70	171.20	316.55	132.75
SW-48	87.70	171.20	316.55	132.75
SW-49	74.05	85.15	290.40	128.15
SW-50	87.70	171.20	316.55	132.75
SW-51	104.50	202.95	292.80	100.15
SW-52	87.70	171.20	316.55	132.75
SW-53	87.70	171.20	316.55	132.75
SW-54	114.05	220.15	363.10	172.60
SW-55	104.50	202.95	292.80	100.15
SW-56	104.50	202.95	292.80	100.15
SW-57	114.75	249.45	284.70	134.05

Table E12: Changes in streamflow simulation under varying future precipitation

Sub-watershed	Horizon 2020	Horizon 2040	Horizon 2060	Horizon 2080
SW-1	17.42	-2.34	108.90	53.43
SW-2	17.40	-2.13	109.03	53.45
SW-3	0.09	-0.75	-0.39	-0.19
SW-4	15.07	1.71	107.01	51.22
SW-5	14.84	2.85	107.66	51.42
SW-6	11.07	11.51	85.13	39.93
SW-7	3.74	-7.84	23.03	11.75
SW-8	2.14	-3.04	2.67	2.32
SW-9	-0.36	-2.24	0.06	-0.39
SW-10	2.86	-1.07	4.11	3.48
SW-11	11.68	14.90	85.11	40.57
SW-12	4.03	-5.01	23.28	12.28
SW-13	-0.23	-1.10	0.01	-0.14
SW-14	4.00	-4.51	23.54	12.41
SW-15	0.13	-1.06	1.64	0.86

SW-16	3.89	-3.38	21.91	11.57
SW-17	12.09	16.97	85.13	40.86
SW-18	3.89	-3.31	21.81	11.53
SW-19	11.88	23.00	77.61	37.13
SW-20	11.59	22.46	77.35	36.89
SW-21	3.69	-1.52	19.11	10.10
SW-22	0.60	-5.08	7.82	4.07
SW-23	0.20	-1.77	2.66	1.41
SW-24	0.39	-3.10	4.83	2.51
SW-25	13.24	24.84	73.03	35.98
SW-26	0.14	-1.24	1.89	0.99
SW-27	3.20	-1.33	18.42	9.51
SW-28	2.09	0.18	11.65	5.60
SW-29	0.14	-1.10	1.72	0.89
SW-30	-0.82	0.96	4.60	1.60
SW-31	0.23	-1.80	2.82	1.47
SW-32	16.03	28.52	71.21	32.88
SW-33	0.93	0.06	4.41	2.67
SW-34	14.65	28.22	63.56	29.27
SW-35	1.30	1.40	6.13	2.86
SW-36	-0.50	0.70	3.22	1.14
SW-37	15.10	28.10	59.54	27.75
SW-38	11.97	24.19	45.20	21.14
SW-39	2.82	3.57	12.89	5.96
SW-40	1.89	2.03	8.89	4.16
SW-41	0.60	1.17	2.49	1.17
SW-42	0.97	1.93	4.04	1.89
SW-43	10.22	20.70	37.91	17.76
SW-44	1.00	1.97	4.10	1.97
SW-45	8.73	17.76	31.76	14.87
SW-46	0.66	1.30	2.72	1.30
SW-47	1.34	2.68	5.56	2.63
SW-48	7.27	14.84	25.68	12.00
SW-49	1.38	1.48	6.49	3.01
SW-50	5.51	11.31	18.30	8.54
SW-51	0.97	2.01	3.19	1.32
SW-52	1.51	3.19	5.55	2.43
SW-53	1.26	2.51	5.28	2.49
SW-54	3.95	8.01	12.51	6.01
SW-55	2.81	5.84	8.48	3.88
SW-56	1.06	2.16	3.42	1.43
SW-57	1.03	2.21	2.70	1.46

Table E13: Changes in sediment yield simulation under varying future precipitation

Sub-watershed	Horizon 2020	Horizon 2040	Horizon 2060	Horizon 2080
SW-1	4.08	-0.14	79.75	41.62
SW-2	1.03	-0.02	20.46	10.69
SW-3	0.00	0.00	0.00	0.00
SW-4	2.53	1.32	54.08	27.32
SW-5	0.89	0.47	19.02	9.62
SW-6	0.48	0.80	5.18	2.54
SW-7	0.66	-1.24	6.14	3.42
SW-8	0.14	0.09	0.16	0.17
SW-9	0.00	0.00	0.00	0.00
SW-10	0.00	0.00	0.00	0.00
SW-11	1.87	3.53	18.65	9.23
SW-12	0.81	-1.47	7.44	4.15
SW-13	0.00	0.00	0.00	0.00
SW-14	5.77	-8.64	58.16	32.14
SW-15	0.00	0.00	0.00	0.00
SW-16	4.79	-7.28	49.40	27.32
SW-17	5.76	8.96	43.09	21.09
SW-18	2.06	-1.13	14.30	7.78
SW-19	0.01	0.10	0.45	0.04
SW-20	2.51	5.62	19.08	9.29
SW-21	0.09	-0.03	0.66	0.36
SW-22	0.00	-0.05	0.09	0.05
SW-23	0.00	0.00	0.00	0.00
SW-24	0.00	-0.08	0.13	0.07
SW-25	-0.22	0.28	2.14	-0.82
SW-26	0.00	0.00	0.00	0.00
SW-27	0.01	0.00	0.10	0.05
SW-28	0.00	0.00	0.03	0.02
SW-29	0.00	0.00	0.00	0.00
SW-30	0.00	0.00	0.00	0.00
SW-31	0.00	0.00	0.00	0.00
SW-32	0.58	1.05	2.00	1.09
SW-33	0.00	0.00	0.00	0.00
SW-34	1.01	1.80	3.24	1.80
SW-35	0.00	0.00	0.00	0.00
SW-36	0.00	0.00	0.00	0.00
SW-37	1.41	2.40	4.11	2.34
SW-38	0.60	1.00	1.59	0.94
SW-39	0.01	0.02	0.07	0.03
SW-40	0.00	0.00	0.00	0.00
SW-41	0.00	0.00	0.00	0.00
SW-42	0.00	0.00	0.00	0.00
SW-43	0.89	1.41	2.15	1.31
SW-44	0.00	0.00	0.00	0.00
SW-45	3.54	5.39	8.01	5.02

SW-46	0.00	0.00	0.00	0.00
SW-47	0.50	0.61	0.81	0.60
SW-48	0.15	0.37	0.62	0.31
SW-49	0.00	0.00	0.00	0.00
SW-50	0.94	2.26	3.63	1.76
SW-51	0.00	0.00	0.00	0.00
SW-52	0.02	0.05	0.09	0.04
SW-53	0.00	0.00	0.00	0.00
SW-54	0.02	0.06	0.09	0.04
SW-55	0.02	0.04	0.06	0.03
SW-56	0.00	0.00	0.00	0.00
SW-57	0.00	0.00	0.00	0.00

Table E14: Changes in evapotranspiration simulation under varying future precipitation

Sub-watershed	Horizon 2020	Horizon 2040	Horizon 2060	Horizon 2080
SW-1	18.05	0.15	-5.90	-26.80
SW-2	20.35	0.25	-5.15	-26.00
SW-3	18.80	3.95	-0.10	-13.85
SW-4	20.15	0.80	-4.00	-23.55
SW-5	22.60	7.10	3.20	-10.35
SW-6	14.55	-2.80	-9.40	-14.25
SW-7	21.25	4.75	-0.50	-15.00
SW-8	17.50	3.85	0.95	-11.75
SW-9	12.55	-4.95	-9.40	-13.45
SW-10	22.50	3.60	-2.25	2.15
SW-11	18.40	3.20	-5.80	-11.90
SW-12	22.60	5.90	1.20	-15.00
SW-13	18.50	0.90	-11.60	-20.90
SW-14	13.05	-2.50	-5.85	-9.35
SW-15	10.75	6.55	-6.25	-2.55
SW-16	10.75	6.45	-5.60	-2.00
SW-17	19.85	4.65	-4.30	-10.55
SW-18	12.65	18.15	21.55	34.45
SW-19	18.90	5.70	1.55	-1.45
SW-20	17.75	2.45	-4.85	-10.60
SW-21	24.05	2.70	-5.05	-2.65
SW-22	12.30	9.15	-5.40	-0.90
SW-23	11.40	8.00	-7.15	-4.35
SW-24	12.35	9.00	-7.35	-3.35
SW-25	12.05	8.45	-6.85	-2.75
SW-26	11.55	8.20	-3.55	0.40
SW-27	10.85	7.15	-7.60	-5.30
SW-28	11.40	7.60	-8.80	-6.10
SW-29	10.90	5.80	-5.50	-2.45
SW-30	21.85	16.40	17.30	3.75
SW-31	10.85	5.80	-5.65	-2.70

SW-32	15.00	21.65	17.60	31.25
SW-33	8.45	14.85	-5.00	-7.75
SW-34	11.30	9.45	-5.35	-1.20
SW-35	15.30	20.15	0.50	-6.30
SW-36	19.05	14.35	15.50	2.05
SW-37	15.05	19.35	2.35	-1.50
SW-38	17.35	29.70	13.00	-3.35
SW-39	14.35	18.65	2.05	-2.25
SW-40	14.90	19.95	-0.70	-7.45
SW-41	17.35	32.05	11.30	-9.20
SW-42	17.90	29.65	11.15	-7.25
SW-43	19.05	29.85	13.05	-4.05
SW-44	17.00	28.15	9.85	-8.90
SW-45	18.75	27.70	10.65	-7.45
SW-46	17.50	29.55	12.55	-4.55
SW-47	17.30	26.30	9.05	-9.00
SW-48	19.00	28.90	11.45	-6.65
SW-49	14.75	20.20	-0.45	-6.25
SW-50	18.60	27.05	10.50	-6.95
SW-51	23.95	34.85	23.80	3.35
SW-52	17.50	29.00	9.80	-10.60
SW-53	18.25	29.55	10.40	-9.25
SW-54	18.65	33.40	12.80	-9.25
SW-55	23.75	34.20	17.30	-11.90
SW-56	22.10	32.40	18.25	-6.25
SW-57	13.00	29.30	12.00	-8.10

Table E15: Changes in water yield simulation under varying future precipitation

Sub-watershed	Horizon 2020	Horizon 2040	Horizon 2060	Horizon 2080
SW-1	27.33	-123.00	-89.22	-12.08
SW-2	25.29	-122.26	-89.70	-12.39
SW-3	10.51	-89.41	-46.03	-22.11
SW-4	25.23	-121.41	-89.53	-12.14
SW-5	7.07	-91.15	-47.19	-20.78
SW-6	-21.17	-120.52	2.02	-20.98
SW-7	8.45	-89.69	-45.67	-19.56
SW-8	12.17	-89.01	-45.46	-22.41
SW-9	-19.24	-117.95	3.38	-20.56
SW-10	100.90	-37.19	144.95	122.80
SW-11	-25.40	-125.39	-0.74	-19.59
SW-12	7.15	-91.23	-45.88	-18.50
SW-13	-26.06	-125.26	1.03	-16.28
SW-14	-18.81	-117.75	4.18	-18.60
SW-15	9.10	-70.40	110.48	58.27
SW-16	8.95	-70.70	110.21	57.93
SW-17	-26.80	-127.25	-1.99	-21.12

SW-18	10.00	-68.55	109.91	58.53
SW-19	-24.68	-124.18	-0.07	-20.68
SW-20	-24.49	-124.00	-0.09	-19.87
SW-21	99.65	-38.49	143.85	122.50
SW-22	7.25	-72.80	109.26	56.53
SW-23	8.20	-72.25	109.72	58.75
SW-24	7.15	-73.40	109.58	56.44
SW-25	7.10	-72.80	110.40	57.09
SW-26	8.15	-71.70	109.72	57.67
SW-27	8.75	-72.00	109.39	58.23
SW-28	7.85	-72.70	110.04	58.39
SW-29	9.00	-69.80	109.92	57.46
SW-30	-25.82	30.95	147.24	51.54
SW-31	9.15	-70.00	110.60	58.54
SW-32	5.96	-75.48	109.36	56.21
SW-33	43.65	3.30	207.47	126.35
SW-34	7.90	-73.80	108.31	54.88
SW-35	60.85	65.80	286.65	133.14
SW-36	-23.02	33.26	150.98	53.33
SW-37	60.05	67.60	285.45	130.99
SW-38	73.40	145.70	302.00	139.90
SW-39	61.45	68.50	286.40	131.39
SW-40	60.55	65.25	286.06	134.30
SW-41	72.80	141.25	302.90	141.95
SW-42	72.25	144.60	302.75	141.35
SW-43	71.20	144.20	300.70	138.75
SW-44	75.10	146.50	304.55	147.05
SW-45	71.55	145.95	303.20	141.40
SW-46	73.60	145.10	303.25	144.75
SW-47	73.55	147.35	305.10	143.80
SW-48	70.60	144.75	302.15	140.50
SW-49	60.70	65.35	285.90	132.77
SW-50	72.60	148.55	305.25	143.25
SW-51	83.40	172.05	272.95	112.90
SW-52	72.75	144.30	303.15	144.55
SW-53	72.70	144.15	302.80	143.45
SW-54	97.85	185.70	345.70	183.55
SW-55	84.55	171.30	274.20	116.80
SW-56	85.20	173.50	275.75	114.80
SW-57	103.00	220.05	269.25	145.45

E4: Combined land use and climate change impacts assessment on SWAT simulation

Table E16: Changes in streamflow simulation under combined impact analysis

Sub-watershed	Horizon 2020	Horizon 2040	Horizon 2060	Horizon 2080
SW-1	18.02	-1.78	109.36	53.88
SW-2	17.96	-1.56	109.54	53.90
SW-3	-0.01	-0.85	-0.48	-0.28
SW-4	16.23	2.86	108.02	52.16
SW-5	16.16	4.06	108.77	52.45
SW-6	11.92	12.26	85.87	40.65
SW-7	4.12	-7.42	23.34	12.03
SW-8	1.57	-3.59	2.14	1.84
SW-9	-0.39	-2.28	0.02	-0.43
SW-10	2.73	-1.20	3.96	3.34
SW-11	12.39	15.52	85.73	41.18
SW-12	4.42	-4.58	23.62	12.58
SW-13	-0.17	-1.04	0.06	-0.10
SW-14	4.40	-4.08	23.89	12.72
SW-15	-0.14	-1.35	1.38	0.60
SW-16	4.56	-2.64	22.52	12.14
SW-17	12.66	17.44	85.64	41.38
SW-18	4.55	-2.57	22.41	12.10
SW-19	12.19	23.25	77.90	37.45
SW-20	12.01	22.79	77.75	37.30
SW-21	4.40	-0.72	19.79	10.74
SW-22	0.78	-4.90	7.97	4.20
SW-23	0.16	-1.82	2.60	1.33
SW-24	0.49	-3.00	4.91	2.58
SW-25	13.29	24.81	73.07	36.08
SW-26	0.27	-1.10	2.01	1.10
SW-27	3.95	-0.49	19.14	10.20
SW-28	2.81	0.98	12.35	6.28
SW-29	0.23	-1.00	1.80	0.97
SW-30	-0.82	0.96	4.60	1.61
SW-31	0.28	-1.75	2.86	1.50
SW-32	15.37	27.78	70.53	32.32
SW-33	1.13	0.30	4.63	2.89
SW-34	13.76	27.21	62.64	28.48
SW-35	1.45	1.57	6.28	2.99
SW-36	-0.54	0.67	3.19	1.11
SW-37	14.50	27.38	58.90	27.21
SW-38	11.46	23.58	44.66	20.70
SW-39	2.72	3.46	12.78	5.86
SW-40	2.15	2.32	9.15	4.41
SW-41	0.66	1.24	2.55	1.23
SW-42	0.99	1.95	4.06	1.90
SW-43	9.68	20.07	37.35	17.30

SW-44	0.94	1.90	4.04	1.92
SW-45	8.26	17.20	31.27	14.47
SW-46	0.60	1.23	2.66	1.25
SW-47	1.20	2.51	5.41	2.50
SW-48	6.95	14.44	25.34	11.73
SW-49	1.45	1.56	6.56	3.07
SW-50	5.43	11.20	18.21	8.49
SW-51	0.92	1.93	3.12	1.28
SW-52	1.50	3.17	5.54	2.43
SW-53	1.29	2.54	5.31	2.52
SW-54	3.88	7.92	12.44	5.96
SW-55	2.75	5.77	8.42	3.84
SW-56	1.01	2.10	3.37	1.40
SW-57	1.03	2.21	2.71	1.46

Table E17: Changes in sediment yield simulation under combined impact analysis

Sub-watershed	Horizon 2020	Horizon 2040	Horizon 2060	Horizon 2080
SW-1	4.47	0.20	80.06	42.00
SW-2	1.13	0.07	20.54	10.79
SW-3	0.00	0.00	0.00	0.00
SW-4	3.01	1.77	54.53	27.78
SW-5	1.06	0.63	19.19	9.78
SW-6	0.52	0.82	5.21	2.57
SW-7	0.74	-1.15	6.22	3.48
SW-8	0.13	0.09	0.16	0.17
SW-9	0.00	0.00	0.00	0.00
SW-10	0.00	0.00	0.00	0.00
SW-11	1.96	3.61	18.74	9.32
SW-12	0.91	-1.35	7.54	4.23
SW-13	0.00	0.00	0.00	0.00
SW-14	7.13	-7.19	59.49	33.31
SW-15	0.00	0.00	0.00	0.00
SW-16	5.95	-6.03	50.54	28.32
SW-17	5.99	9.15	43.29	21.32
SW-18	2.57	-0.55	14.87	8.24
SW-19	0.02	0.10	0.45	0.04
SW-20	2.57	5.66	19.13	9.36
SW-21	0.12	0.00	0.69	0.38
SW-22	0.00	-0.05	0.09	0.05
SW-23	0.00	0.00	0.00	0.00
SW-24	0.00	-0.08	0.13	0.08
SW-25	-0.09	0.28	2.18	-0.82
SW-26	0.00	0.00	0.00	0.00
SW-27	0.02	0.00	0.10	0.06
SW-28	0.01	0.00	0.04	0.02
SW-29	0.00	0.00	0.00	0.00

SW-30	0.00	0.00	0.00	0.00
SW-31	0.00	0.00	0.00	0.00
SW-32	0.57	1.03	1.99	1.07
SW-33	0.00	0.00	0.00	0.00
SW-34	0.99	1.77	3.22	1.78
SW-35	0.00	0.00	0.00	0.00
SW-36	0.00	0.00	0.00	0.00
SW-37	1.38	2.36	4.08	2.32
SW-38	0.59	0.99	1.58	0.93
SW-39	0.01	0.02	0.07	0.03
SW-40	0.00	0.00	0.00	0.00
SW-41	0.00	0.00	0.00	0.00
SW-42	0.00	0.00	0.00	0.00
SW-43	0.88	1.38	2.13	1.29
SW-44	0.00	0.00	0.00	0.00
SW-45	3.50	5.30	7.95	4.97
SW-46	0.00	0.00	0.00	0.00
SW-47	0.50	0.60	0.80	0.59
SW-48	0.15	0.37	0.62	0.31
SW-49	0.00	0.00	0.00	0.00
SW-50	0.94	2.25	3.65	1.78
SW-51	0.00	0.00	0.00	0.00
SW-52	0.03	0.05	0.09	0.04
SW-53	0.00	0.00	0.00	0.00
SW-54	0.02	0.06	0.09	0.04
SW-55	0.02	0.04	0.06	0.03
SW-56	0.00	0.00	0.00	0.00
SW-57	0.00	0.00	0.00	0.00

Table E18: Changes in evapotranspiration simulation under combined impact analysis

Sub-watershed	Horizon 2020	Horizon 2040	Horizon 2060	Horizon 2080
SW-1	-29.75	-51.10	-58.05	-80.45
SW-2	-43.65	-65.45	-72.55	-94.40
SW-3	31.45	16.50	12.20	-1.95
SW-4	-28.55	-51.20	-59.05	-81.95
SW-5	-22.20	-38.30	-42.70	-57.35
SW-6	-10.75	-28.65	-34.85	-39.90
SW-7	7.15	-9.30	-14.50	-29.00
SW-8	20.25	4.45	-1.60	-17.55
SW-9	-8.80	-27.50	-32.75	-37.90
SW-10	-35.45	-57.80	-66.00	-63.85
SW-11	-38.65	-55.80	-65.05	-72.30
SW-12	8.40	-9.00	-14.80	-32.05
SW-13	-0.35	-18.10	-30.00	-38.70
SW-14	-55.05	-73.55	-78.45	-83.85
SW-15	-3.45	-7.20	-24.55	-21.90

SW-16	-23.00	-27.90	-42.20	-39.90
SW-17	-14.80	-31.75	-43.10	-52.20
SW-18	-312.20	-317.50	-330.25	-329.15
SW-19	-105.20	-123.60	-130.85	-137.35
SW-20	-44.90	-63.10	-70.85	-78.35
SW-21	12.20	-11.15	-19.35	-17.65
SW-22	-25.20	-29.10	-46.20	-43.10
SW-23	-14.05	-17.75	-34.00	-31.85
SW-24	3.65	1.30	-18.80	-15.50
SW-25	-39.15	-45.75	-58.85	-56.20
SW-26	-48.55	-54.50	-67.30	-65.30
SW-27	-3.95	-7.05	-23.65	-21.45
SW-28	-21.15	-27.65	-41.20	-39.40
SW-29	-20.00	-26.65	-38.25	-35.90
SW-30	10.25	4.35	4.65	-9.75
SW-31	-22.00	-28.10	-40.70	-38.75
SW-32	-185.60	-186.55	-200.40	-194.20
SW-33	-19.65	-15.60	-34.80	-38.60
SW-34	26.15	24.30	4.10	7.30
SW-35	5.60	9.75	-9.75	-16.10
SW-36	9.10	3.85	4.70	-9.80
SW-37	-7.95	-4.45	-22.40	-27.35
SW-38	-2.25	9.55	-8.25	-25.65
SW-39	15.10	20.65	1.50	-4.90
SW-40	0.40	4.40	-15.60	-22.25
SW-41	10.25	24.10	3.95	-15.75
SW-42	8.35	19.60	0.75	-18.20
SW-43	7.65	18.60	0.70	-17.55
SW-44	-9.65	1.85	-18.70	-40.25
SW-45	13.50	22.45	4.75	-13.95
SW-46	-31.50	-19.60	-40.05	-61.65
SW-47	14.40	24.35	5.45	-14.45
SW-48	54.20	69.40	47.25	23.70
SW-49	5.90	10.95	-9.75	-15.55
SW-50	0.60	8.95	-8.90	-28.45
SW-51	-87.45	-76.85	-93.90	-123.95
SW-52	11.10	21.75	2.55	-17.90
SW-53	11.00	22.05	2.70	-17.10
SW-54	8.90	23.60	2.30	-20.60
SW-55	8.15	18.40	0.25	-30.70
SW-56	-33.55	-23.80	-40.60	-70.25
SW-57	-13.35	2.85	-15.65	-37.05

Table E19: Changes in water yield simulation under combined impact analysis

Sub-watershed	Horizon 2020	Horizon 2040	Horizon 2060	Horizon 2080
SW-1	10.73	-136.23	-102.37	-23.81
SW-2	14.29	-131.29	-98.03	-19.48
SW-3	-1.04	-101.20	-57.66	-33.34
SW-4	22.90	-123.40	-90.88	-13.17
SW-5	12.36	-86.43	-43.24	-17.85
SW-6	-16.67	-116.13	5.88	-17.79
SW-7	12.53	-86.01	-42.67	-17.51
SW-8	-26.43	-126.01	-79.41	-52.55
SW-9	-20.62	-119.82	1.52	-22.24
SW-10	96.20	-41.98	139.65	117.85
SW-11	-16.14	-115.94	7.94	-13.31
SW-12	4.73	-93.79	-48.25	-20.83
SW-13	-19.54	-118.78	6.80	-11.76
SW-14	-17.48	-116.58	4.42	-19.13
SW-15	-9.20	-90.00	93.16	40.92
SW-16	4.30	-75.60	105.19	52.91
SW-17	-36.81	-137.77	-12.09	-30.13
SW-18	-2.15	-81.70	97.55	46.46
SW-19	-13.44	-112.68	9.96	-11.74
SW-20	-14.80	-114.29	8.23	-12.17
SW-21	89.70	-47.59	134.05	113.10
SW-22	2.50	-78.00	104.86	51.96
SW-23	6.75	-74.80	107.29	55.47
SW-24	-8.45	-90.85	93.90	41.39
SW-25	27.25	-50.70	129.34	75.91
SW-26	15.15	-64.05	116.05	62.95
SW-27	0.15	-81.60	100.52	48.17
SW-28	26.15	-52.50	127.75	75.54
SW-29	14.30	-63.75	115.34	63.05
SW-30	-25.94	31.12	147.40	51.96
SW-31	11.10	-68.05	111.96	59.89
SW-32	10.92	-69.68	114.23	61.88
SW-33	53.20	14.95	218.85	136.54
SW-34	-26.57	-109.42	76.39	23.78
SW-35	67.80	73.75	292.90	140.15
SW-36	-24.67	31.86	149.73	52.28
SW-37	61.75	68.45	286.55	132.29
SW-38	74.05	146.40	303.00	140.35
SW-39	44.85	49.30	268.75	114.48
SW-40	68.80	74.20	294.60	141.96
SW-41	80.00	149.45	309.86	149.15
SW-42	73.85	146.15	304.50	143.10
SW-43	69.40	142.50	299.30	137.30
SW-44	70.30	140.65	300.45	142.85
SW-45	70.05	144.40	302.65	140.45

SW-46	67.00	137.95	296.95	139.60
SW-47	63.55	136.90	294.60	134.30
SW-48	32.15	99.10	261.05	104.55
SW-49	64.15	68.20	289.29	136.37
SW-50	70.75	145.70	303.40	142.55
SW-51	78.65	165.50	267.40	109.83
SW-52	76.20	149.15	307.40	148.10
SW-53	74.05	146.55	304.65	144.80
SW-54	97.00	185.00	344.20	182.35
SW-55	83.10	169.60	272.75	116.35
SW-56	81.25	168.85	271.35	112.45
SW-57	103.10	220.05	269.80	145.80

VITA

Name	: **Santosh Subhash Palmate**
Address	: Room No. F-24, Azad Bhawan IIT Roorkee, Roorkee Dist. Haridwar, Uttarakhand – 247667 India
Email ID	: psubhash@wr.iitr.ac.in; santoshpalmate@gmail.com
Educational Qualifications	: B.Tech. (Agricultural Engineering), June-2011 MAU Parbhani, Maharashtra, India M.Tech. (Irrigation Water Management), June-2013 IIT Roorkee, Uttarakhand, India

Publications from the Ph.D. research work

Peer-reviewed Journal

1. Pandey, A., & **Palmate, S.S.** (2019). Assessing future water-sediment interaction and critical area prioritization at sub-watershed level for sustainable management. *Paddy and Water Environment (Springer Publication)*. https://doi.org/10.1007/s10333-019-00732-3 (**IF: 1.379**)
2. **Palmate S. S.**, Pandey A., & Mishra, S. K. (2017). Modelling spatiotemporal Land dynamics for a trans-boundary river basin using an integrated Cellular Automata and Markov Chain approach. *Applied Geography (Elsevier Publication), 82: 11-23.* https://doi.org/10.1016/j.apgeog.2017.03.001 (**IF: 3.844**)

Conference

3. **Palmate, S.S.,** & Pandey, A. (2019). Effectiveness of Best Management Practices on Dependable Flow in a River Basin. *ASABE Annual International Meeting 2019, Boston, US,* July 7-10.
4. **Palmate, S.S.**, Wagner, P.D., Pandey, A., & Fohrer, N. (2018). Effects of land use change on the water resources of the Basoda basin using the SWAT model. *International SWAT conference 2018, IIT Madras, India,* January 8-12.
5. **Palmate, S.S.,** & Pandey, A. (2017). Monitoring crop land greening and degradation using remotely sensed MODIS time-series data. *EGU General Assembly 2017, Vienna, Austria,* Vol. 19: p. 1284, April 23-28.
6. **Palmate, S.S.**, Pandey, A., Suryavanshi, S., & Himanshu, S.K. (2016). Relationship between Climate Variability and Runoff in the Betwa River Basin. *International Conference on Climate Change and Rural Development, Aurangabad, India,* January 21-23.

Other publications during Ph.D. study

Journal

1. Pandey, A., & **Palmate, S. S.** (2018). Assessments of spatial land cover dynamic hotspots employing MODIS time-series datasets in the Ken River Basin of Central India. *Arabian Journal of Geosciences*, 11(17), 479. https://doi.org/10.1007/s12517-018-3812-z (**IF: 0.860**)

2. **Palmate, S.S.**, Pandey, A., Kumar, D., Pandey, R.P., & Mishra, S.K. (2017). Climate change impact on forest cover and vegetation in Betwa Basin, India. *Applied Water Science (Springer)*, 7(1): 103-114. https://doi.org/10.1007/s13201-014-0222-6

3. Kumar, D., Gautam, A. K., **Palmate, S. S.**, Pandey, A., Suryavanshi, S., Rathore, N. & Sharma, N. (2017). Evaluation of TRMM multi-satellite precipitation analysis (TMPA) against terrestrial measurement over a humid sub-tropical basin, India. *Theoretical and Applied Climatology*, 129(3-4): 783-799. https://doi.org/10.1007/s00704-016-1807-9 (**IF: 2.321**)

Conference

4. Dayal, D., Pandey, A., Himanshu, S.K., & **Palmate, S.S.** (2018). Long Term Historic Changes of Precipitation and Aridity Index over an Indian River Basin. *ASCE World Environmental and Water Resources Congress 2018, Minneapolis, Minnesota, USA,* pg. 262-272, June 3-7. https://doi.org/10.1061/9780784481417.026

5. Pandey, A., & **Palmate, S.S.** (2017). Assessment of Land Degradation and Greening in Ken River Basin of Central India. *EGU General Assembly 2017, Vienna, Austria,* Vol. 19: p. 3846, April 23-28.

6. Abdelfattah, A.A., Pandey, A., & **Palmate, S.S.** (2017). Evaluation of Temperature Based Evapotranspiration Models in Subtropical Humid Climate of India. *ASABE 2017 Annual International Meeting, Spokane, Washington, USA,* July 16-19.

List of Ph.D. manuscript(s) under review

- Palmate, S. S., Wagner, P. D., Fohrer, N., & Pandey, A. Assessment of uncertainties in modelling land use change with an integrated Cellular Automata−Markov Chain model. *(*In *Journal of Environmental Informatics; Manuscript ID.: 18JM11240118)*
- Palmate, S. S., Pandey, A., Pandey, R. P., & Mishra, S. K. Assessing the land cover dynamic response to changes in hydro-climatic variables using a conceptual framework. (In *Environmental Earth Sciences; Manuscript ID: ENGE-D-19-00196*)